Residual stresses in composite materials

Related titles:

Non-destructive evaluation (NDE) of polymer matrix composites
(ISBN 978-0-85709-344-8)

Developments in fiber-reinforced polymer (FRP) composites for civil engineering
(ISBN 978-0-85709-234-2)

Advanced fibre-reinforced polymer (FRP) composites for structural applications
(ISBN 978-0-85709-418-6)

Details of these books and a complete list of titles from Woodhead Publishing can be obtained by:

- visiting our web site at www.woodheadpublishing.com
- contacting Customer Services (e-mail: sales@woodheadpublishing.com; fax: +44 (0) 1223 832819; tel.: +44 (0) 1223 499140 ext. 130; address: Woodhead Publishing Limited, 80, High Street, Sawston, Cambridge CB22 3HJ, UK)
- in North America, contacting our US office (e-mail: usmarketing@woodheadpublishing.com; tel.: (215) 928 9112; address: Woodhead Publishing, 1518 Walnut Street, Suite 1100, Philadelphia, PA 19102–3406, USA)

If you would like e-versions of our content, please visit our online platform: www.woodheadpublishingonline.com. Please recommend it to your librarian so that everyone in your institution can benefit from the wealth of content on the site.

We are always happy to receive suggestions for new books from potential editors. To enquire about contributing to our Composites Science and Engineering series, please send your name, contact address and details of the topic/s you are interested in to gwen.jones@woodheadpublishing.com. We look forward to hearing from you.

The team responsible for publishing this book:

Commissioning Editor: Francis Dodds
Publications Coordinator: Lucy Beg
Project Editor: Kate Hardcastle
Editorial and Production Manager: Mary Campbell
Production Editor: Mandy Kingsmill
Project Manager: Annette Wiseman, RCL
Copyeditor: Jo Egré
Proofreader: Annette Wiseman
Cover Designer: Terry Callanan

Woodhead Publishing Series in Composites Science and Engineering:
Number 48

Residual stresses in composite materials

Edited by
Mahmood M. Shokrieh

Oxford Cambridge Philadelphia New Delhi

Published by Woodhead Publishing Limited,
80 High Street, Sawston, Cambridge CB22 3HJ, UK
www.woodheadpublishing.com
www.woodheadpublishingonline.com

Woodhead Publishing, 1518 Walnut Street, Suite 1100, Philadelphia, PA 19102-3406, USA

Woodhead Publishing India Private Limited, 303, Vardaan House, 7/28 Ansari Road,
Daryaganj, New Delhi – 110002, India
www.woodheadpublishingindia.com

First published 2014, Woodhead Publishing Limited

British Library Cataloguing in Publication Data
A catalogue record for this book is available from the British Library.

Library of Congress Control Number: 2013947979

ISBN 978-0-85709-270-0 (print)
ISBN 978-0-85709-859-7 (online)
ISSN 2052-5281 Woodhead Publishing Series in Composites Science and Engineering (print)
ISSN 2052-529X Woodhead Publishing Series in Composites Science and Engineering (online)

The publisher's policy is to use permanent paper from mills that operate a sustainable forestry policy, and which has been manufactured from pulp which is processed using acid-free and elemental chlorine-free practices. Furthermore, the publisher ensures that the text paper and cover board used have met acceptable environmental accreditation standards.

Typeset by RefineCatch Limited, Bungay, Suffolk
Printed by Lightning Source

Contributor contact details

(* = main contact)

Editor

M. M. Shokrieh
Composites Research Laboratory
Center of Excellence in
Experimental Solid Mechanics
and Dynamics
School of Mechanical Engineering
Iran University of Science and
Technology
Narmak
Tehran 16846-13114, Iran

E-mail: shokrieh@iust.ac.ir

Chapters 1, 2 and 3

M. M. Shokrieh* and A. R. Ghanei
Mohammadi
Composites Research Laboratory
Center of Excellence in
Experimental Solid Mechanics
and Dynamics
School of Mechanical Engineering
Iran University of Science and
Technology
Narmak
Tehran 16846-13114, Iran

E-mail: shokrieh@iust.ac.ir

Chapter 4

A. R. Ghasemi
Department of Mechanical
Engineering
University of Kashan
Kashan 87317-51167, Iran

F. Taheri-Behrooz and M. M.
Shokrieh*
Composites Research Laboratory
Center of Excellence in
Experimental Solid Mechanics
and Dynamics
School of Mechanical Engineering
Iran University of Science and
Technology
Narmak
Tehran 16846-13114, Iran

E-mail: shokrieh@iust.ac.ir

Chapter 5

M. M. Shokrieh* and S. Akbari
Composites Research Laboratory
Center of Excellence in
Experimental Solid Mechanics
and Dynamics
School of Mechanical Engineering
Iran University of Science and
Technology
Narmak
Tehran 16846-13114, Iran

E-mail: shokrieh@iust.ac.ir

Chapter 6

H. Aben* and A. Errapart
Institute of Cybernetics
Tallinn University of Technology
21 Akadeemia tee
12618 Tallinn, Estonia

E-mail: aben@cs.ioc.ee

J. Anton
GlasStress Ltd
21 Akadeemia tee
12618 Tallinn, Estonia

Chapter 7

M. M. Shokrieh* and S. M. Kamali Shahri
Composites Research Laboratory
Center of Excellence in Experimental Solid Mechanics and Dynamics
School of Mechanical Engineering
Iran University of Science and Technology
Narmak
Tehran 16846-13114, Iran

E-mail: shokrieh@iust.ac.ir

Chapter 8

M. M. Shokrieh*
Composites Research Laboratory
Center of Excellence in Experimental Solid Mechanics and Dynamics
School of Mechanical Engineering
Iran University of Science and Technology
Narmak
Tehran 16846-13114, Iran

E-mail: shokrieh@iust.ac.ir

M. Safarabadi
School of Mechanical Engineering
College of Engineering
University of Tehran
North Amirabad
Tehran, 1135716914, Iran

E-mail: msafarabadi@ut.ac.ir

Chapter 9

M. M. Aghdam* and S. R. Morsali
Thermoelasticity Center of Excellence
Department of Mechanical Engineering
Amirkabir University of Technology
Hafez Ave.
Tehran, Iran

E-mail: aghdam@aut.ac.ir

Chapter 10

H. Wu
Department of Materials
Loughborough University
Leicestershire LE11 3TU, UK

E-mail: h.wu2@lboro.ac.uk

Chapter 11

R. Jaeger* and C. Koplin
Biomedical Materials and Implants Group
Fraunhofer Institute for Mechanics of Materials IWM
Freiburg, Germany

E-mail: raimund.jaeger@iwm.fraunhofer.de; christof.koplin@iwm.fraunhofer.de

Chapter 12

F. Dai
Center for Composite Materials and Structures
Harbin Institute of Technology
92 West Dazhi Street
Nan Gang District
Harbin, People's Republic of China 150001

E-mail: daifh@hit.edu.cn

Chapter 13

M. M. Shokrieh*, S. Akbari and A. Daneshvar
Composites Research Laboratory
Center of Excellence in Experimental Solid Mechanics and Dynamics
School of Mechanical Engineering
Iran University of Science and Technology
Narmak
Tehran 16846-13114, Iran

Email: shokrieh@iust.ac.ir

Woodhead Publishing Series in Composites Science and Engineering

1 **Thermoplastic aromatic polymer composites**
F. N. Cogswell
2 **Design and manufacture of composite structures**
G. C. Eckold
3 **Handbook of polymer composites for engineers**
Edited by L. C. Hollaway
4 **Optimisation of composite structures design**
A. Miravete
5 **Short-fibre polymer composites**
Edited by S. K. De and J. R. White
6 **Flow-induced alignment in composite materials**
Edited by T. D. Papthanasiou and D. C. Guell
7 **Thermoset resins for composites**
Compiled by Technolex
8 **Microstructural characterisation of fibre-reinforced composites**
Edited by J. Summerscales
9 **Composite materials**
F. L. Matthews and R. D. Rawlings
10 **3-D textile reinforcements in composite materials**
Edited by A. Miravete
11 **Pultrusion for engineers**
Edited by T. Starr
12 **Impact behaviour of fibre-reinforced composite materials and structures**
Edited by S. R. Reid and G. Zhou
13 **Finite element modelling of composite materials and structures**
F. L. Matthews, G. A. O. Davies, D. Hitchings and C. Soutis
14 **Mechanical testing of advanced fibre composites**
Edited by G. M. Hodgkinson
15 **Integrated design and manufacture using fibre-reinforced polymeric composites**
Edited by M. J. Owen and I. A. Jones
16 **Fatigue in composites**
Edited by B. Harris
17 **Green composites**
Edited by C. Baillie

18 **Multi-scale modelling of composite material systems**
Edited by C. Soutis and P. W. R. Beaumont
19 **Lightweight ballistic composites**
Edited by A. Bhatnagar
20 **Polymer nanocomposites**
Y-W. Mai and Z-Z. Yu
21 **Properties and performance of natural-fibre composite**
Edited by K. Pickering
22 **Ageing of composites**
Edited by R. Martin
23 **Tribology of natural fiber polymer composites**
N. Chand and M. Fahim
24 **Wood-polymer composites**
Edited by K. O. Niska and M. Sain
25 **Delamination behaviour of composites**
Edited by S. Sridharan
26 **Science and engineering of short fibre reinforced polymer composites**
S-Y. Fu, B. Lauke and Y-M. Mai
27 **Failure analysis and fractography of polymer composites**
E. S. Greenhalgh
28 **Management, recycling and reuse of waste composites**
Edited by V. Goodship
29 **Materials, design and manufacturing for lightweight vehicles**
Edited by P. K. Mallick
30 **Fatigue life prediction of composites and composite structures**
Edited by A. P. Vassilopoulos
31 **Physical properties and applications of polymer nanocomposites**
Edited by S. C. Tjong and Y-W. Mai
32 **Creep and fatigue in polymer matrix composites**
Edited by R. M. Guedes
33 **Interface engineering of natural fibre composites for maximum performance**
Edited by N. E. Zafeiropoulos
34 **Polymer-carbon nanotube composites**
Edited by T. McNally and P. Pötschke
35 **Non-crimp fabric composites: Manufacturing, properties and applications**
Edited by S. V. Lomov
36 **Composite reinforcements for optimum performance**
Edited by P. Boisse
37 **Polymer matrix composites and technology**
R. Wang, S. Zeng and Y. Zeng
38 **Composite joints and connections**
Edited by P. Camanho and L. Tong
39 **Machining technology for composite materials**
Edited by H. Hocheng
40 **Failure mechanisms in polymer matrix composites**
Edited by P. Robinson, E. S. Greenhalgh and S. Pinho
41 **Advances in polymer nanocomposites: Types and applications**
Edited by F. Gao

42 **Manufacturing techniques for polymer matrix composites (PMCs)**
Edited by S. Advani and K-T. Hsiao
43 **Non-destructive evaluation (NDE) of polymer matrix composites: Techniques and applications**
Edited by V. M. Karbhari
44 **Environmentally friendly polymer nanocomposites: Types, processing and properties**
S. S. Ray
45 **Advances in ceramic matrix composites**
Edited by I. M. Low
46 **Ceramic nanocomposites**
Edited by R. Banerjee and I. Manna
47 **Natural fibre composites: Materials, processes and properties**
Edited by A. Hodzic and R. Shanks
48 **Residual stresses in composite materials**
Edited by M. M. Shokrieh
49 **Health and environmental safety of nanomaterials: polymer nanocomposites and other materials containing nanoparticles**
Edited by J. Njuguna, K. Pielichowski and H. Zhu

Introduction

Residual stresses are self-balanced stresses that exist in engineering components, even when they are not under external loads. Although residual stresses exist in many engineering components, due to the complexity of their nature some designers ignore them in the design process. Often the magnitude of these stresses is significant and ignoring them at the design stage may result in a risky design. However, residual stresses can be useful and improve the performance of the component under load-bearing conditions. Therefore, methods of determination, measurement, simulation and reduction of residual stresses are important research topics.

In composite materials, micro-residual stresses are created during the manufacturing process, due to the mismatch of the physical and mechanical properties of the matrix and reinforcement. The shrinkage of the matrix after curing is also another source of such stresses. In laminated composites, the physical and mechanical properties of each ply are functions of the direction of the reinforcement. This is the source of macro-residual stresses in laminated composites. Also, heat treatment processes after manufacturing, machining and environmental conditions, such as absorption or release of the moisture, are some of the other sources of residual stresses.

Although residual stresses can occasionally be beneficial, they are usually detrimental. In some circumstances these stresses can cause warping, undesired distortion and dimensional instability in composite specimens. Experimental observations show that residual stresses can cause matrix cracking. Although this mode of failure is not catastrophic, cracks can be a dangerous source of failure initiation; especially when the specimen is under cyclic loading conditions. Also, matrix cracking can be a source of delamination in laminated composites, which is a catastrophic mode of failure.

There are different experimental methods for measuring residual stresses in various materials. Measurement of residual stresses can be performed by destructive, semi-destructive and non-destructive techniques. As a general classification, these methods can be categorized as mechanical, optical, diffraction and stress-relevant properties methods. By considering the physical and

mechanical properties of composite materials, special methods for measurement of residual stresses in these types of materials are available. Among different measurement techniques for measuring the residual stresses, mechanical techniques are those most often used by various researchers for measurement of residual stresses in composites.

Application of the other techniques for measurement of the residual stresses in composite materials can sometimes be very difficult or even impossible. A deeper understanding of the physics and mechanics of these stresses in composites and finding suitable techniques for their measurement are still needed. As already mentioned, there are many complexities and difficulties in the use of some of the experimental techniques for the measurement of residual stresses in composites and further research is also needed to eliminate these obstacles.

There are also various mathematical (analytical and numerical) methods for calculation of residual stresses in composite materials. These methods have been developed based on assumptions made on the curing process of composites. The generality of the model and the proper characterization of the constituent materials (reinforcement and matrix) play important roles in successful simulation of the process. For this purpose, a precise characterization of the matrix and the reinforcement properties with time and temperature is necessary. Studies on the mechanisms of generation of additional residual stresses due to tool-part interaction are an ongoing research area and their influence on the final residual stresses should be understood. Thus, there are many unanswered questions in the mathematical modeling of residual stresses that need to be clarified by further research.

There are a few techniques available in the literature for reduction of residual stresses. One of these techniques is heat treatment after the curing process of composites. Addition of nanoparticles to the matrix, to reduce the mismatch of the physical and mechanical properties of the matrix and the reinforcement (also reducing the shrinkage behavior of the matrix), is a new method that has been recently studied by some authors. This field also seems attractive for further research.

In this book, the latest available results of research in the field of residual stresses in polymer, metal and ceramic matrix composites are comprehensively reviewed and provided. The present state of knowledge and the future trends of research on this subject are analyzed and interpreted. A comprehensive review of the available knowledge of residual stresses in composite materials shows that further research is required, in modeling and experimental characterization, for a proper and deeper understanding of this complicated subject.

Mahmood M. Shokrieh

1

The importance of measuring residual stresses in composite materials

M. M. SHOKRIEH and A. R. GHANEI MOHAMMADI,
Iran University of Science and Technology, Iran

DOI: 10.1533/9780857098597.1.3

Abstract: This chapter discusses categories of residual stress in composite materials, their effects and the importance of their measurement. It also summarizes issues in measuring residual stresses and introduces the range of techniques available.

Key words: composite materials, residual stress, measurement, experimental techniques.

1.1 Introduction

In the modern world there is an increasing need for high strength, lightweight materials such as composites for a wide range of applications, including the aerospace and automotive industries, civil infrastructure, sporting goods, etc. In order to get the best out of such materials, a good understanding of the different aspects of their behavior is required. An important aspect that needs proper investigation is the effect of the manufacturing process on the mechanical behavior of the material. A good example is residual stresses in materials created by processes such as heating. Such stresses have played an important role in manufacture since the beginning of civilization. In the manufacture of sword blades, for example, repeated hammering at a controlled elevated temperature creates a thin layer of compressive residual stress which strengthens the blade.

Residual stresses can be defined as stress fields that exist in the absence of any external loads and are the result of any mechanical process which can cause deformation. As an example, non-uniform heating or cooling causes thermal strain. Incompatible deformation is induced by plastic deformation, and mismatched thermal expansion coefficients produce discontinuity in deformation due to temperature change. The two main factors that affect residual stress are the processes that the component has undergone, and the material properties that relate the mechanical process to deformation behaviour (Cheng and Finnie, 2007).

Operations, such as mechanical forming procedures, heat treatment or welding, can cause residual stresses during manufacture and/or use. Processes resulting in stress concentrations close to surfaces can boost failure resistance.

Manufacturing processes, such as shot peening, chemical surface treatment and laser surface hardening, are used to induce useful surface compression to improve resistance to fatigue failure. However, those leading to surface tension normally facilitate the formation of cracks, which can cause untimely fracture (Colpo, 2006; Fitzpatrick and Lodini, 2003). The distortion of laminate composites is typically the result of residual stresses. This makes it particularly important to understand, measure, model and control residual stresses in composite and other materials.

Residual stresses arise for several reasons: on the macroscopic scale, they may emanate from heat treating, machining and secondary processing, and assembly. On the microscopic scale, they usually result from the discontinuities between the thermal expansion coefficients, yield stresses, rigidities or phase changes (e.g. cure shrinking) of different constituents. In any component or material, both kind of stress may co-exist (Colpo, 2006).

A fiber reinforced polymer (FRP) composite is usually subject to a process wherein the resin is heated, the fibers are wetted and cure is performed at high temperatures. The need for high temperatures in the curing process results in formation of residual stresses in the final laminate structure. These residual stresses have two major causes: the mismatch in thermal expansion of the constituents, and chemical shrinkage of the polymers in the composite. Measurement and characterization of these stresses is complex (Liu, 1999). Residual stresses typically arise due to the discrepancies between the mechanical properties of the matrix and the reinforcing fibers. Other mechanisms that cause residual stresses include cure shrinkage, moisture, ageing, elevated post-cure temperature, differences in material properties at the microscopic scale, differences in fiber volume across the matrix and non-uniform degree of cure (Tsouvalis *et al.*, 2009).

1.2 Categories of residual stresses

Barnes and Byerly (1994) explained the various types of residual stress at work in continuous carbon-fiber-reinforced thermoplastic composites. They identified three levels of stress in laminated structures: the 'micro-stresses' present between distinct fibers within each ply, the 'macro-stresses' forming in multi-axial laminates at the ply-to-ply scale, and a third, more prevalent level of stress resulting from different thermal histories of distinct parts of a laminate during the cooling stage.

The discontinuity between the thermal expansion coefficients of the fiber and matrix, along with the development of chemical shrinkage, create residual strains and stress at the ply scale. As a lamina is cured, its matrix constituent is subject to polymerization. Epoxy resins undergo condensation polymerization, where two reacting monomers are put together to form a new molecule of the compound in question (Gibson, 1994). For many advanced structural composites, this process

happens in two steps. Prepreg tape is produced by wetting the fibers and allowing the matrix to partially cure. When these prepreg materials are arranged into the desired stacking sequences and then heated to the desired cure temperature, the polymerization process is complete. During this process, the matrix undergoes a volumetric change known as chemical shrinkage, while the fibers stay volumetrically unchanged. This heightens the mismatch in expansion of the fibers and matrix, where the matrix undergoes greater expansion and contraction than the fiber (Myers, 2004).

Residual stresses arise when the expansion of the lamina is limited. As the angles of the lamina vary from ply to ply, the lower contraction of the fiber constrains the contraction of the matrix. When temperatures are lowered, the matrix attempts to contract but is subjected to tensile stress opposing this deformation. If all of the fibers are aligned with each other, there will be no stress on the ply scale. A cross-ply [0/90] stacking sequence leads to the highest level of residual stress (Myers, 2004).

All three scales of residual stresses must be taken into account when determining the overall state of stress. At the macro- or structural-scale, residual stresses arise due to the counteraction of one part of the structure against another, which may occur when one component experiences different thermal strains from another, or because of external constraints. At the meso- or laminate-scale, residual stresses arise through individual laminae experiencing different thermal and hygroscopic strains from those of neighboring laminae. This may be due to temperature and moisture variation throughout the laminate and from inter-lamina differences in material characteristics or orientations. The fibers and matrix are equally strained at both the macro- and meso-scales; therefore, the effects of residual stresses at these scales are not distinguishable from mechanical stresses. However, at the micro- or lamina-scale, this does not hold true. At this scale, stresses in the fiber and matrix counteract, even when the lamina appears not to be loaded at larger scales. In this situation the residual stresses arise from discrepancies in the unconstrained thermal and hygroscopic strains of the fibers and the matrix.

Polymerization cure shrinkage of the matrix sets up additional residual stresses at this scale. Residual stresses are set up both parallel and perpendicular to the fiber direction. Nevertheless, the fibers can significantly restrain the free movement of the resin system and align it with the fiber length. The stresses in this direction are thereby considerably greater than those perpendicular to the fiber direction. Consequently, the magnitude of the latter stresses is not important, particularly as these stresses are not aligned in a direction to increase environmentally assisted cracking of the laminate (Reid and Paskaramoorthy, 2009).

The residual stresses at the micro-scale, along with the overall stress state arising from both the mechanical loading and the macro- and meso-scale residual stresses, alter the overall stress state. Tensile residual stresses at the micro-scale

tend to assist in opening microcracks in the polymer matrix before the crack may promote the flow of corrosive media to the glass fibers, potentially heightening crack growth rate. This is prevalent as corrosion equipment is usually cured at room temperature and then exposed to post-cure at higher temperatures for the enhancement of the chemical resistance of the resin system (Stone *et al.*, 1997). Therefore, the relatively high thermal contraction of the resin system as the laminate cools to room temperature is significantly hindered by the stiff fibers. Moreover, the fibers can inhibit the free shrinkage of the resin due to the additional polymerization reactions through post-cure. Therefore the resin system is loaded in tension while the fibers become compressed. The tensile stress in the resin increases its predisposition to microcracking. Furthermore, the reduction in tensile stress in the fibers lowers their tendency to fracture. As a result, the increased percolation of corrosive media to the fibers can be offset by the longer time required for flaws of critical size to form in the fibers (Reid, 2009).

Another basic mechanism taking place when a laminate with a low coefficient of thermal expansion (CTE) is cured on a tool with a much higher CTE, is tool-laminate interaction. Cure shrinkage is another basic mechanism creating residual stresses. It is a chemical effect occurring through curing when the polymer volume decreases leading to a high level of locked in stress (Stamatopoulos, 2011).

The sources of residual stresses are classifiable as intrinsic (concerning material, lay-up and structure shape) or extrinsic (concerning processing and tooling). Non-consistent thermal expansion is one of the basic mechanisms affecting all three of the above-mentioned levels of residual stresses. At the micro-mechanical (intra-laminar) level, the thermal expansion coefficient discrepancies between the fibers and the matrix is the chief factor for development of residual stresses. Cooling through the curing cycle leads to a volumetric shrinkage of the matrix considerably greater than that of the fibers. A second level of stress in continuous-fiber-reinforced composites forms on the ply-to-ply scale (inter-laminar) in multi-axial laminates, because of the non-consistent CTEs of the individual plies in different directions. These are regarded as ‘macro-stresses’ (macro-mechanical or lamination residual stresses according to Parlevliet *et al.*, 2006), which exist on a ply-to-ply scale as a result of lamina anisotropy (Twigg *et al.*, 2004). At the laminate level, residual stresses arise throughout the thickness and are typically parabolically distributed. Such stresses in uni-axial laminates can be about 40 MPa, affecting the mechanical response of the composite. Moreover, dimensional tolerance problems in asymmetrically cooled laminates might be caused by such stresses. One important point concerning the stresses arising at this level is that they can be stopped by raising the composite above the glass transition temperature (T_g) of the matrix, and permitting relaxation processes to take effect (Twigg *et al.*, 2004).

1.3 Effects of residual stresses

The failures of composite materials are largely associated with residual stresses. The normal residual stress of the fiber-matrix interface seriously influences fiber matrix debonding and pull-out, the most prevalent failure mechanisms (Liu *et al.*, 1999; Nath *et al.*, 2000; Warrier *et al.*, 1999). Residual stress has also been proven to influence some other performance characteristics, including matrix cracking (Deve and Maloney, 1991), yield strength (Nakamura and Suresh, 1993; Zheng, 2000) and dimensional stability (Jain and Mai, 1996).

Failures through fatigue, creep, wear, stress corrosion cracking, fracture, buckling, etc., are mainly caused by residual stresses. Furthermore, residual stresses regularly lead to dimensional instability, an example of which is distortion following heat treating or machining of a part. In parts without external loads, residual stresses can be located. All manufacturing processes can bring about residual stresses, and correlated loads are exaggerated with residual stresses. Residual stresses are subtle as they compensate equilibrium and thus remove all outer traces of their presence. It is necessary to be aware of residual stresses in all engineering structures in which safety factors are a problem, as residual stresses contribute to failures. Residual stresses brought about by different manufacturing processes can be predicted or modeled and much research is underway in this area (Prime, 1999a,b).

The discharges of residual stresses cause deformation, be it an inconspicuous process leading to the formation of a crack on a simple clay vase or an agitation of the Earth by a massive earthquake which causes great destruction. It is generally very difficult to predict failures resulting from residual stresses. The existence of residual stresses has a significant effect on the integrity of the mechanical components at work, in such circumstances as a nuclear reactor over an extended period of time, or in systems of high security-sensitivity, such as an airplane. The existence of residual tensile stresses close to the surface is regarded as one of the major contributing factors leading to the slow and ongoing formation of cracks in parts of objects that are exposed to radiation. Containers that are welded and sealed completely (Masubushi, 1980; Prime 1999a,b) and those containing nuclear waste, the radioactive level of which continues to be dangerously high for many centuries, are more subject to these sorts of residual stresses. Machining by turning, which is an operation performed on most shafts and rods, generally causes tensile residual stresses close to the surface (Brinksmeier *et al.*, 1982). These stresses are destructive to fatigue life under the pressure of cyclic loads. In addition, the compressive residual stress present close to the surface has been proven to lengthen fatigue life and prevent stress corrosion cracking (Cheng and Finnie, 2007).

Not only does residual stress affect the formation of surface cracks, it also changes the path and the extension of a crack beneath the surface. The first reason for this is that the compressive stress beneath the surface in all cases balances the

tensile stress close to the surface. Thus it significantly slows down the growth of a crack as it reaches the region of compressive stress. The second reason is that with the extension of the crack, the stiffness or compliance of the area changes, resulting in the release of the previously trapped-in load. An example of the first case would be a surface crack, which is exposed to uni-axial tension. Such a crack will enlarge and infiltrate a plate, as the width of the crack reaches a size of nearly four times its thickness (Raju and Newman, 1979). However, a crack loaded by the same outer pressure from above, with a considerable residual stress beneath its surface, will extend more quickly on the surface, with a width to depth ratio greater than ten. Consequently, the crack takes longer to penetrate the object, despite the fact that the component continues to lose strength with the further extension of the crack upon the surface. For a pressurized vessel under such circumstances, any leakage taking place may be a sign of a quickly growing crack (Finnie *et al.*, 1990).

It is usual for parts to become deformed upon welding or heat-treatment during manufacturing processes, and the understanding of this is an indicator of the extent to which engineers are experienced (Prime, 1999a,b). Analyses of the fundamental mechanics and measurement of residual stresses under different circumstances have substantially increased our knowledge about residual stresses throughout the past century, allowing us to assess and boost the integrity of current components. The behavior of materials and components is crucially affected by the existence of residual stresses.

Residual stresses can lead to defects in composite structures, such as fiber waviness, cracking, delamination, warpage, dimensional instability and spring-in (Stamatopoulos, 2011). Fiber waviness in uni-directional materials occurs when the fibers deviate from the average direction of the laminate, creating a pattern that can usually be mathematically represented by a sine wave (Fig. 1.1). Fiber

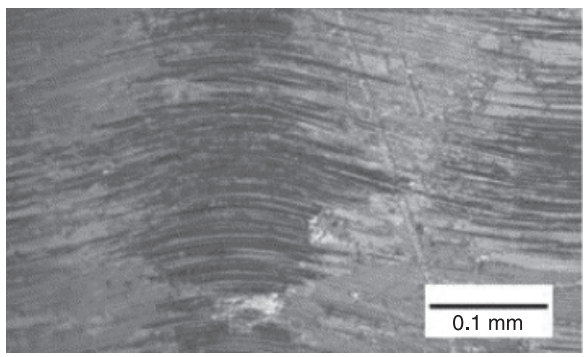

1.1 Micrograph of a composite laminate showing fiber waviness (Parlevliet *et al.*, 2007).

waviness arises through the manufacturing of a composite structure when the fibers undergo compressive axial loads resulting in thermal residual stresses. Since the matrix cannot provide any crosswise support, the fibers become deformed (micro-buckling), leading to waviness. The strength of the structure and the overall quality of the composite material will be reduced by fiber waviness (Parlevliet *et al.*, 2007).

Thermal residual stresses exceeding the yield strength of the resin can lead to the formation of cracks in composite materials. Cracks multiply along the interface when the fiber-matrix interface bond is weak. When the interface is strong, cracks can grow into the matrix. The thermal residual stresses can reach values near to those of the transverse ply strength, which can lead to the premature cracking of the ply during processing. Such cracks, which are commonly referred to as microcracks, are sometimes visible in transparent composites and create failure initiation sites in ensuing service life. Microcracks might propagate into transverse ply cracks, forming initiation points for delamination and the ultimate failure of the laminate, in the same manner as longitudinal splitting. More significantly, they can entail premature failure in cyclic loading conditions (Parlevliet *et al.*, 2007).

Besides the formation of transverse cracks, the difference in the magnitude of residual stresses between 0-degree and 90-degree plies in cross-ply laminates can also cause delamination. Inter-laminar failure of composite materials is indicated by gradual propagation of the delamination, eventually leading to loss of stiffness and structure strength. The free edge effect is another mechanism causing delamination, which also entails matrix cracking. Delamination at free edges is related to high inter-laminar stresses, developing because of the non-uniform features at the free edges. Delamination may also take place around any geometric concentration of stress, for instance around holes, cut-outs and changes in section. This significantly reduces the composite structure's capability to bear loads (Parlevliet *et al.*, 2007).

An important factor for affordable composite manufacturing is the ability to produce composite structures within tight dimensional tolerances. Residual stresses develop through the processing of composite structures and often entail dimensional changes, warpage of structures framed on flat tooling, and spring-in of flanges on angled sections. These sorts of defects can be observed more clearly in thin laminates, in which the magnitude of the deformation is often greater, particularly in the case of warpage. Warpage, or dimensional instability, may be the outcome of unbalanced cooling and tool-part interaction. Tool-part interaction has been proven to significantly contribute to warpage, for thin pieces especially. Furthermore, a differential temperature distribution in the mold can result in warpage (Fig. 1.2) (Parlevliet *et al.*, 2007).

The main outcomes of residual stresses are strength reduction and shape distortion. Stresses at the fiber-matrix, lamina-laminate and structural levels all influence the strength of the component, while only lamina-laminate and structural level stresses influence dimensional stability to any great degree.

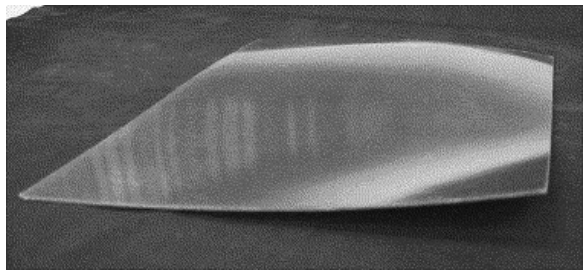

1.2 Distorted glass fiber reinforced polyetherimide (Cetex®) due to non-uniform cooling of the hot plate press (Parlevliet *et al.*, 2007).

1.4 The importance of residual stress measurement

In recent years, the growing employment of advanced laminated composites has drawn a lot of attention to process-induced residual stresses. Explaining such residual stresses has therefore been a subject of great interest (Liu, 1999). While the reliable measurement and prediction of residual stresses is a challenge, their distribution and size are the critical factors in determining how a composite will behave (Colpo, 2006).

The residual stresses developing through processing and operating conditions cannot be neglected. They can significantly compromise a laminate's strength. If these stresses are not precisely understood, they may result in material failures where the tensile stresses developed in the matrix surpass its critical tensile strength. Once this has occurred, microcracks could develop, permitting hydrogen to seep into the core. The formation of microcracks in other structures exposes the fibers to possibly degrading environmental conditions and possible chemical attack in storage facilities (Myers, 2004). These stresses are usually small; however, they may be comparable with those generated by mechanical loads due to the low stresses imposed by the design codes. Thus if the residual stresses are not taken into account, the overall stress state is misrepresented, potentially increasing the risk of failures related to environmentally assisted cracking (Reid and Paskaramoorthy, 2009).

The residual stress state must be superimposed on any stress state resulting from external loading, in order to estimate the actual stress state existing when a structure undergoes external loading. When the overall stress surpasses the design stress limit of the material, this combined stress can entail premature structural failure. Thus it is important to evaluate residual stresses in order to predict the failure mode of a composite (Seif and Short, 2002; Seif *et al.*, 2006). If residual stresses are not taken into account throughout the structural design phase, a higher safety factor should be considered for the structure, usually resulting in overweight and over-designed structures (Stamatopoulos, 2011).

1.5 Issues in the measurement of residual stresses

It is difficult to measure the specific residual stress contributing to matrix-fiber failures with sufficient spatial resolution to predict their effects. The development of residual stress implies nonlinear material behavior and often entails material discharge, phase transformations, and mechanical and thermal problems. For most problems, predictive capabilities are inadequate. Therefore, being able to measure residual stress is essential to satisfy two goals:

1. minimizing failures pertaining to residual stresses; and
2. to promote the development of predictive capabilities through the verification of models.

Residual stresses can be investigated through empirical methods, or by modeling of production mechanisms (Prime, 1999a,b). Empirical methods may or may not be destructive. The methods which are considered destructive normally entail cutting or drilling processes, in order to relax the residual stresses. Then residual stresses are calculated considering the changes of dimension that have taken place. For the non-destructive methods, diffraction techniques are employed (Prime, 1999a,b).

Since advanced structural composites were developed, the need to understand their behavior has led to a large body of research in residual stress determination. Many existing methods have been developed for the characterization of residual stresses and their effects. Some of these methods have been developed from existing tests performed on other materials, and some are completely new. Existing methods are often categorized into two broad groups: destructive and non-destructive. Destructive testing implies damaging or removing a section of material so that the specimen may no longer be usefully employed. Non-destructive tests are often preferred to destructive tests for these reasons. Furthermore, with non-destructive testing, tests can be repeated on the same specimen in order to improve accuracy. Generally, the latter methods also offer the means to test the specimen over time (Myers, 2004).

1.6 Techniques for measuring residual stress in composites

There are a wide range of experimental methods to measure the residual stresses. These methods can be categorized into four main groups (Reid, 2009):

1. *Methods considering the response to released residual stresses*: Methods that monitor the elastic response of a laminate to the release of residual stresses are probably the most widely used measurement techniques. A variety of methods for releasing residual stresses within a laminate are available. These include layer removal, Sachs method, hole drilling, ring-core method, deep-hole drilling, incremental slitting method, contour method, sectioning method,

radial cutting method, matrix removal methods and micro-indentation techniques.
2. *Methods considering changes due to failure*: The estimation of residual stresses through the measurement of the change in apparent failure strength can, in principle, be applied to any material with a well-defined failure (or yield) strength. However, the method appears only to have been applied to the measurement of transverse residual stresses in composite materials and in the form of the 'first ply failure method'.
3. *Methods considering changes in the material structure*: Methods that rely on changes in the material structure include X-ray diffraction, neutron diffraction, Raman spectroscopy, photoelasticity, and the use of acoustic waves. Only the use of acoustic waves requires contact with the specimen and all methods are potentially non-destructive.
4. *Methods considering the response to changes in temperature*: These methods include measurement of curvature, Cure referencing method, and Local heating methods.

Each of these methods has its own advantages and shortcomings (Reid, 2009).

From another perspective, experimental methods for the estimation of residual stresses can be divided into two categories, destructive and non-destructive. Furthermore, the non-destructive methods are divided into those that use the inherent material properties, those that use sensors, and finally those that use in-plane and out-of-plane deformation. The non-destructive methods in general can provide results for large areas a laminate, whereas the measurements acquired using destructive methods concern only a small area of the structure. Some of the existing non-destructive methods make use of the inherent material properties of the composites, since some material properties change when the material is exposed to stresses or stains. Photoelasticity, Micro-Raman spectroscopy and measurement of electrical conductivity of fibers are three methods of this kind (Stamatopoulos, 2011). Several methods are based on in-plane and out-of-plane deformations, such as methods based on interferometry, warpage of asymmetrical composite materials, Neutron diffraction and X-ray diffraction.

There are also destructive methods that attempt to estimate the residual stresses. The main disadvantage of the non-destructive methods described above is that they do not provide information on the distribution of global residual stresses in the composite or along the plies. The methods which can measure the distribution of residual stresses are based mainly on destructive techniques. The general principle shared by all destructive methods is that some stressed material is removed and the resulting deformations (usually displacements or strains) are measured (Schajer and Prime, 2006). The destructive methods include first-ply failure, layer removal method, the incremental hole-drilling method, the deep-hole method and the crack compliance method (Stamatopoulos, 2011). The following chapters review the range of destructive and non-destructive techniques.

1.7 References

Barnes, J. A. and Byerly, G. E. (1994) Formation of residual stresses in laminated thermoplastic composites, *Composites Science and Technologies*, **51**(4), 479–94.

Brinksmeier, E., Cummett, J. T., Leskovar, P., Knig, W., Peters, J. and Tnshoff, H. K. (1982) Residual stresses – measurement and causes in machining processes, *Annals of CIRP*, **31**, 491–510.

Cheng, W. and Finnie, I. (2007) *Residual Stress Measurement and the Slitting Method*, New York, Springer.

Colpo, F. (2006) *Residual Stress Characterization in a Single Fibre Composite Specimen by Using FBG Sensor and the OLCR Technique*, PhD Thesis, Lausanne, EPFL.

Deve, H. E. and Maloney, M. J. (1991) On the toughening of intermetallics with ductile fibers – role of interfaces, *Acta Mettallurgica et Materialia*, **39**(10), 2275–84.

Finnie, I., Cheng, W. and McCorkindale, K. J. (1990) Delayed crack propagation in a steel pressure vessel due to thermal stresses, *International Journal of Pressure Vessels and Piping*, **42**, 15–31.

Fitzpatrick, M. E. and Lodini, A. (eds) (2003) *Analysis of Residual Stress by Diffraction using Neutron and Synchrotron Radiation*, London, Taylor & Francis, Inc.

Gibson, R. F. (1994) *Principles of Composite Material Mechanics*, New York, McGraw-Hill.

Jain, L. K. and Mai, Y. W. (1996) On residual stress induced distortions during fabrication of composite shells, *Journal of Reinforced Plastics and Composites*, **15**(8), 793–805.

Liu, H. Y., Zhang, X., Mai, Y. W. and Diao, X. X. (1999) On steady-state fibre pull-out. Part II: Computer simulation, *Composite Science and Technology*, **59**(15), 2191–9.

Liu, S. C. (1999) *Residual Stress Characterization for Laminated Composites*, Ph.D. Thesis, University of Florida. Available at: etd.fcla.edu/UF/amp7373/liu.pdf

Masubushi, K. (1980) *Analysis of Welded Structures: Residual Stresses, Distortion and their Consequences*, Oxford, Pergamon Press.

Myers, D. G. (2004) *Method for Measurement of Residual Stress and Coefficient of Thermal Expansion of Laminated Composites*, MSc Thesis, University of Florida.

Nakamura, T. and Suresh, S. (1993) Effects of thermal residual stresses and fiber packing on deformation of metal-matrix composites, *Acta Metallurgica et Materialia*, **41**(6), 1665–81.

Nath, R. B., Fenner, D. N. and Galiotis, C. (2000) The progressional approach to interfacial failure in carbon reinforced composites: Elasto-plastic finite element modeling of interface cracks, *Composites: Part A*, **31**(9), 929–43.

Parlevliet, P. P., Bersee, E. N. and Beukers, A. (2006) Residual stresses in thermoplastic composites – a study of the literature. Part I: Formation of residual stresses, *Composites: Part A*, **37**(11), 1847–57.

Parlevliet, P. P., Bersee, E.N. and Beukers, A. (2007) Residual stresses in thermoplastic composites – a study of the literature. Part III: Effects of thermal residual stresses, *Composites: Part A*, **38**, 1581–96.

Prime, M. B. (1999a) Measuring residual stress and the resulting stress intensity factor in compact tension specimens, *Fatigue and Fracture of Engineering Materials and Structures*, **22**(3), 195–204.

Prime, M. B. (1999b) Residual stress measurement by successive extension of a slot: the crack compliance method, *Applied Mechanics Reviews*, **52**(2), 75–96.

Raju, I. S. and Newman, J. C. (1979) Stress-intensity factors for a wide range of semi-elliptical surface cracks in finite-thickness plates, *Engineering Fracture Mechanics*, **11**(4), 817–29.

Reid, R. G. (2009) *The Measurement of Longitudinal Residual Stresses in Unidirectional Glass Fibre Reinforced Plastic*, PhD Thesis, University of the Witwatersrand, Johannesburg.

Reid, R. G. and Paskaramoorthy, R. (2009) A novel method to measure residual stresses in unidirectional GFRP, *Composite Structures*, **88**, 388–93.

Schajer, G. S. and Prime, M. B. (2006) Use of inverse solutions for residual stress measurement, Los Alamos National Laboratory, Engineering Sciences and Applications Divisions, LA-UR–04–5890, *Journal of Engineering Materials*, **40**(3), 375–82.

Seif, M. A. and Short, S. R. (2002) Determination of residual tresses in thin-walled composite cylinders, *Experimental Techniques*, **26**(2), 43–6.

Seif, M. A., Khashaba, U. A. and Rojas-oviedo, R. (2006) Residual stress measurements in CFRE and GFRE composite missile shells, *Composite Structures*, **79**(2), 261–9.

Stamatopoulos, K. (2011) *Measurement of Residual Stresses on Composite Materials with the Incremental Hole Drilling Method*, Diploma Thesis, National Technical University of Athens, School of Naval Architecture and Marine Engineering, Athens.

Stone, M. A. Schwartz, I. F. and Chandler, H. D. (1997) Residual stresses associated with post-cure shrinkage in GRP tubes, *Composites Science and Technology*, **57**(1), 47–54.

Tsouvalis, N., Margelis, G. and Dellis, D. (2009) *Residual Stresses in Composite Materials: A Review*, NTUA Report No. MAR-R4–3-ntua–24(2) for MARSTRUCT.

Twigg, G., Poursartip, A. and Fernlund, G. (2004) Tool-part interaction in composites processing. Part I: Experimental investigation and analytical model, *Composites: Part A*, **35**, 121–33.

Warrier, S. G., Rangaswamy, P., Bourke, M. A. M. and Krishnamurthy, S. (1999) Assessment of the fiber/matrix interface bond strength in Sic/Ti–6Al–4V composites, *Materials Science and Engineering A*, **259**(2), 220–7.

Zheng, M. H. (2000) Strength formulae of unidirectional composites including thermal residual stresses, *Materials Letters*, **43**(1–2), 36–42.

2

Destructive techniques in the measurement of residual stresses in composite materials: an overview

M. M. SHOKRIEH and A. R. GHANEI MOHAMMADI,
Iran University of Science and Technology, Iran

DOI: 10.1533/9780857098597.1.15

Abstract: Existing methods of measuring residual stresses in composite materials are often categorized into two broad groups: destructive and non-destructive. Destructive testing implies damaging or removing a section of material so that the specimen may no longer be usefully employed. This chapter aims to introduce the main methods that fall into the category of destructive methods. For each method, the notable contributions are discussed in detail.

Key words: composite materials, residual stress, measurement, destructive techniques.

2.1 Introduction

This chapter reviews the following destructive methods for testing residual stresses in composite materials:

- the layer removal method;
- the Sachs (boring) method;
- hole-drilling methods;
- the ring-core method;
- the cutting method;
- the contour method;
- the ply sectioning method;
- the radial cutting method;
- matrix removal methods;
- micro-indentation methods;
- the slitting method;
- the first-ply failure method;
- the measurement of curvature method;
- heating methods.

2.2 The layer removal method

The layer removal method was first considered as early as the 1940s (Letner, 1953; Richards, 1945; Timoshenko, 1941) and was originally developed by Treuting and Read (1951) for isotropic materials such as metals, but has been modified for use with composites. It depends on the removal of thin layers of material from one surface of a plate. The internal stresses originally present in this layer are thus eliminated and the plate consequently curves to restore force equilibrium. By measuring the strain and curvature of the laminate as successive layers are removed, it is possible to derive the stress profile of the original laminate (Reid, 2009; Stamatopoulos, 2011).

Abrasion or milling can be used to remove one or more plies of the composite material. Removal of composite layers can also be done by machining (Cowley and Beaumont, 1997; Eijpe and Powell 1997; Jeronimidis and Parkyn, 1988), splitting with a knife (Ersoy and Vardar, 2000) or by placing separation films within a laminate during cure (Chapman *et al*., 1990; Manson and Seferis, 1992). The use of methods such as abrasion can reduce the accuracy of the technique. This is because during the layer removal, the surface temperature increases and microcracks are created, and this results in the relaxation of residual stresses. Moreover, the irregularities caused at the plies from abrasion, for example alteration of the thickness of the plies, influence the final shape of the resulting deformation. In order to prevent any damage to the laminate, the Process Simulated Laminates (PSL) technique is used. PSL composite materials consist of prepreg plies and other thin separating films placed between the plies. The plies between two thin separating films create a constitutive laminate (CL) (Fig. 2.1). These CLs may be removed from the composite material after manufacturing (Parlevliet *et al*., 2006). The use of separation films provides more reproducible data than machining (Chapman *et al*., 1990; Reid, 2009).

There are two methods for calculating residual stresses. The first uses the CL deformation technique, that is, the measurement of the dimension changes (curvature) of the PSLs and CLs before and after their removal. The second is by the PSL-strain gage technique, where strain gages are attached to the surface of the composite. These monitor the strain changes as CLs are removed from the other side (Parlevliet *et al*., 2006). The PSL-strain gage technique is more precise. The layer removal method cannot be used to measure the micro-scale residual stresses in a uni-directional glass fiber-reinforced plastic (GFRP) laminate. Each layer that is removed has a thickness far larger than the fiber diameter and consequently it is not possible to remove either matrix material or fibers individually (Reid, 2009).

Jeronimidis and Parkyn (1988) investigated residual stresses in APC-2 cross-ply laminates using a number of experimental techniques, including the layer removal method. They showed that accurate predictions can be made, provided that the changes in thermo-elastic properties of the materials with temperature are

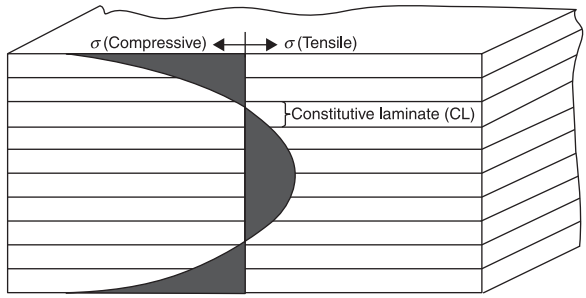

2.1 Schematic view of the process simulated laminate (PSL) configuration with constitutive laminates (CLS) for determination of laminate skin-core residual stress distribution (gray area) through this type of layer removal method (Parlevliet *et al.*, 2007).

taken into account. Chaoui *et al*. (1988) evaluated residual stress distribution in a medium density polyethylene (MDPE) pipe using a modified layer removal procedure. Paterson and White (1989) analysed residual stresses in parallel-sided polymer moldings. Chapman *et al*. (1990) analysed the macroscopic in-plane residual stress state of uni-directional graphite (AS4) reinforced polyetheretherketone (PEEK) laminates.

Crasto and Kim (1993) studied the curing-induced strains in graphite/epoxy (AS4/3501-6) composites at different temperatures. These results were used to predict the stress at first-ply and ultimate failure of $[0_2/90_2]_s$ laminates. Güngör and Ruiz (1996) used layer removal methods to measure residual stresses in continuous fiber composites. Cowley and Beaumont (1997) carried out experiments to measure the residual stresses in a thermoplastic matrix and a toughened thermosetting matrix, both reinforced with carbon fiber. They showed that, under certain conditions, the residual tensile stress can approach closely to the transverse ply tensile strength. Eijpe and Powell (1997, 1998) validated the modified layer removal method using a compression-molded continuous-fiber laminate (PEI/glass) and an injection-molded short-fiber-reinforced laminate (PC/glass). They showed that the modified layer removal method produced good results. Ersoy and Vardar (2000) also used a layer removal technique to measure macroscopic residual stresses in layered composites,

2.3 The Sachs (boring) method

The Sachs method (also known as the boring method) is similar to the layer removal method, except that it is applied to rods and tubes rather than plates. In this method, tube-shaped parts are progressively removed from the center of a circular section of the material. As each radial increment is removed, the residual stresses within this material are released and the remaining material responds

elastically. Axially and circumferentially aligned strain gages are used to record the response on the outer surface of the section (Reid, 2009). An alternative way of using this method is to remove material from the outer surface of tubes. In this case, the strain gages are placed on the inner surface of the tube (Kovač *et al*., 1989; Stacey and Webster, 1988). Despite the fact that these techniques can be used for measuring the residual stresses in laminated composite tubes, the Sachs method cannot be used to find the micro-scale residual stresses in a uni-directional GFRP laminate, since the technique cannot differentiate between fiber and matrix stresses (Reid, 2009).

The Sachs method technique allows axial, circumferential and radial residual stresses to be determined (Chen *et al*., 2000; Garcia-Granada *et al*., 2001; Sachs, 1927; Sharman *et al*., 1997). It has been used to measure residual stress distribution in metal and ceramic components (Hung, 1989; Jones and Martin, 1977; Kovač *et al*., 1989; Kuboki *et al*., 2000; Lacarac *et al*., 2004; Olson and Bert, 1966; Özdemir and Edwards, 1996; Rasty *et al*., 2007; Smith *et al*., 1998; Stacey and Webster, 1988; Voyiadjis and Hartley, 1987; Voyiadjis *et al*., 1985; Waki *et al*., 2003; Yamada *et al*., 1990). However, the technique does seem to have been used for composite materials.

2.4 Hole-drilling methods

2.4.1 The hole-drilling method

The hole-drilling technique for determining residual stresses was first proposed by Mathar (1934). When a hole is introduced into a stressed body the stresses relax, which leads to a change in the surrounding strain field that can be measured and correlated to the relaxed stresses. There are three variations of this method:

1. Center-hole drilling involves drilling a hole normal to a surface to investigate surface strain;
2. Through-hole drilling is used to measure uniform through-thickness residual stresses; and
3. Incremental-hole drilling is used to measure residual stresses varying through the thickness, by drilling in successive depth increments (Reid, 2009).

Originally, this semi-destructive method was restricted to macroscopically homogeneous isotropic materials, but attempts have been made to extend it to anisotropic, fiber reinforced composites (Prasad *et al*., 1987) and, since the mid-1960s, to orthotropic materials (Lake *et al*., 1970; Rendler and Vigness, 1966), but it is numerically intense and several assumptions must be made to simplify the resulting solutions. The highly orthotropic nature of composites further complicates the measurements themselves, because it is extremely difficult to obtain measurement precision around the hole, particularly in the fiber direction, even with high precision techniques, such as Moiré interferometry (Nicoletto, 1991).

Bert and Thompson (1968) developed the theoretical basis for relating measured strains to residual stresses in orthotropic materials applying an approximate calculation procedure. Later a precise formulation for uniform through-thickness residual stresses in a limited class of orthotropic materials was proposed by Schajer and Yang (1994). Sicot and Gong (2003, 2004) made an approximate analysis of the residual stresses in orthotropic composite laminates using the incremental hole-drilling method. An exact formulation of the through-hole method enabling the measurement of uniform through-thickness residual stresses in a generic orthotropic laminate was published by Pagliaro and Zuccarello (2007). The effects of macro-scale residual stresses acting on symmetrical orthotropic laminates can also be considered using this method.

The hole-drilling method most commonly uses strain gages, which must be correctly positioned relative to the hole. Although not so widely used, optical methods have an advantage over strain gages in that positioning of the hole is less important. A technique has been developed to determine residual stresses in orthotropic materials using Moiré interferometry for any alignment of Moiré gratings (Càrdenas-Garcìa, 2005). Dual beam shearography yields the in-plane strain directly, since the axes of symmetry in the measured fringe pattern correspond to the axes of the principal stresses. In spite of this advantage over Moiré interferometry, measuring residual stress in orthotropic materials using shearography combined with the hole-drilling technique appears to be limited. Qualitative measurements have been obtained on composite panels. In an effort to speed up measurement, micro-indentation (whereby a small indent is pressed into the measurement surface) has been used instead of the hole-drilling process (Hung, 1999), but this process again has only yielded qualitative measurements.

All the current analytical methods used with hole drilling assume the material within a single ply to be homogeneous, and are therefore unable to resolve the micro-scale residual stresses within a heterogeneous ply. However, since fibers are cut when a hole is drilled into a composite laminate, residual stress is released at the cut and an elastic response occurs in the adjoining material. It is thus potentially possible to use the hole-drilling technique for measuring micro-scale residual stress in GFRP. The region over which a significant elastic response takes place is, nonetheless, extremely small (Nairn, 1997). Since the maximum diameter of E-glass reinforcement fibers is often less than 27 μm, measurements must be taken within a small distance of the edge of the hole (Corning, 2003), which causes problems if the smallest commercially available strain gages are used. If extremely small special gages were developed to overcome the problem of sensitivity, they would simply introduce another problem due to self-heating. GFRP is not a good conductor of heat, therefore the localized heating effect of such a small gage becomes important (Reid, 2009).

Fiber optic Bragg gratings have been employed for measuring residual stresses in a composite laminate in a modified version of the hole-drilling method, with the

Bragg gratings embedded within the laminate (Guemes and Menéndez, 2002). They avoid the self-heating effect, but are too long to be used for measuring stress relief around individual fiber breaks. In addition, the analytical method used to interpret the measured response must accommodate the stiffening effect of the transducer. It seems unlikely that reliable measurements of the stress relief relative to a fiber break could be made with this method (Reid, 2009).

The use of optical methods present two important problems that are prevalent, irrespective of the instrumentation technique employed (Reid, 2009). The first significant problem arises from the introduction of residual stresses in drilling the hole. The strains measured are those resulting from the release of residual stress superimposed on those caused by the hole-drilling process, and the two sets of strains cannot be separated from each other. EDM would minimize the residual stresses caused by making the hole, but only where the fibers and matrix are conductive, and unfortunately neither the fiber nor the matrix in GFRP satisfies this criterion (Reid, 2009). It might be possible to avoid the introduction of residual stresses during hole drilling through the micro-indentation process (Hung, 1999), but the interpretation of the strain measurements would be complicated by the heterogeneity of the material at small scales (Reid, 2009). Thus the hole-drilling method, and variations of it, cannot be directly used or adapted for use in finding the micro-scale residual stresses in uni-directional GFRP (Reid, 2009).

Buchmann *et al*. (2000) describe a novel approach to simulating the thermal spraying process by modeling a moving heat source combined with the material transfer and deposition process. Their quantified stresses and deformations agree with experimental residual stress measurements by the advanced hole-drilling method. According to Prasad *et al*. (1987), the semi-destructive hole-drilling technique for measuring residual stresses is well established for isotropic materials and they have made attempts to extend this method to orthotropic composite materials. Pagliaro and Zuccarello (2007) dealt with the development and application of the through-hole drilling method for residual stress analysis in orthotropic materials.

Balalov *et al*. (2007) discussed in detail the main features inherent in a simplified approach to residual stress determination in cylindrical shells and tubes with external diameters of not less than 60 mm, by combining the hole-drilling method and reflection hologram interferometry. Stefanescu *et al*. (2006) presented results advancing and improving the usefulness, accuracy and efficiency of incremental center-hole drilling as a method of measuring close-to-surface residual stress fields. Shokrieh and Kamali (2005) studied the residual stresses in thermoset polymer composites. Shokrieh and Ghasemi (2007a,b) presented a new method (simulated hole-drilling method) for calculating the calibration factors for measuring the residual stresses in different material systems. Baldi (2007) analyzed the problem of residual stress determination in an orthotropic material using the hole-drilling technique combined with non-contact, full-field optical

methods. Schajer (1988, 2007) and Schajer and Yang (1994) presented an effective procedure allowing for stable hole-drilling residual stress calculations using strain data from measurements taken at many small increments of hole depth. Schajer (1988, 2007) described the use of Tikhonov regularization to reduce the noise sensitivity characteristic of a fine-increment calculation, and combined this mathematical procedure with the Morozov criterion to identify the optimal amount of regularization that balances the competing tendencies of noise reduction and stress solution distortion.

Schajer and Yang (1994) used the hole-drilling method to measure residual stresses in an orthotropic material. Sicot *et al*. (2003) presented a new method for measuring residual stress in composite laminates, using three cooling conditions to produce different residual stress levels. Shokrieh and Ghasemi (2007a,b) determined that the calibration factors for orthotropic plates are based on an exact solution method. Bert and Thompson (1968) and Lake *et al*. (1970) extended a method to include orthotropic materials by introducing new coefficients of calibration, and investigated the applicability of the semi-destructive hole-drilling technique to the experimental determination of residual stresses in relatively thin rectangular orthotropic materials.

2.4.2 The incremental hole-drilling method

The incremental hole-drilling method takes account of the non-uniformity of the stress distribution through the thickness. The basic principle for the calculation of stresses is the same as with the hole-drilling method, but in this case drilling is performed gradually. The measured strains are processed by an appropriate model and the residual stresses are calculated (Oettel, 2000; Parlevliet *et al*., 2006; Sicot *et al*., 2003).

The incremental, high-speed hole-drilling and circular-milling technique has several advantages that make it suitable for measuring residual stress on coating composites. The measuring set-up is comparatively small (Fig. 2.2), offers high flexibility and can be applied to a variety of complex machine parts. The measurement of surface strains by means of strain gages is a well-known technique with a reasonably high accuracy (errors are in the range of 2 to 5% (Häusler *et al*., 1987)). The stepwise removal of material in increments of 5 to 20 μm leads to a good depth resolution. In comparison with the conventional hole-drilling method, the combination of high-speed drilling and circular milling (Fig. 2.2) reduces the mechanical loading of the material at the bottom of the bore-hole, the plastic deformation in the center of the hole, and the thermal input into the material. Therefore, manipulation of the intrinsic residual stresses during measurement is reduced and the accuracy of results is increased. Difficulties in applying the hole-drilling method are mainly due to preparation of the surface by grinding without influencing the residual stresses, and the adhesion of the strain gages to the surface (Wenzelburger *et al*., 2006).

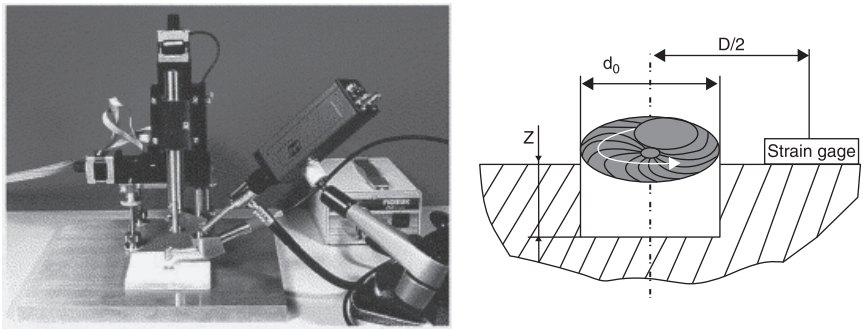

2.2 Measurement set-up of the incremental-step, circular hole-drilling and milling method (pneumatic turbine, motors for three-axis position control, LCD-camera, strain gage data acquisition), and illustration of the method (Wenzelburger *et al.*, 2006). Notation: z, depth; d_0, diameter of bore hole; D, diameter of circle on which strain gage rosette is positioned.

A disadvantage of the incremental hole-drilling method is that the size of a typical strain gage rosette is two to four times larger than the diameter of the hole, making the area covered by the rosette very large compared to the stress field (Fig. 2.3). Another frequent problem is eccentric drilling, such as when the hole is not drilled exactly at the center of the rosette. The hole-drilling method has been applied in combination with Moiré interferometry, holographic interferometry and speckle interferometry, as well as in combination with finite element modeling for determination of the residual stresses. Incremental hole-drilling can be utilized to study residual stresses in between adjacent plies, but optimal drilling and translation speeds must be found (Margelis *et al*., 2010; Parlevliet *et al*., 2006).

Tsouvalis *et al*. (2009) proposed a new method of calibration showing how finite element analysis can be used to determine the correlation coefficients, and take account of the effects of changes in the hole geometry, which they reported can cause a significant error in the experimental data. Sicot *et al*. (2003, 2004) described an application of the incremental hole-drilling method to measure residual stress in a uni-directional and a $[0/90]_s$ carbon/epoxy laminate with thicknesses of the order of 1 mm, measuring tensile and compressive residual stresses in the fiber direction and transverse direction up to a magnitude of about 100 MPa. Sicot *et al*. (2004) studied the effect of two experimental parameters: the depth of each drilled increment and the effect of the relative position of the strain gages compared with the radius of the hole drilled.

Manson and Seferis (1992) applied the PSL technique to develop a method to evaluate the distribution of process-induced residual stresses, making use of a strain gage that was attached to the laminate. Grant *et al*. (2002) provided a practical guide to achieving better measurements, drawing together some

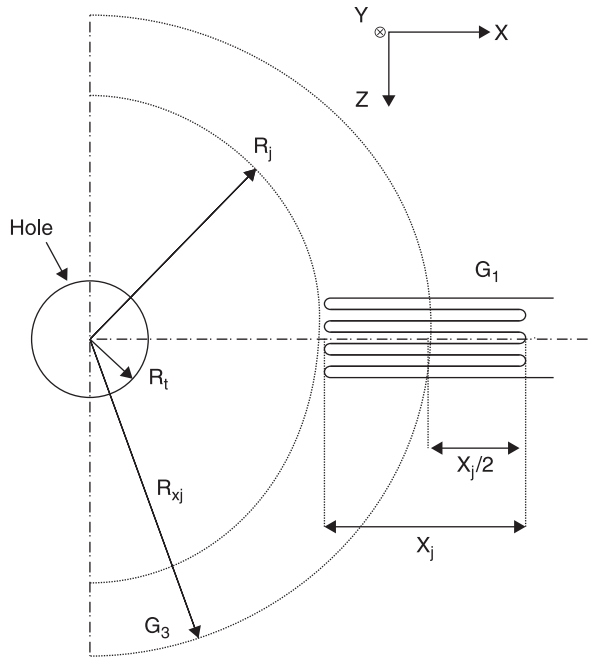

2.3 Relative location of the hole and the strain gages (Sicot *et al.*, 2004). Notation: R_t, hole radius; R_j, radius of outside strain gage; R_{xj}, radius of middle strain gage; G_1 and G_3, first and third strain gages; X_j, gage length

background to the technique, discussing the current standards and highlighting a number of key issues crucial to obtaining good measurements, based on input from UK experts and some of the findings from a recent UK hole-drilling residual stress inter-comparison exercise. Wenzelburger *et al*. (2006) described and compared the most common residual stress measurement techniques, focusing on incremental hole drilling and milling, and their application to industrial machine parts.

2.4.3 The deep hole-drilling method

The deep hole-drilling (DHD) method is used to measure residual stress in isotropic materials, but it can also be applied to orthotropic materials such as thick laminated composites. For large structures, it is considered non-destructive, because a small hole does not affect the structural integrity. In this method, the formulation is mainly based on the calculation of the hole distortion in a plate under the effect of remote loading. For isotropic materials, there are suitable closed-form solutions; however, for orthotropic materials, a finite element approach should be used (Stamatopoulos, 2011).

DHD allows the resolution of residual stresses through even very thick components. In this method, a hole with a narrow diameter is drilled through a part that has residual stresses. The diameter of the hole is then measured carefully (typically using an air gage) as a function of depth and angular position inside the hole. The residual stresses are then released by co-axially removing a core of larger diameter from around the hole. The release of residual stress causes the shape of the reference hole to change. The diameter of the hole is then re-measured at the same angular positions and depths as in the original measurements and using the same equipment. Changes in the shape of the hole are then related to the residual stresses that were present before the hole was drilled (Reid, 2009).

The main assumption of this technique is that the introduction of the reference hole has little effect on the residual stress state, and that cutting the core allows residual stresses around the hole to thoroughly relax (Mirzaee-Sisan, 2007). Another assumption is that the core is comprised of many independent lengths. Therefore, a thick part can be approximated as a set of stacked layers unconnected by through-thickness shear stresses (Bateman *et al*., 2005). The alterations in the core length can be considered as a measure of through-thickness residual stresses as the outer core depth increases (Procter and Beaney, 1987). The DHD technique has been utilized occasionally in cases of welds in metal parts (Bouchard *et al*., 2005; Brown *et al*., 2006; George and Smith, 2005; Mirzaee-Sisan, 2007), railway track (Stefanescu *et al*., 2003) and rolls in steel mills (Kingston and Smith, 2005).

This method has also been used to measure residual stresses in a laminated carbon-fiber composite (Bateman *et al*., 2005). In this case, the removal of the core around the hole could not be performed using EDM, and as an alternative, a diamond encrusted hole saw was used. The analysis technique was extended to account for orthotropic material to allow the change in hole shape to be related to the original residual stresses.

The basic assumption of the DHD method is that the material at each depth can be treated as a continuum. When this technique is applied to a laminated composite, averages of the stresses within the fiber and matrix are measured. As a result, this method cannot be directly used to measure the micro-scale residual stresses. The method is only able to resolve meso-scale residual stresses, which in unloaded uni-directional laminates are non-existent (Reid, 2009). Drilling a small diameter hole results in the cutting of fibers on the hole wall. Consequently, the micro-scale residual stresses in the fibers are released and the material near the ends of the fibers responds in an elastic way. By carefully monitoring this phenomenon, it is possible to modify this method to measure the longitudinal micro-scale residual stresses in uni-directional GFRP (Reid, 2009).

Attempting to modify the technique poses at least three major difficulties (Reid, 2009), first that the mechanical methods of creating the hole create cutting stresses on the hole wall. These occur at the same place where the breaks in the fibers occur, so the elastic responses from cutting stresses and from the release of micro-scale residual stresses are coincident. These two effects cannot clearly be

distinguished from each other, making an accurate measurement difficult. Second, it is not easy to measure the profile of the hole wall at scales smaller than that of the diameter of the glass fiber, due to problems with measurement resolution. Third, the material that tends to move radially inwards in response to the fiber being cut cannot be removed in the process of making the hole, and consequently the profile of the hole wall cannot be monitored properly. The DHD technique cannot be used to measure the micro-scale residual stresses present in the fiber direction of uni-directional GFRP directly, and every modification of the technique leads to additional problems (Reid, 2009).

Initial development of the DHD method was carried out by Zhandanov and Gonchar (1978), Beaney (1978) and Jesensky and Vargova (1981). Zhadanov and Gonchar (1978) used the DHD method to measure residual stresses in steel welds. Beaney's (1978) methodology was later improved by Procter and Beaney (1978) with the introduction of non-contacting capacitance gages to measure the hole diameter. Jesensky and Vargova (1981) measured residual stresses in steel welds using strain gages attached to the sides of the hole to measure the strain relaxation following trepanning.

Bateman *et al*. (2005) described an extension to the DHD method for the evaluation of residual stresses in thick section composite laminated plates. Leggatt *et al*. (1996) described the development of a DHD method, based on earlier techniques, for measuring the through-thickness distribution of residual stresses. Some researchers have made improvements to the DHD method, by gun-drilling a hole of 3 mm nominal diameter and measuring the change in diameter of the hole using an air probe. Trepanning the core was carried out using an electro-discharge machining (EDM) operation (Bonner and Smith, 1996; George *et al*., 2000, 2002; George and Smith, 2000).

2.5 The ring-core method

The ring-core method (Fig. 2.4) follows a procedure similar to the hole-drilling technique. Instead of residual stresses being released by drilling a hole and monitoring the elastic response of the neighboring material, the ring-core method releases stress by cutting an annular groove into the surface of a part containing residual stress. A strain gage rosette is used to measure the elastic response on the end of the core within the groove. An incremental increase in the depth of the groove makes it possible to determine the stress variation through the thickness (Keil, 1992). The through-thickness stresses can be determined by monitoring the change in core length with increasing groove depth (Wern *et al*., 1997; Wern, 1997).

Compared with the hole-drilling method, the ring-core method offers a number of benefits. Since the strains are more fully relaxed, the measured response is considerably larger. There is no stress concentration effect in the annulus and as a result, this method can measure residual stresses up to the yield stress of the

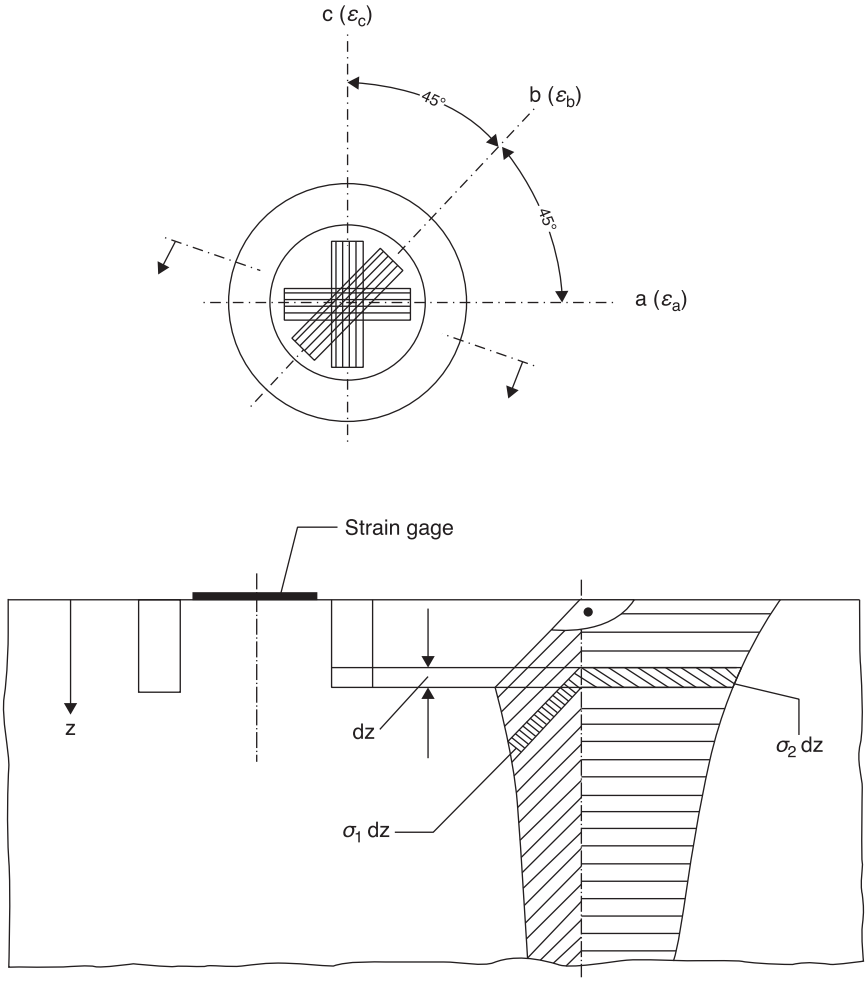

2.4 Principle of the ring-core method for determination of plane residual stress (Keil, 1992). Notation: dz, amount of step-by-step milling of annular groove; z, depth of groove; ε_a, strain in direction a; σ_1 and σ_2, stress acting in principal directions 1 and 2 respectively.

material. The relaxation of strain that occurs on the end of the separated core is uniform, so this method is less sensitive to errors in the strain gage rosette positioning (Reid, 2009). As the ring-core method ruptures the fibers while the groove is being formed, it is possible to monitor the elastic response of the neighboring material in order to measure the magnitude of micro-scale residual stresses (Reid, 2009).

Despite these benefits, the ring-core method has not been employed extensively. This could be because it was not widely known until 1988 (Keil, 1992). It could

also be due to common use of the standard hole-drilling technique for measuring residual stresses in FRPs. It is not practical to use EDM, since composite materials are either non-conducting or are poor conductors of electricity, and this complicates the conditions for composites (Reid, 2009). This method has been applied to large cast steel parts and forgings (Keil, 1992), forged aluminum parts (Witt *et al*., 1983), welds in stainless steel (Roy *et al*., 2005) and hot rolled laminates of stainless and carbon steel (Schröder *et al*., 1995). The ring-core method can also be used in regions with high stress gradients, such as laser welds (Ren and Li, 2007) and ultrasonic spot welds (Li *et al*., 2007). Lu (1996) devoted a part of his book to this method.

2.6 The cutting method

The cutting method is based on similar principles to those in the hole-drilling method. Once more, stress is relaxed by the removal of material. This time a notch is removed from a specimen, resulting in the creation of a free edge. A Moiré interferometry grating can be applied to the specimen to record the resulting strain field (Filiou *et al*., 1992; Lee *et al*., 1989), which is then calculated and related to the residual stresses using finite element analysis (Myers, 2004).

This method is not without its faults and needs modifications to be totally accepted in the experimental community. Niu (1999) posed many questions regarding the application of the grating. Since the grating was applied after an edge of the composite had been trimmed, some of the residual stresses were released prior to data recording and a complex strain field was created under the surface. The resulting measurements thus contained data based on a stress field different from the original residual stress (Myers, 2004).

Lee *et al*. (1989) studied the residual strain distribution in a thick composite ring experimentally using interferometric techniques. The specimen was a segment of a graphite/epoxy composite cylinder, with the fibers orientated in the hoop and axial directions. Casari *et al*. (2006) presented a method for the characterization of residual stresses in thick filament wound tubes. A second technique derived to employ the cutting method was proposed by Sunderland *et al*. (1995). Their successive grooving technique involved cutting a groove through the thickness at successive depths. Strain gages were placed opposite the groove and recorded the changing strain field. The residual stress was then calculated from the strain by use of a numerical 2D model for each layer (Myers, 2004).

2.7 The contour method

The contour method is used to measure 2D residual stresses. In this method, a part which contains residual stresses is cut through by a planar surface. This results in the release of the residual stresses across the plane and consequently the new

surface undergoes an out-of-plane deformation (Reid, 2009). These out-of-plane deformations are measured and the original residual stresses across the cut are determined using the finite element method. In order to do this, displacement boundary conditions (equal to the negative of the measured deflections) are imposed on the cut surface. The method has proved to be efficient in mapping complicated residual stress fields, such as in railway track (Kelleher, 2003) and welds (Prime *et al*., 2006; Zhang *et al*., 2003), as well as those caused by hypersonic impact (Martineau *et al*., 2004).

This procedure is mainly ideal for measuring existing longitudinal residual stresses in uni-directional GFRP materials. The heterogeneous structure of GFRP is easy to model using the finite element method, and with accurate measurement of out-of-plane displacements in the vicinity of the fibers using methods such as laser probe scanning (Prime *et al*., 2004), the fiber residual stresses can be determined easily.

The main requirement of the contour method is that the planar section must be cut through the material under stress with great care. Mechanical methods tend to create cutting stresses and trim down out-of-plane deflections while they are being observed, so electric discharge wire machining (EDWM) is commonly used as a suitable alternative. The advantage of this method is that it only removes material at the tip of the cut and no significant cutting stresses are created. Unfortunately, EDWM cannot be utilized to create the cut in GFRP materials, because neither constituent is conducting. The contour method therefore cannot be applied to the measurement of longitudinal micro-scale residual stresses in GFRP (Reid, 2009).

Prime (2001) presented a powerful new method for residual stress measurement, concluding that the contour method was more powerful than other relaxation methods because it could determine an arbitrary cross-sectional area map of residual stress, yet at the same time simpler, because the stresses could be determined directly from the data without an inversion technique. He verified this method with a numerical simulation, and then experimentally validated it, using a steel beam with a known residual stress profile. Zhang *et al*. (2003) performed contour measurements on a MIG 2024-T351 aluminum alloy welded plate. They compared their results with the results from neutron and synchrotron X-ray and observed a favorable agreement between them.

Prime *et al*. (2006) joined plates of aluminum alloys 7050-T7451 and 2024-T351 in a butt joint by friction stir welding (FSW). In their work, a 54 mm long test specimen was removed from the parent plate, and cross-sectional maps of residual stresses were measured using neutron diffraction and the contour method. Martineau *et al*. (2004) impacted a thick plate of high-strength low-alloy (HSLA-100) steel with tungsten carbide spheres travelling at velocities ranging from 0.8 to 2.5 km/s. Good agreement was shown between the numerical simulation of the impact event and the experimental data. Prime *et al*. (2004) described noncontact scanning using a confocal laser probe to measure surface contours for applications in residual stress measurement.

2.8 The ply sectioning method

The ply sectioning method is a destructive technique used to study residual stresses in laminated composites (Joh *et al*., 1993). This method uses Moiré interferometry, and measures the deformation due to sectioning and releasing a layer from the constraints imposed by an adjacent layer. The deformation strains are used to calculate the resulting release of stress. This technique overcomes the problems resulting from the cutting method by obtaining a small strip specimen from the edge of the larger specimen, which leads to creation of a plane stress state. Ply sectioning can also be used to study the nature of warping observed in an unbalanced composite laminate. The outside layers of a laminate can be machined away, resulting in an unbalanced, warped structure (Chapman *et al*., 1990; Manson and Seferis, 1992). The resulting warpage is measured and can be used as an input in classical lamination theory (CLT) to calculate the corresponding residual stresses (Myers, 2004).

In the sectioning method, removing sections of interest is performed in such a way that it can be reasonably assumed that the final stress state is zero. The total change in strain from the original state to the unstressed state corresponds to the negative of the strain in the component prior to testing (Reid, 2009). In one variation of this method, strain gage rosettes are used. In this case, the section is cut as close as possible to the edges of the rosette, so that it is secluded from the neighboring parts to make sure that the final stress state is negligible. If the variation of the through-thickness stress is needed, more gages are attached to the surfaces that have been newly exposed. Further cuts can then be made to part sub-sections, each with its own gage. This approach is known as the 'slice-and-dice' method (Reid, 2009).

Strain gages cannot be used when the stiffness of the removed section is low. Under such circumstances, Moiré interferometry can be used to measure the released strains, because this measurement system applies no loading to the removed section. Moiré interferometry has consequently been used to measure the residual stresses in individual plies of cross-ply laminates (Gascoigne, 1994; Joh *et al*., 1993) and thick-walled cross-ply cylinders. The sectioning method is not considered suitable for measuring micro-scale residual stresses in uni-directional FRPs. This is because the thickness of each removed section is much larger than the fiber diameters. Therefore, this method fails to achieve a resolution sufficient to give a clear understanding of the stresses at the micro-scale (Reid, 2009).

The sectioning method has been used extensively to measure residual stresses in metallic components. The residual stress variations across a welded steel H section, (Tebedge *et al*., 1973) in cold-bent steel plate (Weng and White, 1990), welded seams (Kovač, 1995) and in filament wound tubes (Casari *et al*., 2006) have all been measured using this technique. A finite element method can also be used to predict the tri-axial stresses at points away from strain gages. This approach has been simulated in the residual stress analysis of a welded joint (Hill and Nelson 1995, 1996).

Gascoigne (1994) used high-sensitivity Moiré interferometry and linearized strain-displacement equations to measure released displacements and residual strains. Joh *et al*. (1993) developed a novel concept of layer separation to measure quantitatively and precisely the tensile residual stresses in thick plates with layered distribution of residual stresses. Chapman *et al*. (1990) presented a model to predict the macroscopic in-plane residual stress state of semi-crystalline thermoplastic composite laminates induced by process cooling. Their model predictions were in good agreement with experimental residual stress measurements for uni-directional graphite (AS4) reinforced PEEK laminates.

2.9 The radial cutting method

The radial cutting method is a different version of the sectioning method. It has been used extensively to determine the residual stresses in fiber reinforced tubes (Cohen, 1997; Ganley *et al*., 2000; Seif and Short, 2002, Seif *et al*., 2006) and rings (Aleong and Munro, 1991; Roy, 1991). Based on the assumption that the residual stresses in such structures are invariant with axial and circumferential position, a single axial cut can result in their release. The extent of a laminate's opening or closure can be considered as a measure of the variation in circumferential and radial residual stresses through the laminate (Reid, 2009).

In the radial cutting method, the amount of relative deformation is measured when the cylindrical structure is cut radially. Fourney (1968), Dewey and Knight (1969) and Aleong and Munro (1991) used elasticity equations to transform the measured relative strain either on the inner surface or on the outer surface during the radial cut into the residual stresses and residual strains in filament-wound composite rings. When material properties in the thick fabric composite cylinder are homogeneous, both the Sachs' boring method and the radial cutting method give similar results (Lee, 2004), and consequently the radial cutting method is preferred over the Sachs method, because it is simpler and less expensive than the boring method.

Current analytical methods related to this method are confined to laminates, which are balanced with respect to the cylindrical coordinate system. As a result, the residual shear stresses are taken to be zero. According to Kaddour *et al*. (2003), this assumption does not necessarily hold true. Thin filament-wound laminates exhibit a change in axial displacement across the cut. This implies the existence of a built-in twist with corresponding residual shear stresses (Reid, 2009). The radial cutting method is based on measuring the elastic response of the laminate as a whole and also on the assumption of homogeneous materials. Both of these conditions prevent the resolution of residual stresses at the micro-scale (Reid, 2009).

Kaddour *et al*. (2003) conducted a preliminary study to investigate the residual stresses developed in hot cured thin-walled angle-ply filament wound tubes made of E-glass/epoxy, Kevlar/epoxy and carbon/epoxy materials. Kim *et al*. (2006) developed a smart cure method with cooling and reheating to reduce residual

stresses in thick-wound composite cylinders made of carbon phenolic woven composite. Roy (1991) presented thermal stress analysis of a thick laminated ring. Kim and Lee (2007) measured the residual stresses in thick cylinders made of carbon fabric phenolic composites by a new radial-cut cylinder-bending method.

2.10 Matrix removal methods

Matrix removal methods are based on the fact that residual stresses are mutually self-equilibrated. In uni-directional laminates, stresses within the fibers are opposed by stresses in the matrix. If the matrix material is removed, the stresses within the fibers are released. The consequent elastic response of the fiber allows the residual stresses to be measured (Reid, 2009).

As long as the fibers are not damaged, the matrix material can be removed using a variety of techniques, and it is worth noting that the technique selected depends greatly on the type of composite material. Strong acids can be used to etch away metal matrices, acid digestion is utilized for the removal of polymer matrices surrounding carbon and aramid fibers, while polymer matrices surrounding glass fibers are vaporized with the aid of high temperatures (American Society for Testing and Materials, 2002).

Another method that employs the matrix removal procedure relies on the micro-buckling of the fibers (Zong and Marcus, 1991). In metal matrix composites, the stress in reinforcement fibers is compressive at room temperature, thus the matrix material around the fibers provides them with enough support to prevent buckling. In absence of the matrix, the fibers can buckle freely. In this method, the lengths of buckled and unbuckled fibers are determined after a small portion of metal matrix is etched away from the surface of a composite plate and the underlying fibers are exposed. Using these lengths, the 'clamped-clamped' Euler buckling stress is determined, which corresponds to the residual fiber stress. The major shortcoming is that a parameter known as the 'knock-down factor' needs to be introduced to take initial fiber imperfections and misalignment into account, and the use of this method is greatly restricted by the uncertainty concerning this parameter (Reid, 2009).

Another complication that is sometimes troublesome relates to the bending of the fibers after matrix dissolution (Ramamurty *et al*., 1996). Since a portion of the fiber length is inclined to the length direction, the extension of the fiber appears shorter than it actually is. In addition, this bending phenomenon alters their obvious location on the reference plane. It is not possible to align the reference plane completely normal to the measurement axis; the change in position alters the apparent change in length relative to the reference plane. Regardless of these issues, the method has been used to investigate the residual stresses within silicon-carbide reinforced titanium alloys (Fang *et al*., 2000; Güngör, 2002).

Fiber reinforced plastics have not been subjected to the etching technique as a method of residual stress measurement. This is most likely due to two main

factors; the low elastic modulus of polymers and the small diameter of the fibers used with polymer matrices (Reid, 2009). Since the modulus of polymers is notably lower than that of metals, polymer matrix composites retain lower residual strain in the fibers compared to metal matrix composites. Thus in order to obtain acceptable resolution in the displacement of the fiber ends, the matrix must be removed over a greater fiber length. This increases the chances of bending in exposed fibers, the effect of which is greatly exacerbated by their small diameter in comparison to those used in the metal matrix composites studied previously (Fang *et al*., 2000; Güngör, 2002; Ramamurty *et al*., 1996). Significant bending of the fibers reduces the accuracy of the measured change in fiber length, and consequently this method is of limited helpfulness for fiber reinforced plastics.

Another problem that limits the use of this method with GFRP is that if strong acids are used to remove the matrix, the fibers might corrode or crack (Jones and Chandler, 1985). Using high temperatures to vaporize or burn off the polymer matrix are possible alternatives (American Society for Testing and Materials, 2002). However, the residual stress state in the material will be altered, because the high temperatures employed to vaporize the matrix between the slits will affect the neighboring material. Therefore, if this method must be used for GFRPs, the entire matrix should be burned off simultaneously. Achieving a measure of the original residual stress in the material is possible through a comparison between the length of the glass fiber prior to and after matrix removal (Reid, 2009). Modifications to the etching process could thus allow the measurement of the longitudinal fiber stresses within GFRP. However, bending of fibers and the need to vaporize rather than etch the matrix away, causes the measurement to be less accurate. The practicality of this method is therefore questionable (Reid, 2009).

The etching or dissolution method has been used extensively to quantify fiber stress in silicon-carbide reinforced titanium alloys. The method was first used by Cox *et al*. (1990), who dissolved the matrix from the central part of long rectangular specimens and subsequently measured their change in length. The change in length was then related back to the average fiber strain resulting from the release of residual stresses.

The etching technique has been enhanced since it was first proposed. Pickard *et al*. (1995) presented a simplified experimental technique to determine the axial fiber residual strain in continuously-reinforced metal matrix composites. Kendig *et al*. (1995) measured residual stresses in Ti-15-3/SCS-9 composites with controlled matrix and interfacial microstructures. The FEMUR test was used to measure axial residual strains in the reinforcing fibers. Ramamurty *et al*. (1996) modified the method by preparing a flat face perpendicular to the fiber direction, at the end of a composite specimen, which acted as a reference surface. This method was accurate and simple to implement. In addition, it completely released the strains in every fiber, thereby allowing the residual stress in individual fibers to be determined.

Güngör (2002) measured the residual stresses in two Ti/SiC uni-directional composite panels with thick cladding using two experimental methods, crack compliance to measure the variation of in-plane residual stresses in the cladding of the materials, and matrix etching to measure the longitudinal fiber strains. By combining the results of both methods, the out-of-plane stresses were also determined, so that the full stress state in the reinforced section of the material could be obtained. Fang *et al*. (2000) applied a method based on matrix etching for calculating residual stresses in continuous fiber reinforced titanium matrix composites.

2.11 Micro-indentation methods

Micro-indentation techniques are micro-mechanical methods that are used to analyze the interfacial characteristics of composites (Kalton *et al*. 1998; Parthasarathy *et al*., 1991). Micro-indentation techniques do not require the use of model composite systems (Ramanathan *et al*., 2001). Single fiber push-in and single fiber push-out are two micro-indentation methods. Both of these methods include exerting a compressive longitudinal load at the end of a single fiber using a small indenter. The end of the fiber is exposed by cutting the composite perpendicular to the direction of the fibers and then polishing the cut surface. The test relies inherently on the heterogeneous nature of a composite material, but allows measurements of micro-scale residual stresses (Lara-Curzio and Ferber, 1994; Ramanathan *et al*., 2001).

In push-in tests, a backing plate is positioned on the reverse face of the specimen, and the compressive load on the fiber causes an increase in interface stress between the fiber and matrix. The loading is increased until the interface finally fails and debonding occurs at the fiber end. As the load is further increased, the debonding extends progressively along the fiber. However, since the fiber is long, the debonding length never extends beyond a small fraction of the length of the embedded fiber. In push-out tests, the specimen is less thick, and the debonding length can consequently extend over the complete length of the fiber. As a result, the fiber is pushed out of the rear side of the specimen (Lara-Curzio and Ferber, 1994).

Several mechanical properties of the fiber and matrix affect the beginning and propagation of the debonding, including the strength and fracture toughness of the interface, and the friction between fiber and matrix. Residual stresses that appear in the form of radial clamping stress and longitudinal stresses need to be considered. Analytical predictions are generally used to characterize the interface properties (Zhou *et al*., 2001). It is simple to visualize the influence of longitudinal residual stresses on the measurements. The release of longitudinal residual compression in the fiber with increasing debond length causes the fiber to extend. The extension and the applied compressive loading are in opposition, therefore the displacement of the fiber end is less for a given applied load than if longitudinal residual stresses were not present (Reid, 2009).

The analytical techniques developed for use with the single-fiber push-in and push-out methods allow them to be applied directly to measuring micro-scale longitudinal residual stresses. There are problems applying these methods to glass fiber, and the majority of cases where these techniques have been applied have made use of large diameter (>100 μm) fibers (Belnap and Shetty, 2005). Accuracy in measurement of longitudinal residual stress at this scale is of prime importance. Unlike small diameter fibers (Lara-Curzio and Ferber, 1994), measuring longitudinal residual stresses in larger diameter fibers does not show much scatter in the results (Belnap and Shetty, 2005; Huang *et al*., 1995; Parthasarathy *et al*., 1991). This implies that scatter is more related to fiber size than to the distribution of longitudinal stress (Reid, 2009).

Least-squared methods are used to infer the residual stress simultaneously with a number of other interfacial characteristics in the fibers, rather than measuring them directly. Due to the nature of the problem, it is possible to obtain a reasonable fit to the measured data, even if some of the interfacial characteristics are poorly determined (Lara-Curzio and Ferber, 1994). It follows that inadequacies in analytical technique can result in faulty measurements of residual stress.

Although the fiber push-in and push-out techniques are capable of measuring micro-scale residual stresses in GFRP, there are a number of problems with these approaches. The measurement system can be costly and may result in considerable scatter in the measurements. In addition, the residual stresses are not measured directly but are inferred along with a number of other interfacial characteristics, which makes the method susceptible if there are insufficiencies in the analysis technique used (Reid, 2009).

Ramanathan *et al*. (2001) investigated the effect of the acidic and basic nature of surface-activated carbon fibers in epoxy and PPS matrices on fiber/matrix adhesion using fiber push-out and push-in micro-indentation methods. Lara-Curzio and Ferber (1994) determined the interfacial properties of a glass-ceramic matrix composite (SiC/CAS) from single-fiber push-out tests using the interfacial test system. The coefficient of friction, μ, the residual clamping stress, σ_c, and fiber axial residual stress, σ_z, were extracted by fitting the experimental stress versus fiber-end displacement curves using the models of Hsueh (1992, 1993) and Kerans and Parthasarathy (1991).

Huang *et al*. (1995) characterized the interfacial mechanical properties of SiC monofilament-reinforced β'-SiAlON composites using a single fiber push-out technique. Belnap and Shetty (2005) used two different techniques to assess interfacial sliding friction and residual stresses in sapphire filament reinforced epoxy matrix composite. They measured stresses in filaments bridging a steady-state matrix crack using a laser microprobe to stimulate fluorescence from the sapphire filaments, and load-displacement records in filament push-in tests using a mechanical microprobe. Olivas *et al*. (2006) measured the surface residual stresses in SiC particle-reinforced Al matrix composites using a nano-indentation technique. Suresh and Giannakopoulos (1999) proposed a simple method for

measuring residual stress with sharp indenters, based on the difference in contact area of stressed and stress-free materials indented to the same depth.

Swadener *et al*. (2001) presented a new technique based on spherical indentation, which can be more sensitive to residual stress than measurements with sharp indenters in certain deformation regimes. Experiments have verified that this method is accurate to within 10 to 20% of the specimen yield strength and can be useful for making localized measurements.

Rossington *et al*. (1984) examined indentation-induced delamination between thin films of ZnO and Si substrates. They determined that the crack path is influenced by the indenter load and the film thickness, as well as by residual stresses formed during deposition. Marshall and Oliver (1990) analyzed fiber sliding in the presence of residual stresses in ceramic composites, and found that measurements of the force-displacement relation for an indenter loaded onto the end of a fiber can be used to quantify the magnitude of the residual axial stress in the fiber. The technique is applied to calculate residual stresses generated by thermal cycling of SiC-glass ceramic composites.

Marshall and Lawn (1977) analyzed fiber sliding in the presence of residual stresses in ceramic composites, and found that measurements of the force-displacement relation for an indenter loaded onto the end of a fiber can be used to calculate the magnitude of the residual axial stress in the fiber. The technique is applied to measuring residual stresses generated by thermal cycling of SiC-glass ceramic composites.

2.12 The slitting method

The incremental slitting method is another stress relaxation technique, often called ‘crack compliance’, ‘compliance’ or ‘slitting’. It is also found in the literature as the successive cracking method, the slotting method, and as a fracture mechanics based approach (Prime, 1999a,b). This method was introduced in 1971 by Vaidyanathan and Finnie and developed by Cheng and Finnie (1985, 1986, 1992, 1998) and Cheng *et al*. (1991).

In this approach, a slot or multiple slots (also called grooves or slits) are incrementally cut into a component with residual stress. The slot releases the residual stresses normal to the plane of the slot and the part deforms in order to restore force equilibrium. It is possible to determine the original residual stresses as a function of depth by measuring the deformations as the slot depth increases. A single slot only permits the measurement of residual stresses perpendicular to its plane. To measure a bi-axial stress field, two orthogonal slots are applied (Ersoy and Vardar, 2000; Prime and Hill, 2002).

An essential assumption of the incremental slitting method is that stresses are consistent in the direction of the slot width, which allows the material removed by the slot to be treated as a homogeneous continuum. If the heterogeneous structure of a fibrous composite is treated as homogeneous (Ganley *et al*., 2000; Kim *et al*.,

2002), the measured residual stresses will be averages of the matrix and reinforcement stresses (Prime and Hill, 2004). This implies that only residual stresses at the meso-scale can be found in the fiber direction. Thus the incremental slitting method needs to be modified to account for material heterogeneity, if micro-scale residual stresses in the fiber direction are to be quantified (Reid, 2009).

If the heterogeneous nature of the material is to be taken into account, the method chosen must have sufficient resolution to control the elastic response to the release of residual stress from individual fibers. In addition, as the fiber stresses return to far-field conditions over a few fiber diameters, the measurement system must function over a small scale (Reid, 2009).

Deformations resulting from the relaxation of stresses are measured with strain gages to determine the residual stresses through the thickness (Fig. 2.5). This is a destructive method, but offers a high degree of accuracy and does not require any specific specimen preparation (Parlevliet *et al*., 2006).

The method employed to create a cut of increasing depth has evolved from sawing (Ersoy and Vardar, 2000; Ganley *et al*., 2000; Johnson *et al*., 1985; Kang *et al*., 1989; Neubrand, 2002) and milling (Cheng and Finnie 1985, 1986) to EDM (Cheng *et al*., 1994). Sawing and milling are universally applied but the cutting can cause an undesirable temperature increase and plastic deformation close to the bottom of the cut. As material is removed, residual stresses are introduced into the tip of the slot. These cutting stresses can influence the strain readings obtained from the gage on the front face (Prime, 1999a,b). Mechanical methods of cutting the slot also impose cutting stresses on the interior surfaces of the slit. This is the exact region where the elastic response to the release of fiber residual stresses is highest, and so the elastic response due to cutting stresses and those resulting from residual stresses in the fibers cannot be distinguished from each other. If feasible, saws should be avoided if near surface stresses are to be measured. The back face strain-gage is relatively insensitive to cutting stresses and so it is feasible to obtain reasonable through-thickness results if the temperature is allowed to stabilize before measurements are taken (Prime, 1999a,b). In order to reduce the influence

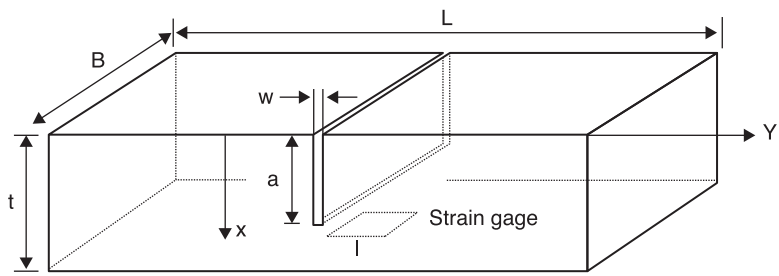

2.5 Slitting method schematic. Notation: t, specimen thickness; L, specimen length; B, specimen width; a, slit depth; w, slit width; l, strain gage length..

of clamping force on the measurement, the plane of cut should be placed far enough away from the fixture. When sawing is used, an accurate measurement of the depth of cut is more difficult, and the release of a compressive residual stress may generate substantial 'binding' on the cutter, even to breakage, often ending measurement prematurely.

EDWM is the best method for cutting the slot (Güngör, 2002; Prime, 1999a,b; Prime and Hill 2002), since the use of a fine wire keeps the slot narrow and minimizes the residual stresses introduced by the cutting process, for instance by minimizing the clamping force needed to secure the specimen. Moreover, because the part is usually submerged under deionized water during the cutting process, it is simple to take all strain measurements at a constant temperature.

For wire EDM, the location and depth of cut is precisely controllable and cutting can resume in most cases after rethreading the wire if it breaks. For close-to-surface measurement on a curved surface, conventional EDM is uniquely qualified to make a cut of approximately uniform depth by use of a sheet of electrode with a profile matching the curved surface. As the electrode wears out gradually during cutting, the measurement of cut depth must be carefully calibrated for the material and cutting conditions.

There are two situations requiring special attention throughout measurements. When a thin cut is created by a wire through a region with high compressive stress, the deformation that results from releasing the stress may be so great that it puts the faces of the cut into contact, hence invalidating the assumption of the superposition principle. This is easily avoided by cutting backwards in order to prevent contact. A thin cut in a region of high tensile stress can initiate the propagation of cracks near the cut tip, and thus prematurely terminate the test. Despite these restrictions, EDM continues to be the best method for making a high precision cut of progressively increasing depth for electrically conductive materials. The only important disadvantages of EDWM are that it can only be used on conducting materials, so it is not applicable to GFRP, and that it cannot be used for field applications (Cheng and Finnie, 2007).

The use of a focused ion beam (Kang *et al*., 2004; Sabaté, 2006a,b) permits the incremental slitting method to be applied to tiny components, as extremely fine slots can be cut, and this method has been used to cut slots of 10 μm long, 0.35 μm wide and 0.3 μm deep (Sabaté, 2006a). Its main disadvantage is that since it is restricted to the creation of very small slots, it is not so useful for large components (Reid, 2009). However, the widths of these slots are also substantially smaller than the size of a typical glass fiber, and it has been reported that introducing narrow and deep slots using a focused ion beam is problematic. Therefore it appears that this approach is not useful for cutting through a single glass fiber, no matter what the surrounding matrix material may be (Reid, 2009). However, the use of a focused ion beam could introduce a flaw of sufficient size in a glass fiber causing it to fracture, and an analytic method could be developed to relate the elastic response of the matrix material around the fiber break to the residual stress

in the fiber. The technique would need the heterogeneity of the material at small structural scales to be taken into account. Because the sub-surface structure is not known directly, but still affects the elastic response on the surface, the method would rely on information that is not available. Therefore, neither the incremental slitting method, nor adaptations of it are applicable to measure uni-directional micro-scale longitudinal residual stresses GFRP (Reid, 2009).

Deformation resulting from releasing residual stress through a cut with progressively increasing depth is measureable as the change of displacements and/or strain. Several methods can be used to measure the elastic response to the introduction of the slot, including Moiré interferometry (Güngör, 2002; Neubrand *et al*., 2002), the measurement of crack mouth opening displacement (Lim *et al*., 2003; Prime, 1999a,b) and digital image correlation (DIC) of high resolution micrographs of the surface adjacent to the crack mouth (Kang *et al*., 2004, Sabaté, 2006a,b). However, the use of strain gages is the most commonly employed technique, owing to the wide availability of high precision electric-resistance strain gages of different sizes and patterns. The gages are positioned perpendicular to the slot to maximize their response. Placing a strain gage on the back face, opposite the entrance of the slot, makes it possible to measure residual stresses all the way through the thickness. Residual stresses immediately below the surface can be best measured using a gage placed on the front face close to the slot (Kang *et al*., 2004). As the response of the gage on the front face saturates at some depth, a back face strain gage is always needed, unless only residual stresses near the surface are required (Reid, 2009).

Fortunately, in most cases, the slitting method requires measurement of strain at just one or two locations. When selecting a strain gage, it is essential to match the thermal expansion coefficient of the strain gage with that of the surface on which the gage is supposed to be installed. Also, the gage length must be short enough to reduce the effect of strain gradient and heighten the measurement sensitivity (Cheng and Finnie, 2007).

Although strain measurement using strain gages is more sensitive and reliable than most displacement based measurements, it has some limitations (Cheng and Finnie, 2007), because measurement is restricted to a few fixed locations, with an increase in the number of strain gages, soldering and cabling the gages becomes time-consuming, and the gage is sensitive to temperature variation if its thermal expansion coefficient does not match that of the specimen adequately.

Analysis consists of forward and inverse solutions. The forward solution, often referred to as the compliance calculation, determines the response of the part as the slot depth increases over a range of familiar stress distributions. The inverse solution involves finding the residual stress distribution best matching the experimentally measured response. The inverse solution is often carried out using a series expansion incorporating a least squares approach. If this approach is employed, the calculated solution does not have to exactly match the measurements (Prime, 1999a,b) and is thus tolerant of small measurement errors (Reid, 2009).

Analytical techniques include Reid's beam-bending approximation, the series expansion approach and the fracture mechanics approach. Reid's beam-bending approximation is substantially imprecise, whereas both the series expansion approach and the fracture mechanics approach function well, but have different advantages and disadvantages. The fracture mechanics approach depends on the approximation of the slot as a mathematical crack. This approximation has proved valid for slots with a depth-to-width ratio larger than five. The residual stress results are commonly precise except for extremely deep cracks. The calculations need a weight function solution for the given geometry and differentiation of the calculated strains, and thus efforts must be made to minimize errors. With slot depth-to-width ratios of less than five, some errors may arise in near-surface measurements, as the method assumes a mathematical crack (Prime, 1999a,b).

In the series expansion approach, the residual stress profile is determined from the measured strains, using a technique developed originally for hole-drilling measurements. First, the unknown residual stresses are written as a series expansion. Then the strains, called compliances, are calculated for each term (basis function) of this series. Eventually, a least-squares fit is carried out between the calculated and measured strains, providing the coefficients of the series expansion terms. The unknown residual stresses therefore result from the series expansion equation. With this method, the residual stress profile is determinable precisely, with some restrictions depending on the choice of the series' basic functions. This approach is particularly tolerant to strain measurement errors, and it is simple to account for the finite width slot, permitting near-surface measurements (Prime, 1999a,b).

Schajer and Prime (2007) used equilibrium constraints to extrapolate the stress field through the entire thickness; the maximum depth was limited to approximately 90 to 95% of the thickness in the slitting method. Prime *et al*. (2000, 2004) measured micro-scale residual stress using the incremental slitting method transversely. Shokrieh and Akbari (2012) investigated the influence of shear stresses on the determination of residual stresses in isotropic and orthotropic materials by the slitting method. Seif *et al*. (2006) developed a simple, sensitive, non-contact, quantitative technique combining the slitting method with image processing analysis to measure displacements caused by relieving residual stresses, which was used to evaluate residual stresses in composite missile components. The technique was applied to two types of composites, filament wound carbon/epoxy and filament wound glass/epoxy.

Prime (1999a,b) reviewed the technical literature around determining residual stress profiles by successive extension of a slot, and measurement of the resulting strains or displacements. Ersoy and Vardar (2000) investigated the macroscopic residual stresses in layered composites, paying particular attention to implementing a reliable experimental technique for measuring through-the-thickness residual stresses in layered composite plates. Residual stresses in $(0_{10}/90_{10})_S$ APC-2 laminate were measured using layer removal and compliance methods and

comparing the results with those obtained by a numerical model developed by other researchers. Güngör (2002) measured the residual stresses in two Ti/SiC uni-directional composite panels with thick cladding, using a crack compliance method to measure the variation of in-plane residual stresses in the cladding of the materials and infer the average fiber stresses from the results, and finite element analysis to confirm the applicability of a simple bending theory for the calculation of the residual stresses from curvature measurements made using matrix etching. Hermann (1995) investigated the growth of cracks under far-field cyclic compressive loading in aluminum-lithium (Al-Li) alloys reinforced with SiC particulates in notched compact tension (CT) specimens. He used the slitting method in a particulate-reinforced metal-matrix composite and treated the composite as an isotropic material.

Hill and Lin (2002) applied the slitting method to a ceramic–metallic graded material and presented experimental measurements of the through-thickness distribution of residual stress in a ceramic–metallic functionally graded material (FGM). Seif and Short (2002) discussed a straightforward method for experimentally deducing the residual stresses in a thin-walled, axially symmetrical round cylinder. They used the slitting technique along with an optical technique to measure the deflection of a slit ring originally sectioned from a thin-walled cylinder.

2.13 The first ply failure method

The first-ply failure method uses the maximum stress criterion to quantify the residual stresses present (Hahn, 1976; Kim and Hahn, 1979). Kim and Hahn (1979) recorded strains and loads while loading a cross-ply [0/90] specimen to failure. Elastic assumptions were employed to quantify the load at which the first ply failed. This load was compared to the corresponding strength of a uni-directional specimen with the difference being referred to as the residual stress. Kam (1995) considered the viscoelastic effect in this methodology.

Thermal contraction in symmetrical cross-ply composites entails the development of tensile residual stresses in the transverse (90-degree) plies. When the composite material is transversely loaded, its tensile $\sigma^{t}_{0/90}$ strength (t represents the transverse direction) is lower than the tensile strength of a similar uni-directional composite in the longitudinal (0-degree) direction $\sigma_{0/0}$. The tensile strength is quantified through acoustic emission of the first crack, hence the term 'first-ply failure'. The difference between the tensile strengths provides a rough calculation of the residual stresses between plies (interlaminar residual stresses) σ_R, where $\sigma_R = \sigma_{0/0} - \sigma^{t}_{0/90}$. The 90-degree plies are positioned at the external surface to guarantee the cracking noise is not suppressed (Parlevliet *et al*., 2006).

Cracking of transversely loaded plies has been used to estimate transverse residual stresses in cross-ply laminates (Cowley and Beaumont, 1997; Jeronimidis and Parkyn, 1988; Kim and Hahn, 1979). This technique depends on measuring

the difference between the perceptible transverse tensile strength of uni-directional material and the stress needed to instigate transverse cracking when the same material is embedded in a cross-ply laminate. It is assumed that the transverse strength continues to be constant and hence tensile residual stresses reduce the additional stress needed to cause failure (Reid, 2009).

Although this approach can offer good results (Jeronimidis and Parkyn, 1988), it has been shown that transverse tensile strength is not a built-in ply feature (Flaggs and Kural, 1982). The transverse strain in plies perpendicularly orientated to the applied load is restricted by neighboring plies, which are more aligned with the load. Consequently, the apparent strength of the transversely loaded plies increases. The restricting effect is most substantial when plies aligned with the load sandwich a single ply perpendicularly orientated to the load. The strength has been shown to increase by a factor of 2.48 in a $(0_2/90)_s$ laminate (Flaggs and Kural, 1982). In order to reduce the restricting influence of adjacent plies, residual stress measurements are thus limited to the outer plies of the laminate (Reid, 2009).

The method depends completely on the assumption that the transverse stresses in a uni-directional laminate are zero. This is valid at the meso-scale, but does not hold true at the micro-scale, where the residual stress field in the plane perpendicular to the fibers is obviously complex. The method is thus restricted to the measurement of meso-scale residual stresses in the transverse direction (Reid, 2009).

The residual strain field of a uni-directional material is uniform at points far from the fiber ends, in the longitudinal direction. Therefore, this approach could potentially be modified to measure the micro-scale residual stresses aligned with the fibers by loading the laminate in the fiber direction. Measurements of the strain needed to initiate resin cracking could indicate the longitudinal residual stresses, because the strain to failure of glass fibers is greater than that of some thermoset resins. However, this approach requires knowledge of the strain needed to initiate resin cracking when no longitudinal residual stresses exist. As there is no way of knowing when the residual stresses in a laminate are zero, the information needed to apply this method cannot be obtained. The strain to failure of unreinforced resin is also inapplicable, because the tri-axial state of stress experienced within the laminate is different from the uni-axial stress state in a tensile test of pure resin (Lee and Schile, 1982). The cracking stress of the resin in a laminate is hence different from that of unreinforced resin, so the method is not applicable (Reid, 2009).

Kim and Hahn (1979) described an experimental technique for detecting the first ply-failure in laminated composites using a combination of long strain gages and acoustic emission measurement. The material system chosen for this study was T300/5208 graphite/epoxy laminates of $[0/90_3]_S$, $[\pm 45/90_2]_S$ and $[0/\pm 45/90]_S$ orientations. The experimental data for all three types of laminates agreed fairly well with the analytical predictions with and without residual stresses present.

2.14 The measurement of curvature method

Warpage is a common indication of residual stresses in asymmetrical composites. Thus, a relatively simple method for quantifying residual stresses is to measure out-of-plane deformations in asymmetrical or angle-ply laminates, as the residual stresses can be relieved by these deformations. Monitoring out-of-plane deformations may be undertaken during or after cooling from the processing temperature. The greater the curvature of a composite material with a specific thickness, the higher the magnitude of the residual stresses (Parlevliet *et al*., 2006). Cutting the specimen in narrow strips and measuring both the deviation at the center and the chord length is the most common method for measuring curvature. Using narrow strips simplifies the measurements because, unlike the whole specimen, there is just one dominant curvature.

A disadvantage of the curvature method is that the results may considerably deviate for equal laminates under similar conditions. This is explained by accuracy of curvature measurement, non-symmetry of ply thickness, disorientation of the plies, and deviations in the alignment of the fibers. Nor does this method provide any information for the spatial variation of residual stresses at the micro-mechanical level, due to varying fiber distribution, variable thermal contraction, etc. (Parlevliet *et al*., 2006; Tsouvalis *et al*., 2009).

Warpage leads to the formation of unbalanced, asymmetrical multi-directional laminates. The destructive method of Joh *et al*. (1993) used this fact in its quantification of stress from deformation strain due to sectioning. Asymmetrical laminates can also be manufactured for the warpage to be measured. This method has been an area of extensive study (Fakuda *et al*., 1995; Hyer, 1981; Jain and Mai. 1995; Kim and Hahn, 1989, 1979; Wang *et al*., 1992). The stresses are normally calculated from the observed warpage by CLT.

The combination of warpage and CLT has also been used to devise a method for measuring and calculating polymer matrix cure shrinkage (Daniel and Wang, 1989; Daniel *et al*., 1989). Daniel manufactured a laminate directly onto an existing and previously cured identical laminate with the same CTE and manufacturing procedure. Any resulting warpage was strictly due to chemical shrinkage. The curvature was measured and stresses were again quantified using CLT, and the resulting stresses were related directly to chemical shrinkage (Myers, 2004).

Measurement of the temperature-related change in curvature has been employed frequently to study residual stresses within asymmetrical laminates (Cowley and Beaumont, 1997; Nairn and Zoller, 1985; Unger and Hansen, 1993; Wisnom *et al*., 2006). The method is based on the same phenomenon seen in thermostats using bi-metallic strips. The curvature of an asymmetrical laminate changes with temperature, if the thermal expansion coefficient in a specific direction changes from ply to ply. This variation is predictable using CLT, which can typically predict simultaneous curvature in the two reference directions. However, thin laminates are bi-stable, meaning that the laminate assumes a cylindrical shape with its axis swapping between two directions. This takes place because curvature

in one direction tends to restrict curvature in the other. Therefore, curvature measurements are carried out on thin strips aligned in the direction of interest. The short dimension across the strip minimizes the displacements, and the consequential limiting effects, due to secondary curvature (Jeronimidis and Parkyn, 1988).

The technique depends on finding the stress-free temperature. This is typically carried out through measuring the curvature at a number of temperatures and then extrapolating these measurements to find the temperature at which the laminate flattens. When the stress-free temperature is found, the meso-scale stresses at other temperatures can be determined using CLT (Jeronimidis and Parkyn, 1988). It is also possible to determine the micro-scale residual stresses within a ply if a mathematical model such as that of Nairn (1985) is applied. It is essential to know the stress-free temperature and the temperature-dependent elastic features of the constituent materials (Reid, 2009).

Symmetrical laminates do not curve with temperature changes. However, symmetrical laminates have been cured onto a thin steel sheet (Kim *et al*., 2006) acting like a 'dummy ply'. This can create an asymmetrical laminate, permitting the measurement of the stress-free temperature and thus the micro-scale residual stresses (Reid, 2009). A dummy ply therefore permits the measurement of micro-scale residual stresses in uni-directional laminates. However, this only holds true in cases where the laminate is cured onto the dummy ply. Under these conditions, the laminate is flat when both the micro-scale and meso-scale residual stresses are zero. Nonetheless, this approach is not applicable for work on composite laminates, because the dummy ply must be removed from the GFRP specimens before their immersion in a corrosive medium, in order that the rate of environmentally assisted crack growth can be measured. This hinders measurement of the residual stresses in the specimens as the test terminates. This is an important restriction, since moisture diffuses into the laminate as it is immersed in the corrosive medium, changing the state of residual stress (Reid, 2009).

Gigliotti *et al*. (2003) alluded to another problem with the use of a dummy ply. Thermal expansion differences entail shear stresses at the interface between a composite specimen and a tool surface. These stresses generate non-thermoelastic strain, possibly because of viscous flow throughout the curing process. As the dummy ply is equivalent to a tool in this situation, it is expected that the non-thermoelastic strains artificially affect the measured stress-free temperature (Reid, 2009).

A dummy ply also cannot be used with laminates made for purposes other than residual stress measurements, for example, to prevent residual stress measurements in failure studies. Although this limitation is not important, since this method cannot be applied to investigating the rate of environmentally assisted cracking, an alternative approach is needed. It would be of benefit if this method could also be used on existing laminates (Reid, 2009).

Although the most widely used technique for measuring the residual curvature of asymmetrical laminates, this method cannot be applied to symmetrical laminates and only provides a global approach to residual stress (Sicot *et al*.,

2003). This method is effective for validating residual stress models; however, it can be used only for asymmetrical ply sequences, which are rarely used in practice.

Yu *et al*. (2006) described an investigation of residual stresses in epoxy-steel systems using a bi-material beam. Gigliotti *et al*. (2003) monitored the development of residual stresses in [0/90] asymmetrical flat laminates (AS4/8552 composite system) by stopping the cure cycle at pre-determined points and evaluating the related level of deformation. Dano and Hyer (1998) presented a methodology to predict the displacements, particularly the out-of-plane component, of flat asymmetrical epoxy-matrix composite laminates as they are cooled from their elevated cure temperature. Cho *et al*. (1998) examined slippage effects resulting from the interaction between the laminates and the tool-plate, which had been ignored in previous studies. White and Hahn (1990) measured warpage of $[0_4/90_4]_T$ cross-ply specimens to monitor residual stress build-up. Harper and Weitsman (1985) presented an experimental and theoretical investigation of moisture effects in graphite/epoxy composites. Tarsha-Kurdi and Olivier (2002) examined the effects of autoclave curing pressure and cooling rate on the room-temperature curvature of carbon/epoxy $[0°_2/90°_2]$ laminated strips. Di Landro *et al*. (1995) studied the residual thermal stresses in composite laminates due to curing cycles.

Kim and Hahn (1989) carried out intermittent curing of an asymmetrical laminate to monitor the residual stress development. The resulting warpage was measured to assess the extent of residual stresses. Peeters *et al*. (1996) experimented on both cross-ply and angle-ply laminates over a wide range of laminate dimensions. Zewi *et al*. (1987) fabricated symmetric and asymmetrical glass-fabric-reinforced laminates to study the residual stresses. The laminate material was fully characterized by determining its physical and mechanical properties at room and elevated temperatures. Jun and Hong (1990) investigated the effects of width-to-thickness, aspect ratio, number of layers and stacking sequence on the shapes of the asymmetrical cross-ply $[0_n/90_n]_T$ (n = 1,2,. . .) family of laminates. Fukuda *et al*. (1995) also performed warpage measurements on laminated composites.

Timmerman *et al*. (2003) used a model prepreg system to evaluate the effect of cure temperature on microcracking in polymeric composite materials exposed to cryogenic cycling. Kesler *et al*. (1998) studied residual stresses in plasma-sprayed coatings using three experimental techniques, curvature measurements, neutron diffraction and X-ray diffraction. They investigated two distinct material classes:

1. single-material coatings (molybdenum); and
2. bi-material composites (nickel_alumina and NiCrAlY_yttria-stabilized zirconia), with and without graded layers.

Wisnom *et al*. (2006) considered the mechanisms involved in residual stresses and distortions and discussed the way they develop during the cure. Youssef and Denault (1998) characterized the microstructure, mechanical features and residual stresses in glass fiber reinforced polypropylene (PP) composites with regard to the

thermoforming parameters and as a function of the fiber-matrix interface quality. Fernlund *et al*. (2003) presented an overview of residual stress build-up and shape distortions in autoclaved composite laminates, discussing the sources of stress build-up and shape distortions and presenting experimental results that identify the parameters driving shape distortions. Palerosi and Muller de Almeida (2007) held that studying the changes in curvature of asymmetrical composite laminates with temperature offers a measure of the magnitude of the thermal stresses and the mechanical behavior of the material with temperature. Lange *et al*. (1995) utilized a bilayer-beam bending technique and parallel-plate rheometry to investigate the onset of stresses in epoxy films.

2.15 Heating methods

To avoid the problems caused by drilling a hole, an alternative technique that makes use of localized heating to achieve the same result has been developed (Pechersky *et al*., 2000). A small spot (2 mm diameter) on the surface of a steel subject is heated to around 200°C for a short time using an infra-red laser. The elevated temperature in this region causes the localized reduction of yield strength. As a result, plastic flow can occur, which leads to the release of some of the residual stress. The resulting surface deformations in the surrounding material are measured using electronic speckle pattern interferometry when the subject has cooled to ambient conditions. The measured surface deformations are then processed to determine the strain relief and hence the residual stresses prior to heating (Pechersky, 2002).

A few factors complicate the use of this technique. The method relies critically on the variation in yield stress, elastic modulus and coefficient of thermal expansion with temperature (Vikram, 1996). As with the original method, the response would need to be calibrated against a finite element model with special parameters required as the input. Heating of the matrix can cause viscous flow to occur, particularly when the stresses are high. It is consequently improbable that non-linear behavior can be avoided, and the method needs major modifications to be applicable to composite materials. Pechersky (2002) presented a new technique for measuring residual stresses based on strain measurements following thermal stress relaxation. According to Reid and Paskaramoorthy (2009), there are a few methods available for measuring residual stresses in the simplest possible composites structure, unconstrained uni-directional laminate. However, none of them are suitable for use on GFRP.

2.16 Conclusions

In recent years, the growing use of advanced laminated composites has drawn a lot of attention to process-induced residual stress, and it is essential to develop methods for measuring and predicting residual stresses in composite materials.

Explaining quantities and qualities of residual stresses has therefore been the subject of much research. While measuring and predicting residual stresses reliably is a considerable challenge, their distribution and size are critical to understanding how composites behave. Optimizing material quality and minimizing component weight also require a more thorough understanding of the significance of residual stresses. This chapter provided a comprehensive overview of the destructive techniques in measuring the residual stresses in composite materials. It was shown that a wide range of such methods exist that have been investigated by different researchers, each having its own benefits and shortcomings.

2.17 References

Aleong, C. and Munro, M. (1991) Evaluation of the radial-cut method for determining residual strains in fiber composite rings, *Experimental Techniques*, **15**(1), 55–8.

American Society for Testing and Materials (2002) ASTM Standard D-3171-06, *Standard Test Methods for Constituent Content of Composite Materials*, American Society for Testing and Materials.

Balalov, V. V., Pisarev, V. S. and Moshensky, V. G. (2007) Combined implementing the hole-drilling method and reflection hologram interferometry for residual stresses determination in cylindrical shells and tubes, *Optics and Lasers in Engineering*, **45**(5), 661–76.

Baldi A. (2007) Full field methods and residual stress analysis in orthotropic material. Part I: Linear approach, *International Journal of Solids and Structures*, **44**(25–26), 8229–43.

Bateman, M. G., Miller, O. H., Palmer, T. J., Breen, C. E. P., Kingston, E J. *et al*. (2005) Measurement of residual stress in thick section composite laminates using the deep-hole method, *International Journal of Mechanical Sciences*, **47**(11), 1718–39.

Beaney, E. M. (1978) *Measurement of Sub-Surface Stress*, CEGB Report Rd/B/N4325.

Belnap, J. D. and Sketty, D. K. (2005) Interfacial properties of sapphire/epoxy composites: comparison of fluorescence spectroscopy and fiber push-in techniques, *Composites Science and Technology*, **65**(11–12), 1851–60.

Bert, C. W., and Thompson, G. L. (1968) A method for measuring planar residual stresses in rectangularly orthotropic materials, *Journal of Composite Materials*, **2**(2), 244–53.

Bonner, N. W. and Smith, D. J. (1996) Measurement of residual stresses using the deep-hole method, *Pressure Vessels and Piping*, **327**, 53–65.

Bouchard, P. J., George, D., Santisteban, J. R., Bruno, G., Dutta, M. *et al*. (2005) Measurement of the residual stresses in a stainless steel pipe girth weld containing long and short repairs, *International Journal of Pressure Vessels and Piping*, **82**(4), 299–310.

Brown, T. B., Dauda, T. A., Truman, C. E., Smith, D. J., Memhard, D. and Pfeiffer, W. (**4**) Predictions and measurements of residual stress in repair welds in plates, *International Journal of Pressure Vessels and Piping*, **83**(11–12), 809–18.

Buchmann, M., Gadow, R. and Tabellion, J. (2000) Experimental and numerical residual stress analysis of layer coated composites, *Materials Science and Engineering*, **A288**, 154–9.

Càrdenas-Garcìa, J. F., Ekwaro-Osire, S., Berg, J. M. and Wilson, W. H. (2005) Nonlinear least-squares solution to the Moiré hole method problem in orthotropic materials. Part I: Residual stresses, *Experimental Mechanics*, **45**(4), 301–13.

Casari, P., Jacquemin, F., and Davies, P. (2006) Characterization of residual stresses in wound composite tubes, *Composites – Part A: Applied Science and Manufacturing*, **37**(2), 337–43.

Chaoui, K., Moet, A. and Chudnovsky, A. (1988) Strain gage analysis of residual stress in plastic pipes, *Journal of Testing and Evaluation*, **16**(3), 286–90.

Chapman, T. J., Gillespie, J. W., Pipes, R. B., Manson, J. E. and Seferis, J. C. (1990) Prediction of process-induced residual stresses in thermoplastic composites, *Journal Composite Materials*, **24**, 616–43.

Chen, J., Terasaki, T., Akiyama, T. and Kishitake, K. (2000) New concept of equivalent inherent strain for measuring axisymmetric residual stresses, *Journal of Manufacturing Science and Engineering – Trans ASME*, **122**, 304–9.

Cheng, W. and Finnie, I. (1985) A method for measurement of axisymmetric residual stresses in circumferentially welded thin-walled cylinders, *ASME Journal of Engineering Materials and Technology*, **106**, 181–5.

Cheng, W. and Finnie, I. (1986) Measurement of residual hoop stresses in cylinders using the compliance method, *ASME Journal of Engineering Materials and Technology*, **108**, 87–92.

Cheng, W. and Finnie, I. (1992) Deformation of an edge cracked strip subjected to arbitrary shear surface traction on the crack faces, *Engineering Fracture Mechanics*, **43**, 33–9.

Cheng, W., and Finnie, I. (1998) The single slice method for measurement of axisymmetric residual stresses in solid rods or hollow cylinders in the region of plane strain, *ASME Journal of Engineering Materials and Technology*, **120**, 170–6.

Cheng, W. and Finnie, I. (2007) *Residual Stress Measurement and the Slitting Method*, New York, Springer.

Cheng, W., Finnie, I., and Vardar, Ö. (1991) Measurement of residual stresses near the surface using the crack compliance method, *ASME Journal of Engineering Materials and Technology*, **113**, 199–204.

Cheng, W., Gremaud, M., Prime, M., and Finnie, I. (1994) Measurement of near surface residual stress using electric discharge wire machining, *ASME Journal of Engineering Materials and Technology*, **116**, 1–7.

Cho, M., Kim, M. H., Choi, H. S., Chung, C. H., Ahn, K. J. and Eom, Y. S. (1998) A study on the room-temperature curvature shapes of unsymmetric laminates including slippage effects, *Journal of Composite Materials*, **32**(5), 460–82.

Cohen, D. (1997) Influence of filament winding parameters on composite vessel quality and strength, *Composites – Part A: Applied Science and Manufacturing*, **28**(12), 1035–47.

Corning, O. (2003) *Pultrusion of Glass Fibre Composite – A Technical Manual*, Publication No. 5-PL-58644.

Cowley, K.D. and Beaumont, P.W.R. (1997) The measurement and prediction of residual stresses in carbon-fibre/polymer composites, *Composites Science and Technology*, **57(**11**)**, 1445–55.

Cox, B. N., James, M. R., Marshall, D. B. and Addison Jr., R. C. (1990) Determination of residual stresses in thin sheet titanium aluminide composites. *Metallurgical Transactions A (Physical Metallurgy and Materials Science)*, **21A**(10), 2701–7.

Crasto, A. S. and Kim, R. Y. (1993) On the determination of residual stresses in fiber–reinforced thermoset composites, *Journal of Reinforced Plastics and Composites*, **12**(5), 545–57.

Daniel, I. M. and Wang, T. (1989) Determination of chemical cure shrinkage in composite laminates, *Journal of Composites Technology & Research*, **12**(3), 172–6.

Daniel, I. M., Wang, T. M., Karalekas, D. and Gotro, J. T. (1989) Determination of chemical cure shrinkage in woven-glass/epoxy laminates, *Annual Technical Conference – Society of Plastics Engineers*, New York, **1–4**, 632–4.

Dano, M. L. and Hyer, M. W. (1998) Thermally-induced deformation behavior of unsymmetric laminates, *International Journal of Solids and Structures*, **35**(17), 2101–20.

Dewey, B. R. and Knight, C. E. (1969) Residual strain distribution in layered rings, *Journal of Composite Materials*, **3**, 583–5.

Di Landro, L., Palonca, A. and Sala, G. (1995) Residual thermal stresses in bismaleimide/carbon fiber composite laminates, *Polymer Composites*, **16**(4), 276–83.

Eijpe, M. P. I. M. and Powell, P. C. (1997) Residual stress evaluation in composites using a modified layer removal method, *Composite Structures*, **37**(3–4), 335–42.

Eijpe, M. P. I. M. and Powell, P. C. (1998) Determination of residual shear stresses in composites by a modified layer-removal method, *Journal of Materials Science*, **33**, 2019–26.

Ersoy, N. and Vardar, Ö. (2000) Measurement of residual stresses in layered composites by compliance method, *Journal of Composite Materials*, **34**(7), 575–98.

Fakuda, H., Takahashi, K. and Toda, S. (1995) Thermal deformation of anti-symmetric laminates at cure, *Proceedings of ICCM-10*, Whistler, BC, Canada, **3**, 141–8.

Fang, Q., Sidky, P. S. and Hocking, G. M. (2000) Residual stresses in titanium matrix composites (TMC) in thermomechanical cycling using matrix etching, *Materials Science and Engineering A – Structural Materials: Properties, Microstructure and Processing*, **288**(2), 293–7.

Fernlund, G., Poursartip, A., Twigg G. and Albert, C. (2003) Residual stress, spring-in and warpage in autoclaved composite parts, *14th International Conference of Fiber Materials* (ICCM-14).

Filiou, C., Galiotis, C. and Batchelder, D. N. (1992) Residual stress distribution in carbon fiber/thermoplastic matrix pre-impregnated composite tapes, *Composites*, **23**(1), 28–38.

Flaggs, D. L. and Kural, M. H. (1982) Experimental determination of the *in situ* transverse lamina strength in graphite/epoxy laminates, *Journal of Composite Materials*, **16**(2), 103–16.

Fourney, W. I. (1968) Residual strain in filament-wound rings, *Journal of Composite Materials*, **2**, 408–11.

Fukuda, H., Takahashi, K. and Toda, S. (1995) Thermal deformation of antisymmetric laminates at cure, *Proceedings of the ICCM-10*, **3**, 141–8.

Ganley, J. M., Maji, A. K. and Huybrechts, S. (2000) Explaining spring-in in filament wound carbon fiber/epoxy composites, *Journal of Composite Materials*, **34**(14), 1216–39.

Garcia-Granada, A. A., Lacarac, V. D., Smith D. J. and Pavier, M. J. (2001) A new procedure based on Sachs' boring for measuring non-axisymmetric residual stresses: Experimental application, *International Journal of Mechanical Sciences*, **43**(12), 2753–68.

Gascoigne, H.E. (1994) Residual surface stresses in laminated cross-ply fiber-epoxy composite materials, *Experimental Mechanics*, **34**(1), 27–36.

George, D. and Smith, D. J. (2000) The application of the deep-hole technique for measuring residual stresses in autofrettaged tubes, *ASME PVP High Pressure Technology*, **406**, 25–31. Available at: *ohttp://members.asme.org/catalog/ItemView.cfm? ItemNumber ¼ H011744*

George, D. and Smith, D. J. (2005) Through thickness measurement of residual stresses in a stainless steel cylinder containing shallow and deep weld repairs, *International Journal of Pressure Vessels and Piping*, **82**(4), 279–87.

George, D., Bouchard, P. J. and Smith, D. J. (2000) Evaluation of through wall residual stresses in stainless steel weld repairs, *Materials Science Forum*, **347–9**, 646–51.

George, D., Kingston, E. and Smith, D. J. (2002) Measurement of through-thickness stresses using small holes, *Journal of Strain Analysis*, **37**, 125–39.

Gigliotti, M., Wisnom, M. R. and Potter, K. D. (2003) Development of curvature during the cure of AS4/8552 [0/90] unsymmetric composite plates, *Composites Science and Technology*, **63**(2), 187–97.

Grant, P. V., Lord, J. D. and Whitehead, P. S. (2002) The measurement of residual stresses by the incremental hole drilling technique, *NPL Good Practice Guide 53*, Materials Centre, UK, National Physical Laboratory (NPL).

Guemes, J. A. and Menéndez, J. M. (2002) Response of Bragg grating fiber-optic sensors when embedded in composite laminates, *Composites Science and Technology*, **62**(7–8), 959–66.

Güngör, S. (2002) Residual stress measurements in fiber reinforced titanium alloy composites, *Acta Materialia*, **50**(8), 2053–73.

Güngör, S. and Ruiz, C. (1996) Measurement of thermal residual stresses in continuous fibre composites, in: *Ceramic and Metal Matrix Composites*, San Sebastian, Spain. *Key Engineering Materials*, Switzerland, Trans Tech Publications, **127–31**, 851–60.

Hahn, H. T. (1976) Residual stresses in polymer matrix composite laminates, *Composite Materials*, **10**, 265–77.

Harper, B. D. and Weitsman, Y. (1985) On the effects of environmental conditioning on residual stresses in composite laminates, *International Journal of Solids and Structures*, **21**(8), 907–26.

Häusler, H., König, G. and Kockelmann, H. (1987) In: E. Macherauch and V. Hauk (eds), *Residual Stresses in Science and Technology*, DGM, Oberursel, **1**, 257.

Hermann, R. (1995) Crack growth and residual stress in Al-Li metal matrix composites under far-field cyclic compression, *Journal of Materials Science*, **30**(15), 3782–90.

Hill, M. R. and Nelson, D. V. (1995) Inherent strain method for residual stress determination and its application to a long welded joint, *Proceedings of the 1995 Joint ASME/JSME Pressure Vessels and Piping Conference*, Honolulu, 343–52.

Hill, M. R. and Nelson, D. V. (1996) Determining residual stress through the thickness of a welded plate, *Proceedings of the 1996 ASME Pressure Vessels and Piping Conference*, Montreal, Canada, 29–36.

Hill, M. R., and Lin, W. Y. (2002) Residual stress measurement in a ceramic- metallic graded material, *ASME Journal of Engineering Materials and Technology*, **124**(2), 185–91.

Hsueh, C. H. (1992) Interfacial debonding and fiber pull-out stresses of fiber-reinforced composites. Part VII: Improved analyses for bonded interfaces, *Materials Science and Engineering: A*, **154**(2), 125–32.

Hsueh, c. h. (1993) evaluation of interfacial properties of fiber-reinforced ceramic composites using a mechanical properties microprobe, *Journal of the American Ceramic Society*, **76**(12), 3041–50.

Huang, Chao M., Zhu, D., Xu, Y., Mackin, T. and Kriven, W. M. (1995) Interfacial properties of SiC monofilament reinforced β'-SiAlON composites, *Materials Science & Engineering A – Structural Materials: Properties, Microstructure and Processing*, **A201**(1–2), 159–68.

Hung, N. P. (1989) Use of an automatic data-acquisition system for the Sachs' residual stress measurement method, *Experimental Techniques*, **13**(4), 24–6.

Hung, Y. Y. (1999) Applications of digital shearography for testing of composite structures, *Composites: Part B*, **30**(7), 765–73.

Hyer, M. W. (1981) Calculation of room-temperature shapes of unsymmetrical laminates, *Journal Composite Materials*, **15**, 296–310.

Jain, L. K., and Mai, Y. W. (1995) On residual stress induced distortions during fabrication of composite shells, *Proceedings of the American Society for Composites – Tenth Technical Conference*, Santa Monica, CA, **18**–**20**, 261–70.

Jeronimidis, G. and Parkyn, A. T. (1988) Residual stresses in carbon fibre thermoplastic matrix laminates, *Journal of Composite Materials*, **22**(5), 401–15.

Jesensky, M. and Vargova, J. (1981) Calculation and measurement of stresses in thick-walled pressure vessels, *Svaracske Spravy*, **4**, 79–87.

Joh, D., Byun, K. Y. and Ha, J. (1993) Thermal residual stresses in thick graphite/epoxy composite laminates-uniaxial approach, *Experimental Mechanics*, **33**, 70–6.

Johnson, M. R., Robinson, R. R., Opinsky, A .J., Joerms, M. W. and Stone, D. H. (1985) *Calculation of Residual Stresses in Wheels from Saw Cut Displacement Data*, Technical Report 85-WA/RT-16.

Jones, B. K. and Martin J. W. (1977) Residual stress distribution in nitrided En41B steel as function of case depth, *Metals Technology*, **4**(11), 520–23.

Jones, R .L. and Chandler, H. D. (1985) Strength loss in E-glass fibres after exposure to hydrochloric, hydrobromic and hydriodic acids, *Journal of Materials Science*, **20**(9), 3320–4.

Jun, W. J. and Hong, C. S. (1990) Effect of residual shear strain on the cured shape of unsymmetric cross-ply thin laminates, *Composites Science and Technology*, **38**(1), 55–67.

Kaddour, A. S., Al-Hassani, S. T. S. and Hinton, M. J. (2003) Residual stress assessment in thin angle ply tubes, *Applied Composite Materials*, **10**(3), 169–88.

Kalton, A. F., Howard, S. J., Janczak-Rusch, J. and Clyne, T. W. (1998) Measurement of interfacial fracture energy by single fibre push-out testing and its application to the titanium-silicon carbide system, *Acta Materialia*, **46**(9), 3175–89.

Kam, T. Y. (1995) Nonlinear and first-ply failure analyses of laminated composite cross-ply plates, *Journal of Composite Materials*, **29**(4), 463–82.

Kang, K. J., Song, J. H. and Earmme, Y. Y. (1989) A method for the measurement of residual stresses using a fracture mechanics approach, *Journal of Strain Analysis*, **24**, 23–30.

Kang, K. J., Darzens, S. and Choi, G. S. (2004) Effect of geometry and materials on residual stress measurement in thin films by using the focused ion beam, *Journal of Engineering Materials and Technology, Transactions of the ASME*, **126**(4), 457–64.

Keil, S. (1992) Experimental determination of residual stresses with the ring-core method and an on-line measuring system, *Experimental Techniques*, **16**(5), 17–25.

Kendig, K .L., Soboyejo, W. O. and Miracle, D. B. (1995) Measurement of residual stresses in Ti-15-3 SCS-9 continuously reinforced composites using X-ray diffraction and a matrix etching technique, *Scripta Metallurgica et Materialia*, **32**(5), 669–74.

Kerans, R. J. and Parthasarathy, T. A. (1991) Theoretical analysis of the fiber pullout and pushout tests, *Journal of the American Ceramic Society*, **74**(7), 1585–96.

Kesler, O., Matejicek, J., Sampath, S., Suresh, S., Gnaeupel-Herold, T. *et al*. (1998) Measurement of residual stress in plasma-sprayed metallic, ceramic and composite coatings, *Materials Science and Engineering*, **A257**, 215–24.

Kim, B. S., Bernet, N., Sunderland, P. and Manson, J. A. E. (2002) Numerical analysis of the dimensional stability of thermoplastic composites using a thermoviscoelastic approach, *Journal of Composite Materials*, **36**(20), 2389–403.

Kim, J. W. and Lee, D. G. (2007) Measurement of residual stresses in thick composite cylinders by the radial-cut-cylinder-bending method, *Composite Structures*, **77**(4), 444–56.

Kim, J. W., Lee, J. H., Kim, H. G., Kim, H. S. and Lee, D. G. (2006) Reduction of residual stresses in thick-walled composite cylinders by smart cure cycle with cooling and reheating, *Composite Structures*, **75**(1–4), 261–6.

Kim, K. S. and Hahn, H. T. (1989) Residual stress development during processing of graphite/ epoxy composite, *Composite Science and Technology*, **36**, 121–32.

Kim, R. Y. and Hahn, H. T. (1979) Effect of curing stresses on the first ply-failure in composite laminates, *Journal Composite Materials*, **13**, 2–16.

Kingston, E. and Smith, D. J. (2005) Residual stress measurements in rolling mill rolls using deep hole drilling technique, *Ironmaking and Steelmaking*, **32**(5), 379–80.

Kovač, M. (1995) Method for residual stress measurement in welded seams, *Journal of Materials Processing Technology*, **52**(2–4), 503–14.

Kovač, M., Miyano, Y. and Woo, T. C. (1989) Residual-stress measurement in SS304 seamless tube, *Experimental Mechanics*, **29**(2), 209–13.

Kuboki, T., Akiyama, M., Neishi, Y. and Kuroda K. (2000) Effect of final drawing with light reduction on the levelling of residual stress distribution in cold bar drawing, *Proceedings of the Institution of Mechanical Engineers, Part C: Journal of Mechanical Engineering Science*, **214**(11), 1389–400.

Lacarac, V., Smith, D .J. and Pavier, M .J. (2004) Residual stress creep relaxation around cold expanded holes in an aluminium alloy, *AIAA Journal*, **42**(7), 1444–9.

Lake, B. R., Appl, F. J. and Bert, C. W. (1970) An investigation of the hole-drilling technique for measuring planar residual stress in rectangularly orthotropic materials, *Experimental Mechanics*, **10**, 233–9.

Lange, J., Toll, S., Manson, J. A. E. and Hult, A. (1995) Residual-stress build-up in thermoset films cured above their ultimate glass-transition temperature, *Polym*er, **36**(16), 3135–41.

Lara-Curzio, E. and Ferber, M. K. (1994) Methodology for the determination of the interfacial properties of brittle matrix composites, *Journal of Materials Science*, **29**(23), 6152–8.

Lee, D. G. (2004) *Evaluation Method of Residual Stresses on Heat-Resisting Composite Axi-Symmetric Structures*, Agency for Defense Development in Korea, Technical Report.

Lee, J., Czarnek, R. and Guo, Y. (1989) Interferometric study of residual strains in thick composites, *Proceedings of the 1989 SEM Conference on Experimental Mechanics*, Cambridge, MA, 356–64.

Lee, S. M. and Schile, R. D. (1982) Investigation of material variables of epoxy resins controlling transverse cracking in composites, *Journal of Materials Science*, **17**(7), 2095–106.

Leggatt, R. H., Smith, D .J., Smith, S. D. and Faure, F. (1996) Development and experimental validation of the deep-hole method for residual stress measurements, *Journal of Strain Analysis*, **31**, 177–86.

Letner, H. R. (1953) Application of optical interference to the study of residual surface stresses, *Proc. Soc. Exp. Stress Analysis*, **10**(2), 23–36.

Li, K., Xiao, B. and Feng, Z. (2007) Interferometric strain rosette and incremental ring-core cutting applied to residual stress measurement on a spot weld, in: *Proceedings of the SEM Annual Conference and Exposition on Experimental and Applied Mechanics*, Springfield, MA **3**, 2021–31.

Lim, W. K., Song, J. H. and Sankar, B. V. (2003) Effect of ring indentation on fatigue crack growth in an aluminum plate, *International Journal of Fatigue*, **25**(9–11), 1271–7.

Liu, H. Y., Zhang, X., Mai, Y. W. and Diao, X. X. (1999) On steady-state fibre pull-out. Part II: Computer simulation, *Composite Science and Technology*, **59**(15), 2191–9.

Lu, D. J. (1996) *Handbook of Measurement of Residual Stresses*, Lilburn, GA, The Fairmont Press, Inc.

Manson, J. A. E. and Seferis, J. C. (1992) Process Simulated Laminate (PSL), a methodology to internal stress characterization in advanced composite materials, *Journal Composite Materials*, **26**(3), 405–31.

Margelis, G., Stamatopoulos, K. and Tsouvalis, N. (2010) *Measurement of Residual Stresses in Typical Marine Composite Materials using the Incremental Hole Drilling Method*, NTUA Report No MAR-R4-3-NTUA-28(1) for MARSTRUCT.

Marshall, D. B. and Lawn, B. R. (1977) An indentation method for measuring residual stresses in tempered glass surfaces, *Journal of the American Ceramic Society*, **60**(1–2), 86–7.

Marshall, D. B. and Oliver, W. C. (1990) An indentation method for measuring residual stresses in fiber-reinforced ceramics, *Materials Science and Engineering*, **A126**, 95–103.

Martineau, R .L., Prime, M .B. and Duffey, T. (2004) Penetration of HSLA-100 steel with tungsten carbide spheres at striking velocities between 0.8 and 2.5 km/s, *International Journal of Impact Engineering*, **30**(5), 505–20.

Mathar, J. (1934) Determination of initial stress by measuring the deformations around drilled holes, *Transactions of ASME*, **56**, 249.

Mirzaee-Sisan, A., Fookes, A. J., Truman, C. E., Smith, D .J., Brown, T. B. and Dauda, T. A. (2007) Residual stress measurement in a repair welded header in the as-welded condition and after advanced post-weld treatment, *International Journal of Pressure Vessels and Piping*, **84**(5), 265–73.

Myers II, D. G. (2004) *Method for Measurement of Residual Stress and Coefficient of Thermal Expansion of Laminated Composites*, MSc Thesis, University of Florida.

Nairn, J. A. (1985) Thermoelastic analysis of residual stresses in uni-directional, high performance composites, *Polymer Composites*, **6**(2), 123–30.

Nairn, J. A. (1997) On the use of shear-lag methods for analysis of stress transfer in unidirectional composites, *Mechanics of Materials*, **26**(2), 63–80.

Nairn, J. A. and Zoller, P. (1985) Matrix solidification and the resulting residual thermal stresses in composites, *Journal of Materials Science*, **20**(1), 355–67.

Neubrand, A., Chung, T. J., Rodel, J., Steffler, E. D. and Fett, T. (2002) Residual stresses in functionally graded plates, *Journal of Materials Research*, **17**(11), 2912–20.

Nicoletto, G. (1991) Moiré interferometry determination of residual stresses in the presence of gradients, *Experimental Mechanics*, **31**(3), 252–6.

Niu, X. (1999) *Process Induced Residual Stresses and Dimensional Distortions in Advanced Laminated Composites*, PhD Thesis, University of Florida.

Oettel, R. (2000) The determination of uncertainties in residual stress measurement (using the hole drilling technique). Part I: *Manual of Codes of Practice for the Determination of Uncertainties in Mechanical Tests on Metallic Materials*, Code of Practice No. 15, Standards Measurement & Testing Project No. SMT4-CT97-2165.

Olivas, E. R., Swadener, J. G. and Shen, Y. L. (2006) Nanoindentation measurement of surface residual stresses in particle-reinforced metal matrix composites, *Scripta Materialia*, **54**, 263–8.

Olson, W. A. and Bert, C. W. (1966) Analysis of residual stresses in bars and tubes of cylindrically orthotropic materials, *Experimental Mechanics*, **6**(9), 451–7.

Özdemir, A. T. and Edwards, L. (1996) Measurement of the three-dimensional residual stress distribution around split-sleeve cold-expanded holes, *Journal of Strain Analysis for Engineering Design*, **31**(6), 413–21.

Pagliaro, P. and Zuccarello, B. (2007) Residual stress analysis of orthotropic materials by the through-hole drilling method, *Experimental Mecha*nics, **47**(2), 217–36.

Palerosi, A. C. and Muller de Almeida, S. F. (2007) Thermoelastic evaluation of composite laminates using digital imaging processing, *Composites: Part A*, **38**, 2283–93.

Parlevliet, P. P., Bersee, E. N. and Beukers, A. (2007) Residual stresses in thermoplastic composites – A study of the literature. Part II: Experimental techniques, *Composites: Part A*, **38**, 651–65.

Parthasarathy, T .A., Jero, P. D. and Kerans, R. J. (1991) Extraction of interface properties from a fiber push-out test, *Scripta Metallurgica et Materialia*, **25**(11), 2457–62.

Paterson, M. W. and White, J. R. (1989) Layer removal analysis of residual stress, Part II: A new procedure for polymers moldings with depth varying Young's modulus, *Journal of Materials Science*, **24**(10), 3521–8.

Pechersky, M. J. (2002) Determination of residual stresses by thermal relaxation and speckle correlation interferometry, *Strain*, **38**(4), 141–9.

Pechersky, M. J., Estochen, E. G. and Vikram C. S. (2000) Improved measurement of low residual stresses by speckle correlation interferometry and local heat treating. In: *SEM IX International Congress on Experimental Mechanics*, Orlando, FL.

Peeters, L .J. B., Powell, P .C. and Warnet, L. (1996) Thermally-induced shapes of unsymmetric laminates, *Journal of Composite Materials*, **30**, 603–26.

Pickard, S. M., Miracle, D. B., Majumdar, B. S., Kendig, K. L., Rothenflue, L. and Coker, D. (1995) Experimental study of residual fiber strains in Ti-15-3 continuous fiber composites, *Acta Metallurgica et Materialia*, **43**(8), 3105–12.

Prasad, C. B., Prabhakaran, R. and Tompkins, S. (1987) Determination of calibration constants for the hole-drilling residual stress measurement technique applied to orthotropic composites. Part H: Experimental evaluations, *Composite Structures*, **8**, 165–72.

Prime, M. B. (1999a) Measuring residual stress and the resulting stress intensity factor in compact tension specimens, *Fatigue and Fracture of Engineering Materials and Structures*, **22**(3), 195–204.

Prime, M. B. (1999b) Residual stress measurement by successive extension of a slot: the crack compliance method, *Applied Mechanics Reviews*, **52**(2), 75–96.

Prime, M. B. (2001) Cross-sectional mapping of residual stresses by measuring the surface contour after a cut, *Journal of Engineering Materials and Technology, Transactions of the ASME*, **123**(2), 162–8.

Prime, M. B. and Hill, M. R. (2002) Residual stress, stress relief, and inhomogeneity in aluminum plate, *Scripta Materialia*, **46**(1), 77–82.

Prime, M. B. and Hill, M. R. (2004) Measurement of fiber-scale residual stress variation in a metal-matrix composite, *Journal of Composite Materials*, **38**(23), 2079–95.

Prime, M. B., Rangaswamy, P. and Bourke, M. A. M. (2000) Measuring spatial variation of residual stresses in a MMC using crack compliance. In: D. Hui (ed.), *Proceedings of the Seventh International Conference on Composites Engineering*, Denver, CO, 711–12.

Prime, M. B., Sebring, R. J., Edwards, J. M., Hughes, D. J., and Webster, P. J. (2004) Laser

surface-contouring and spline data-smoothing for residual stress measurement, *Experimental Mechanics*, **44**(2), 176–84.

Prime, M. B., Gnäupel-Herold, T., Baumann, J. A., Lederich, R. J., Bowden, D. M., and Sebring, R. J. (2006) Residual stress measurements in a thick, dissimilar aluminum alloy friction stir weld, *Acta Materialia*, **54**(15), 4013–21.

Procter, E. and Beaney, E. M. (1978) Trepan or ring-core method, centre-hole method, Sach's method, blind hole methods, deep hole technique. In: *Advances in Surface Treatment: Technology – Application and Effects*, New York, Pergamon Press, *Residual Stresses*, **4**, 165–98.

Ramamurty, U., Dary, F. C. and Zok, F. W. (1996) Method for measuring residual strains in fiber-reinforced titanium matrix composites, *Acta Materialia*, **44**(8), 3397–406.

Ramanathan, T., Bismarck, A., Schulz, E. and Subramanian, K. (2001) Investigation of the influence of surface-activated carbon fibres on debonding energy and frictional stress in polymer-matrix composites by the micro-indentation technique, *Composites Science and Technology*, **61**(16), 2511–18.

Rasty, J., Le, X., Baydogan, M. and Càrdenas-Garcìa, J. F. (2007) Measurement of residual stresses in nuclear-grade Zircaloy-4(R) tubes. Effect of heat treatment, *Experimental Mechanics*, **47**(2), 185–99.

Reid, R. G. (2009) *The Measurement of Longitudinal Residual Stresses in Unidirectional Glass Fibre Reinforced Plastic*, PhD Thesis, University of the Witwatersrand, Johannesburg.

Reid, R. G. and Paskaramoorthy, R. (2009) A novel method to measure residual stresses in unidirectional GFRP, *Composite Structures*, **88**, 388–93.

Ren, W. and Li, K. (2007) Application of miniature ring-core and interferometric strain/slope rosette to determine residual stress distribution with depth. Part II: Experiments, *Journal of Applied Mechanics, Transactions ASME*, **74**(2), 307–14.

Rendler, N. J., and Vigness, I. (1966) Hole-drilling strain-gage method of measuring residual stresses, *Experimental Mechanics*, **6**(12), 577–86.

Richards, D. G. (1945) A study of certain mechanically-induced residual stresses, *Proc. Soc. Exp. Stress Analysis*, **3**(1), 40–61.

Rossington, C., Evans, A. G., Marshall, D. B. and Khuri-Yakub, B. T. (1984) Measurements of residually stressed thin films by indentation. Part II: Experiments with ZnO/Si, *Journal of Applied Physics*, **56**(10), 2639–44.

Roy, A. K. (1991) Response of thick laminated composite rings to thermal stresses, *Composite Structures*, **18**(2), 125–38.

Roy, A. K., Venkatesh, A., Dronavalli, S., Marthandam, V., Wells, D. *et al*. (2005) Residual stress measurements in welded and plastically deformed target structural materials, *Journal of ASTM International*, **2**(6), 67–79.

Sabaté, N., Vogel, D., Gollhardt, A., Keller, J., Cané, C. *et al*. (2006a) Measurement of residual stress by slot milling with focused ion-beam equipment, *Journal of Micromechanics and Microengineering*, **16**(2), 254–9.

Sabaté, N., Vogel, D., Gollhardt, A., Keller, J., Michel, B, *et al*. (2006b) Measurement of residual stresses in micromachined structures in a microregion, *Applied Physics Letters*, **88**(7), 071910.

Sachs, G. (1927) Der nachweiss innerer spannungen in stangen und rohren, *Zeitschrift für Metallkunde*, **19**, 352–7.

Schajer, G. S. (1988) Measurement of non-uniform residual-stresses using the hole drilling method. Part I: Stress calculation procedures, *Journal of Engineering Materials and Technology, Trans ASME*, **110**(4), 338–43.

Schajer, G. S. (2007) Hole-drilling residual stress profiling with automated smoothing, *Journal of Engineering Materials and Technology*, **129**(3), 440–5.

Schajer, G. S., and Yang, L. (1994) Residual-stress measurement in orthotropic materials using the hole-drilling method, *Experimental Mechanics*, **34**(4), 324–33.

Schajer, G. S. and Prime, M. B. (2007) Residual stress solution extrapolation for the slitting method using equilibrium constraints, *Journal of Engineering Materials and Technology*, **129**(2), 227–32.

Schröder, J., Keuter, J. M., and Priesmeyer, H. G. (1995) Residual stress investigations on a hot-rolled plane sandwich-type composite X5 Cr Ni 18 9-C45-X5 Cr Ni 18 9 by means of neutron diffraction, *Journal of Strain Analysis for Engineering Design*, **30**(1), 15–20.

Seif, M. A. and Short, S. R. (2002) Determination of residual stresses in thin-walled composite cylinders, *Experimental Techniques*, **26**(2), 43–6.

Seif, M. A., Khashaba, U. A. and Rojas-oviedo, R. (2006) Residual stress measurements in CFRE and GFRE composite missile shells, *Composite Structures*, **79**(2), 261–9.

Sharman, D. J., Stark, H. L. and Kelly, D. W. (1997) Benchmarking of a destructive technique to determine residual stresses in thick-walled axisymmetric components, *Journal of Strain Analysis*, **32**, 87–96.

Shokrieh, M. M. and Akbari, R. S. (2012) Effect of residual shear stresses on released strains in isotopic and orthotropic materials measured by the slitting method, *Journal of Engineering Materials and Technology*, 134/011006-1.

Shokrieh, M. M. and Kamali, S. M. (2005) Theoretical and experimental studies on residual stresses in laminated polymer composites, *Journal of Composite Materials*, **39**(24), 2213–25.

Shokrieh, M. M. and Ghasemi, A. R. (2007a) Determination of calibration factors of the hole drilling method for orthotropic composites using an exact solution, *Journal of Composite Materials*, **41**(19), 2293–311.

Shokrieh, M. M. and Ghasemi, A. R. (2007b) Simulation of central hole drilling process for measurement of residual stresses in isotropic, orthotropic and laminated composites plates, *Journal of Composite Materials*, **41**(4), 435–52.

Sicot, O., Gong, X .L., Cherouat, A. and Lu, J. (2003) Determination of residual stress in composite laminates using the incremental hole-drilling method, *Journal of Composite Materials*, **37**(9), 831–44.

Sicot, O., Gong, X. L., Cherouat, A. and Lu, J. (2004) Influence of experimental parameters on determination of residual stress using the incremental hole-drilling method, *Composites Science and Technology*, **64**(2), 171–80.

Smith, D. J., Poussard, C. G. C. and Pavier, M. J. (1998) Assessment of the Sachs' method for measuring residual stresses in cold worked fastener holes, *Journal of Strain Analysis for Engineering Design*, **33**(4), 263–74.

Stacey, A. and Webster, G. A. (1988) Determination of residual stress distributions in autofrettaged tubing, *International Journal of Pressure Vessels and Piping*, **31**(3), 205–20.

Stamatopoulos, K. (2011) *Measurement of Residual Stresses in Composite Materials with the Incremental Hole Drilling Method*, Diploma Thesis, National Technical University of Athens, School of Naval Architecture and Marine Engineering.

Stefanescu, D., Browne, P., Truman, C. E. and Smith D. J. (2003) Residual stress measurement within a European UIC60 rail using integrated drilling techniques, *Materials Science Forum*, **440–1**, 85–92.

Stefanescu, D., Truman, C. E. and Smith, D .J. (2006) Improvements in residual stress measurement by the incremental centre hole drilling technique, *Experimental Mechanics*, **46**, 417–27.

Sunderland, P., Yu, W. J., and Manson, J. E. (1995) A technique for the measurement of process-induced internal stresses in polymers and polymer composites, *Proceedings of ICCM-10*, Whistler, BC, Canada, **3**, 125–32.

Suresh, S. and Giannalopoulos A. E. (1999) Determination of elastoplastic properties by instrumented sharp indentation, *Scripta Materialia*, **409**(10), 1191–8.

Swadener, J. G., Taljat, B. and Pharr, G. M. (2001) Measurement of residual stress by load and depth sensing indentation with spherical indenters, *Journal of Materials Research*, **16**(7), 2091–102.

Tarsha-Kurdi, K. E. and Olivier, P. (2002) Thermoviscoelastic analysis of residual curing stresses and the influence of autoclave pressure on these stresses in the carbon/epoxy laminates, *Composites Science and Technology*, **62**, 559–65.

Tebedge, N., Alpsten, G. and Tall, L. (1973) Residual-stress measurement by the sectioning method, *Experimental Mechanics*, **13**(2), 88–96.

Timmerman, J. F., Hayes, B. S. and Seferis, J. C. (2003) Cure temperature effects on cryogenic microcracking of polymeric composite materials, *Polymer Composites*, **24**(1), 132–9.

Timoshenko, S. (1941) *Strength of Materials*, Part II, London, MacMillan.

Treuting, R. G. and Read, Jr. W. T. (1951) A mechanical determination of biaxial residual stress in sheet materials, *Journal of Applied Physics*, **22**(2), 130–4.

Tsouvalis, N., Margelis, G. and Dellis, D. (2009) Residual stresses in composite materials, a review. Part I: Experimental investigation and analytical model, *Composites: Part A*, **35**, 121–33.

Unger, W. J. and Hansen, J. S. (1993) Effect of cooling rate and annealing on residual stress development in graphite fibre reinforced PEEK laminates, *Journal of Composite Materials*, **27**(2), 108–37.

Vaidyanathan, S. and Finnie, I. (1971) determination of residual stresses from stress intensity factor measurements, *Journal of Basic Engineering*, **93**, 242–6.

Vikram, C. S., Pechersky, M. J., Feng, C. and Engelhaupt, D. (1996) Residual-stress analysis by local laser heating and speckle-correlation interferometry, *Experimental Techniques*, **20**(6), 27–30.

Voyiadjis, G. Z. and Hartley, C. S. (1987) Residual stress determination of concentric layers of cylindrically orthotropic materials, *Experimental Mechanics*, **27**(3), 290–7.

Voyiadjis, G. Z., Kiousis, P. D. and Hartley, C. S. (1985) Analysis of residual stresses in cylindrically anisotropic materials, *Experimental Mechanics*, **25**(2), 145–7.

Waki, H., Ogura, K., Nishikawa, I. and Kashihara, Y. (2003) Residual stress measurement of plasma-sprayed coatings, *JSME International Journal, Series A: Solid Mechanics and Material Engineering*, **46**(4), 590–7.

Wang, T. M., Daniel, I. M., and Gotro, J. T. (1992) Thermoviscoelastic analysis of residual stresses and warpage in composite laminates, *Journal of Composite Materials*, **26**(6), 883–99.

Weng, C. C. and White, R. N. (1990) Residual stresses in cold-bent thick steel plates, *Journal of Structural Engineering*, **116**(1), 24–39.

Wenzelburger, M., López, D. and Gadow, R. (2006) Methods and application of residual stress analysis on thermally sprayed coatings and layer composites, *Surface and Coatings Technology*, **201**, 1995–2001.

Wern, H. (1997) New approach to triaxial residual stress evaluation by the hole drilling method, *Strain*, **33**(4), 121–5.

Wern, H., Cavelius, R. and Schlaefer, D. (1997) New method to determine triaxial

nonuniform residual stresses from measurements using the hole drilling method, *Strain*, **33**(2), 39–45.

White, S. R. and Hahn, H. T. (1990) Mechanical property and residual stress development during cure of a graphite/BMI composite, *Polymer Engineering and Science*, **30**(22), 1465–73.

Wisnom, M. R., Gigliotti, M., Ersoy, N., Campbell, M. and Potter, K. D. (2006) Mechanisms generating residual stresses and distortion during manufacture of polymer-matrix composite structures, *Composites Part A: Applied Science and Manufacturing*, **37**(4), 522–9.

Witt, F., Lee, F. and Rider, W. (1983) Comparison of residual-stress measurements using blind-hole, abrasive-jet and trepan-ring methods, *Experimental Techniques*, **7**(2), 41–4.

Yamada, T., Yokoi, K. and Kohno, A. (1990) Effect of residual stress on the strength of alumina-steel joint with Al-Si interlayer, *Journal of Materials Scie*nce, **25**(4), 2188–92.

Youssef, Y. and Denault, J. (1998) Thermoformed glass fiber reinforced polypropylene: Microstructure, mechanical properties and residual stresses, *Polymer Composites*, **19**(3), 301–9.

Yu, Y., Ashcroft, I. A. and Swallowe, G. (2006) An experimental investigation of residual stresses in an epoxy–steel laminate, *International Journal of Adhesion and Adhesives*, **26**, 511–19.

Zewi, I. G., Daniel, I. M. and Gotro, J. T. (1987) Residual stresses and warpage in woven-glass/epoxy laminates, *Experimental Mechanics*, **27**(1), 44–50.

Zhandanov, I. M. and Gonchar, A. K. (1978) Determining the residual welding stresses at depth in metals, *Automatic Welding*, **31**, 22–4.

Zhang, Y., Ganguly, S., Stelmukh, V., Fitzpatrick, M. E. and Edwards, L. (2003) Validation of the contour method of residual stress measurement in a MIG 2024 weld by neutron and synchrotron X-ray diffraction, *The Journal of Neutron Research*, **11**(5), 181–5.

Zhou, X. F., Wagner, H. D. and Nutt, S. R. (2001) Interfacial properties of polymer composites measured by push-out and fragmentation tests, *Composites – Part A: Applied Science and Manufacturing,* **32**(11), 1543–51.

Zong, G. and Marcus, H. L. (1991) A microbuckling method for determination of the residual stress in metal matrix composites, *Scripta Metallurgica et Materialia*, **25**(2), 277–82.

3

Non-destructive testing (NDT) techniques in the measurement of residual stresses in composite materials: an overview

M. M. SHOKRIEH and A. R. GHANEI MOHAMMADI,
Iran University of Science and Technology, Iran

DOI: 10.1533/9780857098597.1.58

Abstract: Non-destructive testing (NDT) includes a wide group of techniques utilized in science and industry to evaluate the properties of a material (such as residual stresses) without causing any major damage. Since NDT does not cause any permanent changes in the material being inspected, it is a valuable technique that can save both money and time in evaluation and research. This is why non-destructive tests are often preferred to destructive ones. This chapter discusses the main methods that fall into the category of non-destructive methods of residual stress measurement. Also, for each method, the notable contributions are discussed in detail.

Key words: composite materials, residual stress, measurement, experimental technique, non-destructive testing (NDT) techniques.

3.1 Introduction

This chapter looks at a range of non-destructive techniques used to measure residual stresses in composite materials. Techniques discussed include the following:

- the X-ray diffraction method;
- the neutron diffraction method;
- the Raman spectroscopy method;
- the photoelasticity method;
- other optical methods;
- the acoustic wave method;
- methods based on interferometry;
- the cure referencing method;
- measurement methods using sensors;
- the electrical resistance method.

3.2 The X-ray diffraction method

X-ray diffraction is a method that can be used with materials having a crystalline structure (Lu and Retraint, 1998). Residual stresses in crystalline materials can be

measured to a maximum depth of about 0.05 mm. Layer removal such as etching is required for deeper measurements, making this method a form of destructive testing (Prime, 1999a,b). According to Parlevliet *et al.* (2006), X-ray diffraction can measure through the thickness of a specimen with metallic inclusions to a depth of 0.3 to 0.5 mm. Soft X-rays are most commonly used, although X-rays from synchrotron sources have greater penetration (Fiori, 2004). However, soft X-rays have a small penetration depth and only permit measurement of strains to a depth of about 50 μm (Rangaswamy, 1999).

X-ray diffraction measures strains in the crystal lattice of polycrystalline materials by examining variations in the inter-planar spacing. In addition to the requirement for sampled material to be macroscopically isotropic and homogeneous (Lu and Retraint, 1998), it must also be crystalline. The method can be directly applied to metal matrix composites. Micro-scale residual stresses in silicon-carbide reinforced titanium alloys have been analysed (Cox *et al.*, 1990; Kendig *et al.*, 1995; Rangaswamy *et al.*, 1999).

X-ray diffraction has also been used for fiber reinforced polymer composites (Albertini *et al.*, 1999; Hauk and Macherauch, 1984; Tsouvalis *et al.*, 2009). However, because the polymer matrix is non-crystalline, small metallic particles of almost the same size as the fiber diameter must be incorporated into the matrix (Bateman, 2005). The stress in these particles is then measured by applying X-ray diffraction. However, it is essential to relate the measured stress in the particles to the residual stress in the surrounding matrix. Consequently, additional experiments are required to develop a 'stress transmission tensor'. All the components of the stress field can then be determined (Meske and Schnack, 2001).

Bacon *et al.* (2011) used high-energy synchrotron X-ray diffraction to measure the internal strain evolution in the matrix and of steel-based metal matrix composites reinforced with particulate titanium diboride (TiB_2). The results were in agreement with those from Eshelby modeling for the elastic loading of the material. The elastic internal strain response of the 316-based material was not affected by heat treatment. Rotundo and Korsunsky (2009) measured residual strain profiles in shot peened specimens of 2124-T4 aluminum alloy matrix composite reinforced with particulate silicon carbide (SiCp). In order to evaluate the effect of nano-sized dispersoid on the microscopic stress distribution of multilayered composite, Adachi *et al.* (2003) studied two kinds of multi-layered composites, Al_2O_3/3 mol% Y_2O_3-stabilized ZrO_2 (3Y-TZP) and Al_2O_3/3Y-TZP (SiC). Rangaswamy *et al.* (1999) studied continuous fiber reinforced SiC/Ti–6Al–4V titanium matrix composites (TMC) by applying X-ray and neutron diffraction with finite element predictions.

Abuhasan *et al.* (1990) have determined residual strains and stresses in hot-pressed α-Al_2O_3 composites. Chevalier *et al.* (2005) studied the residual internal thermal stress in an Al_2O_3–ZrO_2 nanocomposite. X-ray and neutron diffraction measured values for the residual stress parallel to the fibers in the matrix of SiC-Ti

alloy matrix composites have been reported by James *et al.* (1993a,b). Ghonem *et al.* (1994) have assessed the axial thermal residual stress in the matrix of the continuously reinforced metal matrix composite. They concluded that the development of the thermal residual stress depends upon cooling rate, while the relaxation of this stress depends on the magnitude of the visco-plastic strain generated in the matrix material.

Barrett and Predecki (1976, 1980) and Predecki and Barrett (1979) first applied the method to polymeric and other materials. Fenn *et al.* (1993) extended their work to measure residual stresses using metal particles as part of the matrix material. Larsson and Odén (2004) used X-ray diffraction to assess functionally graded WC-Co composites. Benedikt *et al.* (2002) studied residual stresses in uni-directional and fabric graphite/PMR-15 composite specimens. Benedikt *et al.* (2004a,b) investigated uni-directional and woven graphite fiber (T650-35)/polyimide (PMR-15) composites with embedded aluminum inclusions to determine residual strains and stresses as a function of ageing. Their work showed that ageing conditions noticeably affected residual strains and stresses. Meske and Schnack (2003) used X-ray diffraction to investigate inter-laminar stresses in fiber reinforced composites. Widjaja (2001) measured residual strains in the matrix of laminated SiC fiber-reinforced barium magnesium aluminosilicate (BMAS) glass-ceramic matrix composites using X-ray diffraction. He attributed the increase in the compressive residual stress in the matrix to the effectiveness of high-temperature creep conditioning. Benedikt *et al.* (2005) have studied residual thermal stresses in high temperature graphite/polyimide composites subjected to external loads and ageing. Benedikt *et al.* (2006) have also monitored average residual stresses in aged high temperature uni-directional and woven graphite fiber/PMR-15 composites. Fenn *et al.* (1993) measured tri-axial residual strains in a thermosetting resin used in high performance fiber composite materials.

Balasingh and Singh (2000) reviewed the various factors leading to the formation of residual stresses and described the X-ray diffraction technique for the measurement of residual stresses. They emphasized the recent developments permitting the estimation of:

- tri-axial stresses;
- stresses in the various phases of a multiphase material, such as ceramic composites; and
- the stresses in composites containing non-crystalline or poorly crystalline materials, such as BE polymer matrix composites.

Willemse *et al.* (2000) reported residual stress measurements for a continuous SiC fiber-Ti 1100 matrix composite. Watts *et al.* (2011) employed X-ray diffraction to measure the stresses arising in the ZrB_2 matrix and SiC dispersed particulate phase in ZrB_2–30 vol% SiC composites produced by hot pressing. Delfosse *et al.* (1997) determined compressive residual stresses using X-ray

diffraction in the WC phase of bi-layer and tri-layer samples of Cu-Ni, CrNi-ZrO_2 and WC-Co composites. Meske and Schnack (2001) measured strain fields in silver inclusions embedded in the polymer matrix of a graphite/epoxy composite.

3.3 The neutron diffraction method

Neutron diffraction is a crystallographic method mainly used to study the atomic and/or magnetic structure of a material. The method is an elastic scattering in which the neutrons exiting the experiment have approximately the same energy as the incident neutrons. This technique is comparable to X-ray diffraction, although it provides complementary information because of the different type of radiation (Stamatopoulos, 2011). In this technique, a sample is positioned in a beam of thermal or cold neutrons and the intensity pattern around the sample provides information about the structure of the material. One practical application of elastic neutron scattering/diffraction is the accurate measurement of the lattice constant of metals and other crystalline materials. Together with an accurately aligned micro-positioner, a map of the lattice remaining constant through the material can be derived. This can be easily converted to the stress field experienced by the material (Tsouvalis *et al.*, 2009).

Neutron radiation provides far greater penetration than X-rays (Albertini *et al.*, 1999). Consequently, the neutron diffraction technique can measure residual stresses to depths of about 50 mm in engineering materials. The technique is limited in resolution and not capable of measuring residual stress variations over distances smaller than around 1 mm (Prime, 1999a,b).

Although the method has been used to measure residual stresses in silicon-carbide reinforced titanium alloys (Rangaswamy *et al.*, 1999), no direct way of utilizing it for measuring the residual stresses in glass fibre-reinforced plastic (GFRP) is available. This is because neither the fiber nor the matrix of the material are crystalline and the neutron diffraction method can only measure residual stresses in crystalline materials (Prime, 1999). The measurement of the residual stresses may be made possible by incorporating small metallic particles into a GFRP laminate.

According to Hauk and Macherauch (1984), X-rays applied for stress determination usually penetrate a few tens of micrometres into the material, while neutron radiation can penerate several tens of millimetres into most relevant materials. Neutron diffraction is an effective, non-destructive technique for measuring strain in polycrystalline materials, including metal matrix composites, because thermal neutrons penetrate deeply (3–4 cm) into most engineering materials and permit bulk average measurements (Allen *et al.*, 1985; Bourke *et al.*, 1992; Kupperman *et al.*, 1992; Stacey *et al.*, 1985).

3.4 The Raman spectroscopy method

Another experimental method for the determination of residual strains is Micro-Raman Spectroscopy (MRS), which is based on an intrinsic material property and is another method for measuring the residual thermal stresses in Raman active materials. Raman spectroscopy uses scattered light (usually visible wavelength laser light) to probe the vibrational energy levels of chemical bonds (Skoog *et al.*, 1998). It is based on the stress (strain) sensitivity of most Raman vibrational modes in crystalline phases. The difference in energy between the incident photon and the Raman scattered photon equals the energy of vibration of the scattering molecule. A Raman spectrum is produced by plotting the scattered light intensity against the energy difference (Fig. 3.1).

The method is applicable for determining strain in carbon fibers embedded in a translucent polymer matrix. When strain is applied, some peaks in the Raman spectrum of the fiber will change. For instance, the Raman peaks of the fiber in an unloaded polyetheretherketone (PEEK) prepreg will shift to higher peak positions. This represents a compressive fiber strain due to the thermal residual strains imposed by the surrounding matrix. The shift of the 2660 cm^{-1} peak with compressive strain (−0.65% vs 0%) is illustrated in Fig. 3.1. Initially, a calibration

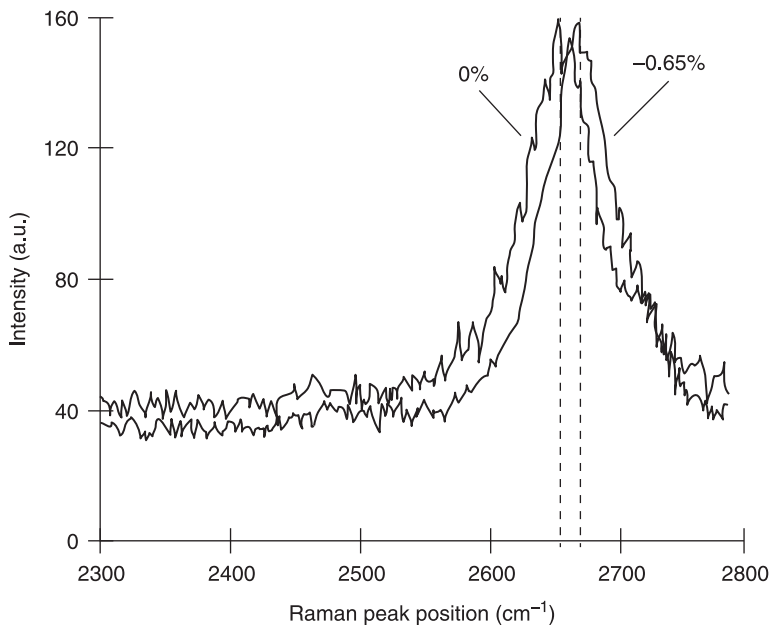

3.1 Raman spectrum which presents the shift of the 2660 cm^{-1} peak for AS4 carbon fibers embedded in PEEK matrix (Nielsen and Pyrz, 1988).

curve should be established on single fibers in air to relate the change in the Raman peak position to the magnitude of the fiber thermal residual strain inside the composite. This method can be used in uni-directional composite prepreg layers (PEEK) with fiber volume fractions of 60% or higher, or in composites with more uni-directional plies. Some amorphous fibers, such as glass, have a very weak Raman response and therefore cannot be used as strain sensors. In such cases, a small amount of aramid fibers can be embedded in glass fiber reinforced composites, as these have strong Raman responses.

The Raman spectroscopy method is also applicable for the determination of inter-ply stresses in cross-ply laminates (macro-mechanical stresses). The residual strains can be measured in small steps down to 1 to 2 $\mu\varepsilon$ with the MRS method. No analytical models are needed to predict the macroscopic residual stresses. However, the contribution of the matrix to the Raman peaks should be taken into account, to avoid over-estimation of the residual stresses (Parlevliet *et al.*, 2006; Tsouvalis *et al.*, 2009).

Stress-induced frequency change has been extensively used to investigate the deformation micromechanics of aramid, carbon and ceramic fiber-reinforced composites in polymer matrices (Bannister *et al.*, 1995; Goutianos *et al.*, 2002; Thomsen and Pyrz, 1999; Yallee and Young, 1998). These studies apply a technique known as MRS, in which an area substantially smaller than the fiber diameter is illuminated. By moving the illuminated area along the length of the fiber, the stress change along the fiber length can be determined. This technique has also been directly applied to measure the residual stresses in ceramic fibers (Yang and Young, 1994).

However, MRS is not ideal for measuring residual stresses in GFRP. Intensity peaks in Raman spectra are well defined for crystalline materials, although they are broadly spread for amorphous solids (Ward *et al.*, 2004), and as glass is amorphous, it has no well-defined Raman spectra (Young *et al.*, 2001). The band shifts of amorphous materials are also very small (Nielsen and Pyrz, 2002), thus preventing accurate measurement of the frequency shift. Only one study involving the measurement of stress in glass fiber is presented in the literature (Young *et al.*, 2001). In some studies, the fibers were coated with a specially synthesised coating, so that well-defined Raman spectra could be obtained from the fiber–matrix interface. This coating prevents the use of Raman spectroscopy. Changes in the glass fiber are not desirable, as they may interfere with the mechanisms involved in environmentally assisted cracking.

The distribution of molecular orientations in amorphous polymers determines the intensity of Raman scattering from polarized light (Nielsen and Pyrz, 2002). The stress in the matrix can be determined by measuring the angular variation in the intensity of Raman scattering. However, this approach measures strain rather than stress in the matrix. Even above the yield limit, the relationship between strain and intensity is linear (Nielsen and Pyrz, 2002). This is not a matter of concern where the matrix is in the elastic range, but polymer matrices are

visco-elastic (Kominar, 1996). In room-temperature post-curing of the resins generally used in corrosion applications, the polymer is heated to a high temperature. The resultant thermal stresses due to expansion cause mismatches between the fiber and resin and may give rise to a viscous flow in the resin.

This indicated that 'strains' are locked in, even when the stress state does not exist. The technique is therefore inapplicable in these cases or those in which any other non-linear resin behavior is expected.

3.5 The photoelasticity method

Photoelasticity is one of the classical optical methods of static stress analysis. A transparent or translucent matrix is needed to determine the stress field in composite materials. When such materials are stressed, their molecular orientation distribution changes and affects the polarization of light (Nielsen and Pyrz, 2002). To determine the magnitude of residual stresses, the measurement of retardation (phase difference between two light vectors travelling at different velocities) is required. The residual stress components can then be calculated by means of the stress-optic or Brewster's Law. Photoelasticity can be utilized to determine the thermal residual stress distribution in the matrix, when a uni-directional specimen with fibers in the 0-degree direction is rotated between crossed polarizers. The matrix region then forms a fringe indicating a unique principal stress direction. Maximum extinctions are found at 0 and 90 degrees, which indicates that the principal stress directions are parallel and perpendicular to the fiber direction (Parlevliet *et al.*, 2006).

Photoelasticity exploits this effect to determine the direction of and the difference between the principal stresses (Hendry, 1966). The technique yields results in the form of a fringe pattern over the area of study. It is possible to resolve this pattern over small regions by using a microscope (Reid, 2009).

Photoelasticity has been widely applied to investigate the stress fields surrounding single fibers embedded in a polymer matrix (Kim and Nairn, 2002; Sjögren *et al.*, 1999; Zhao *et al.*, 2003). Although most of these studies have been directed at the bonding between fiber and matrix, residual stresses around single fibers have been quantified (Yan and Ohsawa, 1994; Xu and Ashbee, 1994).

Residual stresses have also been investigated in typical uni-directional composite materials (Nairn and Zoller, 1985a,b). Andersson *et al.* (2000) investigated the transverse residual stresses in a cross-section of GFRP containing thousands of fibers. However, the observed fringe pattern did not change with the application of external loading in this investigation. It was deduced that the fringe pattern does not reflect the existing stresses, but rather the stress history of the matrix. This effectively means that the method does not accurately reflect the residual stresses in the laminate (Reid, 2009).

Nairn and Zoller (1985a,b) investigated the residual stresses in carbon fiber reinforced polysulfane and epoxy. It was clear from their investigation that the principal residual stresses are aligned with, and perpendicular to, the fiber direction. The stress difference between the principal stresses in the matrix was also determined in both cases. It was not possible to determine the principal stresses individually without making an assumption regarding one of these values. Although the thickness of the laminate was not stated, it was necessary to keep the fiber volume fraction fairly low so that regions of transparency could be found between fibers (Reid, 2009).

Although the studies of Andersson *et al.* (2000) and Nairn and Zoller (1985a,b) demonstrate that micro-scale residual stresses in uni-directional composites could be investigated using the photoelastic technique, they also highlighted some serious concerns (Reid, 2009), as the photoelastic technique may not reflect the residual stress state in real laminates. The technique allows the difference in principal stresses to be determined, although it is not possible to measure these stresses individually. This problem can be resolved by using holographic interferometry in conjunction with conventional photoelasticity (Seif *et al.*, 2002, 2006). However, this technique is more complex than the conventional approach and has not been widely used since being proposed in 1994.

This method may only be used in thin composites with low fiber volume fraction (i.e. <40 vol%), if any effects in the matrix are to be observed. The residual stress patterns in both matrix and reinforcing phase in the cross-section of uni-directional composites with regular (high) fiber volume fraction can be observed if a thin slice of the cross-section is cut and held between crossed polarizers in transmitted polarized light (Parlevliet *et al.*, 2006).

3.6 Other optical methods

Lubineau (2008) proposed a simple method using optical microscopy on the basis of observation of the displacement field in relation to the creation of a transverse crack in a crosswise laminate. This displacement field can be subsequently re-interpreted in accordance with the model in use to build the quantity required.

Berezhinsky *et al.* (2007) offered an optical method for registering internal stresses in composite materials based on modulation of the polarization of laser radiation reflected from anisotropic media and its anisotropy parameters were defined by this modulation. Using this method, they studied residual stresses on the border of SiC/SiC + 20% TiB_2 which resulted from the difference of temperature expansion coefficients. The experimental curve of stress distribution agreed qualitatively with the theoretical calculation. The stress magnitude obtained by this method agreed well with the values offered by the Raman scattering method and the diffraction of X-ray radiation.

3.7 The acoustic wave method

Acoustic waves possess the important property of undergoing changes in velocity and polarization under the effect of stresses. Thus by measuring the alterations in these parameters, residual stresses can be measured. Where there is no stress, the waves stay in phase but where the polarization alters, interference between the waves increases. The underlying stresses can be measured, taking into account the resulting patterns of interference, regardless of the temperature (Ostertag and Drescher-Krasicka, 1999).

Using acoustic waves to measure residual stress in heterogeneous materials poses particular problems. The wavelength must be long enough to be influenced by microstructure features inside the laminate. This allows propagation of the wave but effectively means that the samples appear homogeneous (Ostertag and Drescher-Krasicka, 1999), so causing limitations in the corresponding resolution. The effective measured stress is the average stress over the path of the wave and nothing can be gathered about the stress state in the fiber or matrix

Instead of propagating waves in the plane perpendicular to the fibers, it is possible to measure the longitudinal micro-scale residual stresses in GFRP by propagating longitudinal waves down their length and measuring the stress related changes in the wave properties. However, compatibility between strains in the fiber and the surrounding matrix means that the wave must propagate at the same speed in both constituents. The wave must accordingly disperse into the surrounding matrix, acting in the same manner as a longitudinal wave propagating through a homogeneous composite material. Only information regarding the average stress in the composite material can be obtained in this way. Since this stress is zero, irrespective of the micro-scale residual stress state, the approach is not satisfactory (Reid, 2009).

It is therefore obvious that the propagation of acoustic waves, both in the plane perpendicular to the fibers and in the fiber direction, is associated with a lack of resolution. The use of acoustic waves for quantifying the micro-scale residual stresses in GFRP is accordingly prevented (Reid, 2009).

3.8 Methods based on interferometry

Interference with light waves reflected from an object generates an optical pattern, which may be used to determine deformations. Some of the methods using this phenomenon have been employed to quantify residual stresses in composite materials. The Moiré effect is based on an interference pattern, which develops when light passes through two gratings rotated at a small angle to each other. When one of the gratings alters because of deformation, the resulting interference (Moiré) pattern also alters (Parlevliet *et al.*, 2006). Moiré interferometry is applicable for monitoring both in-plane and out-of-plane displacements. A grating should be applied to the surface of the specimen for in-plane displacements. This is not necessary for out-of-plane displacements, as the

grating may be projected onto the surface at an angle to the viewing direction (Parlevliet *et al.*, 2006)

The cure reference method was developed to measure the thermal residual strains on thermoset materials using Moiré interferometry. This is a highly accurate and sensitive laser-based optical technique, permitting the development of a contour map of the in-plane displacements (Post *et al.*, 1994). It is a full-field laser method, which monitors the development of strains on the surface of a composite laminate throughout the cooling process. A grating is applied to the material during curing to act as a reference to the stress-free condition just prior to the stress-free temperature. The interference results in a characteristic pattern of light and dark fringes, which are used to determine the in-plane-displacements in symmetrical laminates. The residual stresses can then be quantified using lamination theory. This non-contact full-field method provides highly accurate results, has high displacement and strain sensitivity, high spatial resolution and high signal-to-noise ratio. However, it only provides information for strains on the surface of the specimen and an interference image is required when no strains exist. This may prove difficult in thermoplastic composites (Parlevliet *et al.*, 2006).

3.9 The cure referencing method

The cure referencing method was developed at the University of Florida by Niu *et al.* (1999) to record process-induced strains. It is a non-destructive novel testing method designed to accurately determine the process-induced and residual strains associated with manufacturing, cure and thermal loading. This method uses the full-field laser based optical method of Moiré interferometry to measure strains on the surface of laminates, which are initiated during the high temperature curing process. The method involves replicating a high frequency diffraction grating on the specimen whilst it is in the autoclave during the cure cycle (Myers, 2004).

The cure referencing method measures the residual strains associated with the curing of polymer composites (Schulz *et al.*, 2005). Attempts to measure these strains using methods such as embedding strain gages and fiber optic Bragg gratings have been subject to criticism, as it was unclear as to whether they measured the residual stress in the laminate or the influence of the sensors on the residual stress (Ifju *et al.*, 1999). The cure referencing method avoids this problem by replicating a Moiré diffraction grating onto the surface of a laminate prior to gelation of the resin in an autoclave. The grating is thus applied to the laminate in its stress-free state. After curing, Moiré interferometry is used to measure the strains associated with this condition. The polymerisation cure shrinkage can be isolated from the thermal strains by measuring the residual strain at the cure temperature (Reid, 2009).

The method can easily be used to find the longitudinal residual stresses in a uni-directional laminate. As the fibers and matrix are bonded together, they have the same longitudinal strain as the laminate. However, in an unstressed condition,

they would experience strain to different degrees. The difference between the laminate strain and the unstressed strain of each constituent consequently defines its micro-scale residual strain (Reid, 2009).

However, this method cannot be used efficiently with room temperature cured laminates that are later post-cured. The post-curing process involves heating the resin system to promote further cross-linking, which therefore does not take place at a constant temperature. As the polymer matrices are viscoelastic, the high temperatures combined with the associated thermal stresses may be expected to promote some viscous flow prior to full cross-linking of the resin. The temperature at which the Moiré grating remains undeformed therefore cannot be taken as corresponding to the temperature of the stress-free state. An additional difficulty is the requirement to apply the Moiré grating during manufacture. Consequently, the method can only be applied to laminates that are specifically made for the purpose of measuring residual stress (Reid, 2009).

3.10 Measurement methods using sensors

Sensors are capable of measuring variations in the residual strains of a composite through change of its features, where there is an appropriate mechanical interaction between the composite and the sensors. Strain gages and optic sensors are used for the analysis of inter-laminar stresses in angle-ply laminates and intra-laminar stresses in uni-directional laminates (Parlevliet *et al.*, 2006). There are three general methods in this category.

3.10.1 Embedded strain gages

Embedded strain gages in thermoset composites have been shown to provide accurate results in heating and cooling, but are inapplicable to thermoplastic composites due to the high processing temperatures (Tsouvalis *et al.*, 2009). In one case, a strain gage was melt-embedded in the center of the surface plies of a uni-directional carbon fiber/PEEK (CF/PEEK) laminate to measure residual strain development directly from both thermal and crystallisation effects (Parlevliet *et al.*, 2006).

The most widely-used devices are electrical resistance and fiber optic strain gages (Myers, 2004). Daniel and Liber (1975, 1977) made the first attempts to measure residual stress by this method. High temperature electrical resistance strain gages were directly cured in the laminate by placing them between the lamina plies. The strain gages were therefore directly exposed to any deformation of the laminate. A compensation method was derived to account for the changing features of the gage over a certain temperature range. The main disadvantage of this method is the introduction of a foreign body to the laminate, which can substantially change the material features at the location and create a void leading to incorrect measurements (Myers, 2004).

3.10.2 Embedded fiber optical sensors

Fiber Optical Sensors (FOSs) can be embedded inside a composite material, where they monitor the residual strains. These sensors are small and lightweight and can be embedded in a composite laminate without substantially compromising its structural integrity (Karalekas *et al.*, 2008). These sensors can be used in both uni-directional and angle-ply laminates. There are a number of different FOSs, among which the Fiber Bragg Grating (FBG) and Extrinsic Fabry–Perot Interferometric (EFPI) sensors are the most frequently used for monitoring the formation of residual stresses. An EFPI sensor quantifies strain through a change in cavity length, which is related to a phase change between the input/output signals and the reflection of the optical fibers (Fig. 3.2) (Parlevliet *et al.*, 2006). When embedded parallel to the reinforcing fibers, FOSs are minimally disruptive, provided that the thickness of the ply matches the diameter of the optical fiber. They will usually not entail any degradation of macroscopic features. However, this does not hold true when an FOS is embedded perpendicular to the fiber direction. In this case, an eye-shaped defect is created, which causes stress concentration and deterioration of the mechanical features. One fiber usually contains many sensors (FBGs), therefore an array of FOSs can be embedded inside a laminate (known as 'multiplexing') to provide information on the residual stress distribution throughout the laminate on both a macro-mechanical and a global level. The strain resolution is higher than 1 $\mu\varepsilon$ (Parlevliet *et al.*, 2006).

3.10.3 Embedded metallic particles

This technique measures the deformation of thermoset polymer matrix by applying X-ray diffraction to metallic particles embedded within it. In composite materials, aluminum, copper and silver particles present a deflection in the peak angle. Using Bragg's law, this deflection can be related to changes in the spacing of the crystal lattice resulting from the residual strains. The measured strain can be connected with the residual stresses by Hooke's law or via a stress transmission tensor. The regularly shaped aluminum particles give a high degree of accuracy. This technique can only measure to a thickness of 0.3 to 0.5 mm and can therefore only

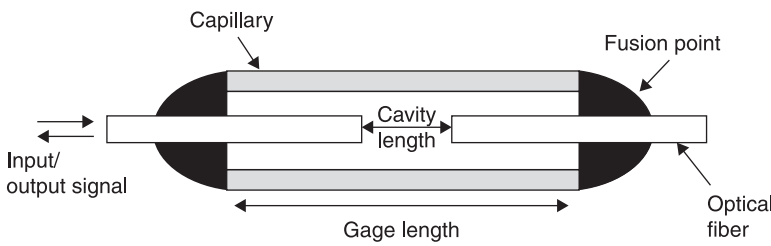

3.2 Schematic view of EFPI sensor (Zhou and Sim, 2002).

provide information about the surface features of thicker specimens (Parlevliet *et al.*, 2006).

The method is used mainly in thermoset matrices, as these do not have a crystalline structure that changes in response to X-rays when strained. Thermosets therefore require crystalline fillers. In semi-crystalline thermoplastics, the lattice spacing between the crystals and the change due to straining can be measured by X-ray diffraction. This was shown to be feasible for PEEK reinforced with carbon and glass fillers, but the technique has not yet been examined for continuous fiber reinforced thermoplastics (Tsouvalis *et al.*, 2009).

3.11 The electrical resistance method

This method measures the electrical resistance of materials. As it requires an electrically conductive material, the method is not suitable for polymers with insulating properties. To overcome this difficulty, electrically conductive fillers are used in the polymers. In the case of composites, continuous carbon fibers are used to reinforce, as they are electrically conductive (Chung, 2000).

Graphite and carbon fibers are electrical conductors and therefore a laminate made from these substances will have a measure of electrical conductivity and resistance (Myers, 2004). It is an important property of carbon fiber composite materials that the electrical properties such as resistance are influenced by strain, damage and temperature. Embedded sensors increase the cost and may reduce the strength of the structure, while monitoring the electric resistance of a composite material provides information on the stresses and the temperature without these disadvantages. Electrical resistivity measurements make it possible to determine differences in the inter-laminar residual stresses (Parlevliet *et al.*, 2006). The electrical resistivity of the composite in the fiber direction increases under the influence of structural transition in the matrix (i.e. glass transition, melting, solid-state curing) on the fiber morphology (e.g. fiber waviness). The thermal stress leads to an increase in the degree of fiber waviness or a decrease in the degree of fiber alignment. Therefore, the measurement of electrical conductivity of the fibers may reveal information concerning the residual stresses, structural transitions, thermal damage, etc. (Chung, 2000).

3.12 Conclusions

In recent years, the growing use of advanced laminated composites has focused attention on process-induced residual stress. The development of methods for measuring and predicting residual stresses in composite materials is therefore essential, and considerable effort has gone into understanding their quantities and qualities. Reliable measurement and prediction of such stresses is a considerable challenge. The distribution and size are decisive in understanding the behavior of composites, as these affect the quality and performance of the target structural

material. It is therefore necessary to take the residual stresses into account when designing a component. The optimization of the material quality and the minimization of the component weight require a more thorough understanding of the significance of residual stresses.

This chapter has attempted to categorize the non-destructive experimental techniques of residual stress measurement in composite materials. It was shown that a considerable number of such methods have been tried, based on different properties related to these stresses. There seems to be considerable scope for future research in this field of study.

3.13 References

Abuhasan, A., Balasingh, C. and Predecki, P. (1990) Residual stresses in alumina/silicon carbide (whisker) reinforced composite by X-ray diffraction, *Journal of the American Ceramic Society*, **73**, 2474–84.

Adachi, T., Sekino, T., Nakayama T., Kusunose, T. and Niihara K. (2003) Measurement of microscopic stress distribution of multilayered composite by X-ray stress analysis, *Materials Letters*, **57**, 3057–62.

Albertini, G., Bruno, G., Carrado, A., Fiori, F., Rogante M. and Rustichelli, F. (1999) Determination of residual stresses in materials and industrial components by neutron diffraction, *Measurement Science and Te*chnology, **10**(3), R56–R73.

Allen, A. J., Hutchings, M. T. and Windsor, C. G. (1985) Neutron diffraction methods for the study of residual stress fields, *Advances in Physics*, **34**(4), 445–73.

Andersson, B., Sjögren, A. and Berglund, L. (2000) Micro- and meso-level residual stresses in glass-fiber/vinyl-ester composites, *Composites Science and Technology*, **60**(10), 2011–28.

Bacon, D. H., Edwards, L., Moffatt, J. E. and Fitzpatrick, M. E. (2011) Synchrotron X-ray diffraction measurements of internal stresses during loading of steel-based metal matrix composites reinforced with TiB2 particles, *Acta Materialia*, **59**, 3373–83.

Balasingh, C. and Singh, A. K. (2000) Residual stresses and their measurements by X-ray diffraction methods, *Metals Materials And Processes*, **12**(2–3), 269–80.

Bannister, D. J., Andrews, M. C., Cervenka, A. J. and Young R. J. (1995) Analysis of the single-fiber pull-out test by means of Raman spectroscopy. Part II: Micromechanics of deformation for an aramid/epoxy system, *Composites Science and Technology*, **53**(4), 411–21.

Barrett, C. S. and Predecki, P. (1976) Stress measurement in polymeric materials by X-ray diffraction, *Polymer Engineering and Sc*ience, **16**, 602–8.

Barrett, C. S. and Predecki, P. (1980) Stress measurement in graphite/epoxy uniaxial composites by X-rays, *Polymer Composites*, **1**, 2–6.

Bateman, M. G., Miller, O. H., Palmer, T. J., Breen, C. E. P., Kingston, E .J. *et al.* (2005) Measurement of residual stress in thick section composite laminates using the deep-hole method, *International Journal of Mechanical Sciences*, **47**(11), 1718–39.

Benedikt, B., Predecki, P. K., Kumosa, L., Rupnowski, P. and Kumosa, M. (2002) Measurement of residual stresses in fiber reinforced composites based on X-Ray diffraction, JCPDS-International Centre for Diffraction Data, *Advances in X-ray Analysis*, **45**, 218–24.

Benedikt, B., Kumosa, M., Armentrout, D., Kumosa, L., Sutter, J. K. and Predecki, P. K. (2004a) Analysis of stresses in aluminum particles embedded inside uni-directional and

woven graphite/polyimide composites subjected to large bending loads, *Mechanics of Advanced Materials and Structures*, **11**(1), 31–49.

Benedikt, B., Gentz, M., Kumosa, L., Rupnowski, P., Sutter, J. K. *et al.* (2004b) X-ray diffraction experiments on aged graphite fiber/polyimide composites with embedded aluminum inclusions, *Composites: Part A*, **35**, 667–81.

Benedikt, B., Kumosa, M. and Predecki, P.K. (2005) An evaluation of residual stresses in graphite/PMR-15 composites by X-ray diffraction, *Acta Materialia*, **53**, 4531–43.

Benedikt, B., Lewis, M., Rangaswamy, P., Kumosa, M., Predecki, P. *et al.* (2006) Residual stress analysis in aged graphite/PMR-15 composites using X-ray diffraction, *Materials Science and Engineering A*, **421**, 1–8.

Berezhinsky, L. I., Berezhinsky, I. L., Grigorev, O. N., Serdega, B. K. and Ukhimchuk, V.A. (2007) Investigation of residual stresses on the boundary of SiC/SiC + 20% TiB2 composite materials joining by optic modulation–polarization method, *Journal of the European Ceramic Society*, **27**, 2513–19.

Bourke, M. A. M., Goldstone, J. A. and Holden, T. M. (1992) In: M. T. Hutchings and A.D. Krawitz (eds), *Measurement of Residual and Applied Stress using Neutron Diffraction*, London, Kluwer, 369.

Chevalier, J., Deville, S., Fantozzi, G., Bartolomé, J. F., Pecharroman, C. and Moya, J. S. (2005) Nano-structured ceramic oxides with a slow crack growth resistance close to covalent materials, *Nano Letters*, **5**, 1297–301.

Chung, D. D. L. (2000) Thermal analysis of carbon fiber polymer-matrix composites by electrical resistance measurement, *Thermochimica Acta*, **364**, 121–32.

Cox, B. N., James, M. R., Marshall, D. B. and Addison Jr., R. C. (1990) Determination of residual stresses in thin sheet titanium aluminide composites, *Metallurgical Transactions A (Physical Metallurgy and Materials Science*), **21A**(10), 2701–7.

Daniel, I. M. and Liber, T. (1975) *Lamination Residual Stresses in Fiber Composites*, IITRI Report D6073-I, for NASA-Lewis Research Center, NASA CR-134826.

Daniel, I. M. and Liber, T. (1977) Effect of laminate construction on residual stresses in graphite/polyimide composites, *Experimental Mechanics*, **1**, 21–5.

Delfosse, D., Cherradi, N. and Ilschner, B. (1997) Numerical and experimental determination of residual stresses in graded materials, *Composites Part B: Engineering*, **28B**, 127–41.

Fenn, R. H., Jones, A. M. and Wells, G. M. (1993) X-ray diffraction investigation of triaxial residual stresses in composite materials, *Journal of Composite Materials*, **27**(14), 1338–51.

Fiori, F., Albertini, G., Girardin, E., Giuliani, A., Manescu, A. and Rustichelli, F. (2004) Neutron and synchrotron radiation non-destructive methods for the characterisation of materials for different applications, *Journal of Alloys and Compounds*, **382**(1), 39–45.

Ghonem, H., Wen, Y. and Zheng, D. (1994) An interactive simulation technique to determine the internal stress states in fiber reinforced metal matrix composites, *Materials Science and Engineering*, **A177**, 125–34.

Goutianos, S., Peijs, T. and Galiotis, C. (2002) Comparative assessment of stress transfer efficiency in tension and compression, *Composites Part A: Applied Science and Manufacturing*, **33**(10), 1303–9.

Hauk, V. M. and Macherauch, E. (1984) A useful guide for X-ray stress evaluation (XSE), *Advances in X-ray Analysis*, **27**, 81–99.

Ifju, P. G., Niu, X., Kilday, B. C. and Liu, S. C. (1999) A novel means to determine residual stresses in laminated composites, *Journal of Composite Materials*, **33**(16), 1511–24.

James, M. R., Bourke, M. A., Goldstone, J. A. and Lawson, A. C. (1993a) *Advances in X-Ray Analysis*, New York, Plenum Press, 481.

James, M. R., Bourke, M. A., Goldstone, J. A. and Lawson, A. C. (1993b) Diffraction measurements of residual stress in titanium matrix composites. In: E. V. Barrera and I. Dutta, I. (eds), *Residual Stresses in Composites, Measurement, Modeling and Effects on Thermo- Mechanical Behavior*, The Minerals, Metals and Materials Society, 177–85.

Karalekas, D., Cugnoni, J. and Botsis, J. (2008) Monitoring of process induced strains in a single fibre composite using FBG sensor: a methodological study, *Composites: Part A*, **39**, 1118–27.

Kendig, K. L., Soboyejo, W. O. and Miracle, D. B. (1995) Measurement of residual stresses in Ti-15-3 SCS-9 continuously reinforced composites using X-ray diffraction and a matrix etching technique, *Scripta Metallurgica et Materialia*, **32**(5), 669–74.

Kim, B. W. and Nairn, J. A. (2002) Experimental verification of the effects of friction and residual stress on the analysis of interfacial debonding and toughness in single fiber composites, *Journal of Materials Science*, **37**(18), 3965–72.

Kominar, V. (1996) Thermo-mechanical regulation of residual stresses in polymers and polymer composites, *Journal of Composite Materials*, **30**(3), 406–15.

Kupperman, D. S., Majumdar, S., Singh, J. P. and Saigal, A. (1992) In: M. T. Hutchings and A. D. Krawitz (eds), *Measurement of Residual and Applied Stress Using Neutron Diffraction*, London, Kluwer, 439.

Larsson, C. and Odén, M. (2004) X-ray diffraction determination of residual stresses in functionally graded WC–Co composites, *International Journal of Refractory Metals and Hard Materials*, **22**, 177–84.

Lu, J. and Retraint, D. (1998) Review of recent developments and applications in the field of X-ray diffraction for residual stress studies, *Journal of Strain Analysis for Engineering Design*, **33**(2), 127–36.

Lubineau, G. (2008) Estimation of residual stresses in laminated composites using field measurements on a cracked sample, *Composites Science and Technology*, **68**, 2761–9.

Meske, R. and Schnack, E. (2001) A micromechanical model for X-ray stress analysis of fiber reinforced composites, *Journal of Composite Materials*, **35**(11), 972–98.

Meske, R. and Schnack, E. (2003) Particular adaptation of X-ray diffraction to fiber reinforced composites, *Mechanics of Materials*, **35**(1–2), 19–34.

Myers, D. G. (2004) *Method for Measurement of Residual Stress and Coefficient of Thermal Expansion of Laminated Composites*, MSc Thesis, University of Florida.

Nairn, J. A. and Zoller, P. (1985a) Matrix solidification and the resulting residual thermal stresses in composites, *Journal of Materials Science*, **20**(1), 355–67.

Nairn, J. A. and Zoller, P. (1985b) Residual thermal stresses in semicrystalline thermoplastic matrix composites, *Fifth International Conference on Composite Materials*, San Diego, USA.

Nielsen, A. S. and Pyrz, R. (1998) The effect of cooling rate on thermal residual strains in carbon/polypropylene micro composites, *Science Engineering Composite Materials*, **7**(1–2), 1–22.

Nielsen, A. S. and Pyrz, R. (2002) A novel approach to measure local strains in polymer matrix systems using polarised Raman microscopy, *Composites Science and Technology*, **62**(16), 2219–27.

Niu, X. (1999) *Process Induced Residual Stresses and Dimensional Distortions in Advanced Laminated Composites*, PhD thesis, University of Florida.

Ostertag, C. P. and Drescher-Krasicka, E. (1999) Novel residual stress measurement techniques to measure residual stresses in fiber reinforced composites, *Journal of Materials Science*, **34**(3), 557–63.

Parlevliet, P. P., Bersee, E. N. and Beukers, A. (2007) Residual stresses in thermoplastic composites – A study of the literature. Part II: Experimental techniques, *Composites: Part A*, **38**, 651–65.

Post, D., Han, B. and Ifju, P. G. (1994) High sensitivity Moiré: Experimental analysis for mechanics and materials, *Mechanical Engineering Series*, New York, Springer-Verlag.

Predecki, P. and Barrett, C. S. (1979) Stress measurement in graphite/epoxy composites by X-ray diffraction from fillers, *Journal of Composite Materials*, **13**(1), 61–71.

Prime, M. B. (1999a) Measuring residual stress and the resulting stress intensity factor in compact tension specimens, *Fatigue and Fracture of Engineering Materials and Structures*, **22**(3), 195–204.

Prime, M. B. (1999b) Residual stress measurement by successive extension of a slot: The crack compliance method, *Applied Mechanics Reviews*, **52**(2), 75–96.

Rangaswamy, P., Prime, M. B., Daymond M., Bourke, M. A. M., Clausen, B. *et al.* (1999) Comparison of residual strains measured by X-ray and neutron diffraction in a titanium (Ti–6Al–4V) matrix composite, *Materials Science and Engineering*, **A259**, 209–19.

Reid, R. G. (2009) *The Measurement of Longitudinal Residual Glass Fibre Reinforced Plastic*, PhD Thesis, University of Witwaterstrand, Johannesburg.

Rotundo, F. and Korsunsky, A. M. (2009) Synchrotron XRD study of residual stress in a shot peened Al/SiCp composite, *Procedia Engineering*, **1**, 221–4.

Schulz, W. A., Myers, D. G., Singer, T. N., Ifju P. G. and Haftka R. T. (2005a) Determination of residual stress and thermal history for IM7/977-2 composite laminates, *Composites Science and Technology*, **65**(13), 2014–24.

Seif, M.A. and Short, S. R. (2002) Determination of residual stresses in thin-walled composite cylinders, *Experimental Techniques*, **26**(2), 43–6.

Seif, M. A., Khashaba, U. A. and Rojas-oviedo, R. (2007) Residual stress measurements in CFRE and GFRE composite missile shells, *Composite Structures*, **79**(2), 261–9.

Sjögren, A., Joffe, R., Berglund, L. and Mäder, E. (1999) Effects of fiber coating (size) on properties of glass fiber/vinyl ester composites, *Composites – Part A: Applied Science and Manufacturing*, **30**(8), 1009–15.

Skoog, D. A., Holler, F. J. and Nieman, T. A. (eds) (1998) *Principals of Instrumental Analysis*, Philadelphia, Harcourt Brace, **5**, 429–35.

Stacey, A., MacGillivray, H. J., Webster, G. A., Webster, P. J. and Ziebeck, K. R. K. (1985) Measurement of residual stresses by neutron diffraction, *The Journal of Strain Analysis for Engineering Design*, **20**, 93–100.

Stamatopoulos, K. (2011) *Measurement of Residual Stresses in Composite Materials with the Incremental Hole Drilling Method*, Diploma Thesis, National Technical University of Athens, School of Naval Architecture and Marine Engineering, Athens.

Thomsen, J. S. and Pyrz, R. (1999) Creep of carbon/polypropylene model composites, a Raman spectroscopic investigation, *Composites Science and Technology*, **59**(9), 1375–85.

Tsouvalis, N., Margelis G. and Dellis, D. (2009) *Residual Stresses in Composite Materials: a Review*, NTUA Report No MAR-R4-3-NTUA-24(2) for MARSTRUCT.

Ward, Y., Young, R. J. and Shatwell, R. A. (2004) Application of Raman microscopy to the analysis of silicon carbide monofilaments, *Journal of Materials Science*, **39**(22), 6781–90.

Watts, J., Hilmas, G., Fahrenholtz, W. G., Brown, D. and Clausen, B. (2011) Measurement of thermal residual stresses in ZrB2–SiC composites, *Journal of the European Ceramic Society*, **31**, 1811–20.

Widjaja, S. (2001) Determination of creep-induced residual stress in fiber-reinforced glass–ceramic matrix composites by X-ray diffraction, *Materials Characterization*, **47**, 47–54.

Willemse, P. F., Mulder, F. M., Wei, W., Rekveldt, M. Th. and Knight, K. S. (2000) Residual stress measurements in an SiC continuous fiber reinforced Ti matix composite, *Scripta materialia*, **42**, 775–9.

Xu, Z. R. and Ashbee, K. H. G. (1994) Photoelastic study of the durability of interfacial bonding of carbon fiber-epoxy resin composites, *Journal of Materials Science*, **29**(2), 394–403.

Yallee, R. B. and Young, R. J. (1998) Micromechanics of fiber fragmentation in model epoxy composites reinforced with α-alumina fibers, *Composites – Part A: Applied Science and Manufacturing*, **29**(11), 1353–62.

Yan, X. and Ohsawa, T. (1994) Measurement of the internal local stress distribution of composite materials by means of laser imaging methods, *Composites*, **25**(6), 443–50.

Yang, X. and Young, R. J. (1994) Model ceramic fibre-reinforced glass composites: residual thermal stresses, *Composites*, **25**(7), 488–93.

Young, R. J., Thongpin, C., Stanford, J. L. and Lovell, P. A. (2001) Fragmentation analysis of glass fibers in model composites through the use of Raman spectroscopy, *Composites – Part A: Applied Science and Manufacturing*, **32**(2), 253–69.

Zhao, F., Hayes, S. A., Patterson, E. A., Young, R. J. and Jones, F. R. (2003) Measurement of micro stress fields in epoxy matrix around a fiber using phase-stepping automated photoelasticity, *Composites Science and Technology*, **63**(12), 1783–7.

Zhou, G. and Sim, L. M. (2002) Damage detection and assessment in fiber reinforced composite structures with embedded fiber optic sensors, *Smart Material Structures*, **11**(6), 925–39.

4

Measuring residual stresses in composite materials using the simulated hole-drilling method

A. R. GHASEMI, University of Kashan, Iran and
F. TAHERI-BEHROOZ and M. M. SHOKRIEH,
Iran University of Science and Technology, Iran

DOI: 10.1533/9780857098597.1.76

Abstract: The calibration coefficients for each stage of drilling are determined by simulating the incremental hole-drilling process. As described in this chapter, different samples of laminated composites with various lay-ups were evaluated experimentally. The residual stresses in each layer of composite samples were determined using simulation of the integral hole-drilling method process and measuring the released strains in consecutive steps of the drilling. The experimental measurements were then compared with the predictions of the classical laminate theory. The agreements between the two results validate the integral method for calculating the residual stresses in laminated composite materials.

Key words: residual stress, hole drilling, simulation, laminated composite, calibration factors.

4.1 Introduction

Residual stresses are self-equilibrating stresses inside a component, or assembly of parts if the specimen is not placed under an external load. As a result, some of the strength of the specimen is used to oppose these stresses. In metals, residual stresses can arise from deformation during heat treatment, machining, cold working or processing operations that transform the shape or change the properties of a material. In composite materials, mismatches between the thermal expansion coefficients of fibers and matrix, contraction and expansion of different layers due to differences in their material directions, and temperature gradients in the manufacturing process cause residual stresses. The magnitude of these stresses depends on the lay-up configuration, material properties and manufacturing process. Residual stresses in laminated composites decrease the performance of the structures and cause early matrix cracking, fiber breakage, delamination and swelling (Crasto and Kim, 1993; Hahn and Pagano, 1975; Hahn, 1976; Hyer, 1989; White and Hahn, 1992).

As the cross-linking takes place, the epoxy shrinks, that is, chemical shrinkage occurs. The resulting deformation of a uni-directional composite in the transverse

direction is much larger than in the longitudinal direction. Therefore, within the laminate the deformation of one ply is constrained by the other plies with different fiber orientations, and hence residual stresses are built up in each ply. However, since most cross-linking takes place at the highest temperature, called the cure temperature, the epoxy can still be viscous enough to allow complete relaxation of the residual stresses. Thus the cure temperature can be taken as the stress-free temperature. However, the stress-free temperature will vary with the employed cure process, because the property change during curing is time-dependent. The cure temperature can serve as the stress-free temperature as long as almost all cures take place at the cure temperature.

Consider a $[0/90]_s$ laminate being cooled from the cure temperature to room temperature. Suppose for a moment that the 0-degree plies and the 90-degree plies can deform unconstrained by each other (Fig. 4.1). For convenience, only one 0-degree ply and one 90-degree ply are shown in the figure. As the temperature is lowered, the 0-degree ply deforms by e_x^T, while the 90-degree ply undergoes a thermal strain e_y^T in the same direction. Since e_x^T and e_y^T are different from each other, there will be a geometrical mismatch between the 0-degree and 90-degree plies. However, in the actual $[0/90]_s$ laminates, such a mismatch is not allowed. Therefore, residual stresses σ_x^R and σ_y^R are internally exerted to the 0-degree and 90-degree plies, respectively, to bring about the geometrical compatibility. The final strain ε_x^R and ε_y^R of the laminates is called the laminate curing strain and

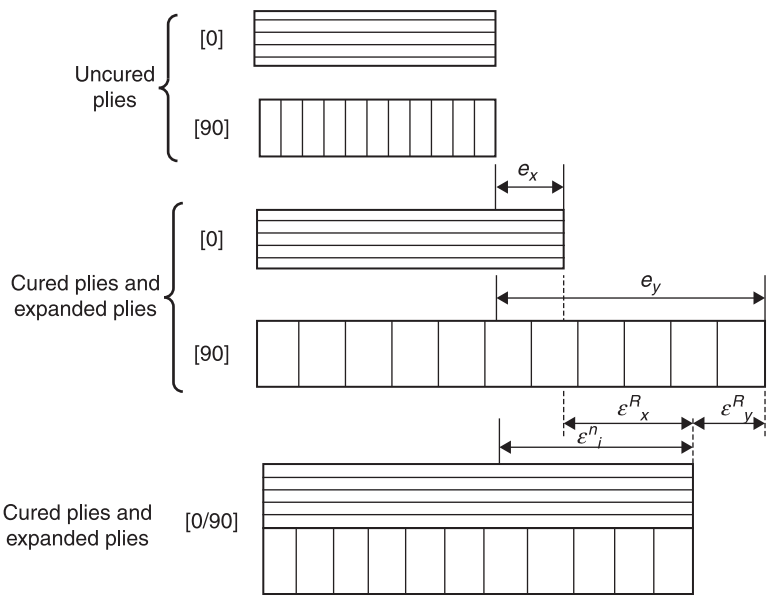

4.1 Build up of residual stresses after fabrication.

depends on e_x^T and e_y^T as well as on the elastic modulus (Tsai and Hahn, 1980; Tsai, 1988). The materials scientist and the engineer can now access a large number of residual stress measurement techniques. Some are destructive, while others can be used without significantly altering the component; some have excellent spatial resolution, whereas others are restricted to near surface stresses or to specific classes of material (Withers and Bhadeshia, 2001).

One of the most useful and widely used methods of residual stress measurement is the central hole-drilling method. This method is a well-established, popular technique for measuring residual stresses in isotropic materials. It is easy to use, reliable in operation, and involves only limited damage to the specimen (ASTM E837-01, 1999; Beaney, 1976; Rendler and Vigness, 1966). The most common use of this method involves the application of a special three-element strain-gage rosette onto the surface of the component at the measurement location. A small shallow hole, usually with a depth equal to the diameter and about 0.8 mm to 3.2 mm in diameter, is made in the specimen through the center of the rosette. The production of the hole in the material causes a redistribution of strains to occur near the hole, which can be detected and measured by the strain gages. These strain measurements can be then related to the original residual stresses at the hole location. The response of the strain gages is sensitive to the diameter of the hole (D_0) and the diameter of the rosette (D). During the hole-drilling process, careful experimental techniques are essential so as to avoid introducing additional localized stresses, particularly in materials which strain harden appreciably (Flaman *et al.*, 1987; Flaman and Boag, 1990; Flaman and Herring, 1985).

Most often, the hole-drilling method is used when the residual stress field is assumed not to vary with depth beneath the surface. In such cases, experimental relaxed strain calibration data from test specimens with known uniform stress fields can be used directly. For many years, there has also been great interest in using the hole-drilling method to measure non-uniform residual stresses. Two stress calculation procedures, the Incremental Strain Method and Average Strain Method, have been widely adopted. The need to use experimental calibration data has limited the theoretical scope of these two stress calculation procedures, and some theoretical shortcomings have recently been identified (Schajer, 1988). Finite element calculation of calibration factors open new possibilities for improved ways of calculating non-uniform residual stresses from incremental relaxed strain data. The Power Series Method (Schajer, 1981) and the Integral Method (Aoh and Wei, 2003; Flaman and Manning, 1985; Niku-Lari, *et al.*, 1985; Schajer, 1988; Shaw and Chen, 1990) both rely on finite element calculated calibration data, and do not have the theoretical shortcomings of the two traditional methods.

The influence of measurement error of residual strains on computed stresses has been investigated by Zuccarello (1999). He showed that in each given depth of hole-drilling step, the error sensitivity depends on the maximum hole depth and sum of the number of hole-drilling increments. Development of the integral

method for isotropic materials was carried out by improvement of the hole geometry (Tootoonian and Schajer, 1995), number and size of drilling step increments (Stefanescu *et al.*, 2006), calibration factors (Beghini and Bertini, 2000; Hwang *et al.*, 2003; Xiao *et al.*, 2011), and the geometry of the strain gage rosette (Schajer and Tootoonian, 1997). The original mechanical deformation measurement method has also been replaced by the use of strain gages and optical techniques, such as Moiré, Holographic Interferometric Techniques, Electronic Speckle Pattern Interferometry (ESPI) and Digital Image Correlation (DIC). The early empirical stress computation procedures have been superseded by finite element calibrations and inverse calculations to accommodate the character and quantity of the newly available measured data (Schajer, 2010a). An overview of the history and progress of the hole-drilling method, along with recent advances in both the measurement and analytical areas, is described by Schajer (2010a,b).

The first application of the method to orthotropic materials was carried out by Bert and Thompson (1968) and Lake *et al.* (1970), using an approximate calculation procedure. Subsequent developments and applications to orthotropic materials have been carried out by Prasad *et al.* (1987a,b). The approximate approach, proposed in Bert and Thompson (1968) and Lake *et al.* (1970), was used also by Sicot *et al.* (2003, 2004) to the residual stresses measurement on orthotropic composite laminates. More recently, Schajer and Yang (1994) have proposed an exact formulation based on the analytical solution of the displacement field of an orthotropic plate with a hole, valid for a limited class of orthotropic materials. Shokrieh and Kamali (2005) employed Schajer and Yang's (1994) results for determination of residual stresses in the first layer of laminated composite materials. Later, Shokrieh and Ghasemi (2007) presented an exact solution for determining calibration factors of the hole-drilling method for an orthotropic plate. Pagliaro and Zuccarello (2006) applied the hole-drilling method for the residual stress analysis in orthotropic materials. Ghasemi and Shokrieh (2008) developed the integral hole-drilling method to calculate the residual stresses in laminated composites materials. Later, Ghasemi *et al.* (2013) verified their model by experimental measurements on various laminated composites.

This chapter reviews modeling of the central hole-drilling process for measurement of residual stresses in isotropic, orthotropic and laminated composite plates. The integral method has been extended and simulated to calculate the residual stresses in laminated composites materials. Integral method calibration factors have been determined using simulation integral hole-drilling (SIHD) technique. For model verification, composite specimens with various arrangements were fabricated. Subsequently, by installing a rosette strain gage on the surface of each sample, and measuring the incremental strains, the residual stresses in each layer are determined and compared with the values predicted by theoretical methods.

4.2 The hole-drilling method in isotropic materials

4.2.1 Theory

The hole-drilling method is one of the most used techniques for measuring residual stresses in metallic components. The method was originally proposed by Matahr (1934) for the measurement of through-thickness uniform residual stresses in homogeneous isotropic materials. A thin plate of infinite length and width with a circular hole is shown in Fig. 4.2. The plate is subjected to a uniform tensile type load, which produces a uniform stress σ_0 in the y-direction at $r=\infty$. The distribution of the stresses about the hole, along the x- and y-axis, can be determined by using the Airys stress function approach.

The boundary conditions to be satisfied are

$$\sigma_{rr}=\tau_{r\theta}=0 \qquad at\ r=a \qquad (a)$$

$$\sigma_{yy}=\sigma_0 \qquad at\ r=\infty \qquad (b) \qquad [4.1]$$

$$\sigma_{xx}=\tau_{xy}=0 \qquad at\ r=\infty \qquad (c)$$

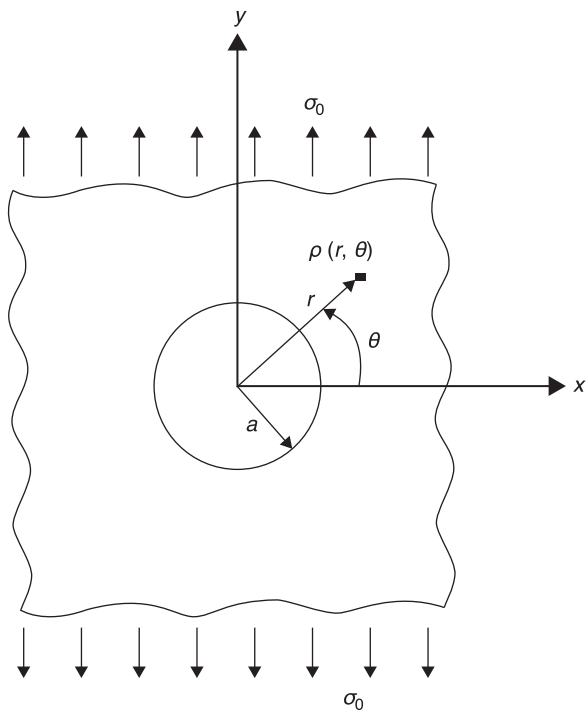

4.2 Infinite plate with a circular hole subjected to a uni-axial tensile stress σ_0.

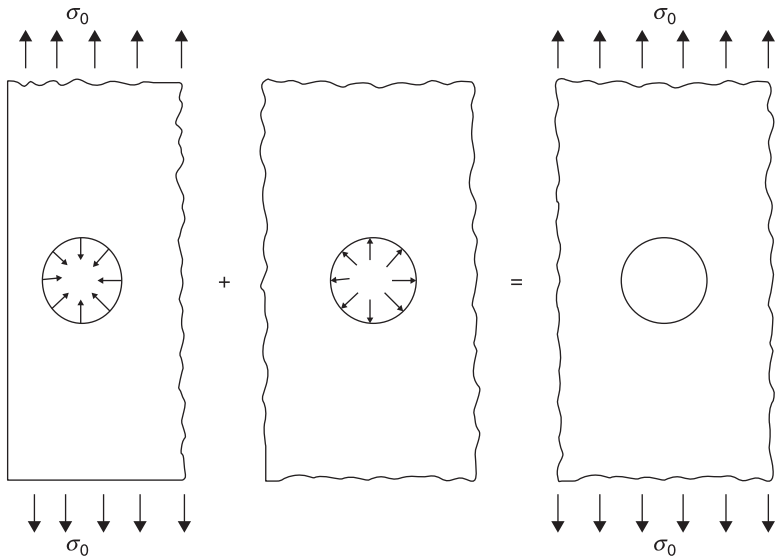

4.3 The method of superposition.

Two different stress functions along with the superposition method are commonly used to solve these equations. The first function is selected such that the stresses associated with it satisfy the boundary condition at $r=\infty$, but in general violate the conditions on the boundary of the hole. The second stress function has associated stresses, which cancel the stresses on the boundary of the hole without influencing the stresses at $r=\infty$. An illustration of this superposition process is presented in Fig. 4.3.

If an imaginary hole of radius a is created in the plate, the stresses σ_{rr}, $\sigma_{\theta\theta}$ and $\tau_{r\theta}$ on the boundary of hole could be computed as

$$\sigma_{rr}^{I} = \frac{\sigma_0}{2}(1-\cos 2\theta)$$
$$\sigma_{\theta\theta}^{I} = \frac{\sigma_0}{2}(1+\cos 2\theta) \qquad [4.2]$$
$$\tau_{r\theta}^{I} = \frac{\sigma_0}{2}\sin 2\theta$$

In the original problem, the boundary conditions at $r=a$ were

$$\sigma_{rr}=\tau_{r\theta}=0$$

The boundary conditions to be satisfied by the stresses associated with the second stress function are

$$\sigma_{rr} = -\frac{\sigma_0}{2}(1-\cos 2\theta) \qquad at\, r = a \qquad \text{(a)}$$
$$\sigma_{rr} = \tau_{r\theta} = \sigma_{\theta\theta} = 0 \qquad at\, r = \infty \qquad \text{(b)}$$
$$\tau_{r\theta} = -\frac{\sigma_0}{2}\sin 2\theta \qquad at\, r = a \qquad \text{(c)} \qquad [4.3]$$

Substituting and solving the above equations using Airys stress function gives

$$\sigma_{rr}^{II} = -\frac{\sigma_0 a^2}{2r^2}\left[1+\left(\frac{3a^2}{r^2}-4\right)\cos 2\theta\right]$$
$$\sigma_{\theta\theta}^{II} = \frac{\sigma_0 a^2}{2r^2}\left(1+\frac{3a^2}{r^2}\cos 2\theta\right) \qquad [4.4]$$
$$\sigma_{r\theta}^{II} = -\frac{\sigma_0 a^2}{2r^2}\left(\frac{3a^2}{r^2}-2\right)\sin 2\theta$$

The required solution for the original problem is obtained by superposition as

$$\sigma_{rr} = \sigma_{rr}^{I} + \sigma_{rr}^{II} = \frac{\sigma_0}{2}\left(1-\frac{a^2}{r^2}\right)\left[1+\left(\frac{3a^2}{r^2}-1\right)\cos 2\theta\right]$$
$$\sigma_{\theta\theta} = \sigma_{\theta\theta}^{I} + \sigma_{\theta\theta}^{II} = \frac{\sigma_0}{2}\left[\left(1+\frac{a^2}{r^2}\right)+\left(1+\frac{3a^4}{r^4}\right)\cos 2\theta\right] \qquad [4.5]$$
$$\tau_{r\theta} = \tau_{r\theta}^{I} + \tau_{r\theta}^{II} = \frac{\sigma_0}{2}\left(1+\frac{3a^2}{r^2}\right)\left(1-\frac{a^2}{r^2}\right)\sin 2\theta$$

The released stresses in the central hole-drilling method are represented by Eq. 4.4. The released strains associated with released stresses can be computed as

$$\varepsilon_{rr} = \frac{\sigma_{rr}}{E} - \nu\frac{\sigma_{\theta\theta}}{E} = -\frac{\sigma_0 a^2(1+\nu)}{2Er^2}\left(1+\frac{3a^2}{r^2}\cos 2\theta - \frac{4\cos 2\theta}{1+\nu}\right)$$
$$\varepsilon_{\theta\theta} = \frac{\sigma_{\theta\theta}}{E} - \nu\frac{\sigma_{rr}}{E} = -\frac{\sigma_0 a^2(1+\nu)}{2Er^2}\left(1+\frac{3a^2}{r^2}\cos 2\theta - \frac{4\nu\cos 2\theta}{1+\nu}\right) \qquad [4.6]$$
$$\varepsilon_{r\theta} = \frac{1+\nu}{E}\tau_{r\theta} = -\frac{\sigma_0 a^2(1+\nu)}{2Er^2}\left(\frac{3a^2}{r^2}-2\right)\sin 2\theta$$

In the central hole-drilling method, a rosette strain gage is mounted on a sample containing residual stresses. Then, using a drill, a small diameter hole with a depth slightly more than the diameter is located in the center of the strain gage. The strains are thus released around the hole area and measured by the three strain gages of the rosette. For isotropic materials, the released strains measured by each strain gage, located at the angle of θ with respect to the x-axis, are expressed by

$$\varepsilon_r = A(\sigma_x+\sigma_y) + B(\sigma_x-\sigma_y)\cos 2\theta + C\tau_{xy}\sin 2\theta \qquad [4.7]$$

where θ is the angle of each arbitrary point with respect to the x-axis, and A, B and C are constant values called calibration constants. σ_x, σ_y and τ_{xy} are the residual stresses trapped in the sample. In Fig. 4.4, the central hole-drilling apparatus and a rosette strain gage are shown. If the rosette is clockwise and the strain gages are located at 0, 135 and 270 degrees, then

$$\begin{bmatrix} A+B & 0 & A-B \\ A & -C & A \\ A-B & 0 & A+B \end{bmatrix} \begin{Bmatrix} \sigma_x \\ \tau_{xy} \\ \sigma_y \end{Bmatrix} = \begin{Bmatrix} \varepsilon_1 \\ \varepsilon_2 \\ \varepsilon_3 \end{Bmatrix} \quad [4.8]$$

By measuring the strains ε_1, ε_2 and ε_3 and using Eq. 4.8, the residual stresses are calculated. The responses of the strain gages are sensitive to the diameter of the hole (D_o) and the diameter of the rosette (D) (Fig. 4.4). The depth of the hole is about $0.4D$, or slightly more. However, for a material where the thickness is less than $1.2D$, a through-the-thickness hole must be applied. Maximum sensitivity for a rosette occurs when the diameter of the hole is maximum. By increasing the ratio of D_o/D the sensitivity of the method increases in proportion to $(D_o/D)^2$. The following relation should be used for the ideal ratio of D_o/D:

$$0.3 < \frac{D_0}{D} < 0.5 \quad [4.9]$$

The calibration constants A, B, and C are dependent on the material properties, geometry of the rosette and the depth of the hole. The important issue of determining the calibration constants can be carried out by experimental and numerical methods. In isotropic materials $C=2B$ and, for a counterclockwise rosette, $-C$ in Eq. 4.8 is changed to C.

4.2.2 Simulation

In this section, a computational procedure is explained to simulate the hole-drilling process in isotropic materials and obtain the calibration constants. These constants are dimensionless and could be used for determination of the residual stresses in a real experiment. A commercial finite element software, ANSYS, is used for stress analysis and simulating the process. A steel specimen ($E=200$ GPa, and $\nu=0.3$) under plane stress conditions is considered. Eight-node plane stress solid (plane 82) elements are used. The location of the strain gage with a 1.59 mm length and a 5.13 mm diameter was meshed precisely. Also the location of the hole with different diameters from $0.3D$ to $0.5D$ was meshed (Fig. 4.5).

The dimension of the specimen is 150 mm by 150 mm. The number of elements in the model is 2217, with 36 elements that were used for each of the three strain gages of the rosette. In order to verify the stability of the presented results, the number of elements was increased to achieve the convergence for the results. The mesh refinement is performed for all finite element models presented in this study.

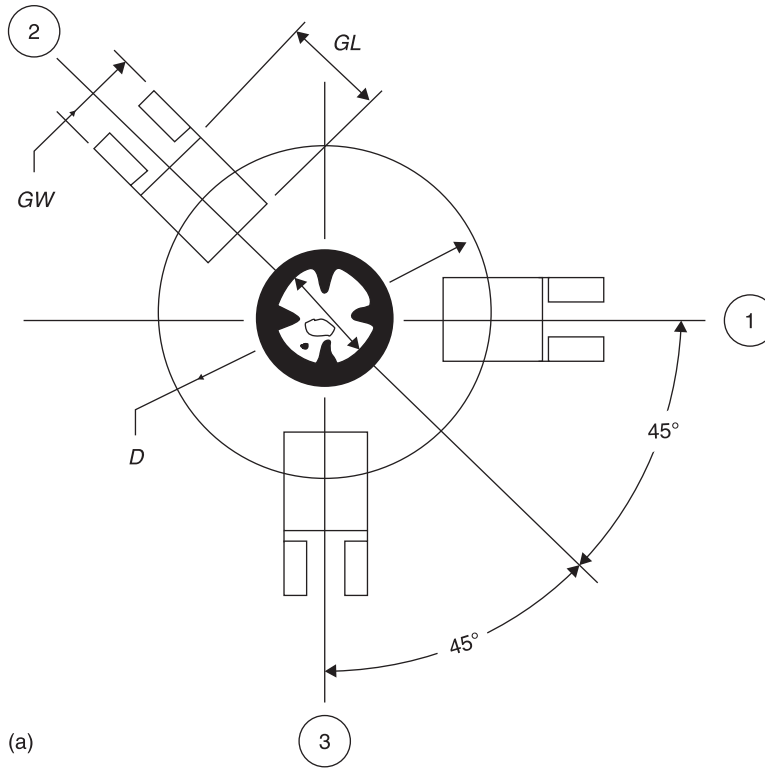

(a)

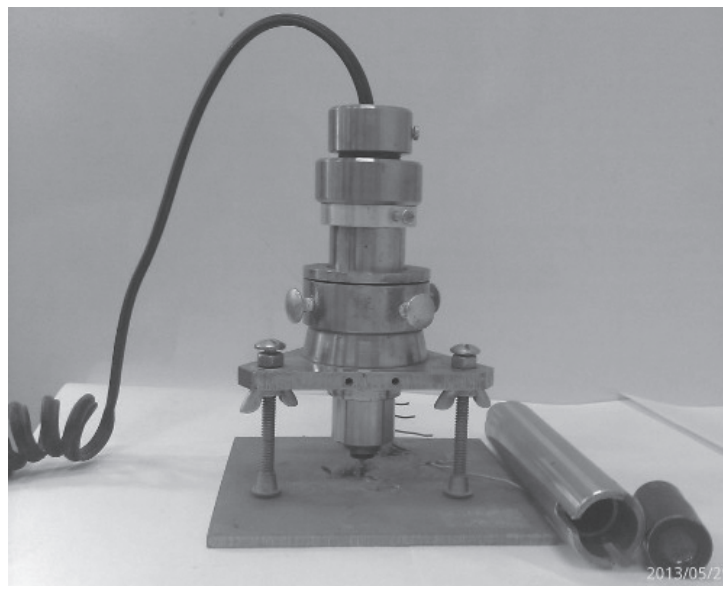

(b)

4.4 (a) Rosette strain gage; numbers 1 to 3 show strain gages; *GW* and *GL* are the width and length of any strain gage of the rosette. (b) The central hole-drilling apparatus.

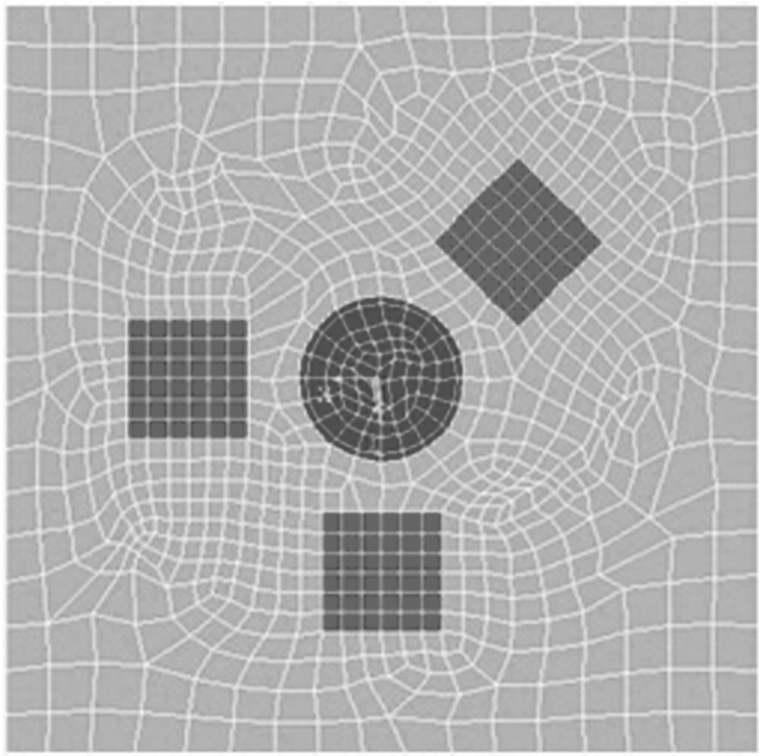

4.5 Finite element model of the specimen, rosette and the hole area.

After applying the initial stress as the residual stress to the model, in order to simulate the hole-drilling process, the elements under the area of the hole must be removed. However, to achieve the element elimination effect, the ANSYS program does not actually remove deleted elements. Instead, it deactivates them by multiplying their stiffness (or conductivity, or other analogous quantity) by a severe reduction factor. This factor is set to 10^{-6} by default, but can be given other values. For this purpose the magnitude of stiffness values of the removed element is decreased to 10^{-6} of its initial magnitude.

After simulation of the hole-drilling process, the software calculates the released strains on the hole region under the area of the strain gages. The strains for each strain gage are averaged from the magnitude of the strains on the Gauss points, under the area of the strain gage. Using this method, the calibration constants are calculated and compared with the available data in the standards. Also by using the ASTM standard, the calibration constants for a through-the-thickness hole are available (ASTM E837-01, 1999). In Table 4.1, the strains obtained by the simulation central hole-drilling (SCHD) method and the standard

Table 4.1 A comparison between the strains obtained by the SCHD method and the standard

	ASTM		SCHD				
D_0/D	A	B	A	B	ASTM μm/m	SCHD μm/m	Error %
0.30	0.089	0.278	0.0891	0.2784	19.69	19.71	0.10
0.35	0.121	0.364	0.1211	0.3642	26.07	26.08	0.07
0.40	0.158	0.454	0.1582	0.4541	32.97	32.99	0.06
0.45	0.200	0.544	0.2002	0.5438	40.20	40.21	0.02
0.50	0.247	0.629	0.2481	0.6303	47.51	47.64	0.27

are compared. A comparison of the calibration factors obtained by the standard method and the SCHD method (Table 4.1) shows that these magnitudes are very near to each other and the percentage of error is very small. In Table 4.1, the strains measured by the SCHD method are also compared with those measured by the standard calibration factors. The small differences between these magnitudes confirm the accuracy of the proposed model.

By considering that the rosette is attached to the surface of the specimen, the variation of the strain due to the hole-drilling process should be monitored on the surface. After the first step of the drilling, the released strains in the next step are influenced by the existing residual stresses in the depth of the specimen and the variation of the geometry of the hole. Therefore, even if the new depth of the hole is free of stress, the process of strain releasing would be continued.

For three-dimensional (3D) simulation of the hole-drilling process in isotropic materials, the 3D 20-node solid element (Solid86) is used. The location of the drilling with a diameter of 2.052 mm (0.4D) is meshed. Specimens with three different thicknesses of 1, 1.5 and 2 mm were modeled. A uni-axial stress equal to 20 MPa was applied to the specimens as the residual stress. Figure 4.6 shows the distribution of the released strain in the direction of the applied load for the specimen. The thickness of the specimen in this case is equal to the hole diameter (2 mm).

In order to find the released strain under the strain gages, the strains for all nodes of all elements under the strain gages were averaged. For instance, based on the ASTM standard, the strain along the load direction measured by one strain gage in that direction is equal to 32.97 μm/m. The released strains for three specimens with three different thicknesses are simulated by the SCHD method and compared with those available by the ASTM standard (ASTM E837-01, 1999) (Table 4.2). The results show that there is a good agreement between the two methods. The maximum error obtained for the 3D case is equal to 5.6%, for the case of thickness equal to the hole diameter. As shown in

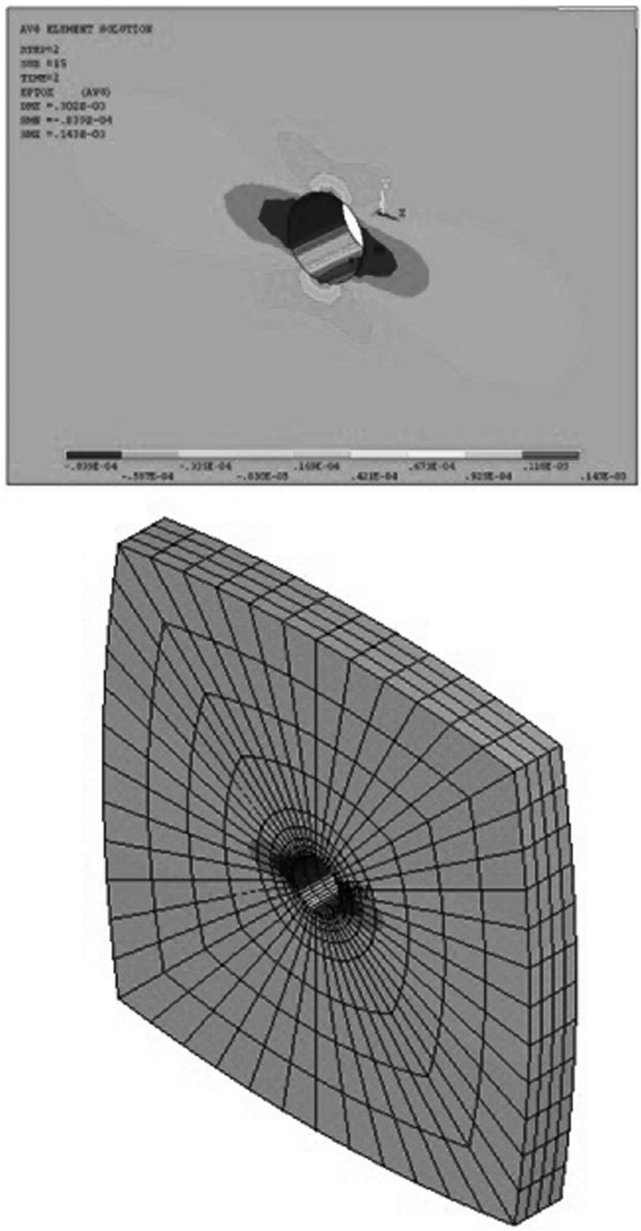

4.6 Distribution of the released strain in the direction of the applied load for the specimen (thickness = hole diameter).

Table 4.2 The released strains obtained by three-dimensional SCHD compared with the ASTM standard

Thickness (mm)	Strain (μm/m) (ASTM)	Strain (μm/m) (SCHD)	Error %
1.0	32.97	33.55	1.7
1.5	32.97	34.14	3.5
2.0	32.97	34.81	5.6

the table, while the ASTM standard predicts similar residual stresses for all thicknesses, the SCHD method predicts different residual stresses for different thicknesses.

4.3 The hole-drilling method in orthotropic materials

4.3.1 Theory

For plane stress conditions of orthotropic materials, five elastic constants (E_x, E_y, G_{xy}, ν_{xy}, ν_{yx}) are needed to relate strains to the stresses. E_x and E_y are the longitudinal and transverse stiffness, G_{xy} is the in-plane shear stiffness, and ν_{xy} and ν_{yx} are the Poisson's ratios. Where the x- and y-coordinate axes are the material axes, then the generalized Hookes law is

$$\begin{aligned}\varepsilon_x &= \frac{\sigma_x}{E_x} - \nu_{xy}\frac{\sigma_y}{E_y}\\ \varepsilon_y &= \frac{\sigma_y}{E_y} - \nu_{yx}\frac{\sigma_x}{E_x}\\ \gamma_{xy} &= \frac{\tau_{xy}}{G_{xy}}\end{aligned} \qquad [4.10]$$

Only four of the five elastic constants are independent, because of the following elastic symmetry relationship:

$$\frac{\nu_{xy}}{E_x} = \frac{\nu_{yx}}{E_y} \qquad [4.11]$$

Orthotropic materials in 3D cases have nine elastic constants, of which eight are independent. These materials also have three symmetrical planes. For isotropic materials, $E_x = E_y = E$, $\nu_{xy} = \nu_{yx} = \nu$ and $G_{xy} = G = E/[2(1+\nu)]$. Therefore, isotropic materials have only two independent elastic constants.

The central hole-drilling method is also used for orthotropic materials. A simple assumption for calculation of strains in the hole-drilling method is that the released strains for orthotropic materials are similar to those of the isotopic materials

trigonometrically (Bert and Thompson, 1968; Lake *et al.*, 1970; Prasad *et al.*, 1987a,b). Therefore, it is assumed that Eq. 4.7 is still valid and the strain gages 1 and 3 are in the symmetrical directions of the orthotropic materials. In this case, all calibration constants (A, B and C) are independent.

It was shown (Schajer and Yang, 1994; Shokrieh and Kamali, 2005; Shokrieh and Ghasemi, 2007) that equation $C=2B$ is not valid for orthotropic materials. By assuming a homogeneous continuity of the microstructure of orthotropic materials and using the equations of the released displacements, the relationship between the residual stresses and the released strains around the hole was shown. Increasing the orthotropy behavior of the materials leads to more deviation from Eq. 4.7. For better correlation of the residual stresses and the released strains in orthotropic materials, nine calibration factors are defined. These calibration factors can be found by closed form, numerical and experimental methods. In order to relate the released strains to the stresses, the following equation is used:

$$\frac{1}{\sqrt{E_X E_Y}}\begin{bmatrix} C_{11} & C_{12} & C_{13} \\ C_{21} & C_{22} & C_{23} \\ C_{31} & C_{32} & C_{33} \end{bmatrix}\begin{Bmatrix} \sigma_{11} \\ \sigma_{12} \\ \sigma_{22} \end{Bmatrix} = \begin{Bmatrix} \varepsilon_1 \\ \varepsilon_2 \\ \varepsilon_3 \end{Bmatrix} \qquad [4.12]$$

in which the compliances C_{ij} are independent of the trigonometric constants A, B and C. The term $\frac{1}{\sqrt{E_X E_Y}}$ is used in Eq. 4.12, in order to make the compliance terms (C_{ij}) non-dimensional. If x and y are the principal elastic directions of the orthotropic material, then the terms C_{12} and C_{32} are zero.

The elastic coefficients in Eq. 4.12 are dependent on the orthotropic material properties of the sample, depth of the hole and the geometry of the strain gage. The holes depth effect for an orthotropic material is dependent on the ratio of the out-of-plane shear modulus to the in-plane longitudinal stiffness of the material. Decreasing this ratio leads to decreasing the effective depth of the hole.

In order to calculate the calibration coefficients C_{11}, C_{21} and C_{31}, load was applied in the longitudinal direction, and also load was applied in the transverse direction to calculate calibration coefficients C_{13}, C_{23} and C_{33}. Moreover, by applying the in-plane shear load, calibration coefficients C_{12}, C_{22} and C_{32} were calculated. In the following section, these three groups of calibration coefficients are calculated by simulation method.

4.3.2 Simulation

In order to simulate the central hole-drilling process for orthotropic materials, ANSYS finite element software was employed. For an orthotropic material with the dimensions of 150 mm by 150 mm, the location of the strain gage and the hole

are modeled. The type of the element used is a second-order eight-node Plane82 solid element. The number of elements for the two-dimensional (2D) modeling is 2054 and for the meshing of the area under the strain gages, 9 elements are used. After applying the initial stress as the residual stress, in order to simulate the hole-drilling process, the elements in the area of the strain gage are removed. By knowing the magnitude of the initial stress applied to the specimen and the released strain on the strain gage area, the calibration coefficients are calculated. The strain in each direction is calculated by averaging the strains on element Gaussian points under the strain gage area.

After applying the initial stress (as residual stress) to the plate, the first load step was run and strains in the three strain gages were measured. For this purpose, the strains in all the elements within the strain gage areas were calculated and averaged. These were the strains without drilling of a hole. Subsequently, a hole was introduced in the model geometry. In order to simulate the hole-drilling process in ANSYS, the elements under the area of the hole must be removed. To achieve this element elimination effect in ANSYS, elements were not deleted. Instead the concept of 'Element Death' was implemented by 'Killing' the elements. ANSYS kills the elements by multiplying their stiffness values by a severe reduction factor (10^{-6} in this case). The elements thus 'killed' acted as deleted elements in the structure. After introducing the hole, the second load step was run and strains were calculated in strain gage areas with the hole drilled. The difference in the recorded strains of respective gages during first and second steps resulted in relieved strains due to drilling of hole.

In order to calculate the coefficients of Eq. 4.12 for orthotropic materials, first the model is loaded in the first principal direction (i.e. longitudinal direction). Then the hole-drilling process is simulated and the strains for all three strain gages are calculated and averaged for each gage. Then the model is loaded in the second principal direction (i.e. transverse direction) and the previous process is repeated. Finally, a shear stress is applied to the model and again the whole process is repeated. By changing the mechanical properties of the model, the mentioned modeling process is repeated. In Fig. 4.7, the stress distributions in the x- and y-directions due to the applied shear stress on the model are presented.

For calculation of the coefficient matrix, it was assumed that the plane stress condition existed and a uni-axial stress was applied to a uni-directional composite ply. In this case, the stress distribution in the thickness of the sample is uniform. In order to remove the elements in the area of the hole, their stiffness is reduced by a factor of 10^{-6}. In order to calculate the compliance coefficients C_{11}, C_{21} and C_{31}, a simulation of the tensile test, by applying a known stress in the direction of strain gage No. 1, is performed. Strain gages No. 1, 2 and 3 are located in the fiber direction, matrix direction, and at 45 degrees with respect to the fiber direction, respectively (Fig. 4.8).

By calculating the released strains ε_1, ε_2 and ε_3, using the finite element method, and applying Eq. 4.12, compliance coefficients C_{11}, C_{21} and C_{31} are calculated as

$$\sigma_{11} = \sigma, \qquad \sigma_{22} = \sigma_{12} = 0$$

$$C_{11} = \sqrt{E_x E_y}\,\frac{\varepsilon_1}{\sigma}, \qquad C_{21} = \sqrt{E_x E_y}\,\frac{\varepsilon_2}{\sigma}, \qquad C_{31} = \sqrt{E_x E_y}\,\frac{\varepsilon_3}{\sigma} \qquad [4.13]$$

Again, in order to calculate the compliance coefficients C_{13}, C_{23} and C_{33}, a simulation of the tensile test by applying a known stress in the direction of the strain gage No. 3 is performed (Fig. 4.9).

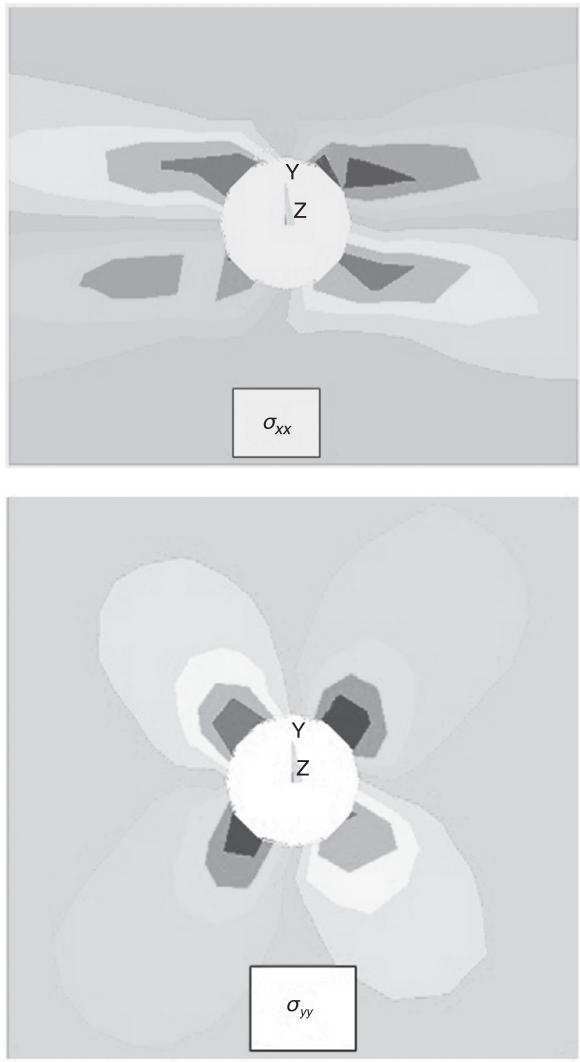

4.7 Stress distribution of an orthotropic material due to hole drilling by applying shear stress: (a) stress in fiber direction, σ_{xx} and (b) stress perpendicular to fiber direction, σ_{yy}.

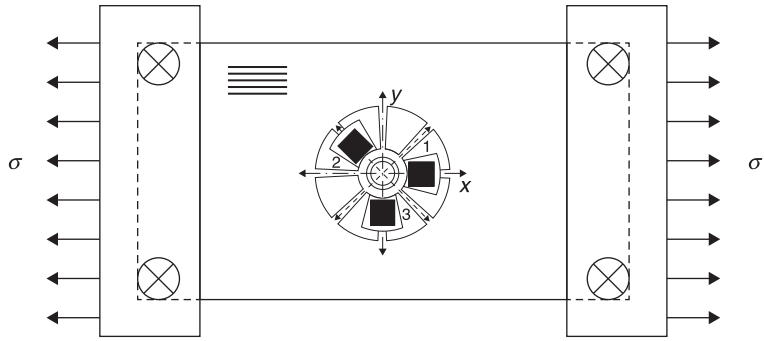

4.8 Simulation of loading in fiber direction for calculation of coefficients C_{11}, C_{21} and C_{31}.

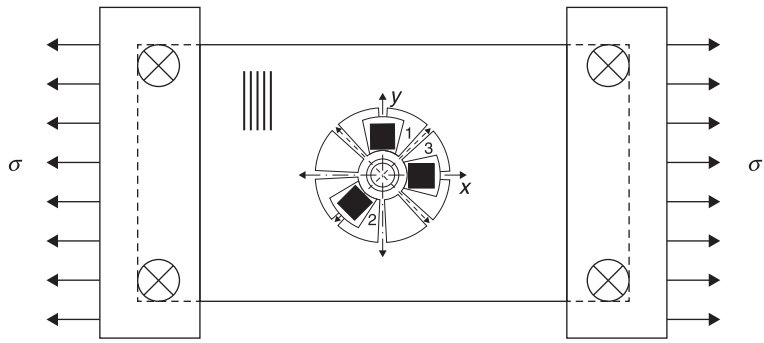

4.9 Simulation of loading in transverse direction for calculation of coefficients C_{13}, C_{23} and C_{33}.

By calculating the released strains ε_1, ε_2 and ε_3, using the finite element method, and applying Eq. 4.12, compliance coefficients C_{13}, C_{23} and C_{33} are calculated as

$$\sigma_{22} = \sigma, \qquad \sigma_{11} = \sigma_{12} = 0$$

$$C_{13} = \sqrt{E_x E_y}\,\frac{\varepsilon_1}{\sigma}, \qquad C_{23} = \sqrt{E_x E_y}\,\frac{\varepsilon_2}{\sigma}, \qquad C_{33} = \sqrt{E_x E_y}\,\frac{\varepsilon_3}{\sigma} \qquad [4.14]$$

Finally, in order to calculate the compliance coefficient C_{22}, a simulation of the shear test is performed by applying a known shear stress to the specimen (Fig. 4.10).

By calculating the released strains ε_2, using the finite element method and applying Eq. 4.12, compliance coefficient C_{22} is calculated as

$$\sigma_{12} = \sigma, \qquad \sigma_{11} = \sigma_{22} = 0$$

$$C_{12} = 0, \qquad C_{22} = \sqrt{E_x E_y}\,\frac{\varepsilon_2}{\sigma}, \qquad C_{32} = 0 \qquad [4.15]$$

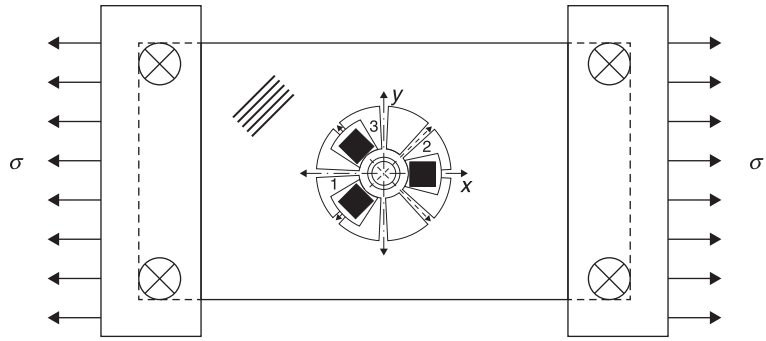

4.10 Simulation of shear test or loading in 45-degree direction for calculation of coefficient C_{22}.

In order to study the variation of calibration factors with respect to the variation of normal and shear modulus of elasticity, a fixed Poisson's ratio equal to 0.25 is considered and the magnitudes of both modulus were changed. Using the SCHD method, the coefficient matrix was obtained. In Table 4.3, the results obtained by the SCHD method for a constant Poisson's ratio are summarized. In order to study the variation of the Poisson's ratio, the modulus of elasticity in two directions (x and y) are assumed to be constant and equal ($E_x = E_y$). The ratio of the

Table 4.3 Results obtained by the SCHD method for a Poisson's ratio of $\upsilon = 0.25$

E_x/E_y	G_{xy}/E_y	C_{11}	C_{13}	C_{21}	C_{22}	C_{23}	C_{31}	C_{33}
1	0.1	−0.567	0.115	−0.316	1.045	−0.316	0.115	−0.567
1	0.2	−0.489	0.137	−0.205	0.755	−0.205	0.138	−0.490
1	0.3	−0.449	0.149	−0.159	0.640	−0.159	0.149	−0.449
1	0.4	−0.423	0.156	−0.133	0.577	−0.133	0.156	−0.423
2	0.15	−0.436	0.114	−0.247	1.047	−0.359	0.144	−0.719
2	0.30	−0.385	0.138	−0.159	0.771	−0.232	0.166	−0.607
2	0.45	−0.359	0.150	−0.124	0.662	−0.181	0.176	−0.551
2	0.60	−0.342	0.158	−0.104	0.602	−0.152	0.183	−0.516
4	0.20	−0.338	0.106	−0.204	1.120	−0.444	0.162	−0.922
4	0.40	−0.305	0.130	−0.131	0.833	−0.289	0.183	−0.762
4	0.60	−0.288	0.142	−0.101	0.720	−0.227	0.192	−0.683
4	0.80	−0.277	0.150	−0.084	0.659	−0.193	0.198	−0.635
8	0.30	−0.254	0.100	−0.152	1.146	−0.511	0.179	−1.129
8	0.60	−0.235	0.122	−0.096	0.871	−0.340	0.197	−0.913
8	0.90	−0.224	0.133	−0.073	0.765	−0.272	0.204	−0.811
8	1.20	−0.217	0.140	−0.060	0.707	−0.235	0.208	−0.749
16	0.40	−0.193	0.088	−0.119	1.253	−0.634	0.187	−1.416
16	0.80	−0.181	0.108	−0.072	0.964	−0.430	0.202	−1.121
16	1.20	−0.174	0.118	−0.053	0.853	−0.350	0.208	−0.983
16	1.60	−0.170	0.125	−0.043	0.792	−0.307	0.211	−0.901

Table 4.4 Results obtained by the SCHD method for $E_x = E_y$ and $G_{xy}/E_x = 0.1$ and varying Poisson's ratio

υ_{xy}	C_{11}	C_{22}	C_{21}	C_{13}
0	−0.574	0.161	−0.295	1.128
0.25	−0.567	0.115	−0.316	1.045
0.50	−0.559	0.068	−0.336	0.961
0.75	−0.550	0.020	−0.355	0.877

shear modulus to the normal modulus is assumed to be 0.1 ($G_{xy}/E_x = 0.1$). In Table 4.4, the results obtained by the SCHD method are summarized.

The deviation of the released strains of an orthotropic material from the trigonometry behavior of Eq. 4.7 is shown by the following numerical example. Consider an orthotropic material with $E_x = 200\,\text{GPa}$, $E_y = 50\,\text{GPa}$, $G_{xy} = 40\,\text{GPa}$ and $\upsilon_{xy} = 0.25$. Using the SCHD method, the coefficient matrix is obtained as

$$\begin{bmatrix} C_{11} & C_{12} & C_{13} \\ C_{21} & C_{22} & C_{23} \\ C_{31} & C_{32} & C_{33} \end{bmatrix} = \begin{bmatrix} -0.277 & 0 & 0.150 \\ -0.084 & 0.659 & -0.193 \\ 0.198 & 0 & -0.635 \end{bmatrix} \quad [4.16]$$

For isotropic materials, in Eq. 4.8, $C_{11} = C_{33}$, $C_{21} = C_{23} = (C_{11} + C_{31})/2 = (C_{13} + C_{33})/2$ and $C_{13} = C_{31}$. Note that Eq. 4.16 does not show these relations for an orthotropic material.

Another example that shows the deviation of the released strains of an orthotropic material from the existing equation for an isotropic material, is the different behavior of the orthotropic material in different directions. For instance, suppose a tensile load is applied in the principal elastic direction of an orthotropic material ($\sigma_x = 1$, $\sigma_y = \tau_{xy} = 0$). Then, by the SCHD method, the following results are obtained: $A = (C_{11} + C_{31})/2 = -0.0395$, and $B = (C_{11} - C_{31})/2 = -0.2375$. Whereas, if a tensile load is applied in the normal direction of the principal elastic direction of an orthotropic material ($\sigma_y = 1$, $\sigma_x = \tau_{xy} = 0$), then by the SCHD method, the following results would be obtained: $A = (C_{33} + C_{13})/2 = -0.2425$ and $B = (C_{33} - C_{13})/2 = -0.3925$. These results show another deviation of the released strains of an orthotropic material from the trigonometry behavior of Eq. 4.7.

4.4 The hole-drilling method in laminated composites

4.4.1 Theory

The central hole-drilling method can be improved to predict intensity and signs of stress deep into the materials. The incremental hole-drilling method is

recommended to achieve the non-uniform distribution of stress deep inside the isotropic materials. In order to determine the stress non-uniform distribution at depth, in the incremental hole-drilling method, first (similar to the central drilling method) the rosette strain-gage is installed at the sample level. By gradually increasing the depth of the hole, which is generated in the rosette center, the strains released are read in equal gaps. Then the stresses that existed at each increment of the depth of the hole would be calculated. It was presumed that the strain released at each step has totally been due to the stress in the same step of the depth of the hole. For each step of the depth, different calibration factors must be applied to get correct results. The calibration factors normally are determined analytically, numerically or experimentally per step of the hole depth.

Generation of a hole on a plane, where the residual stresses are confined, results in releasing of residual stresses around the hole. The residual stresses released are expressed through the differentiated distribution of residual stresses on the plane before and after establishment of such hole. Thus, presuming the elastic release of the strains, the difference between the planes, strains after drilling and strains of the same plate prior to the drilling, indicates the released strains. Using the superposition principle, and applying equal and opposite stress distribution in the sample, the strains released shall be equal to the strains measured by the hole-drilling method.

The calibration factors convert the measured strains to the residual stresses in the part sampled. Such factors are obtained using the theoretical, numerical and experimental methods. Such factors are independent of the loading and may be used in a real test to determine the residual stresses. The condition of force balance is a logical and essential condition for the residual stresses confined in a structure, including metals or composites. Stress non-uniformity at the thickness of the laminated composites requires development of the incremental hole-drilling method in the composites.

Notwithstanding the popularity of this method, there are important theoretical defects associated with the same. The presumption that the strain released per step totally belongs to the residual stresses of the same phase is not valid. After completion of the first phase, the strain released at the next phase is affected by two factors:

1. residual stresses in such depth; and
2. change of the holes geometry.

Changing of the hole geometry provides the possibility of more released strains to the sample in comparison with the previous phases (Schajer, 1988). Thus, even if the new hole depth is totally free from stress, by increasing the depth, releasing strains would be continued. In addition, according to the Saint–Venant principle, the strain responses on the surface become rapidly insensitive to the released internal stresses deep into the sampled part. Hence, the major

error that may have appeared in such method is due to the physical limitations in the incremental hole-drilling method. In the central and incremental hole-drilling method, the rosette is attached on the samples surface and the strains on the parts surface are read, while the non-uniform stresses are deep into the sample.

In this part of the sample, the matrix relation Eq. 4.12 was developed to consider the stress and strain relationship for each step of the incremental hole-drilling process. Equation 4.12 for the single layer is expressed as

$$C_{ij}\sigma_j = \varepsilon_i \qquad i,j = 1,2,3 \qquad [4.17]$$

It is important to note that whenever progress in depth of each step is equal to the thickness of one layer of the laminate, the released strains due to the drilling of each layer should be proportional to the residual stresses confined in such layer. However, generally, released strains of each layer is a function of strains and vertical position (depth) of that layer, thus increase in the depth of the laminate during the incremental hole-drilling process must be accounted for in the calculations.

The strain changes at each layer of the laminated composite due to the incremental hole-drilling may be expressed as

$$(C_{ij})_{mn} * (\sigma_j)_n = (\varepsilon_i)_{tm} \qquad i,j = 1,2,3,\ 1 \le n \le m \qquad [4.18]$$

where n denotes the position of each layer at the laminated composite, and m denotes the step of drilling at the incremental hole-drilling of a laminated composite. The index 't' denotes the total of the released strains per step. By removing each layer at the incremental hole-drilling method, the total strains released on the surface are changed. The strains measured at each step are indicated by $(\varepsilon_i)_{tm}$, where i denotes the number of each of the three strain-gages of the rosette. $(\sigma_j)_n$ denotes the plane stresses of each orthotropic layer, and $(C_{ij})_{mn}$ denotes the calibration factors.

Using the calibration factors at each step of drilling, Eq. 4.18 may be extended for consecutive drilling of the layers per laminated composites. For instance, for a four-layered composite, we have

$$\begin{aligned}
&(C_{ij})_{11}.(\sigma_j)_1 = (\varepsilon_i)_{t1} && \text{first layer}\\
&(C_{ij})_{21}.(\sigma_j)_1 + (C_{ij})_{22}.(\sigma_j)_2 = (\varepsilon_i)_{t2} && \text{second layer}\\
&(C_{ij})_{31}.(\sigma_j)_1 + (C_{ij})_{32}.(\sigma_j)_2 + (C_{ij})_{33}.(\sigma_j)_3 = (\varepsilon_i)_{t3} && \text{third layer}\\
&(C_{ij})_{41}.(\sigma_j)_1 + (C_{ij})_{42}.(\sigma_j)_2 + (C_{ij})_{43}.(\sigma_j)_3 + (C_{ij})_{44}.(\sigma_j)_4 = (\varepsilon_i)_{t4} && \text{fourth layer}
\end{aligned} \qquad [4.19]$$

In the incremental hole-drilling process simulation, for each $(C_{ij})_{mn}$ matrix factor, apart from m and n values, loading are applied in x-, y- and x-y-directions for each layer.

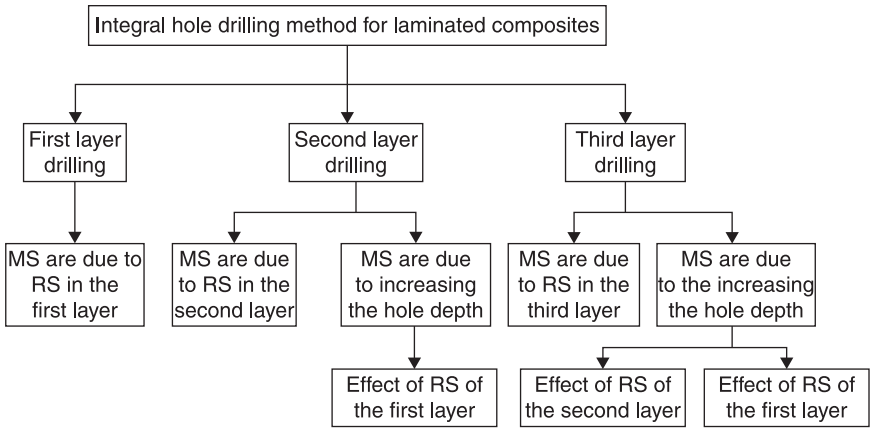

4.11 Relation between measured strains and residual stresses in the integral hole-drilling method (MS: measured strains; RS: residual stresses).

Three steps of the incremental hole-drilling modeling of a laminated composite and their associated calibration factor matrices are shown in Fig. 4.11. At the first step of incremental hole-drilling, the first layer is drilled and then strains released from the same layer due to the residual stresses of the first layer are measured. At the second step, the second layer is drilled and the released strains may be classified into two groups: the strains released due to hole depth increase, which are associated to the $(C_{ij})_{21}$ matrix and the strains resulted from the second layer residual stresses, which are proportional to the $(C_{ij})_{22}$ matrix. By increasing the hole depth via drilling the third layer, the strains released due to the depth increase are classified into two groups:

1. the effect of the first layer stresses on the third step strains as $(C_{ij})_{31}$; and
2. the effect of the second layer stresses on the third step strains as $(C_{ij})_{32}$.

Also, the effect of the residual stresses confined in the third layer is shown by the $(C_{ij})_{33}$ matrix. The effect of the depth increase on calculation of the residual stresses in other lower layers may also be expressed in the same above-mentioned manner.

4.4.2 Simulation

In order to determine the calibration factor values of the incremental hole-drilling method in laminated composites, a computer program has been written and developed, using the ANSYS finite element method to simulate the integral hole-drilling process. The results of this program will be used to calculate the residual

stresses in laminated composites. In modeling of each sample, apart from suitability of the elements shapes, the number of the elements has also been optimized in this model.

The laminated composites are modeled in ANSYS software using the Solid46 3D element, and the Surf154 3D structural element has been used to apply pressure to the hole walls. Three steps of the simulation of hole-drilling modeling of a laminated composite are shown in Fig. 4.12. The installed rosette on the surface of the part measures the strains released per step, which is denoted by $(\varepsilon_i)_{tm}$.

The incremental calibration factors together with the progressive solution would convert the measured strains to the residual stresses confined at each layer. Using Eq. 4.19, the strains resulted from the residual stresses confined in each layer can be calculated. For instance, in the drilling of the third layer we may have

$$\begin{aligned}(C_{ij})_{33}.(\sigma_j)_3 &= (\varepsilon_i)_{t3} - (C_{ij})_{31}.(\sigma_j)_1 - (C_{ij})_{32}.(\sigma_j)_2 \\ (C_{ij})_{33}.(\sigma_j)_3 &= (\varepsilon_i)_{t3} - (\varepsilon_i)_{31} - (\varepsilon_i)_{32}\end{aligned} \qquad [4.20]$$

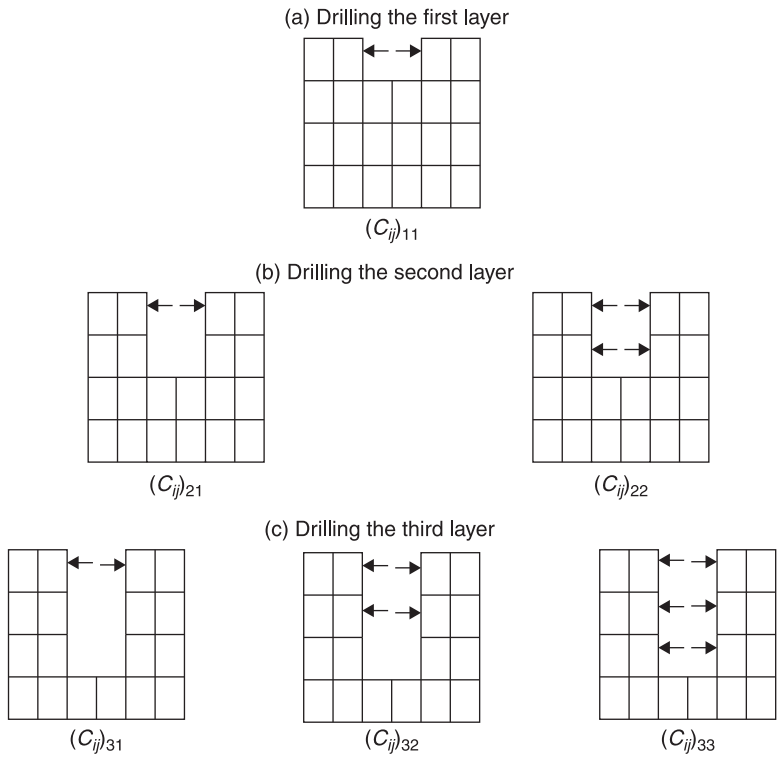

4.12 Three stages of drilling a composite laminate.

Thus, the residual strains resulted from the residual stresses confined in each layer may be separated from the total strains measured on the surface by rosette using the following relation:

$$(\varepsilon_i)_m = (\varepsilon_i)_{tm} - \sum_{n=1}^{n=m-1} \left(\varepsilon_i\right)_{mn} \quad [4.21]$$

where $(\varepsilon_i)_{tm}$ is the total of the strains measured on the surface at the mth drilling step, and $\sum_{n=1}^{m-1}\left(\varepsilon_i\right)_{mn}$ is that part of the strain released due to the hole's changed geometry. In other words, $(\varepsilon_i)_{mn}$ will be the share of the upper layers in the released strains due to the removal of the last layer and $(\varepsilon_i)_m$ denotes the strains measured resulting from the residual stresses confined in each layer. Thus, the residual strains in each layer may be expressed by $(\varepsilon_i)_m$.

However, in the given method, the effect of the geometrical changes and the residual strains of each layer have been considered as separate and continuous. Because of the similarity of this method to the integral method of isotropic materials, hereafter this method will be referred to as the integral hole-drilling method of the laminated composite materials. In such a method, in order to determine calibration coefficients, the effect of hole depth increase, direction and position of each layer, elastic properties, residual stresses confined in each layer and the effect of the upper layers residual stresses, have all been considered.

It should be mentioned that in Fig. 4.12, for better illustration of the hole-drilling steps, the measurement scale for the hole diameter and the depth have not been chosen equally. Also such a process has been shown in three steps of hole-drilling for a laminated composite. The aforementioned process may be continued for all the internal layers in laminated composites with more thickness and layers. Whereas the strain responses on the part surface rapidly become insensitive with respect to the effects of the internal stresses deep in the part, the final limit of the hole depth in the hole-drilling method will be approximately equal to the hole's diameter. Thus, major errors may appear in this method due to the physical limitations of the hole-drilling test method. Hence, the above-mentioned process may be repeated for the laminated composites up to a depth equal to the hole diameter.

4.5 Key issues in using the hole-drilling method

4.5.1 Specimen preparation and test set-up

The simulated central hole-drilling (SCHD) method in isotropic and orthotropic materials has been described in the preceding sections. By developing the simulated method in laminated composites, the simulated incremental hole-drilling (SIHD) process in laminated composite materials was performed. In this section, the residual stresses in the depth of laminated composites will be

Table 4.5 Elastic constants of glass/epoxy uni-directional ply

E_x (GPa)	E_y (GPa)	G_{xy} (GPa)	V_{xy}	α_x (μ/°C)	α_y (μ/°C)
25	9	4.8	0.26	5.4	26

determined by using the calibration factors obtained from the SIHD process in the laminated composites. In order to complete the incremental hole-drilling operations and compare the results, several experimental specimens with cross-ply and quasi-isotropic configurations were considered. Glass/epoxy specimens, with properties mentioned in Table 4.5, in sizes of 15 by 15 cm have been made by the hand lay-up method. During manufacturing, the vacuum bagging technique was used to uniformly distribute resin and remove excess resin in the presence of heat. All specimens were cured under a temperature of 120 °C for 10 hours. The thickness of each layer was 0.2 mm and the thickness of the specimens were 1.6 ± 0.1 mm, with a fiber volume fraction of $\upsilon_F = 60\%$.

According to ASTM standards, surface preparation will induce a significant residual stress in the pieces (ASTM E837-01, 1999). Thus, the surface of the specimen was polished with sandpaper No. 600, and acetone was used to clean grease and superfluous particles from the surface of the piece. Finally, the rosette-type strain gage was installed on the sample's surface precisely where the rosette strain gages No. 1 and 3 were located in the fibers and matrix directions, respectively. An eight-channel UPC601 unit (made by Validyne Co.) was employed to measure released strains during the hole-drilling process. The experiments were performed in a temperature and humidity controlled room. The temperature compensation circuit was not used, as there was no variation in the ambient and sample surface temperatures. The input voltage of the I/O card was equivalent to 4 V and the 6-wire strain gage input method (Fig. 4.13) has been used to connect the circuit of strain gages in the Watson bridge to consider the exact voltage of each circuit. Table 4.6 shows the specifications of the strain gages used in this experiment, which were produced by TML Co. A cyanoacrylate-type liquid glue, with trade name of CN, was used for attaching the strain gages to the specimen surface.

At the start of the hole-drilling process, the data acquisition system was activated and the exact voltage applied to the Watson bridge, with the strain values

Table 4.6 Strain gage rosette characterization

Type	Gage length	Gage factor	Gage resistance	Transverse sensitivity	Test condition
FRS - 2	1.5 mm	2.08	120 ± 0.5 Ohms	0.9%	23 °C, 50% RH

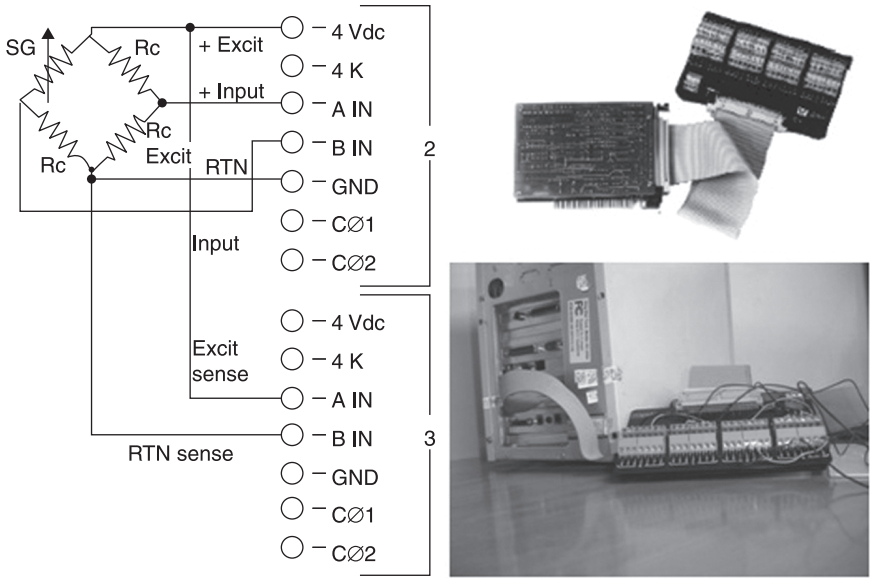

4.13 UPC601 and Watson bridge circuit.

at each step being recorded. The relation between output voltage variations of the Watson bridge and the released strains are expressed by Eq. 4.22. In this relation, E is input voltage in the Watson bridge and Δe represents the output voltage variations. K is the strain gage factor (gage factor) and ε is the strain released:

$$\Delta e = \frac{E}{4} K\varepsilon \qquad [4.22]$$

Various methods have been used to perforate the specimens (Flaman and Herring, 1985; Flaman *et al.*, 1987; Flaman and Boag, 1990; Andersen, 2002). Flaman and Herring (1985) used the high speed turbine and carbide milling blades to measure the residual stresses. Andersen (2002) used the normal milling method on thick isotropic samples, regardless of its effect on the measurement precision of the strains released in his study. He indicated that the normal hole-drilling method could be used to calculate the residual stresses deep in the specimens, with no effect on the accuracy of the measurements. The hole-drilling of multi-layer composites at a milling speed of 5000 rpm and a feed rate of 10 μm per second has been performed by Sicot *et al.* (2003).

The hole drilling of multi-layer composites were carried out using a high speed CNC milling machine during this investigation (Fig. 4.14). This machine enabled researchers to perform the hole-drilling process at a constant speed and feed rate and measure the released strains of each separate layer precisely. Furthermore, despite rotational motion of the drill, there was the possibility of stopping the

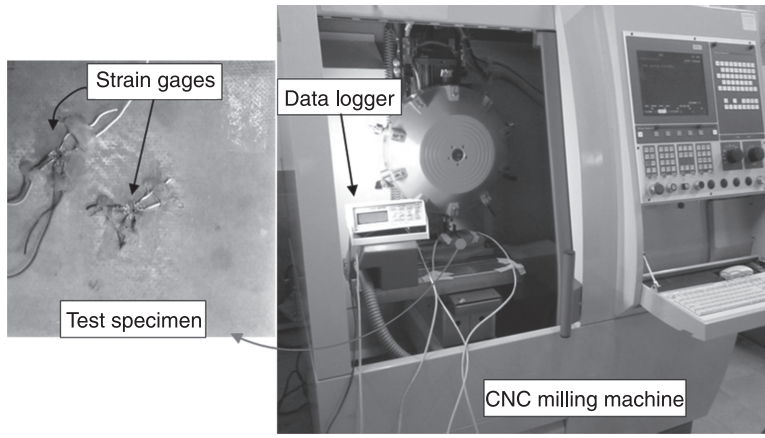

4.14 Incremental hole-drilling test set-up.

machine feed rate during the hole-drilling operation at each step. A drilling speed of 8000 rpm was used during this research. The end mill drilling used in this research was made of carbon with 1.5 mm diameter. During the incremental hole-drilling process, a considerable time gap was left between each drilling increment to enable the released strains of each step to become stable and be recorded. During each drilling step, the average of the recorded strains was considered as the representative of released strains of the layer in question.

4.5.2 Measurement of released strains

Symmetrical cross-ply samples, $[0_2/90_2]_S$

Due to the lay-up symmetry in the symmetrical cross-ply laminates, only half of the thickness of the specimens was perforated at the center of the rosette strain gage and released strains were recorded. The released strains were converted to the residual stresses using the calibration factors matrices. The released strains due to the perforation of a symmetrical cross-ply sample are shown in Fig. 4.15. In the figure, numbers 1, 3, 5 and 7 represent the hole-drilling steps, and steps 2, 4, 6 and 8 are the strain relaxation times when the feed rate was zero and drilling was stopped.

As shown in Fig. 4.15, during the hole-drilling period, the released strains were fluctuating, while during the time of strain releasing, the released strains reached a relatively stable value and variations became damped. In this study, the average value of the released strains, which were recorded during strain releasing times, was taken as the average of the released strains of each layer in the laminate. The horizontal axis in Fig. 4.15 illustrates the drilling and strain releasing times and steps.

During the hole-drilling process of cross-ply samples, the attached strain gage in a zero direction recorded an increasing and a decreasing released strain during

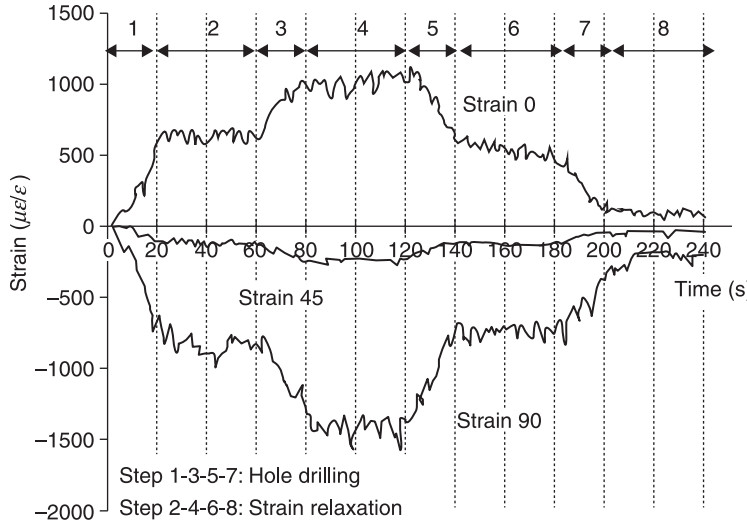

4.15 Incremental hole-drilling and released strains of cross-ply laminate, $[0_2/90_2]_S$.

perforation of 0-degree and 90-degree plies, respectively. The hole-drilling behavior of cross-ply laminates were reversed in strain gages installed in a 90-degree direction (Fig. 4.15). The 90-degree installed strain gage showed a decreasing released strain in the first two steps, which is continued with an increasing released strain in the last two steps. The third strain gage, which was installed in a 45-degree direction, recorded a decreasing released strain during drilling of 0-degree plies, which was followed with an increasing released strain during drilling of 90-degree plies. However, strain variations in this strain gages are almost negligible in comparison with the other strain gages. Five specimens were tested and the same pattern was observed during incremental hole-drilling process. The average of the recorded data from five specimens in each step was presented as the average value of the released strain (Table 4.7). Data presented in the table will later be used to calculate the residual stress of each layer.

Table 4.7 Average value of released strains of symmetric cross-ply laminates $[0_2/90_2]_S$ ($\mu\varepsilon$)

	Average released strain value			
Gage direction	First layer	Second layer	Third layer	Fourth layer
0-degree	629	1003	542	122
45-degree	–140	–245	–142	–65
90-degree	–850	–1367	–770	–149

Asymmetrical cross ply samples, [$0_4/90_4$]

Asymmetrical composite laminates deform from the flat state during the curing process. According to the 'Classical Lamination Plate Theory' (CLPT), the cured shape of asymmetrical laminates should always be saddle-like, because while considering parameters such as specimen lengths and cure temperatures, they may lead to two cylindrical shapes. The cured shape of the composite shells is mainly dependent on the stacking sequences, mold radius, layer thickness and cure temperature. During the experiment of asymmetrical samples due to out-of plane deformations, variation in the value of recorded released strains was more than that observed for symmetrical laminates.

In order to determine the non-uniform residual stresses in the thickness of asymmetrical laminate, we need to perform the hole-drilling process in all layers of the laminate. The depth of the hole-drilling process in asymmetrical cross-ply [$0_4/90_4$] samples at each step was equal to two-layers thickness and thus the number of hole-drilling steps was limited to four steps. The released strains due to the hole-drilling of the asymmetrical cross-ply laminate are shown in Fig. 4.16. During the drilling of asymmetrical cross-ply laminate, the strain gage installed in the 0-direction recorded a decreasing strain during drilling of the first two layers, which continued to increase to a positive value during drilling of the third and fourth layers. Subsequently, released strains remained negative during drilling of the 90-degree layers. The strain gage

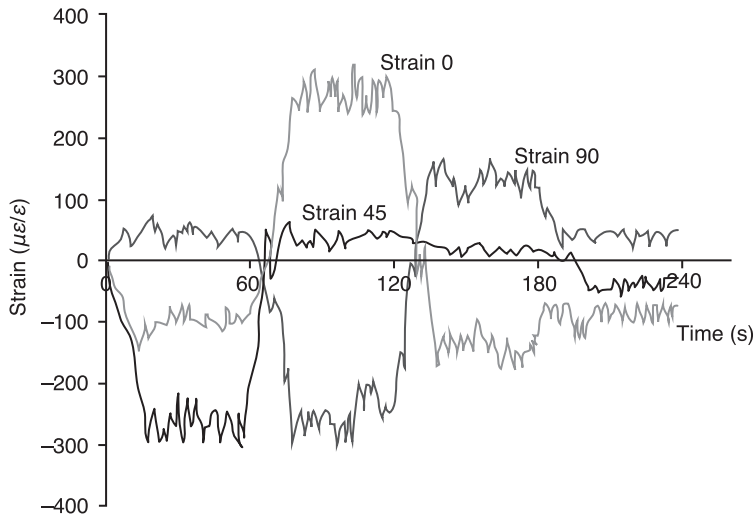

4.16 Incremental hole-drilling and released strains of asymmetrical cross-ply laminate [$0_4/90_4$].

Table 4.8 Average value of released strains of unsymmetrical cross-ply laminates $[0_4/90_4]$ ($\mu\varepsilon$)

Gage direction	Average value of released strains			
	First layer	Second layer	Third layer	Fourth layer
0-degree	–253	272	–128	–86
45-degree	–92	33	11	–33
90-degree	42	–246	138	39

installed in the 90-degree direction recorded released strain entirely contrary to what was recorded by the strain gage installed in the 0-degree direction. The strain gage installed in the 45-degree direction during steps 1 and 4 recorded negative released strains; however, in steps 2 and 3, positive released strains were recorded.

The released strain values recorded from all of the asymmetrical specimens were very close to each other. Average values of recorded released strains, obtained from testing of five specimens, were averaged for each step separately and are tabulated in Table 4.8.

Comparison between the recorded strains of the hole-drilling process for symmetrical and asymmetrical samples showed that the released strain values in asymmetrical samples were less than in the symmetrical samples. However, local variations and fluctuations in the asymmetrical samples were much more than in the symmetrical samples, even when the drill was not advancing to depth.

Symmetrical quasi-isotropic samples, $[0/\pm 45/90]_S$

Hole-drilling processes were performed on quasi-isotropic symmetrical samples $[0/\pm 45/90]_S$ by four steps. The hole depth was equal to half of the specimen thickness and the hole-drilling operation was continued up to the symmetry plane of the samples. The released strains, due to the hole-drilling of quasi-isotropic symmetrical samples in $[0/\pm 45/90]_S$ stacking sequence, are shown in Fig. 4.17. During the hole-drilling of 45-degree layers, the released strains are changed in the strain gage located in the 45-degree direction, while the strain gages in 0- and 90-degree directions recorded little change in their values. Whereas during the hole-drilling of the 0- and 90-degree layers, the strain variations in the 45-degree strain gage were small, the gages in 0- and 90–degree directions reported severe strain changes. The average values of released strains gathered from testing of five quasi-isotropic samples in each step were calculated and are expressed in Table 4.9.

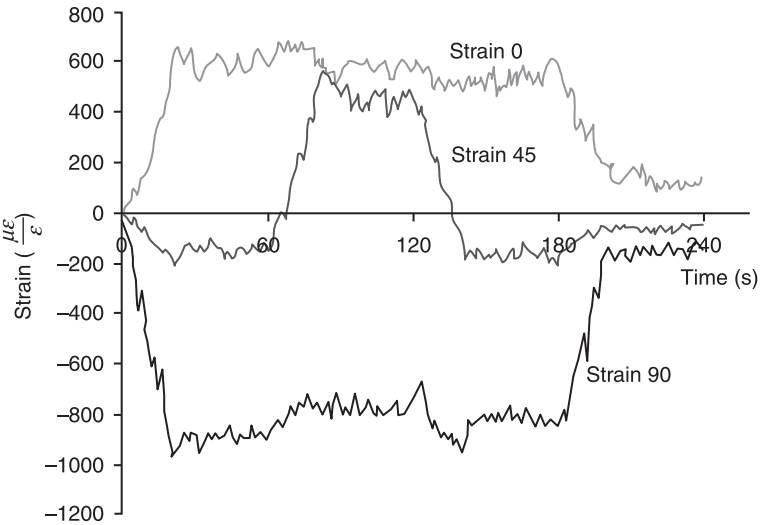

4.17 Incremental hole-drilling and released strains of quaso-isotropic laminate $[0/\pm 45/90]_S$.

Table 4.9 Average value of released strains of symmetric quasi isotropic laminates $[0/\pm 45/90]_S$ ($\mu\varepsilon$)

	Average value of released strains			
Gage direction	First layer	Second layer	Third layer	Fourth layer
0-degree	602	583	543	118
45-degree	–144	476	–167	–50
90-degree	–892	–792	–834	–148

4.5.3 Calibration factors calculations

Symmetrical cross-ply samples, $[0_2/90_2]_S$

Table 4.10 presents the calculated calibration factors of $[0_2/90_2]_S$ laminates under four drilled steps of the hole-drilling process. Each single layer inside the cross-ply laminate, as well as the total laminate, was taken as an orthotropic material. In addition, undrilled layers during incremental hole-drilling process are orthotropic. By installing strain gages in on-axis directions of the first layer, calibration factor terms such as C_{12} and C_{32} in all matrices would be equal to zero.

The calibration factors matrix associated with the released strains due to the residual stress of each layer is expressed by $(C_{ij})_{mm}$. The calibration factors matrix associated with the released strains induced from increase in the depth of the hole

Table 4.10 Calibration factors of symmetrical cross-ply $[0_2/90_2]_S$

(a) *Calibration factors of first layer*

$$\begin{bmatrix} -29.334 & 0 & 15.635 \\ -5.699 & -56.815 & -15.146 \\ 16.158 & 0 & -47.680 \end{bmatrix}$$

$$(C_{ij})_{11}$$

(b) *Calibration factors of second layer*

$$\begin{bmatrix} -26.570 & 0 & 14.116 \\ -5.158 & -52.697 & -14.189 \\ 14.785 & 0 & -44.239 \end{bmatrix} \qquad \begin{bmatrix} -19.905 & 0 & 11.163 \\ -3.623 & -40.355 & -10.084 \\ 11.832 & 0 & -32.792 \end{bmatrix}$$

$$(C_{ij})_{21} \qquad (C_{ij})_{22}$$

(c) *Calibration factors of third layer*

$$\begin{bmatrix} -26.495 & 0 & 14.095 \\ -5.134 & -52.613 & -14.167 \\ 14.774 & 0 & -44.159 \end{bmatrix} \quad \begin{bmatrix} -20.441 & 0 & 11.471 \\ -3.752 & -41.129 & -10.240 \\ 12.063 & 0 & -33.537 \end{bmatrix} \quad \begin{bmatrix} -22.346 & 0 & 12.030 \\ -4.392 & -43.267 & -10.592 \\ 12.371 & 0 & -35.059 \end{bmatrix}$$

$$(C_{ij})_{31} \qquad (C_{ij})_{32} \qquad (C_{ij})_{33}$$

(d) *Calibration factors of fourth layer*

$$\begin{bmatrix} -26.493 & 0 & 14.094 \\ -5.133 & -52.609 & -14.165 \\ 14.773 & 0 & -44.154 \end{bmatrix} \quad \begin{bmatrix} -20.457 & 0 & 11.477 \\ -3.756 & -41.153 & -10.252 \\ 12.068 & 0 & -33.576 \end{bmatrix} \quad \begin{bmatrix} -22.191 & 0 & 11.975 \\ -4.357 & -43.086 & -10.555 \\ 12.311 & 0 & -34.909 \end{bmatrix} \quad \begin{bmatrix} -21.736 & 0 & 11.858 \\ -4.214 & -42.532 & -10.432 \\ 12.211 & 0 & -34.47 \end{bmatrix}$$

$$(C_{ij})_{41} \qquad (C_{ij})_{42} \qquad (C_{ij})_{43} \qquad (C_{ij})_{44}$$

and geometry change is expressed by $(C_{ij})_{mn}$ in which $m \neq n$. For instance, consider the matrix of calibration factors $(C_{ij})_{11}$, $(C_{ij})_{21}$ and $(C_{ij})_{22}$. Calibration factors matrices $(C_{ij})_{11}$ and $(C_{ij})_{22}$ are associated with the released strains due to the residual stress of the first and second layers. However, the calibration factor matrix $(C_{ij})_{21}$ is induced because of an increase in the depth of the hole and a change in the geometry. By increasing the depth of the hole, the effects of the upper layers on the bottom layers were reduced. These differences are illustrated in calibration factors matrices, $(C_{ij})_{31}$, caused by the effect of first layer stresses on drilling of the third layer strains, and calibration factors matrices, $(C_{ij})_{21}$, due to the effect of first layer stresses on drilling of the second layer strains. Reduction in the numerical values fluctuations of the matrix components indicate the reducing effects of upper layers stresses with further distance on drilling of the lower layers.

Asymmetrical cross-ply samples, [0_4/90_4]

In asymmetrical laminates, by increasing the number of hole-drilling steps, the number of calibration factor matrices will increase rapidly. Selecting drilling increments equal to the thickness of a single layer is ideal and enhances the accuracy of the test results; however, for the sake of simplicity, drilling increments are taken to be equal to the thickness of two layers. In the asymmetrical cross-ply laminate, [0_4/90_4], by considering the depth of the increment to be equal to the thickness of two layers, 8 by 8 diagonal calibration factor matrices reduces to 4 by 4 diagonal calibration factors matrices.

The calibration factor matrices obtained by incremental hole-drilling of asymmetrical laminate [0_4/90_4] are presented in Table 4.11. In the calibration factor matrices of asymmetrical cross-ply laminates, terms C_{12} and C_{32} in all matrices were zero. Also, as has been depicted by the matrices, by increasing the depth of the hole, the effects of the upper layer stresses with further distance, on drilling of the lower layers, has been reduced.

Symmetrical quasi-isotropic samples, [0/± 45/90]$_S$

Calibration factor matrices of quasi-isotropic laminates [0/± 45/90]$_S$, obtained from drilling half of the thickness of the laminate, are presented in Table 4.12. Although each separate layer and total quasi-isotropic laminated were orthotropic, calibration factors terms, C_{12} and C_{32}, in none of the matrices were zero. Calibration factors terms, C_{12} and C_{32}, are the effect of the shear residual stresses on the measured strains along the 0- and 90-degree strain gages. Therefore, during drilling of the first layer, the effect of adjacent layers in a 45-degree direction has prevented the terms C_{12} and C_{32} from becoming zero. By increasing the hole depth, the effect of released strains in depth reduced on the surface. Therefore, by increasing the depth, and values of indices $n = m$, numerical values of the calibration factor matrices have been reduced.

Table 4.11 Calibration factors of unsymmetrical cross-ply laminate $[0_4/90_4]$

(a) *Calibration factors of first step*

$$\begin{bmatrix} -49.093 & 0 & 17.247 \\ -15.353 & -58.798 & -5.633 \\ 16.390 & 0 & -29.852 \end{bmatrix}$$

$$\left(C_{ij}\right)_{11}$$

(b) *Calibration factors of second step*

$$\begin{bmatrix} -45.151 & 0 & 15.499 \\ -14.288 & -54.048 & -5.124 \\ 14.709 & 0 & -26.968 \end{bmatrix} \qquad \begin{bmatrix} -31.150 & 0 & 11.199 \\ -9.574 & -38.688 & -3.657 \\ 10.714 & 0 & -19.514 \end{bmatrix}$$

$$\left(C_{ij}\right)_{21} \qquad \left(C_{ij}\right)_{22}$$

(c) *Calibration factors of third step*

$$\begin{bmatrix} -44.949 & 0 & 15.431 \\ -14.233 & -53.831 & -5.097 \\ 14.633 & 0 & -26.833 \end{bmatrix} \quad \begin{bmatrix} -32.171 & 0 & 11.580 \\ -9.831 & -39.781 & -3.769 \\ 11.133 & 0 & -20.159 \end{bmatrix} \quad \begin{bmatrix} -34.537 & 0 & 12.390 \\ -10.462 & -43.164 & -4.444 \\ 12.038 & 0 & -22.562 \end{bmatrix}$$

$$\left(C_{ij}\right)_{31} \qquad \left(C_{ij}\right)_{32} \qquad \left(C_{ij}\right)_{33}$$

(d) *Calibration factors of fourth step*

$$\begin{bmatrix} -44.932 & 0 & 15.427 \\ -14.228 & -53.817 & -5.095 \\ 14.628 & 0 & -26.826 \end{bmatrix} \quad \begin{bmatrix} -32.242 & 0 & 11.600 \\ -9.852 & -39.838 & -3.774 \\ 11.154 & 0 & -20.192 \end{bmatrix} \quad \begin{bmatrix} -34.306 & 0 & 12.275 \\ -10.406 & -42.850 & -4.396 \\ 11.940 & 0 & -22.327 \end{bmatrix} \quad \begin{bmatrix} -33.940 & 0 & 12.051 \\ -10.337 & -42.249 & -4.301 \\ 11.770 & 0 & -21.915 \end{bmatrix}$$

$$\left(C_{ij}\right)_{41} \qquad \left(C_{ij}\right)_{42} \qquad \left(C_{ij}\right)_{43} \qquad \left(C_{ij}\right)_{44}$$

Table 4.12 Calibration factors of symmetrical quasi-isotropic $[0/\pm 45/90]_S$

(a) *Calibration factors of first layer*

$$\begin{bmatrix} -28.305 & -0.806 & 15.130 \\ -5.605 & -58.515 & -15.986 \\ 15.864 & -0.927 & -48.273 \end{bmatrix}$$

$$(C_{ij})_{11}$$

(b) *Calibration factors of second layer*

$$\begin{bmatrix} -26.051 & -0.769 & 13.838 \\ -5.050 & -54.026 & -14.929 \\ 14.727 & -0.848 & -45.127 \end{bmatrix} \qquad \begin{bmatrix} -18.051 & -2.409 & 10.554 \\ -3.400 & -43.979 & -12.480 \\ 11.736 & -2.773 & -35.584 \end{bmatrix}$$

$$(C_{ij})_{21} \qquad (C_{ij})_{22}$$

(c) *Calibration factors of third layer*

$$\begin{bmatrix} -25.991 & -0.735 & 13.816 \\ -5.025 & -53.924 & -14.889 \\ 14.711 & -0.834 & -45.041 \end{bmatrix} \quad \begin{bmatrix} -18.614 & -2.345 & 10.816 \\ -3.520 & -44.761 & -12.584 \\ 11.961 & -2.741 & -36.146 \end{bmatrix} \quad \begin{bmatrix} -20.193 & -2.705 & 11.469 \\ -4.190 & -47.140 & -13.346 \\ 12.493 & -3.235 & -37.970 \end{bmatrix}$$

$$(C_{ij})_{31} \qquad (C_{ij})_{32} \qquad (C_{ij})_{33}$$

(d) *Calibration factors of fourth layer*

$$\begin{bmatrix} -25.989 & -0.753 & 13.815 \\ -5.025 & -53.921 & -14.888 \\ 14.710 & -0.834 & -45.037 \end{bmatrix} \quad \begin{bmatrix} -18.635 & -2.357 & 10.823 \\ -3.526 & -44.780 & -12.590 \\ 11.965 & -2.729 & -36.173 \end{bmatrix} \quad \begin{bmatrix} -20.080 & -2.703 & 11.414 \\ -4.153 & -46.949 & -13.286 \\ 12.439 & -3.195 & -37.809 \end{bmatrix} \quad \begin{bmatrix} -19.670 & -2.701 & 11.295 \\ -4.001 & -46.411 & -13.162 \\ 12.353 & -3.201 & -37.410 \end{bmatrix}$$

$$(C_{ij})_{41} \qquad (C_{ij})_{42} \qquad (C_{ij})_{43} \qquad (C_{ij})_{44}$$

When $n \neq m$, the calibration factors matrix represents the released strains, due to the geometry change of the hole during drilling. Whenever the differences between m and n increases, the change of the numerical values of calibration factors are decreased, which means decreasing the effects of the upper layers with further distance on the released strains of the lower layers.

Comparison between data provided in Tables 4.10 to 4.12 revealed two majors points:

1. By increasing the hole depth, measured strains on the surface in comparison to the released strains in the depth will be rapidly reduced, which is illustrated by decreasing numerical values of the calibration factors matrices. This phenomenon indicates that there must be a limitation on the depth of the hole. According to Saint–Venant principles, the hole depth cannot be more than the hole diameter.
2. By increasing the hole depth, the effect of upper plies with further distance on the released strain of the lower plies due to the drilling of the lower plies would be decreased. Therefore we may conclude that increase in released strains of the lower plies due to the depth increase is more related to the released strains of the upper adjacent plies. This finding is important and simplifies the integration method in layered composites.

As it was explained in the previous section, increasing the number of hole-drilling increments will rapidly increase the number of calibration factor matrices. Usually the number of calibration factor matrices is the same as the number of hole-drilling increments. For instance, in the fourth and eighth increments of a hole-drilling process, the numbers of calibration factor matrices are 4 and 8, respectively.

This section has proved that the residual stresses of each ply has an effect on the released strain of ply underneath during the hole-drilling process and its effect on the released strain of the other plies is negligible. Therefore, calibration factor matrices of each hole-drilling step are summarized in two matrices. The first matrix results from releasing residual stresses due to hole drilling of each orthotropic ply. The second matrix is due to the increase of the hole depth and expresses the effect of the residual stress of an upper given ply on the released strain of its underlying ply. With this result, in each row of the lower triangular matrix $(C_{ij})_{mn}$, only two matrices have been changed, and other calibration factor matrices remain constant.

4.5.4 Residual stresses calculations

Symmetrical cross-ply samples, $[0_2/90_2]_S$

Residual stresses are not uniform throughout the thickness of the laminated composites, and their values change ply by ply. During this research it was

assumed that the amount of residual stress along the thickness of a single orthotropic ply was constant and uniform. The average of released strains of each hole-drilling increment are presented in Table 4.7, and calibration factors presented in Table 4.10 along with Eq. 4.18 are used to calculate the residual stresses of $[0_2/90_2]_S$ laminates. These results are presented in Table 4.13. Because of the symmetry of the laminate, residual plane stress values are presented only for four out of eight plies of the laminate.

Asymmetrical cross-ply samples, $[0_4/90_4]$

Residual stresses of $[0_4/90_4]$ laminates were calculated using calibration factors of the simulation models presented in Table 4.11, and average of released strains in any step of hole-drilling increment (Table 4.8) are calculated and given in Table 4.14. Plane stress values in the table are related to the each increment of hole-drilling process, starting from the surface of the sample and continuing through the hole.

Symmetrical quasi-isotropic samples, $[0/\pm 45/90]_S$

Residual stress values of $[0/\pm 45/90]_S$ laminates were calculated and are presented in Table 4.15, using the calibration factors and average of the released strains of each hole-drilling increment, as presented in Tables 4.12 and 4.9, respectively. The plane stress values in Table 4.15 are related to the separate orthotropic plies of the sample started from the sample surface toward its symmetry plane.

4.5.5 Comparisons

The CLPT calculates the macroscopic residual stresses in the laminated composites by assuming plane stress conditions and linear elastic behavior for each ply. Due to the different coefficients of thermal expansion values of different plies, thermal loads are extended inside the laminate during cooling from curing temperature to the ambient conditions. Subsequently, thermal loads induce residual stresses inside the laminate.

We may calculate the coefficient of thermal expansions in the off-axis direction of an orthotropic ply as

$$\alpha^{(k)} = \begin{Bmatrix} \alpha_1 \\ \alpha_2 \\ \alpha_6 \end{Bmatrix}^{(k)} = \begin{bmatrix} m^2 & n^2 & -mn \\ n^2 & m^2 & mn \\ 2mn & -2mn & m^2 - n^2 \end{bmatrix} \begin{Bmatrix} \alpha_x \\ \alpha_y \\ 0 \end{Bmatrix} \quad [4.23]$$

where α_x, α_y and α_1, α_2, α_6 are the thermal expansion coefficients in on- and off-axis directions, respectively, and k is the number of each layer. Thus, the

Table 4.13 Average value of symmetrical cross-ply laminates residual stresses $[0_2/90_2]_S$ (MPa)

Stress	First layer			Second layer			Third layer			Fourth layer		
	A	B	C	A	B	C	A	B	C	A	B	C
σ_x	–14.57	–13.90	4.8	–14.86	–13.90	6.9	14.50	13.90	4.3	11.89	13.90	14.46
σ_{xy}	0.49	0	–	1.01	0	–	–0.87	0	–	0.41	0	–
σ_y	12.89	13.90	7.27	12.36	13.90	11.08	–12.24	–13.90	11.94	–13.89	–13.90	0.07

A: present research
B: theory
C: % error

Table 4.14 Average value of unsymmetrical cross-ply laminates residual stresses (MPa)

Stress	First layer			Second layer			Third layer			Fourth layer		
	A	B	C	A	B	C	A	B	C	A	B	C
σ_x	5.77	5.52	4.53	–13.71	–13.88	1.22	7.20	7.04	2.27	1.52	1.33	14.29
σ_{xy}	–0.11	0	–	–0.33	0	–	0.25	0	–	0.45	0	–
σ_y	1.76	1.33	32.33	6.99	7.04	0.71	–13.64	–13.88	1.73	4.96	5.52	10.14

A: present research
B: theory
C: % error

Table 4.15 Average value of symmetrical quasi isotropic laminates residual stresses (MPa)

Stress	First layer			Second layer			Third layer			Fourth layer		
	A	B	C	A	B	C	A	B	C	A	B	C
σ_x	–13.82	–13.90	0.57	0.20	0	–	–0.20	0	–	13.62	13.90	2.06
σ_{xy}	–0.2	0	–	–13.96	–13.90	0.43	13.89	13.90	0.07	0.30	0	–
σ_y	13.94	13.90	0.29	0.02	0	–	–0.06	0	–	–13.85	–13.90	0.36

A: present research
B: theory
C: % error

thermal load in the off-axis plane for laminated composite materials can be expressed as

$$\left(N_1^T, M_1^T\right) = \sum_{k=1}^{N} (\overline{Q}_{11}^{(k)}\alpha_1^{(k)} + \overline{Q}_{12}^{(k)}\alpha_2^{(k)} + \overline{Q}_{16}^{(k)}\alpha_6^{(k)})\Delta\, T^{(k)}(t_k, t_k\, \overline{z}_k) \qquad [4.24]$$

$$\left(N_2^T, M_2^T\right) = \sum_{k=1}^{N} (\overline{Q}_{21}^{(k)}\alpha_1^{(k)} + \overline{Q}_{22}^{(k)}\alpha_2^{(k)} + \overline{Q}_{26}^{(k)}\alpha_6^{(k)})\Delta\, T^{(k)}.(t_k, t_k\, \overline{z}_k) \qquad [4.25]$$

$$\left(N_6^T, M_6^T\right) = \sum_{k=1}^{N} (\overline{Q}_{61}^{(k)}\alpha_1^{(k)} + \overline{Q}_{26}^{(k)}\alpha_2^{(k)} + \overline{Q}_{66}^{(k)}\alpha_6^{(k)})\Delta T^{(k)}.(t_k, t_k\, \overline{z}_k) \qquad [4.26]$$

where $\alpha_i^{(k)}$ and $\overline{Q}_{ij}^{(k)}$ are the thermal expansion coefficients and the stiffness matrix indexes, respectively. $\Delta T^{(K)}$, t_k and $\bar{z}_k$ are the temperature difference between the ambient and the stress free temperatures, ply thickness and lamina mid-plane height, respectively.

If the thermal resultant forces and the moments are defined as $N_T=(N^T_1, N^T_2, N^T_3)$ and $M^T=(M^T_1, M^T_2, M^T_3)$, then the strain and the curvature of the mid-plane are calculated as

$$\begin{bmatrix} \varepsilon^\circ \\ k^\circ \end{bmatrix} = \begin{bmatrix} A & B \\ B & D \end{bmatrix}^{-1} \begin{bmatrix} N \\ M \end{bmatrix} \qquad [4.27]$$

where *A, B* and *D* are extensional, coupling and bending stiffness matrices, respectively. Using the strain and the curvature of the mid-plane, the residual strains and stresses of each layer in the off-axis coordinate system were calculated as

$$\varepsilon_r^{(k)} = (\varepsilon^\circ + \bar{z}_k k^\circ - \alpha^{(k)}\Delta T) \qquad [4.28]$$

$$\sigma_r^{(k)} = \overline{Q}^{(k)}\, \varepsilon_r^{(k)}) \qquad [4.29]$$

In the rest of this section, the experimentally obtained residual stresses (Section 4.5.4) will be compared with the values predicted by CLPT method.

Symmetrical cross-ply samples, $[0_2/90_2]_S$

Results of obtained analytical and experimental data of stress components σ_x, σ_y and σ_{xy} in each layer of laminated composite, $[0_2/90_2]_S$, are compared in Table 4.13. In the upper half of the laminate where the rosette was installed, a good agreement between experimental and theoretical results was obtained. By increasing the depth of the hole, the error percentage was increased, which in return resulted in a higher difference between the experimental and theoretical values. The maximum observed error value was 14% and occurred in the fourth layer. The maximum measured shear stress of $[0_2/90_2]_S$ laminates was equal to 1 MPa,

which was negligible in comparison to its analytical value based on the CLPT method, which was zero.

The comparison of analytical and experimental results of stress components σ_y of $[0_2/90_2]_S$ laminate in Table 4.13 show that the maximum differences between numerical and experimental results were less than 12% and related to the results of the stress analysis in the third layer. The equilibrium condition of the residual stresses in the thickness of the laminates is an essential and logical constraint, which results in equal tensile and compressive stresses in the thickness of the laminate. The summation of the stress components in all directions and along the thickness of the laminate by using CLPT was zero. According to the obtained experimental results, the summation of σ_x, σ_y and σ_{xy} stress components in the *x, y* and *x-y* directions and along the thickness of the laminate were 3, 0.88 and 1 MPa, respectively. These values were close to the analytical values, which were zero according to CLPT.

Asymmetrical cross-ply samples, [0$_4$/90$_4$]

A comparison between analytical and experimental results of σ_x, σ_y and σ_{xy} stress components for each step of the incremental hole-drilling process of $[0_4/90_4]$ laminates are shown in Table 4.14. Experimental results in the thickness of the laminates show good agreement with the theoretical results. The maximum differences between theoretical and experimental values of stress components σ_x and σ_y occurred in the fourth step and were equal to 14 and 10%, respectively. Also, the summation of experimental stress components σ_x and σ_y in the *x*- and *y*-directions and along the thickness of the laminate, were obtained as 0.78 and 0.07 MPa, respectively.

Maximum of the measured shear stress in $[0_4/90_4]$ laminates is equal to 0.45 MPa and the sum of stress components σ_{xy} in the laminates thickness is 0.26 MPa. As mentioned above, the summation of residual stress components in the *x*-, *y*- and *x-y*-directions along the thickness of the laminate are in good agreement compared to the CLPT results, which were zero.

Symmetrical quasi-isotropic samples, [0/± 45/90]$_S$

Table 4.15 explains the differences between experimental and analytical stress components σ_x, σ_y and σ_{xy} obtained from the incremental hole-drilling process in each layer of the laminate, $[0/\pm 45/90]_S$. Experimental results show good agreement with the theoretical results and the maximum error in measurement is 0.28 MPa. While the CLPT predicts the shear stress, σ_{xy}, in the fourth layer as equal to zero, the measured value was 0.3 MPa, which of course is close to zero. Summation of the residual stress components in the *x-*, *y*- and *x-y* directions and along the thickness of the laminate were negligible.

4.6 Conclusions

Several reasons can cause the trapping of residual stresses inside laminated composites, such as mismatch between thermal expansion coefficient of the fiber and the matrix, different thermal expansion coefficient in longitudinal and transverse directions of a layer, different expansion and contraction of consecutive layers as a result of their different arrangements, and non-uniform freezing. The central hole-drilling method is one of the most successful methods for measuring residual stresses described by the ASTM standard (ASTM E837-01, 1999). In the central hole-drilling method, the released strains are related to the residual stresses by using the calibration factors. For correlation of the residual stresses and the released strains in orthotropic materials, nine calibration factors are defined. These calibration factors can be found by closed form, numerical and experimental methods.

In this chapter, a method called the simulated central hole-drilling (SCHD) method is established. The simulation of the hole-drilling process for the orthotropic materials, with different Poisson's ratios, shear modulus, and longitudinal and transverse modulus are performed. The results are compared with the available analytical results. Through developing the hole-drilling process simulation in laminated composites, the incremental hole-drilling method has been extended to determine the non-uniform residual stresses in laminated composites. In the incremental hole-drilling method, the strains relaxed in each step are divided into strains released due to releasing the residual stresses confined in the drilled layer, and an increase in the hole depth. Since in the method presented in the current study, the effects of the changes of geometry and residual strains of each layer are taken into account separately and continuously, the method is called the integral method in laminated composite materials.

In order to determine the calibration factor matrices at each step, simulation of the integral hole-drilling (SIHD) process in the laminated composites is performed. Through applying an equal and opposite stress distribution in place of the confined residual stress distributed in the sample, the simulation of the integral method in composite laminates is performed. In modeling the integral method for laminated composite materials, the relation between measured strains on the surface and residual stresses are presented. By increasing the hole depth, the number of the calibration factor matrices increases. One of these matrices expresses the relation of measured strains and residual stresses for each layer, and the rest express the relation between strains due to increase in the hole depth and measured strains.

By increasing the hole depth, measured strains on the surface in comparison to the released strains in the depth will be reduced rapidly, which is illustrated by the decreased numerical values of the calibration factors matrices. This phenomenon indicates that there must be a limitation to the depth of the hole that cannot be

more than the hole diameter. Also, the effect of upper plies with further distance on the released strain of the lower plies, due to the drilling of the lower plies, would be decreased. Therefore we may conclude that increased released strain of the lower plies is due to the depth increase and is more related to the released strain of the upper adjacent plies. Therefore, the residual stresses of each ply has an effect on the released strain of its underlying ply during the hole-drilling process and its effect on the released strain of the other plies is negligible. Therefore, calibration factor matrices of each hole-drilling step are summarized in two matrices: The first matrix results from releasing residual stresses due to hole-drilling of each orthotropic ply. The second matrix results from the increase in hole depth and expresses the effect of the residual stress of an upper given ply on the released strain of its underlying ply.

Finally, some composite samples with various arrangements have been made. Also the integral method calibration factors have been determined using the SIHD. Subsequently, by installing a rosette strain gage on the surface of each sample, and measuring the incremental strains, the residual stresses in each layer are determined and compared with the values predicted by the theoretical methods.

4.7 References

Andersen, L.F. (2002) Experimental method for residual stress evaluation through the thickness of a plate, *Engineering Materials and Technology*, **124**(4), 428–33.

ASTM, (1999) *Determining Residual Stresses by the Hole-Drilling Strain-Gage Method*, American Society for Testing and Materials (ASTM), Standard E837-01.

Aoh, J. N. and Wei, C. S. (2003) On the improvement of calibration coefficients for hole-drilling integral method. Part II: Experimental validation of calibration coefficients, *Engineering Materials and Technology*, **125**(2), 107–15.

Beaney, E. M. (1976) Accurate measurement of residual stress on any steel using the central hole method, *Strain Journal*, **12**(3), 99–106.

Beghini, M. and Bertini, L. (2000) Analytical expressions of the influence functions for accuracy and versatility improvement in the hole-drilling method, *Strain Analysis for Engineering Design*, **35**(2), 125–35.

Bert, C. W. and Thompson, G. L. (1968) A method for measuring planar residual stresses in rectangularly orthotropic materials, *Composite Materials*, **2**(2), 244–53.

Crasto, A. S. and Kim, R. Y. (1993) On the determination of residual stresses in fiber-reinforced thermoset composites, *Reinforced Plastics and Composites*, **12**(5), 545–58.

Flaman, M. T. and Herring, J. A. (1985) Comparison of four hole-producing techniques for the center-hole residual-stress measurement method, *Experimental Techniques*, **9**(8), 30–33.

Flaman, M. T. and Manning, B. H. (1985) Determination of residual-stress variation with depth by the hole-drilling method, *Experimental Mechanics*, **25**(3), 205–7.

Flaman, M. T. and Boag, J. M. (1990) Comparison of residual-stress variation with depth-analysis techniques for the hole-drilling method, *Experimental Techniques*, **30**(4), 352–5.

Flaman, M. T., Mills, B. E. and Boag, J. M. (1987) Analysis of stress-variation with-depth measurements procedures for the center-hole method of residual stress measurement, *Experimental Techniques*, **11**(6), 35–7.

Ghasemi, A. R. and Shokrieh, M. M. (2008) Development of an integral method for determination of non-uniform residual stresses in laminated composites, *Polymer Science and Technology*, **21**(4), 355–47.

Ghasemi, A. R. Taheri-behrooz, F. and Shokrieh, M. M. (2013) Determination of non-uniform residual stresses in laminated composites using integral hole-drilling method: Experimental evaluation, *Composite Materials*, available online 22 January.

Hahn, H. T. (1976) Residual stresses in polymer matrix composite laminates, *Composite Materials*, **10**(6), 266–78.

Hahn, H. T. and Pagano, N. J. (1975) Curing stresses in composite laminates, *Composite Materials*, **9**(1), 91–106.

Hwang, B. W., Shu, C. M. and Kim, S. H. (2003) Finite element analysis of calibration factors for the modified incremental strain method, *Strain Analysis for Engineering Design*, **38**(1), 45–51.

Hyer, M. W. (1989) Mechanics of unsymmetrical laminates, in: *Handbook of Composites*, Ch. 2, Structures and design, Elsevier Science Publisher., 85–114.

Lake, B. R., Appl, F. J. and Bert, C. W. (1970) An investigation of the hole-drilling technique for measuring planar residual stress in rectangularly orthotropic materials, *Experimental Mechanics*, **10**(6), 233–9.

Matahr, J. (1934) Determination of initial stresses by measuring deformation around drilled holes, *Transactions of ASME*, **56**(4), 249–54.

Niku-Lari, A., Lu, J. and Flavenot, J. F. (1985) Measurement of residual stress distribution bythe incremental hole-drilling method, *Experimental Mechanics*, **25**(2**)**, 175–85.

Pagliaro, P. and Zuccarello, B. (2006) Residual stress analysis of orthotropic materials by the through hole-drilling method, *Experimental Mechanics*, **47**(2), 217–36.

Prasad, C. B., Prabhakaran, R. and Thompkins, S. (1987a) Determination of calibration constants for the hole-drilling residual stress measurement technique applied to orthotropic composites. Part I: Theoretical considerations, *Composite Structures*, **8**(2), 105–18.

Prasad, C. B., Prabhakaran, R. and Thompkins, S. (1987b) Determination of calibration constants for the hole-drilling residual stress measurement technique applied to orthotropic composites. Part II: Experimental evaluations, *Composite Structures*, **8**(3), 165–72.

Rendler, N. J. and Vigness, I. (1976) Hole-drilling strain-gage method of measuring residual stresses, *Experimental Mechanics*, **6**(12), 577–86.

Schajer, G. S. (1981) Application of finite element calculations to residual stress measurement, *Engineering Materials and Technology*, **103**(2), 157–63.

Schajer, G. S. (1988) Measurement of non-uniform residual stresses using the hole-drilling method. Part I: Stress calculation procedures. Part II: Practical application of the integral method, *Engineering Materials and Technology*, **110**(4), 338–49.

Schajer, G. S. (2010a) Hole-drilling residual stress measurements at 75: Origins, advances, opportunities, *Experimental Mechanics*, **50**(2), 245–53.

Schajer, G. S. (2010b) Advances in hole-drilling residual stress measurements. *Experimental Mechanics*, **50**(2), 159–68.

Schajer, G. S. and Yang, L. (1994) Residual-stress measurement in orthotropic materials using the hole-drilling method, *Experimental Mechanics*, **34**(4), 324–33.

Schajer, G. S. and Tootoonian, M. (1997) A new rosette design for more reliable hole-drilling residual stress measurements, *Experimental Mechanics*, **37**(3), 299–306.

Shaw, D. and Chen, H. Y. (1990) A finite element technique to analyze the data measured by the hole-drilling method, *Experimental Techniques*, **30**(2), 120–3.

Shokrieh, M. M. and Kamali, S. M. (2005) Theoretical and experimental studies on residual stresses in laminated polymer composites, *Composite Materials*, **39**(24), 2213–25.

Shokrieh, M. M. and Ghasemi, A. R. (2007) Determination of calibration factors of the hole-drilling method for orthotropic composites using an exact solution, *Composite Materials*, **41**(19), 2293–311.

Sicot, O., Gong, X. L., Cherouat, A. and Lu, J. (2003) Determination of residual stress in composite laminates using the incremental hole-drilling method, *Composite Mat*erials, **37**(9), 831–43.

Sicot, O., Gong, X. L., Cherouat, A. and Lu, J. (2004) Influence of experimental parameters on determination of residual stress using the incremental hole-drilling method, *Composite Science and Technology*, **64**(2), 171–80.

Stefanescu, D., Truman, C. E., Smith, D. J. and Whitehead, P. S. (2006) Improvements in residual stress measurement by the incremental centre hole-drilling technique, *Experimental Mechanics*, **46**(4), 417–27.

Tootoonian, M. and Schajer, G. S. (1995) Enhanced sensitivity residual-stress measurements using taper-hole-drilling, *Experimental M*echanics, **35**(2) 124–9.

Tsai, S. W. (1988) *Composites Design*, 4th edition, Dayton, OH, Think Composites.

Tsai, S. W. and Hahn, H. T. (1980) *Introduction to Composite Materials*, Westport, Technomic.

White, S. R. and Hahn, H. T. (1992) Process modeling of composite materials: residual stress development during cure. Part I: Model formulation. Part II: Experimental validation, *Composite Materials*, **26**(16), 2402–53.

Withers, P. J. and Bhadeshia, H. K. D. H. (2001) Overview residual stress, Part I: Measurement techniques. Part II: Nature and origins, *Materials Science and Technology*, **17**(4), 355–75.

Xiao, B., Li, K. and Rong, Y. (2011) Automatic determination and evaluation of residual stress calibration coefficients for hole-drilling strain gauge integral method, *Strain*, **47**(1), 525–34.

Zuccarello, B. (1999) Optimal calculation steps for the evaluation of residual stress by the incremental hole-drilling method, *Experimental Mechanics*, **39**(2), 117–24.

5

Measuring residual stresses in composite materials using the slitting/crack compliance method

M. M. SHOKRIEH and S. AKBARI, Iran University of Science and Technology, Iran

DOI: 10.1533/9780857098597.1.121

Abstract: This chapter discusses the theoretical and experimental aspects of residual stress measurement through the thickness of laminated composites using the slitting method (or crack compliance method). First, the common methods of approximation of residual stress distribution when using the slitting method are discussed. Then a finite element method is presented to calculate compliance coefficients of laminated composites. Furthermore, effects of residual shear stresses when measuring residual normal stresses by the slitting method are investigated. Finally, the chapter presents a practical application of the slitting method to measure the residual stresses in carbon/epoxy laminated composites.

Key words: laminated composites, residual stress measurement, slitting method, compliance coefficients, finite element method.

5.1 Introduction

Over the past 25 years, the slitting method has been employed for residual stress determination in a vast variety of materials, such as stainless steel, functionally graded materials, polymer and metal matrix composites, aluminum alloys, friction stir welds, etc. In this method, a narrow slit is progressively cut through the thickness of a stressed component. The released strains around the slit are measured using strain gages bonded either on the top or back surfaces of the specimen. Residual stress distribution is then calculated using recorded strains and calculated compliance coefficients.

The main aim of this chapter is to review the slitting method, focusing on its application to laminated polymer composites. First, a brief history of slitting determination of residual stresses is presented. Then, the basic elements of the slitting method, such as different approximations for residual stress distribution, are discussed. Moreover, a finite element model is presented for the calculation of compliance coefficients of laminated composites. Different parameters influencing the calculation of compliance coefficients are also investigated. A literature survey on the slitting measurement of the residual stresses reveals that only the stress component perpendicular to the slit face is considered by other researchers, but in this chapter it is shown that the residual shear stresses may have considerable

effects on the measured strain. At the end of this chapter, a case study of slitting residual stress measurement in a carbon/epoxy laminated composite is presented.

5.2 The development of the slitting method

Since the beginning of the 20th century, various destructive methods (also known as relaxation methods) for measuring residual stresses have been developed. Substantial advances have been made in different aspects of these methods, including specimen shapes and material removal geometry, material cutting arrangement, deformation measurement technology and stress calculation techniques (Schajer, 2010). Some of the destructive methods have a wide range of application, while others are very specific. The most commonly used methods are slitting and hole-drilling. The slitting method is conceptually similar to the hole-drilling method, but uses a slit instead of a hole. Unlike hole-drilling, slitting can measure a full through-thickness stress profile, regardless of the specimen thickness. The slitting method is also more sensitive and has a better spatial resolution than the hole-drilling method.

Although the slitting method was introduced by Vaidyanathan and Finnie (1971), due to experimental difficulties, its wide application was postponed until the mid–1980s. Over the past 25 years, considerable effort has been devoted to improve theoretical and experimental aspects of this method. In their book, Cheng and Finnie (2007) have provided a complete coverage of analytical and computational techniques of both near-surface and through-thickness residual stress measurements by the slitting method. Also, a good source for a review on this method is provided by Prime (1999).

The vast majority of applications of the slitting method are to monolithic metals; however, its reported applications to orthotropic materials are very limited. Hermann (1995) employed the slitting method in a metal matrix composite, but he treated the composite as an isotropic material. By using this method, Ersoy and Vardar (2000) determined residual stresses in a cross-ply thermoplastic laminate. Hill and Lin (2002) applied the slitting method to a ceramic-metallic graded material. Prime and Hill (2004) used an eigenstrain-based extension of the slitting method to measure a localized depth profile of residual stresses in a metal matrix composite.

5.3 Theoretical basis

In the basic implementation of the slitting method, a slit of progressively increasing depth is cut through the thickness of the stressed specimen and the released strain on the specimen top or back surface are measured after each step. Then the stress component normal to the slit face can be calculated from the measured strains and compliance coefficients. This incremental procedure allows the stress profile within the slit depth to be calculated.

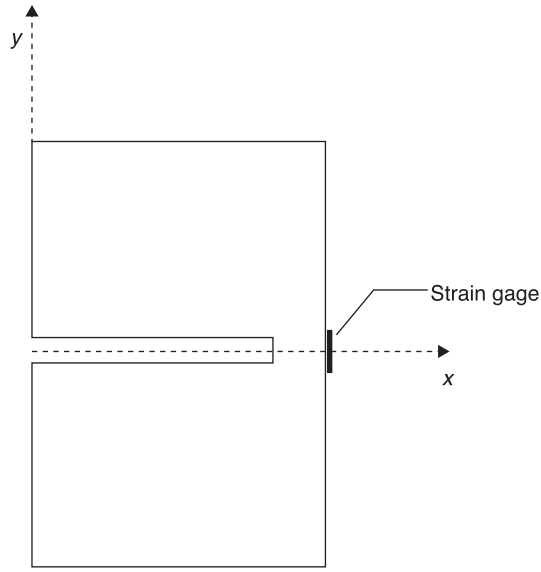

5.1 Slitting method schematic.

5.3.1 Background and terminology

Figure 5.1 shows the typical geometry of the slitting method with a back surface strain gage. The geometry of the slitting method includes the specimen thickness t, the specimen length L, the specimen width B, the slit depth a, the slit width w and the strain gage length l. The strain gages bonded on the back surface of the stressed part directly opposite the slit are sensitive to all residual stress within the specimen thickness and thus generally used for through-thickness measurements. However, strain gages bonded on the top surface near the slit are only sensitive to near surface residual stress (usually up to 20–25% of the thickness) and therefore are appropriate for near surface measurements.

The slit starts from the top surface of the specimen and is extended in successive increments towards the back surface. For the configuration shown in Fig. 5.1, the slitting method will determine unknown normal residual stress component perpendicular to the slit plane, $\sigma_{yy}(x)$, using the y-strain measured by the back surface or top surface strain gages.

Major assumptions of the slitting method include:

- On the slit face, the residual stresses only vary in the depth direction, and not in the transverse direction. If the stress varies in both directions, the slitting method is not applicable.
- The measured strains result only from stress component normal to the slit face; relaxed residual shear stresses do not have any effect on the recorded

data. It is shown in Section 5.5 that this assumption is not valid for top surface strain gages used for near surface measurements. This point is of considerable importance, particularly for laminated composites, because significant values of residual shear stresses might be created in these materials due to their heterogeneous structure.

- Material remains linearly elastic in the entire slitting process, so the principle of superposition is valid. By using a fracture mechanics approach, Prime (2010) showed that plasticity effects are not considerable in the slitting method.
- In the conventional slitting method applied to monolithic materials, it is assumed that the residual stress can be fitted by a continuous function of the spatial variables. Due to stress discontinuity in the layers boundaries, this assumption is not applicable to laminated composites.

5.3.2 Estimation of residual stresses

A difficulty of destructive methods of residual stress measurement, for example the slitting method, is that the relationship between the residual stresses released along the slit face and the measured strains does not have a simple one-to-one form. This is because the measured strains depend on the released stresses within the whole specimen thickness and not just those at a specific depth (Schajer, 2001). As a result, for the slitting method and other methods based on the incremental material removal, the relationship between the residual stresses and the measured strain data has the following integral form (Schajer and Prime, 2006):

$$\varepsilon_{yy}(a_i) = \int_0^{a_i} G(x, a_i)\sigma_{yy}(x)\,dx \qquad [5.1]$$

in which $\varepsilon_{yy}(a_i)$ is the measured y-strain when the slit is cut to a depth a_i. The Kernel function, $G(x,a_i)$, describes the strain response due to a unit stress at depth x within a slit of depth a_i. Kernel function can be determined analytically only for some simple geometries. It is usually obtained using a finite element method (FEM).

Equation 5.1 shows that the measured strains on the surface, $\varepsilon_{yy}(a_i)$, depend on the combination of residual stresses, $\sigma_{yy}(x)$, originally contained at all depths and not just the stresses at the last increment. The equation is called an 'inverse problem', because the unknown stresses, $\sigma_{yy}(x)$, are within the integral and the known measured strains are outside of it. An undesirable feature of the solutions to inverse equations is that they tend to amplify noise in the measurement data. Therefore, small measurement errors can result in much larger relative errors in the calculated stress. A physical reason of this phenomenon is the spatial separation of the location of the strain measurement and the location of calculated residual stress (Schajer, 2010). Mathematical techniques, such as least squares (Cheng and Finnie, 1985) and Tikhonov regularization (Schajer and Prime, 2006; Schajer,

2007), can be used to stabilize the residual stress solution and reduce the noise sensitivity.

In order to solve Eq. 5.1, an initial distribution for the residual stress must be considered. It is important to note that the form of initial stress distribution not only dictates how the compliance coefficients will be defined but also has a significant effect on the estimated residual stress. The most important estimations include continuous polynomials and strip loads, which will be reviewed in the next sections. Also piecewise polynomials, which are extension to continuous polynomials, are discussed.

Approximation using continuous polynomials

When the unknown residual stress could be reasonably assumed to be continuous along the thickness of the part, it may be approximated by a continuous polynomial with unknown coefficients. This approach was initially developed by Schajer (1981) for the incremental-hole-drilling method and was first applied to the slitting method by Cheng and Finnie (1985). For this purpose, various types of polynomials are used. The type of polynomial is determined by two important factors. First, the assumed polynomial should satisfy the equilibrium conditions of zero resultant force and moment along the thickness of the specimen. Second, the effect of error in strain measurement on estimated stress is directly related to the type of polynomial.

Many researchers use Legendre polynomials, because the equilibrium conditions can be easily satisfied by removing the first and the second terms of Legendre series. However, Cheng and Finnie (2007) showed that the use of a Legendre polynomial leads to a significantly improved condition of the compliance matrix over that of other kinds of polynomials. Therefore, residual stress distribution can be expressed as (dropping the *yy* subscript for convenience):

$$\sigma(x) = \sum_{j=2}^{n} A_j P_j(x) \qquad [5.2]$$

in which A_j are unknown coefficients and $P_j(x)$ are known Legendre basis functions. The solution for $\sigma(x)$ from measured strain is thus reduced to finding values for the basis function coefficients. Substituting Eq. 5.2 into Eq.5.1 gives

$$\varepsilon(a_i) = \frac{1}{E'}\int_0^{a_i} G\left(x, a_i\right)\sum_{j=2}^{n} A_j P_j(x)\, dx = \frac{1}{E'}\sum_{j=2}^{n} A_j \int_0^{a_i} G(x, a_i) P_j(x)\, dx = \sum_{j=2}^{n} A_j C_{ij} \qquad [5.3]$$

Thus, C_{ij} or the elements of compliance matrix are expressed by

$$C_{ij} = \frac{1}{E'}\int_0^{a_i} G(x, a_i) P_j(x)\, dx \qquad [5.4]$$

Comparison to Eq. 5.1 indicates that a specific element of the compliance matrix, C_{ij}, is the measured strain at the strain gage location for a slit of depth a_i when

residual normal stress distribution along the specimen thickness is equal to Legendre polynomial term P_j:

$$C_{ij} = \varepsilon(a = a_i, \sigma(x) = P_j(x)) \quad [5.5]$$

Equation 5.3 can be rewritten using matrix notation:

$$\{\varepsilon\} = [C]\{A\} \quad [5.6]$$

The number of the polynomial terms in the stress expansion is usually less than the number of measured strains. The system in Eq. 5.6 is therefore over-determined, and a least squares solution is pursued by inverting Eq. 5.6 to minimize the error between the strains given by Eq. 5.6 and the vector of measured stains:

$$\{A\} = ([C]^T [C])^{-1} [C]^T \{\varepsilon\} \quad [5.7]$$

In this equation, the inverse of $[C'] = [C]^T[C]$ has been used. Dependent on the type of polynomial and its order, matrix $[C']$ may be unstable. In other words, its condition number may be large and consequently a small error in measured strain, $\{\varepsilon\}$, will result in significant errors in polynomial coefficients, $\{A\}$, and consequently in estimated stress. It has been shown that compared with other types of polynomials, Legendre polynomials generally produce matrix $[C']$ with a smaller condition number (Cheng and Finnie, 2007). Since Legendre polynomials satisfy equilibrium conditions and the solution based on these polynomials is more stable, many researchers use it for the residual stress approximation in the slitting method.

Approximation using piecewise polynomials

In some cases, the residual stress profile cannot be precisely fitted with continuous polynomials. For example, the residual stress in laminated composites will be discontinuous across layers boundaries. However, in many engineering applications such as shot peening, the residual stress variation may be sharp and consequently the estimation using a continuous stress distribution will require a high order of approximation that becomes unstable in estimation. In such cases, two alternative approaches can be employed, including piecewise polynomials and strip loads. This section reviews the piecewise polynomials method.

Piecewise polynomials were initially used by Gremaud *et al.* (1994) in the slitting method. An approximation based on polynomials usually gives a better stress estimation near the center of the sub-interval than at the ends. Therefore, in order to produce acceptable results, Gremaud *et al.* (1994) divided the region of residual stress variation into a series of overlapping subintervals; points between two adjacent subintervals were shared. The residual stress in each interval is approximated by a linear or quadratic or cubic polynomial. Therefore, an overlapping piecewise function for a specific subinterval may be expressed as

$$\sigma(x) = \sum_{i=0}^{n_j} A_i^j L_i^j \left(\frac{x - x_{aj}}{x_{bj} - x_{aj}}\right) = \sum_{i=0}^{n_j} A_i^j L_i^j(s) \qquad j = 1, \ldots, N \qquad [5.8]$$

where x_{aj} and x_{bj} are the jth sub-interval endpoints. The ith order polynomial $L_i^j(s)$ is defined by the normalized local distance $0 \le s \le 1$ in the jth sub-interval.

Gremaud *et al.* (1994) used a numerical example to show the effectiveness of piecewise polynomials compared with continuous polynomials. They considered a third-order polynomial distribution for residual stress through the thickness of an isotropic specimen. Based on this residual stress distribution, they calculated the released strain in the strain gage location. This can be easily done using FEM or other analytical methods such as the body force method. Again, they used a second-order continuous polynomial, as well as first- and second-order piecewise polynomials, to calculate the residual stress from the strain data.

It was shown that the piecewise polynomials result in better approximations. Even results of first-order piecewise polynomial are more precise than those using a second-order continuous polynomial. Thus, it can be concluded that piecewise polynomials improve the accuracy of approximation by reducing the size of the intervals.

Approximation using strip loads

The second common inverse solution for estimating discontinuous stress profiles is to solve for the stress variation expressed as a series of strip loads. In other words, a uniform stress for each increment of slit depth is considered. This is the oldest and still most common approach for obtaining a residual stress profile and has its roots in the hole-drilling method (Schajer, 1988). This method is also known as the 'incremental stress method' (Prime, 1999) and 'pulse method' (Schajer and Prime, 2006). The stress is thus expressed as the sum of a series of pulse functions:

$$\sigma(x) = \sum_{j=1}^{n} A_j U_j(x) \qquad [5.9]$$

$U_j(x)$ are unit pulses and are defined as

$$U_j(x) = \begin{cases} 1 & a_{j-1} \le x \le a_j \\ 0 & x \le a_{j-1}, x \ge a_j \end{cases} \qquad [5.10]$$

The solution involves determining the unknown coefficients A_j corresponding to the stress value within the jth increment. Substituting Eq. 5.9 into Eq. 5.1 gives

$$\varepsilon(a_i) = \frac{1}{E'} \int_0^{a_i} G(x, a_i) \sum_{j=1}^{n} A_j U_j(x) dx = \frac{1}{E'} \sum_{j=1}^{n} A_j \int_{a_j}^{a_{j-1}} G(x, a_i) U_j(x)\, dx = \sum_{j=1}^{n} A_j C_{ij} \qquad [5.11]$$

Thus, C_{ij} or the elements of compliance matrix can be defined by

$$C_{ij} = \frac{1}{E'} \int_{a_j}^{a_{j-1}} G(x, a_i) U_j(x) dx \qquad [5.12]$$

Comparing with Eq. 5.1 indicates that C_{ij} is the measured strain by the strain gage for a slit of depth a_i when residual normal stress distribution at the domain $a_{j-1} \le x \le a_j$ is equal to the unit load:

$$C_{ij} = \varepsilon(a = a_i, \sigma(x) = U_j(x)) \qquad [5.13]$$

The difference of compliance coefficients for the strip loads method and continuous polynomials method (Eqs 5.5 and 5.13) should be noted. The physical interpretation of the compliance matrix for the strip loads method is shown in Fig. 5.2. This matrix is a lower triangular.

In the strip loads method, the number of known strains and unknown stresses are identical and using least squares fit is not possible. As a result, contrary to piecewise and continuous polynomials methods, the strip loads method is more sensitive to experimental noise in the measured strains. Numerical techniques can be used to solve this issue. For example, Schajer and Prime (2006) used Tikhonov regularization to reduce the effect of measurement noise. Tikhonov regularization was also used by Schajer (2007) in the hole-drilling method.

The main advantage of the strip loads approximation is that it requires no explicit assumption for the residual stress distribution. Therefore, they can be used for laminated composites. A successful application of this method to the hole-drilling residual stress measurement in carbon/epoxy laminates was reported by Sicot *et al.* (2003). Overall, the use of the strip loads or piecewise polynomials is mandatory for laminated composites, because discontinuity of the mechanical properties across the layer interfaces results in discontinuity of residual stresses.

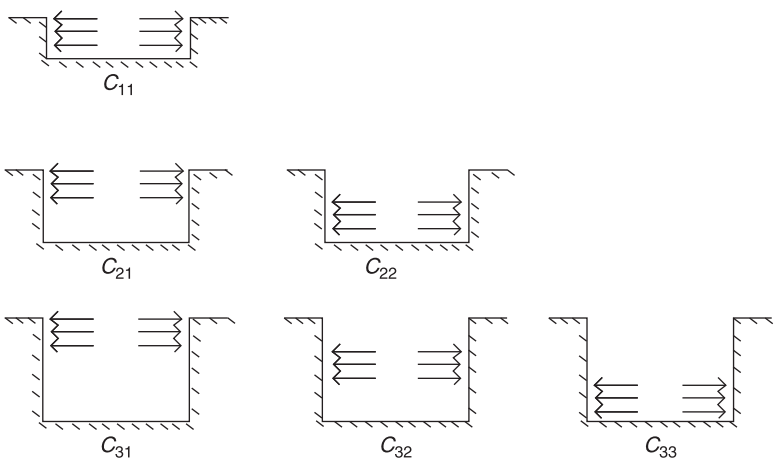

5.2 Physical interpretation of compliance coefficients C_{ij} of the strip loads method.

5.4 The finite element method (FEM) for calculation of compliance functions

Compliance coefficients for each method of approximation depend on the geometry of the slit, the strain gage length and its relative position, stacking sequence of the laminate and mechanical properties of the uni-directional ply. Researchers use any of a variety of analytical methods, such as the body force method and the linear elastic fracture mechanics method (LEFM) (Cheng and Finnie, 2007), to calculate the compliance coefficient. In the LEFM, the slit is treated as a crack, but the body force method includes the finite width of the slit. The analytical solutions have two major disadvantages, in that they are generally for isotropic materials. Lee and Hill (2007) presented a table of compliance coefficients for the back surface gage on the isotropic beam. In addition, analytical methods can only be employed for simple geometries, such as plates, beams and disks. For orthotropic materials, such as laminated polymer composites, the finite element is the only available method. For these materials, compliance coefficients must be calculated for each specimen separately. Shokrieh and Akbari (2011) explained FEM calculations of the calibration coefficients for the laminated composites.

5.4.1 Linear elasticity and superposition principle

In order to calculate compliance coefficients, almost all researchers use a simple superposition principle. According to this principle, when a slit is introduced to a specimen with the residual stress, the released strain is the same as that produced by applying the same residual stress profile with an opposite sign to the faces of the slit of a specimen without residual stress. This principle is an extension of Bueckner's superposition principle (Bueckner, 1973), which was developed for the crack propagation.

5.4.2 General considerations in finite element mesh

In this section, the concept of the simulated slitting method for isotropic materials and laminated composites is explained. The calculations are carried out using the commercial code ANSYS [Ver. 21]. It should be noted that all compliance functions calculated in this section are related to the continuous polynomials, obtained according to Eq. 5.5. The following finite element models can also be employed for calculating compliance coefficients related to the strip loads method and piecewise polynomials method; only loading will be different. Because the run time of the three-dimensional (3D) computation is large, two-dimensional (2D) models are often used. The modeling of rectangular samples such as plates and beams are simplified by using the plane strain symmetric models (Prime, 1999).

Because of symmetry, only half of the model is simulated. In Fig. 5.3, the 2D symmetric model used for the simulation of the slitting process is shown. This

simple model has been used by many researchers (Ersoy and Vardar, 2000; Hill and Lin, 2002; Lee and Hill, 2007). The slit width is assumed to be negligible, therefore the slit is approximated by a crack. Because of the symmetry, the nodes along the slit plane were initially constrained in the y-direction. The node at $x/t = 1$ and $y = 0$ is also constrained in the x-direction to prevent a rigid body motion. The crack extension is simulated on the left side of the model, by releasing nodes along the plane of symmetry. The crack surface is thus indicated by the unconstrained nodes on the crack plane. In this model, the crack extended to a depth of $a_{max}/t = 0.95$. The strain gage is considered on the back surface and the elastic modulus was taken as 1 Pa and Poisson's ratio as 0.3. The type of the element used is the four-node *Plane42* solid element. Since the change of released strain on the strain gage location is of interest, a finer mesh should be used on the area near the slit. For simplicity, all dimensions used in this study are normalized by the thickness to have a non-dimensional model. The normalized dimensions for this model are $L = 4$, $l = 0.2$, $w = 0$ and $B = 0$ (plane stress).

The discretization of a continuous load on the nodes along the surface of the crack may result in a small residue in the resultant force. Thus, mesh refinement was investigated, and the models are adequately converged such that a major increase in the mesh density results in a negligible change in the compliance functions. The efficiency of a 2D symmetric model can be investigated by comparing results with a 3D model. The process of the slitting was repeated with 3D eight-node solid elements (ANSYS type *Solid45*). The specimen depth was taken as $B = 3$. The model is thus under the plane strain conditions and for comparison with the plane-stress 2D model, the results should be multiplied

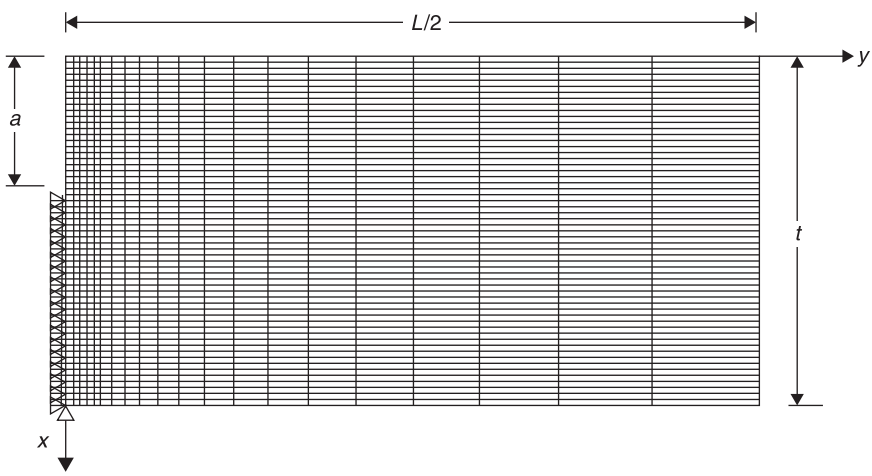

5.3 A two-dimensional finite element mesh used to calculate compliance coefficients of an isotropic specimen.

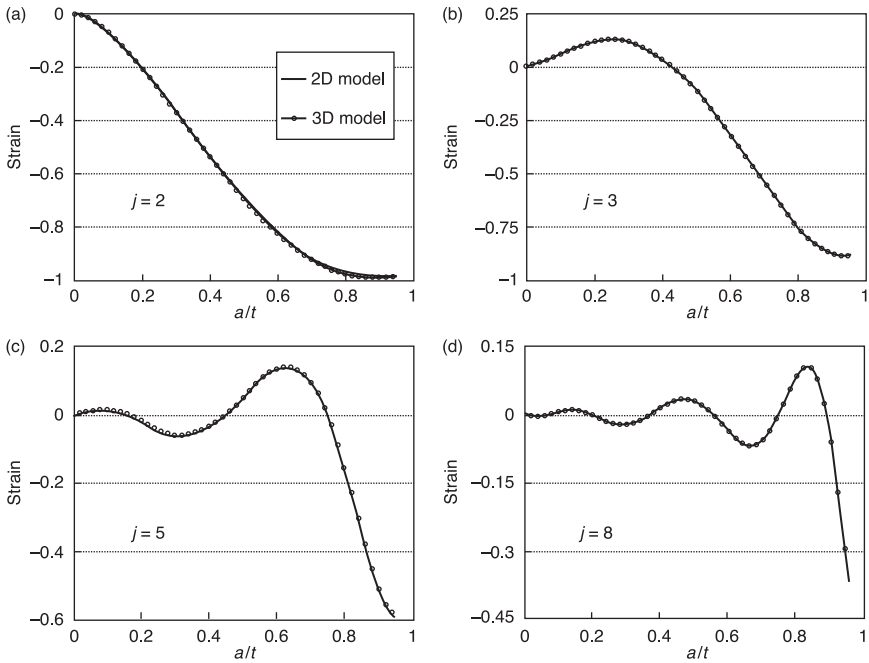

5.4 Comparison of compliances for 2- and 3D models: (a) $j = 2$; (b) $j = 3$; (c) $j = 5$; and (d) $j = 8$.

by $1/(1 - \upsilon^2)$. In Fig. 5.4, the extracted compliances of the 2- and 3D simulations are plotted versus the slit depth to the thickness ratio (a/t) for $l/t = 0.2$ and Legendre polynomial order $j = 2$, 3, 5 and 8. It can be observed that the results of the 3D model fit the 2D data well.

Although the 3D modeling is more time-consuming, it has advantages in comparison with a 2D modeling:

- With 3D models, compliance functions can also be obtained for parts with a varying width such as disk.
- In a 2D finite element analysis, it is usually assumed that the state of deformation is either in plane-stress for a thin specimen or in plane-strain conditions for a long specimen. However, many components have a width that falls between these two limits. Thus, a deformation assumed to be in either state will deviate from the actually measured ones.

Effect of slit width

In most applications of the slitting method, the slit width is assumed to be small relative to the thickness of the specimen and the slit is approximated by an

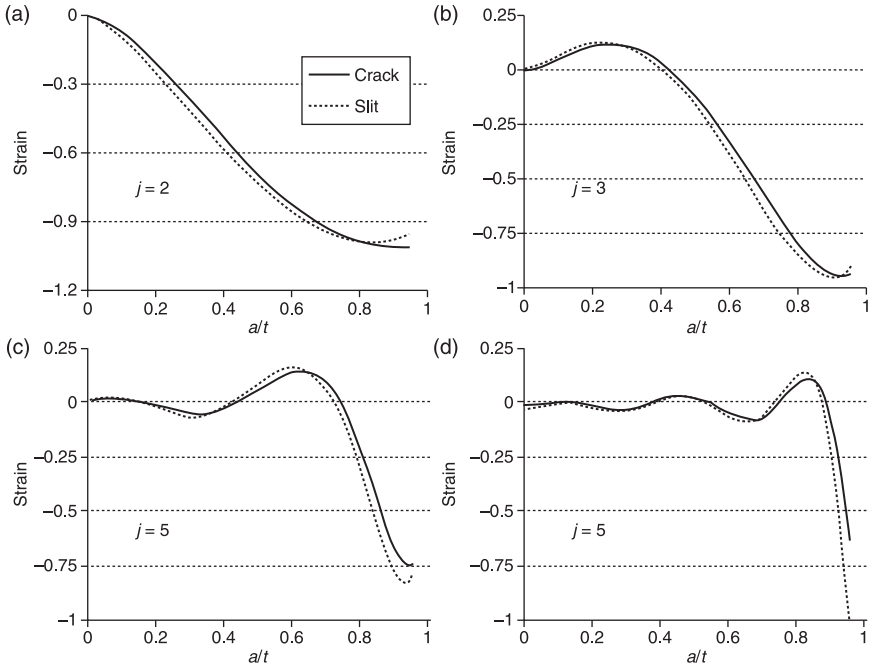

5.5 Comparison of compliances for crack and slit: (a) $j = 2$; (b) $j = 3$; (c) $j = 5$; and (d) $j = 8$.

extending crack. In this section, a more general problem is considered in which the slit width is considerable and cannot be ignored. In order to show the dependence of the compliances on the slit width, these coefficients are calculated for the 2D model used in Section 5.4.2, with a slit of a finite width. Taking the width of the slit as 10% of the thickness ($w/t = 0.1$), the compliance functions of the slit for $j = 2$, 3, 5 and 8 are obtained. Unlike a crack, for which an increment in depth is achieved by releasing nodes ahead of the crack tip, an advance of the slit has to be simulated by removing the elements at the bottom of the slit at each step.

A comparison with the compliance functions for a crack is shown in Fig. 5.5. A noticeable difference is observed between the results of a crack and a slit. Therefore, a slit of finite width cannot be approximated by a crack, especially for thin specimens such as composite laminates. This is because in such parts, the width of the slit is not very small relative to the thickness, and the width of the slit has to be taken into account in computing the compliance functions.

5.4.3 Compliance functions of a cross-ply laminate

In the process of the simulated slitting method for composite materials, the unidirectional lamina is considered as a transversely isotropic material. A cross-ply

glass/epoxy laminate is considered and its mechanical properties are given in Table 5.1.

Unlike the previous section, the full model without symmetry assumption is considered for a better precision. This is because during the slitting experiment the part is clamped in one side and is not symmetrical (Fig. 5.6).

A glass/epoxy $[0_2/90_2]_s$ laminated composite with a top strain gage is modeled. The normalized dimensions of the model (with respect to the thickness of the laminated composite) include $B = 3$, $L = 6$, $l = 0.5$ and $w = 0.1$. The normalized distance between the center of the gage and the slit edge is 0.6. Three-dimensional eight-node layered solid elements (*Solid46*) are used for the mesh modeling.

Figure 5.7 shows the top view of a mesh scheme of the composite laminate and the strain gage. Each layer of this composite laminate is modeled separately. So each layer has its own mechanical properties, fiber direction and thickness. Due to cantilever boundary condition, all nodes at the left edge of the model are completely constrained. The compliance function is calculated by removing the elements in the slit area.

In simulation of the slitting method and other methods of measuring residual stresses based on incremental material removal such as the hole-drilling method and the layer removal method, it is necessary to remove elements related to the removed material. A common way of removing elements is by using the ANSYS Elements Birth and Death feature by EKILL command. It deactivates desired elements by multiplying their stiffness matrix by 10^{-6}. Many researchers used this method for 2- and 3D modeling of different methods of residual stress measurement (Ersoy and Vardar, 2000; Shokrieh and Ghasemi, 2007). Using this method, dead elements still technically exist; they just have almost

Table 5.1 Elastic constants of glass/epoxy uni-directional ply

E_x (GPa)	G_{xy} (GPa)	E_y (GPa)	ν_{xy}
38.6	4.14	8.27	0.26

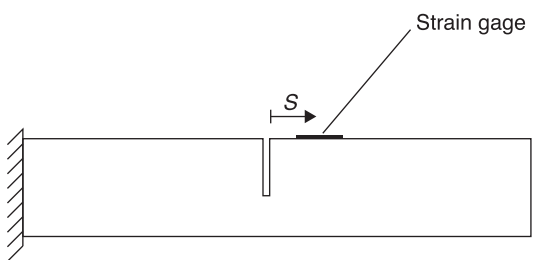

5.6 A specimen with cantilever boundary condition.

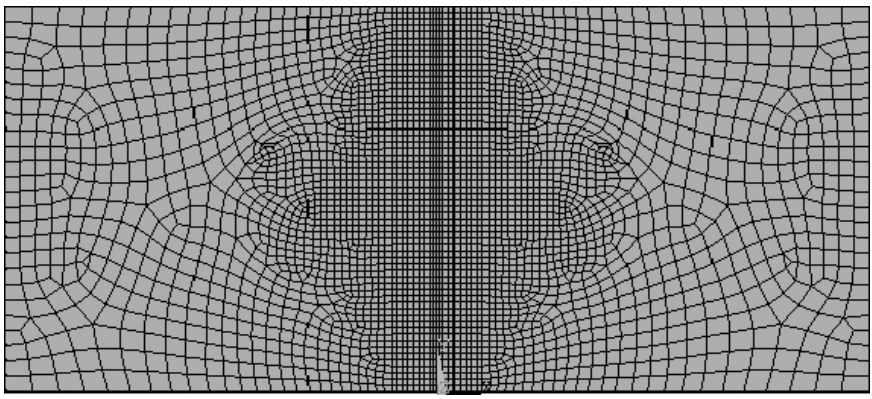

5.7 Top view of 3D finite element mesh used to calculate compliances in laminated composites.

zero stiffness and thus have no affect on the model. Therefore, this feature may be useful in situations when we may need to activate dead elements again. For example, we may use this method in a thermal-structural analysis to deactivate elements reaching their melting point, because they have no structural effect. Then we can activate melted elements again when they reach their freezing point. However, in simulation of the slitting method, we need to delete slit elements permanently.

Also, using this feature for 3D modeling greatly increases the run time. That is mostly because this method needs non-linear solution requirements. To cope with this problem, another approach was used; the area of the slit was modeled apart from remainder of the model. Also, every layer of the composite laminate at the area of the slit was simulated separately. Thickness of every layer was considered equal to the increment of depth in each step. Then all parts of the model were merged together. Finally, for creating the slit at each depth, volume elements in the slit area were easily deleted by the VCLEAR command. Then the related unmeshed volume was removed by the VDELE command. Applying this method is much more convenient than the previous one. It does not need non-linear adjustments. In addition, it decreases run time significantly.

In the meshing of the composite laminate, the area near the slit was meshed denser than the other areas of the model. After applying the distributed load, the y-strain at the gage location is calculated by averaging the strains on element nodal points under the strain gage area (strain-based method). For this laminate, compliance functions of continuous polynomials method are plotted in Fig. 5.8 for $j = 2$, 3, 5 and 8. This figure indicates that for this special configuration and dimensions, the released strain has no significant change with stress distribution applied in depths of more than $a/t > 0.2$. Therefore, for laminated composites, residual stress measurement in larger depths with top surface strain gage is

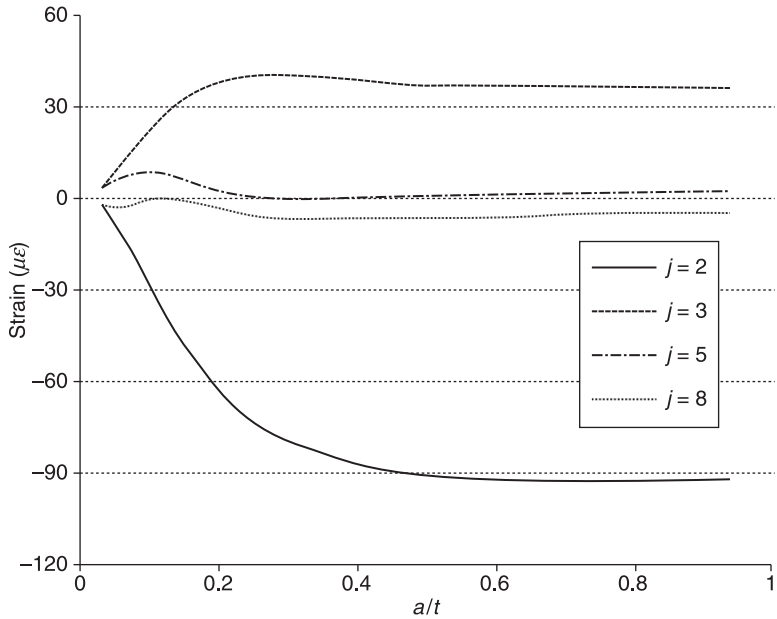

5.8 Compliance functions for a glass/epoxy $[0_2/90_2]_s$ composite laminate.

not possible. This behavior is similar to isotropic materials. Although the presented finite element model was employed for calculating compliance coefficients of continuous polynomials method, it can also be used for other methods in a similar way.

5.5 Residual shear stresses: effects on measured strains

According to Eq. 5.1, an important assumption considered in the slitting method is that the measured strains are only a function of the released stress perpendicular to the slit face. Based on this assumption, a great deal of research effort is focused on the incremental slitting determination of the residual stress component normal to the slit face. However, the slitting process will also release two components of shear stress, which may influence the measured strains.

Considering the heterogeneous structure of laminated composites, higher amounts of residual shear stresses are likely to be created in these materials. In this section, the effect of the residual shear stresses on measured strains in the slitting method is investigated. Only angle-ply laminates are considered, because in cross-ply laminates residual shear stress would not be created. For this purpose, hypothetical distributions for normal and shear stresses should be

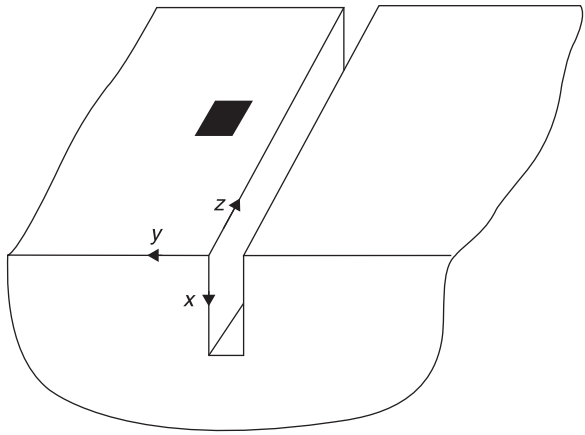

5.9 Coordinate system considered for stress distributions.

considered. In order to create comparable results, assumed stress distributions must satisfy force and moment equilibrium equations as well as boundary conditions. These distributions should also have the same maximum value to facilitate a comparison between effects of different components of residual stresses.

According to Fig. 5.9, in addition to residual normal stress (σ_{yy}), two components of residual shear stress (τ_{yz} and τ_{yx}) are also released during slitting. Considering the laminated structure of a laminated composite, τ_{yz} is named as the in-plane shear stress and τ_{yx} as the out-of-plane shear stress. It is assumed that σ_{yy} and τ_{yx} vary only in the x-direction and τ_{yz} varies only in the z-direction.

Dimensions of the specimen are the same as those used in Section 5.3. The residual out-of-plane shear stress $\tau_{yx}(x)$ vanishes at both upper and lower free surfaces. An expression for this stress component must satisfy the following equations:

$$\begin{cases} \int_0^1 \tau_{yx}(x)\,dx = 0 & \text{Force balance} \\ \tau_{yx}(0) = \tau_{yx}(1) = 0 & \text{Boundary conditions} \end{cases} \quad [5.14]$$

Also, the residual in-plane shear stress $\tau_{yz}(z)$ vanishes at both front and back free surfaces:

$$\begin{cases} \int_0^3 \tau_{yz}(z)\,dz = 0 & \text{Force balance} \\ \tau_{yz}(0) = \tau_{yz}(3) = 0 & \text{Boundary conditions} \end{cases} \quad [5.15]$$

Moment balance for τ_{yz} and τ_{yx} is always satisfied.

For $\sigma_{yy}(x)$, these conditions are defined as

$$\begin{cases} \int_0^1 \sigma_{yy}(x)\,dx = 0 & \text{Force balance} \\ \int_0^1 x\,\sigma_{yy}(x)\,dx = 0 & \text{Moment balance} \end{cases} \quad [5.16]$$

Also, $\sigma_{yy}(x)$ has no boundary condition. According to Eqs 5.14 to 5.16, stress distributions can be assumed as

$$\begin{aligned} &\sigma_{yy}(x) = 10(6x^2 - 6x + 1) \quad \text{MPa} \quad 0 \le x \le 1 \\ &\tau_{yx}(x) = 10\sin(2\pi x) \quad \text{MPa} \quad 0 \le x \le 1 \\ &\tau_{yz}(z) = 10\sin\left(\frac{2\pi}{3}z\right) \quad \text{MPa} \quad 0 \le z \le 3 \end{aligned} \quad [5.17]$$

All these distributions have a maximum magnitude of 10 MPa.

Although already mentioned, distributions satisfy boundary conditions as well as force and moment balance, but they do not satisfy the following equilibrium equation:

$$\frac{\partial \tau_{xy}}{\partial x} + \frac{\partial \sigma_{yy}}{\partial y} + \frac{\partial \tau_{yz}}{\partial z} = 0 \quad [5.18]$$

Based on this equation, two components of shear stress cannot exist independently. As a result, contrary to assumed distributions in Eq. 5.17, shear stress components could not be the function of only one spatial variable. At least one of them changes in both the *x*- and *z*-directions. Because it is hard to find distributions that would satisfy all conditions simultaneously, distributions presented in Eq. 5.17 are used for simplicity. The results are reliable, because the assumed stress distributions satisfy equilibrium condition for each stress component separately. The calculations are carried out using the finite element model described in the Section 5.4.3. In order to apply the shear stress to the faces of layered elements at the slit location, structural surface effect elements (*Surf154*) should be overlaid onto the area faces of surface elements of the slit face.

5.5.1 Effect on back surface measurements

Consider a glass/epoxy $[\pm 45]_s$ laminate and a steel specimen ($E = 200$ GPa and $\nu = 0.3$). For the stress distributions mentioned in Eq. 5.19, released strains on the back surface are plotted versus *s* (distance from the center of the slit (Fig. 5.8)) for four different depths in Figs 5.10 and 5.11. Strains are calculated at the mid-depth ($Z = 1.5$) of the finite element models.

Results show that on both sides of the slit, strains due to the normal stress are symmetrical. However, strains due to both in-plane and out-of-plane shear stresses are almost anti-symmetrical.

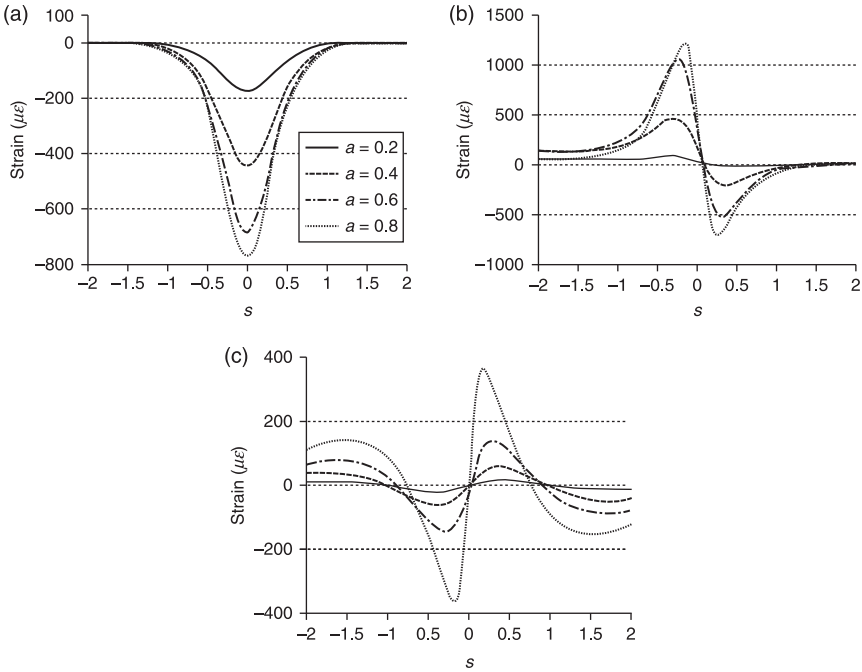

5.10 Distribution of released strain on back surface for a glass/epoxy $[\pm 45]_s$ laminate due to: (a) residual normal stress: $\sigma_{yy} = 10(6x^2 - 6x + 1)$ MPa; (b) residual out-of-plane shear stress: $\tau_{yx} = 10 \sin(2\pi x)$ MPa; and (c) residual in-plane shear stress: $\tau_{yz} = 10 \sin(2\pi z/3)$ MPa.

Figures 5.10 and 5.11 show that when measuring with a back gage, strains due to τ_{yx} and τ_{yz} may be significant compared with strains due to σ_{yy}. However, there are two reasons that the released strains due to τ_{yx} and τ_{yz} on the back surface are not important and will not influence strain measurements in a real experiment:

1. Around the slit at the domain $-1 \leq s \leq 1$, strain distribution due to σ_{yy} is symmetrical, but due to the τ_{yx} and τ_{yz} is not, and strains vary from positive to negative at $s = 0$. The back face strain gage is usually bonded directly opposite the slit and its center is at $s = 0$. Also, because the strain measured by a strain gage is essentially the average strain under the area of the strain gage, positive and negative strains on both sides of the slit neutralize each other in a large part and thus reduce the strain value recorded by the strain gage. It is important to note that this result is based on the assumption that the strain gage is bonded completely opposite the slit.
2. The maximum magnitudes of τ_{yx} and τ_{yz} are assumed to be equal to σ_{yy}, which in practice it is unlikely to occur. For example, in Fig. 5.10, at each depth, the maximum strain obtained due to τ_{yz} is seen as less than 40% of that due to σ_{yy}.

If the maximum magnitude of τ_{yz} is not more than a quarter of that of σ_{yy}, the maximum error in the released strain measured in the presence of the shear stress will not be more than 10%.

It is important to note that unlike the strains due to in-plane shear stress, strains due to out-of-plane shear stress are not completely equal and anti-symmetrical in both sides of the slit. As shown in Fig. 5.6, the left side of the finite element model is constrained in order to simulate the real boundary condition. Therefore, it can be concluded that in a real slitting experiment with the cantilever boundary condition, released strains due to τ_{yx} would have larger values on one side of the slit, where the constrained boundary condition is located. However, modeling with a free boundary condition for both sides of the slit results in a completely equal and anti-symmetrical distribution of strains due to τ_{yx}.

Results of this simulation agree with results of an analytical approach used by Cheng and Finnie (1992). They showed that τ_{yx} has no effect on the measured strains on the back surface. For this purpose, they applied Castigliano's theorem

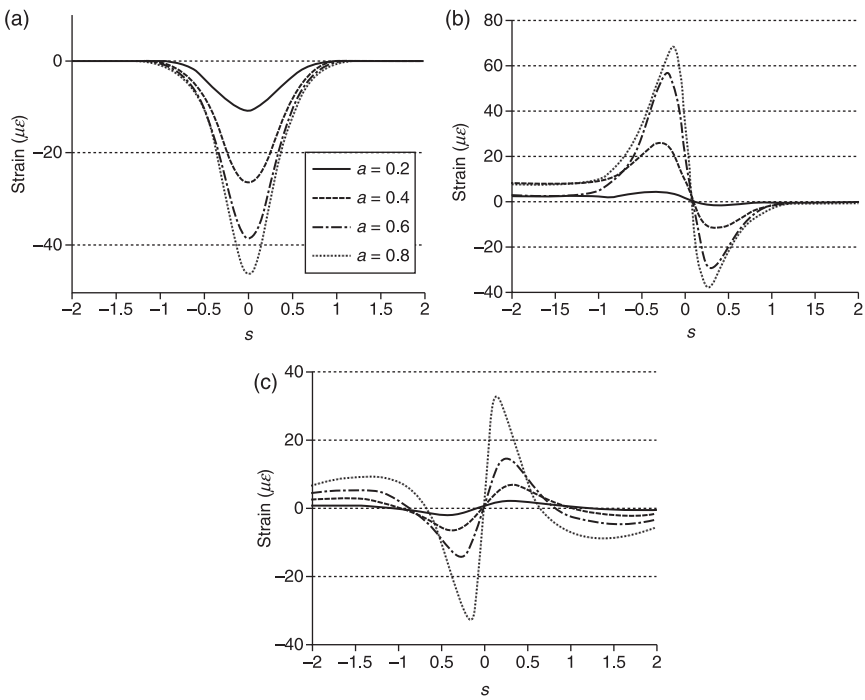

5.11 Distribution of released strain on the back surface for a steel specimen due to: (a) residual normal stress: $\sigma_{yy} = 10(6x^2 - 6x + 1)$ MPa; (b) residual out-of-plane shear stress: $\tau_{yx} = 10 \sin(2\pi x)$ MPa; and (c) residual in-plane shear stress: $\tau_{yz} = 10 \sin(2\pi z/3)$ MPa.

to a homogeneous semi-infinite plane with symmetrical boundary condition. Consequently, distribution of released strains due to τ_{yx} around the slit was completely equal and anti-symmetrical. They used the same procedure in other research (Cheng *et al.*, 1991) to calculate strains due to τ_{yz} with uniform, linear and quadratic distributions. These distributions do not satisfy equilibrium equations and boundary conditions. Generally, these results show that the strains measured by the back surface strain gages correspond only to the normal residual stress and will not be affected by the presence of any component of residual shear stress on the plane of the slit.

5.5.2 Effect on top surface measurements

In this section, the effect of the in-plane and out-of-plane shear stresses, τ_{yz} and τ_{yx}, on the released strain on the top surface are investigated. In Figs 5.12 and 5.13, distribution of the released strains on the upper surface are plotted versus s for a

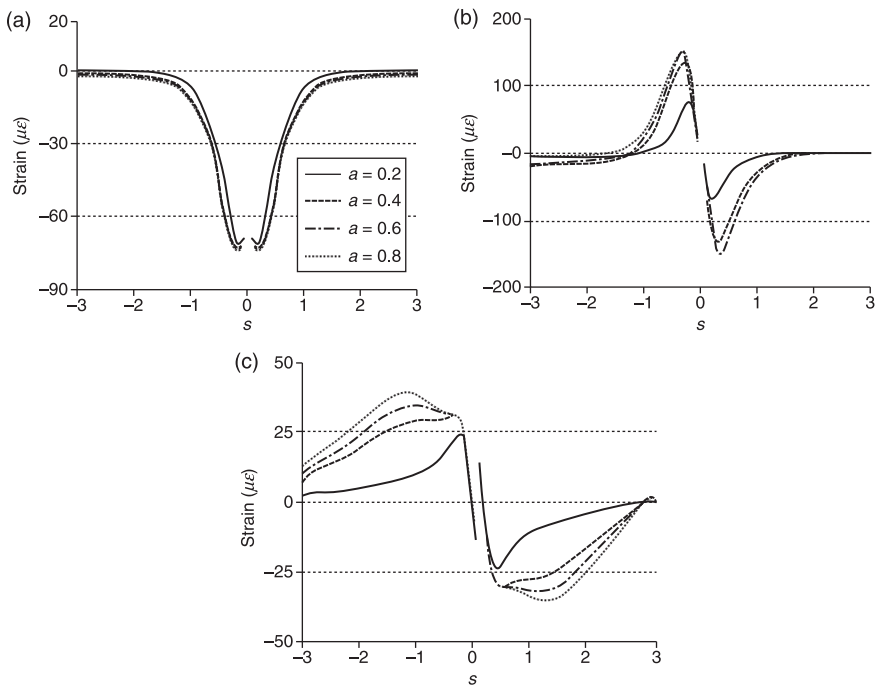

5.12 Distribution of released strain on the top surface for a carbon/epoxy [0/±45/90]s laminate due to: (a) residual normal stress: $\sigma_{yy} = 10(6x^2 - 6x + 1)$ MPa; (b) residual out-of-plane shear stress: $\tau_{yx} = 10 \sin(2\pi x)$ MPa; and (c) residual in-plane shear stress: $\tau_{yz} = 10 \sin(2\pi z/3)$ MPa.

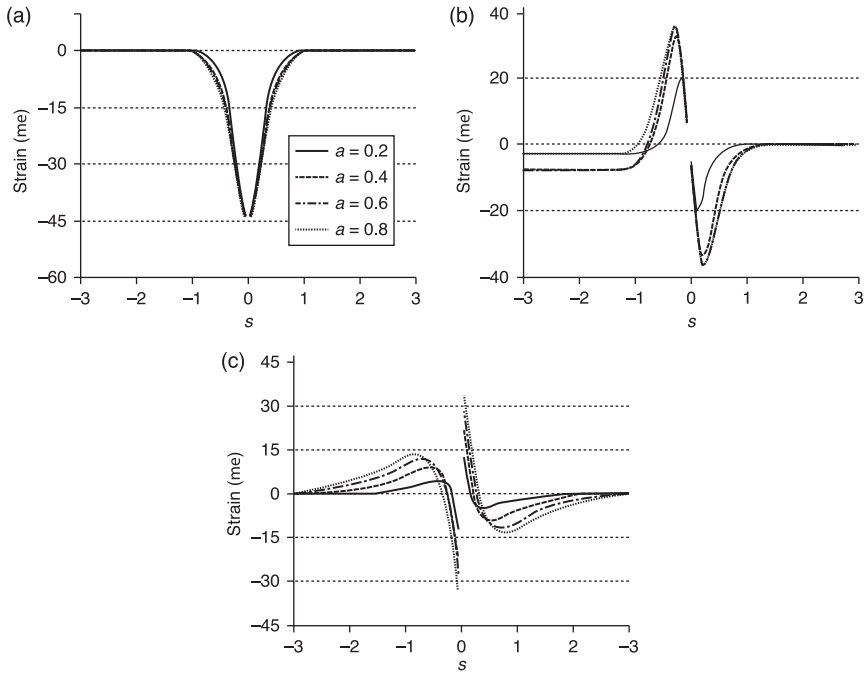

5.13 Distribution of released strain on the top surface for a steel specimen due to: (a) residual normal stress: $\sigma_{yy} = 10(6x^2 - 6x + 1)$ MPa; (b) residual out-of-plane shear stress: $\tau_{yx} = 10 \sin(2\pi x)$ MPa; and (c) residual in-plane shear stress: $\tau_{yz} = 10 \sin(2\pi z/3)$ MPa.

carbon/epoxy $[0/\pm45/90]_s$ laminate and a steel specimen for four different depths. Results show that on the top surface, like the back surface, at the domain $-1 \leq s \leq 1$, strain distribution due to normal stress is symmetrical. Also, strain distribution due to both in-plane and out-of-plane shear stresses are completely anti-symmetrical. Therefore, presence of both residual normal and shear stresses causes the asymmetrical distribution of the released strain. In addition, Figs 5.12 and 5.13 show that as the depth of slit increases, released strains due to in-plane and out-of-plane shear stresses also increase, but due to the normal stress remain basically constant, which indicates that with increasing the depth, the contribution of shear stresses in measured strains increases.

Based on the results, we can see that for the assumed stress distributions, at $a = 0.8$, the maximum released strain in glass/epoxy laminate due to the in-plane and out-of-plane shear stresses is almost equal to the maximum magnitude of released strain due to the normal stress. Similar behavior is observed in other specimens. This point shows that existence of residual shear stresses deserves special attention for the top surface strain gage measurements for both isotropic and orthotropic materials.

Therefore, when measuring released strains with top surface strain gages, the stress components other than the normal stress on the faces of the slit may affect the measured strain, and a computation based on normal stresses alone will result in error.

5.5.3 Separation of residual shear stress effects

According to the discussion in the previous section, the assumption of the negligible effect of shear stress on the measured strains can result in a significant error when using top surface strain gages. For a more precise measurement, the effects of the residual normal and shear stresses on the measured strains should be separated from each other. It was shown that strain distribution on the top surface due to the normal stress is symmetrical, but the strain distribution due to shear stresses is anti-symmetrical. We can use this point to separate the effects of normal and shear stresses from each other. For this purpose, two strain gages should be attached on both sides of the slit at equal distances from the slit edge. Two different configurations are considered. In the first case (Fig. 5.14(a)), it is assumed that there is only the normal stress at the slit location. In the second case (Fig. 5.14(b)), it is assumed that there is only the shear stress at the slit location (only the out-of-plane shear stress has been shown in Fig. 5.14(b)).

Referring to the previous discussion, we have:

$$\varepsilon_1 = \varepsilon_2, \quad \varepsilon_1' = -\varepsilon_2' \qquad [5.19]$$

Generally, both normal and shear stresses are released in the plane of the slit (Fig. 5.15) and strain gages indicate different values.

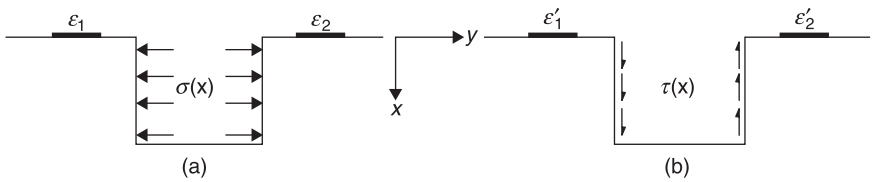

5.14 (a) Residual normal stress; and (b) residual shear stresses acting on the plane of the slit.

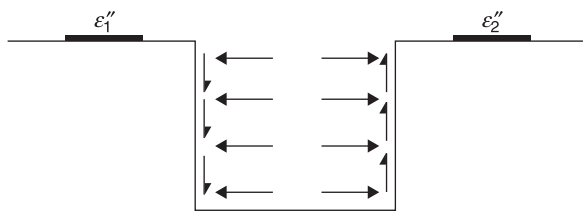

5.15 Both normal and shear stresses exist in the plane of the slit.

Using the principle of superposition results in

$$\varepsilon_1'' = \varepsilon_1 + \varepsilon_1' \quad , \quad \varepsilon_2'' = \varepsilon_2 + \varepsilon_2' \qquad [5.20]$$

Regarding Eqs 5.19 and 5.20, we can conclude that

$$\begin{cases} \varepsilon_1 = \varepsilon_2 = \dfrac{\varepsilon_1'' + \varepsilon_2''}{2} \\ \varepsilon_1' = -\varepsilon_2' = \dfrac{\varepsilon_1'' - \varepsilon_2''}{2} \end{cases} \qquad [5.21]$$

With this method, strains due to the residual normal stress can be separated from those due to shear stresses.

Hosseinzadeh *et al.* (2010) measured released strains on opposite sides of the slit in a welded compact tension specimen using two gages, which registered significantly different strain readings. The presence of significant shear stresses along the slit face has probably been the most important reason for the differences in the top gage readings. This strong evidence shows that it is important to take into account the shear stresses effects when measuring the residual stress by the slitting method. However, they did not separate the released strains due to shear and normal stresses and used the back gage readings to calculate the residual stresses.

The conclusions of this section can be summarized as:

- On the back surface, although the strains due to the in-plan and out-of-plane shear stresses have considerable values, their effects can be ignored; because they have different signs on both sides of the slit and neutralize each other. Therefore, the residual normal stress determined by using back surface strain gages will not be affected by the residual shear stresses.
- On the top surface, from a comparison of the measured strain distribution due to the in-plane and out-of-plane shear stresses with those due to the normal stress, it was found that both components of shear stresses result in significant values of released strains and might have noticeable contribution to the measured strains and therefore cannot be ignored.
- Also, the in-plane and out-of-plane shear stresses have almost opposite effects on the opposite sides of the slit on the top surface. However, normal stresses have approximately equal effect. Therefore, significant shear stress values would be recognizable in the measured strains and using two strain gages located on opposite sides of the slit will allow strains due to normal and shear stresses to be separated.

5.6 Case study: residual stress measurement in a carbon/epoxy laminate

The incremental slitting method was applied for the determination of residual stresses in symmetrical laminated composites. A detailed description of the method is presented in this section.

5.6.1 Material preparation

In this research, $[0_4/90_4]_s$ carbon/epoxy laminate was selected. The material used was T300 uni-directional carbon fibers with epoxy resin LY-5052 and hardener Aradure-830. This is a high performance composite used mostly in the aeronautical and aerospace industries. The curing process involved temperature stages of 100 °C during 6 hours, followed by 120°C for 6 hours. The heating and cooling rates were 4°C/min. The results of the characterization tests are shown in Table 5.2. The longitudinal tensile test, transverse tensile test and shear test were carried out according to ASTM (30–31).

The surface of the specimens is not abraded; it is only degreased with acetone. This is because manual abrasion can change the residual stress state of the specimen. The composite specimens prepared for the slitting experiment are shown in Fig. 5.16. Dimensions of these specimens are given in Table 5.3.

Table 5.2 Elastic constants of uni-directional carbon/epoxy ply

E_x (GPa)	G_{xy} (GPa)	E_y (GPa)	ν_{xy}
104.6	3.8	7.5	0.31

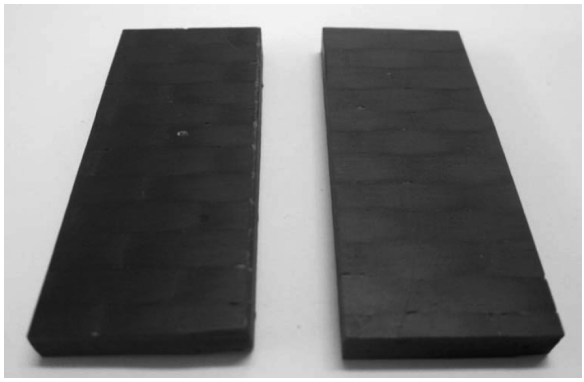

5.16 Composite specimens prepared for slitting experiment.

Table 5.3 Dimensions of the composite specimen (mm)

Width (B)	Length (L)	Thickness (t)	Slit width (w)
20	60	4.80	0.25

5.6.2 Experimental procedure

The slitting process may introduce significant amounts of residual stress to the part. Stresses induced by the slitting have a very small effect on the back surface gage measurements. However, a top surface gage is much more sensitive to slitting induced stresses, so the method used to make a slit of increasing depth is of special importance, especially for near-surface measurements. Saw, milling cutter and wire electrical discharge machining (wire EDM) are common ways of making a slit in the slitting method. Using wire EDM is preferred, because contrary to mechanically machining methods, wire EDM is less likely to introduce additional residual stresses to the part. Also, a much finer slit with a very small width can be created (Cheng *et al.*, 1994). However, using wire EDM in polymer composites is not possible, as it only cuts electrical conductive materials. Therefore, a mechanical method of cutting has to be considered. In this study, a computer numerical control (CNC) milling machine with a circular saw blade of thickness 0.2 mm was used to create a slit in depth-direction with 0.1 mm increments. The translation speed was fixed at 3 mm/s and the disk speed at 5000 rpm. The cutter advance-plane was parallel to the fiber direction. The experimental set-up of the slitting test is shown in Fig. 5.17.

Careful attention was paid to several aspects of the slitting experiment. The slit location was selected to be at least twice the specimen thickness from the sample edges. In addition, between each slitting increment the strains were allowed to relax for 1 minute. In this experiment, the slit was cut through the half of the specimen thickness. Precise alignment of the slit to the strain gage is preferred, although it is not mandatory, because compliance coefficients for the actual gage location can always be calculated precisely using a finite element model.

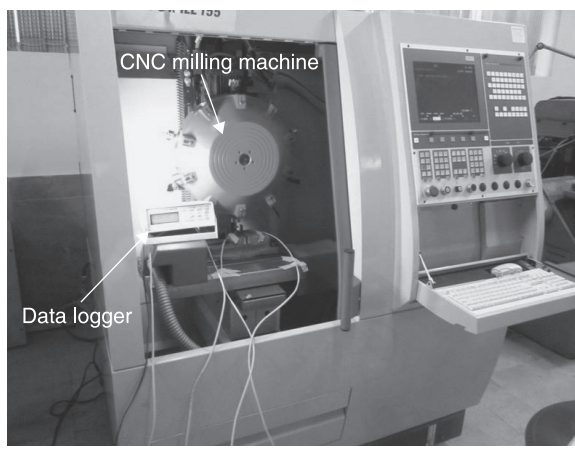

5.17 Experimental set-up used for the slitting experiment.

As mentioned in previous sections, the strain gage can be bonded onto the back surface of the specimen (back surface strain gage) or onto the top surface near the slit (top surface strain gage). A back surface gage is used in this research for several reasons:

- When using the top surface strain gage, the slit must be cut as close as possible to the slit edge, so that the strain gage records higher amounts of strain. In some cases, the top surface gage results are not reliable. According to the previous discussion, the slitting process can introduce additional residual stress and influence the top gage results.
- Top gage results are more susceptible to plasticity effects. These effects cause larger strains to be measured and then greater stresses to be calculated. However, Prime (2010) showed that these effects are not considerable.
- According to the discussion presented in Section 5.5, two components of residual shear stresses released in the slit face can influence the recorded strains. Contrary to the top surface strain gage, the back surface gage is not subjected to these effects and its results are more reliable.
- As shown in Figs 5.12 and 5.13, top gages are only sensitive to near surface residual stress. The stresses released in depths of more than 0.2 of the thickness do not affect the gage readings.

For these reasons, the back surface gage is preferred in this study. The relative positions of the strain gage and cutter in the slitting experiment are shown in Fig. 5.18.

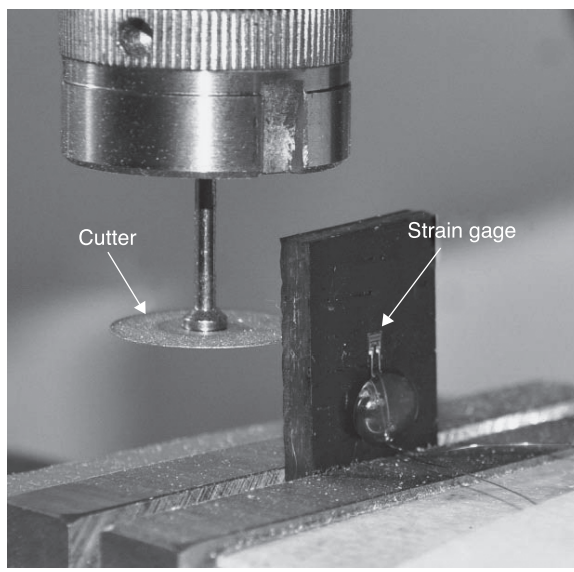

5.18 Relative position of strain gage and cutter in the slitting experiment.

In order to minimize the effect of averaging of the strain over the gage length and to increase the precision of strain readings at the gage location, the gage with smallest gage length available from different types of gages was selected. Type UBFLA-03 strain gage having gage length of 0.3 mm, gage width of 1.9 mm, nominal resistance of 120 W, and gage factor 2.35, supplied from TML Company, were precisely attached to the back surface of the specimen using epoxy resin. The released strains were measured by a commercial Wheatstone bridge strain indicator. The strain gage was connected to the strain indicator in a quarter-bridge using the three-wires technique. This technique allows the system to be calibrated so that temperature variations do not influence the measured strains. The specimen was clamped from one side away from the slit and gage so the other side could deform freely and recorded strains are correct. All required dimensions of the composite specimen, including the distance from the center of the slit to the center of the strain gage grid, final slit depth and slit width, were measured after the slitting process using a microscope. Such measurement of the actual geometry is necessary to obtain precise results from finite element model.

5.6.3 Results and discussion

Figure 5.19 shows the distribution of the back surface measured strains as a function of slit depth. For shallow slit, the strain sensitivity of the back surface strain gage is low. As the slitting progresses deeper, the change in the measured strains becomes more significant. The final slit depth was 2.4 mm. The division of the increments must match as closely as possible the layers boundaries.

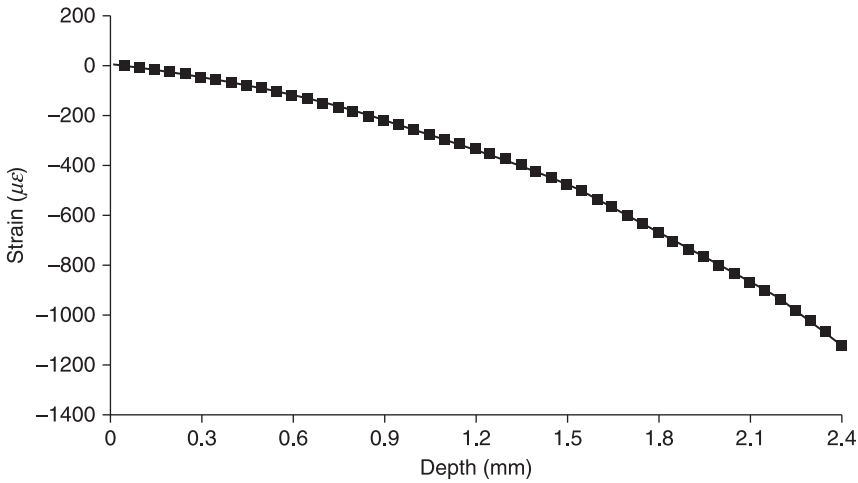

5.19 Measured strains in slitting experiment.

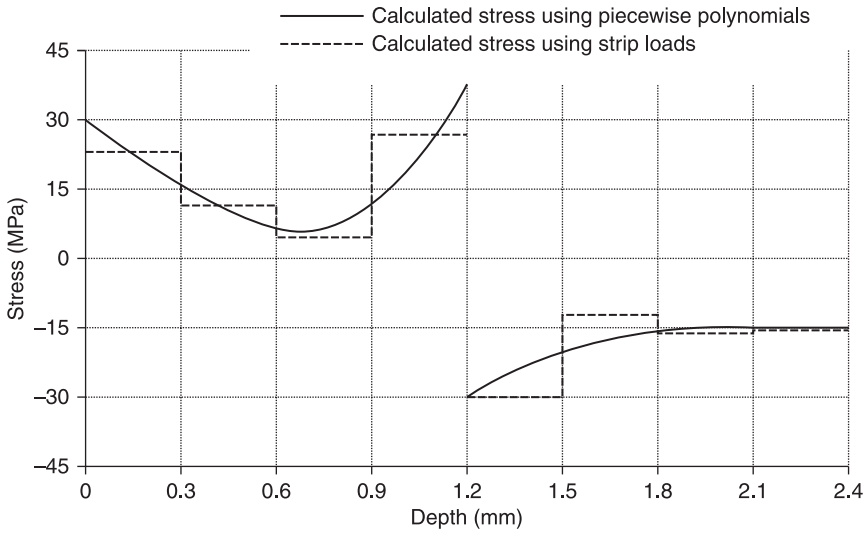

5.20 Residual stress computed using two different approaches.

Figure 5.20 shows the residual stress profile calculated using strip loads and piecewise polynomials approaches. The compliance coefficients for both approaches were determined using an FEM. The stress results of two approaches show a good general agreement. This figure shows the stresses within half the specimen thickness.

In the piecewise polynomials method, two polynomials were used to calculate residual stresses in 0-degree layers and 90-degree layers separately. In 0-degree layers, the average of fourth- and fifth-order Legendre polynomials and in the 90-degree layers, the average of fifth- and sixth-order Legendre polynomials were used for the stress calculation. Such averaging between the successive orders is a common method of reducing endpoint instability in the continuous and piecewise polynomials methods. According to Fig. 5.20, the stresses are tensile through the 0-degree layers and compressive through the 90-degree layers. A local stress maximum occurs at the boundary of 0/90-degree layers. At this point, there exists a remarkable stress concentration.

It was observed that in the strip loads method, the reduction of increment size will create some scatter in calculated stresses. This point shows that the reduction in the depth of each increment rapidly increases the influence of error in measured strains on estimated stresses. This is because in the strip loads method, the number of known strains and unknown stresses are identical and errors in measured strains will be directly reflected in the calculated stress. To obtain a stable estimation we had to omit two-thirds of the measured data; only recorded strains at layers boundaries were used in stress calculation.

However, the piecewise polynomials method is immune to this drawback. We can use this method to make full use of the measured strains and improve the estimation of the stress in each increment. In this method, an increase in the number of increments and a corresponding reduction in the depth of each increment makes it possible to increase the sensitivity of the method and results in greater measuring precision, particularly near the 0/90-degree boundary.

5.7 Conclusions and future trends

The slitting method for determining residual stress profile can give good results, both near the surface and through the thickness of the stressed specimens. This method provides a versatile methodology that can be applied to a wide range of specimen geometries and generally gives accurate and reliable results. Features of the slitting method often make it attractive, even though some specimen damage is caused. This method is much more sensitive than the hole-drilling method for near-surface residual stress measurement and also permits accurate measurement of stresses below the surface.

Over the past decades, great advances in technologies related to material cutting, deformation measurement and computing power have resulted in advances not only in measurement reliability and accuracy, but also in the range of applications; much greater detail in residual stress measurement is now available using the slitting method.

In the application of the slitting method to isotropic materials, continuous polynomials are generally used for the estimation of residual stresses. But for residual stresses in laminated composites, which are affected by the discontinuity of the material properties, the use of the continuous polynomials is not possible. In this chapter, we have discussed two alternative approaches for approximation of residual stresses when employing the slitting method in laminated composites. These approaches include the strip loads method and piecewise polynomials method. The residual stress in a cross-ply carbon/epoxy laminate was successfully determined using these two approaches. Comparison of results showed acceptable agreement.

An important complementary computational approach for destructive methods is the ‘eigenstrain’ method. This method is based on the determination of permanent strains created during inelastic processes, such as thermal expansion mismatch between different parts of a component and plastic deformations. Thus, determining eigenstrain distribution from the slitting strains is an intermediate step to determine the residual stress distribution. An important advantage of the application of this method to laminated composites is that it will give stress discontinuities and might be able to fit the data well. Future work should be performed to determine the residual stress in laminated composites using the eigenstrain method. However, a major issue limiting the application of this approach is that the information about eigenstrain distributions is not always readily accessible.

5.8 References

ANSYS Help System, *Analysis Guide and Theory Reference*, Version 12.

ASTM, Standard test method for tensile properties of polymer matrix composite materials, ASTM d 3039/d 3039m.00. Technical report, American Society for Testing and Materials (ASTM).

ASTM, Standard test method for in-plane shear response of polymer matrix composite materials by test of a g45o laminate, ASTM d 3518/3518m–94. Technical report, American Society for Testing and Materials (ASTM).

Bueckner, H. F. (1973) Field singularity and integral expressions, in: G. C. Sih, (ed.), *Methods of Analysis and Solutions of Crack Problems*, Ch. 5, Groningen, Noordhoff International Publishing, 239.

Cheng, W. and Finnie, I. (1985) A method for measurement of axisymmetric residual stresses in circumferentially welded thin-walled cylinders, *ASME Journal of Engineering Materials and Technology*, **107**, 181–5.

Cheng, W. and Finnie, I. (1992) Deformation of an edge cracked strip subjected to arbitrary shear surface traction on the crack faces, *Engineering Fracture Mechanics*, **43**, 33–9.

Cheng, W. and Finnie, I. (2007) *Residual Stress Measurement and the Slitting Method*, New York, Springer.

Cheng, W., Finnie, I., and Vardar, Ö. (1991) Measurement of residual stresses near the surface using the crack compliance method, *ASME Journal of Engineering Materials and Technology*, **113**, 199–204.

Cheng, W., Finnie, I., Gremaud, M. and Prime, M. B. (1994) Measurement of near surface residual stresses using electric discharge wire machining, *ASME Journal of Engineering Materials and Technology*, **116**(1), 1–7.

Ersoy, N. and Vardar, O. (2000) Measurement of residual stresses in layered composites by compliance method, *Journal of Composite Materials*, **34**(7), 575–98.

Gremaud, M., Cheng, W., Finnie, I. and Prime. M. B. (1994) The compliance method for measurement of near surface residual stresses – analytical background, *ASME Journal of Engineering Materials and Technology*, **116**, 550–5.

Hermann, R. (1995) Crack growth and residual stress in al-li metal matrix composites under far-field cyclic compression, *Journal of Materials Science*, **30**(15), 3782–90.

Hill, M. R. and Lin, W. Y. (2002) Residual stress measurement in a ceramic-metallic graded material, *ASME Journal of Engineering Materials and Technology*, **124**(2), 185–91.

Hosseinzadeh, F., Bouchard, P. J. and James, J. A. (2010) Measurements of residual stress in a welded compact tension specimen using the neutron diffraction and slitting techniques, *Materials Science Forum*, **652**, 210–15.

Lee, M. J. and Hill, M. R. (2007) Effect of strain gage length when determining residual stress by slitting, *ASME Journal of Engineering Materials and Technology*, **129**(1), 375–82.

Prime, M. B. (1999) Residual stress measurement by successive extension of a slot: the crack compliance method, *Journal of Applied Mechanics*, **52**(2), 75–96.

Prime, M. B. (2010) plasticity effects in incremental slitting measurement of residual stresses, *Engineering Fracture Mechanics*, **77**(10), 1552–66.

Prime, M. B. and Hill, M. R, (2004) Measurement of fiber-scale residual stress variation in a metal-matrix composite, *Journal of Composite Materials*, **38**(23), 2079–95.

Schajer, G. S. (1981) Application of finite element calculations to residual stress measurement, *ASME Journal of Engineering Materials and Technology*, **103**(2), 157–63.

Schajer, G. S. (1988) Measurement of non-uniform residual stresses using the hole-drilling method, *ASME Journal of Engineering Materials and Technology*, **110**, 338–49.

Schajer, G. S. (2001) Residual stresses: Measurement by destructive testing, in: *Encyclopedia of Materials: Science and Technology*, Amsterdam, Elsevier, 8152–8.

Schajer, G. S. (2007) Hole-drilling residual stress profiling with automated smoothing, *ASME Journal of Engineering Materials and Technology*, **129**(3), 440–5.

Schajer, G. S. (2010) Relaxation methods for measuring residual stresses: techniques and opportunities, *Experimental Mechanics*, **50**(8), 1117–27.

Schajer, G. S. and Prime, M. B. (2006) Use of inverse solutions for residual stress measurements, *ASME Journal of Engineering Materials and Technology*, **128**(3), 375–82.

Shokrieh, M. M. and Ghasemi, A. R. (2007) Simulation of central hole drilling process for measurement of residual stresses in isotropic, orthotropic and laminated composites plates, *Journal of Composite Materials*, **41**, 435–52.

Shokrieh, M. M. and Akbari R. S. (2011) Simulation of slitting method for calculation of compliance functions of laminated composites, *Journal of Composite Materials*, **46**(9), 1101–9.

Sicot, O., Gong, X. L., Cherouat, A. and Lu, J. (2003) Determination of residual stress in composite laminates using the incremental hole-drilling method, *Journal of Composite Materials*, **37**(9), 831–43.

Vaidyanathan, S. and Finnie, I. (1971) Determination of residual stresses from stress intensity factor measurements, *Journal of Basic Engineering*, **93**, 242–6.

6

Measuring residual stresses in homogeneous and composite glass materials using photoelastic techniques

H. ABEN and A. ERRAPART, Tallinn University of Technology, Estonia and J. ANTON, GlasStress Ltd, Estonia

DOI: 10.1533/9780857098597.1.152

Abstract: This chapter gives a review of the modern photoelastic techniques for residual stress measurement in homogeneous and composite glass articles, including glass articles of complicated shape. For residual stress measurement in axisymmetrical glass articles, integrated photoelasticity is being used. In the case of non-axisymmetrical glass articles of complicated shape, photoelastic tomography is to be used. As for automotive and architectural glass panels used in buildings, surface stress can be measured with the mirage method. More complete stress analysis can be carried out with the scattered light method.

Key words: glass, photoelasticity, residual stress.

6.1 Introduction

Glass is the oldest man-made material. Its invention about 5000 years ago should be considered as one of the crucial events in the history of mankind. Besides traditional applications of glass in buildings and in tableware, glass is now used in the most sophisticated technologies: glass fibres helped create a revolution in telecommunications and glass is used in many modern electronic devices. Two peculiarities of glass should be pointed out. The first is fragility – it breaks easily because of tensile stresses. The second is that in every glass item there exists residual stresses because of the complicated technological process during which glass changes from the state of a viscous liquid at high temperature into a solid state upon cooling. During the cooling process, the temperature field in the glass is inhomogeneous. As a result, residual stresses appear that can considerably reduce or increase the strength of the article. Therefore, measurement and control of the residual stresses are inseparable parts of glass technology.

The photoelastic effect in glass was discovered at the beginning of the 19th century by Estonian-German physicist Seebeck (1813, 1814). Since then, photoelasticity has been widely used for the estimation of residual stress in glass. However, until the middle of the previous century, this estimation has been mostly qualitative, based on the observation of the interference colours in simple polariscopes. Later, many quantitative photoelastic techniques for glass stress

analysis have been elaborated. An exhaustive review can be found in Aben and Guillemet (1993). The aim of this chapter is to give a brief overview of the various photoelastic techniques used today for the measurement of residual stress in homogeneous and composite glass articles.

6.2 Measuring residual stresses in axisymmetric glass articles

6.2.1 Integrated photoelasticity

One of the techniques that can be used for stress measurement in glass articles of complicated shape is integrated photoelasticity (Aben, 1979). In this technique, the test object is placed in an immersion tank and a beam of polarised light is passed through it (Fig. 6.1a). The light rays, which pass the axisymmetrical hollow glass article parallel to the mid-surface, between points A and B, are the most informative. This is termed illumination by tangential incidence.

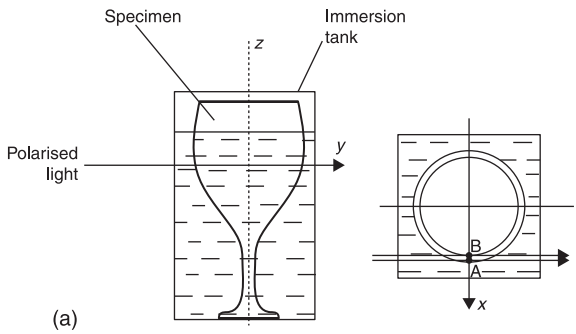

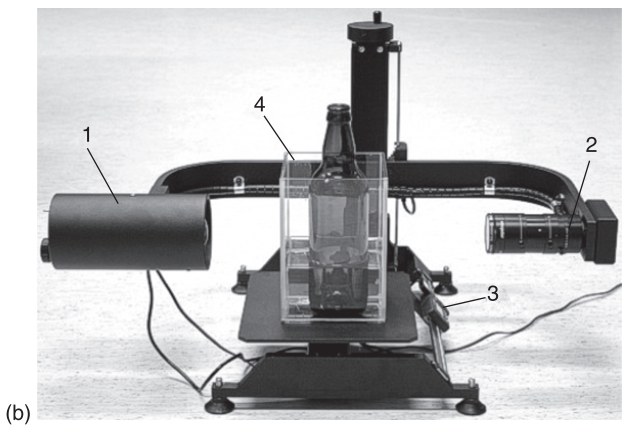

6.1 (a) Experimental set-up in integrated photoelasticity; and (b) automatic polariscope AP-07. 1 – box of the light source; 2 – CCD camera; 3 – coordinate device; 4 – immersion tank with the specimen.

Measurements are carried out with a computer-controlled polariscope (Fig. 6.1b). Transformation of the polarisation of light in the specimen is measured on many light rays. The box of the light source 1 contains a set of polaroids and quarter-wave plates that permit precise photoelastic measurements by using the phase-stepping method (Aben *et al.*, 1999a; Patterson and Wang, 1991). As the values and directions of the principal stresses vary on the light rays, optical phenomena in integrated photoelasticity are complicated and the relationships between the measurement data and parameters of the stress distribution are non-linear. However, it has been shown (Aben *et al.*, 1989: Aben and Guillemet, 1993) that if birefringence is weak or rotation of the principal stress directions on the light rays is weak, a three-dimensional (3D) specimen can be investigated in a conventional transmission polariscope similar to two-dimensional (2D) specimens. On every light ray it is possible to determine the parameter of the isoclinic φ and the optical retardation δ. The latter are related to the components of the stress tensor on the ray by simple integral relationships:

$$\delta\cos 2\varphi = C\int(\sigma_z - \sigma_x)dy, \quad \delta\sin 2\varphi = 2C\int\tau_{zx}dy \qquad [6.1]$$

where C is the photoelastic constant and σ_x, σ_z, and τ_{zx} are components of the stress tensor in the plane perpendicular to the light ray, y. Equations 6.1 expresses the integral Wertheim law. They are valid if either optical retardation is less than one-third of the wavelength or rotation of the principal stress along the light ray is less than $\pi/6$. If no rotation of the principal stress axes is present, Eqs. 6.1 are always valid. The integral Wertheim law is a generalization of the classical Wertheim law, used in 2D photoelasticity, for the case of 3D photoelasticity when stresses on the light beam are not constant.

It has been shown that if the parameter of the isoclinic φ and optical retardation δ have been measured on many light rays in two parallel sections, perpendicular to the z-axis of the axisymmetrical specimen, then radial distribution of the axial stress σ_z and shear stress τ_{rz} can be determined (Aben and Guillemet, 1993). Using the equilibrium equation and the sum rule, all the stress components can be determined (Aben *et al.*, 1999b; Ainola and Aben, 2000).

6.2.2 Stress measurement in tempered glass

In strongly tempered drinking glasses, birefringence is high and often many fringes can be observed in a circular polariscope. Figure 6.2a shows the geometry of a tempered tumbler and Fig. 6.2b the physical and digitised fringe patterns. In this case, the fringe pattern is digitised and by using this information the stresses are calculated (Fig. 6.2c). This figure shows that high compressive axial stresses σ_z are created both at the external and internal surface of the tumbler. Thus this tumbler does not break when, by handling it, certain tensile stresses are created.

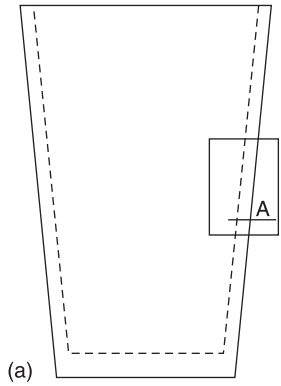

(a)

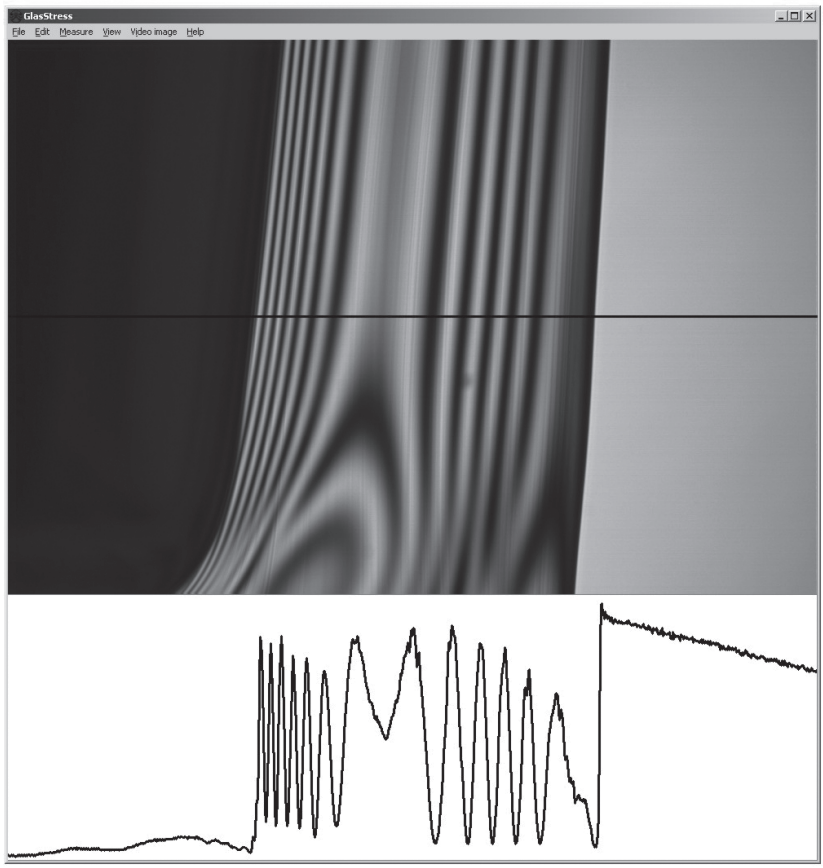

(b)

6.2 (a) Geometry of a tempered tumbler; (b) physical fringe pattern in the investigated area (above) and digitised fringe pattern (below) in section A; and (c) axial stress distribution in section A (Aben *et al.*, 2005).

(*Continued*)

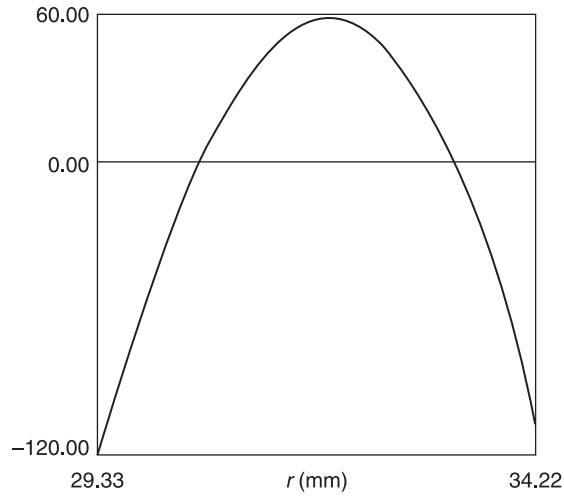

6.2 Continued

6.2.3 Stress measurement in annealed glass

In annealed glass, no fringes can be observed. In this case, photoelastic measurements are carried out with the phase-stepping method (Aben *et al.*, 1999a). Figure 6.3 shows results of stress measurement near the knuckle of a bottle. For bottles, high compressive stresses at the external surface near the bottom are common.

6.2.4 Composite glass articles

The photoelastic measurement technique described above can also be used for residual stress measurement in composite glass articles. Figure 6.4a shows the geometry of a cathode ray tube (CRT) glass bulb. The panel, the funnel and the neck tube all are made of different glasses, which have different thermal expansion coefficients. Due to this, additional residual stresses are created. In the case of CRT bulbs, a critical region is the neck tube near the neck seal.

By investigating an axisymmetrical glass article, light can be passed through the latter perpendicular to different meridional sections (Fig. 6.5). In case of axisymmetrical residual stress distribution, the data obtained should be the same with all measurements (differing no more than the measurement errors), and interpretation of the data should give similar stress distribution all over the perimeter. Practical measurement of the residual stress in many bottles, tumblers, CRTs, neck tubes and other axisymmetrical glass articles has shown that mostly that is not the case.

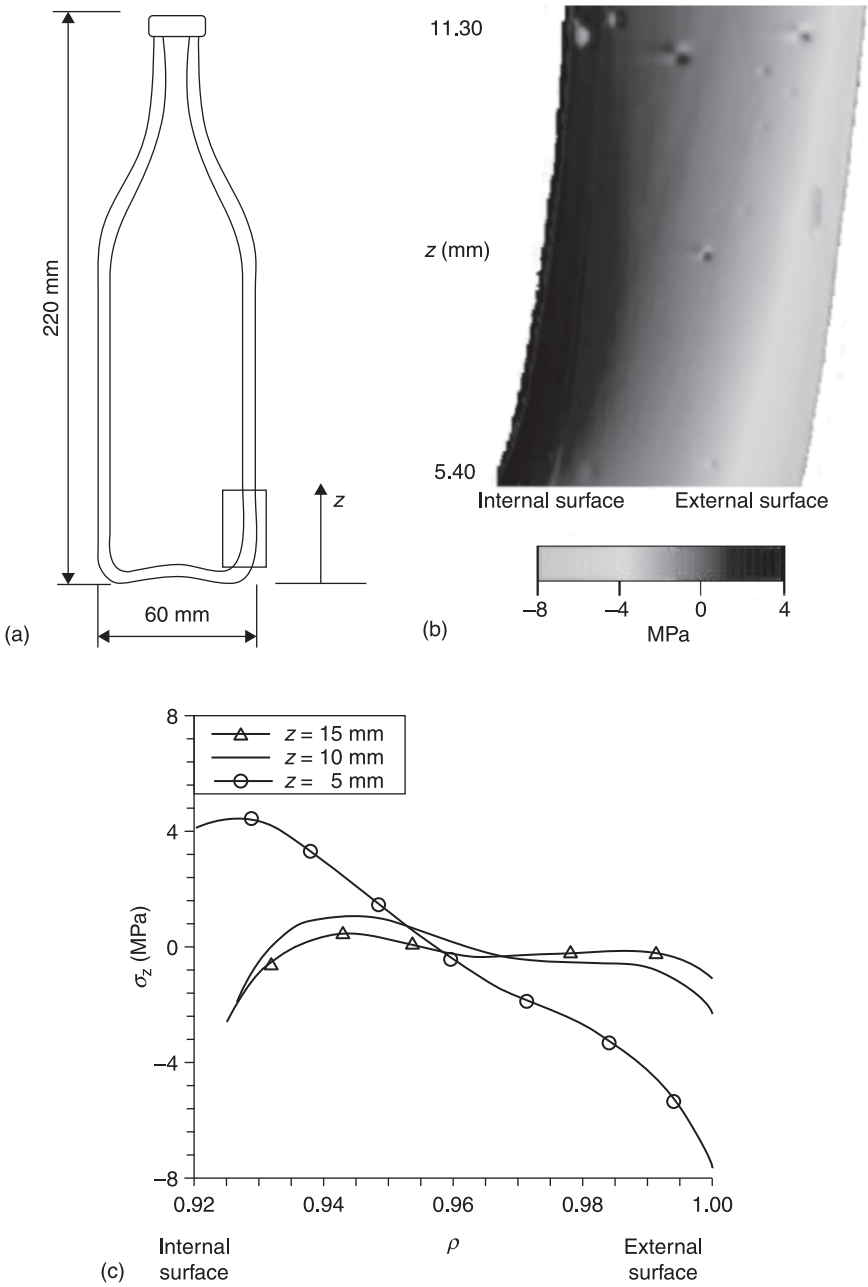

6.3 (a) Geometry of the bottle; (b) axial stress field near the knuckle; and (c) axial stress distribution in the wall in three sections, ρ is dimensionless radius (Aben *et al.*, 2008).

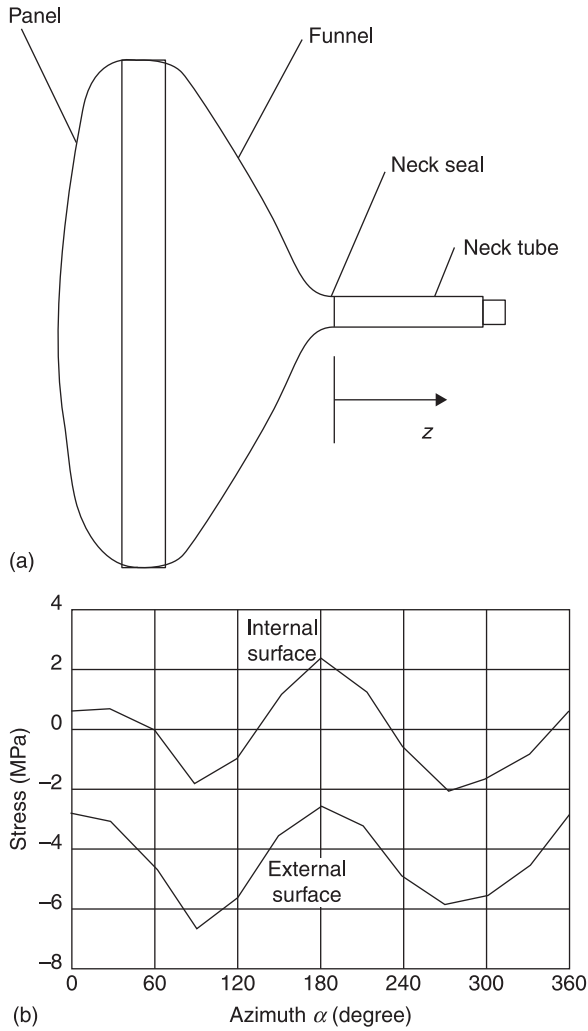

6.4 (a) Geometry of a CRT glass bulb; and (b) distribution of the axial surface stress σ_z over the perimeter in the neck tube at 5 mm from the neck seal (Aben *et al.*, 2008).

Almost always the residual stress distribution deviates from the axisymmetrical one, often considerably, due to non-even cooling conditions of glass articles on the production line. A method for measuring non-axisymmetrical stress distribution in axisymmetrical glass articles has been developed (Aben *et al.*, 1996). Figure 6.4b shows distribution of the axial stress over the perimeter on the surfaces of the CRT neck tube (Fig. 6.4a), at 5 mm from the neck seal. Thus, photoelastic measurements should be carried out for various azimuths of the light beam, in order to establish the real character of the stress distribution.

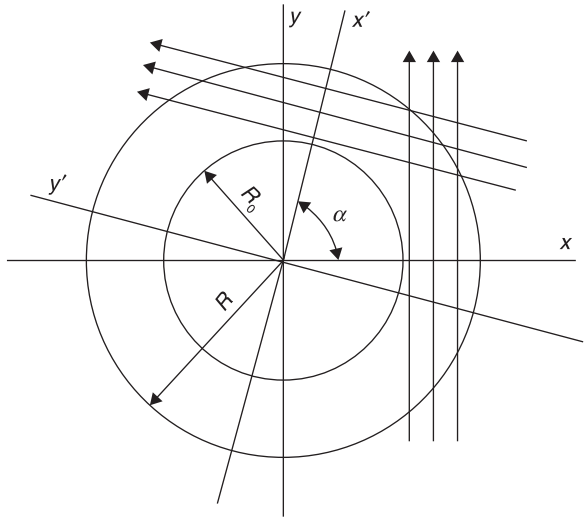

6.5 At measurements, the light can be passed through the axisymmetrical article perpendicular to different meridional sections determined by the azimuth α.

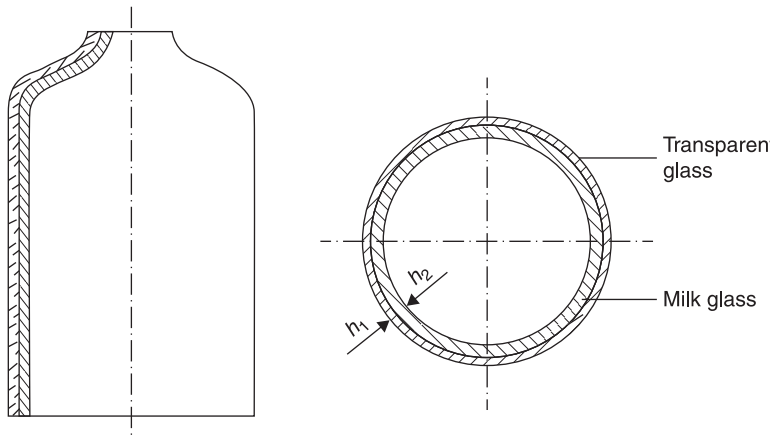

6.6 A two-layer lighting fixture.

As another example of stress measurement in composite glass articles, we consider a sandwich shell. Two-layer lighting fixtures with the inner layer of milk glass and the outer layer of transparent glass are widely used (Fig. 6.6). In production, such lighting fixtures often crack during annealing or when in use. The reason for this lies in the incompatibility of the glasses of the layers with respect to the coefficients of thermal expansion. For the adjustment of the production process, a method is needed to quickly determine stresses in the lighting fixtures. For this, the so-called ring-probe (Jebsen-Marwedel and

Brückner, 1980) is not accurate enough, since it gives only a qualitative estimate of the stresses. It turns out that from an investigation of the outer layer of the lighting fixture by tangential incidence, stresses in both layers can be determined as well as the difference of the coefficients of thermal expansion.

The membrane stresses caused by uniform cooling of a two-layer shell may be expressed as (Timoshenko, 1959)

$$\sigma_{ym}^{(1)} = \sigma_{\theta m}^{(1)} = -\frac{(\alpha_1 - \alpha_2)\delta T}{1-\mu_0}\frac{E_1 E_2 h_2}{E_1 h_1 + E_2 h_2} \quad [6.2]$$

$$\sigma_{ym}^{(2)} = \sigma_{\theta m}^{(2)} = \frac{(a_1 - a_2)\delta T}{1-\mu_0}\frac{E_1 E_2 h_1}{E_1 h_1 + E_2 h_2} \quad [6.3]$$

$$\mu_0 = \frac{\mu_1 \dfrac{E_1 h_1}{1-\mu_1^2} + \mu_2 \dfrac{E_2 h_2}{1-\mu_2^2}}{\dfrac{E_1 h_1}{1-\mu_1^2} + \dfrac{E_2 h_2}{1-\mu_2^2}} \quad [6.4]$$

where the superscript indices 1 and 2 denote the inner and the outer layer of the shell, respectively, α_i are the thermal expansion coefficients, δT is the temperature interval by cooling, E_i are the moduli of elasticity, h_i are the thickness of the layers, μ_i are Poisson's ratios of the layers, and μ_0 is the reduced Poisson's ratio.

The determination of the stresses is as follows. By passing the light tangentially through the outer layer the membrane ($\sigma_{ym}^{(2)}$) and the bending ($\sigma_{yb0}^{(2)}$), stresses in that layer are determined.

For the known temperature interval δT and thickness, and the elasticity coefficients of the layers, Eq. 6.2 allows calculation of the difference of the thermal expansion coefficients α_1–α_2. Now, the membrane stresses in the inner layer may be calculated from Eq. 6.3.

If the elasticity coefficients of the layers are not very different, the axial bending stress at the inner surface of the shell ($\sigma_{yb0}^{(1)}$) is

$$\sigma_{yb0}^{(1)} = -\sigma_{yb0}^{(2)} \quad [6.5]$$

Thus, an examination with the tangential incidence of only the outer layer of the shell permits us to determine stresses in both layers of the shell, as well as the difference of the coefficients of thermal expansion. Since the method described is non-destructive, it can be readily used in factories.

6.3 Measuring residual stresses in glass articles of arbitrary shape

6.3.1 Conventional tomography

Tomography is a powerful method for the analysis of the internal structure of different objects, from human bodies to parts of atomic reactors (Herman, 1980;

Kak and Slaney, 1988). In tomography, a certain radiation (X-rays, protons, acoustic waves, light, etc.) is passed through a section of the object in many directions, and properties of the radiation after it has passed the object (intensity, phase, deflection, etc.) are measured on many rays. Experimental data $g(l,\theta)$ for different values of the angle θ (Fig. 6.7a) are termed projections.

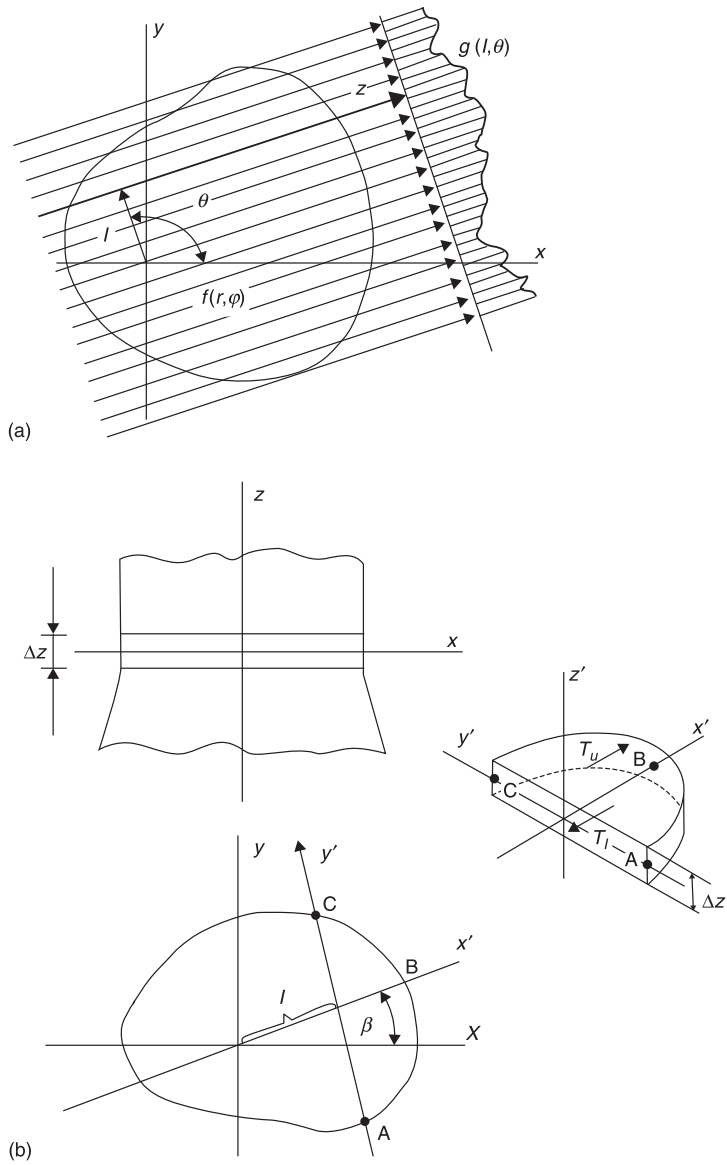

6.7 (a) Schematic of tomographic measurements; and (b) illustration explaining derivation of Eq. 6.12 (Aben *et al.*, 2005).

If $f(r,\varphi)$ is the function that determines the distribution of a certain parameter of the field, experimental data for a real pair l, θ can be expressed by the Radon transform of the field:

$$g(l,\theta) = \int_{-\infty}^{\infty} f(r,\varphi)\mathrm{d}z \qquad [6.6]$$

When projections for many values of θ have been recorded, the function $f(r,\varphi)$ is determined from the Radon inversion:

$$f(r,\varphi) = \frac{1}{2\pi^2}\int_0^{\pi}\mathrm{d}\theta\int_{-E}^{E}\frac{\partial g(l,\theta)}{\partial l}\frac{\mathrm{d}l}{r\cos(\theta-\varphi)-l} \qquad [6.7]$$

Many numerical algorithms for solving Eq. 6.7 have been elaborated. The question arises, whether it is also possible to determine tomographically stress fields in 3D objects. This problem is not trivial because the classical tomography considers only determination of scalar fields, that is, every point of the field is characterised by a single number (the coefficient of attenuation of the X-rays, acoustical or optical index of refraction, etc.). As stress is a tensor, in stress field tomography, every point of the field is characterised by a second rank tensor, which is determined by six numbers. Thus the problem is much more complicated in principle (Sharafutdinov, 1994). The peculiarities of the stress field tomography have been considered by Aben *et al.* (1992, 2005, 2008).

6.3.2 Photoelastic tomography in linear approximation

In the case of axisymmetrical glass articles, for stress measurement it is sufficient to pass the light through the article in only one direction (Fig. 6.1a). For stress measurement in glass articles of arbitrary shape, tomographic photoelastic measurements are to be carried out for many azimuths of the light beam (Fig. 6.7). Let us assume that in two parallel sections, $z=z_0$ and $z=z_0+\Delta z$, of an arbitrary 3D test object, tomographic photoelastic measurements have been carried out for many azimuths β of the light beam (Fig. 6.7b). Let us write Eq. 6.1 for the section $z=z_0$ in the following form:

$$V_1 = \Delta\cos 2\varphi = C\int(\sigma_{x'}-\sigma_{z'})\mathrm{d}y' \qquad [6.8]$$

$$V_2 = \Delta\sin 2\varphi = C\int\tau_{x'z'}\mathrm{d}y'. \qquad [6.9]$$

For the auxiliary section $z=z_0+\Delta z$, we denote V_1 and V_2 as V'_1 and V'_2.

Using Eqs 6.8 and 6.9, we limit ourselves with linear approximation of integrated photoelasticity, such that either the birefringence or the rotation of the principal stress axes must be weak. Considering the equilibrium of the 3D segment ABC in the direction of the x'-axis (Fig. 6.7b), we may write:

$$\Delta z\int_A^C \sigma_{x'}\,\mathrm{d}y' = T_u - T_l \qquad [6.10]$$

where T_u and T_l are the shear forces on the upper and lower surfaces of the segment, respectively:

$$T_u = \frac{1}{2C}\int_l^B V_2'\,\mathrm{d}x', \qquad T_l = \frac{1}{2C}\int_l^B V_2\,\mathrm{d}x'. \qquad [6.11]$$

Taking into consideration Eqs 6.10 and 6.11, Eq. 6.8 reveals:

$$\int_A^C \sigma_{Z'}\mathrm{d}y' = \frac{1}{2C\Delta z}\left(\int_l^B V_2'\;\mathrm{d}x' - \int_l^B V_2\;\mathrm{d}x'\right) - \frac{V_1}{C} \qquad [6.12]$$

As tomographic photoelastic measurement data can be obtained for all the light rays y', Eq. 6.12 expresses the Radon transform of the field of the stress σ_z. Thus we have reduced a problem of tensor field tomography to a problem of scalar field tomography for a single stress component $\sigma_{z'}$. The field of $\sigma_{z'}$ can be determined using any of the well-known Radon inversion techniques (Herman, 1980; Kak and Slaney, 1988). By rotating the specimen by tomographic measurements around the x- and y-axes, the fields of σ_x and σ_y can also be determined.

Equation 6.12 shows that if the stress gradient in the direction of the z-axis is absent, $V_2 = 0$ and the axial stress field can be measured with methods of scalar field tomography. Summing up, essential features of photoelastic tomography in linear approximation are:

- Determination of the stress field is decomposed to the measurement of a single stress component at a time.
- For the measurement of the field of a single stress component, the specimen is rotated around only one axis.
- Distribution of the normal stress in a section of the specimen is determined by using algorithms of scalar field tomography.
- By tomographic photoelastic measurements, the parameter of the average isoclinic φ and the integral optical retardation δ should be measured in two parallel sections. Thus the photoelastic measurements are similar to those used by investigating 2D problems.

If assumptions of the linear approximation are not valid, photoelastic tomography should be based on the general non-linear relationships of integrated photoelasticity. An algorithm of non-linear photoelastic tomography has been developed (Aben and Errapart, 2007).

6.3.3 Examples

Figure 6.8 shows the geometry of a high-pressure lamp and normal stress distribution in the critical section AB. Figure 6.9 shows the axial stress field in a

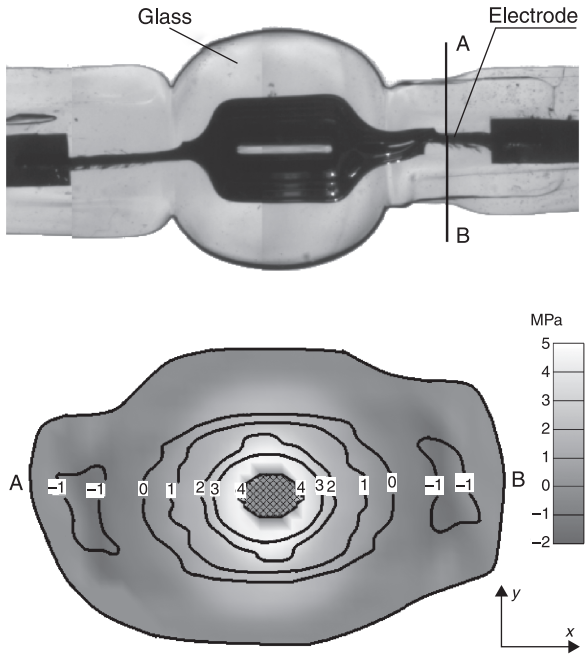

6.8 Geometry of the high-pressure lamp and axial stress field in section AB of the stem obtained with 180 projections (Aben *et al.*, 2005).

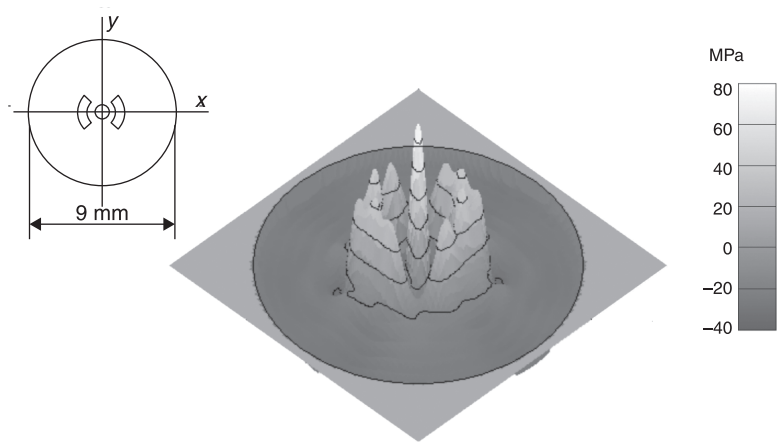

6.9 Cross-section of a bow-tie optical fibre preform and axial stress distribution obtained with 180 projections (Aben *et al.*, 2005).

bow-tie optical fibre preform. In this case, residual stress and birefringence is intentionally introduced into the fibre by inclusions of a different glass. Such a birefringent fibre preserves better polarisation of light that is important in communication technology.

6.4 Measuring residual stresses in automotive and building glass

6.4.1 Application of 2D photoelasticity

Certain information about the residual stress in flat glass panels, and in automotive and building glass, can be obtained with 2D photoelasticity. For example, in float glass ribbons, the residual membrane stresses can be automatically measured on the production line (Redner, 2002). By tempering glass panels, a large number of jets are used to cool down the panel with cool air. Therefore, the residual stress field is not homogeneous and by inspection in a polariscope, such panels exhibit a complicated fringe pattern (Fig. 6.10). The fringe pattern in Fig. 6.10 characterises only the general inhomogeneity of the cooling conditions and gives no information about the tempering stresses through the thickness of the panel. Value and distribution of the edge stresses are important characteristics of automotive glazing. Figure 6.11 shows the geometry of a car side window and edge stress distribution, measured with the polariscope shown in Fig. 6.1b. For measuring edge stresses, specialised apparatus is also available (Redner, 2003).

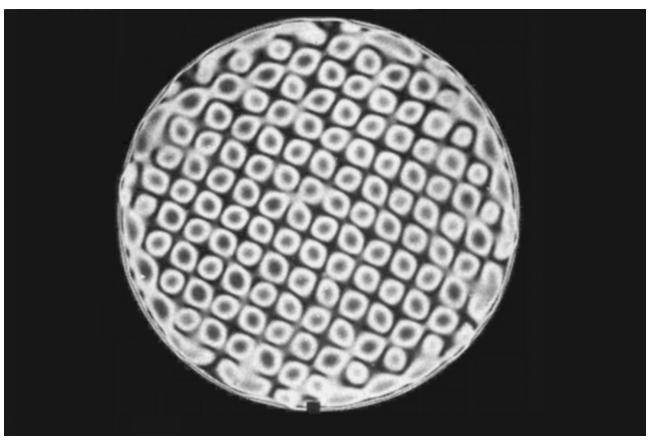

6.10 Typical fringe pattern of a tempered glass panel in a circular polariscope.

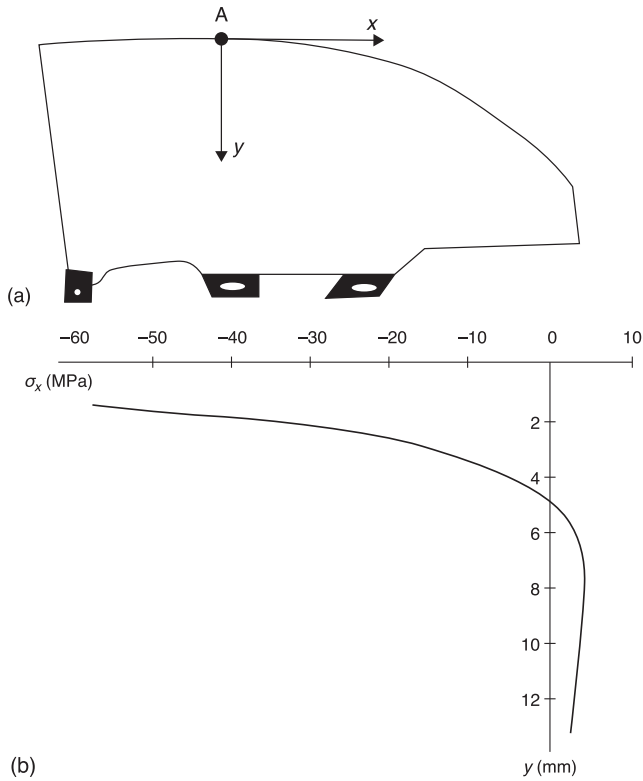

6.11 (a) Geometry of a car side window and (b) distribution of the edge stress near the point A (Aben *et al.*, 2008).

6.4.2 Surface stress measurement

Differential refractometry

In differential refractometry, a glass prism with a high refractive index is placed on the surface of the glass plate coated with an oil film. When convergent monochromatic light is conveyed through the prism, it falls on the surface of the stressed sample. The reflected light is then collected in a telescope through a polariser. Two parallel boundaries between dark and light areas are observed in the telescope. The observation of either boundary depends upon whether the polarization plane is parallel or perpendicular to the plane of incidence. The distance between the two boundaries constitutes a measure of the difference between the two critical angles of total reflection. This difference is proportional to the surface stress.

In 1962, Guillemet and Acloque suggested using a special prism made of two parts separated by a screen (Fig. 6.12). This enables us to collect only the evanescent waves in the telescope and thus we do not observe two boundaries between dark and light in the focal plane, but two thin fringes that can be located more accurately.

The idea of this method is very simple but it has some limitations. First, it needs a rather flat surface, as otherwise the observations will not be clearly defined. Second, even if this condition is fulfilled, the precision is limited by the magnifying power of the telescope. If the magnification is ten times, a variation in the critical angle as small as ten seconds can be measured. However, if the ratio between the refractive index of the sample and that of the prism is close to 1 (i.e. 0.99), then the smallest birefringence that can be determined is approximately equal to 3×10^{-6}. This value corresponds to a stress equal to 2 MPa.

The mirage method

Float glass has an astonishing property resulting from its forming process. During contact with molten tin, Sn ions spread into the glass, by entering the tin side. This diffusion of tin produces gradients of various physical properties perpendicular to the surfaces for up to about 10 micrometers. Thus, close to the tin side, the float glass is a stratified medium. In particular, the refractive index decreases from the surface (n_0) to the core (n_c): the drop amounts to about 4×10^{-3} (Fig. 6.13a). This gradient of the refractive index causes the resurgence of the rays out of the panel (Fig. 6.13b). If the incident light beam is polarised, the state of polarisation of the

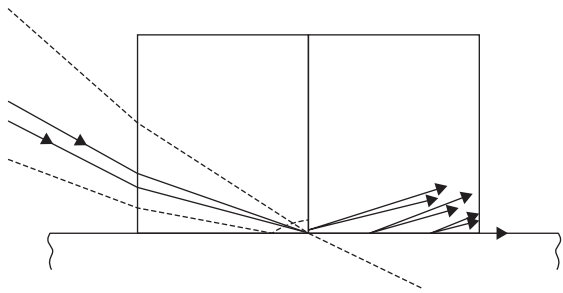

6.12 Surface stress measurement with a prism containing a screen.

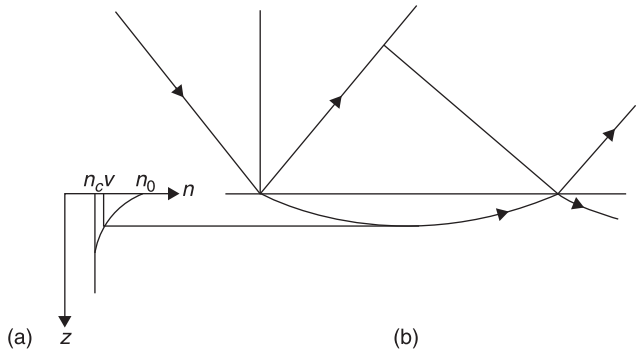

6.13 Gradient of the refractive index near the surface of the glass panel (a) evokes the mirage effect (b).

emergent beam depends on the stresses in the surface layer and on the distance between the points of incidence and emergence. Polarisation of emergent rays gives information about the stress near the surface. Figure 6.14 illustrates the measurement scheme and Fig. 6.15 shows device GASP-LCD for surface stress measurement ('GASP' is a registered trademark of Strainoptics, Inc.).

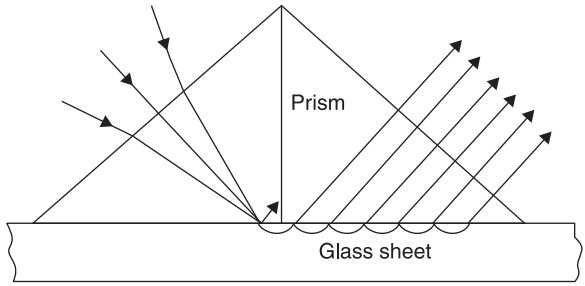

6.14 Mirage effect and resurgence of the light propagating in the outermost layers of a glass panel.

6.15 Grazing angle polariscope GASP-LCD (courtesy of Strainoptics, Inc.).

6.4.3 The scattered light method

If a laser beam passes through a glass panel, the light is scattered in the plane, perpendicular to the direction of the beam. The intensity of the scattered light depends on the birefringence caused by the stresses. This opens up the possibility to measure the distribution of the residual stresses through the thickness of glass panels (Aben and Guillemet, 1993; Hundhammer *et al.*, 2002; Laufs *et al.*, 2002; Lochegnies *et al.*, 2005).

Figure 6.16a shows the scattered light measurement scheme. A laser beam is directed into the glass panel perpendicular to an inclined surface of a glass prism to avoid refraction of the light. Usually the angle α is equal to 45 degrees. A thin layer of immersion liquid between the prism and the panel improves the optical contact.

Because of stresses, the polarisation of the laser beam varies when it passes through the panel. Variation of the polarisation also means variation of the intensity of the scattered light. The latter is recorded with the CCD camera and based on this measurement data the stress profile in the glass panel is calculated. Figure 6.16b shows a photograph of a compact scattered light polariscope SCALP–04. Figure 6.17 shows distribution of the normal stresses σ_x and σ_y through the thickness of a tempered architectural glass panel in a particular case.

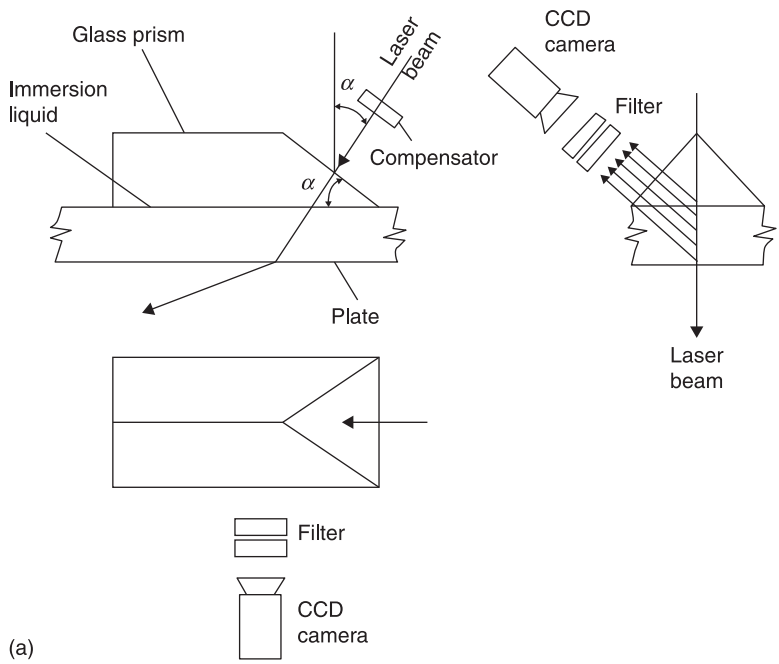

6.16 (a) Scattered light measurement scheme and (b) scattered light polariscope SCALP-04 of GlasStress Ltd (Anton *et al.*, 2011).

(*Continued*)

(b)

6.16 Continued

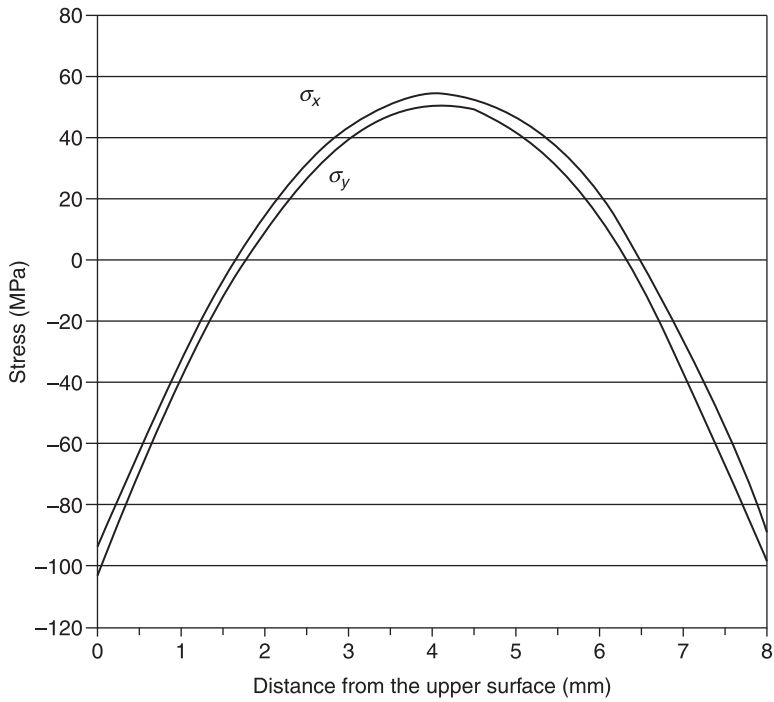

6.17 Distribution of normal stresses σ_x and σ_y through the thickness of a tempered architectural glass panel (Anton *et al.*, 2011).

Stresses σ_x and σ_y are almost equal to each other, which is typical for middle parts of tempered glass panels.

6.5 Conclusions

This review shows that contemporary photoelastic technology possesses efficient methods for residual stress measurement in homogeneous and composite glass articles of various kinds. Integrated photoelasticity makes it possible to measure residual stress in axisymmetrical glass articles. Photoelastic tomography can be used for stress measurement in glass articles of arbitrary complicated shape. Devices have been developed for residual stress measurement, either at the surface or through the thickness of architectural and automotive glass panels. Precise information about the residual stresses permits the glass technologists to improve the glass manufacturing technology in order to meet the demands of the variety of glass consumers.

6.6 Acknowledgement

The support of the Estonian Science Foundation (grant No. 7840) is gratefully acknowledged.

6.7 References

Aben, H. (1979) *Integrated Photoelasticity*, New York, McGraw-Hill.

Aben, H. K., Josepson, J. I. and Kell, K.-J. E. (1989) The case of weak birefringence in integrated photoelasticity, *Opt. Lasers Eng.*, **11**, 145–57.

Aben, H. K., Idnurm, S., Josepson, J. I., Kell, K.-J. E. and Puro, A. (1992) Optical tomography of the stress tensor field, in: G. G. Levin, *Analytical Methods for Optical Tomography*, Proc. SPIE, **1843**, 220–9.

Aben, H. K. and Guillemet, C. (1993), *Photoelasticity of Glas*s, Berlin, Springer-Verlag.

Aben, H. K., Anton, J. and Josepson, J. I. (1996) Nonaxisymmetric residual stress distribution in axisymmetric glass articles, *Glastechnische Berichte – Glass Science and Technology*, **69**(3), 75–81.

Aben, H. K., Ainola, L. and Anton, J. (1999a) Half-fringe phase-stepping with separation of the principal stress directions, *Proc. Estonian Acad. Sci. Eng.*, **5**, 198–211.

Aben, H. K., Ainola, L. and Anton, J. (1999b) Sum rules for photoelastic residual stress measurement in axisymmetric glass articles, *Proceedings of the International Confererence on Advanced Technology in Experimental Mechanics ATEM'99*, Ube, **2**, 629–34.

Aben, H. K., Errapart, A., Ainola, L. and Anton, J. (2005) Photoelastic tomography for residual stress measurement in glass, *Opt Eng*, **44**(9), 093601–1–8.

Aben, H. K. and Errapart, A. (2007) A non-linear algorithm of photoelastic tomography for the axisymmetric problem, *Exp. Mech.*, **47**(6), 821–30.

Aben, H. K., Anton, J. and Errapart, A. (2008) Modern photoelasticity for residual stress measurement in glass, *Strain*, **44**(1), 40–8.

Ainola, L. and Aben, H. K. (2000) Hybrid mechanics for axisymmetric thermoelasticity problems, *J. Thermal Stresses*, **23**(7), 685–97.

Anton, J., Errapart, A., Paemurru, M., Lochegnies, D., Hödemann, S. and Aben, H. K. (2011) On the inhomogeinity of residual stresses in tempered glass panels, *Proceedings of the Conference on Glass Performance Days*, Tampere, 119–21.

Guillemet, C. and Acloque, P. (1962) New optical methods for the determination of the stresses near the surfaces, *Rev. Franc Méc*, **4**, 157–63.

Herman, C. T. (1980) *Image Reconstruction from Projections*, New York, Academic Press.

Hundhammer, I., Lenhart, A. and Pontesch, D. (2002) Stress measurement in transparent materials using scattered laser light, *Glass Sci. Technol.*, **75**, 236–42.

Jebsen-Marwedel, H. and Brückner, R. (eds) (1980) *Glastechnische Fabrikationsfehler*, Berlin, Springer Verlag.

Kak, C. A. and Slaney, M. (1988) *Principles of Computerized Tomography*, New York, IEEE Press.

Laufs, W., Sedlacek, G., Mohren, R. and Völling, B. (2002) Structural use of glass – stress distribution in tempered panels, *Proceedings of the Conference on Modelling of Glass Forming and Tempering*, Valenciennes, 254–9.

Lochegnies, D., Romero, E., Anton, J., Errapart, A. and Aben, H. K. (2005) Measurement of complete residual stress fields in tempered glass plates, *Proceedings of the Conference on Glass Processing Days*, Tampere, 88–91.

Patterson, E. A. and Wang, Z. F. (1991) Towards full field automated photoelastic analysis of complex components, *Strain*, **27**, 49–56.

Redner, A. S. (2002) Stress measuring methods for quality control and process optimization in glass, *Proceedings of the International Colloquium on Modelling of Glass Forming and Tempering*, Valenciennes, Presses Universitaires de Valenciennes, 269–75.

Redner, A. (2003) Automated measurement of edge stress in automotive glass, *Proceedings of the Conference on Glass Processing Days*, Tampere, 578–99.

Seebeck, T. J. (1813) Einige neue Versuche und Beobachtungen über Spiegelung und Brechung des Lichtes, *Journal Chemie Physik*, **VII**(3), 259–98, 382–4.

Seebeck, T. J. (1814) Von den entoptischen Farbenfiguren und den Bedingungen ihrer Bildung in Gläsern, *J Chemie Physik*, **XII**, 1–16i.

Sharafutdinov, V. A. (1994) *Integral Geometry of Tensor Fields*, Utrecht, VSP.

Timoshenko, A. (1959) *Theory of Plates and Shells*, 2nd ed., New York, McGraw-Hill.

7

Modeling residual stresses in composite materials

M. M. SHOKRIEH and S. M. KAMALI SHAHRI,
Iran University of Science and Technology, Iran

DOI: 10.1533/9780857098597.1.173

Abstract: In this chapter, the analytical models on evaluation of the ply scale or macro residual stresses in polymeric composite materials are reviewed. It is shown that the ability of the model to describe the behavior of the polymer matrix during the cure is crucial for the accuracy of the analysis. Due to complex thermo-chemo-rheological viscoelastic behavior of the resin, the common approximations to achieve an accurate constitutive model are studied. A modified classical laminate theory (CLT) model with consideration of resin chemical shrinkage contribution is introduced.

Key words: elastic, viscoelastic, constitutive model, analysis, residual stress.

7.1 Introduction

Process-induced stresses, or generally called 'residual stresses', in composite materials are a consequence of different parameters: the thermal expansion mismatch between the fiber and the matrix during cooling, the chemical shrinkage of the resin during polymerization, the non-uniform curing of the laminate, post-moisture absorption and also mechanical tool-part interaction. These stresses can be high enough to cause cracking within the matrix, even before mechanical loading. This microcracking of the matrix can expose the fibers to degradation by chemical attack and consequently degrade the material strength of the component. Eventually the part fails earlier than expected. In addition, these stresses may cause component warpage and often make it very difficult to achieve the specified dimensions.

The state of the residual stresses in a composite structure after processing and before part usage should be known and an optimum curing cycle must be found in order to minimize the residual stresses and the production time and maximize the composite mechanical properties. For thermoset polymer composites, a typical curing process consists of two steps: curing at a constant elevated temperature and thermal cooling from the curing temperature to room temperature. During curing, the polymer shrinks as a result of a purely chemical reaction (polymerization) and its material characteristics change dramatically through the transition from a liquid to a solid state while the reinforcement remains unchanged. For thermal cooling, both polymer and reinforcement contract but by different amounts and in

addition the polymer may change its stiffness significantly. Therefore, the build-up of residual stress over time is governed by the change of volume and material properties during the complete cure process. Exact study of cure cycle and control of the stress governing parameters could lead to lower residual stresses.

To control these stresses, first it is necessary to estimate their magnitude, and then relate this number to the processing conditions. One of the key parameters to finding the residual stresses analytically or numerically is the temperature at which these stresses start building up in the laminate during its cure. Under this condition, generally it is assumed that the maximum deflection of an asymmetrical laminate is reduced to zero and the relevant temperature defined as stress-free or strain-free temperature (the gel point). The residual stresses are assumed to be generated by cooling down from this temperature. The temperature difference between the stress-free temperature and the service temperature is a major driving force for the formation of residual stresses.

For fiber reinforced polymers (FRPs), residual stresses exist on three different scales:

1. *The fiber–matrix (constituent) scale or micro stresses*: The mismatch in shrinkage between the matrix and fibers is the main source for the development of residual strains on the micro-mechanical or constituent level.
2. *The ply scale or macro stresses*: Residual stresses on a ply-to-ply scale arise due to an anisotropic difference in the transverse and longitudinal ply coefficients of thermal contraction:
3. *The global (structural) scale. Residual stresses* through the thickness of a composite laminate, which are the result of a variation in shrinkage through the thickness.

Intrinsic sources generate residual stress at the constituent level and the effect is integrated up through the length scales. Extrinsic sources generate stress at the boundaries of the structure and the effect is migrated down through the length scales. Thus intrinsic sources act from the 'inside and outwards' and extrinsic sources act from the 'outside and inwards'. Intrinsic sources have in general the largest effect on fiber matrix level stresses and extrinsic sources have the largest effect on the structural level stresses (Fig. 7.1) (Fernlund *et al.*, 2003). Fiber-matrix, lamina-laminate and structural levels all affect the strength of the component, whereas only lamina-laminate and structural level stresses affect dimensional fidelity to any significant degree. Figure 7.1 shows a schematic of the relationship between the source of stress, the length scale at which it is acting and the effect of that stress.

In this chapter, we deal with and go through the detailed investigation on the ply scale or macro residual stresses. In order to determine the residual stresses, analytical, numerical and experimental approaches can be applied. The analytical (sometimes mixed with numerical) method history is explained and one of the most recently developed methods is reviewed in detail.

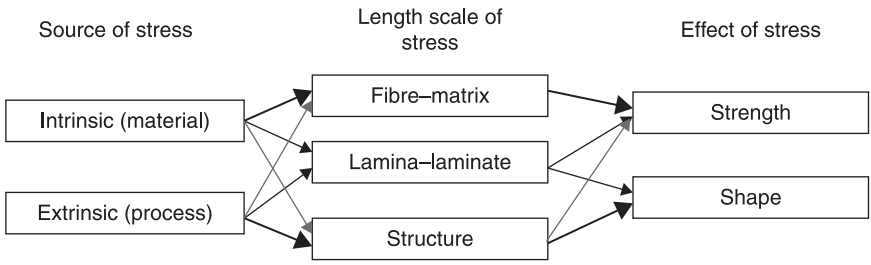

7.1 Schematic relationship between stress source, length scale of stress and the effect of residual stress. Thicker arrows indicate a stronger relationship (Fernlund *et al.*, 2003).

7.2 Selecting an appropriate model

7.2.1 Introduction: selecting model behavior

Numerous mathematical approaches have been developed to determine residual stresses in composite materials, which basically depend to the cure process assumptions. The ability of the model to describe the behavior of the polymer matrix during cure is crucial for the accuracy of the analysis. The mechanical behavior of a thermoset polymer during cure is viscoelastic and thermo-rheologically complex. There is much research described in the literature to show that polymers display viscoelastic behavior, which is more serious at higher temperatures. Around the mid–1960s, Schapery published several papers on the constitutive modeling of viscoelastic media under the influence of temperature. In Schapery's 1968 paper, by utilizing the corresponding principle, the author clearly defined the general form of the stress-strain relationship for anisotropic composite materials with a linear viscoelastic and thermo-rheologically simple assumption. Examples of some other prominent works are Tobolsky (1958), Leaderman (1958) and Ferry (1980).

The viscoelastic behavior during cure and in particular thermo-rheologically complex behavior is difficult to characterize and model accurately for a composite. To obtain a simpler description, some researchers have approximated the viscoelastic behavior as thermo-rheologically simple. Also, this description has some problems, because use of anisotropic viscoelastic models requires extensive material characterization and for numerical simulations, they lead to long calculation times and require a large memory for storage of internal state variables. For these reasons, elastic models have also been used for residual stress calculation. For obtaining more accurate replies by elastic models, incremental elastic relations have been used in some analyzes (Zobeiry, 2006).

Figure 7.2a shows a typical cure cycle for a thermoset composite, where the approximate material behavior is indicated in italics. Before gelation, the matrix is viscous and no residual stresses can be carried by the matrix. After gelation, the

matrix is a rubbery viscoelastic solid with short relaxation times. At the end of the final temperature hold, the matrix is fully cured and behaves as a viscoelastic glassy solid with a long relaxation time (Fig. 7.2b). The majority of the residual stress is generated during the cool-down from the final hold temperature. These stresses are the easiest to predict, as the material can be treated as being thermo-elastic with fairly good accuracy. Stresses built up earlier in the cure cycle, for example due to cure shrinkage and tool-part interaction, are more difficult to estimate (Fernlund *et al.*, 2003).

During cure, the polymer transforms from a liquid to a rubber-like solid (gelation), which finally transforms to a solid in the glassy state (vitrification) and there are three material phases in each typical curing cycle. This means a dramatic change in mechanical properties. The Young's modulus and the shear modulus are approximately 100 times lower in the rubbery than in the glassy state and the coefficient of thermal expansion is approximately 2 to 3 times higher in the rubbery than in the glassy state. Much of the shrinkage due to cross-linking occurs while the resin is a liquid and therefore (in most cases) without stress development, but shrinkage in the later stages of cure (after gelation) leads to residual stresses. A common approximation is to assume the chemical shrinkage of the resin to be linearly dependent on degree of cure (Svanberg and Holmberg, 2004).

Taking into account the complexities of the materials, a proper constitutive model is needed in the residual stress modeling of the composite. Such a model needs to be accurate by taking into consideration different aspects of the material behavior and also efficiency, due to the size of the problems normally encountered in real-world applications. Generally most of the models can be classified into two categories, elastic models and viscoelastic models. Also, other denominations such as CHILE models (this term was introduced by Johnston (1997) to denote Cure Hardening Instantaneously Linear Elastic) or PVE models (this term was introduced by Zobeiry *et al.* (2006) to denote Pseudo-ViscoElastic), are used for

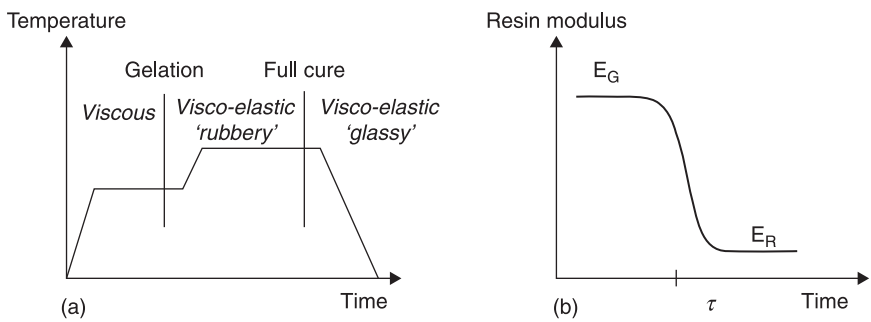

7.2 (a) Schematic of a typical cure cycle showing the material behavior at different times; and (b) schematic of relaxation behavior of resin after gelation. E_G = glassy modulus; E_R = rubbery modulus; τ = characteristic relaxation time (Fernlund *et al.*, 2003).

some of the elastic methods in which the modulus of elasticity changes as a function of temperature and degree of cure.

7.2.2 Model dimension

One important aspect of the model is its dimensionality. The majority of the studies have used the one-dimensional (1D) model in their analyses (Adolf and Martin, 1996; Djokic *et al.*, 2001; Lange *et al.*, 1996, 1997; Loos and Springer, 1983; Prasatya *et al.*, 2001). Some others have assumed that the effect of one of the directions does not significantly change the behavior of the material and modeled the material by 2D analyses (Bogetti and Gillespie, 1991, 1992; Johnston *et al.*, 2001). At the same time, more recent studies have modeled the material in 3D (Poon *et al.*, 1998; Zhu *et al.*, 2001, 2003) to be able to analyze composite parts of any shape. These models offer a better representation of the geometry and the state of stress in the material and therefore are more desirable. However, it should be noted that due to the complexity of the constitutive models employed in the available research works, these approaches have normally been very time-consuming (Zobeiry, 2006).

7.2.3 Numerical or analytical model

Another important consideration in process modeling is the method used to solve the relevant equations over the domain of interest. Some have used Laminated Plate Theory (LPT) based models for stress analysis. LPT-based models are simpler methods and, as clear from their names, are based on the theory of thin plates. This approach can be used to model different lay-ups and material behavior, but is not able to model complex shapes or boundary conditions. However, the method of choice for most recent studies on composite materials is the finite elements method (FEM). This method enables modeling of more complex cases and is not limited to the assumptions made by LPT. Several researchers have used elastic FE analysis to calculate the cool-down stresses. However, modeling the whole cure cycle has been more limited in the literature. This is perhaps due to the complexity and requirement of larger computation of FE-based methods (Zobeiry, 2006).

In earlier works on residual stress assessment, the researchers modeled only the final cool-down section of the curing process. The recent works model the entire cure cycle for the calculation of stresses and take into account other sources of residual stress generation, such as cure shrinkage strains or tool-part interaction, thus producing more complex and accurate models.

Different aspects of residual stress calculation in process modeling are discussed above and some of the complexities of the problem were described. Taking such complexities of behavior into account, we need a suitable approach to properly simulate the response of composite materials during processing. This underlines

the importance of the accuracy of the employed models and their ability to take into account different complexities of the process in a comprehensive fashion. In addition, process models usually involve significant numerical runs, consistent with the size and complexity of the relevant composite parts. This makes efficiency of the model a crucial factor in controlling the modeling costs. In the following, the different kinds of models used in the literature to model the residual stresses analytically or numerically are described and the major aspects in each methodology are discussed.

7.3 The elastic behavior models

Hahn and Pagano (1975) applied an elastic analysis for a thermoset matrix composite to model the in-plane residual stresses based on Classical Lamination Theory (CLT). This was the first attempt to assess the residual stresses of composites with a mathematical method. In another study, Hahn (1976) showed that the effect of swelling due to moisture absorption can reduce the residual stresses. Two years after their first publication, Pagano and Hahn (1977) modified their analysis, proposing a new concept as the stress free temperature. Now, it is proven that some assumptions in their work were not valid. The stress-free temperature was proposed to be the same as the cure temperature. Also the viscoelastic behavior, as well as the chemical shrinkage of the polymer, were not considered. Due to these problems, the relative error between prediction and experimental results with the proposed analysis could be as high as 25%. This is a large discrepancy, which would need drastic reduction in order to gain confidence in the values predicted by the model. The CLT with the mentioned assumptions is commonly used as a 'ballpark' technique to calculate the residual stresses only during the cool-down stage and to make sure that experimental results are in the right area, or to show if a particular material/configuration should be considered.

Since this work, many other studies have been carried out on the topic, which have taken various complexities of the manufacturing process into account and have used different approaches. In a later experimental study, Hahn (1984) noted that stress free temperature is higher than curing temperature and the cool-down rate apparently has no effect on the residual stresses. Also, data showed that lowering the gelation point reduces the residual stresses. An extension to the CLT by the energy method was proposed by Hyer (1981a,b,c, 1989) to investigate the elastic residual stresses and warpage in thin laminates. The method included the geometrically nonlinear terms in the formulation, which provided further insight into the nature of residual stress deformation. CLT predicts the room-temperature shapes of all cross-ply asymmetrical laminates to be a saddle, but the predictions of the modified method by Hyer are well coincident with the experiments.

Shokrieh and Kamali (2005) and also Tuttle *et al.* (1996), in their slight modification on Hyer's developed model, reported excellent agreement between the measured curvature and the estimated values. Also other groups, such as Zewi

et al. (1987), Jun and Hong (1992) and Teng and Ossward (1994), used similar approaches to investigate the elastic residual stresses and warpage in thin laminates. By assuming stress-free conditions in the final shape, Radford and Diefendorf (1993) developed a simple mathematical formula to predict the spring-forward of curved-shape parts.

Jeronimidis and Parkyn (1988) applied the CLT for a thermoplastic composite and compared the results with experimental data. They showed that accurate predictions can be made, provided that the changes in thermoplastic properties of the materials with temperature are taken into account. However, they did not consider the time effects and concluded that the importance of viscoelasticity in thermoplastic matrixes is greater than thermosetting materials. Kim and Hahn (1989) compared the warpage of a non-symmetrical $[0_4/90_4]_T$ graphite-epoxy laminate strip calculated by their elasticity-based approach with the experimental data. The analytical prediction of the warpage was greater than the measured values during the early stages of the cure. It was suggested that viscoelastic relaxation of the uncured epoxy matrix reduced the residual stresses and eventually the warpage. Schulte and Hahn (1990) adopted the experimental technique of Kim and Hahn (1989) and showed that the laminate curvature increased as the cooling rate decreased. Also, it was observed that the stress-free temperature decreased with increasing the process cooling rate.

The matrix shrinkage due to thermoset resin cross-linking and thermoplastic resin crystallization should be considered, in addition to the thermal expansion in the residual stress assessment, especially in thick composites. Bogetti and Gillespie (1989, 1991, 1992, 1994) coupled the CLT with a 1D cure simulation model to estimate the residual stresses during processing of a composite laminate focusing on matrix shrinkage. Their model calculated the increments in stress and deformation in the laminate over each time step, from the incremental total strains based on cure-dependent resin modulus and resin chemical shrinkage. According to their study, the matrix shrinkage significantly influenced the prediction of the residual stress distribution. However, their work did not take viscoelasticity into account.

Crasto and Kim (1993) determined the stress free temperature of an asymmetrical graphite/epoxy composite at different curing temperatures, by observing zero deflection of the laminate. For both cure temperatures of 121 °C and 177 °C, the stress free temperature was 15 °C higher than the cure temperature. The difference between the maximum processing temperature and stress free temperature was attributed to the chemical shrinkage stresses. At the maximum cure temperature, all the thermal stresses were relieved, but the residual deflection was related to shrinkage of the thermosetting matrix. Further thermal increase above the stress free temperature caused the reverse deflection due to additional thermal stresses. Also, a significant reduction in residual stresses was observed by reduced cure temperature. A similar trend in behavior was noted by Nairn and Zoller (1985).

CLT can be applied only for the thin composite structures. As the composite becomes thicker, the thin plate assumption used in deriving CLT is no longer valid and edge effects would be more significant. Li *et al.* (1997) developed an FE residual stress model by combining a generalized plane-strain elasticity analysis and the modified standard linear solid model, which was capable of estimating the thermal and chemical residual stresses throughout a thick composite cross-section.

Jain and Mai (1997a,b) developed a mechanics-based model using modified shell theory, and predicted spring-forward and residual stresses in anisotropic cylindrical shells. Chen *et al.* (1998) conducted an analysis on the basis of a systematic Hamiltonian thermoelastic theory in conjunction with a semi-analytical FEM. Liu *et al.* (1998), by their experimental approach, show that depending on the lay-up, there could be up to 22% of final residual stress induced by the chemical shrinkage. Due to this fact, some other researches implemented some modifications on the CLT in order to improve the predictive capability of the model by considering the chemical shrinkage. For instance, Wijskamp *et al.* (2003) predicted the residual stresses using the CLT approach including thermal shrinkage and contraction of the resin due to cross-linking. This showed that the model gives sensible results when the chemical shrinkage is corrected for shrinkage occurring before the vitrification point.

Schulz *et al.* (2005), by modification of CLT, considered the material properties as a function of temperature, as most mechanical properties tend to vary over large temperature ranges. In addition, they included uni-directional chemical shrinkage information by calculating the strain present on the panel when returned to the cure temperature. It was found that once the chemical shrinkage term is decoupled and defined, the computer based analytical tool of the CLT can be used to predict the development of strains anywhere in a given temperature range with acceptable accuracy. Also the chemical shrinkage can be treated in calculations as a one-time event, completely independent of temperature effects. Furthermore, we can predict the behavior of a multi-directional laminate based solely on the behavior of a uni-directional sample of the same material system. Based on our survey in the literature, it is suggested that more precise representation of the mechanical behavior of the composites can be achieved based on a viscoelastic model.

7.4 The viscoelastic behavior models

Nearly all commonly used polymer matrix composites exhibit some viscoelastic properties. When the service temperature of the composite is high, it is usually necessary to cure the composite at an even higher temperature to achieve the desired thermal stability at the service temperature. In this case, the viscoelastic behaviors, such as stress relaxation and creep, will be highly accelerated due to the time temperature dependence of polymer matrix (Schapery, 1974).

Weitsman (1979) and Harper and Weitsman (1981, 1985) developed a method for assessing the residual stresses in cross-ply graphite-epoxy laminates, considering linear viscoelasticity during the entire cool-down phase. Based on a comparison of results obtained from elasticity and viscoelasticity analyses, the viscoelastic relaxation of the epoxy matrix reduced the residual stresses to about 20%. Also, they measured the curvature of asymmetrical cross-ply laminates, in which the elasticity analysis over-estimated the curvature of the laminates, while the viscoelasticity analysis was able to accurately predict the curvatures. However, their work was only limited to the cooling stage of the curing cycle.

Weitsman (1980) investigated the effect of the temperature profile on the curing cycle, both analytically and experimentally, and attempted to obtain an optimal cooling path to minimize the residual stresses. Stango and Wang investigated inter-laminar stresses at the free edge of the laminate due to cool-down using thermoelastic-based (1984) and viscoelastic-based (1987) approaches. Using the numerical method, they demonstrated the 3D (in-plane and inter-laminar) nature of residual stresses, their severity near the free edges, inconstancy in-plane stresses within each lamina and finally the effect of a stacking sequence on inter-laminar residual stresses. None of the mentioned results can be achieved by the elastic CLT.

White and Hahn (1990) studied the development of residual stresses through the whole cure cycle. It was shown that transversal stiffness and strength, which are matrix dependent, develop only after the polymer degree of cure reached 0.83 in IM6/CYCOM 3100 graphite/BMI composites. It was shown that post-cure causes increase in the residual stresses, which was attributed to shrinkage due to additional cure and loss of moisture or volatiles. The inter-laminar stress in viscoelastic composites due to hygro-thermal loading were also analyzed by Lin and Yi (1991). Wang *et al.* (1992) studied residual stresses and warpage in asymmetrical woven-glass-epoxy laminates using linear thermo-viscoelastic laminate theory. They considered a thermo-rheologically simple model and time-temperature superposition in their analysis. Chemical shrinkage and thermal expansion were considered in calculating stresses and the formulation of a stress-strain relationship was presented. The authors did not consider the matrix and fiber separately and did not examine the cure kinetics of the system. Consequently, the model was not able to depict the evolution of curing in terms of degree of cure. Instead, the time coordinates along a certain temperature profile was used to describe the evolution of the chemical reaction. Once the temperature profile is determined, the degree of cure should be a unique function of time. Finally, they qualitatively compared the results of the viscoelastic analysis with the experimentally data and the results were satisfactory.

Most of the aforementioned elastic and viscoelastic analyses have neglected the stresses developed before cool-down and focused merely on the cool-down stage. Only a relatively few papers have considered the development of residual stresses during the entire cure cycle. Lee and Sohn (1994) investigated the residual stress

distribution in a uni-directional graphite-epoxy laminate. They divided the curing process into a polymerization phase and a cool-down phase. By adding the polymerization stress developed in the polymerization phase and the thermal stress in the cool-down phase, they obtained the total residual stress.

Lange *et al.* (1996, 1997) studied stress build-up in thermoset films cured below their ultimate glass transition temperatures. They used a Maxwell model to simplify the viscoelastic analysis. They used the double beam method to verify analysis predictions. It was shown that contribution of cure volume changes to final residual stresses depends on amount of resin shrinkage beyond gelation and density of cross-linking. They indicated that stresses from cure shrinkage vary from 1 to 30% of the final residual stresses, depending to the polymer under consideration and on cure cycle.

A comprehensive study was carried out by White and Hahn (1992a–b, 1993) and by White and Kim (1998), who used viscoelastic constitutive relations with time-dependent and degree-of-cure-dependent material properties. They studied the residual stress development during the curing of thin laminates, both numerically and experimentally. Their viscoelastic model based on the CLT included the effects of chemical and thermal strains. Together with a 2D finite difference thermo-chemical model, they predicted the stress development in a graphite-epoxy composite. Thermal strains were shown to remain relatively constant during cure. Chemical strains occurred early in the cure cycle and were completed before cure fully developed. At low cure states, the creep response was significant. As full cure was approached, the material became predominantly elastic. Based on the measured input data, the viscoelastic analysis showed that the contribution of chemical strains to residual stress was less than 4% for a typical cure cycle. A good correlation was obtained between model predictions and experimental warpage data for the cure cycle investigated.

Kim and White (1997) also studied the effect of mandrel structure on the process-induced residual stresses in cylinder composite structure. Adolf and Martin (1996) presented a comprehensive linear viscoelastic constitutive model for a cross-linked polymer to calculate the process-induced stresses. Their analysis applied for thermo- and chemo-rheologically simple polymers and for time-dependent strain histories where the total strain at any time is not large, such that linear viscoelasticity can be used. It was suggested to use time-cure superposition to account for non-isothermal cure viscoelasticity. It was indicated that changing cure cycle for a given polymer may affect significantly the contribution of cure shrinkage to final residual stress. Experimental data for the viscoelastic material properties and the cure kinetic model parameters were obtained from matrix resin specimens to model the whole composite material system (fibers and matrix). So it is doubtful that the models could represent the composite systems well.

A simplified viscoelastic model was developed by Wiersma *et al.* (1998) to study the spring-forward behavior in an L-shaped laminate. The viscoelastic behavior of the composite was described by characterizing the fiber as an elastic

spring and the matrix as a Maxwell element, consisting of an elastic spring and a viscous damper. Viscoelastic behavior of the composite during the cure cycle had an important influence on the spring-forward. The prediction of spring-forward with the viscoelastic model was sensitive to the amount of cure shrinkage and the viscosity profile during the cure cycle. The heating rate of the cure cycle had almost no influence on spring-forward according to the viscoelastic model. It was concluded that a better prediction is possible by modeling the complete cure cycle, with the composite modeled as a viscoelastic material. Although the aforementioned work did take the whole curing process into account, the models used are either elastic or simplified viscoelastic, and do not accurately reflect the actual material behavior.

Wisnom *et al.* (1999) numerically analyzed the residual stresses throughout the cure cycle in thick filament wound tubes considering the effects of thermal expansion, chemical shrinkage, orthotropic viscoelasticity, and the gelation and cure process. A good correlation with measured strains was obtained, provided that gelation was modeled. The results showed the importance of modeling gelation, and allowing resin flow prior to the gel point, which was rarely considered in residual stress analyses. Ignoring this fact, the axial strains at different points through the thickness would all be the same, and the strong effect of differential contraction seen in the experimental results would not be reproduced. It was shown that inter-laminar stresses during the cure cycle were generally low. However, if three-dimensional (3D) constraints are presented, significant stresses can arise due to the relatively high bulk modulus of the material, even in the partially cured state. Since the strength was low early in the cure cycle, it is postulated that these stresses may be responsible for delamination. For the resin considered, viscoelastic effects proved to be unimportant, and an elastic analysis with fully relaxed properties was adequate.

Liu (1999) considered both the mismatch of the CTE between the fibers and matrix, and chemical curing shrinkage of thermoset resins to be two major mechanisms in formation of residual stresses. Using a viscoelastic constitutive equation to describe the stress-strain behavior of a polymer matrix composite laminate, CLT and the time temperature superposition (TTS) principle (Ferry, 1980) were employed to construct the equation. A new technique, which focused on measuring only the post-gel chemical shrinkage of thermoset resins, was developed particularly for the purpose of residual stress characterization. The study proved that the chemical curing shrinkage of polymer matrix contributes to a large portion of residual strains and only the shrinkage occurring after the solidification will contribute to the residual stresses in composite materials.

The nature of the thermo-chemo-viscoelastic problem often involves complex part geometry and boundary conditions, yielding strong 3D effects and precluding the use of CLT or 2D models. Furthermore, the tooling material plays a significant role in warpage and residual stress development. Warpage, shrinkage and residual stresses are caused by the complex interplay of heat transfer, curing and

viscoelastic properties. To understand how these phenomena interact, a model that accounts for all three effects is required.

Zhu and Geubelle (2001) presented a fully 3D coupled thermo-chemo-viscoelastic FE model to simulate the heat transfer, curing and residual stress development during the manufacturing cycle of thermoset composite parts. Special emphasis has been placed on capturing the complex evolution of the material response throughout the cure cycle. FE simulations have been conducted to study two phenomena, the warpage of thin cross-ply laminates and the spring-forward observed in curved parts. The predicted values of curvature for thin cross-ply graphite-epoxy laminates agreed well with experimental observations. In particular, the FE code was able to capture the sharp increase in residual stresses during the gelation process. The numerical result indicated that a significant fraction of residual stress develops before cool-down. Simulations of the spring-forward phenomenon in L-shaped graphite-epoxy composites have shown that the value of the spring-forward found by the thermo-chemo-viscoelastic model is much larger than that predicted by an elastic model, or by a viscoelastic model of the cool-down process only. This emphasizes the need to simulate the entire curing process. Their study also indicates that mold design and thermal expansion play an important role in spring-forward. Finally, unlike conventional elastic models, the thermo-chemo-viscoelastic model was able to capture the strong effect of the part thickness on the spring-forward phenomenon.

Zhu and Geubelle (2002) formalized the design process by integrating process modeling, design sensitivity analysis and numerical optimization into a single framework, in order to optimizing the tool shape used in thermoset composite manufacturing. The process modeling was based on a transient coupled thermo-chemo-viscoelastic FE scheme, which accurately captured the evolution of residual stresses throughout the manufacturing process, and their effect on the final shape of the composite part. The method provided a systematic way to predict the optimal tool geometry that leads to the minimum difference between desired and final shapes of the manufactured part. Optimization results were presented for two specific applications involving mold design for cross-ply laminates and L-shaped composite parts. The described approach was an efficient and accurate way to achieve dimensional accuracy in manufacturing thermoset composites and can be used for a wide range of shape design problems involving viscoelastic materials.

Xia *et al.* (2002) evaluated the evolution of residual stresses by a numerical 3D viscoelastic micromechanics model. The analysis showed high cooling rate resulted in the initial high residual stresses. The residual stresses would relax with time and tend to a smaller certain value independent of cool-down rate. Zhao *et al.* (2007) studied the process-induced residual stress in FRP-matrix composites by thermo-viscoelastic micromechanical analysis. The constitutive behavior of the epoxy matrix was described by a cure and temperature-dependent viscoelastic material model. They found that compared to an elasticity solution, a reduction in

residual stress was predicted due to the stress-relaxation caused by the viscoelastic behaviour of the epoxy matrix.

Guo *et al.* (2008) determined the residual stresses analytically by a linear viscoelastic model and utilized the temperature-independent mechanical properties of the materials, in addition to an experiment method on a T300/5222A carbon fiber/epoxy prepreg. Considering the good agreed results of the model with experimental values, they concluded that the viscoelasticity of composites should be considered in calculating the residual stresses.

7.5 Modified classical lamination theory (CLT) for modeling residual stresses

Classical Lamination Theory (CLT) is a commonly used predictive tool, which evolved in the 1960s, which makes it possible to analyze complex coupling effects that may occur in composite laminates. It is able to predict strains, displacements and curvatures that develop in a laminate as it is mechanically and thermally loaded. The method is similar to isotropic plate theory, with the main difference appearing in the lamina stress-strain relationships. As with any analytical technique, some assumptions must be made in order to make the problem solvable:

1. The plate consists of orthotropic lamina bonded together, with the principal material axes of the orthotropic lamina orientated along arbitrary directions with respect to the *x*-*y* axes.
2. The thickness of the plate, t, is much smaller than any characteristic dimension.
3. The displacements u, v, and w are small compared with t.
4. The in-plane strains ε_x, ε_y, and γ_{xy} are small compared with unity.
5. Transverse shear is negligible, $\gamma_{xz} = \gamma_{yz} = 0$ (plane stress in each ply).
6. Displacements u and v are assumed to be linear functions of the thickness coordinate z (no warping).
7. Assumptions 5 and 6 together define the Kirchhoff hypothesis.
8. Transverse normal strain ε_z is negligible.
9. Each ply obeys Hooke's Law.
10. The plate thickness is constant throughout the laminate.
11. Transverse shear stresses τ_{xz} and τ_{yz} vanish on the laminate surfaces $z = \pm t/2$.

These assumptions lay the foundation for the theory and enable prediction of composite laminate behavior. More details will follow, so that we can understand the modifications made to the existing methodology.

As reviewed in the literature, there would be up to almost 25% chemical shrinkage due to curing process and based on this, an error of up to 25% is normal in calculating the residual stresses with the original CLT. Another problem is that at the cure temperature of the composite, CLT predicts a zero strain state, yet there

is a significant amount of experimentally measured strain. This is due to the discussed chemical shrinkage phenomenon, which CLT does not account for. Therefore, modification should be implemented on the original CLT to compensate for the error. By modifying the original CLT formulation to include variations in material properties as a function of temperature as well as chemical shrinkage contributions, we can predict the behavior of a multi-directional laminate based solely on the behavior of a uni-directional sample of the same material system. A simple method used for consideration of chemical shrinkage in calculating residual stresses with CLT is to measure the stress-free temperature experimentally and consider the measured temperature in the calculations instead of curing temperature, and by this way the chemical strains would not be entered into the calculations.

7.5.1 Predicting residual stresses with modified CLT

Due to thermal loading and chemical contraction of the curing process, the total strains at any point may be related to the laminate's reference plane and curvatures as

$$\begin{Bmatrix} \varepsilon_x^{(k)} \\ \varepsilon_y^{(k)} \\ \gamma_{xy}^{(k)} \end{Bmatrix} = \begin{Bmatrix} \varepsilon_x^0 \\ \varepsilon_y^0 \\ \gamma_{xy}^0 \end{Bmatrix} + z \begin{Bmatrix} \kappa_x \\ \kappa_y \\ \kappa_{xy} \end{Bmatrix} - \begin{Bmatrix} \varepsilon_x^T \\ \varepsilon_y^T \\ \gamma_{xy}^T \end{Bmatrix} - \begin{Bmatrix} \varepsilon_x^S \\ \varepsilon_y^S \\ \gamma_{xy}^S \end{Bmatrix} \quad [7.1]$$

where $\{\varepsilon\}^0$, $\{\kappa\}$, $\{\varepsilon\}^T$, $\{\varepsilon\}^S$ are the mid-plane strain, mid-plane curvature, thermal strain and chemical shrinkage, respectively.

The thermal strain $\{\varepsilon\}^T$ and chemical shrinkage $\{\varepsilon\}^S$ are calculated by the following formulas respectively:

$$\begin{Bmatrix} \varepsilon_x^T \\ \varepsilon_y^T \\ \gamma_{xy}^T \end{Bmatrix} = [T_2]_{\theta_k} \times \begin{Bmatrix} \alpha_1 . \Delta T \\ \alpha_2 . \Delta T \\ 0 \end{Bmatrix} \quad [7.2]$$

$$\begin{Bmatrix} \varepsilon_x^S \\ \varepsilon_y^S \\ \gamma_{xy}^S \end{Bmatrix} = [T_2]_{\theta_k} \times \begin{Bmatrix} \psi_1 \\ \psi_2 \\ 0 \end{Bmatrix} \quad [7.3]$$

where $[T_2]\theta_k$ is the transformation matrix and is determined by

$$[T_2]_{\theta_k} = \begin{bmatrix} \mathrm{Cos}^2\theta & \mathrm{Sin}^2\theta & \mathrm{Cos}\,\theta\mathrm{Sin}\,\theta \\ \mathrm{Sin}^2\theta & \mathrm{Cos}^2\theta & -\mathrm{Cos}\,\theta\mathrm{Sin}\,\theta \\ -2\mathrm{Cos}\,\theta\mathrm{Sin}\,\theta & 2\mathrm{Cos}\,\theta\mathrm{Sin}\,\theta & \mathrm{Cos}^2\,\theta - \mathrm{Sin}^2\,\theta \end{bmatrix} \quad [7.4]$$

Also, $\alpha_{1,2}$ and $\psi_{1,2}$ are the coefficients of thermal expansion and chemical shrinkage in principal directions, respectively. The contribution of the chemical shrinkage is less transparent; the amount of shrinkage after the vitrification point, often assumed as the point where the resin becomes elastic and is able to pick up stress, is generally not available and requires extensive chemo-rheological characterization. Nevertheless, the total chemical shrinkage is presumed as stress-inducing for a first guess. The coefficients $\psi_{1,2}$ are derived with micro-mechanical rules for uni-directional (UD) plies (Shapery, 1968; Wijskamp *et al.*, 2003):

$$\{\psi\} = \begin{Bmatrix} \psi_1 \\ \psi_2 \\ \psi_3 \end{Bmatrix} = \begin{Bmatrix} \dfrac{V_m E_m}{V_f E_f + V_m E_m} \\ (1+\nu_m)V_m - \dfrac{V_m E_m (V_f \nu_f + V_m \nu_m)}{V_f E_f + V_m E_m} \\ (1+\nu_m)V_m - \dfrac{V_m E_m (V_f \nu_f + V_m \nu_m)}{V_f E_f + V_m E_m} \end{Bmatrix} . \varepsilon_{cure}^{resin} \qquad [7.5]$$

where V_m and V_f are the volume fractions, E_m and E_f are the stiffness, ν_m and ν_f are the Poisson's ratios of matrix and fiber, respectively and $\varepsilon_{cure}^{resin}$ represents the chemical shrinkage of the matrix.

The force resultants along the cross-section of the lamina are given by

$$\begin{Bmatrix} N_x \\ N_y \\ N_z \end{Bmatrix} = \int_{-h/2}^{h/2} \begin{Bmatrix} \sigma_x^{(k)} \\ \sigma_y^{(k)} \\ \tau_{xy}^{(k)} \end{Bmatrix} dz = \sum_{k=1}^{n} \int_{z_{k-1}}^{z_k} \begin{Bmatrix} \sigma_x^{(k)} \\ \sigma_y^{(k)} \\ \tau_{xy}^{(k)} \end{Bmatrix} dz = \sum_{k=1}^{n} \int_{z_{k-1}}^{z_k} [\bar{Q}]_{\theta_k} \begin{Bmatrix} \varepsilon_x^{(k)} \\ \varepsilon_y^{(k)} \\ \gamma_{xy}^{(k)} \end{Bmatrix} dz$$

$$= \sum_{k=1}^{n} \int_{z_{k-1}}^{z_k} \left[\bar{Q}\right]_{\theta_k} \left(\begin{Bmatrix} \varepsilon_x^0 \\ \varepsilon_y^0 \\ \gamma_{xy}^0 \end{Bmatrix} + z \begin{Bmatrix} \kappa_x \\ \kappa_y \\ \kappa_{xy} \end{Bmatrix} - \begin{Bmatrix} \varepsilon_x^T \\ \varepsilon_y^T \\ \gamma_{xy}^T \end{Bmatrix} - \begin{Bmatrix} \varepsilon_x^S \\ \varepsilon_y^S \\ \gamma_{xy}^S \end{Bmatrix} \right) dz$$

$$= [A] \begin{Bmatrix} \varepsilon_x^0 \\ \varepsilon_y^0 \\ \gamma_{xy}^0 \end{Bmatrix} + [B] \begin{Bmatrix} \kappa_x \\ \kappa_y \\ \kappa_{xy} \end{Bmatrix} - \int_{-\frac{h}{2}}^{\frac{h}{2}} [\bar{Q}]_{\theta_k} \cdot [T_2]_{\theta_k} \begin{Bmatrix} \alpha_1 \Delta T + \psi_1 \\ \alpha_2 \Delta T + \psi_2 \\ 0 \end{Bmatrix} dz \qquad [7.6]$$

Here [*A*] is the laminate extensional stiffness and [*B*] is the bending-stretching coupling stiffness. They are only related to material properties. Similarly, the resultant moments are derived by

$$\begin{Bmatrix} M_x \\ M_y \\ M_z \end{Bmatrix} = \int_{-h/2}^{h/2} \begin{Bmatrix} \sigma_x^{(k)} \\ \sigma_y^{(k)} \\ \tau_{xy}^{(k)} \end{Bmatrix} z\,dz = \sum_{k=1}^{n} \int_{z_{k-1}}^{z_k} \begin{Bmatrix} \sigma_x^{(k)} \\ \sigma_y^{(k)} \\ \tau_{xy}^{(k)} \end{Bmatrix} z\,dz = \sum_{k=1}^{n} \int_{z_{k-1}}^{z_k} [\bar{Q}]_{\theta_k} \begin{Bmatrix} \varepsilon_x^{(k)} \\ \varepsilon_y^{(k)} \\ \gamma_{xy}^{(k)} \end{Bmatrix} zdz$$

$$= \sum_{k=1}^{n} \int_{z_{k-1}}^{z_k} \left[\bar{Q}\right]_{\theta_k} \left(\begin{Bmatrix} \varepsilon_x^0 \\ \varepsilon_y^0 \\ \gamma_{xy}^0 \end{Bmatrix} + z \begin{Bmatrix} \kappa_x \\ \kappa_y \\ \kappa_{xy} \end{Bmatrix} - \begin{Bmatrix} \varepsilon_x^T \\ \varepsilon_y^T \\ \gamma_{xy}^T \end{Bmatrix} - \begin{Bmatrix} \varepsilon_x^S \\ \varepsilon_y^S \\ \gamma_{xy}^S \end{Bmatrix} \right) zdz$$

$$= [B] \begin{Bmatrix} \varepsilon_x^0 \\ \varepsilon_y^0 \\ \gamma_{xy}^0 \end{Bmatrix} + [D] \begin{Bmatrix} \kappa_x \\ \kappa_y \\ \kappa_{xy} \end{Bmatrix} - \int_{-\frac{h}{2}}^{\frac{h}{2}} [\bar{Q}]_{\theta_k} \cdot [T_2]_{\theta_k} \begin{Bmatrix} \alpha_1 \Delta T + \psi_1 \\ \alpha_2 \Delta T + \psi_2 \\ 0 \end{Bmatrix} zdz \qquad [7.7]$$

where $[D]$ is the laminate bending stiffness, which is only a function of material properties. Since there are no external forces applied to the laminate, the resultant stresses derived in Eqs 7.6 and 7.7 are equal to 0, so, we have

$$[A] \begin{Bmatrix} \varepsilon_x^0 \\ \varepsilon_y^0 \\ \gamma_{xy}^0 \end{Bmatrix} + [B] \begin{Bmatrix} \kappa_x \\ \kappa_y \\ \kappa_{xy} \end{Bmatrix} - \int_{-\frac{h}{2}}^{\frac{h}{2}} \left[\bar{Q}\right]_{\theta_k} \cdot \left[T_2\right]_{\theta_k} \begin{Bmatrix} \alpha_1 \cdot \Delta T + \psi_1 \\ \alpha_2 \cdot \Delta T + \psi_2 \\ 0 \end{Bmatrix} dz = \begin{Bmatrix} 0 \\ 0 \\ 0 \end{Bmatrix} \qquad [7.8]$$

$$[B] \begin{Bmatrix} \varepsilon_x^0 \\ \varepsilon_y^0 \\ \gamma_{xy}^0 \end{Bmatrix} + [D] \begin{Bmatrix} \kappa_x \\ \kappa_y \\ \kappa_{xy} \end{Bmatrix} - \int_{-\frac{h}{2}}^{\frac{h}{2}} \left[\bar{Q}\right]_{\theta_k} \cdot \left[T_2\right]_{\theta_k} \begin{Bmatrix} \alpha_1 \cdot \Delta T + \psi_1 \\ \alpha_2 \cdot \Delta T + \psi_2 \\ 0 \end{Bmatrix} zdz = \begin{Bmatrix} 0 \\ 0 \\ 0 \end{Bmatrix} \qquad [7.9]$$

In Eqs 7.8 and 7.9, only 3 mid-plane strains and 3 laminate curvatures are unknowns, which could be solved from the 6 available equations. Then, from Eq. 7.1 the values of the residual strains $\{\varepsilon^{(k)}\}$ are given. The residual stresses in each layer are evaluated by

$$\left\{\sigma_r^{(k)}\right\} = \left[\bar{Q}\right]_{\theta_k} \left\{\varepsilon^{(k)}\right\} \qquad [7.10]$$

7.5.2 Predicting room-temperature shapes with CLT

For asymmetrical laminated composites, the process-induced stresses are not balanced internally. The composite warps to reach a new internal residual stress balance. Because the residual stresses cause warpage on the asymmetrical laminated composites and also cause an unexpected shape of the final product, composites with asymmetrical stacking sequences are not practical. The applications of asymmetrical laminates are mainly confined to academic research.

The curvature of the warped composite can be related to the residual stresses with analytical solutions. CLT is normally used to calculate the residual stresses from the curvature. Hyer (1981) has documented the room temperature shapes of asymmetrical laminates and found that the room-temperature shapes of some thin asymmetrical laminates are closely approximated by right circular cylinders. In addition, some thin laminates have two room-temperature cylindrical shapes. These results were in contrast to the predictions of the CLT, which predicts the room temperature shapes of all asymmetrical laminates to be a saddle with unique (single-values) curvature characteristics. Specifically, Hyer found that the cylindrical shape could be snapped into another cylindrical shape, which had the same characteristic as the first shape, named snap-through or oil-canning phenomenon. The theory proposed by Hyer was based on an extension of CLT, which accounted for geometric nonlinearities. A rigorous explanation of the theory and formulation is shown in his article published in 1981.

In curved composite parts, the out-of-plane distortions known as 'spring back' or 'spring in' cannot be predicted by CLT. This phenomenon is mostly caused by the orthortropy of the composites and the difference between the in-plane and the out-of-plane material properties cause these distortions.

7.6 Future trends

In previous sections, the importance of a suitable approach to properly simulate the response of composite materials during processing was discussed. The model should have the ability to take into account different complexities of the process and also be efficient concurrently. This makes efficiency of the model a crucial factor in controlling the modeling costs. The following subjects would be the areas for further research.

A precise characterization of the development of the resin properties with time and temperature is necessary for the visco-thermo-elastic modeling of composite materials, which is rarely available. In these experiments the possibility of the nonlinear behavior of the material should be explored. Using the viscoelastic model and utilizing the temperature-independent mechanical properties of the materials, would make the possibility of evaluation of residual stresses. In such a study, the influence of the temperature on the material properties is ignored but the model complexity is decreased.

Further research would include the application of the viscoelastic model, utilizing the temperature-dependent mechanical properties of the materials and taking the matrix shrinkage into account in the analysis. This method is the most rigorous modeling available to evaluate the residual stresses in composite materials and can be called thermo-chemo-viscoelastic modeling. Comparison on the accuracy of the described models and the introduced modified CLT is of great importance, which should be comprehensively studied. Studies on the mechanisms

of generation of additional residual stresses due to tool-part interaction are an ongoing research and their influence on the final residual stresses should be realized.

7.7 References

Adolf, D. and Martin, J. E. (1996) Calculation of stresses in cross-linking polymers, *Journal of Composite Materials*, **30**(1), 13–34.

Bogetti, T. A. and Gillespie. J. W. Jr. (1989) Process-induced stress and deformation in thick-section thermosetting composite laminates, *SAMPE Technical Conference*. **21**, 947–59.

Bogetti, T. A. and Gillespie, J. W. Jr. (1991) Two-dimensional cure simulation of thick thermosetting composites, *Journal of Composite Materials*. **25**(3), 239–73.

Bogetti, T. A. and Gillespie, J. W. Jr. (1992) Process-induced stress and deformation in thick-section thermoset composite laminates, *Journal of Composite Materials*, **26**(5), 626–60.

Bogetti, T. A. and Gillespie, J. W. Jr. (1994) Influence of processing on the development of residual stresses in thick-section thermoset composites, *International Journal of Materials and Product Technology*, **9**(1–3), 170–82.

Chen, H., Yang, Z., Jemah, A. K. and Williams, F. W. (1998) Process-induced stress analysis of composite laminates using semi-analytical Hamiltonian method, *Composite Structures*, **41**(1), 49–55.

Crasto, A. S. and Kim, R. Y. (1993) On the determination of residual stresses in fiber-reinforced thermoset composites, *Journal of Reinforced Plastics and Composites*, **12**, 545–58.

Djokic, D., Hojjatic, M., Johnston, A. and Lee-Sullivan, P. (2001) Process optimization for reduction of composite patch repair residual stress, *Proceedings of the 33rd International SAMPE Technical Conference*, Seattle, WA.

Fernlund, G., Poursartip, A., Twigg, G. and Albert, C. (2003) Residual stress, spring-in and warpage in autoclaved composite parts, *ICCM14 Conference*.

Ferry, J. D. (1980) *Viscoelastic Properties of Polymers*, New York, John Wiley and Sons Inc.

Guo, Z. S., Zhang, J., Guo, X and, Hu, H. (2008) Theoretical and experimental characteristics on residual stresses of advanced polymer composites, *Proceedings of SPIE. 6934.* **693409**, 1–8.

Hahn, H. T. (1976) Residual stresses in polymer matrix composite laminates, *Journal of Composite Materials*, **10**, 266–78.

Hahn, H.T. (1984) Effect of residual stresses in polymer matrix composites, *Journal of Astronautical Science*, **32**(3), 253–67.

Hahn, H.T. and Pagano, N. J. (1975) Curing stresses in composite laminates, *Journal of Composite Materials*, **9**, 91–106.

Harper, B. D. and Weitsman, Y. (1981) Residual thermal stresses in an unsymmetrical cross-ply graphite/epoxy laminate, *Proceedings of AIAA/ASME/ASCE/AHS 22nd Structures, Atlanta, GA: Structural Dynamics and Materials Conference*, 6–8 April, 325–32.

Harper, B. D. and Weitsman, Y. (1985) On the effects of environmental conditioning on residual stresses in composite laminates, *International Journal of Solids and Structures*, **21**(8), 907–26.

Hyer, M. W. (1981a) An inherent instability in fiber-reinforced composite laminates, in: S. S. Wand and W. J. Renton (eds), *Advances in Aerospace Structures and Materials, ASME AD–01*, New York, American Society of Mechanical Engineers, 239–46.

Hyer, M. W. (1981b) Calculation of the room-temperature shapes of unsymmetric laminates, *Journal of Composite Materials*, **15**, 296–310.

Hyer, M. W. (1981c) Some observations on the cured shape of thin unsymmetric laminates, *Journal of Composite Materials*, **15**, 175–94.

Hyer, M. W. (1989) Mechanics of unsymmetric laminates, in: C. T. Herakovich and Y. M. Tarnopol'skii, *Handbook of Composites*, Ch. 2, vol. 2, *Structures and design*, Elsevier Science Publishing, 85–114.

Jain, L. K. and Mai, Y. W. (1997a) Stress and deformations induced during manufacturing. Part I: Theoretical analysis of composite cylinders and shells, *Journal of Composite Materials*, **31**(7), 672–95.

Jain, L. K. and Mai, Y. W. (1997b) Stress and deformations induced during manufacturing. Part II: A study of the spring-in phenomenon, *Journal of Composite Materials*, **31**(7), 696–719.

Jeronimidis, G. and Parkyn, A. T. (1988) Residual stress in carbon fibre thermoplastic matrix laminates, *Journal of Composite Materials*, **22**(5), 401–15.

Johnston, A. (1997) *An Integrated Model of the Development of Process-Induced Deformation in Autoclave Processing of Composite Structures*, PhD Thesis, The University of British Columbia, Canada.

Johnston, A. J., Reza V. and Anoush, P. (2001) A plane strain model for process-induced deformation of laminated composite structures, *Journal of Composite Materials*, **35**(16), 1435–69.

Jun, W. J. and Hong, C. S. (1992) Cured shape of unsymmetric laminates with arbitrary lay-up angles, *Journal of Reinforced Plastics and Composites*, **11**(12), 1352–66.

Kim, K. S. and Hahn, H. T. (1989) Residual stress development during processing of graphite/epoxy composites, *Composite Science and Technology*, **36**, 121–32.

Kim, Y. K. and White, S. R. (1997) Secondary structure effects on the process-induced residual stress development of cylinder structure, in: *The 11th International Conference on Composite Materials (ICCM–11)*, vol. IV, Composites processing and microstructure, Gold Coast, Australia, 360–9.

Lange, J., Manson, J. A. E. and Hult, A. (1996) Build-up of structure and viscoelastic properties in epoxy and acrylate resins cured below their ultimate glass transition temperature, *Polymer*, **37**(26): 5859–68.

Lange, J., Toll, S. and Manson, J. A. E. (1997) Residual stresses build-up in thermoset films cured below their ultimate glass transition temperature, *Polymer*, **38**(4), 809–15.

Leaderman, H. (1958) Viscoelasticity phenomena in amorphous high polymeric systems, in: F. R. Eirick (ed.), *Rheology, Theory and Applications*, New York, Academic Press, Inc., 1–61.

Lee, S. S. and Sohn, Y S. (1994) Viscoelastic analysis of residual stresses in a unidirectional laminate, *Structural Engineering and Mechanics*, **2**(4), 383–93.

Li, M. C., Wu, J. J., Loos, A. C. and Morton, J. (1997) A plane-strain finite element model for process-induced residual stresses in a graphite/PEEK composites, *Journal of Composite Materials*, **31**, 212–43.

Lin, K. Y. and Yi, S. (1991) Analysis of inter-laminar stresses in viscoelastic composites, *International Journal of Solids Structures*, **27**(7), 929–45.

Liu S. C. (1999) Residual Stress Characterization for Laminated Composites, PhD Thesis, University of Florida.

Liu, S. C., Niu, X. and Ifju, P. (1998) Residual stress characterization by Moiré interferometry, *Proceedings of the SEM Spring Conference of Experimental and*

Applied Mechanics and Experimental/Numerical Mechanics in Electronic Packaging III, Houston, TX, 176–8.

Loos, A. C. and Springer, G. S. (1983) Curing of epoxy matrix composites, *J. Compos. Mater.*, **17**, 135–69.

Nairn, J. A. and Zoller, P. (1985) Matrix solidification and the resulting residual thermal stresses in composites, *Journal of Material Sciences*, **20**, 355–67.

Pagano, N. J. and Hahn, H. T. (1977) Evaluation of composite curing stresses, *Composite Materials: Testing and Design (Fourth Conference*), ASTM STP 617, 317–29.

Poon, H. and Ahmad, M. F. (1998) A material point time integration procedure for anisotropic, thermo theologically simple, viscoelastic solids, *Computational Mechanics*, **21**(3), 236–42.

Prasatya, P. (2001) A viscoelasic model for predicting isotropic residual stresses in thermosetting materials: Effects of processing parameters, *Journal of Composite Materials*, **35**(10), 826–48.

Radford, D. W. and Diefendorf, R. J. (1993) Shape instabilities in composites resulting from laminate anisotropy, *Journal of Reinforced Plastics and Composites*, **12**(1), 58–75.

Schapery, R. A. (1968) Thermal expansion coefficients of composite materials based on energy principles, *Journal of Composite Materials*, **2**, 380.

Schapery, R. A. (1974) Viscoelastic behavior and analysis of composite materials, in: G. P. Sendeckyi (ed.), *Mechanics of Composite Materials*, New York, Academic Press, 85–167.

Schulte, K. J. and Hahn, H. T. (1990) Annealing of residual stresses in Gr/PEEK laminate, *Proceedings of the 5th Tech. Conf., American Society for Composites*, 81–9.

Schulz, W. A., Myers, D. G., Singer, T. N., Ifju, P. G. and Haftka, R. T. (2005) Determination of residual stress and thermal history for IM7/977–2 composite laminates, *Composite Science and Technology*, **65**, 2014–24.

Shokrieh, M. M. and Kamali Shahri, S. M. (2005) Theoretical and experimental studies on residual stresses in laminated polymer composites, *Journal of Composite Materials*, **39**, 2213–25.

Stango, R. J. and Wang, S. S. (1984) Process-induced residual thermal stress in advanced fiber-reinforced composite laminates, *Journal of Engineering for Industry*, **106**(1), 48–54.

Stango, R. J. and Wang, S. S. (1987) Viscoelastic analysis of post-cure processing stresses in advanced composite laminates, Invited paper, *Symposium on Applied Mechanics Problems in Composite Manufacturing and Processing: Polymer Matrix Composites*, ASME Winter Annual Meeting, Boston, MA.

Svanberg, J. M. and Holmberg, J. A. (2004) Prediction of shape distortions. Part I: Fe-implementation of a path dependent constitutive model, *Composites Part A: Applied Science and Manufacturing*, **35**(6), 711–21.

Teng, S. C. and Ossward, T. A. (1994) Prediction of shrinkage and warpage of fiber reinforced thermoset composite parts, *Journal of Reinforced Plastics and Composites*, **13**(8), 698–721.

Tobolsky, A. (1958) Stress relaxation studies of the viscoelastic properties of polymers, in: F. R. Eirick (ed.), *Rheology, Theory and Applications*, New York, Academic Press, Inc., 63–81.

Tuttle, M. E., Koehler, R. T. and Keren, D. (1996) Controlling thermal stresses in composites by means of fiber pre-stress, *Journal of Composite Materials*, **30**, 486–502.

Wang, T. M., Daniel, I. M. and Gotro, J. T. (1992) Thermo-viscoelastic analysis of residual

stresses and warpage in composite laminates, *Journal of Composite Materials*, **26**(6), 883–99.

Weitsman, Y. (1979) Residual thermal stresses due to cool-down of epoxy-resin composites, *Journal of Applied Mechanics*, **46**, 563–7.

Weitsman, Y. (1980) Optimal cool-down in linear viscoelasticity, *Journal of Applied Mechanics*, **47**, 35–9.

White, S. R. and Hahn, H. T. (1990) Mechanical property and residual stress development during cure of a graphite/BMI composite, *Polymer Engineering and Science*, **30**(22), 1465–72.

White, S. R. and Hahn, H. T. (1992a) Process modeling of composite materials: residual stress development during cure. Part I: Model formulation, *Journal of Composite Materials*, **26**(16), 2402–22.

White, S. R. and Hahn, H. T. (1992b) Process modeling of composite materials: residual stress development during cure. Part II: Experimental validation, *Journal of Composite Materials*, **26**(16), 2423–53.

White, S. R. and Hahn, H. T. (1993) Cure cycle optimization for the prediction of processing-induced residual stresses in composite materials, *Journal of Composite Materials*, **27**(14), 1352–78.

White, S. R. and Kim, Y. K. (1998) Process-induced residual stress analysis of AS4/3501–6 composite material, *Mechanics of Composite Materials and Structures*, **5**, 153–86.

Wiersma, H. W., Peeters, J. B. and Akkerman, R. (1998) Prediction of spring-forward in continuous-fiber/polymer L-shaped parts, *Composite: Part A*, **29A**(11), 1333–42.

Wijskamp, S., Akkerman, R. and Lamers, E. A. D. (2003) Residual stresses in non-symmetrical carbon/epoxy laminates, *ICCM14 Conference*.

Wisnom, M. R., Stringer, L. G., Hayman, R. J. and Hinton, M. J. (1999) Curing stresses in thick polymer composite components. Part I: Analysis, *Proceedings of the 12th ICCM*, Paris, 5–9 July, Ref. CD-ROM, paper 861.1–10.

Xia, Z., Zhang, Y. and Ellyin, F. (2002) Thermal residual stresses induced during manufacturing process of fiber reinforced polymeric composites, *2002 ASME Pressure Vessels and Piping Conference*, Vancouver, BC, **443**(2), 171–5.

Zewi, I. G., Daniel, I. M. and Gotro, J. T. (1987) Residual stresses and warpage in woven-glass/epoxy laminate, *Experimental Mechanics*, **27**(1), 44–50.

Zhao, L. G., Warrior, N. A. and Long, A. C. (2007) A thermo-viscoelastic analysis of process-induced residual stress in fiber reinforced polymer–matrix composites, *Materials Science and Engineering A*, **452–3**, 483–98.

Zhu, Q. and Geubelle, P. H. (2002) Dimensional accuracy of thermoset composites: Shape optimization, *Journal of Composite Materials*, **36**(6), 647–72.

Zhu, Q., Geubelle, P. H., Li, M and, Tucker, III C. L. (2001) Dimensional accuracy of thermoset composites: Simulation of process-induced residual stresses, *Journal of Composite Materials*, **35**(24), 2171–205.

Zhu, Q., Shrotriya, P., Sottos, N. R. and Geubelle, P. H. (2003) Three-dimensional viscoelastic simulation of woven composite substrates for multilayer circuit boards, *Composites Science and Technology*, **63**(13), 1971–83.

Zobeiry, N. (2006) *Viscoelastic Constitutive Models for Evaluation of Residual Stresses in Thermoset Composites During Cure*, PhD Thesis, The University of British Columbia.

8

Understanding residual stresses in polymer matrix composites

M. SAFARABADI, University of Tehran, Iran and
M. M. SHOKRIEH, Iran University of Science and Technology, Iran

DOI: 10.1533/9780857098597.2.197

Abstract: This chapter presents a review of the formation and effects of thermal residual stresses, as well as methods of measuring and predicting them. The first part of this chapter focuses on the factors responsible for residual stress formation in composites. The second part discusses the effects of thermal residual stresses on composites and their material properties. After identification of the effective parameters for thermal residual stress build-up and the effects of these stresses on composite shape and material properties, the methods for residual stresses measurement are presented, including destructive and non-destructive techniques. Finally, analytical and numerical methods for prediction of thermal residual stresses are studied and a comparison of experimental and theoretical methods is performed in the last section of this chapter.

Key words: residual stress, fiber, matrix, composite laminate, measurement, prediction.

8.1 Introduction

Residual stresses or process-induced stresses can be defined as those stresses existing within a body in the absence of external loading or thermal gradients. Therefore, residual stresses in a structural material or component are those stresses which remain after the original cause of the stresses (external forces, heat gradient) has been removed. These stresses can be present in any mechanical structure for a variety of reasons, including inelastic deformations and heat treatment. Generally, in metallic components manufacturing and fabricating processes such as casting, welding, machining, molding, heat treatment and plastic deformation during bending, rolling or forging induce residual stresses into the manufactured object. As an example, welding is one of the most significant causes of residual stresses and typically produces large tensile stresses whose maximum value is approximately equal to the yield strength of the materials being joined. Also, residual stresses could be caused by localized yielding of the material, because of a sharp notch or from certain surface treatments such as shot peening or surface hardening. For these reasons, sometimes residual stresses are defined as the internal stresses created inside a component during the manufacturing process.

Thermal-induced residual stresses are primarily due to differential expansion when a metal is heated or cooled. The two factors that control this are thermal treatment (heating or cooling) and restraint. Material shrinkage during injection molding can be conveniently demonstrated with a free quenching example, in which a part with uniform temperature is suddenly sandwiched by cold mold walls. During early cooling stages, when the external surface layers cool and start to shrink, the bulk of the polymer at the hot core is still molten and free to shrink. However, as the internal core cools, local thermal contraction is constrained by the already-rigid external layers. This results in a typical state of stress distribution with tension in the core balanced by compression in the outer layers (Fig. 8.1).

In composite laminates, after the curing process and subsequent cooling from the relatively high processing temperature to the room temperature, residual stresses arise due to chemical and thermal reasons. During solidification, chemical contraction leads to resin shrinkage (Callister, 1994). Since the chemical shrinkage of the polymer matrix is small, chemical effects are often neglected in the residual stress prediction, while thermal residual stresses are performed because of the inherent inhomogeneous nature of polymeric composites. Consequently, these stresses are named as the curing or thermal residual stresses. For example, when a composite laminate is subjected to a temperature decrease during solidification, the various layers will shrink differently due to incoherence of their orientations. In reality, all the layers are bounded together. Consequently, thermal residual stresses are performed. The schematic view of the out-of-plane deformation of a laminated composite is shown in Fig. 8.2.

However, moisture conditions throughout the thickness of the composite laminate or structure may result in a residual stress distribution throughout the thickness of the laminate (Barnes and Byerly, 1994). Polymer matrix

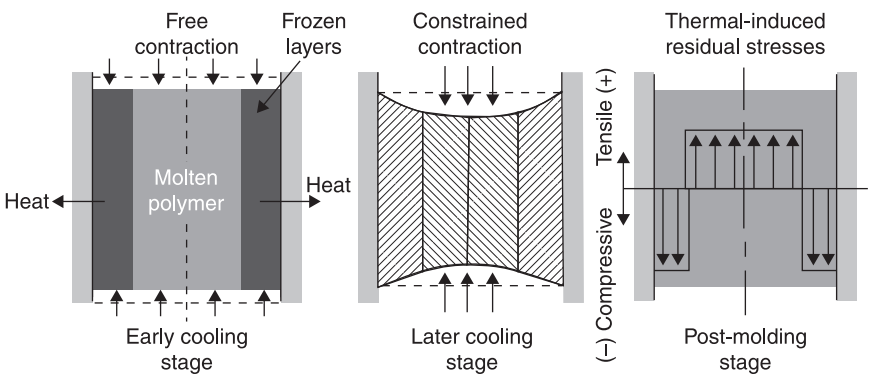

8.1 The development of residual thermal stress in a 'free-quenching' part.

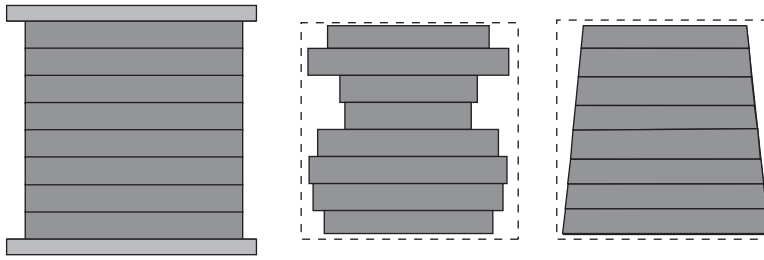

8.2 Schematic view of out-of-plane deformation of a laminated composite (Harris, 1999).

composites tend to absorb moisture in wet environments. Since the rate of moisture absorption is very low, the residual stress distribution is non-uniform. These stresses can reduce or inactivate the thermal residual stresses effects (Tsai and Hahn, 1980).

8.2 Formation of residual stresses

Residual stresses in continuous fiber reinforced composites exist in the laminate or composite structure immediately after processing and subsequent cooling to the service temperature. They can be regarded at three different levels, based on their origins.

8.2.1 Micro-residual stresses

On the micro-mechanical level, or constituent level, the mismatch in coefficient of thermal expansion between the fibers and the matrix is the governing parameter. Unlike a thermoset matrix, the thermoplastic matrix is heated to a processing temperature above its glass or melting temperature and subsequently solidified upon cooling to the service temperature (often ambient conditions), where no chemical reaction should take place. The cooling involves volumetric shrinkage of the thermoplastic matrix, which is significantly higher than the fibers shrinkage. This represents an important driving force for the development of residual strains in fibers and the surrounding matrix. Assuming that fiber–matrix bonding presents during the cooling stage, Fig. 8.3 shows that the result is a residual compressive stress in the fiber along the longitudinal axis as well as in the radial direction, and a residual tensile stress in the matrix in the longitudinal and radial direction (Li *et al.*, 1997).

Also, in a series of previous publications, Papanicolaou *et al.* (2002) presented the concept as well as the effect of the boundary interphase on several properties of composite materials. In all these publications, the following definition for the interphase area was adopted:

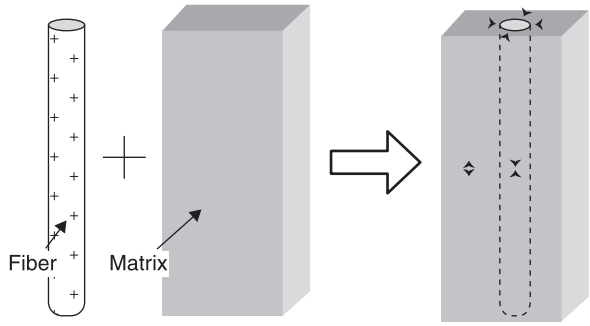

8.3 Schematic view of the effect of cooling on the matrix around a fiber (Li *et al.*, 1997).

> . . . around an inclusion embedded in a matrix a rather complex situation develops consisting of areas of imperfect bonding, where mechanical stresses are abundantly developed due to shrinkage and high stress gradients or even stress singularities due to the geometry of the inclusion are apparent and finally voids, microcracks and other similar discontinuities may be created. In this case the composite may be considered as consisting of three phases, that is the two actual phases and a third one, which may also arise during thermal treatment of the material, because of component interaction. This extra phase is what we call 'interphase' and it is obviously inhomogeneous.

The existence of the interphase is not an assumption. Its existence has already been experimentally proved by a number of researchers and its properties have already been experimentally measured and theoretically modeled (Papanicolaou *et al.*, 2002). Figure 8.4 illustrates the possible variation of the modulus of elasticity and the coefficient of thermal expansion at the micro-mechanical level.

Bonding conditions

It has been proven that the adhesion conditions on material interfaces also play an important role in thermal residual stresses fields. Imperfect adhesion conditions lead to stress discontinuity at the fiber-interphase and interphase-matrix interfaces. These bonding imperfections do not primarily separate material phases, but decrease the capability for transmitting and sustaining loading as well as the structural stiffness. In this way, interfacial compatibility and continuity conditions on displacements and stresses remain, but interphase material properties are much softer than those of the fiber and tend to matrix properties. This difference depends on the degree of imperfect adhesion between the fiber and matrix. Shokrieh and Safarabadi (2011, 2012) investigated the influences of the interphase region on

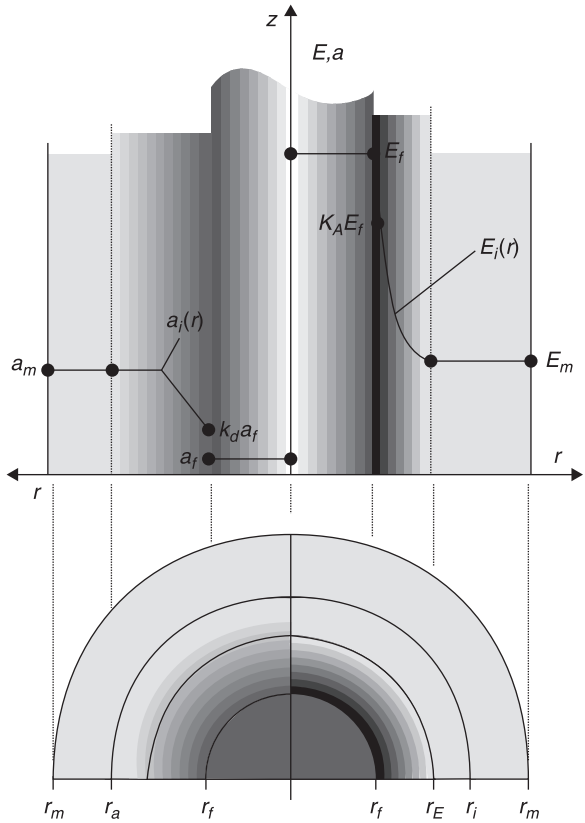

8.4 Variation of interphase modulus of elasticity and coefficient of thermal expansion along radial direction (Papanicolaou *et al.*, 2002).

micro-residual stresses in polymeric composites. The results demonstrated that the degree of imperfect adhesion affects the micro-mechanical residual stresses significantly.

Reinforcing fibers and matrix behavior

Both aramid and carbon fibers show highly anisotropic thermal expansion behavior, with small shrinkage in the fiber longitudinal direction when heated. So these reinforcing fibers have transversely isotropic behavior, while the glass fiber is isotropic. The thermal expansion behavior of anisotropic fibers can be described by separate coefficients of thermal expansion (CTEs) in the directions parallel (often negative) and perpendicular (positive) to the fiber axis (Nairn and Zoller, 1985; Wardle, 2001). In general, the CTE of the fibers is much lower

than that of the matrices, which results in a large difference in expansion behavior between the matrix and the reinforcing fibers in the longitudinal direction. The perpendicular (radial) fiber shrinkage upon cooling was shown to be a relatively insignificant contribution to the formation of residual stresses (Barnes and Byerly, 1994). Also, the shrinkage in thermoplastic polymers depends on the matrix morphology, such as amorphous or semi-crystalline. The total shrinkage for semi-crystalline matrices was found to be approximately ten times higher than that of the amorphous matrices (Barnes, 1993; Barnes, *et al.*, 1991). This matter has an important effect on micro-residual stress fields.

Processing conditions

Cooling rate is the most important processing condition that affects the residual stress formation. For amorphous polymer matrices, the high cooling rate in the glass transition region leads to formation of higher residual stresses. Studies have shown that for amorphous matrix (CF/PEI) composites, the radial residual stresses indeed increase upon increasing cooling rate (DiLandro and Pegoraro, 1996). In contrast, for semi-crystalline thermoplastics, a higher cooling rate will give a lower peak crystallization temperature and lower crystallinity levels (Guillen and Cantwell, 2002). This leads to a lower stress-free temperature and less shrinkage. Therefore, it was concluded that residual stresses due to crystallization could be reduced by increasing the cooling rate (Deshpande and Seferis, 1996). Also, the processing environment may prove to have a significant effect on formation of residual stresses. Applied pressure may affect the polymer thermal properties, which in turn influence the formation of residual stresses (Young and Lovell, 1991).

In addition, the Young's modulus of semi-crystalline matrix is cooling rate dependent. A higher cooling rate generates a lower level of highly elastic crystals, hence the resulting Young's modulus will be lower (Young and Lovell, 1991). Consequently, the mismatch in the fiber and matrix elastic properties increases, which can give rise to higher residual stresses.

8.2.2 Macro-residual stresses

Macro-mechanical or lamination residual stresses present on a ply-to-ply scale, due to the difference in material directions of each ply of composite laminates (Kim and Mai, 1998). During cooling from curing temperature to the room temperature within a laminate, the deformation of one ply is constrained by the other plies with different fiber orientations. Hence, residual stresses are built up in each ply. Consequently, the layers are under tension and compression and therefore thermal loads are induced. For example, with cross-ply composites, the 90-degree fibers impose a mechanical constraint on the 0-degree

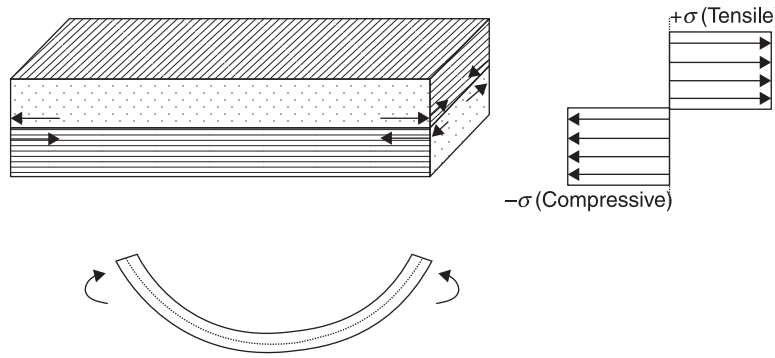

8.5 Schematic view of residual stress formation and front view of out-of-plane deformation in unbalanced cross-ply laminate. (Li *et al.*, 1997). M: Bending moment.

fibers during cooling and vice versa, because of differences in thermal shrinkage directions (Harris, 1999). Figure 8.5 shows that the 90-degree fibers are under compression, while the 0-degree fibers experience tension. The anisotropic shrinkage resembles the behavior of a bi-metallic strip, if unbalanced and unconstrained, and curvature of the laminate may be the result (Shokrieh and Kamali, 2005).

Parameters that influence the magnitude of a laminate macro-residual stresses are listed below:

- temperature difference (between the curing and ambient temperatures);
- fiber volume fraction;
- fiber waviness;
- processing condition (curing and cooling rate);
- thickness and fiber orientation of each layer in the laminate;
- lamination sequence;
- coefficient of the thermal expansion of each layer in the longitudinal and transverse directions;
- on-axis mechanical properties of each layer.

Residual stresses increase as the curing temperature is further away from the ambient temperature. Considering the fiber volume fraction, a few conclusions were obtained in the literature. It was found that for higher fiber volume fractions, the macro-residual strains were lower (Wagner and Nairn, 1997). An optimum in fiber volume may exist when the laminate is subjected to external loads (Jones, 1999). For cross-ply composites, it was stated that the residual interlaminar stresses increase with increasing fiber volume fraction (Wang *et al.*, 2004). An increase in the fiber waviness lowers the difference in CTE in the transverse and longitudinal directions, consequently for uni-directional (UD) as well as

angle-ply laminates, the residual stresses are lower (Karami and Garnich, 2005). In addition, the optimum processing cycle, giving the lowest residual stresses and maximizing the mechanical properties of the composite, was found to be different for each lay-up (Li *et al.*, 1997). Other parameters listed above affect the lamination residual stresses significantly according to the composite lay-up.

8.2.3 Global residual stresses

In thick composite laminates, a gradient in cooling rate, temperature or moisture throughout the thickness of the composite laminate leads to a residual stress distribution through the thickness of the laminate. This type of residual stress is named as 'skin-core' residual stress. Generally, in thick laminates, the cooling rate in middle plies is slower than that at the plies near the surface. This will gives rise to compressive residual stresses in the near-surface plies and tensile stresses in the middle plies (Fig. 8.6) (Manson and Seferis, 1992). Consequently, a complex three-dimensional (3D) residual stress state within a composite laminate exists.

As mentioned above, cooling rate plays a significant role in the formation of global residual stresses. It was shown that with higher cooling rates, the residual stresses are higher and the distribution is more significant. Most of the fast cooled or quenched composites such as PEEK/CF and PET/CF show almost a parabolic residual stress profile, with the surface plies under compression of a higher magnitude than the tensile residual stresses in the centre plies (Domb and Hansen, 1994; Ersoy and Vardar, 2000; Hsiao and Kikuchi, 1999; Sunderland *et al.*, 2001).

Annealing is typically executed on thick laminates to reduce the skin-core residual stresses through relaxation of the stresses. Annealing can be accomplished by raising the composites' temperature above the glass transition temperature of the matrix and allowing relaxation processes to take place (Chung, 2001).

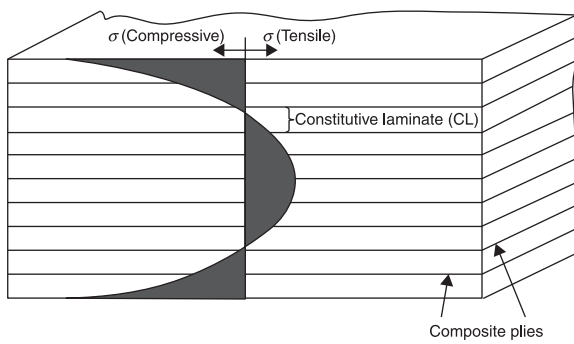

8.6 Laminate skin-core residual stress distribution (Manson and Seferis, 1992).

8.3 Effects of residual stresses

Residual stresses can cause several defects in composite laminates and structures. For example, on the micro-mechanical level for a UD ply, the compressive axial residual stress of the fiber can lead to fiber buckling (Shokrieh and Safarabadi, 2011). Also, several microcracks are performed in the tensile residual stress of the matrix. Consequently, micro-residual stresses are able to affect the mechanical properties of the orthotropic layer. This section discusses the residual stress-induced defects and the effects of thermal residual stresses on the material properties of composite structures.

8.3.1 Effects on fiber–matrix bonding

In thermoset composites, the interphase region is formed with chemical bonds, whereas in thermoplastic composites, the fiber–matrix adhesion primarily occurs due to the shrinkage of the matrix around the fiber and thereby increases the Van der Waals bonds between the fiber and the matrix (Warnet, 2000). The residual stresses in turn influence the fiber–interphase and interphase–matrix interfacial shear strengths significantly (Shokrieh and Safarabadi, 2011). It was found that by increasing radial residual stresses, the fiber–matrix interfacial bond became stronger, due to mechanical locking (Walther, 1998). However, the fiber–matrix interfacial debonding parallel to the fiber axis may occur due to residual stresses alone, if the (chemical) fiber–matrix bond strength is too weak (Sjogren *et al.*, 1999). It was found that in semi-crystalline composites, such as carbon/polyetheretherketone (PEEK), the mismatch in thermal shrinkage behavior between the matrix and the fiber can cause strain induced crystallization. This can lead to the formation of a transcrystalline layer (Li *et al.*, 2000).

8.3.2 Fiber waviness

Micro-mechanical analysis predicts that the fiber axial residual stress is compressive, while the matrix is unable to provide a transverse rigid support for the fiber (Shokrieh and Safarabadi, 2011). This cause fiber micro-buckle and consequently waviness will develop. The global residual stresses due to high temperature gradients through the thickness of the laminates can cause fiber waviness. Fiber waviness in UD laminates is often represented mathematically as a sine wave (Bhalerao, 1996) (Fig. 8.7). Fiber waviness development is affected the most by tool plate material (the difference in CTE between the tool and the composite part), and also by cooling rate and length (Kugler and Moon, 2002).

Fiber waviness can degrade the compressive strength (Wisnom and Atkinson, 2000). In addition, it has found by analysis that the fiber waviness can increase buckling load when the composite is subjected to compressive loads (Shokrieh and Safarabadi, 2011) and has considerable effects on the thermal expansion of the laminate (Karami and Garnich, 2005).

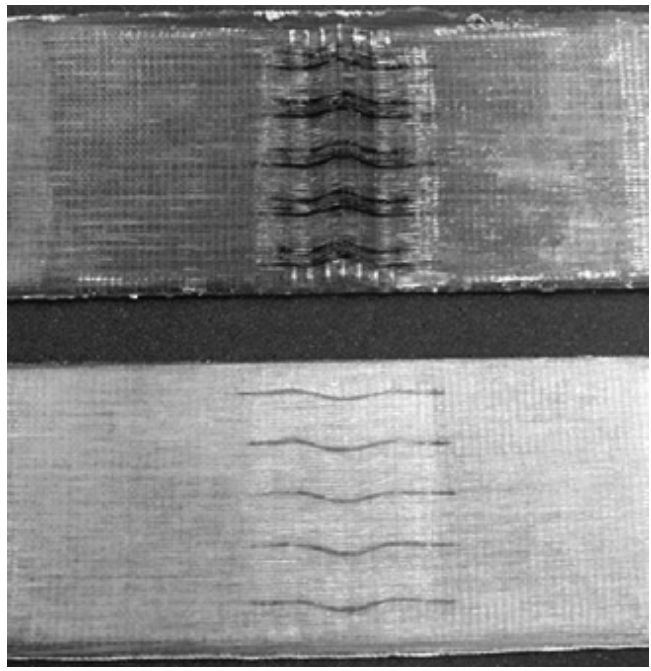

8.7 Glass/epoxy laminates with one surface and four layers of in-plane waviness (Wang, 2001).

8.3.3 Transverse cracking

Thermal residual stresses are able to initiate transverse microcracks in composite laminates. If the thermal residual stress in the matrix exceeds the yield strength of the resin and/or the fiber–matrix bond strength, matrix cracking or fiber–matrix shearing will occur. Generally, the polymer matrix is very weak and consequently after cooling from the curing condition to the room temperature, a solid composite with several microcracks is obtained. Low bond strengths at the fiber-interphase and interphase-matrix interfaces lead to crack propagation along the interphase region. Figure 8.8 shows crack initiation and its progress, which gives rise to fiber–matrix debonding. If a strong interphase exists, cracks may propagate into the matrix.

Microcracks should be noticed during the cyclic (fatigue) loading, which can lead to a longitudinal splitting. First, a fiber–matrix debonding/matrix cracking occurs, and then growing of matrix cracks/fiber–matrix debonds preform microcracks. Microcracks may grow into transverse ply cracks, which finally form initiations of delamination and subsequent failure of the laminate. These stages may take place during the service life.

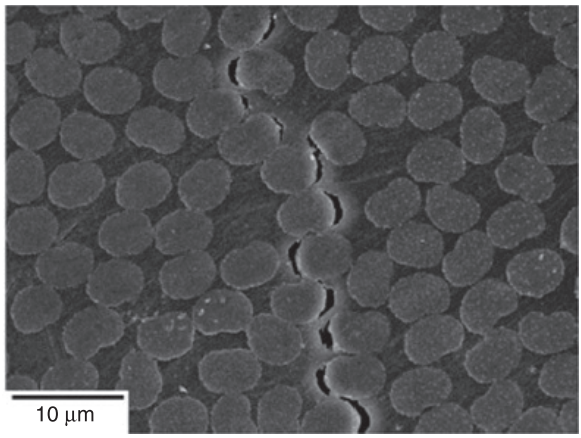

8.8 Fiber–matrix debonding in a woven carbon fiber polyimide composite (Gentz *et al.*, 2004).

8.9 Transverse cracks in a woven graphite fiber polyimide composite laminate (Gentz *et al.*, 2004).

Often cracks initiate at the vicinity of the free edges, because of the stress singularity (Fig. 8.9). For example, on the micro-mechanical level, there are radial and shear stress concentrations at composite ends, which can cause the fiber–matrix debonding initiation.

In general, higher interlaminar residual stresses result in a higher microcrack density within the composite (Nairn and Hu, 1994). In addition, residual stresses

may cause a greater susceptibility to solvents, leading to environmental stress cracking. In addition, various analytical models were developed, from which crack formation due to thermal residual stresses or due to external loading in the presence of residual stresses can be predicted (McCartney, 2005; Nairn, 1997; Park and Manus, 1996).

Transverse cracks cause residual stress relaxation, which in turn lead to redistribution of stresses. Redistribution of thermal residual stresses affects thermal and mechanical properties of the laminates. Some examples include lower transverse mechanical properties (Nairn and Hu, 1992), lower composite stiffness and Young's modulus (especially for quasi-isotropic laminates) (Khatri and Koczak, 1996), reduction of in-plane shear strength and modulus (Weteringe *et al.*, 2002), lower values for Modes I and II interlaminar fracture toughness (Nairn, 1997), initiate sites for delamination during fatigue loading (Highsmith and Reifsnider, 1982), increased deformation during creep loading (Cantwell *et al.*, 1990), lower corrosion resistance (Nairn, 2001) and decrease in the transverse electrical conductivity of carbon fiber reinforced laminates (Chung, 2001). So far, no results have been reported for the relation between residual stress-induced microcracks and impact properties of composites.

8.3.4 Delamination

Stress discontinuity between layers of a laminate can lead to a premature delamination during the life of the component. For example, in a cross-ply laminate, residual stress discontinuity between the 0-degree and 90-degree plies may result in an interlaminar debonding. Interlaminar failure is characterized by progressive delamination of plies of a composite laminate, leading to a loss of stiffness and strength of the structure (Unger *et al.*, 1993). The free-edge effect is one of the mechanisms causing delamination, which can also cause matrix cracking. Free-edge delamination is associated with the high property discontinuities through the thickness at a free edge (Lessard *et al.*, 1996).

8.3.5 Warpage

Interlaminar residual stresses may lead to a curved shape in asymmetrical laminates. As mentioned before, non-symmetrical thermal residual stress gradients through the thickness exist due to the unbalanced cooling and tool–part interaction. These stress gradients could result in a deformation of a laminate (warpage) (Lawrence *et al.*, 1990) or dimensional instability of a composite structure. For cross-ply laminates, the interlaminar residual stresses have more impact on the warpage than the through-the-thickness residual stresses caused by the cooling profile (Sunderland *et al.*, 2001). Tool–part interaction makes a significant contribution to warpage, especially for thin products (Wijskamp, 2005). In addition, a non-uniform temperature distribution in press-plates or moulds may also induce warpage.

8.3.6 Effects on mechanical properties of composite laminates

In cases where the residual stresses and the stresses resulting from external loads are equal in sign, the maximum allowable external load decreases. Consequently, residual stresses must be taken into account in the design of composite structures. The residual stress distribution affects the structural response to different loading regimes, including static and dynamic (fatigue) loadings. So, the aim of this section is to investigate the variation of composite dominant mechanical properties due to the presence of residual stresses.

Tensile properties

Micro-mechanical analysis shows that thermal residual stresses often leave the matrix in a state of tension in the direction parallel to fibers and the reinforcing fibers under the compressive loading. In the radial or transverse direction, the radial stress peaks a positive value at the composite ends due to the edge effect singularity (Papanicolaou *et al.*, 2002; Shokrieh and Safarabadi, 2011). The compressive residual axial stress in fibers should result in an increased tensile strength in the longitudinal direction.

For a UD ply, the longitudinal residual stress is negative, while the transverse residual stress is positive. Therefore, it was found that residual stresses can be detrimental for the transverse tensile loading. When the cross-ply laminate is loaded under tension in one direction, the tensile strength is measured to be lower than for UD transverse tensile strengths. The difference between these values provides an estimate for the interlaminar residual stresses (Kim and Hahn, 1979). Also, differences in residual stresses due to various cooling rates were shown to affect tensile properties of cross-ply IM6 carbon fiber reinforced PEEK composites (Cantwell *et al.*, 1990). Micro-mechanical study of cross-ply laminates showed that even after relaxation, the remaining residual stresses still have a significant influence on the damage evolution during tensile loading (Zhang *et al.*, 2004).

The effect of thermal residual stresses was found to be negligible in the tensile strength of thick glass and carbon fiber reinforced composites. However, the classical lamination theory (CLT) predicts a small increase in ultimate tensile strength for the UD, cross-ply and quasi-isotropic laminates. In thick-section laminates, the residual stresses do not affect the composite Young's modulus (Khatri and Koczak, 1996).

Compressive properties

At the micro-mechanical level, the compressive residual stress of fibers lowers the compressive strength of the UD ply in the longitudinal direction, which in turn

leads to fiber waviness or fiber-matrix debonding (Papanicolaou *et al.*, 2002; Shokrieh and Safarabadi, 2011). Consequently, the residual stresses significantly affect the compressive properties of UD plies. The failure strain will decrease and for materials with different tensile and compressive elastic modulus, the stiffness of the composite will probably be affected by the thermal stresses. Since compressive testing of composites is difficult to perform, not many experimental studies are available.

Shear properties

With the aid of a micro-mechanical unit cell analysis and finite element methods (FEMs), the interfacial shear residual stresses are approximately zero along the fiber length, but peak to a significant value at the vicinity of the fiber ends. Therefore, there is a considerable shear stress concentration near the fiber ends, which decreases the shear strength of UD laminates. This may increase the probability of fiber buckling, matrix cracking and fiber-matrix debonding when the composite is subjected to external loads (Shokrieh and Safarabadi, 2011, 2012). On the macro-mechanical and global levels, no studies have been published that investigate the relation between shear properties and residual stresses. However, it seems most likely that interlaminar mechanical properties are affected due to the discontinuity in the macroscopic stress field between plies in angle-ply laminates.

Flexural properties

UD laminates have compressive axial residual stresses in the longitudinal direction. Consequently, when the laminate is subjected to bending loads, the layers located above the neutral axis have different behavior compared to the layers under this axis. The compressive residual stress is able to increase the negative bending stresses significantly, which results in a lower flexural strength of composite laminate. In a UD glass fiber reinforced PP laminate, the residual stresses were found to comprise between 37 and 45% of the 90-degree flexural strength (~26 MPa). This also resulted in a lower flexural strength for 0-degree flexural loading (Guillen and Cantwell, 2002). To the best knowledge of the authors, no studies have been published that investigate the relation between flexural properties and residual stresses.

Modes I and II fracture toughness

Most of the studies exhibited that thermal residual stresses must be considered in predicting fracture toughness properties of composite laminates, since these stresses significantly decrease the fracture toughness properties of a composite (Unger and Hansen, 1998). In order to understand the effects of residual stresses

on composite toughness properties, Nairn (1987) suggested the assumption that the presence of residual stresses could contribute to loss of the toughness by providing a source of thermal strain energy release during the crack propagation. He investigated the role of residual stresses in the mode *I* energy release rate for double cantilever beam specimens and found that there is a significant effect that needs to be taken into account (Nairn, 2000). The residual stresses do not play an important role in transverse fracture properties of UD T300 carbon fiber polysulfide composites, nor on delamination parallel to the fibers in UD laminates. This is because residual stresses are present in both fiber and matrix, but they release no energy as the delamination propagates (Nairn, 1997).

Interlaminar delamination due to the free-edge effect was studied in cross-ply laminates. The effects of thermal residual stresses were significant for the total strain energy release rate versus the applied axial strain. It was calculated that the failure strains, when considering the residual stresses, are only 73% of the failure strains when residual stresses were neglected during axial loading. For mixed mode *I/II* failure strain, the same trend was observed (Unger and Hansen, 1998).

For UD and cross-ply carbon fiber thermoplastic laminates, the interlaminar critical matrix cracking strain (mode *II*) is small due to high residual thermal stresses in low temperatures (Huang *et al.*, 1997).

Fatigue and creep properties

In thermoplastic composites, thermal residual stresses cause a significant reduction in the specimen's fatigue delamination strain due to free-edge delamination (Unger *et al.*, 1993). For cross-ply carbon fiber reinforced laminates, creep behavior at room temperature is more significant for fast cooled samples (high residual stresses), whereas for UD laminates loaded in the transverse direction, no difference in creep behavior was reported (Cantwell *et al.*, 1990).

8.4 Methods of measurement: destructive methods

Residual stresses may have adverse effects on the mechanical properties of composites. These stresses are often ignored or underestimated in both design and analytical modeling, which can lead to incorrect interpretations of material characteristics and mechanical behavior of composites. Therefore, it is of utmost importance that the thermal residual stresses are taken into the account in both design and analytical modeling of composite structures (Kim and Mai, 1998). Predictive models for thermal residual strains and stresses in composites require verification and validation with experimental results.

In the past, several measurement techniques for residual stress determination in polymer matrix composites have been developed, mostly based on techniques that are frequently applied to metallic structures. Recently, new advanced methods in

the field of experimental residual stress determination for polymer–matrix composite have been developed. For measuring residual stresses, there are two main categories of experimental techniques, destructive methods and non-destructive methods. This section reviews the available experimental techniques, starting with destructive techniques. As the name suggests, the destructive methods render the composites unusable after the testing. After measurements are taken by using destructive methods, the specimens are usually no longer suitable as structural elements. The early-developed experimental techniques are mainly based on destructive evaluation of the residual stresses in composites. These techniques include stress-relaxation based techniques (hole-drilling, cutting/sectioning and layer removal methods, etc.) and the first-ply failure method. They all involve taking a portion out of the specimen to create a free surface and release the stresses on the surface.

8.4.1 Hole-drilling

The central hole-drilling method is one of the methods for measuring residual stresses. This is the only method for measurement of residual stresses that is accepted as an ASTM standard (ASTM E837-01, 1999). This is a simple and reliable method and by considering the small size of the damaged area resulting from the test, it is called a semi-destructive method (Shokrieh and Ghasemi, 2007a). The hole-drilling method for measuring residual stresses was presented in 1934 by Mathar (1934). This method is used when the residual stresses are uniform throughout the thickness of the specimen. This method is established for isotropic and homogeneous materials. Rendler and Vigness (1966) extended this method for any isotropic material by introducing calibration factors.

Traditionally, a strain gage rosette is used with the hole-drilling method to record the strain relief around the hole. Then, using a drill, a small diameter hole with a depth slightly more than the diameter is located in the center of the strain gage. The strains are thus released around the hole area and measured by the three strain gages of the rosette. (Fig. 8.10) The resultant strain changes are recorded and processed in a (semi-empirical) model to deduce the stresses present prior to the hole drilling. In order to obtain the thermal residual stresses, Shokrieh and Ghasemi (2007b) calculated the calibration factors for isotropic, orthotropic and laminated composite plates. One drawback is that the size of a standard strain-gage rosette is two to four times of the hole diameter, making the region covered by the rosette too large compared to the released strain field (Wu and Lu, 2000). In addition, the rosette strain gage is located at the first layer top surface and consequently for the lower layers the measured strains deviate from their actual values. Therefore, the incremental hole drilling method has low accuracy for the lower layers. Also, the eccentric hole drilling error (i.e. the error caused when the hole is not drilled exactly in the centre of the

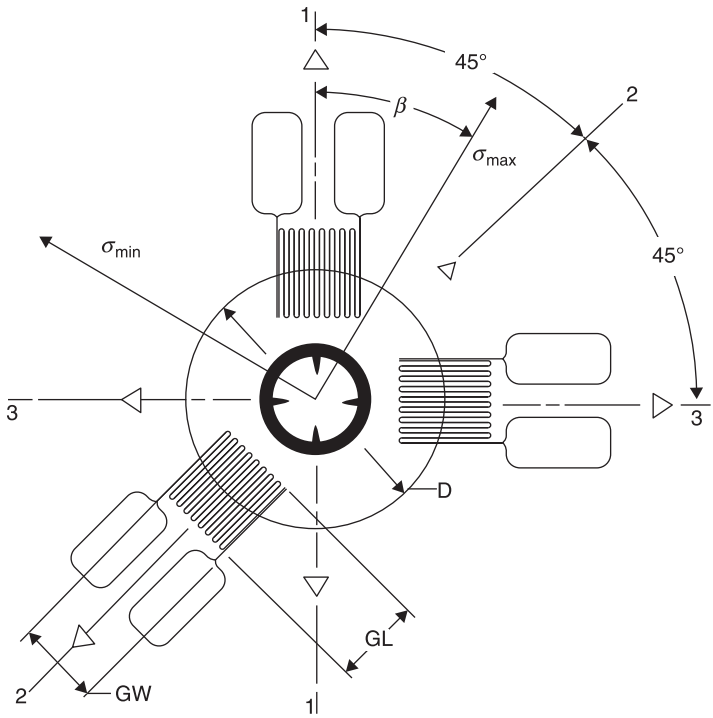

8.10 Schematic diagram showing the geometry of a typical three-element clockwise (CW) strain gage rosette for the hole-drilling method (ASTM E837-01, 1999). GW: Gage width. GL: Gage length.

rosette) is a commonly recognized problem with the strain gage rosette method (ASTM E837-01, 1999).

8.4.2 Cutting

Similar to hole-drilling methods, cutting methods utilize the idea that producing a free surface or separating plies releases residual stresses. Lee *et al.* (1989) and Gascoigne (1994) used Moiré interferometry to record the change of the displacement field before and after cutting. They first replicated a diffraction grating on the lateral surface of the composite specimen, and then used a diamond saw to cut either parallel or perpendicular to the ply interface. The surface residual stresses and the interlaminar residual stresses can be obtained, respectively. Lee and Czarnek, (1991) went one step further. With the data obtained from Moiré interferometry and a FEM post-processor, they claimed that the distribution of the residual strain could be accessed within a single ply. Sunderland *et al.* (1995) introduced another variant of cutting methods called

'successive grooving' or 'slot drilling'. The authors applied strain gages on one side of a thin composite laminate specimen. On the opposite side, they used a diamond saw to cut a groove and let the saw incrementally advance. By monitoring the change of the strain and equilibrium conditions, using classical laminate theory (CLT), the internal stresses (residual stresses) in each layer can be calculated. The cutting method, like the hole-drilling method, also encounters the problem that the stress field around the cut diminishes rapidly for the composite laminates. The strain reading may not be accurate enough to represent the deformation due to the stress relief.

8.4.3 Layer removal (ply sectioning)

Ply sectioning is another destructive method reported in the literature (Chapman *et al.*, 1990; Joh., *et al.* 1993; Manson and Seferis, 1992). Sectioning could be achieved by precise machining or embedding a separating film inside the laminate (the so-called 'process simulated laminate' (PSL)) (Manson and Seferis, 1992)). After the ply removal and stress relief, the unbalanced stresses create out-of-plane deformation on the laminates. Residual stresses were then calculated from laminate theory. The drawback of this method is the difficulty of ply-separation. In order to prevent damaging the composite, as in layer removal by abrasion, the concept of the PSL was described (Manson and Seferis, 1992). The PSL technique consists of several composite prepreg plies separated by thin release plies, such as polyimide foils. The composite plies between two separation films form a constitutive laminate. These laminates can be separated after processing. Lee *et al.* (1989), Gascoigne (1994) and Joh *et al.* (1993) chose Moiré interferometry as the tool for the strain measurement and obtained the displacement contour map around the cuts or sections. This method proved to be inaccurate, because the technique proves sensitive to heat generation and initiation of microcracking due to abrading, both of which may release the internal stresses under investigation (Cowley and Beaumont, 1997). In addition, any irregularity in the layer thickness due to abrasion will affect the resulting curvatures (Jeronimidis and Parkyn, 1988).

8.4.4 First ply failure method

Kim and Hahn (1979) introduced the first-ply failure method. They claimed that the swelling due to moisture absorption could be used to compensate for the effect of curing stress due to CTE mismatch between the matrix and the fibers. When the specimens absorbed the moisture with different degrees of saturation, the tensile strength of the specimen also varied. The relationship between the strength and the swelling could be correlated to obtain the residual stresses of composites. However, waiting for the specimens to become saturated takes a long period of time and the authors' goals were to understand fracture initiation of composites rather than measuring residual stresses.

8.5 Methods of measurement: non-destructive methods

Although the non-destructive methods are more favorable for mechanical testing, the existing non-destructive methods for residual stress measurement are somewhat limited. These techniques include:

- employing inherent material properties of the composite constituents;
- external embedded strain sensors;
- in-plane and out-of-plane deformation monitoring.

More details about these methods are described in the following section.

8.5.1 Employing inherent material properties of the composite constituents

When the material is subjected to strains or stresses, some material properties will change. This section will introduce the experimental techniques that detect the change in material properties due to thermal residual stresses in the composite, such as change in optical or electrical properties.

Photoelasticity

Photoelasticity is one of the oldest methods for experimental stress analysis, but has been overshadowed by the FEM for engineering applications over the past two/three decades. The phenomenon was first observed by David Brewster in the early 19th century in glass and he foresaw the potential of this for stress analysis. This method was applied to the transparent thermoset matrix composites and amorphous thermoplastic matrices (Nielsen and Pyrz, 2002). In amorphous polymers, stress alters the molecular orientation distribution, which affects the polarization state of the light, or in other words, stress results in anisotropic scattering of light and intensity measurements provide information on orientation. For determination of the magnitude of residual stresses, measurement of phase difference between two light vectors travelling at different velocities is required, from which the residual stress components can be calculated by means of the stress-optic law (Dally and Riley, 1991). More details can be found in numerous publications on this topic (Ingersoll, 2004; Nairn and Zoller, 1985; Sjogren *et al.*, 1999).

Micro-Raman spectroscopy

Another technique for the residual strain measurement based on an inherent material property is micro Raman spectroscopy, based on the interaction between light and matter, in which the light is inelastically scattered. The difference in

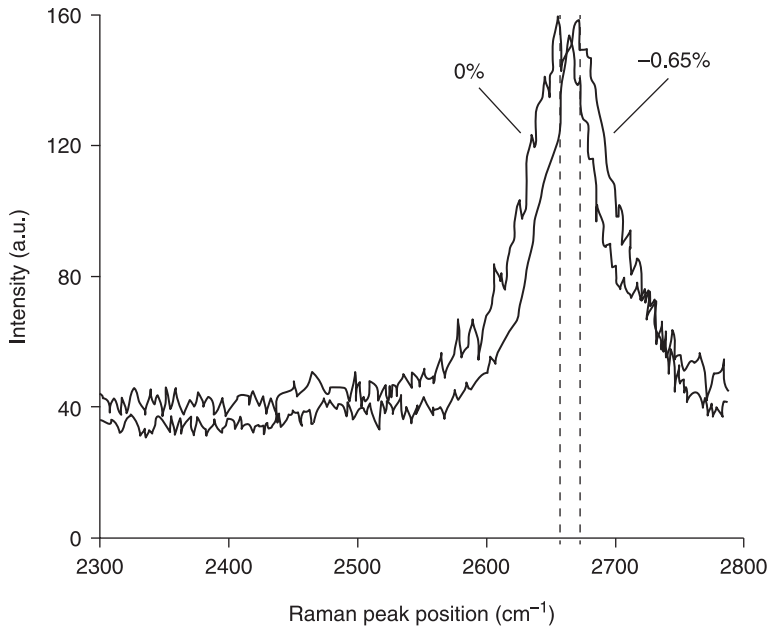

8.11 Compressive strain induced in AS4 carbon fiber embedded in a PEEK matrix (Nielsen and Pyrz, 1998).

energy between the incident photon and the Raman scattered photon is equal to the energy of a vibration of the scattering molecule. The plot of intensity of scattered light versus energy difference is a Raman spectrum (Nielsen and Pyrz, 2002). Certain peak positions in the Raman spectrum of the fiber change with applied strain. For example, the Raman peaks of the fiber in an unloaded PEEK prepreg (Fig. 8.11) show a shift to higher peak positions. This represents a compressive fiber strain due to thermal residual strains imposed by the surrounding matrix (Nielsen and Pyrz, 1998).

Electrical conductivity

In carbon fiber composites, the electrical properties of the composite such as electrical resistance are affected by strain, damage and temperature (Chung, 2001). The electrical resistance can therefore be monitored to indicate strain, damage and temperature. This leads to the possibility of determination differences in the interlaminar residual stresses by means of electrical resistivity measurements of laminates (Chung, 2001). Upon curing of thermoset matrix composites with higher pressures, the electrical conductivity barrier measured as the activation energy increased. This was attributed to increased residual interlaminar stress, because of a higher fiber volume fraction achieved by the higher processing

pressure (Wang *et al.*, 2004). More details are presented in Mei and Chung (2000), Lei Wang *et al.* (2001) and Guerrero and Chung (2002).

8.5.2 External embedded strain sensors

Embedding strain sensors into composites and allowing them to go through the manufacture procedure while monitoring the strain change is another non-destructive method. The sensors can be of any material or shape. Currently used sensors are strain gages, embedded metallic particles and optical fiber strain gages.

Embedded strain gages

In order to maintain the reference for strain measurement, the strain gages and strain indication instruments need to be connected to each other throughout the whole composite curing procedure. Although the strain gages are small (thin), their presence acts to redistribute the residual stress in composites. In thermoset composites, embedded strain gages were shown to give accurate results during heating as well as cooling (Crasto *et al.*, 2002; Kim and Daniel, 2002; Shao-Chun, 1999; Wisnom *et al.*, 2006).

Embedded metallic particles

X-ray diffraction was utilized to measure the residual stress of composites by including metal filler particles into the matrix (Fenn *et al.*, 1993; Predecki and Barrett, 1979). Although the diameter of the filler particles has been reported to be on the same order as the diameter of fibers, the issue is that fillers are distributed throughout the composite and affect the mechanical properties of the composite globally rather than locally, as in embedded strain sensor methods. In addition, the relationship between the residual stress and the results from X-ray diffraction need to be carefully correlated in order to obtain meaningful information. Embedded aluminium (Benedikt *et al.*, 2001a,b; Kumosa, 2003), copper and silver particles show a deflection in peak angle when embedded in a composite (Benedik *et al.*, 2001a,b; Hauk, 1999; Meske and Schnack, 2003). Using Bragg's law, this deflection is related to a change in crystal lattice spacing induced by the residual strain (Benedikt *et al.*, 2001a,b). The measured strain can be related to the residual stress in the polymer matrix using Hooke's law (Benedikt *et al.*, 2001a,b). Regular-shaped aluminium particles gave highest accuracy (Benedikt *et al.*, 2001a,b). Measurement of interlaminar as well as interlaminar residual strain in UD laminates was found to be possible (Benedikt *et al.*, 2001a,b). Since the thermoset matrix does not have a crystalline structure that changes in response to X-rays when strained, this type of experiment is mainly performed on thermoset matrix materials. The main disadvantage of this technique is that it gives information on the surface properties of the sample only.

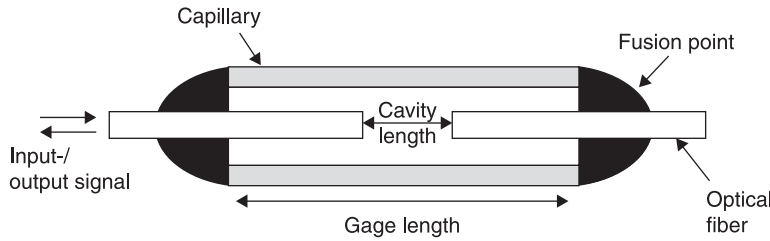

8.12 Schematic view of EFPI sensor (Zhou and Sim, 2002).

Optical fiber strain gages

Recent studies illustrate that optical fiber sensors can be applied as internal 'strain gages' to follow the development of thermal residual strains inside a composite laminate, even during high processing temperature in UD laminates as well as in angle-ply laminates (Sorensen *et al.*, 2004; Vlekken and Parlevliet, 2004). Since the optical fibers have a diameter 10 to 100 times larger than the diameter of a carbon fiber, they can disturb the natural order of the composite (Shao-Chun, 1999). A number of different optical fiber sensors exist (Zhou and Sim, 2002), of which the fiber Bragg grating (FBG) and external Fabry–Perot interferometric (EFPI) sensors were most often applied for following residual stress formation. The working principle of both sensors is explained in Zhou and Sim (2002). An EFPI sensor measures strain through a change in cavity length, which is related to a phase change between the input/output signals and the reflection of the optical fibers (Zhou and Sim, 2002) (Fig. 8.12). Monitoring residual strain development during curing of thermoset laminates was successfully carried out using EFPI sensors as well as a hybrid FBG/EFPI sensor (Lai *et al.*, 1995; Lawrence *et al.,* 1998; Leng and Asundi, 2002; Kang, *et al.*, 2002, 2003). More details about the working principle of the FBG sensors are presented in Zhou and Sim (2002) and Vlekken and Parlevliet (2004).

8.5.3 In-plane and out-of-plane deformation monitoring

Warpage of unsymmetric laminates

Measuring the warpage (i.e. the curvature) of an asymmetrical composite laminate is a widely used method (Fakuda *et al.*, 1995; Hyer, 1981; Jeronimidis and Parkyn, 1988; Kim *et al.*, 1989). There are two methods to produce warped laminates. The most used method involves producing an asymmetrical laminate. Upon cooling, the laminate warps as stresses increase. The second method is to produce a symmetrical laminate and machine off layers from one side to relieve the residual stresses, thus producing a warped laminate. Of course, this will be classified as a destructive method. With CLT, the curvature can be related to the moment resultant

on the laminates. Thus, from the stress-strain relationship, the residual stresses can be calculated.

The disadvantage of this method is that it is unusual to make a structural component out of an asymmetrical laminated composite. Therefore, use of the warpage measurement is greatly limited when dealing with practical situations. Also in this method, the values of curvature may show large variations for equal laminates under similar conditions. This may be due to a multitude of reasons, such as the limits in the precision of curvature measurement, but also fiber alignment, disorientation of the plies or non-symmetry of ply thickness. In addition, it does not provide any information regarding the spatial variation of residual stresses at the micro-mechanical level.

Moiré interferometry

Madhukar *et al.* (1995) measured the residual stress by monitoring the tension development in a single carbon fiber imbedded in epoxy during the curing process. In their paper, the authors clearly demonstrate the interaction between chemical shrinkage and thermal expansion, and proposed the way to optimize the curing cycle to reduce the residual stresses. Nevertheless, those measurements were not taken on a real part or structural element; consequently, the usefulness of the technique is greatly reduced but can still yield valuable information in an academic sense.

In order to overcome the drawbacks in the methods mentioned above, Ifju *et al.* (1996) proposed a novel technique to measure the residual stress for symmetrical fiber reinforced composite laminates using high sensitivity Moiré interferometry. A Moiré diffraction grating is attached to the composite panel during the manufacture process. After cure and separation from the tool, the diffraction grating will deform with the laminate and thus record the dimensional change. By comparing the specimen grating with the reference grating on the tool, the strain information of the composite can be retrieved. However, to obtain the residual stresses from residual strains, the authors used the linear elastic laminate theory, which may be an over-simplified theory for most of the polymer matrix composites (PMCs). In their conclusion, they claimed possible errors due to neglecting visco-elasticity in PMCs.

The Moiré effect is a well-known effect in optics based on an interference pattern that develops when light passes through two gratings rotated over a small angle with respect to each other (Fakuda *et al.*, 1995). When one of the gratings changes due to deformation of the sample, the resulting interference (Moiré) pattern will also change. A good explanation and overview of the applications of Moiré interferometry is available in Han *et al.* (2001). Moiré interferometry can be used to monitor both in-plane and out-of-plane displacements. For in-plane measurements, a grating needs to be applied to the surface of the sample under investigation. For measuring out-of-plane-displacements, there is no need to

apply a grid to the surface. The grating can be projected onto the surface at an angle to the viewing direction.

A method known as the cure reference method (CRM) was developed to determine the thermal strain development in thermoset composites with Moiré interferometry (Ifju *et al.*, 2000). It is a full-field laser-based optical method of Moiré interferometry to monitor strains on the surface of the thermoset laminate that initiate during cooling down. The grating is applied during consolidation and acts as a reference to the stress free condition just prior to the stress free temperature. The result of the interference is a characteristic pattern of light and dark fringes, which can be used to determine the in-plane-displacements in symmetrical laminates from which the residual stresses can be calculated utilizing CLT. The advantages are that it is an accurate and non-contact full-field method. It possesses high displacement and strain sensitivity, high spatial resolution (in the order of 0.5l m) and a high signal-to-noise ratio. However, it only gives information on the residual strain state on the surface and an interference image needs to be captured when no strains are present, which may prove to be difficult for thermoplastic composites (Ifju *et al.*, 1996, 2000).

8.6 Methods of prediction

8.6.1 Analytical methods

In addition to the above-mentioned experimental methods, there have been numerous mathematical models developed to predict residual stresses in composite materials. Many analytical have been performed to study the state of residual thermal stresses in composites. Although analytical approaches offer good results for simple geometries and have an advantage in terms of time and cost, they have limitations concerning complicated geometries and boundary conditions.

Micro-mechanical analysis

Several micro-analytical methods have been developed to determine residual stress fields in polymer composites. These methods include elasticity solution (Huang, 1999; Kurtz and Pagano, 1991; Papanicolaou *et al.*, 2002), cylinder theory (plane strain theory) (Bianchi, *et al.*, 1998; Hashin and Rosen, 1964; Jayaraman and Reifsnider, 1992, 1993; Naik, 1992; Shueh and Becher, 1988), Eshelby theory (Epstein, 2002) and the energy method (Nairn and Zoller, 1985; Quek, 2004; Shokrieh and Safarabadi, 2011, 2012). The theory of elasticity requires the assumption of higher-order displacement fields to obtain greater accuracy for the stresses. This method yields a two-dimensional (2D) solution. Thus, the out-of-plane stress components cannot be obtained. Also, because of complexity, the elasticity solution does not consider the effects of some effective parameters on residual stress fields such as the fiber length or material anisotropy.

Results of the cylinder theory are suitable for plane-strain conditions, which are not suitable to fibers of finite length such as those used in fiber pull- and push-out tests (Quek, 2004). Eshelby theory estimates the strain, stress and minimum strain energy of an inclusion (or inhomogeneity) transforming in a constraining matrix (Hassel and Martin, 2000). The energy method is preferred, because this method considers more general conditions in comparison with other methods. It considers all physical, thermal and mechanical effective parameters on thermal stress fields. In addition, the energy method yields a direct approach to obtain the residual stresses, rather than using an indirect approach.

It has been proven that the adhesion conditions on material interfaces also play an important role in the ability of composites to support and transmit loading. Imperfect adhesion conditions lead to stress discontinuity at fiber-interphase and interphase-matrix interfaces. Localized defects concentrate exclusively inside the interphase. These bonding imperfections do not primarily separate material phases, but decrease the capability for transmitting and sustaining loading as well as structural stiffness. Material (interphase) discontinuities are homogenized at the level of the reference volume. In this way, interfacial compatibility and continuity conditions on displacements and stresses remain, but interphase material properties are much softer than those of fiber and tend to matrix properties. This difference depends on the degree of imperfect adhesion between the fiber and matrix. Inherent complexity of FRPs requires a great number of parameters to completely describe material and geometry features, which in turn require approximate methods to predict the overall material response (Papanicolaou *et al.*, 2002).

Macro-mechanical analysis

At the macro-mechanical level, in order to calculate the residual stresses, there are various analytical methods, of which the CLT is the most simple and applicable one. In addition, the energy method, a modified classical approach can be used to predict the shape of the asymmetrical laminates after curing (Shokrieh and Kamali, 2005).

Hahn and Pagano (1975) proposed a stress-strain-temperature relationship to model the process-induced residual stress based on CLT. This is the first attempt in the literature to assess the residual stresses of composites with a mathematical model. However, since this was the first effort on this topic, the authors made several assumptions, which have proved to be invalid. They assumed the stress-free state was located at the end of highest temperature (cure temperature) stage. Now we know the stress-free state (the gel point) is usually at the beginning or prior to the final hold stage. Their thermal-elastic model was correct for the cooling stage, but apparently could not describe the viscoelastic behavior of the polymer at the cure temperature holding stage. Also, the authors only considered the mechanical and thermal contributions and completely neglected the irreversible

chemical shrinkage of the polymer matrix materials. Wang *et al.* (1992) used linear thermo-viscoelastic laminate theory to calculate the residual stresses and warpage of asymmetrical woven-glass/epoxy laminates.

8.6.2 Numerical methods

Although analytical expressions are preferred in many cases, the pursuit of higher accuracy requires the implementation of numerical analysis. Generally, numerical methods include FEM, finite difference method (FDM) and boundary element method (BEM). In order to predict the micro- and macro-residual stresses, the FE method is more useful in comparison with the two other methods. Several finite element models, such as unit cell models of square and hexagonal arrays with different boundary conditions, have been considered in previous publications (Aghdam and Khojeh, 2003; Chen *et al.*, 2001; Hobbiebrunken *et al.*, 2005; Huang *et al.*, 2008; Karami and Garnich, 2005; Kyo-Kook *et al.*, 2008; Zhao *et al.*, 2007) (Fig. 8.13).

Some experimental methods are simulated using FEM and FDM. For example, a summary of the results presented by different authors show that in order to calculate the residual stresses, experiments must be performed to measure the calibration constant coefficients of the central hole-drilling method. It is clear that the experiments are time-consuming and in most cases expensive. Consequently, a method called the 'simulated central hole-drilling' (SCHD) method was presented by Shokrieh and Ghasemi (2007a,b) to calculate the calibration factors in isotropic, orthotropic and laminated composite plates. This method can be used for simulation of the 2- or 3D central hole-drilling process for isotropic and orthotropic materials, and can be used instead of experimental techniques. The process of hole drilling is simulated by a finite element technique. Bogetti and Gillespie (1992) used a one-dimensional (1D) heat conduction equation and finite difference analysis to stimulate the curing process of a thick thermoset composite laminate.

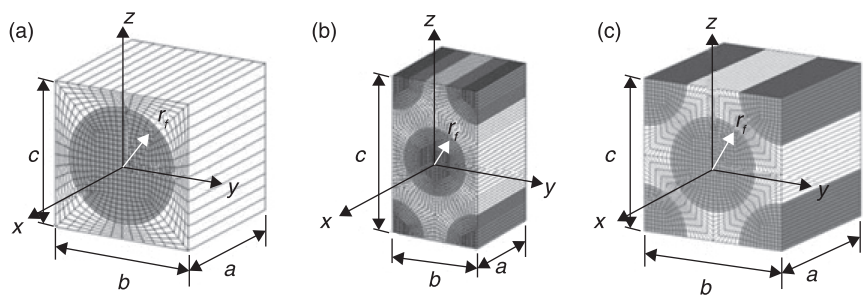

8.13 Finite element model of regular fiber arrays; r_f: radius of fibres; (a) square array; (b) hexagonal array; (c) diamond array (Kyo-Kook *et al.*, 2008).

8.7 Conclusion

Residual stresses may be defined from different point of views, because of various causes of formation such as manufacturing, moisture, curing/cooling, etc. After identification of the most important parameters for residual stress formation with respect to the material properties, it may be concluded that the magnitude of the residual stresses is most dependent on the shrinkage behavior of the thermoplastic matrix during processing, which varies for different processing conditions, such as cooling rate, pressure and environment. Only a few studies have been conducted on the effects of the latter two factors on residual stress formation. On the micro-mechanical level, the effective parameters on residual stress magnitude and its distribution include cooling rate, fiber/matrix bounding efficiency (imperfect adhesion), order of mismatch in thermal and mechanical properties of the fiber and matrix, physical parameters such as the fiber volume fraction and the composite length. At the macro-mechanical and global scales, the stacking sequence, cooling rate and fiber volume fraction are the governing parameters playing important roles in the residual stress distribution.

Regarding the effects of thermal residual stresses in thermoplastic composites, a review of the literature showed that several effects can be identified, such as fiber waviness, warpage, delamination and transverse cracking. Residual stresses affect mechanical properties of composite laminates significantly, which can be beneficial or detrimental, such as increasing/decreasing strength of a UD ply when it is subjected to tensile/compressive external loads. Generally, residual stresses lead to a drastic degradation in mechanical properties of composite structures.

Several experimental techniques can be employed for measuring residual stresses in composites, including destructive and non-destructive methods. Each of the methods has its requirements and drawbacks, which can be applied to a specific level of residual stresses in accordance with Table 8.1. For example, as can be seen from the table, photo-elasticity and Raman spectroscopy can be employed for determination of intra-ply residual stresses in the matrix and the fiber, respectively. The techniques discussed in this review are applicable not only to study thermal residual stresses, but also stresses induced by environmentally induced internal stresses, such as caused by moisture, temperature gradient, solvents, etc.

Theoretical methods include theory of elasticity, generalized plain stain theory (cylinder theory) and the energy method. Between these methods, the energy method is preferred and takes into account more precious assumptions in comparison with the other methods. At the micro-mechanical level, the other methods are only suitable for perfect bonding conditions (which corresponds to a two-phase composite only made of the fiber and matrix), whereas the present solution considers imperfect adhesion between the fiber and matrix (a three-phase

Table 8.1 Overview of experimental techniques for residual stress measurement in composites

Experimental technique	Applicable level of residual stresses	More explanation (requirements, drawbacks, etc.)
Hole-drilling	Macro, global	Low accuracy by increasing hole depth
Cutting	Macro, global	Low accuracy, time-consuming
Layer removal	Macro, global	Low accuracy
First-ply failure	Macro	Works best for unsymmetrical cross-ply laminates
Photoelasticity	Micro	Works for composites with transparent matrix with low fiber volume fraction
Micro-Raman spectroscopy	Micro, macro	Works for composites with transparent matrix, at macro level needs aramid fibers in amorphous material
Electrical conductivity	Macro	Works for composites with electrically conducting fibers
Embedded strain gages	Micro, macro	Redistribution of the residual stress in the composite
Embedded metallic particles	Micro, macro	Particles need to be close to surface
Optical fiber strain gages	Micro, macro, global	Polarization effects
Warpage	Macro	Low accuracy
Moiré interferometry	Macro	Gives only surface information

composite including the fiber and matrix as well as interphase between them). Also the other methods are not able to give the residual shear stress.

Besides using the other methods, the out-of-plane stress components cannot be obtained and the effects of some geometric characteristics such as fiber length are ignored, while the energy method gives a full set of residual stress components. While based on the other solutions, the residual stresses are usually assumed to be independent on the longitudinal coordinate, and the energy based solution assumes that these stresses vary along the fiber length and are functions of longitudinal coordinates. Consequently, the energy method gives a better knowledge of the behavior of residual stress distribution along the fiber length. The other methods do not satisfy some boundary conditions, especially at the ends of the fiber, while the energy method satisfies all boundary conditions. For example, from the other methods the fiber, interphase and matrix axial stresses are not zero at the ends of the fiber, at which stress-free conditions give zero axial and shear stresses. The energy method takes into account the edge effect singularity in contrast with the other methods. Table 8.2 compares the theoretical methods.

Table 8.2 Comparison between theoretical methods for prediction of residual stresses in composites

Method	Assumptions and constraints	Applicable level of residual stresses	More explanations
Theory of elasticity	– Requires the assumption of higher-order displacement fields to obtain greater accuracy for the stresses – Does not consider the effects of some effective parameters on residual stress fields, such as the fiber length or material anisotropy – At the micromechanical level, residual stress distribution is constant along the fiber length	Micro, macro	– At the micromechanical level, is not able to give the residual shear stresses as well as the out-of-plane components – Cannot satisfy stress-free condition
Generalized plain strain theory	– The problem is axisymmetrical – At the micromechanical level, residual stress distribution is constant along the fiber length – Neglects interphase effects	Micro	– Not suitable for fibers of finite length – At the micromechanical level, is not able to give the residual shear stresses as well as the out-of-plane components – Cannot satisfy stress-free condition
Energy method	– The problem is axisymmetrical	Micro, macro, global	– Considers interphase effects – Yields full state of residual stress tensor – Does not have any geometric limit – Micro-residual stresses as a function of longitudinal and radial coordinate – Satisfies all boundary conditions – Takes into account the edge effect singularity

8.8 References

Aghdam, M. M. and Khojeh, A. (2003) More on the effects of thermal residual and hydrostatic stresses on yielding behavior of unidirectional composites, *Composite Structures*, **62**, 285–90.

ASTM Designation: E837-01 (1999) *Standard Test Method for Determining Residual Stresses by the Hole-Drilling Strain Gage Method*, ASTM International.

Bhalerao, M. S. (1996), *On Process-induced Fiber Waviness in Composites: Theory and Experiments*, The University of Texas at Austin.

Barnes, J. A. (1993) Thermal expansion behavior of thermoplastic composites, *Material Science*, **28**(18), 4974–82.

Barnes, J. A. and Byerly, G. E. (1994) The formation of residual stresses in laminated thermoplastic composites, *Composite Science & Technology*, **51**(4), 479–94.

Barnes, J. A., Simms, I. J., Farrow, G. J., Jackson, D., Wostenholm, G. and Yates, B. (1991) Thermal expansion characteristics of PEEK composites, *Material Science*, **26**(8), 2259–71.

Benedikt, B., Predecki, P., Kumosa, L., Armentrout, D., Sutter, J. K. and Kumosa, M. (2001a) The use of X-ray diffraction measurements to determine the effect of bending loads on internal stresses in aluminum inclusions embedded in a unidirectional graphite–fibre/PMR-15 composite, *Composite Science and Technology*, **61**(14), 1995–2006.

Benedikt, B., Kumosa, M., Predecki, P. K., Kumosa, L., Castelli, M. G. and Sutter, J. K. (2001b) An analysis of residual thermal stresses in a unidirectional graphite/pmr–15 composite based on X-ray diffraction measurements, *Composite Science and Technology*, **61**(14), 1977–94.

Bianchi, V., Goursat, P. and Menessier, E. (1998) Carbon-fiber-reinforced YMAS glass ceramic matrix. Part IV: Thermal residual stresses and fiber/matrix interfaces, *Composite Science and Technology*, **58**, 409–18.

Bogetti, T. A. and Gillespie, J. W. J. (1992) Process-induced stress and deformation in thick-section thermoset composite laminates, *Composite Materials*, **26**(5), 626–60.

Callister, W. D. J. (1994) *Materials Science and Engineering – An Introduction*, John Wiley and Sons, Inc.

Cantwell, W. J., Davies, P. and Kausch, H. H. (1990) The effect of cooling rate of deformation and fracture in IM6/PEEK composites, *Composite Structures*, **14**(2), 151–71.

Chapman, T. J., Gillespie, J. W. and Pipes, R. B. (1990) Prediction of process-induced residual stresses in thermoplastic composites, *Composite Materials*, **24**, 616–43.

Chen, Y., Xia, Z. and Ellyin, F. (2001) Evolution of residual stresses induced during curing processing using a viscoelastic micromechanical model, *Composite Materials*, **35**, 522–9.

Chung, D. D. L. (2001), continuous carbon fiber polymer–matrix composites and their joints, studied by electrical measurements, *Polymer Composites*, **22**(2), 250–70.

Cowley, K. D. and Beaumont, P. W. R. (1997) The measurement and prediction of residual stresses in carbon–fibre/polymer composites, *Composite Science and Technology*, **57**(11), 1445–55.

Crasto, A. S., Kim, R. Y. and Russell, J. D. (2002) *In situ* monitoring of residual strain development during composite cure, *Polymer Composites*, **23**(3), 454–63.

Dally, J. W. and Riley, W. F. (1991) Optical methods of stress analysis, in: *Experimental Stress Analysis*, New York, McGraw-Hill, Inc.

Deshpande, A. P. and Seferis, J. C. (1996), Processing characteristics in different semi-crystalline thermoplastic composites using process simulated laminate (PSL) methodology, *Thermoplastic Composite Materials*, **9**(2), 183–98.

DiLandro, L. and Pegoraro, M. (1996) Evaluation of residual stresses and adhesion in polymer composites, *Composites Part A: Applied Science Manufacturing*, **27**(9), 847–53.

Domb, M. M. and Hansen, J. S. (1994) Development of free-edge effect during processing of semi crystalline thermoplastic composites, *AIAA Journal.*, **32**(5), 1029–33.

Epstein, M. (2002) The Eshelby tensor and the theory of continuous distributions of in homogeneities, *Mechanics Research Communications*, **29**(6), 501–6.

Ersoy, N. and Vardar, O. (2000), Measurement of residual stresses in layered composites by compliance method, *Composite Material*, **34**(7), 575–98.

Fakuda, H., Takahashi K. and Toda, S. (1995) Thermal deformation of anti-symmetric laminates at cure, *Proceedings of ICCM-10,* **3**, 141–8.

Fenn, R. H., Jones, A. M. and Wells, G. M. (1993) X-Ray diffraction investigation of triaxial residual stresses in composite materials, *Composite Materials*, **27**(14), 1338–51.

Gascoigne, H. E. (1994) Residual surface stresses in laminated cross-ply fiber-epoxy composite materials, *Experimental Mechanics*, **34**(1), 27–36.

Gentz, M., Armentrout, D., Rupnowski, P., Kumosa, L., Shin, E. and Sutter, J. (2004) In-plane shear testing of medium and high modulus woven graphite fiber reinforced/ polyimide composites, *Composite Science and Technology*, **64**, 203–20.

Guerrero, V. H. and Chung, D. D. L. (2002) Interlaminar interface relaxation upon heating carbon fiber thermoplastic-matrix composite, studied by contact electrical resistivity measurement, *Composite Interface*, **9**(6), 557–63.

Guillen, J. F. and Cantwell, W. J. (2002) The influence of cooling rate on the fracture properties of a thermoplastic-based fibre-metal laminate, *Reinforced Plastic Composites*, **21**(8), 749–72.

Hahn, H. T. and Pagano, N. J. (1975) Curing stresses in composite laminates, *Composite Materials*, **9**, 91–106.

Han, B., Post, D. and Ifju, P. (2001) Moiré interferometry for engineering mechanics: current practices and future developments, *Strain Analysis for Engineering Design*, **36**(1), 101–17.

Harris, B. (1999) Residual strains, in: *Engineering Composite Materials*, London, IOM Communications, 79–83.

Hashin, Z. and Rosen, W. B. (1964) The elastic moduli of fiber reinforced materials, *Applied Mechanics*, **31**, 223–32.

Hassel, L. and Martin, L. D. (2000) Equivalence of Eshelby inclusion theory and Wechsler–Lieberman–Read, Bowles–Mackenzie martensite-crystallography theories, *Materials Science and Engineering A*, **285**, 180–5.

Hauk, V. (1999) Structural and residual stress analysis by X-ray diffraction on polymeric materials and composites, *Materialwissenschaft Und Werkstofftechnik*, **30**(7), 377–84.

Highsmith, A. L. and Reifsnider, K. L. (1982) Stiffness-reduction mechanisms in composite laminates, in: K. Reifsnider (ed.), *Damage in Composite Materials*, Philadelphia, ASTM international, 103–17.

Hobbiebrunken, T., Fiedler, B., Hojo, M., Ochiai, S. and Schulte, K. (2005) Microscopic yielding of CF/epoxy composites and the effect on the formation of thermal residual stresses, *Composites Science and Technology*, **65**, 1626–35.

Hsiao, S. W. and Kikuchi, N. (1999) numerical analysis and optimal design of composite thermoforming process, *Computer Methods in Applied Mechanics Engineering*, **177**(1–2), 1–34.

Huang, Z. M. (1999) Strength formulae of unidirectional composites including thermal residual stresses, *Material Letters*, **40**(4), 164–69.

Huang, X., Gillespie, J. W. and Eduljee, R. F. (1997) Effect of temperature on the transverse cracking behavior of cross-ply composite laminates, *Composites Part B: Engineering*, **28**(4), 419–24.

Huang, Y., Kyo-Kook, J. and Sung, K. H. (2008) Effects of fiber arrangement on mechanical behavior of unidirectional composites, *Composite Materials*, **42**, 1851–6.

Hyer, M. W. (1981) Calculation of room-temperature shapes of unsymmetric laminates, *Composite Materials*, **15**, 296–310.

Ifju, G. P., Kilday, B. C., Liu, S. C. and Niu, X. (1996) measurement of residual stress in laminated composites, *Proceedings of VIII International Congress on Experimental Mechanics and Experimental/Numerical Mechanics in Electronic Packaging*, Nashville, TN, 198–9.

Ifju, G. P., Niu, X., Kilday, B. C., Liu, S. C. and Ettinger, S. M. (2000) Residual strain measurement in composites using the cure-referencing method, *Experimental Mechanics*, **40**(1), 22–30.

Ingersoll, J. (2004) *Photoelastic Stress Analysis*, Durham, NC, Shodor Education Foundation.

Jayaraman, K. and Reifsnider, K. L. (1992) Residual stresses in a composite with continuously varying young's modulus in the fiber/matrix interphase, *Composite Materials*, **26**(6), 770–91.

Jayaraman, K. and Reifsnider, K. L. (1993) The interphase in unidirectional fiber-reinforced epoxies: effect of residual thermal stresses, *Composite Science and Technology*, **47**, 119–29.

Jeronimidis, G. and Parkyn, A. T. (1988) Residual stresses in carbon fiber-thermoplastic matrix laminates, *Composite Materials*, **22**(5), 401–15.

Joh, D., Byun, K.Y. and Ha, J. (1993) Thermal residual stresses in thick graphite/epoxy composite laminates-uniaxial approach, *Experimental Mechanics*, **33**(1), 70–6.

Jones, F. R. (1999) Durability of reinforced plastics in liquid environments, in: G. Pritchard (ed.), *Reinforced Plastics Durability*, Cambridge, Woodhead Publishing, Ltd, 9–96.

Kang, H. K., Kang, D. H., Bang, H. J., Hong, C. S. and Kim, C. G. (2002) Cure monitoring of composite laminates using fiber optic sensors, *Smart Material Structures*, **11**(2), 279–87.

Kang, H. K., Kang, D. H., Hong, C. S. and Kim, C. G. (2003) Simultaneous monitoring of strain and temperature during and after cure of unsymmetrical composite laminate using fiber-optic sensors, *Smart Material Structures*, **12**(1), 29–35.

Karami, G. and Garnich, A. (2005) Micromechanical study of thermo elastic behavior of composites with periodic fiber waviness, *Composites Part B: Engineering*, **36**, 241–8.

Khatri, S. C. and Koczak, M. J. (1996) Thick-section AS4-graphite/E-glass/PPS hybrid composites. Part I: Tensile behavior, *Composite Science and Technology*, **56**(2), 181–92.

Kim, J. K. and Mai, Y. W. (1998) *Engineered Interfaces in Fiber Reinforced* Composites, Oxford, Elsevier Science, Ltd, 308–20.

Kim, R. Y and Hahn, H. T. (1979) Effect of curing stresses on the first-ply failure in composite laminates, *Composite Materials*, **13**, 2–16.

Kim, K. S., Hahn, H. T. and Croman, R. B. (1989) The effect of cooling rate on residual stresses in a thermoplastic composite, *Composites Technology and Research*, **11**(2), 47–52.

Kim, Y. K. and Daniel, I. M. (2002) Cure cycle effect on composite structure manufactured by resin transfer molding, *Composite Materials*, **36**(14), 1725–43.

Kugler, D. and Moon, T. J. (2002) Identification of the most significant processing parameters on the development of fiber waviness in thin laminates, *Composite Materials*, **36**(12), 1451–79.

Kumosa, M. S. (2003) An investigation of damage initiation in woven graphite fiber/polyimide composites subjected to shear, *Advances in Fracture and Damage Mechanics,* **251**, 447–56.

Kurtz, R. D. and Pagano, N. J. (1991) Analysis of the deformation of a symmetrically-loaded fiber embedded in a matrix material, *Composite Engineering*, **1**(1), 13–27.

Kyo-Kook, J., Huang, Y., Young-Hwan, L. and Sung, K. H. (2008) Distribution of micro stresses and interfacial tractions in unidirectional composites, *Composite Materials*, **42**, 1825–34.

Lai, L., Carman, G., Chiou, S., Kukuchek, P. and Echternach, D. (1995) Processing monitoring of carbon phenolic composites using smart sensors, *Smart Material Structures*, **4**(2), 118–25.

Lawrence, W. E., Manson, J. A. E. and Seferis, J. C. (1990) Thermal and morphological skin core effects in processing of thermoplastic composites, *Composites*, **21**(6), 475–80.

Lawrence C. M., Nelson, D. V., Bennett, T. E. and Spingarn, J. R. (1998) An embedded fiber optic sensor method for determining residual stresses in fiber reinforced composite materials, *Intelligent Material System Structures*, **9**(10), 788–99.

Lee, J. and Czarnek, R. (1991) Measuring residual strains in composites laminates using moiré interferometry, *Proceedings of the 1991 SEM Conference on Experimental Mechanics,* Milwaukee, WI, 405–15.

Lee, J., Czarnek, R. and Guo, Y. (1989) Interferometric study of residual strains in thick composites, *Proceedings of the 1989 SEM Conference on Experimental Mechanics*, Cambridge, MA, 356–64.

Lei Wang (2001) *Effects of In-plane Fiber Waviness on the Static and Fatigue Strength of Fiberglass*, MSc thesis, Montana State University, Bozeman.

Leng, J. S. and Asundi, A. (2002) Real-time cure monitoring of smart composite materials using extrinsic Fabry–Perot interferometer and fiber Bragg grating sensors, *Smart Material Structures*, **11**(2), 249–55.

Lessard, L. B., Schmidt, A. S. and Shokrieh, M. M. (1996) Three-dimensional stress analysis of free-edge effects in a simple composite cross-ply laminate, *Solid Structures*, **33**(15), 2243–59.

Li, M. C., Wu, J. J., Loos, A. C. and Morton, J. (1997) A plane-strain finite element model for process-induced residual stresses in a graphite/PEEK composite, *Composite Materials*, **31**(3), 212–43.

Li, T. Q., Zhang, M. Q., Zhang, K. and Zeng, H. M. (2000) Long-range effects of carbon fiber on crystallization of semicrystalline thermoplastics, *Polymer Journal*, **41**(1), 161–8.

Madhukar, M. S., Kosuri, R. P. and Bowles, K. J. (1995) Reduction of curing induced fiber stresses by cure cycle optimization in polymer matrix composites, *Proceedings of ICCM–10*, **3**, 157–64.

Manson, J. A. E. and Seferis, J. C. (1992), Process dimulated laminate (PSL): A methodology to internal-stress characterization in advanced composite materials, *Composite Materials*, **26**(3), 405–31.

Mathar, J. (1934) Determination of initial stresses by measuring the deformation around drilled holes, *Transactions of ASME*, **4**, 249–54.

McCartney, L. N. (2005) Energy-based prediction of progressive ply cracking and strength of general symmetric laminates using an homogenization method, *Composites Part A: Applied Science Manufacturing*, **36**(2), 119–28.

Mei, Z. and Chung, D. D. L. (2000) Thermal stress-induced thermoplastic composite debonding, studied by contact electrical resistance measurement, *Adhesion and Adhesives,* **20**(2), 135–9.

Meske, R. and Schnack, E. (2003) Particular adaptation of X-ray diffraction to fiber reinforced composites, *Mechanics of Materials*, **35**(1–2), 19–34.

Naik, R. A. (1992) Simplified micromechanical equations for thermal residual stress analysis of coated fiber composites, *Composite Technology Research*, **14**(3), 182–6.

Nairn, J. A. (1987) Transverse fracture in unidirectional graphite polysulfide composites, *Composite Materials*, **21**(9), 798–808.

Nairn, J. A. (1997) Fracture mechanics of composites with residual thermal stresses, *Applied Mechanics – Trans ASME*, **64**, 804–15.

Nairn, J. A. (2000) Energy release rate analysis for adhesive and laminate double cantilever beam specimens emphasizing the effect of residual stresses, *Adhesion and Adhesives*, **20**(1), 59–70.

Nairn, J. A. (2001) Matrix micro cracking in composites, in: R. Talreja and J. A. Manson (eds), *Polymer Matrix Composites*, Oxford, Elsevier Science Ltd, 403–32.

Nairn, J. A. and Zoller, P. (1985) Matrix solidification and the resulting residual thermal stresses in composites, *Material Science*, **20**(1), 355–67.

Nairn, J. A. and Hu, S. (1992) The initiation and growth of delaminations induced by matrix micro cracks in laminated composites, *Fracture Journal*, **57**(1), 1–24.

Nairn, J. A. and Hu, S. (1994) Matrix micro cracking, in: R. Talreja (ed.), *Damage Mechanics of Composite Materials*, Amsterdam, Elsevier Science BV, 187–243.

Nielsen, A. S. and Pyrz, R. (1998) The effect of cooling rate on thermal residual strains in carbon/polypropylene micro composites, *Science Engineering Composite Materials*, **7**(1–2), 1–22.

Nielsen, A. S. and Pyrz, R. A. (2002) Novel approach to measure local strains in polymer matrix systems using polarized Raman microscopy, *Composite Science and Technology*, **62**(16), 2219–27.

Papanicolaou, G. C., Michalopoulou, M. V. and Anifantis, N. K. (2002) Thermal stresses in fibrous composites incorporating hybrid interphase regions, *Composites Science and Technology*, **62**, 1881–94.

Park, C. H. and McManus, H. L. (1996) Thermally induced damage in composite laminates: predictive methodology and experimental investigation, *Composite Science and* Technology, **56**(10), 1209–19.

Predecki, P. and Barrett, C. S. (1979) Stress measurement in graphite/epoxy composites by X-ray diffraction from fillers, *Composite Materials*, **13**, 61–71.

Quek, M. Y. (2004) Analysis of residual stresses in a single fiber-matrix composite, *Adhesion and Adhesives*, 24, 379–88.

Rendler, N. J. and Vigness, I. (1966) Hole-drilling strain-gage method of measuring residual stresses, *Experimental Mechanics*, **6**(12), 577–86.

Shao-Chun, L. (1999) *Residual Stress Characterization for Laminated Composites*, PhD thesis, University of Florida.

Shokrieh, M. M. and Kamali, S. M. (2005) Theoretical and experimental studies on residual stresses in laminated polymer composites, *Composite Materials*, **39**(24), 2213–25.

Shokrieh, M. M. and Ghasemi, A. R. (2007a) Simulation of central hole drilling process for measurement of residual stresses in isotropic, orthotropic and laminated composite plates, *Composite Materials*, **41**, 435–52.

Shokrieh, M. M. and Ghasemi, A. R. (2007b) Determination of calibration factors of the hole drilling method for orthotropic composites using an exact solution, *Composite Materials*, **41**, 2293–311.

Shokrieh, M. M. and Safarabadi, M. (2011) Effects of imperfect adhesion on thermal micro-residual stresses in polymer matrix composites, *Adhesion and Adhesives*, **31**(6), 490–7.

Shokrieh, M. M. and Safarabadi, M. (2012) Three-dimensional analysis of micro-residual stresses in fibrous composites based on the energy method: a study including interphase effects, *Journal of Composite Materials*, **46**(6), 727–35.

Shueh, C. H. and Becher, P. F. (1988) Thermal expansion coefficient of unidirectional fiber reinforced ceramics, *American Ceramic Society*, **71**, 438–41.

Sjogren, A., Joffe R., Berglund L. and Mader, E. (1999) Effects of fiber coating (size) on properties of glass fiber vinyl ester composites, *Composites Part A: Applied Science Manufacturing*, **30**(8), 1009–15.

Sorensen, L., Gmur, T. and Botsis, J. (2004) Residual strain development in laminated thermoplastic composites measured using fiber Bragg grating sensors, *Proceedings of Composite Testing 2004 Conference*, Bristol, UK, 21–23 September, 145–6.

Sunderland, P., Yu, W. J. and Manson, J. E. (1995) Technique for the measurement of process-induced internal stresses in polymers and polymer composites, *Proceedings of ICCM–10*, **3**, 125–32.

Sunderland, P., Yu, W. J. and Manson, J. A. (2001) A thermo-viscoelastic analysis of process-induced internal stresses in thermoplastic matrix composites, *Polymer Composites,* **22**(5), 579–92.

Tsai, S. W. and Hahn, H. T. (1980) *Introduction to Composite Materials*, Lancaster, PA, Technomic Publishing Co.

Unger, W. J. and Hansen, J. S. (1998) Method to predict the effect of thermal residual stresses on the free-edge delamination behavior of fiber reinforced composite laminates, *Composite Materials*, **32**(5), 431–59.

Unger, W. J., Hansen, J. S. and Ko, H. Y. S. (1993) *Method of Reducing Residual Stresses in Thermoplastic Laminates,* European patent, USA.

Vlekken, J. and Parlevliet, P. P. (2004) *Fiber Bragg Grating Sensors for Monitoring Thermoplastic Composite Processing*, Personal Communication.

Wagner, H. D. and Nairn, J. A. (1997) Residual thermal stresses in three concentric transversely isotropic cylinders: application to thermoplastic–matrix composites containing a trans crystalline interphase, *Composite Science & Technology*, **57**(9–10), 1289–302.

Walther, B. M. (1998) *An Investigation of the Tensile Strength and Stiffness of Unidirectional Polymer-Matrix, Carbon-Fiber Composites under the Influence of Elevated Temperatures*, Engineering Mechanics, Virginia Polytechnic Institute and State University, Blacksburg, VA.

Wang, T. M., Daniel, I. M. and Gotro, J. T. (1992) Thermo-viscoelastic analysis of residual stresses and warpage in composite laminates, *Composite Materials*, **26**(6), 883–99.

Wang, S. K., Mei, Z. and Chung D. D. L. (2001) Interlaminar damage in carbon fiber polymer-matrix composites, studied by electrical resistance measurement. *Adhesion and Adhesives*, **21**(6), 465–71.

Wang, S. K., Kowalik, D. P. and Chung, D. D. L. (2004) Self-sensing attained in carbon-fiber-polymer–matrix structural composites by using the interlaminar i nterface as a sensor, *Smart Material Structures*, **13**(3), 570–92.

Wardle, M. W. (2001) *Aramid Fiber Reinforced Plastics Properties*, in: R. Talreja and J. A. Manson (eds), *Polymer Matrix Composites*, Oxford, Elsevier Science Ltd, 199–229.

Warnet, L. (2000) *On the Effect of Residual Stresses on the Transverse Cracking in Cross-Ply Carbon-Polyetherimide Laminates*, Mechanical Engineering, University of Twente.

Weteringe, B. J., Bersee, H. E. N. and Beukers, A. (2002) Characterization of micro cracking in PPS laminates. *Proceedings of GO for the Best through Advanced Materials and Processes Conference*, Paris Expo, Porte de Versailles Paris, 9–11 April, 225–36.

Wijskamp, S. (2005) *Shape Distortions in Composites Forming*, The Netherlands, Mechanical Engineering, Division of Design, Production and Manufacturing, University of Twente.

Wisnom, M. R. and Atkinson, J. W. (2000) Fiber waviness generation and measurement and its effect on compressive strength, *Reinforced Plastic Composites*, **19**(2), 96–110.

Wisnom, M. R., Gigliotti, M., Ersoy, N., Campbell, M. and Potter, K. D. (2006) Mechanisms generating residual stresses and distortion during manufacture of polymer-matrix composites structures, *Composites Part A: Applied Science Manufacturing,* **37**(4), 522–9.

Wu, Z. and Lu, J. (2000) Study of surface residual stress by three-dimensional displacement data at a single point in hole drilling method, *Engineering Material Technology – Trans ASME*, **122**(2), 215–20.

Young, R. J. and Lovell, P. A. (1991) *Introduction to Polymers*, London, Chapman and Hall.

Zhang, Y., Xia, Z. and Ellyin, F. (2004) Evolution and influence of residual stresses/strains of fiber reinforced laminates, *Composite Science and Technology*, **64**(10–11), 1613–21.

Zhao, L. G., Warrior, N. A. and Long, A. C. (2007) A thermo-viscoelastic analysis of process-induced residual stress in fiber-reinforced polymer-matrix composites, *Materials Science and Engineering A*, **452–3**, 483–98.

Zhou, G. and Sim, L. M. (2002) Damage detection and assessment in fiber reinforced composite structures with embedded fiber optic sensors, *Smart Material Structures*, **11**(6), 925–39.

www.dc.engr.scu.edu, A culprit in shrinkage and warpage problems.

9

Understanding residual stresses in metal matrix composites

M. M. AGHDAM and S. R. MORSALI,
Amirkabir University of Technology, Iran

DOI: 10.1533/9780857098597.2.233

Abstract: As parts of different engineering structures, the functioning and behaviour of composite materials, particularly metal matrix composites (MMCs), are highly influenced by residual stresses (RS). The presence of tensile RS in the matrix accelerates onset of yielding, while compressive RS at the interface of the fibre and matrix postpones damage of the interface in transverse loading of composites. This chapter presents an overview of various aspects related to RS within the MMCs. In particular, interaction of RS and other factors to determine global behaviour of MMCs are presented. Failure characteristics, initial yield and collapse behaviour for different bi-axial loading in the presence of RS are also presented. Furthermore, effects of RS on high temperature behaviour of MMCs and a brief note on possible future research are presented.

Key words: metal matrix composites (MMCs), thermal residual stresses, interface damage, failure modes, elevated temperature.

9.1 Introduction

Metal matrix composites (MMCs) provide valuable properties, such as high specific modulus and strength in desired directions. Furthermore, high corrosion and temperature resistance also make them attractive for various engineering components, particularly at elevated service temperatures. Proper use of MMCs relies on accurate prediction of the material behaviour under different complicated loading conditions. This is completely dependent on the accurate estimate of the initial state of stresses within the composites. The MMCs are manufactured at high temperature, which is a required condition for diffusion bonding of the fibre–matrix (f/c) interface. For instance, while diffusion bonding takes place at about 550 °C in the SiC/Al system, a temperature of about 850 to 930 °C is needed for SiC/Ti MMC. Subsequently, when they are cooled down to room temperature, residual stresses (RS) are generated in the composite due to the mismatch between the coefficients of thermal expansion (CTE) of the fibre and matrix. In some cases, thermal RS are sufficient to initiate plastic deformation within the matrix immediately around the fibre (Bigelow, 1993; Nimmer *et al.*, 1991; Zahl and McMeeking, 1991).

The magnitude and distribution of the RS in various MMC systems have been estimated using different analytical (Arsenault and Taya, 1987; Brayshaw and

Pindera, 1994; Mikata and Taya, 1985; Yeh and Krempl, 1993) and numerical (Durodula and Derby, 1994; Jeong *et al*., 1994; Rangaswamy and Jayaraman 1994a) micro-mechanical models. Indeed, experimental techniques (Cox *et al.,* 1990; Rangaswamy *et al.*, 1994b) have also been used to measure RS in composites. Details of analytical and numerical modeling procedures together with experimental measurement techniques are discussed in other chapters of this book.

Formation of thermal RS and their effects on the subsequent thermo-mechanical loading of MMCs have attracted many researchers during the past three decades. In particular, existence of RS causes asymmetrical response of MMCs under axial loading in tension and compression (Aghdam *et al*., 2001), which has also been reported by experimental measurments (Clyne and Withers, 1993). Figure 9.1 demonstrates both experimental results and finite element predictions of this asymmetrical behaviour of MMCs subjected to axial loading. While constituent properties of the fibre and matrix are assumed to be symmetrical in tension and compression, the composite behaves asymmetrically due to inclusion of RS effects. However, various parameters, such as weak fibre/matrix interface bonding, constituent properties, fibre coating (f/c), spacing and arrangements, manufacturing

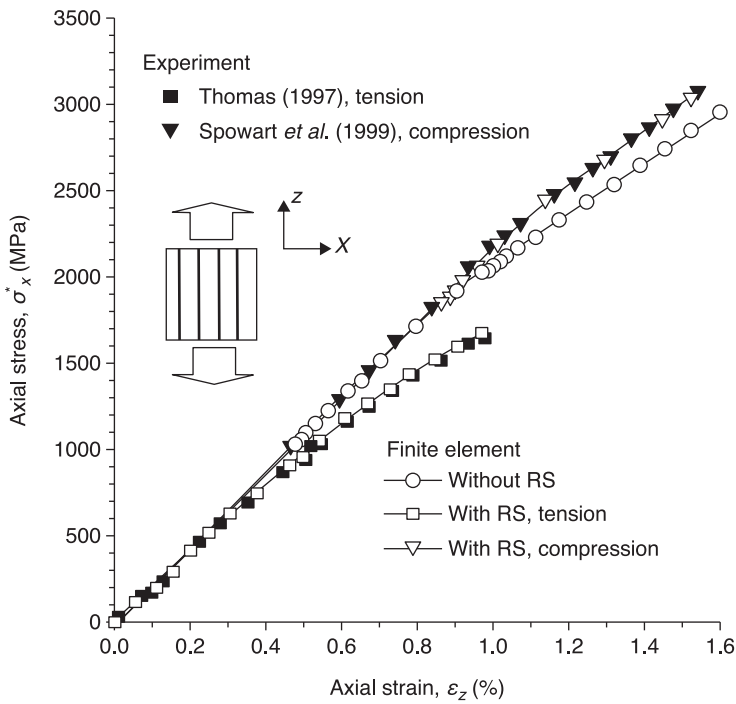

9.1 Asymmetrical behavior of SiC/Ti MMC during axial loading in tension and compression (Aghdam *et al.,* 2001).

process and environmental parameters, influence formation and distribution of RS within the different composite systems.

In this chapter, attention is focused on the effects of RS on the behaviour of MMCs subjected to various thermo-mechanical loadings. Without presenting details of related modeling and/or experiments, effects of various factors on magnitude and distribution of RS and influence of their interactions on global behaviour of MMCs will be discussed. In particular, initial yield and collapse envelopes for different bi-axial loading in the presence of RS will be presented. Considering that MMCs are expected to be used as parts of elevated temperature systems, effects of RS on high temperature behaviour of MMCs are reviewed. Finally, possible future trends in research are also discussed.

9.2 Factors affecting the magnitude and distribution of residual stresses in composites

Distribution and magnitude of RS within the fibre and matrix of MMCs together with other important parameters define the behaviour of the composite system when loaded under different conditions. These parameters mainly include constituent properties, and geometrical and manufacturing process conditions. Therefore, more accurate prediction of the material behaviour depends on a better understanding of the interaction between these parameters and RS. Effects of some of these parameters and RS on behaviour of MMCs will be discussed in the following sub-sections.

9.2.1 Fibre–matrix interface

Apart from thermal RS as a result of the manufacturing process of MMCs, brittle reaction products may be formed at the fibre–matrix interface (f/c) as a result of high temperature. The very thin layer, which is formed through the diffusion of the matrix and reinforcement atoms across their interface during manufacturing process, is known as the interaction layer. Formation of this layer is highly influenced by various parameters such as fibre and matrix material, coating of the fibre, duration of exposure to high temperature during the fabrication process and heat treatment of the MMC. For instance, the interfacial reaction layer is of major concern for titanium alloys reinforced by SiC fibres. These kinds of MMCs contains much thicker interfacial reaction zones than an aluminium matrix, due to the higher manufacturing temperature and the reactivity of the titanium alloy (Li and Wisnom, 1994a). Furthermore, several extensive studies have been carried out to investigate effects of various f/c systems on the reduction of the interaction between fibre and the Ti matrix (Fang *et al.*, 1998; Martineau *et al.*, 1984; Stephenson and Nicholls, 1991). Also, experimental studies were performed by Xun *et al.* (2000) and Yang *et al.* (1999), to explore effects of the high temperature manufacturing process and heat treatment of SiC/Ti on formation and composition of interaction layer.

However, there are some studies in the open literature mainly related to the effects of the interfacial region on the magnitude and distribution of RS within the MMCs. For example, Warrier *et al*. (1999) examined effects of interface properties on RS using both experiment and finite element micromechanical analysis. Hunag *et al*. (2009) found that the interfacial region thickness has an outstanding influence on the hoop and axial stresses in the composite. Thicker interfacial region can reduce most of the thermal RS in the MMC and improve the axial tensile strength of the composite.

Finally, existence of a brittle interaction layer leads to formation of a weakly bonded interface, which plays a crucial role in the behaviour of the material when subsequently subjected to thermo-mechanical loading. The strength of this interface in MMCs, particularly in the SiC/Ti system, is reported to be low (Johnson *et al*., 1990; Majumdar and Newaz, 1992). Therefore, in many practical loading cases, such as uni-axial transverse or off-axis loading, interface damage initiates prior to plastic deformation of the matrix (Lissenden, 1999).

Interaction of thermal RS and weak interface in MMCs are among dominant factors controlling their behaviour in various loading conditions, particularly in the transverse direction. For example, while a level of bonding between fibre and matrix is required for appropriate load transfer to occur, the compressive nature of the RS at the interface improves this load transfer mechanism. Nimmer (1990) and Wisnom's (1990) investigations revealed that the presence of thermally-induced stresses is beneficial for the transverse behaviour of the MMCs, due to generation of compressive radial stresses at the fibre–matrix interface. Figure 9.2 depicts the transverse behaviour of uni-directional SiC/Ti MMCs subjected to uni-axial tension-compression in the transverse direction (Aghdam *et al*., 2001). The figure includes fully bonded and fully de-bonded interface models with and without effects of RS. It is interesting to note that all curves reach a plateau when the matrix becomes fully plastic, regardless of inclusion of RS effects. However, the figure reveals that inclusion of thermal RS in the analysis of the de-bonded interface model significantly improves predictions of the model as RS retarded separation of the matrix from the fibre.

Furthermore, it also shows that experimental results follow the bonded interface model at early stages of loading until failure of the interface occurs and eventually joins the de-bonded model predictions for strains near to failure of the material. Figure 9.2 also implies that in order to have more accurate predictions in comparison with the experiment, an appropriate interface model should be included in the analysis. Many researchers tried to properly include interface damage to their analytical or finite element models. For instance, Li and Wisnom (1994a,b, 1995, 1996) developed an interface element to simulate the interface debonding process, which includes nodes on each side that are coupled with stiff springs. This element initially represents a perfect bond until a certain state of stress is reached when the interface is assumed to fail.

Normal and tangential stresses across the interface are monitored. The springs between node pairs are released when the combination of normal and shear

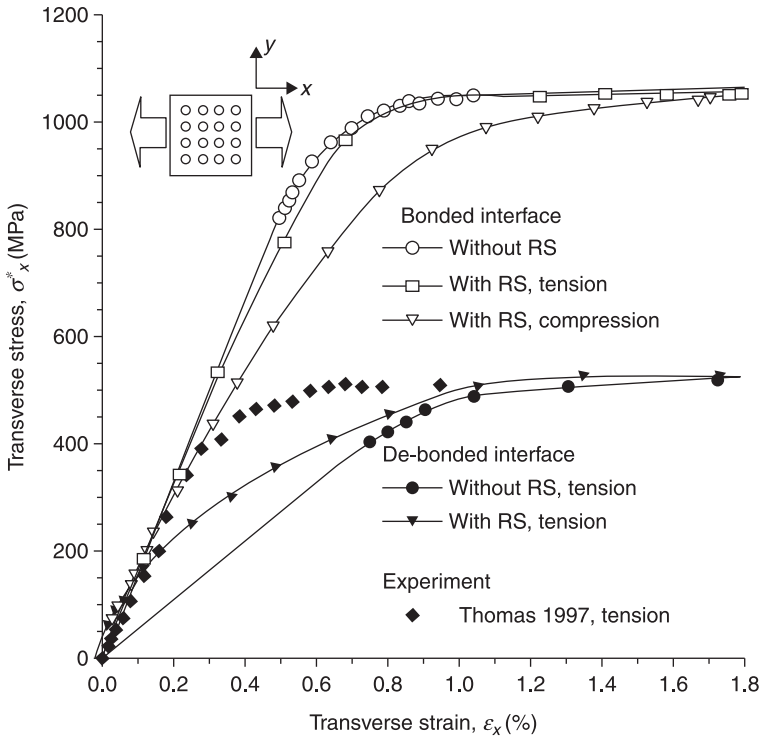

9.2 Predicted and experimental stress–strain curves for transverse loading of SiC/Ti MMC (Aghdam *et al.,* 2001).

stresses at the nodes reaches a predefined criterion. Another unit cell model in combination with the nonlinear finite element technique is employed to investigate the interaction between inelastic matrix deformation and interfacial debonding at the fibre–matrix interface by Ismar *et al*. (2001). They introduced a dimensionless parameter to capture the coupling between normal and tangential debonding.

Another interface model in the finite element code ANSYS together with predefined commands, birth/death of an element, is presented by Aghdam and Falahatgar (2004). They considered two interfaces between f/c and coating/matrix (c/m) to investigate effects of RS and weakly bonded interfaces on the transverse behaviour of SiC/Ti MMCs. Two different failure criteria, which are combinations of normal and shear stresses across the interfaces, were used to predict the failure of the interfaces. Any interface fails as soon as the stress level reaches the interfacial strength. The model was also employed to study bi-axial loading of MMCs in the presence of thermal RS (Aghdam *et al*., 2008). Spring elements were also employed by Lou *et al.* (2010) to simulate interfacial debonding when interfacial radial stress, composed of residual radial stress and radial stress introduced by the applied transverse tensile load, reached interfacial bonding

strength. As indicated, the interfacial region plays a crucial rule in the behaviour of MMCs in different loading conditions. Any improvement in the strength of the interface leads to enhancement of the composite overall load bearing, which is still open to more investigation.

9.2.2 Fibre coating

In order to improve interface strength, different procedures have been proposed. One of the most favoured and possible solutions is to coat the fibres of MMCs with a suitable coating. Various coating systems have been used in different studies to investigate effects of coating on the residual stress distribution, bonding strength of the interface and global behaviour of the composite system in different loading conditions. Carbon can be considered as the most frequently used materials for the coating of SiC fibres. Akser and Choy (2001) found that RS within the carbon-coated SiC fibre composite, SiC/C/Ti–6Al–4V, are generally lower in both compression and tension. A similar trend is also reported by Li and Wisnom (1996), where the residual compressive radial stress at the interface at 0 degrees to the loading direction is reduced by 10 to 20% due to the effect of the carbon coating of SiC fibre. Furthermore, a detailed study on various types of carbon as coating material for SiC fibres was carried out by Haque and Choy (2000).

In another study, Huang *et al.* (2009) investigated the influence of three coating systems including C, C/TiB_2 and no coating, on the distribution of various components of the thermal residual stress within the SiC/Ti MMC. They found that in the interfacial-coating region, the coating system has a significant influence on the hoop stresses (Fig. 9.3). Both in the C coating and C/TiB_2 coating, the hoop stresses in the interfacial region have a peak in the layer adjacent to the matrix.

One of the most detailed finite element simulations of the MMCs with both coating and interface effects was carried out by Li and Wisnom, (1994a,b). Their model includes thermal residual stress and f/c interface effects with a bonded condition assumption for the coating and matrix interface. The predicted results show good agreement with experimental data for relatively small strains of 0.5%. Therefore, the first knee in the transverse stress–strain response, which is correlated to the failure of the coating interface, is well predicted. However, beyond the 0.5% applied strain, the model over-estimates the transverse behaviour of the composite system.

Introducing a second interface between coating and matrix with appropriate failure criteria, Aghdam and Falahatgar (2004) were able to properly predict the second knee in the stress–strain response of the MMC in the transverse direction. A sample of different finite element predictions together with experimental results for transverse behaviour of SiC/Ti composites with coating, thermal residual stress and interface effects is presented in Fig. 9.4. The figure implies that incorporation of the second interface is necessary to obtain more accurate predictions for this composite system. Furthermore, the same approach is used to

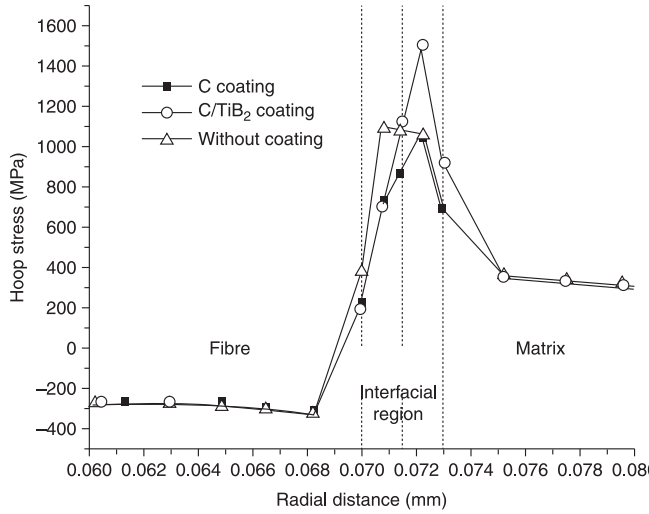

9.3 Distribution of hoop residual stresses along radial direction in SiC/Ti with different coating systems (Huang *et al.*, 2009).

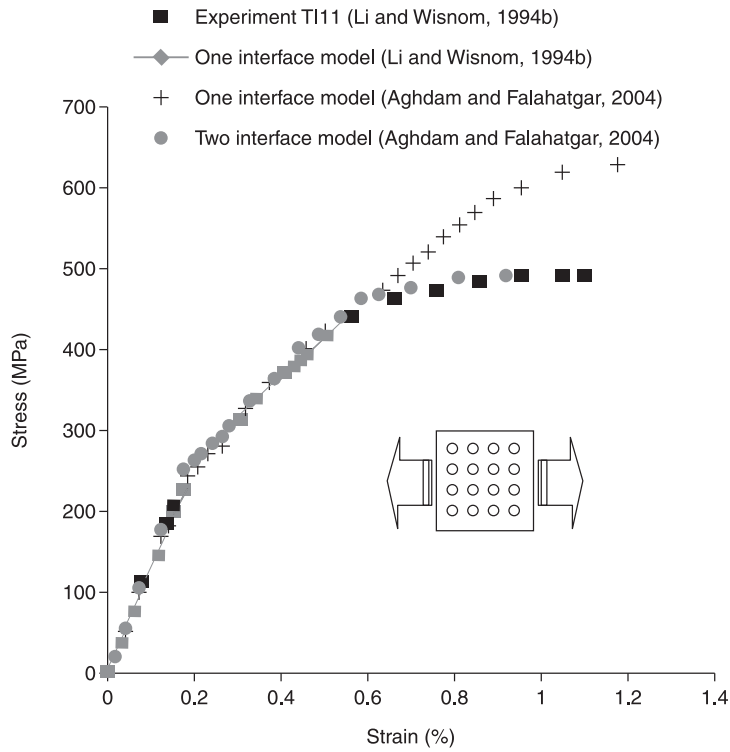

9.4 Comparison of FE models in transverse tension with experiment (Aghdam and Falahatgar, 2004).

develop a three-dimensional (3D) finite element micro-mechanical model to investigate initiation and propagation of interface damage of uni-directional SiC/Ti during combined axial shear and thermal loading (Aghdam *et al*., 2009).

Effects of interface damage and thermal RS on the global axial shear stress–strain response of the composite system are shown in Fig. 9.5. Included in the figure are two limiting cases of fully bonded and de-bonded interface models. As is shown by the figure, while interface damage has a significant influence on the shear response of the system, thermal RS have minor effects on the global shear behaviour and ultimate shear strength of the SiC/Ti composite. However, it should be noted that in the same system, thermal RS have a major influence on the stress distribution within the matrix of the MMC (Aghdam *et al*., 2009). The minor effect of RS on the global shear behaviour of the composite is related to accelerating

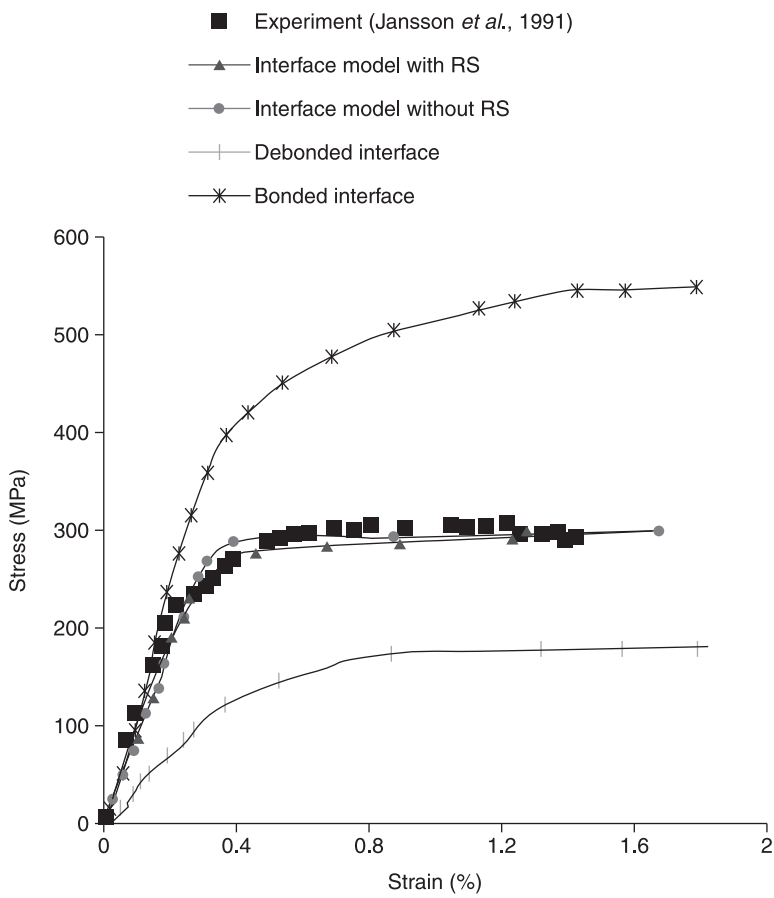

9.5 Stress–strain responses for different interface bonding conditions in SiC/Ti MMC in axial shear loading (Aghdam *et al.*, 2009).

initiation of interface damage when RS are included in the analysis. Furthermore, once interface damage is initiated at the f/c interface, it will quickly propagate through the interface and coating due to the symmetry condition of the axial shear loading. Therefore, the shear response of the composite rapidly flattens.

9.2.3 Viscoplasticity of the matrix, cooling rate and environment

In order to accurately predict the magnitude and distribution of RS within the matrix material of MMCs, viscoplastic behaviour of the metal matrix should be considered. This is mainly due to the difference in the relaxation mechanisms of elastic–plastic and elastic–viscoplastic models. Normally, elastic-plastic models over-estimate the resulting thermal RS at room temperature. Therefore, in modeling studies assuming elastic-plastic behaviour for the matrix, the fabrication temperature is often assumed to be lower than the real manufacturing temperature (typically 70–80% of real temperature) (Haque and Choy, 2000; Huang *et al*., 2008, 2009; Warrior *et al*., 1999). The main problem with this approach is that the model is case sensitive. This means that once the model is validated by experimental measurement of residual stress at room temperature for a particular MMC, it cannot be applied to other types of MMCs or even for the same MMC with other specifications such as fibre volume fraction (FVF). However, using proper elastic-viscoplastic behaviour for the matrix may significantly improve prediction of RS, provided correct creep data is included in the model (Carrere *et al*., 2002; Choo *et al*., 2001; Durodola and Derby, 1994; Li *et al*., 2008; Nimmer *et al*., 1991; Zhijun *et al*., 2006).

The other parameter that affects the formation of RS within the matrix of MMCs is the cooling rate from manufacturing to room temperature. The cooling rate may be considered only when elastic-viscoplastic behaviour is employed for the metal matrix. Results of various modeling studies reveal that for very slow cooling rates there is sufficient time for creep to relax the RS (Choo *et al*., 2001; Durodola and Derby, 1994). Therefore, increasing cooling rate results in increased thermal RS, which may also cause plastic deformation within the matrix of the MMC. Figure 9.6 depicts the average axial residual stress predictions in the matrix of SiC/Ti as a function of cooling rate (Morsali, 2012). As can be seen in the figure, the elastic-plastic model is not sensitive to cooling rate and always over-estimates the RS. However, assuming lower manufacturing temperature, say about 700 °C, reduces the estimated RS to values closer to experimental data. The figure also reveals that thermal RS are not seriously affected for cooling rates over 3 °C/sec.

The other factor that influences the time dependent behaviour of the matrix in MMCs is the environment. Carrere *et al*. (2002) performed experimental and modeling studies to explore damage mechanisms of uni-directional SiC/Ti under transverse creep loading. They found significant difference for time to failure for

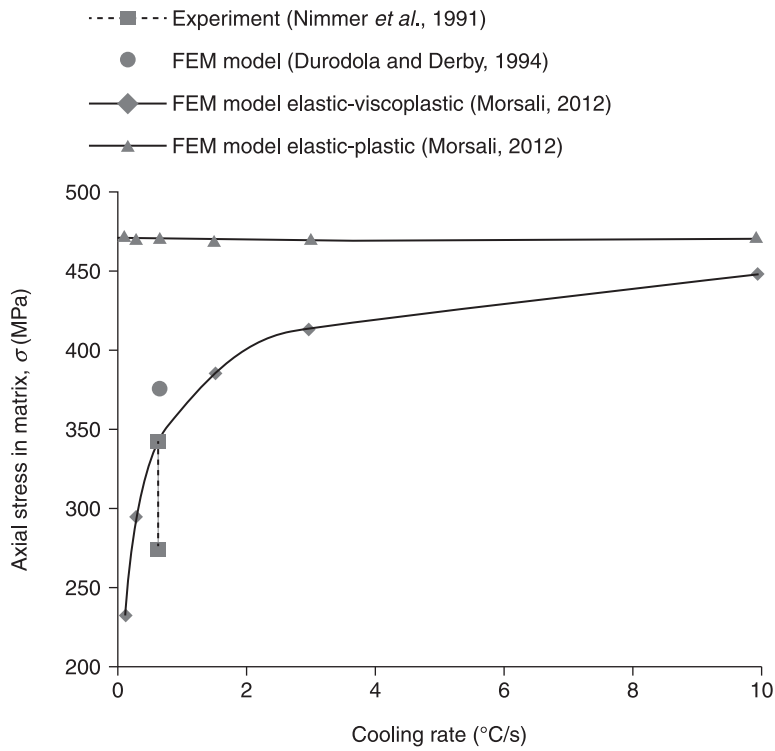

9.6 Average axial stress in matrix of 32% fibre volume fraction SiC/Ti composite (Morsali, 2012).

experiments carried out in vacuum and other reported results in argon and air. In another study, Reis *et al*. (2005) presented detailed experimental data on the influence of the environment on the tensile creep behaviour of titanium alloy. They considered air and nitrogen as environments, together with a temperature range from 500 to 700 °C and a stress range from 14 to 520 MPa. They found that high temperature exposure in a nitrogen atmosphere increases the creep resistance in comparison with an air atmosphere. Using experimental results for titanium alloy in different environments presented by Reis *et al*. (2005), Morsali (2012) investigated the effects cooling rate and environment on the RS in SiC/Ti composite system with coating and interface. Figure 9.7 demonstrates variation of maximum Von-Mises thermal residual stress within the matrix of SiC/Ti MMC during the manufacturing process under different environments and cooling rates. This maximum stress within the matrix occurs at points A and B of the Representative Volume Element (RVE) adjacent to the c/m interface. The figure indicates that relaxation of thermal RS in air is higher than nitrogen, particularly at lower cooling rates.

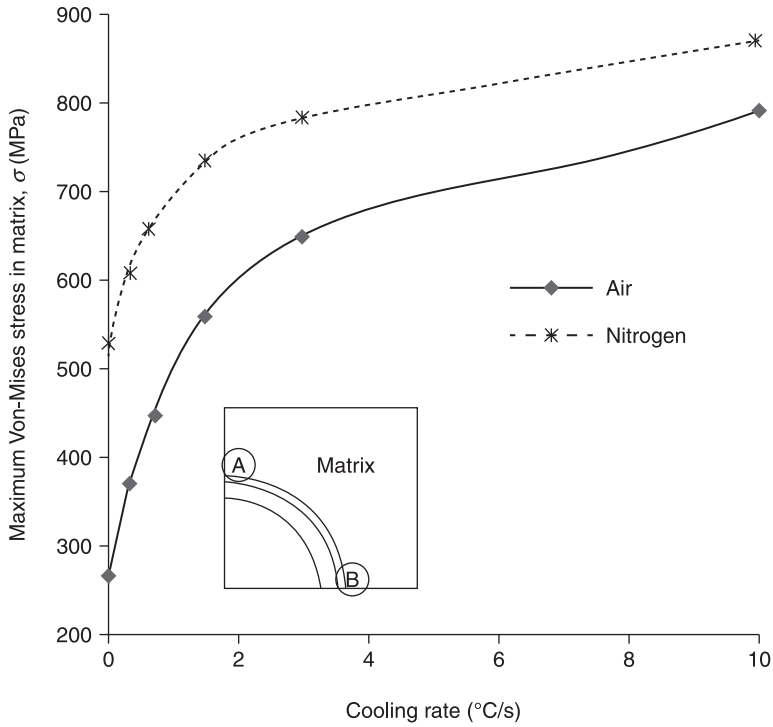

9.7 Variation of maximum Von-Mises equivalent residual stress in the matrix as a function of cooling rate in SiC/Ti MMC for different environments (Morsali, 2012).

9.2.4 Fibre material, volume fraction, arrangement and spacing

It is obvious that different fibre parameters such as material properties, volume fraction, geometrical arrangement and spacing influence thermal RS in the MMCs. Durodula and Derby (1994) determined RS in the Ti reinforced with SiC and Al_2O_3 composites with different volume fractions using the hexagonal array packing model. They also assumed a stress-free temperature of 900 °C and a cooling rate of 0.64 °C/s to room temperature. Figure 9.8 shows the axial residual stress within the fibre and matrix of two composites systems as a function of fibre volume fraction. It should be noted that the axial stress in the fibre is compressive and almost uniform, while in the matrix it is tensile and completely non-uniform.

It is also found that the hexagonal fibre arrangement induces more uniform residual stress distribution in the matrix (Durodula and Derby, 1994; Li and Wisnom, 1995; Nakamura and Suresh, 1993). This is because each fibre is surrounded by six fibres in a hexagonal fibre arrangement, while in square packing

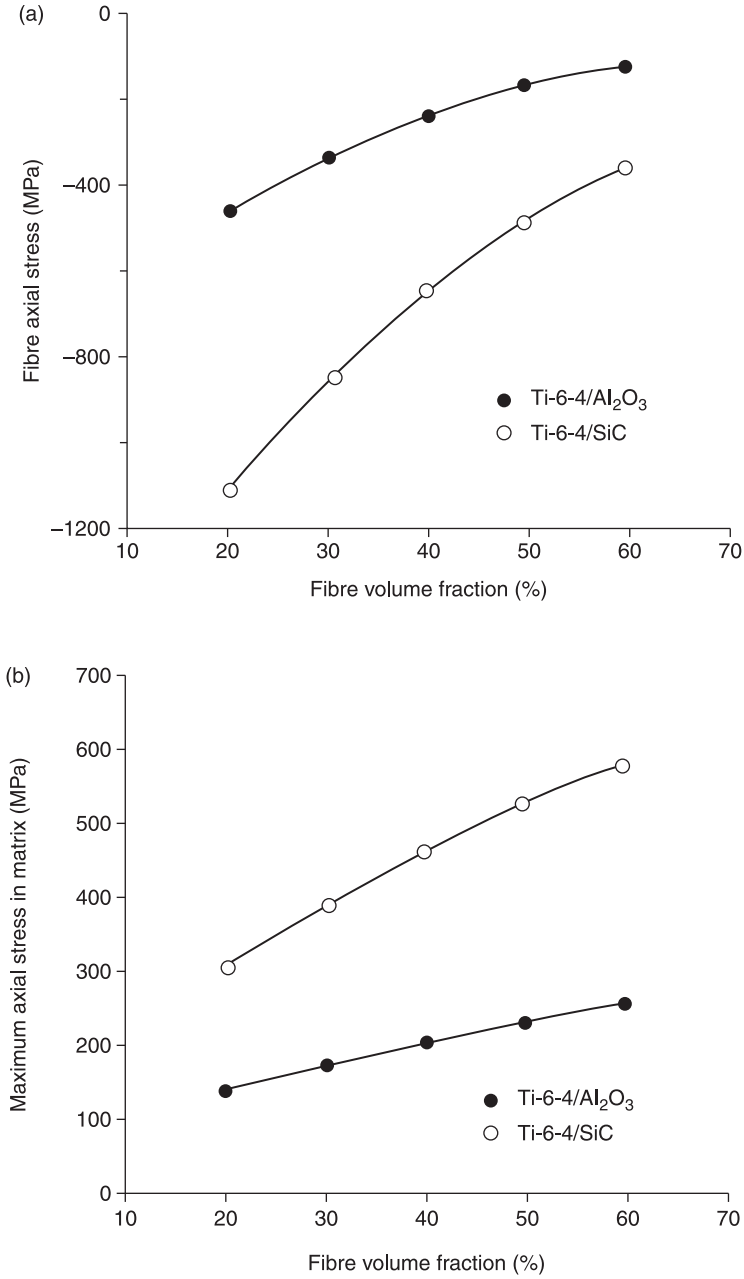

9.8 Variations of (a) axial stress in the fibre; and (b) maximum axial stress in the matrix of SiC/Ti and Al_2O_3/Ti (Durodula and Derby, 1994).

only four fibres surround each fibre (Li and Wisnom, 1995). However, random fibre arrangement may result in higher thermal RS within the matrix (Nakamura and Suresh, 1993).

Finally, for composites with similar fibre volume fraction (FVF), different fibre spacing may exist in the two directions perpendicular to the fibre. This will change the square array with equal spacing in both directions that is transversely isotropic to the rectangular array, which is orthotropic. Nakamura and Suresh (1993) and Nimmer *et al*.'s (1994) studies revealed that fibre spacing can have a pronounced effect on the magnitude of the maximum local RS within the matrix.

9.3 The effects of residual stress on the failure of metal matrix composites (MMCs)

One major target in various analytical, numerical and experimental analyses of composites is to predict yielding and failure of the material under various loading conditions. The strength of the MMCs is limited by different mechanisms such as failure of fibres or interface and plastic deformation of the matrix, depending on the loading of the material. Initial yield and collapse limits are of particular interest. Initial yield normally refers to the stress where the most heavily loaded point of the matrix yields and collapse occurs when the MMC cannot tolerate a higher load. The initial yield stress is too conservative for structural analysis of MMC components, particularly if the RS are taken into account. Obviously, an MMC can support loads higher than those to cause initial yield. Therefore, efficient use of MMCs can take advantage of this additional load-bearing capacity.

Both analytical and numerical studies have been carried out to construct initial yield and collapse envelopes of MMCs in different uni-axial and bi-axial loading conditions. Among early analyses, we refer to the work of Lin *et al*. (1972) and Dvorak *et al*. (1973, 1974), in which initial yield surfaces are predicted for uni-directional composites but effects of RS are included in the latter. They found that in contrast to homogeneous isotropic materials, composites yield under hydrostatic stresses. They also concluded that the effects of a uniform temperature increase (or decrease) on the initial yield surface in stress space is approximately, in Dvorak *et al*. (1973), or exactly, in Dvorak *et al*. (1974), equivalent to a solid translation of the surface in the negative (or positive) direction of the hydrostatic stress axis. The magnitude of this translation was also given as a function of temperature change, the coefficients of thermal expansion and bulk moduli of the constituents. A more detailed comparative study between RS and hydrostatic stress effects on the initial yield envelopes of MMCs is presented by Aghdam and Khojeh (2003).

Dvorak and Bahei-El-Din (1982) employed their vanishing fibre diameter model to explore elastic-plastic behaviour of aligned, continuous fibre reinforced composites. Using their analysis, initial yield surfaces for a boron-aluminium

composite were derived. The analytical method of cells model was employed by Aboudi (1989) to generate initial yield surfaces for a boron-aluminium MMC. Aboudi *et al*. (1994) also proposed a model that predicts the initial yield surface of MMC laminates using temperature-dependent matrix properties. Dvorak and Bahei-El-Din (1987) developed analytical collapse envelopes for a fibrous composite in transverse loading, where both matrix and fibre yield. Zahl *et al*. (1994) used finite element micro-mechanical models to study the collapse behaviour of MMCs in a transverse loading. They examined the effects of matrix hardening and the fibre packing arrangement.

An overview of the initial yield and collapse envelopes for the SiC/Ti MMC in the bi-axial transverse/transverse loading, obtained using finite element analysis, is shown in Fig. 9.9. In this figure, some points at which all the matrix material reaches the yield stress is referred to as gross plasticity. In principle, continuing to load the MMC beyond the state of gross plasticity will eventually result in collapse. In order to demonstrate effects of RS on yielding and failure of MMC, results are shown in two figures; such as with and without residual stress effects. All stresses are normalized with respect to the yield stresses of the matrix. Due to the symmetry condition in the transverse plane of the composite, all curves are symmetrical about the line corresponding to the transverse stresses being equal, that is $\sigma_x = \sigma_y$. While RS reduce the size of the initial yield, the collapse envelope in the bonded case is not affected by RS. The presence of the residual stress shifts both the initial yield and the gross plasticity envelopes in the positive direction corresponding to $\sigma_x = \sigma_y$, and leaves the collapse envelope unaffected. Another observation is that for the de-bonded case with RS, initial yielding is predicted to occur due to these RS alone.

Another sample of initial yield and collapse envelopes is presented in Fig. 9.10 for the bi-axial loading in the axial/transverse directions. Again, for the de-bonded interface in the presence of RS, there is a significant reduction of the size of the initial yield and collapse envelopes, although the size of the collapse envelope is essentially unaltered. Furthermore, the presence of RS shifts both the initial yield and the gross plasticity envelopes in the negative axial direction, while again the collapse envelope remains unaffected.

Furthermore, Table 9.1 provides details of numerical values of the initiation of failure and failure modes in the bi-axial loading of the composite system with effects of thermal RS (Aghdam *et al.*, 2008). RS and failure modes are determined based on two different stress free temperatures (900 and 650 °C). The higher degree is related to the real manufacturing temperature, which leads to over-estimated RS within the matrix due to ignoring stress relaxation within the matrix. As discussed earlier, one way to compensate for this phenomenon is to apply a lower temperature as a stress-free temperature. Therefore, values and failure modes in the brackets are related to assuming 650 °C as the stress-free temperature.

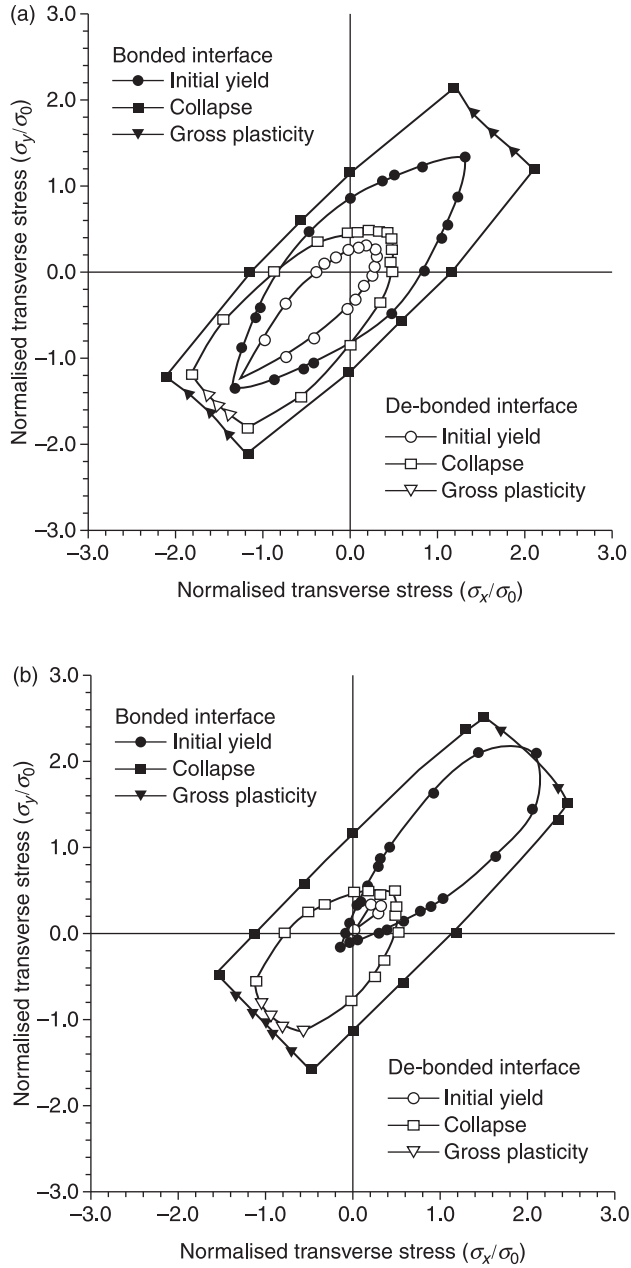

9.9 Comparison of initial yield and collapse envelopes for an MMC in biaxial transverse/transverse loading for fully bonded and fully de-bonded interface conditions: (a) without residual stress; and (b) with residual stress (Aghdam *et al.*, 2000).

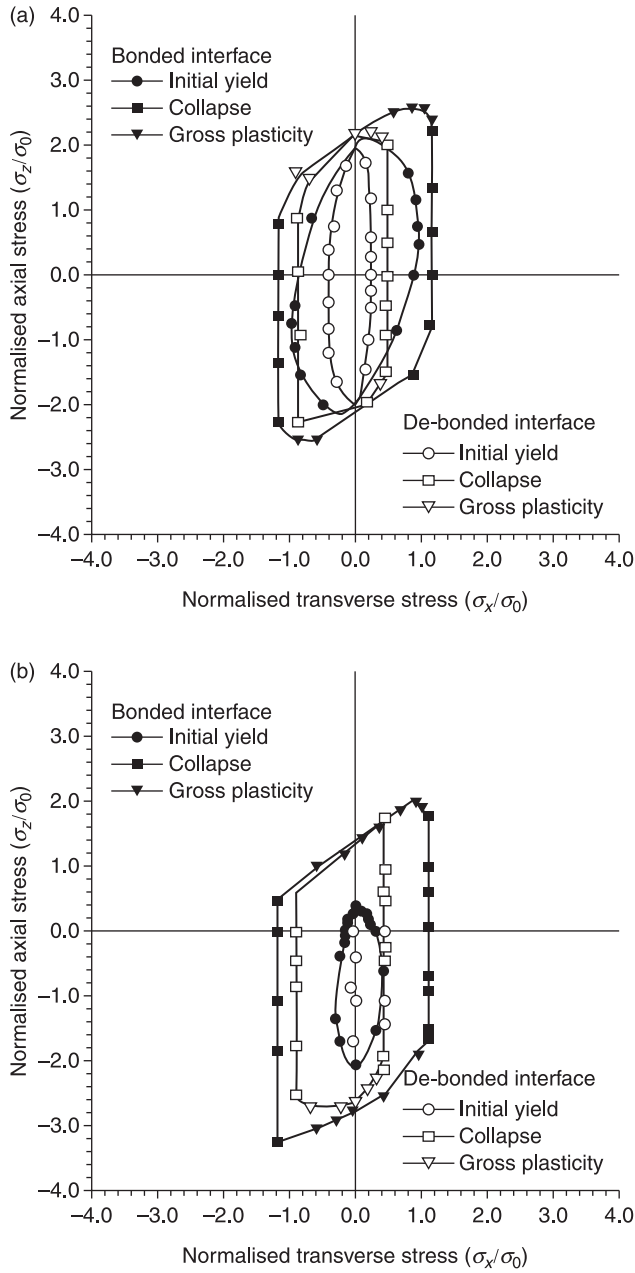

9.10 Comparison of initial yield and collapse envelopes for an MMC in biaxial axial/transverse loading for fully bonded and fully de-bonded interface conditions: (a) without residual stress; and (b) with residual stress (Aghdam *et al.*, 2000).

Table 9.1 Initial damage stress and failure mode of SiC/Ti MMC in axial/transverse loading with residual stress (Aghdam *et al.*, 2008)

Loading conditions	Initial damage* (MPa)	Failure modes*
Uniaxial transverse tension	245 (174)	Interface damage
Uniaxial axial tension	910 (1290)	Matrix yield
Uniaxial transverse compression	–345 (–488)	Matrix yield
Uniaxial axial compression	–1965 (–2020)	Matrix yield
Biaxial tension ($S_z=2S_x$)	235 (185)	
	470 (370)	Interface damage
Biaxial tension ($S_z=3S_x$)	185 (140)	
	555 (420)	Interface damage
Biaxial tension/compression ($S_z=-5S_x$)	202 (160)	
	–1005 (–800)	Interface damage
Biaxial tension/compression ($S_x=-S_z$)	–282 (–320)	
	282 (320)	Matrix yield (interface damage)
Biaxial tension/compression ($S_z=-S_x$)	222 (175)	
	–222 (–175)	Interface damage
Biaxial tension/compression ($S_x=-0.5S_z$)	–228 (–185)	
	456 (370)	Matrix yield (interface damage)
Biaxial compression ($S_z=3S_x$)	–450 (–528)	
	–1350 (–1584)	Matrix yield
Biaxial compression ($S_z=10S_x$)	–195 (–250)	
	–1950 (–2050)	Matrix yield

* Values and modes of failure in parentheses are related to assuming 650 °C as stress free temperature.

9.4 The effects of residual stress on the elevated temperature behaviour of MMCs

MMCs are widely used in various structural components, particularly at elevated service temperatures. Existence of weakly bonded interface and relatively high state of thermal RS affect the behaviour of the MMCs, both at room and elevated temperatures. However, most of published works in the open literature are related to room temperature behaviour of MMCs. Among high temperature studies, we refer to the experimental and micro/macro-mechanical analytical models carried out by Sun *et al*. (1990, 1993), to determine the behaviour of SiC/Ti in off-axis loading at room and high temperatures. They determined strength of the interface at various temperatures by experimental measurements of transverse tensile test, which was then used for different off-axis angles.

Nimmer *et al*. (1991) also studied transverse stress–strain behaviour of SiC/Ti system at different temperatures, using both experiment and the finite element

micro-mechanical model. Fully de-bonded interface with coulomb friction was considered to include effects of weak interface. Later, Nimmer *et al*. (1994) employed the same model to investigate the effect of fibre array geometry on the transverse tensile behaviour of SiC/Ti MMCs at different elevated temperatures. Eggleston and Krempl (1994) performed finite element models to investigate the transverse behaviour of SiC/Ti MMC at 482 °C, using two limiting cases of a perfectly bonded and a fully de-bonded interface with coulomb friction. They also performed experimental tests to obtain transverse stress–strain and the creep behaviour of the material. By comparing with experimental data, they concluded that composite tensile behaviour was best approximated by the model with no interface strength.

Naboulsi (2003) used analytical and numerical (FEM) approaches to determine the transverse behaviour of SiC/Ti MMC at 23 and 427 °C. Again, a fully de-bonded interface was considered to include effects of weak interface. Recently, Lou *et al*. (2010) used a two-dimensional (2D) micro-mechanical model to investigate the effect of temperature on the transverse tensile behaviour of SiC/Ti. Their model consisted of fibre, matrix and an interface with specific bonding strength for all temperatures. They used spring elements to simulate interfacial debonding when interfacial radial stress, composed of residual and applied transverse tensile stress, reaches interfacial bonding strength. However, no experiment validation was provided to verify their predictions.

More recently, Morsali (2012) presented a 2D generalized plane strain micro-mechanical model to investigate the transverse tensile behaviour of SiC/Ti at elevated temperatures. Effects of interface damage, residual stress, coating and temperature dependent matrix properties are considered. Figure 9.11 shows the compressive thermal residual stress and interface damage initiation during transverse loading of SiC/Ti MMC versus service temperature. The figure indicates similar trends of decreasing for both compressive residual stress and damage initiation stress. Furthermore, effects of thermal RS on damage initiation of the interface are depicted in Fig. 9.12. The figure shows that ignoring residual stress in the analysis results in a rapid failure of the interface at the very low stress level of 50 MPa at all elevated temperatures. However, inclusion of RS leads to more realistic predictions in comparison with the experiment. Once the thermal RS are considered, the interface failure is postponed to higher stresses of 220, 148 and 120 MPa for 20, 315 and 427 °C, respectively. It should be noted that the figure includes two different finite element models from Lou *et al.* (2010) and Morsali (2012). The difference between two finite element predictions is due to employing different interfacial strength and failure criteria and inclusion of coated fibres in the second study.

Finally, the other important factor controlling transverse behaviour of the SiC/Ti is the ultimate strength or collapse of the material. The predicted collapse stresses in the presence of RS and weak interface for 34% FVF at different temperatures are tabulated in Table 9.2. Experimental results are also reported in

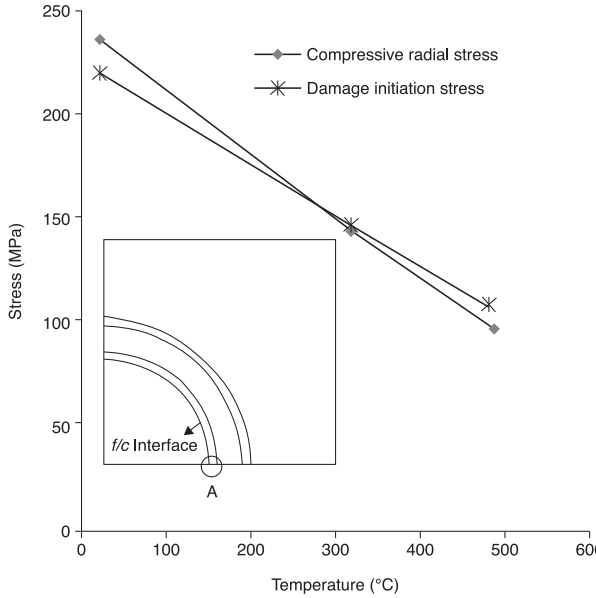

9.11 Compressive radial stress and damage initiation stress at point A in the *f/c* interface as a function of temperature (Morsali, 2012).

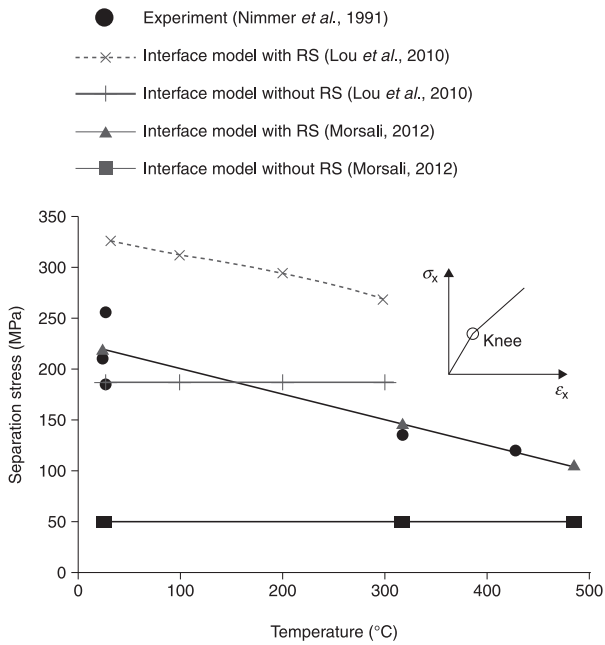

9.12 Comparison of predicted damage initiation stresses with measured experimental knee as a function of temperature, FVF=34% (Morsali, 2012).

Table 9.2 Collapse stress for 34% FVF SiC/Ti MMC in different temperatures (Morsali, 2012)

	Service temperature (°C)		
	23	315	482
Collapse stress (MPa)	450 (443)*	253 (253)*	245

* Values in parentheses are experimental data provided by Nimmer *et al.* (1991)

the parentheses, which are taken from Nimmer *et al.* (1991). The experimental values in Table 9.2 for collapse are taken from the stress points just after the second knee in the experimental stress–strain curves occurred. It should be noted that reported prediction of stress for collapse load is related to the point where all interface elements between coating and matrix of the material are failed. It is visible that collapse stress of the composite substantially decreases at elevated temperatures. This is mainly due to lower strengths of interface and matrix at high temperatures.

9.5 Future trends

As discussed earlier, different concerns arise in MMCs, mainly due to inclusion of a ceramic into a reactive metal matrix. One of the most important concerns is related to the area of the fibre–matrix interface. Since the load on the composite system is transferred from matrix to the reinforcement across the interface, the nature of the interface needs to be clearly explored. Therefore, the interface has a dominant role in determining the load capacity of the MMCs. The elevated temperature during the manufacturing process of MMCs results in formation of a weak interfacial bonding with a brittle reaction layer at the interface.

Although several approaches have been proposed to improve bonding of the interface, considerable technical and experimental research work needs to be carried out to increase load bearing of MMCs. In this regard, attention should be focused on finding efficient manufacturing processes, particularly to reduce processing temperatures or time exposure to high temperatures. The other possible way is to add some alloying material to reduce reactivity of the matrix. However, the best suggestion might be to use appropriate f/c to reduce formation of the brittle reaction layer, thus improving the bonding strength.

9.6 References

Aboudi, J. (1989) Micromechanical analysis of composites by the method of cells, *Appl. Mech. Rev.*, **42**, 193–221.

Aboudi, J., Mirzadeh, F. and Herakovich, C. T. (1994) Response of metal matrix laminates with temperature dependent properties, *J. Comp. Tech. Res.*, **16**, 68–76.

Aghdam, M. M. and Falahatgar, S. R. (2004) Micromechanical modeling of interface damage of metal matrix composites subjected to transverse loading, *Comp. Struct.*, **66**, 415–20.

Aghdam, M. M. and Khojeh, A. (2003) More on the effects of thermal residual and hydrostatic stresses on yielding behaviour of uni-directional composites, *Comp. Struct.*, **62**, 285–90.

Aghdam, M. M., Smith, D. J. and Pavier, M. J. (2000) Finite element micromechanical modeling of yield and collapse behaviour of metal matrix composites, *J. Mech. Phy. Solid*, **48**, 499–528.

Aghdam, M. M., Pavier, M. J. and Smith, D. J. (2001) Micromechanics of off-axis loading of metal matrix composites using Finite Element Analysis, *Int. J. Solids Struct.*, **38**, 3905–25

Aghdam, M. M., Falahatgar, S. R. and Gorji, M. (2008) Micromechanical consideration of interface damage in fibre reinforced Ti-alloy under various combined loading conditions, *Comp. Sci. and Technol.*, **68**, 3406–11.

Aghdam, M. M., Gorji, M. and Falahatgar, S. R. (2009) Interface damage of SiC/Ti metal matrix composites subjected to combined thermal and axial shear loading, *Computational Mater. Sci.*, **46**, 621–31.

Akser, E. O. and Choy, K. L. (2001) Finite element analysis of the stress distribution in a thermally and transversely loaded Ti–6Al–4V/SiC fibre composite, *Comp. Part A*, **32**, 243–51.

Arsenault, R. J. and Taya, M. (1987) Thermal residual stresses in metal matrix composites, *Acta Metall.*, **35**(3), 651–9.

Bigelow, C. A. (1993) Thermal residual stresses in a Silicon-Carbide/Titanium [0/90] laminate, *J. Comp. Technol. Res. JCTRER*, **15**(4), 304.

Brayshaw, J. B. and Pindera, M. J. (1994) The effect of matrix constitutive model on residual thermal stresses in MMC, *J. Eng. Mater. Technol.*, **116**, 505–11.

Carrere, N., Krunch, S., Vassel, A. and Chaboche, J. (2002) Transverse creep loading: experiments and modeling damage mechanisms in uni-directional SiC/Ti composites, *Int. J. Damage Mech.*, **11**, 41–63.

Choo, H., Bourke, M. A. M. and Daymond, M. R. (2001) A finite-element analysis of the inelastic relaxation of thermal residual stress in continuous-fiber-reinforced composites, *Comp. Sci. Technol.*, **61**, 1757–72

Clyne, T. W. and Withers, P. J. (1993) *An Introduction to Metal Matrix Composites*, Cambridge, Cambridge University Press.

Cox, B. N., James, M. R., Marshall, D. B. and Addison, R. C. (1990) Determination of residual stresses in thin sheet titanium aluminide composites, *Metall. Trans. A*, **21A**, 2701–7.

Durodula, J. F. and Derby, B. (1994) An analysis of thermal residual stresses in Ti-6-4 alloy reinforced with SiC and Al_2O_3 fibres, *Acta Metall. Mater.*, **42**(5), 1525–34.

Dvorak, G. J. and Bahei-El-Din, Y. A. (1982) Plasticity analysis of fibrous composites, *J. Appl. Mech.*, **49**, 327–35.

Dvorak, G. J. and Bahei-El-Din Y. A. (1987) A bimodal plasticity theory of fibrous composite materials, *Acta Mechanica*, **69**, 219–41.

Dvorak, G. J., Rao, M. S. M., and Tarn, J. Q. (1973) Yielding in uni-directional composites under external loads and temperature changes, *J. Comp. Mat.*, **7**, 194–216.

Dvorak, G. J., Rao, M. S. M., and Tarn, J. Q. (1974) Generalized initial yield surfaces for uni-directional composites, *J. Appl. Mech.*, **41**, 249–53.

Eggleston, M. R. and Krempl, E. (1994) The transverse creep and tensile behaviour of SCS-6/Ti-6Al-4V metal matrix composites at 482 °C, *Mech. Comp. Mater. Struct.*, **1**, 53–73.

Fang, Q., Sidky, P. S., Hocking, M. G. and Zhang, J. Y. (1998) Cracking behaviour of carbon coating on SIC fibre and residual stresses in Ti/SiC MMCs, *Surf. Coat Technol.*, **100–101**, 264–70.

Haque, S. and Choy, K. L. (2000) Finite element modelling of the effect of a functionally graded protective coating for SiC monofilaments on Ti-based composite behaviour, *Mater. Sci. Eng. A*, **291**, 97–109

Huang, B., Yang, Y., Luo, H., Yuan, M. and Chen, Y. (2008) Effect of the interfacial reaction layer thickness on the thermal residual stresses in SiC_f/Ti–6Al–4V composites, *Mater. Sci. Eng. A*, **489**, 178–86.

Huang, B., Yang, Y., Luo, H. and Yuan, M. (2009) Effects of the coating system and interfacial region thickness on the thermal residual stresses in SiC_f/Ti–6Al–4V composites, *Mater. Design*, **30**, 718–22.

Ismar, H., Schroter, F. and Streicher, F. (2001) Effects of interfacial debonding on the transverse loading behaviour of continuous fibre-reinforced metal matrix composites, *Computers Struct.*, **79**, 1713–22.

Johnson, W. S., Lubowinski, S. J. and Highsmith A. L. (1990) Mechanical characterisation of unnotched SCS6/Ti-15-3 metal matrix composites at room temperature, in: J. M. Kennedy, H. H. Moeller and W. S. Johnson (eds), *Thermal and Mechanical Behaviour of Metal Matrix and Ceramic Matrix Composites*, ASTM STP 1080, American Society for Testing and Materials, Philadelphia, 193–218.

Jeong, G. S., Allen, D. H. and Lasgoudas, D. C. (1994) Residual stress evolution due to cool down in viscoplastic metal matrix composites, *Int. J. Solids Struct.*, **31**(19), 1653–2677.

Li, D. S. and Wisnom M. R. (1994a) Finite element micromechanical modeling of uni-directional fibre-reinforced metal matrix composites, *Comp. Sci. Technol.*, **51**, 545–63.

Li, D. S. and Wisnom, M. R. (1994b) Uni-directional tensile stress-strain response of BP-SiC fibre reinforced Ti- 6Al-4V, *J. Comp. Technol. Res.*, **16**, 225–33.

Li, D. S. and Wisnom, M. R. (1995) Factors controlling the transverse tensile properties of uni-directional SiC/Ti-6Al-4V, *J. Comp. Mater.*, **5**, 235–55.

Li, D. S. and Wisnom, M. R. (1996) Micromechanical modeling of SCS-6 fibre reinforced Ti-6Al-4V under transverse tension-effect of fibre coating, *J. Comp. Mater.*, **30**, 561–99.

Li, T., Olevsky, E. A. and Meyers, M. A. (2008) The development of residual stresses in Ti6Al4V-Al_3Ti metal-intermetallic laminate (MIL) composites, *Mater. Sci. Eng. A*, **473**, 49–57.

Lin, T. H., Salinas, D. and Ito, Y. M. (1972) Initial yield surfaces of a uni-directionally reinforced composites, *J. Appl. Mech.*, **39**, 320–6.

Lissenden, C. J. (1999) Fibre-matrix interracial constitutive relations for metal matrix composites, *Comp. Part B*, **30**, 267–78.

Lou, J. H., Yang, Y. Q., Lou, X., Youan, M. N. and Feng, G. H. (2010) The analysis on transverse tensile behaviour of SiC/Ti–6Al–4V composites by finite element method, *Mater. Design*, **31**, 3942–53.

Majumdar, B. S. and Newaz, G. M. (1992) Inelastic deformation of metal matrix composite: Plasticity and damage mechanisms, *Philosophical Magazine A*, **66**, 187–212.

Martineau, P., Lahaye, M., Pailler, R., Naslain, R., Couzi, M. and Cruege, F. (1984) SiC filament/titanium matrix composites regarded as model composites, *J. Mater. Sci.*, **19**, 2731–48.

Mikata, Y. and Taya, M. (1985) Stress field in a coated continuous fibre composite subjected to thermo-mechanical loadings, *J. Comp. Mater.*, **19**, 554–78.

Morsali, S. R. (2012) *Micromechanics of Interface Damage of Uni-directional Viscoelastic Composite*, Amirkabir University, Tehran, Iran.

Naboulsi, S. (2003) Modeling transversely loaded metal-matrix composites, *J. Comp. Mater.*, **37**, 55–72.

Nakamura, T. and Suresh, S. (1993) Effects of thermal residual stresses and fibre packing on deformation of metal-matrix composites, *Acta Metall. Mater.*, **41**(6), 1665–81.

Nimmer, R. P. (1990) Fibre-matrix interface effect in the presence of thermally induced residual stresses, *J Comp Technol Res*, **12**(2), 64–75.

Nimmer, R. P., Bankert, R. J., Russell, E. S., Smith, G. A. and Wright, P. K. (1991) Micromechanical modeling of fibre/matrix interface effects in transverse loaded SiC/Ti -6Al-4V metal matrix composites, *J. Comp. Technol. Res.*, **16**, 37–46.

Nimmer, R. P., Siemers, P. A. and Eggleston, M. R. (1994) Fibre array geometry effects upon transverse tensile behaviour of SiC/Ti composites, *Comp. Eng.*, **4**, 1289–305.

Rangaswamy, P. and Jayaraman, N. (1994a) Residual stresses in SCS-6/Ti- 24AL-11Nb composite. Part II: Finite element modeling, *J. Comp. Technol. Res. JCTRER*, **16**(1), 54–67.

Rangaswamy, P., Revelos, W. C. and Jayaraman, N. (1994b) Residual stresses in SCS-6/ Ti-24AL-11Nb composite. Part I: Experimental, *J. Comp. Technol. Res.*, **16**(1), 47–53.

Reis, D. A. P., Silva C. R. M., Nono, M. C. A., Barboza, M. J. R., Piorino Neto, F. and Perez, E. A. C. (2005) Effect of environment on the creep behaviour of the Ti–6Al–4V alloy, *Mater. Sci. Eng. A*, **399**, 276–80.

Spowart, J. E. and Clyne, T. W. (1999) The axial compressive failure of titanium reinforced with silicon carbide monofilaments, *Acta Mater.*, **47**, 671–87.

Stephenson, D. J. and Nicholls, J. R. (1991) *Proceedings of the Congo Eurotech Direct 91*, Birmingham, July, Paper C412j074, I. Mech. Eng., 99.

Sun, C. T., Chen, J. L., Sha, G. T. and Koop, W. E. (1990) Mechanical characterization of SCS-6/Ti-6-4 metal matrix composite, *J. Comp. Mater.*, **24**, 1029–59.

Sun, C. T., Chen, J. L., Sha, G. T. and Koop, W. E. (1993) An investigation of the mechanical behaviour of SCS-6/Ti-6-4 metal-matrix composite at elevated temperatures, *Comp. Sci. Technol.*, **49**, 183–90.

Thomas, M. P. (1997) 'Tensile properties of Ti-6-4/SM1240 titanium metal matrix composite with off-axis fibres', SMC Technical Report No. DERA/SMC/SM2/TR 970145, Defence Evaluation and Research Agency, Farnborough, UK.

Warrier, S. G., Rangaswamy, P., Bourke, M. A. M. and Krishnamurthy, S. (1999) Assessment of the fiber/matrix interface bond strength in SiC/Ti-6Al-4V composites, *Mater. Sci. Eng. A*, **259**, 220–7.

Wisnom, M. R. (1990) Factors affecting the transverse tensile strength of uni-directional continuous silicon carbide fibre reinforced 6061 aluminium, *J. Comp. Mater.*, **24**, 707–26.

Xun, Y. W., Tan, M. J. and Zhou, J. T. (2000) Processing and interface stability of SiC fiber reinforced Ti–15V–3Cr matrix composites, *J. Mater. Processing Technol.*, **102**, 215–20.

Yang, Y. Q., Werner, A., Dudek, H. J. and Kumpfert, J. (1999) TEM investigations of interfacial processes in SCS-6 SiC/TiB_2/Super α_2 composites, *Comp. Part A*, **30**, 1209–14.

Yeh, N. M. and Krempl, E. (1993) The influence of cool-down temperature histories on the residual stresses in fibrous metal matrix composites, *J. Comp. Mater.*, **27**, 973–95.

Zahl, D. B. and McMeeking, M. R. (1991) The influence of residual stress on the yielding of metal matrix composites, *Acta Metall. Mater.*, **39**(6), 1117–22.

Zahl, D. B., Schmauder, S. and McMeeking, M. R. (1994) Transverse strength of metal matrix composites reinforced with strongly bonded continuous fibres in regular arrangements, *Acta Metall. Mater.*, **42**, 2983–97.

Zhijun, M., Yanqing, Y., Xianghong, L., Xian, L. and Yan, C. (2006) The effect of matrix creep property on the consolidation process of SiC/Ti–6Al–4V composite, *Mater. Sci. Eng. A*, **433**, 343–6.

10

Understanding residual stresses and fracture toughness in ceramic nanocomposites

H. WU, Loughborough University, UK

DOI: 10.1533/9780857098597.2.256

Abstract: This chapter discusses residual stresses in ceramic nanocomposites and their contribution to the fracture toughness and strength. First, an overview is given on the microstructure of ceramic nanocomposites and their typical mechanical properties, including possible toughening/strengthening mechanisms. A two-dimensional circular disc model is introduced to estimate internal residual stresses and their contribution to stress intensity factor. Exemplary studies of the model are applied on alumina-silicon carbide nanocomposites. Surface residual stress developed by machining is reviewed in alumina/silicon carbide nanocomposites, including their contribution to any improvement of mechanical properties.

Key words: ceramic nanocomposites, nano-dispersants, residual stress, toughening, strengthening, alumina, silicon carbide.

10.1 Introduction

It is generally agreed that a mild toughening, if any, and a possibly significant strengthening can be achieved for ceramic nanocomposites. First, an overview is given on the development of ceramic nanocomposites, followed by describing the most studied alumina/silicon carbide (Al_2O_3/SiC) nanocomposites and some suggested mechanisms of toughening and strengthening that may be applicable to this type of nanocomposites. A two-dimension (2 D) nanocomposite circular disc model (CDM) is then proposed for quantitative estimation of residual stresses in nanocomposites and their contribution to fracture toughness. Compared to other models, the CDM can lead to simple analytic equations correlating residual stresses and fracture toughness contribution to microstructural parameters of the nanocomposites, such as volume fraction and size of nano-dispersants, coefficient of thermal expansion and Young's modulus. Surface residual stress on the machined surface is discussed to highlight the benefits that nano-dispersants can bring to improve mechanical behaviour in an alternative mechanism. Finally, the future research trend will be speculated on.

10.2 Overview of ceramic nanocomposites

Niihara (1991) developed the first ceramic composites with a particulate reinforcement size down to the sub-micron level, even some to less than 100 nm. The volume

fraction of the fine particles ranged from less than 10% to a possible maximum of about 30%. Following Niihara's earlier exploratory work, many researchers have done much further research on ceramic nanocomposites. They have generally agreed that, by incorporating nano-particles into ceramic matrixes, the composites produced have the possibility to exhibit properties superior to those of the matrix materials in monolithic form. This kind of ceramic composite was first called 'ceramic nanocomposite' by Niihar (1991), even though the term 'nanocomposite' was coined in the early 1980s by Roy *et al.* (Komarneni, 1992). Niihara (1991) classified ceramic nanocomposites into four categories, based on their microstructural characteristics:

1. intragranular;
2. intergranular;
3. hybrid of intra- and inter-granular; and
4. nano- to nanocomposites (Fig. 10.1).

In the intra- and inter-granular nanocomposites, the nano-sized particles are dispersed mainly within the matrix grains or at the grain boundaries of the matrix respectively. Throughout this chapter, these dispersed particles are also referred to as dispersants.

Research on ceramic nanocomposites began with the systems Al_2O_3/SiC and Si_3N_4/SiC. Then other systems were investigated, either for structural or for functional interest. Some of the explored systems are listed in Table 10.1 (Sternitzke, 1997). For structural interest, the explored systems include Al_2O_3/SiC, Si_3N_4/SiC, MgO/SiC, Y_2O_3/SiC (Yoshimura *et al.*, 1997), ZrO_2/SiC (Bamba *et al.*, 2003), mullite/SiC (Soraru *et al.*, 2000), Si_3N_4/Al_2O_3 (Zhu *et al.*, 1997), Al_2O_3/TiN (Wang *et al.*, 2006), Si_3N_4/BN (Kusunose *et al.*, 2002), SiC/BN (Kusunose *et al.*, 2004; Wang *et al.*, 2006), AlN/BN (Kusunose *et al.*, 2008), ZrB_2/SiC (Liu *et al.*, 2010) and $Al_2O_3/FeAl_2O_4$ (Mukhopadhyay and Todd, 2010a,b). In the above notation, the material before the forward slash is the matrix, and the one after the nano-dispersant.

Attempts have been made to realise a similar microstructure to ceramic/ceramic nanocomposite in ceramic/metal systems, where nanosized or submicron-sized metal particles are the reinforcements, such as Mo (Nawa *et al.*, 1994), Ni (Sekino *et al.*, 1997), Cr (Ji and Yeomans, 2002), W (Sekino and Niihara, 1997; Hyuga *et al.* (2003), etc. in an Al_2O_3 or other matrices. Typically, a bimodal distribution of metal particles was found with the larger particles (a few microns) on the ceramic grain boundaries and a finer dispersion (in submicrons) within the grains. These larger metal particles are presumably responsible for the increased apparent toughening seen in these materials by a mechanism of crack bridging, compared with ceramic/ceramic nanocomposites. In all of these materials, strengthening can be commonly achieved, but not to an extent any greater than would be expected from the degree of grain refining caused by the second phase particles (Derby, 1998).

To understand ceramic nanocomposites, alumina/silicon carbide nanocomposites have been mostly studied to date. It is therefore necessary to provide enough updated details on this type of nanocomposite, which are presented in the following two sub-sections.

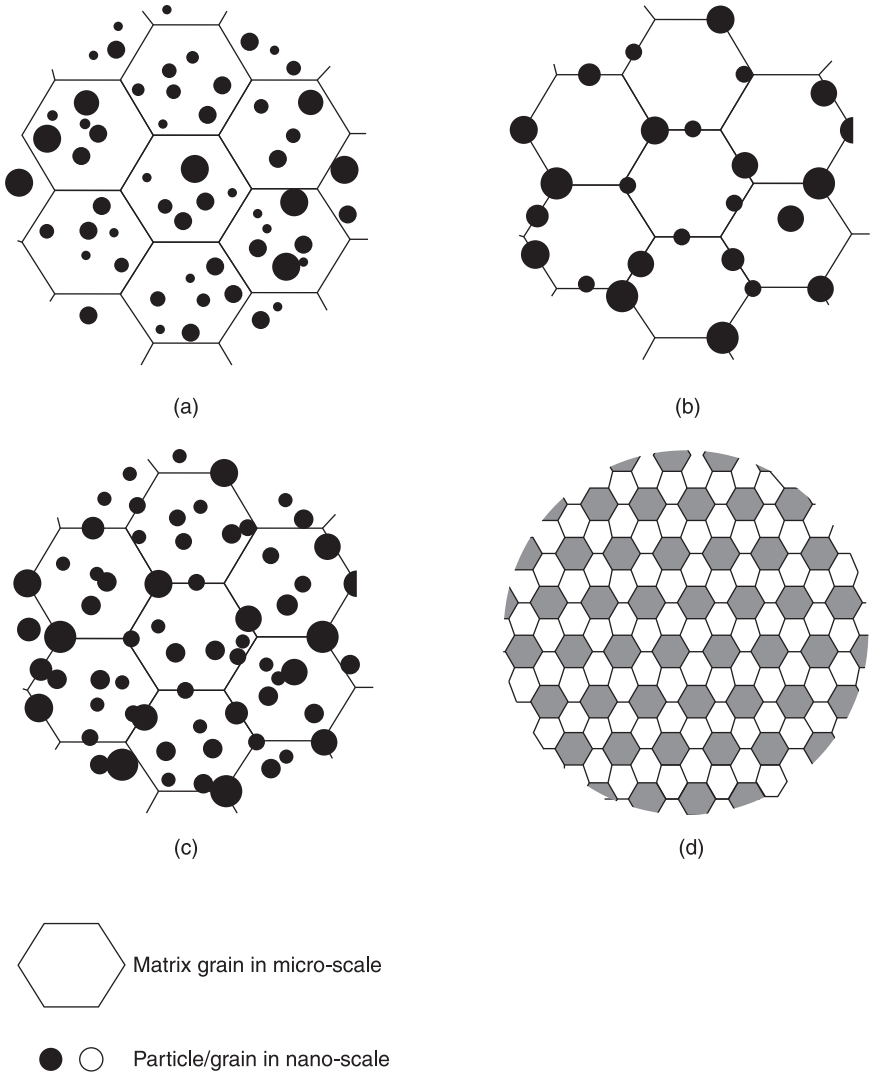

10.1 Schematic types of ceramic nanocomposites classified by Niihara (1991): (a) intragranular; (b) intergranular; (c) hybrid of intra- and intergranular; and (d) nano to nano.

10.2.1 Alumina/silicon carbide nanocomposites

Al_2O_3/SiC nanocomposites have received the most extensive research among the ceramic nanocomposite systems, for the purpose of evaluating mechanisms of mechanical property improvement, investigating microstructural evolution or optimising processing conditions. The typical microstructure for an Al_2O_3/SiC

nanocomposite comprises polycrystalline alumina matrix with an average grain size ranging from 1 to 5 μm, and silicon carbide particles with a size from tens to hundreds nanometers, which exist either inside matrix grains or on the grain boundaries. The volume fraction of the nano-sized SiC particles is constrained by:

- the capability of processing techniques to make a homogeneous distribution of the particles; and
- the limit of densification of the available sintering method.

The most extensively researched Al_2O_3/SiC nanocomposite contains approximately 5 vol% of the SiC particles. This particle fraction (or around) allows the particles to be easily homogeneously dispersed into the matrix by traditional ceramic powder mixing methods (e.g. ball milling and evaporation drying, ball milling and freeze-drying). Also, the composites are able to be fully densified using uni-axial hot pressing at about 1600 to 1800 °C; or be densified to a density of more than 98% of the theoretical value by pressureless sintering at about 1700 °C after a conventional packing method (e.g. cold isostatic pressing or uni-axial pressing). The main property data and processing conditions for such materials from different investigators are summarised in Table 10.1 for Al_2O_3/SiC nanocomposites and the respective reference monolithic Al_2O_3. The most researched properties are briefly outlined in the following sections.

Bend strength

One of the most important conclusions in Niihara's (1991) research on Al_2O_3/SiC nanocomposites was that, by the addition of 5 vol% nano-sized SiC particles, the 3-point bend strength was increased from 320 MPa for monolithic Al_2O_3 as a reference to 1050 MPa for the nanocomposites. Following their research, Zhao *et al.* (1993) tried to repeat this strengthening effect by reproducing a similar microstructure of nanosized SiC-particles dispersed into an Al_2O_3 matrix. They also successfully improved the 4-point bend strength, but only to a level of 800 MPa. Thereafter, other groups carried out more research on the Al_2O_3/SiC system, aiming to repeat the high bend strength of more than 1 GPa and to explore the strengthening mechanisms. Most of them had claimed a strengthening, but only to a level of less than 800 MPa (Borsa *et al.*, 1995; Carroll *et al.*, 1996; Meschke *et al.*, 1997; Wu *et al.*, 1998). Currently, it has been generally agreed that a moderate improvement in bend strength can be achieved in Al_2O_3 incorporated with 5 vol% of SiC particles with a size of less than a sub-micron by controlling the particulate distribution and the densification. The main opinions on possible strengthening mechanisms are given in Section 10.3.

Fracture toughness

As listed in Table 10.1, most of the researchers measured little improvement of fracture toughness in the nanocomposite comparing to referencing alumina, even

Table 10.1 Alumina/silicon carbide nanocomposite properties from different investigators

Researchers	Alumina powder	SiC powder	SiC (vol%)	Processing condition	Relative density	Grain size (μm)	Surface finish	σ_F (MPa)	K_{IC} (MPa.m$^{1/2}$)	σ_F (MPa)	K_{IC} (MPa.m$^{1/2}$)
								As-machined		Annealed	
Niihara *et al.* (1991)	γ-Al_2O_3 0.4 μm	β-SiC <300 nm	0	NA	NA	NA	1 μm	355	3.25		
			5	HP 1600–1900°C	NA	2–3	1 μm	1017	4.7	1540	NA
			10	HP 1600–1900°C	NA	2–3	1 μm	~870	~4.4		NA
			20	HP 1600–1900°C	NA	2–3	1 μm	~870	~4.4		NA
			33	HP 1600–1900°C	NA	2–3	1 μm	~870	~4.4		NA
Zhao *et al.* (1993)	AKP53	SiC β-SiC	0	HP 1400°C		4.8		559 ± 51	2.9 ± 0.1		
	0.2 μm	150 nm	0	PS, 1450°C		3.2		569 ± 72	2.9 ± 0.1		
			5	HP 1640°C	99.9%	4.2	6 μm industry	760 ± 28	3.6 ± 0.1,	1001 ± 102	3.3 ± 0.1
			5	PS 1775°C	98.3%	5.4	6 μm lab.	586 ± 72	27 ± 0.1		
Borsa *et al.* (1995)	AAES11C	α-SiC	0	HP 1500°C	>98%	1.3	3 μm	560 ± 77			
	0.4 μm	200 nm	23.8	HP 1700°C	>98%	1.4	3 μm	730 ± 20			
	AKP53	α-SiC	0	HP 1500°C	>98%	2.9	3 μm	520 ± 10			
	0.2 μm	200 nm	12.1	HP 1700°C	>98%	2.4	3 μm	648 ± 27			
Carroll *et al.* (1996)	AKP53 0.2 μm		0	HP 1550°C	>98%	5.0	3 μm	491 ± 63	3.25 ± 0.27		
		α-SiC 12–115 nm	5	HP 1700°C	98–99.5%	2.1–4.0	3 μm	549–738	2.76–3.46		
Anya and Roberts (1996)	AAES11C	α-SiC	0	PS 1560°C	>99.7%		3 μm		2.88 ± 0.17		
	0.4 μm	200 nm	5	1775°C	>99.7%		3 μm		5.90 ± 0.35		
			15	1775°C	>99.7%		3μm		6.06 ± 0.54		

Meschke *et al.* (1997)	α-Al_2O_3 0.2 μm	β-SiC 180 nm	0	PS1350–1600°C		0.6–8		300–350			
			5	HIP 1550°C	99.2%	1.7	1 μm	1038	2.9 ± 0.1	760	2.2 ± 0.2
			5	HIP 1700°C	98.5%	6.8	1 μm	575	2.7 ± 0.3	424	2.2 ± 0.1
			5	PS 1700°C	97.8%	6.3	1 μm	476	2.9 ± 0.1	380	2.1 ± 0.1
Perez-Rigueiro *et al.* (1998)	Al_2O_3 0.48 μm	SiC 800 nm	0	PS1550–1650°C		2.3–4.6		390–409	3.0–3.2		
			0	HP 1550°C		3.8		480 ± 8	3.3 ± 0.2		
			5	HP 1700°C	3.87	2.6		451 ± 60	3.6 ± 0.2		

HP: hot pressing densification; PS: pressureless sintering densification.σ_F, bend strength; K_{IC}, critical stress intensity factor.

though a few (Niihara, 1991) claimed an increase of 40 to 80%. Fracture toughness should be an inherent parameter, decided only by the basic ceramic substance and its microstructure. However, the most commonly used test methods, for example, indentation fracture and single-edge-notched bending, are hardly able to measure the real fracture toughness, which will make the direct comparison of any marginal differences between materials difficult. Indentation fracture methods are especially notorious for measurements being strongly affected by numerous environmental factors, for example fracture patterns under the indents, plastic deformation properties near the indenter-tip and surface residual stresses.

Fracture mode

Despite the large divergence between different research groups in improvements in bend strength and toughness in Al_2O_3/SiC nanocomposites, there exists one commonly acknowledged effect: a fracture mode transition from intergranular in monolithic alumina to transgranular in nanocomposites. This 'nanocomposite effect' has been achieved in Al_2O_3/SiC nanocomposites with SiC content down to 1 vol% (Kara and Roberts, 2000; Winn and Todd, 1999a), and in those produced by either hot-pressing or pressureless sintering. One of the possible contributors for the fracture mode change could be the residual thermal misfit stress. The residual stress is in compression along the radial direction, and is a maximum at the Al_2O_3 and SiC interface (Levin *et al.*, 1995). If a crack reaches the interface, this compressive residual stress will resist crack propagation. It was expected that this local compression could raise the local K_{IC} by about 50% (Winn and Todd, 1999a), who assumed that this local toughening would be enough to prevent crack propagation along grain boundaries, but only if the SiC particles were dispersed on the grain boundary.

Wear resistance

It has been recognised that grain pull-out (i.e. grain boundary fracture) is the dominant mechanism of catastrophic wear for high purity alumina with a grain size larger than 3 μm; when the grain size is smaller than 2 μm, plastic deformation or chemical removal of material becomes a significant wear process (Miranda-Martinez *et al.*, 1994). It has been found that in pure alumina, material removal rate generally increases with increasing grain size under almost all of the wear modes (Davidge and Riley, 1995; Marshall *et al.*, 1987; Rice and Speronello, 1976; Wiederhorn and Hockey, 1983). In Al_2O_3/SiC nanocomposites, the observed transgranular fracture mode is expected to reduce grain pull-out during grinding, polishing, sliding wear and erosion wear, and thereby should increase the wear resistance of the material. Walker *et al.* (1994) first showed that the nanocomposite was worn at less than one-third of the rate of alumina with comparable grain size, and Davidge *et al.* (1996), Lawrence *et al.* (1998), Winn and Todd (1999a),

Ortiz-Merino and Todd (2005) and Limpichaipanit and Todd (2009) made investigations further confirming the significant improvement of wear resistance by nano-dispersants. Sliding wear of the nanocomposites was tested recently by Rodriguez *et al.* (1999) and Chen *et al.* (2000). It was found that the nanocomposites did not exhibit wear transition behaviour, in contrast to pure alumina that always suffers a transition from mild to severe wear. Rodriguez *et al.* (1999) measured that the wear resistance of nanocomposites was better than for alumina by a factor of 3 to 5.

Machining behaviour

A number of investigators noticed or experimentally demonstrated an improved ease of polish for the Al_2O_3/SiC nanocomposites (Davidge *et al.*, 1997; Kara and Roberts, 2000; Winn and Todd, 1999b; Zhao *et al.*, 1993). Exhibiting less grain boundary fracture and with the remaining transgranular fracture on a relatively smaller scale, a good-quality polished surface could be produced at a quicker rate.

Surface residual stress

Surface residual stress is correlated to some irreversible deformation, for example dislocation activation made by a surface contact operation such as machining (Green, 1983). The near surface ductile deformation in alumina/silicon nanocomposites has been studied in detail with cross-section transmission electron microscopy (TEM) by Wu *et al.* (2001, 2003) and X-ray powder diffraction (Tanner *et al.*, 2005, 2006). The residual compression was approximately 2 GPa inside the ductile deformation layer, as quantified by using Hertzian indentation (Wu *et al.*, 1998, 2001) and fluorescence spectroscopy (Guo *et al.*, 2011; Wu *et al.*, 2008).

Annealing recovery

Another well agreed nanocomposite effect in Al_2O_3/SiC nanocomposites is the strengthening after annealing. Initially, the annealing effect in nanocomposites was somewhat controversial (Luo and Stevens, 1997; Niihara, 1991), because it was shown to involve fracture damage recovery by crack healing (Chou *et al.*, 1996; Thompson *et al.*, 1995; Wu *et al.*, 1998, 2000; Yoshimura *et al.*, 1997).

10.2.2 Toughening and strengthening mechanisms in Al_2O_3/SiC nanocomposites

The first measurement of fracture toughness (by indentation fracture) of ceramic-nanocomposites nanosized SiC particles were dispersed into ceramic matrixes,

Table 10.2 Measured fracture toughness of monolithic ceramics and nanocomposites

System	Monolithic (MPa.m$^{1/2}$)	Nanocomposites (MPa.m$^{1/2}$)
Al_2O_3/SiC	3.5	4.8
MgO	1.2	4.5
Si_3N_4/SiC	4.5	7.5

for example Al_2O_3, MgO or Si_3N_4-showed an obvious increase (Niihara, 1991) (Table 10.2). For brittle materials, the Griffith theory has well established a correlation among the measured bend strength (σ), material toughness (K_{IC}) and critical flaw size (c) as

$$\sigma = Y\frac{K_{IC}}{\sqrt{c}} \qquad [10.1]$$

where Y is a constant relating to the geometry of the flaw. For fully densified and comparable grain-sized monolithic Al_2O_3 and Al_2O_3/SiC nanocomposites, well-polished surfaces presumably contain a similar size of Griffith flaw (or critical flaw). Any increment in toughness should therefore result in a bend strength increase.

However, most other researchers have claimed little change in toughness in Al_2O_3/5vol%SiC nanocomposites (Carroll *et al.*, 1996; Meschke *et al.*, 1997; Perez-Rigueiro *et al.*, 1998; Zhao *et al.*, 1993, 2006). Also, Niihara's measured toughness increment was not enough to account for the measured improvement in bend strength of Al_2O_3/SiC nanocomposites (Eq. 10.1). Therefore, three questions still exist:

1. Does toughening by nano-sized particles exist in nanocomposites?
2. If so, what is the mechanism?
3. In addition to the contribution by toughening (if it exists), what other mechanisms could exist to account for the improvement of bend strength in the nanocomposites?

Niihara (1991) proposed that a primary toughening mechanism was crack deflection by the tensile tangential stress around SiC particles of over 1000 MPa, which arises during cooling down from the sintering temperature due to the thermal expansion misfit (Faber and Evans, 1983a,b). In Al_2O_3/SiC nanocomposites, the observed fracture mode transition from intergranular in monolithic Al_2O_3 to transgranular in nanocomposites, was also supposed to be due to said local stresses. Microcracking toughening was dismissed as a possible toughening mechanism, as the nano-sized particles are far smaller than the critical particle size of initiating microcracking around.

In large-sized (e.g. microns) particulate reinforced ceramic composites, crack deflection by making a crack propagate in a zigzag way leads to an extension of

propagating path; may force the crack to propagate along lattice planes with higher energy. Either effect will increase the total fracture energy or the fracture toughness (i.e. the apparent fracture energy). Detailed analysis of such models has been performed by Faber and Evans (1983a,b).

To investigate possible deflection of cracks by nano-sized SiC particles in alumina, Jiao and Jenkins (1998) made a detailed observation of the crack-particle interaction using TEM. Their results are summarised here. When a crack intersects an intragranular SiC particle directly, interface de-bonding occurs; otherwise, the crack goes straight past the particles without any significant deflection. For intergranular SiC particles, when the acute angle between the crack and the trace of the grain boundary exceeds 60 degrees, the crack was more likely to penetrate the grain boundary and continue to propagate intragranularly. For small angles, it was more likely to be deflected along the grain boundary, even if there were SiC particles on the grain boundary. If the intergranular crack running along a grain boundary inclines to the main propagation direction at a certain angle, the intergranular SiC particles will deflect the crack into the grain. Thus, nano-sized SiC particles can only deflect cracks under very special conditions. Levin *et al.* (1995) suggested that this could be a result of a strong Al_2O_3/SiC interface or a large radial compressive thermal residual stress on the interface. Jiao and Jenkins (1998) observations also indicated that the deflection of the SiC particles did not increase the crack-propagating path significantly, if at all, on the microscale. On the microscale, transgranular fracture in nanocomposites would not increase the length of crack paths, compared to intergranular fracture in monolithic Al_2O_3 ceramics.

Transgranular fracture energy is, in general, higher than intergranular fracture energy. According to the measured fracture energy, Kirchner and Gruver (1979) listed the corresponding critical stress intensity factor for some of the lattice planes in sapphire: $K_{IC(10\ \bar{1}2)} = 2.15\,\text{MPa.m}^{1/2}$, $K_{IC(10\ \bar{1}0)} = 2.4\,\text{MPa.m}^{1/2}$, $K_{IC(11\ \bar{2}6)} = 4.3\,\text{MPa.m}^{1/2}$ and $K_{IC(0001)} > 5.6\,\text{MPa.m}^{1/2}$. The K_{IC} value for transgranular fractured polycrystalline alumina should be some averaged contribution of all the crystal planes, and between 2.5 and $5\,\text{MPa.m}^{1/2}$.

Theoretical calculations have shown that crack deflection can make an increment of $0.12\,K_0$ in toughness (K_0 is the fracture toughness without deflection) (Faber and Evans, 1983a,b; Taya *et al.*, 1990). The change of fracture mode from intergranular to transgranular could give an increment of $0.58\,K_0$ in toughness for monolithic polycrystalline alumina, according to the calculation of Hansson *et al.* (1993), by assuming a weak grain boundary. In the nanocomposites, an additional contribution may be the presence of substantial tensile stress in the alumina matrix, due to thermal misfit of Al_2O_3 and SiC. The existence of this stress has been confirmed with neutron diffraction by Todd *et al.* (1997) and X-ray diffraction (XRD) by Levin *et al.* (1994). Hence the apparent K_{IC} in transgranular fracture may be decreased. By considering the contribution of this thermal residual stress, that is, the compressive in radial and tensile in tangential direction,

Levin *et al.* (1995) calculated that any toughening by the transition of fracture mode will be balanced by the matrix weakening, and the net result of toughness should be decreased by $0.20K_0$ for a nanocomposite with 25 wt% SiC, and $0.05K_0$ for 5 wt% SiC (equal to 5.4 vol%). These calculations indicate that crack deflection and transgranular fracture have little improvement in toughness in the Al_2O_3/SiC nanocomposite, even though there may have such improvement in other ceramics.

Ohji *et al.* (1998) proposed that crack-tip bridging by the particles at short distances behind the crack tip could be one of the primary toughening mechanisms, based on their TEM observations of crack morphology. They believed that the bridging effect could be a result of a perfect crystal structure in the nano-sized SiC particles and in a low boundary energy with a good lattice match between the SiC and Al_2O_3 phases. The peak toughness increment, ΔK, by particle bridging is given by

$$\Delta K = \frac{\sigma_i \pi^{\frac{1}{2}} d^{\frac{1}{2}}}{4\left[\frac{\pi}{6f_p} + 2\left(\frac{\pi}{6f}\right)^{\frac{2}{3}}\right]^{\frac{1}{2}}} \qquad [10.2]$$

where d is the diameter of SiC particles, f_p is the volume fraction of SiC particles and σ_i is the interface fracture stress. By taking away the toughness decrease produced by the residual thermal stress inside the matrix, this bridging model gives a net increment of toughness of about 2 MPa.m$^{1/2}$ at $f_p = 5$ vol% and $d = 50$ nm. They pointed out that the crack-extension distance required to reach a plateau level in toughness is equivalent to the length of the shielding zone – only a few hundred nanometers. This steep rise of fracture resistance in the nanocomposites (i.e. a steep R-curve) was expected to lead to an increase in failure strength. In comparison, the grain bridging and grain pull-out in monolithic Al_2O_3 generate an R-curve slowly rising over about a few hundreds microns, resulting in a smaller failure strength. This comparison can be schematically shown by a linear relationship of K^2 (stress intensity) to Δc (crack extension) with a larger slope for the nanocomposite. The failure strength is proportional to the square root of the slope, and a nanocomposite can achieve higher strengths than alumina, even though both materials have a similar K_{IC}.

By measuring the crack opening displacement (COD), Meschke *et al.* (1997) and Hoffman and Rodel (1997) demonstrated that crack-tip toughness was considerably lower in nanocomposites than in pure alumina, and the proposed R-curve behaviour was unlikely to occur. Meschke *et al.* (1997) measurements of K_{IC} showed that, because of its transgranular failure mode, the grain size in nanocomposites had no effect on the toughness. In contrast, a strong R-curve behaviour (Steinbrech *et al.*, 1990) exists in alumina by crack bridging, as the

fracture is intergranular. The measured R-curve resistance shows a strong dependence on the grain size and grain morphology (Swanson *et al.*, 1987). These measurements show that it is hard to examine the R-curve behaviour in the nanocomposite to support the proposed bridging effect by the nano-sized SiC particles (Ohji *et al.*, 1998). However, lower toughness in nanocomposites may still have a higher bend strength because of short crack extension before failure. The studies seem to imply that the geometric effect of nano-dispersants on the fracture toughness can be ignored, and only the internal residual stress needs to be accounted for in the fracture resistance.

10.3 Residual stress inside ceramic nanocomposites

Residual stresses are developed due to a thermal/mechanical misfit between the nano-dispersant and the matrix, when nanocomposites are cooled down from the high temperatures necessary for densification. Such stresses are widely recognised as the possible source responsible for change in fracture mode, fracture toughness and other mechanical/physical attributes of the ceramic nanocomposites.

The internal residual stresses have been experimentally measured. XRD, neutron diffraction and fluorescence/Raman spectroscopy are the most accepted experimental methods used to directly quantify the internal residual stress in different phases. Theoretical modelling has developed around Shelby's elastic mechanical method in treating secondary inclusions in a matrix. By adapting a basic model of a spherical inclusion embedded inside a concentric spherical shell, analytical solutions are available to predict the stresses inside the dispersant and matrix. When the whole nanocomposite is considered, stacking of the units in the three-dimensional (3D) space is needed, including a consideration of grain size and grain boundaries of the matrix. In this situation, it is unlikely to have simple analytic solutions that can be used conveniently, unless there is a further simplification of the model. In this section, a simplified model is introduced for theoretical quantification. It is expected that analytical solutions can provide enough theoretical convenience to judge the potential impact that nanocomposite microstructure parameters may have on residual stresses and the mechanical property of different ceramic nanocomposite systems.

The widely used 3D model is further simplified as a 2D one, where the dispersant is represented by an inner disc and the matrix by an annular surrounding the inner disc (Fig. 10.2). Such a model has been used successfully by Hsueh *et al.* (2001) for analysing the residual thermal stress of inter-granular two-phase ceramic composites. It is hereafter called 2D CDM of nanocomposites.

In this 2D CDM, the radial (r_d) represents the radial of the nano-dispersants. Between the dispersant and the matrix, a well bonded interface exists to ensure the continuity of the solid. The radial of the whole circle (r_m) is defined by the fraction of dispersants (f) in the composites by

$$f = \frac{r_d^2}{r_m^2 - r_d^2} \qquad [10.3]$$

Hsueh *et al.* (2001) have summarised the process of achieving the analytic equations. Here, the results are adapted to suit the microstructure format of nanocomposites. Residual thermal stresses developed in the nanocomposites can be determined by a procedure of first allowing the two phases to exhibit unconstrained differential thermal strains during the temperature change. Then a radial stress (σ_a) is placed at the interface to restore the displacement continuity at the interface:

$$\sigma_a = \frac{\left(\alpha_m - \alpha_d\right)\Delta T}{\frac{\left(1 - v_d\right)}{E_d} + \frac{\left(\left(r_m^2 + r_d^2\right) / \left(r_m^2 - r_d^2\right)\right) + v_m}{E_m}} \qquad [10.4]$$

where α is the coefficient of thermal expansion, ΔT is the temperature regime from a temperature where property is tested to the highest possible temperature where atomic diffusion is not available to relax any applied stress; E is the Young's

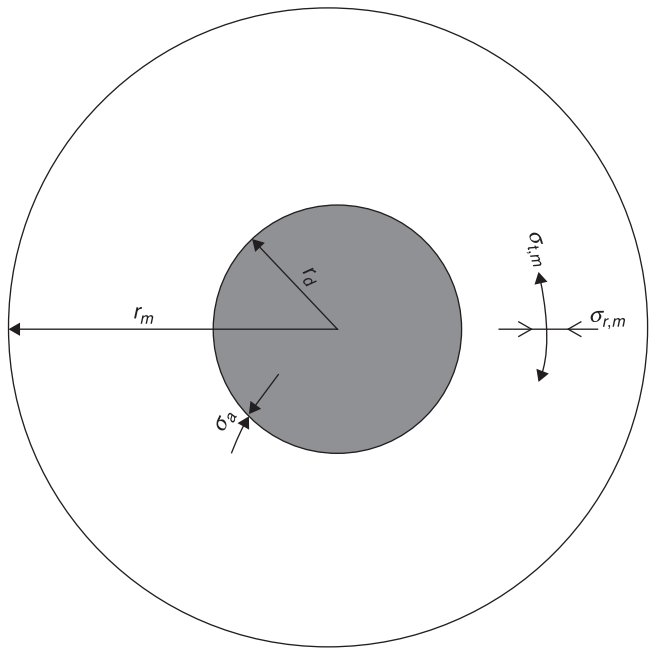

10.2 Schematic showing the 2D nanocomposites circular disc model (CDM).

modulus and ν is the Poisson's ratio; the subscript d and m represent the nano-dispersant and matrix respectively. If only the fraction and size of the nano-dispersants are included in the equation, the radial stress on the interface has the following format:

$$\sigma_a = \frac{E_m E_d \left(\alpha_m - \alpha_P\right) \Delta T}{E_m \left(1 - \nu_d\right) + E_d \left(1 + 2f + \nu_m\right)} \quad [10.5]$$

With an interfacial stress, the radial and the tangential stresses in the dispersant and the matrix are expressed in the following formats, by following the solutions originally given by Timoshenko and Goodier (1970):

$$\sigma_{d,r} = \sigma_{d,t} = \sigma_a \quad [10.6]$$

$$\sigma_{m,r} = \frac{r_d^2 + fr_d^2 - fr^2}{r^2} \times \sigma_a \quad [10.7]$$

$$\sigma_{m,t} = -\frac{r_d^2 + fr_d^2 + fr^2}{r^2} \times \sigma_a \quad [10.8]$$

where $\sigma_{d,r}$, $\sigma_{d,t}$ are the radial and the tangential stresses in the dispersant respectively, and $\sigma_{m,r}$, $\sigma_{m,t}$ the equivalent ones in the matrix; r is the distance from the centre of the nanocomposites circle, satisfying a condition of $r_d \le r \le r_m$.

As per Eqs 10.7 and 10.8, the radial and tangential stresses decline with the increase in distance away from the interface between the dispersant and the matrix. On the boundary of the CDM, the radial stress declines to zero, but the tangential stress will maintain the level of stress invariant. The quantification can give the first stress invariant, that is, the sum of normal stresses, as

$$\sigma_{m,r} + \sigma_{m,t} = -2f\sigma_a \quad [10.9]$$

The stress invariant in the matrix is decided by the thermoelastic misfit of the two phases and the fraction and size of nano-dispersants. However, the one inside the dispersant is less influenced by the fraction of the dispersant, and expressed by

$$\sigma_{d,r} + \sigma_{d,t} = 2\sigma_a \quad [10.10]$$

As an example, the 2D circular model is applied to the alumina/silicon carbide nanocomposites to estimate the residual stress invariant inside the alumina matrix and silicon carbide dispersant, with different fractions and sizes of the dispersants as variables. The thermoelastic constants for each phase of the nanocomposite (Todd *et al.*, 1997) are listed in Table 10.3 for the prediction. The temperature difference is set as 1200 °C. The predicted results are plotted in Fig. 10.3.

To validate the 2D circular model, experimental measurements of residual stress in alumina matrix and silicon carbide dispersants in the nanocomposites with different fraction of SiC dispersants are also included in Fig. 10.3. Results from

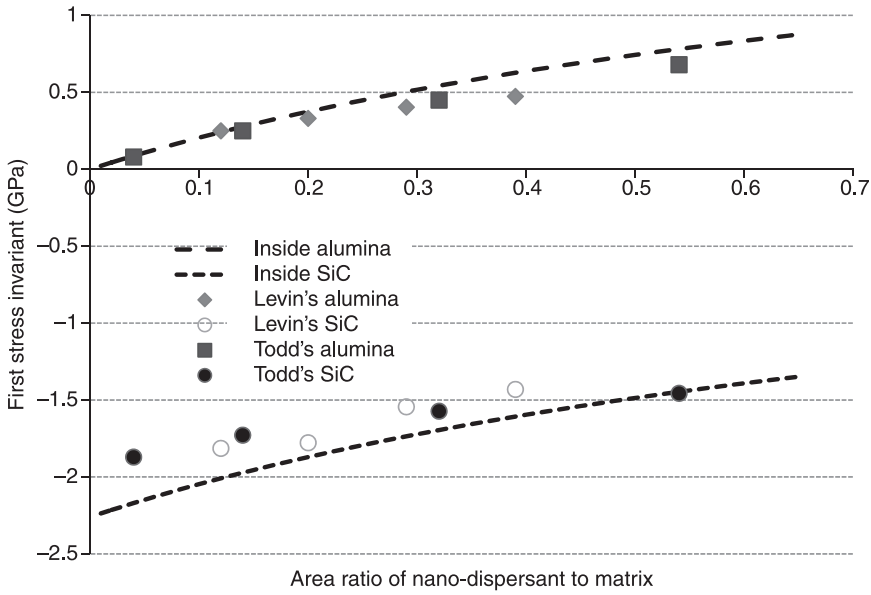

10.3 Predicted stress invariants in alumina matrix and SiC dispersant in Al_2O_3/SiC nanocomposites (dashed lines) by using the 2D circular disc model. Experimental measurements of residual stresses in the composites by Levin *et al.* (1994, 1995) and Todd *et al.* (1997) are included.

Table 10.3 Average values of thermoelastic constants of alumina/silicon carbon nanocomposites

Phase	E (GPa)	ν	α (1/°C)	ΔT (°C)
Alumina	402	0.23	8.9×10^{-6}	1200
Silicon carbide	483	0.17	4.4×10^{-6}	

Todd *et al.* (1997) were measured by using neutron diffraction, which can eliminate the impact by any surface residual stress. Data from Levin *et al.* (1994) were acquired by using X-ray powder diffraction. It is incredible that across a fairly large regime of fraction of silicon carbide dispersants, the measured residual stresses are around the predicted values by using the 2D CDM. It seems that the stress invariant in the matrix is slightly over-estimated at higher fraction, as is the one inside the dispersant at lower fractions. Considering the possible measuring error bars and consistent trend between the prediction and the measurement, the predictions by the 2D CDM should be a reasonable approximation for practical purpose.

It is worth noting that the outer boundary of the CDM has no clear physical meaning yet. It is reasonable to define it as the middle point between the centres of neighbouring nano-dispersants. By having the 2D CDM reasonably validated for the nanocomposites, it is possible to estimate the residual stress in different ceramic nanocomposites and the impact of the fraction and size of nano-dispersant on the residual stress.

10.4 Toughening and strengthening mechanisms in ceramic nanocomposites

The residual stress can be estimated by using Eqs 10.5, 10.7 and 10.8. However, their impact on the fracture toughness should be dependent on the fracture mode. Therefore, the transgranular and intergranular fractures are discussed in the next two sub-sections.

10.4.1 Transgranular fracture

In transgranular fracture mode, the propagation of a crack should follow a path where the highest stress intensity is given under the same loading conditions. When the nano-dispersant is under compression, the whole matrix is likely under tension; in this case, the propagation path of a crack likely goes through the matrix only, which is called a type I transgranular fracture (Fig. 10.4a). If the coefficient of thermal expansion of the matrix phase is smaller than the dispersant, a tensile stress will result inside the dispersant, and a compression into the matrix, in this case, the propagation path may pass though the inclusion or along the interface between the matrix and the inclusion, which is called a type II transgranular fracture (Fig. 10.4b).

Cracking propagation inside the grain is influenced by the fluctuations of the residual stresses. The stress intensity (K) will be reduced for a crack passing

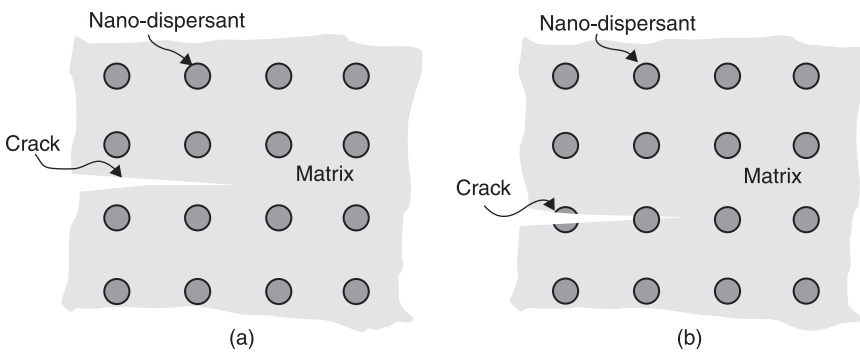

10.4 Transgranular fracture mode: (a) type I – avoid nano-dispersant; and (b) type II – toward the nano-dispersant.

through a compressed region and increased through a tensile region. The change in K_I for a crack propagating through a one-dimensional (1 D) fluctuating residual stress field can be estimated by (Taya *et al.*, 1990)

$$\Delta K_{rI} = 2\bar{\sigma}\left(\frac{2\lambda}{\pi}\right)^{1/2} \quad [10.11]$$

where $\bar{\sigma}$ is the mean residual stress acting over regions of compression or tension, and the wavelength of the stress field is λ. For a type I transgranular fracture, only the stress invariant in the matrix contributes to the stress intensity of a propagating crack, and the amount of stress intensity change can be estimated as

$$\Delta K_{rI} = -8f\left(\frac{\sqrt{\frac{1+f}{f}}r_d}{\pi}\right)^{1/2}\sigma_a \quad [10.12]$$

For a type II transgranular fracture, both the residual stresses inside the dispersant and the matrix contribute to the stress intensity, therefore it should comprise of two parts as

$$\Delta K_{rI} = \Delta K_{rI,m} + \Delta K_{rI,d} = 2\bar{\sigma}_m\left(\frac{2\lambda_m}{\pi}\right)^{1/2} + 2\bar{\sigma}_d\left(\frac{2\lambda_d}{\pi}\right)^{1/2} \quad [10.13]$$

where the λ_m is the nearest distance between the neighbouring dispersant, and λ_d is the diameter of the dispersant. The ΔK_I should have the following relationship with the fraction and size of nano-dispersants:

$$\Delta K_r = -8\left[f\left(\frac{\left(\frac{\sqrt{1+f}}{f}-1\right)r_d}{\pi}\right)^{1/2} - \left(\frac{r_d}{\pi}\right)^{1/2}\right]\sigma_a \quad [10.14]$$

As an example, the contribution of residual stress to the stress intensity is estimated for the alumina/silicon carbide nanocomposites. In these nanocomposites, the transgranular fracture should belong to type I, and only the first stress invariant in the matrix contributes to the stress intensity of a propagating crack and Eq. 10.13 should be used for the estimation. Although type II is unlikely to appear, the estimation is also included for comparison.

The contributions of the residual stress to the stress intensity of the Al_2O_3/SiC nanocomposites are presented in Fig. 10.5. For a type I transgranular fracture (Fig. 10.5(a)), the smaller the SiC dispersants are, the less they contribute to the residual tensile stress. When the fraction of the SiC dispersant is less than about

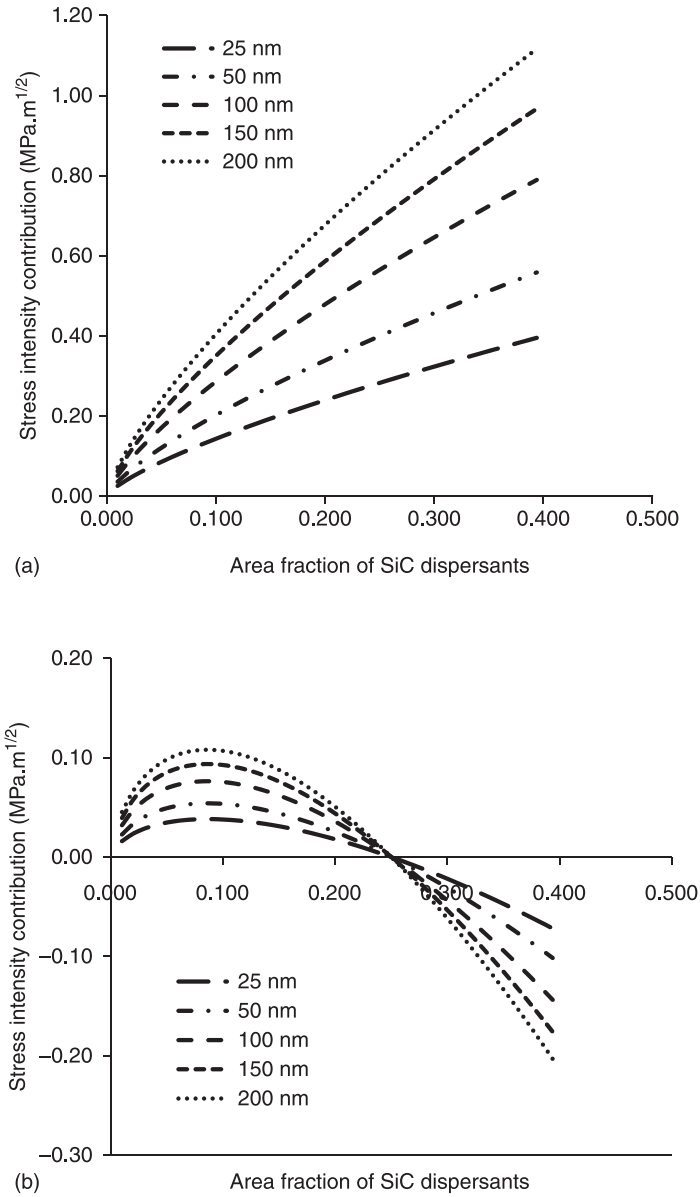

10.5 Stress intensity contribution by the residual stress inside alumina/silicon carbide nanocomposites (sizes in nm) under different transgranular fracture modes: (a) type I mode; and (b) type II mode.

5%, the contribution of the residual stress on the stress intensity is less than 0.1 MPa.m$^{1/2}$ if the size of the dispersant is smaller than 100 nm. When the size of the SiC dispersant is 200 nm, 5 and 25% dispersant can have the fracture toughness reduced by 0.17 and 0.7 MPa.m$^{1/2}$, near 0.05 and 0.2 times the fracture toughness of monolithic alumina (assuming its K_{IC} is 3.5 MPa.m$^{1/2}$), which are similar to the estimation by Levin *et al.* (1995). Therefore, the modelling results imply that to maximise the fracture toughness of alumina/silicon carbide nanocomposites, it is necessary to reduce the size of the dispersants as well as their fraction, whenever the fracture mode is transgranular. If the size and fraction of SiC dispersants are large, the stress intensity could have a reduction of up to 1 MPa.m$^{1/2}$, that is, the fracture toughness of the nanocomposites would be reduced by nearly one-third if we assume that the fracture toughness is 3.5 MPa.m$^{1/2}$ for monolithic ceramics.

For a type II transgranular fracture (Fig. 10.5(b)), the residual stress makes a very limited contribution for the stress intensity from about +0.1 to −0.2 MPa.m$^{1/2}$, regardless of the fraction and size of the dispersants. There exists a critical fraction, f, approximately 0.25, where the residual stresses have zero contribution to the stress intensity. When f is less than 0.25, the fracture toughness is reduced slightly; when f is more than 0.25, the fracture toughness is greater with the increase of the fraction of dispersants, though by only a small amount. Note, for larger dispersants, possible toughening by the geometric effect of the dispersant is not accounted for here.

Now we consider how the residual stress determines the stress intensity if the phase for the matrix is silicon carbide and the dispersant alumina, such as silicon carbide/alumina nanocomposites. The estimated results are shown in Fig. 10.6. When cracking propagation follows type I transgranular mode (Fig. 10.6(a)), the fracture toughness of the nanocomposites increases as the size and fraction of the nano-dispersants increase. If the propagation follows the type II transgranular mode, the residual stresses have very limited impact on the change of the fracture toughness.

For SiC/alumina nanocomposites, as the dispersants are under tension, type II would be the likely fracture mode, rather than type I. Whilst we have no experimental data to validate the prediction on this type of nanocomposite, the modelling does indicate that residual stress would have little impact on the fracture toughness of the nanocomposite (Fig 10.6(b). That means the fracture toughness of the nanocomposite has little change from that of monolithic SiC ceramic.

However, if the cracking propagation did follow type I transgranular mode in silicon carbide, the toughening would become significant. For instance, if 30% of alumina dispersants with a size of 50 nm were dispersed in silicon carbide, an increment of 0.38 MPa.m$^{1/2}$ could be achieved for the fracture toughness of the nanocomposite; if the size of the dispersant is changed to 400 nm with the same amount, the increment would be 1.2 MPa.m$^{1/2}$, which is approximately 50% of the fracture toughness of monolithic silicon carbide ceramics (typically 2.5 MPa.m$^{1/2}$).

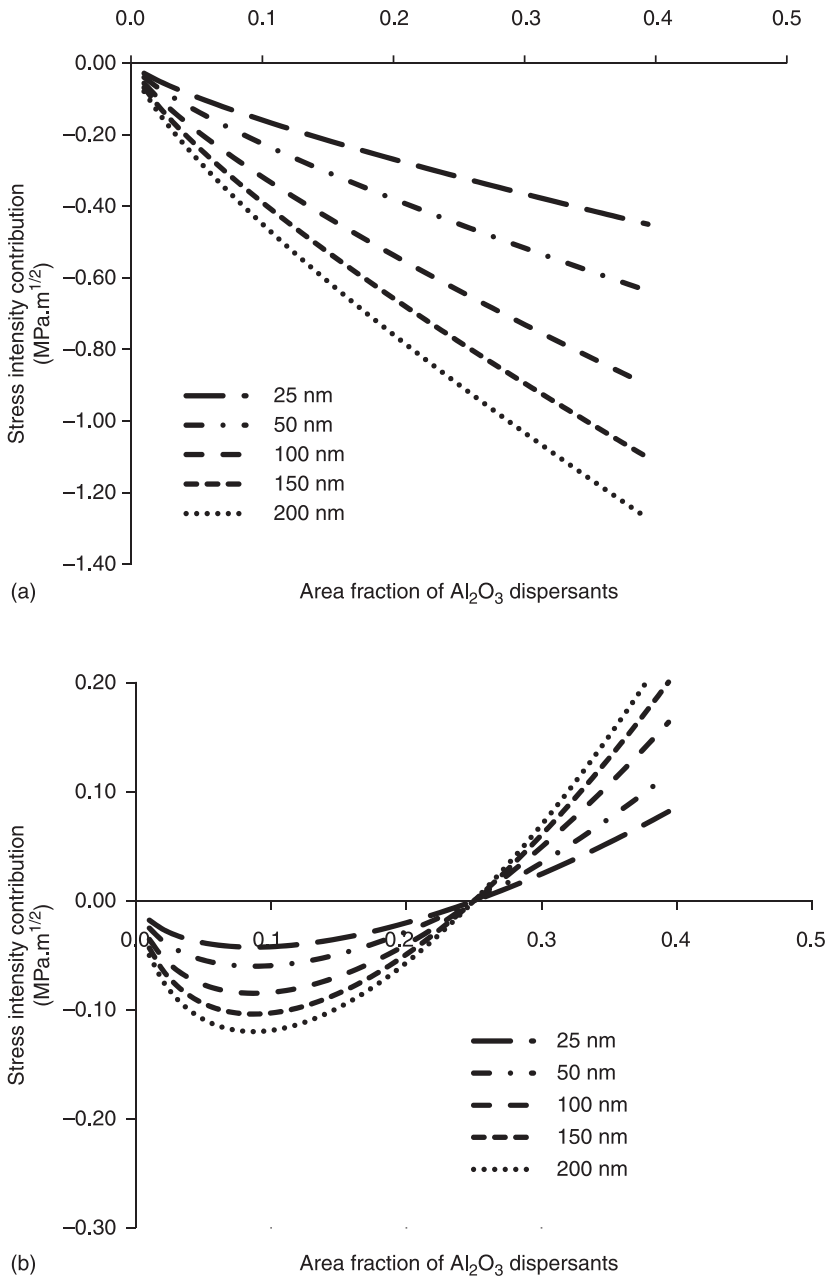

10.6 Stress intensity contribution by the residual stress inside silicon carbide/alumina nanocomposites (sizes in nm) under different transgranular fracture modes: (a) type I mode; and (b) type II mode.

10.4.2 Intergranular fracture

For an intergranular fracture, the location of the nano-dispersants needs to be considered separately. One case is where the dispersants sit right on the grain boundary, and another is where the entire dispersants sit inside the matrix grains but near the grain boundary with a distance of less than r_m from its centre. A schematic of the two types of intergranular fracture is shown in Fig. 10.7.

When nano-dispersants are distributed directly on the grain boundaries, the propagation of a crack through the grain boundary interface and the nano-dispersants should be the equivalent of a type II transgranular fracture, as discussed above. The change of the stress intensity by the existence of nano-dispersants should follow the pattern shown in Fig 10.5(b) if the dispersants are under compression, or Fig. 10.6(b) if the dispersants are under tension. For alumina/silicon carbide nanocomposites, this prediction implies that if there are enough SiC nano-dispersants sitting on the grain boundary, for example more than 0.25, the alumina grain boundaries are toughened by the residual stresses; if the fraction less than 0.25, the boundaries are slightly weakened. Considering that SiC dispersants are obstacles for the growth of alumina grains (Stearns and Harmer, 1996), it is highly likely that more SiC dispersants than average could be trapped on the grain boundaries with a fraction of more than 0.25 in alumina/silicon carbide nanocomposites. However, this point has not drawn the attentions of researchers. For the silicon carbide/alumina nanocomposites, the alumina dispersants are under tension, so a small amount of dispersants on the grain boundary could have a little increase of the fracture toughness of the grain boundary, but more than 0.25 could reduce the fracture toughness.

Now we consider a situation where the nano-dispersants sit near the grain boundary with a distance of less than the radial (r_m) of the CDM. If the radial stress out of the dispersant is tensile, the stress intensity will be increased for a crack propagating along the grain boundary and the grain boundary will be weakened. If the radial stress is compressive, the stress intensity will be reduced, and the grain boundary is toughened. Assuming that the real distance from the centre of the dispersant to the grain boundary is r_{gb}, it can be expressed by

$$r_{gb} = r_d + \phi (r_m - r_d) \qquad [10.15]$$

where ϕ is a parameter set to indicate how close the dispersant is to the grain boundary, with a numerical value between 0 and 1. A smaller ϕ indicates the dispersant is nearer to the grain boundary.

According to Eq. 10.3, r_{gb} can be further expressed as the fraction and size of the dispersant:

$$r_{gb} = \left(1 - \phi + \phi\sqrt{\frac{1+f}{f}}\right) r_d \qquad [10.16]$$

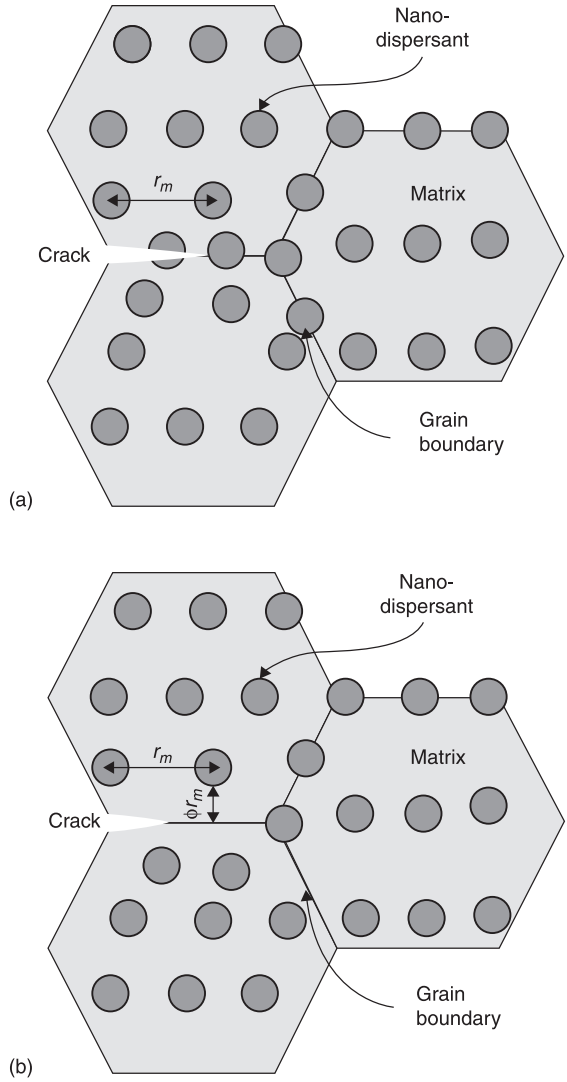

10.7 Intergranular fracture in ceramic nanocomposites: (a) crack propagates along grain boundary and through dispersant sitting right on the grain boundary; and (b) crack propagates along grain boundary with dispersant in the matrix with a distance from the grain boundary less than r_m.

For a specified ϕ, the radial stress applied on the grain boundary face can be estimated by

$$\sigma_{m,r} = \left[\frac{1+f}{\left(1-\phi+\phi\sqrt{\frac{1+f}{f}}\right)^2} - f \right] \times \sigma_a \qquad [10.17]$$

if we assume that only the projected area of the dispersant on the grain boundary is applied by the radial stress. An average radial stress is homogeneously distributed on the period length between the dispersant, i.e. $2r_m$:

$$\bar{\sigma}_{m,r} = \frac{r_d}{r_m}\sigma_{m,r} = \left[\frac{1+f}{\left(1-\phi+\phi\sqrt{\frac{1+f}{f}}\right)^2} - f \right] \times \frac{1}{\sqrt{\frac{1+f}{f}}} \times \sigma_a \qquad [10.18]$$

Then the stress intensity contribution by the radial stress can be estimated by

$$\Delta K_{gb} = 8\left[\frac{1+f}{\left(1-\phi+\phi\sqrt{\frac{1+f}{f}}\right)^2} - f \right] \times \frac{1}{\left(\frac{1+f}{f}\right)^{1/4}} \times \left(\frac{r_d}{\pi}\right)^{1/2} \sigma_a \qquad [10.19]$$

The predictions, based on alumina/silicon carbide composites, are shown in Fig. 10.8. As expected, when ϕ is close to 0, such that the nano-dispersants are close to the grain boundary, there is a significant increase in the fracture toughness of the grain boundary. The increment also increases with the size of the nano-dispersant. For a SiC dispersant with a size of 100 nm, the maximum increase can approach to about 0.6 MPa.m$^{1/2}$ at a fraction of about 0.2; for the dispersant with a size of 600 nm, it can approach to 1.0 MPa.m$^{1/2}$. For the typical fraction of 0.05, the fracture toughness of the grain boundary can be increased by about 0.5 and 0.9 MPa.m$^{1/2}$ for SiC dispersant with a size of 100 and 600 nm.

Modelling has indicated that the SiC nano-dispersants near the grain boundary of alumina make a significant contribution to the improvement of fracture toughness of the grain boundary, compared to those sitting on the grain boundary. The consequence of stronger grain boundary is that the fracture mode will be dominated by the transgranular fracture, even if the fracture in monolithic is dominated by intergranular fracture.

Equation 10.19 is used to estimate the contribution to stress intensity at the grain boundary that can be made by the alumina dispersants in silicon carbide/

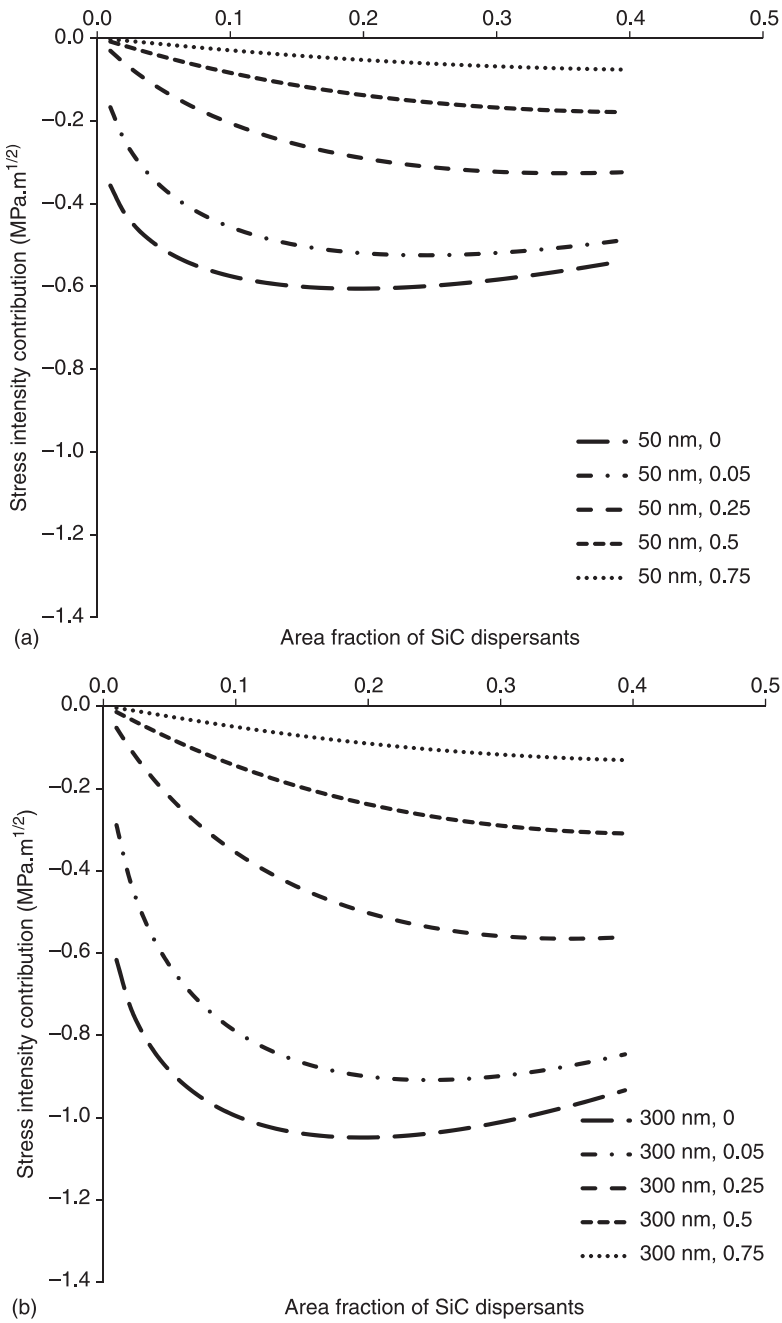

10.8 Estimated contribution to stress intensity of a crack propagating along the grain boundary by the nanodispersants near the grain boundary: (a) the size of the nanodispersant is 50 nm; ϕ values are 0, 0.05, 0.25, 0.5, 0.75; and (b) the size of the nanodispersant is 300 nm; ϕ values are 0, 0.05, 0.25, 0.5, 0.75.

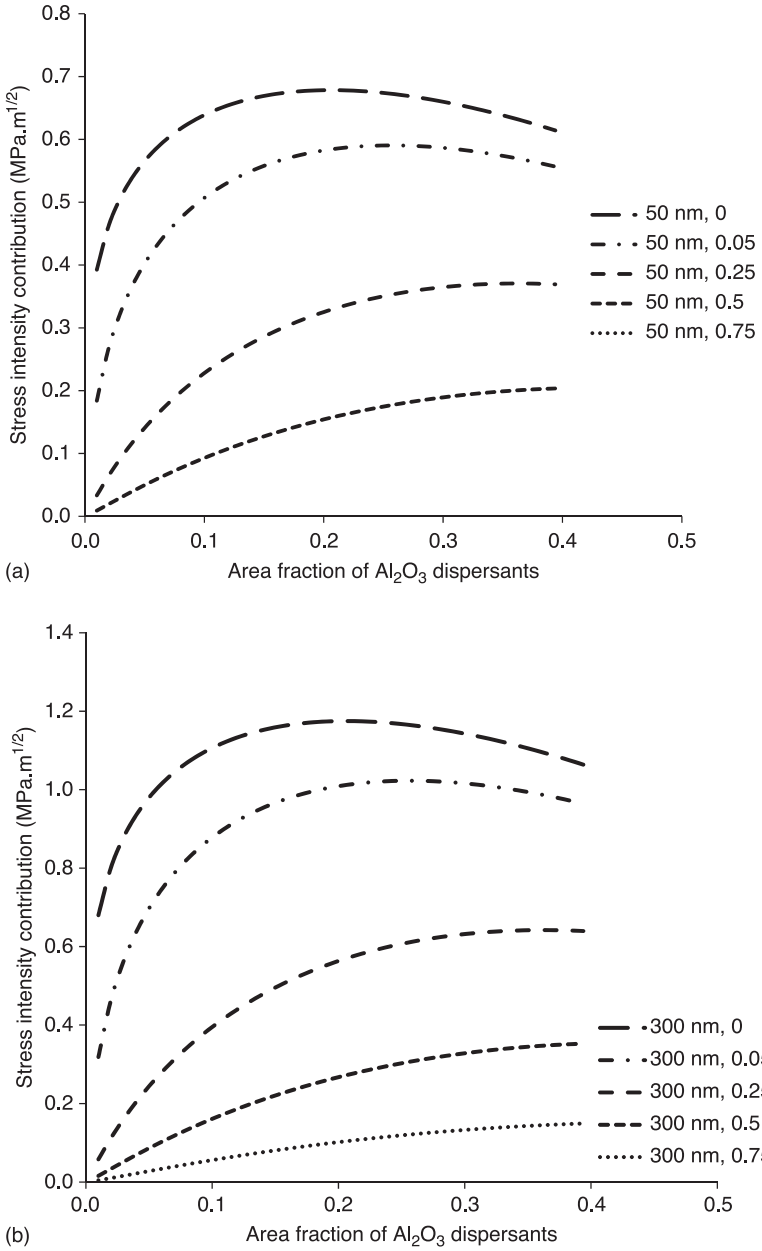

10.9 Estimated contribution to stress intensity of a crack propagating along the grain boundary by the transgranular nanodispersants near the grain boundary in SiC/alumina nanocomposites: (a) the size of the nanodispersant is 50 nm; ϕ values are 0, 0.05, 0.25, 0.5, 0.75; and (b) the size of the nanodispersant is 300 nm; ϕ values are 0, 0.05, 0.25, 0.5, 0.75.

alumina nanocomposites (Fig. 10.9). As noted, the fracture toughness of the grain boundary of silicon carbide can be reduced by up to 0.5 MPa.m$^{1/2}$, even for only 5% alumina dispersants with a size of 100 nm.

10.5 Surface residual stress

10.5.1 The origination of surface residual stress

It has long been acknowledged that machining can introduce a surface compressive residual stress to a depth of tens of microns in many brittle ceramics, such as polycrystalline alumina (Lange *et al.*, 1983), silicon nitride (Immelmann *et al.*, 1997; Johnson *et al.*, 1986; Samuel *et al.*, 1989) and zirconia (TZP) (Johnson *et al.*, 1986, Samuel *et al.*, 1989). The origin of these residual stresses can be understood by regarding a machining process as an accumulation of a large number of isolated sharp particle contact events, similar to indentation. Localised contacts in machining and abrasion cause irreversible deformation and fracture (Hockey, 1971) in brittle materials. It is the permanent deformation that leads to the residual stress. In isolation, the resultant elastic/plastic contact gives rise to a radially compressive residual stress, with tangential tension outside the plastic zone that surrounds the contact site (Marshall and Lawn, 1979). The overlap of residual stress fields from neighbouring damaged sites in a machined surface gives rise to a layer of residual compressive stress.

In alumina/silicon carbide nanocomposites, it has been experimentally demonstrated that much larger residual compression can be left on the machined surfaces (Guo *et al.*, 2011; Wu *et al.*, 1998, 2001, 2008). Unfortunately, there has been little study on other ceramic nanocomposites. Therefore, knowledge on the origination of surface residual stress is to focus on alumina/silicon carbide nanocomposites.

Machining is a necessary procedure in the fabrication of almost all modern structural ceramics, and the introduction of near-surface damage is always unavoidable. This practice not only changes the surface quality of ceramics, but can also have positive and negative impacts on the mechanical properties. To understand the development of the surface residual stress layer, it is necessary to understand the roles of the SiC nano-dispersant and its influence over the ductile deformation and the fracture damage of the alumina matrix.

Under constrained conditions, high shear stress can activate slips in alumina. The possible slip systems in Al_2O_3 crystals are summarised by Snow and Heuer (1973). The self-energy of a dislocation is proportional to the square of its Burgers vector (b^2); the magnitudes of the possible Burgers vectors are in the following order:

$$b_{1/3\langle 11\bar{2}0\rangle} < b_{1/3\langle \bar{1}101\rangle} < b_{1/3\langle \bar{1}021\rangle} < b_{\langle 10\bar{1}0\rangle} < b_{1/3\langle 21\bar{3}1\rangle} < b_{1/3\langle \bar{1}012\rangle} \quad [10.20]$$

Among these, basal slip is expected to have the lowest critical resolved shear stress. Two kinds of twin have been confirmed to operate in the plastic deformation of alumina, basal twins and rhombohedral twins.

It has been demonstrated that all of the main slip systems can be activated under tensile or hydrostatic compression loading at temperatures above the brittle-ductile transition temperature of Al_2O_3, (> ~1100 °C) (Wachtman and Maxwell, 1957). Dislocation slip is generally activated under hydrostatic compression conditions with significant shear components (Chan and Lawn, 1988). Sharp point indentation, scratching and abrasion are produced under such conditions. Twins have been widely found in single or polycrystalline alumina under loading conditions such as grinding or polishing, slide wearing, indentation or scratch, bending tests, uni-axial or hydrostatic compression, and thermal down-shock. Basal twins have been observed far more frequently than rhombohedral twins in all these cases. The thickness of the twins was found to be smaller than a few μm for basal twins and frequently down to tens of nanometres, and for rhombohedral twins, ranged from about 1 μm to about 50 μm. Resolved shear stresses for twinning were measured as 12.6 MPa between 627 and 1100 °C, and 227 MPa at 350 °C (Scott and Orr, 1983).

Due to lack of enough independent slipping systems (typically 5 required), the development of the easiest slips, like twins, can lead to cracking, either due to interactions with the grain boundaries or among themselves. When monolithic alumina is machined, the activated slips likely lead to a fracture surface and only patched ductile deformation could be maintained. Therefore, if the ductile deformation region on a machined surface is well maintained in the ceramic nanocomposites, the slips must be appropriately manipulated to mitigate the possibility of initiating large enough cracks for the dislodgment of plastically deformed regions from the surface.

Experimental evidence has shown that the existence of the SiC dispersant could nucleate dislocations from the interfaces between the dispersant and the matrix (Levin *et al.*, 1995). This is likely due to the elastic residual stress attributed to the thermoelastic misfit, which becomes apparent during cooling down from the processing temperature. These pre-existing dislocations inside the alumina could be activated by shear stress applied by machining. However, the activation of slips may not be enough to support the theory that the ductile deformation layer is less susceptible to being dislodged from the surface, as seen on machined surface of monolithic alumina. Any toughening on the grain boundaries can reduce such susceptibility (Section 10.4) that radial compression beyond the interface of nano-dispersant and matrix can significantly improve the fracture toughness. Of course, any other toughening mechanisms, such as secondary particle deflection of a crack by particles, can also have an influence; however, the size needs to be large enough (Taya *et al.*, 1990).

There is also other evidence to demonstrate that SiC nanodispersants can interfere with the slip systems, to restrain slipping along larger scales to avoid any piling-up of slips on the grain boundary or other slips to generate high enough stress concentration that leads to the development of cracking. When SiC particles are dispersed inside the alumina grains, these particles can act as obstacles to hinder dislocation motion and twin growth. As twinning has been considered to be caused by specific types of slip processes, we simplify the problem here and only consider basal slip in the following analysis.

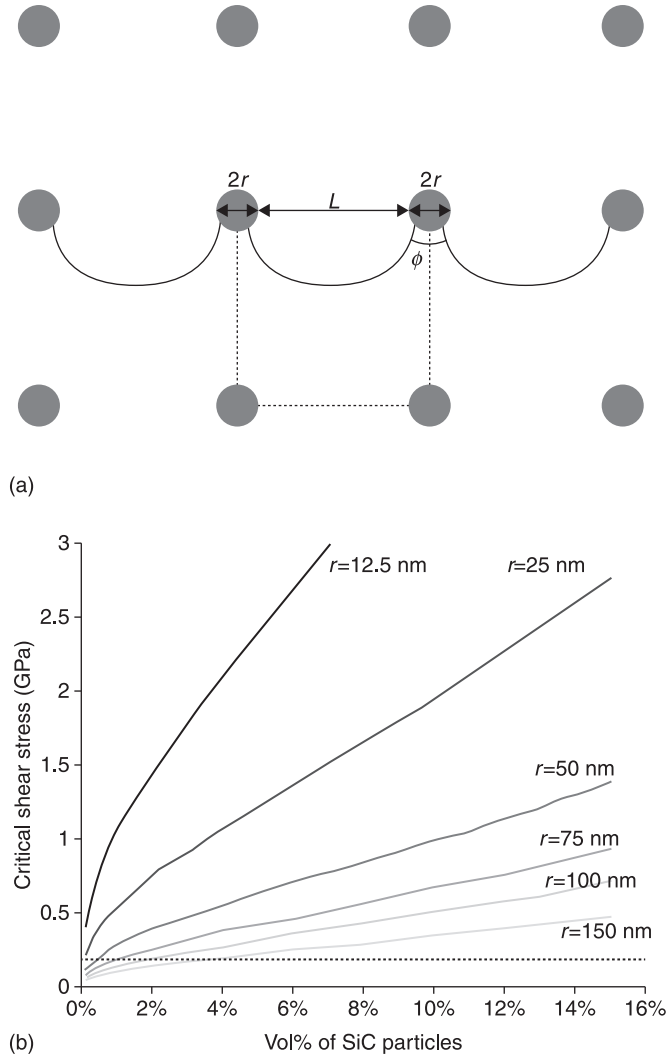

10.10 The effect of SiC particles on the obstacle of dislocation motion in alumina: (a) a simple cubic lattice arrangement of SiC particles with 2*r* as the diameter of the particles, *L* the shortest gap between two particles and ϕ_c the critical angle for dislocations to by-pass the particles under an increasing stress; (b) critical resolved shear stress versus the particle size and volume percent, for dislocations to by-pass the particles in alumina/silicon carbide nanocomposites.

Assume the SiC particles are single-sized spheres with a radius of $2r_d$, and dispersed in an alumina matrix in a simple cubic lattice with a lattice spacing $(2r_d+L)$ (Fig. 10.10a), where each SiC particle occupies one lattice point. The gap

between two particles, L, has the following relationship with the radius of SiC particles, r_d and the volume fraction, f:

$$L = \left[\left(\frac{4\pi}{3f}\right)^{1/3} - 2\right] r_d \qquad [10.21]$$

In order to by-pass SiC particles, dislocation lines assume a curved shape; the maximum shear stress needed to bow a dislocation segment into a semi-circular arc is given by the following (Green, 1998):

$$\Delta\tau = \frac{\mu b}{L}\cos\left(\frac{\phi_c}{2}\right) \qquad [10.22]$$

where ϕ_c is the critical angle for the obstacle to be by-passed by a dislocation, μ is the shear modulus of alumina, and b is the Burgers vector. For alumina, G = 150 GPa, and for basal slip, $b_{1/3<2\bar{1}\bar{1}0>} = 0.476$ nm. The maximum critical shear stress, taking $\phi_c = 0$ (appropriate for hard, impenetrable obstacles), for a dislocation to by-pass the SiC particles is

$$\Delta\tau = \frac{71.4 f^{1/3}}{(1.6 - 2f^{1/3})r} \text{ (GPa)} \qquad [10.23]$$

The modelling results shown in Fig. 10.10 (b) indicate that as little as about 1 vol% SiC particles with a diameter smaller than 150 nm can generate a dislocation motion resistance that is larger than the measured critical shear stress for basal twinning in alumina, 227 MPa at 350 °C (represented by the dashed line in Fig. 10.10(b)). For smaller particle sizes, the resistance to dislocation motion increases more rapidly with the increasing volume fraction.

10.5.2 Toughening and strengthening by the surface residual stress layer

Surface residual stress strengthening can be understood with a simple model. For all of the mechanical surface finishes, the surface residual stress is created by the plastic deformation layer near the top surface. The thickness of this layer and the stress level inside it determine the whole surface residual stress properties. Using a first approximation, we assume the inner stress inside the plastic deformation layer is a constant, as σ_0, and any compensating stress beneath the plastic deformation layer is ignored. The stress intensity for a straight crack under a normal uniform stressing along its surfaces by the plastic deformation layer is (Lawn, 1993)

$$K_I = {}^0K_I - 2\left(\frac{c}{\pi}\right)^{1/2} \int_0^w \frac{\sigma_0}{\sqrt{\left(c^2 - x^2\right)}}\, dx \qquad [10.24]$$

where K_I is the stress intensity with the plastic deformation layer, ${}^0K_I$ is the stress intensity without this layer, c is the Griffith flaw size, and w is the thickness of the plastic deformation layer. Under the critical point of fracture, Eq. 10.24 can be changed to

$$\sigma = {}^0\sigma - \kappa\sigma_0$$

$$\kappa = \frac{2\sin^{-1}\left(\frac{w}{c}\right)}{1.12\pi} \qquad [10.25]$$

where σ is the bend strength with the plastic deformation layer and ${}^0\sigma$ is the bend strength without the deformation layer. The bend strength improvement, $\kappa\sigma_0$, is proportional to the stress level inside the plastic deformation layer by a factor determined by the thickness of the plastic deformation layer, w, and Griffith flaw size, c. From the Hertzian indentation results, a stress level of 1000 to 1500 MPa for the plastic deformed layers can be calculated (Fryer et al., 2001). With $\sigma_0 = -1500$ MPa here, the strength increment for different Griffith flaw sizes are

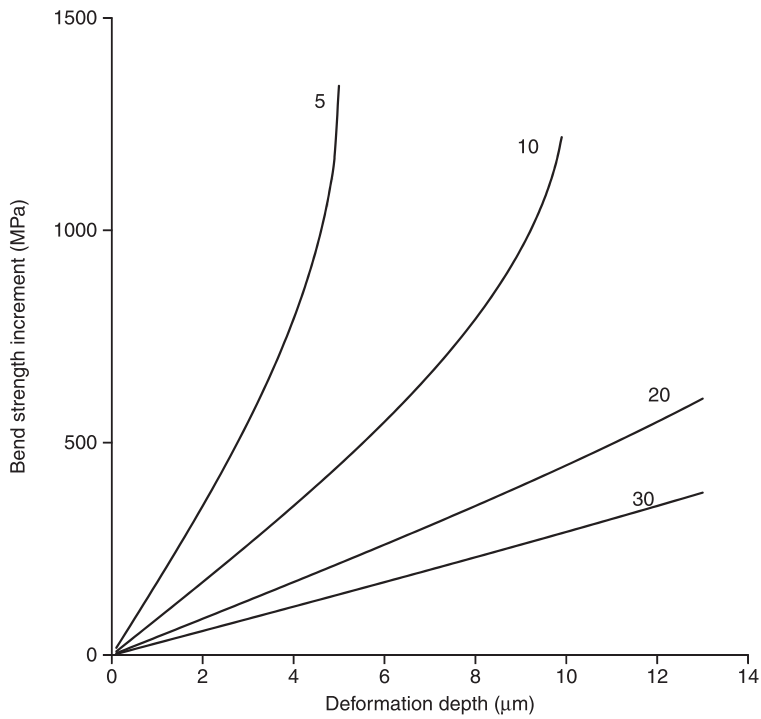

10.11 Predicted bend strength increment versus the plastic deformation depth on the surface. Numbers on the lines represent Griffith flaw size of 5, 10, 20 and 30 μm.

drawn in Fig. 10.11. For a fully plastically deformed surface, as polished by 8 μm diamond grits in the nanocomposite and 3 μm in the alumina, the deformation thickness of 1 to 3 μm, as measured by TEM, can produce a bend strength increase of about 100 to 250 MPa, if the Griffith flaw size is approximately 10 μm. If the fabrication of the nanocomposite is perfectly controlled and its Griffith flaw size is close to one grain size, say 5 μm, the maximum increase could be 550 MPa for a plastic deformation thickness of 3 μm, which is the value measured by cross-section TEM for a nanocomposite polished with 8 μm grit. For a ${}^{0}K_{Ic}$ value of 3.0 MPa.m$^{1/2}$, the maximum bend strength could reach to 1200 MPa. This bend strength is close to the reported highest three-point bend strength of the Al_2O_3/5 vol%SiC nanocomposites by Niihara (1991).

For the ground nanocomposites, assuming a Griffith flaw size of 30 μm, a maximum of about 300 MPa increment in bend strength is expected with the measured maximum plastic deformation thickness of 10 μm, based on an assumption that grinding damage does not change the size of surface critical flaw.

10.6 Future trends

Researchers have been interested in the topic of toughening and strengthening in order to explore and fully understand the potential of ceramic nanocomposites. Unfortunately, some contradictory conclusions have appeared within the literature in the past two decades. This situation can be generally attributed to the following two factors that could influence the validity of claims.

First, it is unlikely that the same microstructure is to be found in the nanocomposites of most studies. As analysed in this chapter, the internal residual stresses, and therefore the change of stress intensity, are tightly correlated to microstructural parameters such as the size of the nano-dispersants and their distribution in the matrix. Whilst most of the literature gives the averaged fraction and size of nano-dispersants, the population of nano-dispersants is likely different in regions such as inside grains, on the grain boundaries and near grain boundaries. The merit of such a distinction is clearly shown by the quantitative estimation of stress intensity that residual stress can contribute to ceramic nanocomposites.

Second, no standard method is conveniently available for all researchers to consistently and accurately quantify the fracture toughness of ceramics. The most used one is Vicker's indentation fracture (VIF). Unfortunately, the ill-defined stress field for a propagating crack makes it impossible to measure the genuine fracture toughness, particularly the value of K_{IC}, and to make any cross-sectional comparison among results from different researchers. Detail on the evaluation of VIF toughness testing is available in Quinn and Bradt (2007). For to be Al_2O_3/SiC nanocomposites, the estimation indicates that any change of K_{IC} is likely to be inside ±50% that of a monolithic alumina, which makes it a challenge when utilising an experimental method like VIF to prove that the possible changes achieved are valid.

When any contribution to fracture toughness by the geometric effect of the nano-dispersant is ignored, the quantitative estimation presented in this chapter leads to the following points that researchers in this area should consider to pay attention to:

- Explore and design novel ceramic nanocomposites. As the thermoelastic misfit is the origin of any change of fracture toughness in the ceramic nanocomposites, the selection of dispersants for a specific matrix should be able to offer such a scope.
- The volume fraction and size of dispersants have a clear impact on the residual stress and then the stress intensity. The aim of optimising these parameters includes not only improving the toughness, but also minimising the possible reduction of toughness wherever this is needed.
- Population of dispersants in regions like inside grain, on grain boundary and near grain boundary should be studied discretely. The analytic solutions presented in this chapter can provide a quantitative guideline in a certain degree.
- To maximise the toughening potential of ceramic nanocomposites, it is necessary to optimise the distribution of dispersants near/on the grain boundaries. Currently, little effort has been spared on this aspect, but results from Winn and Todd (1999a,b) indeed showed the toughening of the grain boundary achieved by large SiC dispersants distributing on the grain boundary of alumina.

Apart from internal residual stress, the contribution of surface residual stress on the mechanical property should not be ignored. It is clear that such residual stress originates from the ductile deformation and the improved sustainability of the deformed layer existing on the surface. Further study is needed to underpin how the nano-dispersants influence the ductile deformation of ceramics and the sustainability of the damage zone on machined surfaces. Regarding the damage resistance, it is worth looking at the behaviour under dynamic loading conditions and severe working environments like neutron irradiation as materials for nuclear reactors. It is speculated that nano-dispersants could provide effective enough interference on the generation of lattice defects and their motion inside crystalline materials.

10.7 References

Bamba, N., Choa, Y. H., Sekino, T. and Niihara, K. (2003) Mechanical properties and microstructure for 3 mol% yttria doped zirconia/silicon carbide nanocomposites, *Journal of the European Ceramic Society*, **23**(5), 773–80.

Borsa, C. E., Jiao, S., Todd, R. I. and Brook, R. J. (1995) Processing and properties of Al_2O_3/SiC nanocomposites, *Journal of Microscopy – Oxford*, **177**, 305–12.

Carroll, L., Sternitzke, M. and Derby, B. (1996) Silicon carbide particle size effects in alumina-based nanocomposites, *Acta Materialia*, **44**(11), 4543–52.

Chan, H. M. and Lawn, B. R. (1988) Indentation deformation and fracture of sapphire, *Journal of the American Ceramic Society*, **71**(1), 29–35.

Chen, H. J., Rainforth, W. N. and Lee, W. E. (2000) The wear behaviour of Al2O3-SiC ceramic nanocomposites, *Scripta Materialia*, **42**(6), 555–60.

Chou, I. A., Chan, H. M. and Harmer, M. P. (1996) Machining-induced surface residual stress behavior in Al_2O_3-SiC nanocomposites, *Journal of the American Ceramic Society*, **79**(9), 2403–9.

Davidge, R. W. and Riley, F. L. (1995) Grain-size dependence of the wear of alumina, *Wear*, **186**(1), 45–9.

Davidge, R. W., Twigg, P. C. and Riley, F. L. (1996) Effects of silicon carbide nano-phase on the wet erosive wear of polycrystalline alumina, *Journal of the European Ceramic Society*, **16**(7), 799–802.

Davidge, R. W., Brook, R. J., Cambier, F., Poorteman, M., Leriche, A. *et al.* (1997) Fabrication, properties, and modelling of engineering ceramics reinforced with nanoparticles of silicon carbide, *British Ceramic Transactions*, **96**(3), 121–7.

Derby, B. (1998) Ceramic nanocomposites: mechanical properties, *Current Opinion in Solid State & Materials Science*, **3**(5), 490–5.

Faber, K. T. and Evans, A. G. (1983a) Crack deflection processes. Part I: Theory, *Acta Metallurgica*, **31**(4), 565–76.

Faber, K. T. and Evans, A. G. (1983b) Crack deflection processes. Part II: Experiment, *Acta Metallurgica*, **31**(4), 577–84.

Green, D. J. (1983) Compressive surface strengthening of brittle materials by a residual-stress distribution, *Journal of the American Ceramic Society*, **66**(11), 807–10.

Green, D. J. (1998) *An Introduction to the Mechanical Properties of Ceramics*, Cambridge, Cambridge University Press.

Guo, S., Limpichaipanit, A. and Todd, R. I. (2011) High resolution optical microprobe investigation of surface grinding stresses in Al_2O_3 and Al_2O_3/SiC nanocomposites, *Journal of the European Ceramic Society*, **31**(1–2), 97–109.

Hansson, T., Warren, R. and Wasen, J. (1993) Fracture-toughness anisotropy and toughening mechanisms of a hot-pressed alumina reinforced with silicon-carbide whiskers, *Journal of the American Ceramic Society*, **76**(4), 841–8.

Hockey, B. J. (1971) Plastic deformation of aluminum oxide by indentation and abrasion, *Journal of the American Ceramic Society*, **54**(5), 223.

Hoffman, M. and Rodel, J. (1997) Suggestion for mechanism of strengthening of 'nano-toughened' ceramics, *Journal of the Ceramic Society of Japan*, **105**(12), 1086–90.

Hsueh, C. H., Becher, P. F. and Sun, E. Y. (2001) Analyses of thermal expansion behavior of intergranular two-phase composites, *Journal of Materials Science*, **36**(1), 255–61.

Hyuga, H., Jones, M. I., Hirao, K. and Yamauchi, Y. (2003) Mechanical and wear properties of Si3N4-W composites using tungsten boride powder, *Journal of Materials Research*, **18**(9), 2262–7.

Immelmann, S., Welle, E. and Reimers, W. (1997) X-ray residual stress analysis on machined and tempered HPSN-ceramics, *Materials Science and Engineering A – Structural Materials Properties Microstructure and Processing*, **238**(2), 287–92.

Ji, Y. and Yeomans, J. A. (2002) Processing and mechanical properties of Al_2O_{3-5} vol.% Cr nanocomposites, *Journal of the European Ceramic Society*, **22**(12), 1927–36.

Jiao, S. and Jenkins, M. L. (1998) A quantitative analysis of crack-interface interactions in alumina-based nanocomposites, *Philosophical Magazine A – physics of Condensed Matter Structure Defects and Mechanical Properties*, **78**(2), 507–22.

Johnson Walls, D., Evans, A. G., Marshall, D. B. and James, M. R. (1986) Residual-stresses in machined ceramic surfaces, *Journal of the American Ceramic Society*, **69**(1), 44–7.

Kara, H. and Roberts, S. G. (2000) Polishing behavior and surface quality of alumina and alumina/silicon carbide nanocomposites, *Journal of the American Ceramic Society*, **83**(5), 1219–25.

Kirchner, H. P. and Gruver, R. M. (1979) Fractographic criterion for subcritical crack-growth boundaries in hot-pressed alumina, *Journal of Materials Science*, **14**(9), 2110–18.

Komarneni, S. (1992) Nanocomposites, *Journal of Materials Chemistry*, **2**(12), 1219–30.

Kusunose, T., Sekino, T., Choa, Y. H. and Niihara, K. (2002) Fabrication and microstructure of silicon nitride/boron nitride nanocomposites, *Journal of the American Ceramic Society*, **85**(11), 2678–88.

Kusunose, T., Sung, R. J., Sekino, T., Sakaguchi, S. and Niihara, K. (2004) High-temperature properties of a silicon nitride/boron nitride nanocomposite, *Journal of Materials Research*, **19**(5), 1432–8.

Kusunose, T., Sakayanagi, N., Sekino, T. and Ando, Y. (2008) Fabrication and characterization of aluminum nitride/boron nitride nanocomposites by carbothermal reduction and nitridation of aluminium borate powders, *Journal of Nanoscience and Nanotechnology*, **8**(11), 5846–53.

Lange, F. F., James, M. R. and Green, D. J. (1983) Determination of residual surface stresses caused by grinding in polycrystalline Al_2O_3, *Journal of the American Ceramic Society*, **66**(2), C16–C17.

Lawn, B. R. (1993) *Fracture of Brittle Solids*, Cambridge, Cambridge University Press.

Lawrence, C. W., Wu, H. Z., Franco, A., Roberts, S. G. and Derby, B. (1998) Erosion resistance of hot pressed $A_{l2}O_3$/SiC nanocomposites, *Silicates Industrials*, **63**(5–6), 73–5.

Levin, I., Kaplan, W. D., Brandon, D. G. and Wieder, T. (1994) Residual-stresses in alumina-SiC nanocomposites, *Acta Metallurgica Et Materialia*, **42**(4), 1147–54.

Levin, I., Kaplan, W. D. and Brandon, D. G. (1995) Effect of SiC submicrometer particle-size and content on fracture-toughness of Alumina-SiC nanocomposites, *Journal of the American Ceramic Society*, **78**(1), 254–6.

Limpichaipanit, A. and Todd, R. I. (2009) The relationship between microstructure, fracture and abrasive wear in Al_2O_3/SiC nanocomposites and microcomposites containing 5 and 10% SiC, *Journal of the European Ceramic Society*, **29**(13), 2841–48.

Liu, Q., Han, W. and Han, J. (2010) Influence of SiCnp content on the microstructure and mechanical properties of ZrB_2-SiC nanocomposite, *Scripta Materialia*, **63**(6), 581–4.

Luo, J. and Stevens, R. (1997) The role of residual stress on the mechanical properties of Al_2O_{3-5} vol% SiC nano-composites, *Journal of the European Ceramic Society*, **17**(13), 1565–72.

Marshall, D. B. and Lawn, B. R. (1979) Residual-stress effects in sharp contact cracking, Part I: Indentation fracture-mechanics, *Journal of Materials Science*, **14**(8), 2001–12.

Marshall, D. B., Lawn, B. R. and Cook, R. F. (1987) Microstructural effects on grinding of alumina and glass-ceramics, *Journal of the American Ceramic Society*, **70**(6), C139–40.

Meschke, F., Alvesriccardo, P., Schneider, G. A. and Claussen, N. (1997) Failure behavior of alumina and alumina silicon carbide nanocomposites with natural and artificial flaws, *Journal of Materials Research*, **12**(12), 3307–15.

Miranda-Martinez, C. M., Davidge, R. W. and Riley, F. L. (1994) The reduction of erosive wear rates of advanced technical ceramics, ceramics in energy applications, *Proceedings of the Institute of Energy's 2nd International Conference*, London, 20–21 April 1994, London, The Institute of Energy, 239–52.

Mukhopadhyay, A. and Todd, R. I. (2010a) Effect of yttria doping on the microstructure and mechanical properties of Al_2O_3-$FeAl_2O_4$ nanocomposites developed via solid state precipitation, *Journal of the European Ceramic Society*, **30**(14), 2905–15.

Mukhopadhyay, A. and Todd, R. I. (2010b) Microstructure and mechanical properties of Al_2O_3 matrix nanocomposites produced by solid state precipitation, *Journal of the European Ceramic Society*, **30**(6), 1359–72.

Nawa, M., Sekino, T. and Niihara, K. (1994) Fabrication and mechanical-behavior of Al_2O_3/MO nanocomposites *Journal of Materials Science*, **29**(12), 3185–92.

Niihara, K. (1991) New design concept of structural ceramics – ceramic nanocomposites, *Journal of the Japanese Ceramic Society*, **99**(10), 974–82.

Ohji, T., Jeong, Y. K., Choa, Y. H. and Niihara, K. (1998) Strengthening and toughening mechanisms of ceramic nanocomposites, *Journal of the American Ceramic Society*, **81**(6), 1453–60.

Ortiz-Merino, J. L. and Todd, R. I. (2005) Relationship between wear rate, surface pullout and microstructure during abrasive wear of alumina and alumina/SiC nanocomposites, *Acta Materialia*, **53**(12), 3345–57.

Perez-Rigueiro, J., Pastor, J. Y., Llorca, J., Elices, M., Miranzo, P. and Moya, J. S. (1998) Revisiting the mechanical behavior of alumina silicon carbide nanocomposites, *Acta Materialia*, **46**(15), 5399–411.

Quinn, G. D. and Bradt, R. C. (2007) On the Vickers indentation fracture toughness test, *Journal of the American Ceramic Society*, **90**(3), 673–80.

Rice, R. W. and Speronello, B. K. (1976) Effect of microstructure on rate of machining of ceramics, *Journal of the American Ceramic Society*, **59**(7–8), 330–3.

Rodriguez, J., Martin, A., Pastor, J. Y., Llorca, J., Bartolome, J. F. and Moya, J. S. (1999) Sliding wear of alumina/silicon carbide nanocomposites, *Journal of the American Ceramic Society*, **82**(8), 2252–4.

Samuel, R., Chandrasekar, S., Farris, T. N. and Licht, R. H. (1989) Effect of residual-stresses on the fracture of ground ceramics, *Journal of the American Ceramic Society*, **72**(10), 1960–6.

Scott, W. D. and Orr, K. K. (1983) Rhombohedral twinning in alumina, *Journal of the American Ceramic Society*, **66**(1), 27–32.

Sekino, T. and Niihara, K. (1997) Fabrication and mechanical properties of fine-tungsten-dispersed alumina-based composites, *Journal of Materials Science*, **32**(15), 3943–9.

Sekino, T., Nakajima, T., Ueda, S. and Niihara, K. (1997) Reduction and sintering of a nickel-dispersed-alumina composite and its properties, *Journal of the American Ceramic Society*, **80**(5), 1139–48.

Snow, J. D. and Heuer, A. H. (1973) Slip systems in Al_2O_3, *Journal of the American Ceramic Society*, **56**(3), 153–7.

Soraru, G. D., Kleebe, H. J., Ceccato, R. and Pederiva, L. (2000) Development of mullite-SiC nanocomposites by pyrolysis of filled polymethylsiloxane gels, *Journal of the European Ceramic Society*, **20**(14–15), 2509–17.

Stearns, L. C. and Harmer, M. P. (1996) Particle-inhibited grain growth in Al_2O_3-SiC. Part I: Experimental results, *Journal of the American Ceramic Society*, **79**(12), 3013–19.

Steinbrech, R. W., Reichl, A. and Schaarwachter, W. (1990) R-curve behavior of long cracks in alumina, *Journal of the American Ceramic Society*, **73**(7), 2009–15.

Sternitzke, M. (1997) Structural ceramic nanocomposites, *Journal of the European Ceramic Society*, **17**(9), 1061–82.

Swanson, P. L., Fairbanks, C. J., Lawn, B. R., Mai, Y. W. and Hockey, B. J. (1987) Crack-Interface grain bridging as a fracture-resistance mechanism in ceramics. Part I: Experimental-study on alumina, *Journal of the American Ceramic Society*, **70**(4), 279–89.

Tanner, B. K., Wu, H. Z. and Roberts, S. G. (2005) Direct evidence for compressive elastic strain at ground surfaces of nanocomposite ceramics, *Applied Physics Letters*, **86**(6), 061909.

Tanner, B. K., Wu, H. and Roberts, S. G. (2006) Sub-surface damage in ground and annealed alumina and alumina-silicon carbide nanocomposites, *Journal of the American Ceramic Society*, **89**(12), 3745–50.

Taya, M., Hayashi, S., Kobayashi, A. S. and Yoon, H. S. (1990) Toughening of a particulate-reinforced ceramic-matrix composite by thermal residual-stress, *Journal of the American Ceramic Society*, **73**(5), 1382–91.

Thompson, A. M., Chan, H. M., Harmer, M. P. and Cook, R. F. (1995) Crack healing and stress-relaxation in Al_2O_3-SiC nanocomposites, *Journal of the American Ceramic Society*, **78**(3), 567–71.

Timoshenko, S. P. and Goodier, J. N. (1970) *Theory of Elasticity*, 3rd edition, New York, McGraw-Hill, Inc.

Todd, R. I., Bourke, M. A. M., Borsa, C. E. and Brook, R. J. (1997) Neutron diffraction measurements of residual stresses in alumina/SiC nanocomposites, *Acta Materialia*, **45**(4), 1791–800.

Wachtman, J. B. and Maxwell, L. H. (1957) Plastic deformation of ceramic-oxide single crystals. Part II, *Journal of the American Ceramic Society*, **40**(11), 377–85.

Walker, C., Borsa, C., Todd, R., Davidge, R. and Brook, R. (1994) Fabrication, charaterisation and properties of alumina-matrix nanocomposites, *British Ceramic Proceedings*, **53**, 249–64.

Wang, L. J., Wu, T., Jiang, W., Li, J. L. and Chen, L. D. (2006) Novel fabrication route to Al_2O_3-TiN nanocomposites via spark plasma sintering, *Journal of the American Ceramic Society*, **89**(5), 1540–3.

Wiederhorn, S. M. and Hockey, B. J. (1983) Effect of material parameters on the erosion resistance of brittle materials, *Journal of Materials Science*, **18**(3), 766–80.

Winn, A. J. and Todd, R. I. (1999a) Microstructural requirements for alumina SiC nanocomposites, *Engineering with Ceramics*, **59**, 153–64.

Winn, A. J. and Todd, R. I. (1999b) Microstructural requirements for alumina-SiC nanocomposites, *British Ceramic Transactions*, **98**(5), 219–24.

Wu, H. Z., Lawrence, C. W., Roberts, S. G. and Derby, B. (1998) The strength of Al_2O_3/SiC nanocomposites after grinding and annealing, *Acta Materialia*, **46**(11), 3839–48.

Wu, H. Z., Titchmarsh, J. M., Roberts, S. G. and Derby, B. (2000) Crack healing in an alumina/silicon carbide nanocomposite after grinding and annealing, *Nanophase and Nanocomposite Materials, Iii*, **581**, 327–32.

Wu, H., Roberts, S. G. and Derby, B. (2001) Residual stress and subsurface damage in machined alumina and alumina/silicon carbide nanocomposite ceramics, *Acta Materialia*, **49**(3), 507–17.

Wu, H. Z., Roberts, S. G., Mobus, G. and Inkson, B. J. (2003) Subsurface damage analysis by TEM and 3 D FIB crack mapping in alumina and alumina/5vol.%SiC nanocomposites, *Acta Materialia*, **51**(1), 149–63.

Wu, H. Z., Roberts, S. G. and Derby, B. (2008) Residual stress distributions around indentations and scratches in polycrystalline Al_2O_3 and Al_2O_3/SiC nanocomposites measured using fluorescence probes, *Acta Materialia*, **56**(1), 140–9.

Yoshimura, M., Ohji, T. and Niihara, K. (1997) Oxidation-induced toughening and strengthening of Y_2O_3/SiC nanocomposites, *Journal of the American Ceramic Society*, **80**(3), 797–9.

Zhao, J. H., Stearns, L. C., Harmer, M. P., Chan, H. M., Miller, G. A. and Cook, R. F. (1993) Mechanical-behavior of alumina silicon-carbide nanocomposites, *Journal of the American Ceramic Society*, **76**(2), 503–10.

Zhao, J., Ai, X. and Lu, Z. (2006) Preparation and characterization of Si_3N_4/TiC nanocomposite ceramics, *Materials Letters*, **60**(23), 2810–13.

Zhu, W. Z., Gao, J. H. and Ding, Z. S. (1997) Microstructure and mechanical properties of a Si_3N_4/Al_2O_3 nanocomposite, *Journal of Materials Science*, **32**(2), 537–42.

11

Measuring and modelling residual stresses in polymer-based dental composites

R. JAEGER and C. KOPLIN, Fraunhofer Institute for Mechanics of Materials IWM, Germany

DOI: 10.1533/9780857098597.2.293

Abstract: The relevance of residual stresses for the marginal integrity of dental fillings is well known but the level of stress is not. An overview of the experimental and theoretical studies on residual stresses in dental composites is given and the underlying phenomena of the development of residual stresses are specified. The experimental and modelling techniques for assessing residual stresses are discussed. A four-parameter-Burgers-model with conversion dependency is introduced as a case study. Examples of further applications of the modelling approach and future trends in research are given.

Key words: internal stresses, viscoelasticity, dental composites, curing shrinkage, material model.

11.1 Introduction

Polymer-based dental composites have found widespread application, since their first introduction to the market in the 1960s. Initially, the dental composites were primarily used for fillings of the incisors, since their tooth-like color offered aesthetic advantages over the commonly used amalgam fillings. In the 1990s, dental composites conquered a large share of the market for dental filling materials, partially due to the concerns regarding the mercury content of amalgam fillings. Although later studies showed that these concerns were not justified, dental composites still dominate the market. Their success is partially due to their continuous improvements, which lead to novel methods of treatment in restorative dentistry, which are nowadays named ‘adhesive dentistry’.

Before curing, dental composites are pliable substances, which can be inserted into a cavity. The curing process is typically photo-initiated. The material transforms within minutes from a paste-like substance to a hard and stiff solid material. The developers of light-curing dental composites initially faced and solved several challenges. A sufficient stability of the color of the composites required appropriate chemical formulation of the used substances. The addition of inorganic filler particles improved the poor abrasion resistance of the early composites and made their use as filling materials for molars possible.

A central problem of dental composites is their tendency to build up internal stresses during the curing process. The composites slightly shrink during the

polymerization reaction – typically by about 2 to 3% of the initial volume – and this volume change results in stresses as soon as the modulus of the material confined in the cavity increases. The stresses are sufficient to cause a separation of the filling from the cavity wall; the 'marginal integrity' of the restoration is lost. Studying the critical stresses which lead to the loss of the marginal integrity remains a challenge. They are highly localized at the edge of the filling, and the reliability of experimental and numerical approaches employed to study the failure of a filling is limited by the knowledge of the local structure of filling and tooth.

Several approaches were taken to improve the marginal stability of dental fillings. A high percentage of fillers – either inorganic fillers or pre-polymerized polymer – reduced the amount of material which undergoes shrinkage. In addition, the inorganic fillers improve the mechanical characteristics of the composites and the addition of nano-fillers facilitates the polishing of the surface of the filling. In order to improve the adhesion strength of the filling, the surface of the dental cavity is treated with bonding agents. The use of bonding agents expanded the range of applications for dental filling materials: the high adhesion strength of the filling to the tooth makes it possible to use dental composites instead of partial crowns in order to restore a tooth. Furthermore, dental composites with alternative chemical compositions were developed. In addition to acrylate-based materials, dental composites based on Ormocers® or siloranes are available.

The research efforts aiming at improving the marginal integrity of dental fillings were able to improve the reliability of the fillings. However, it has up to now not been possible to eliminate residual stresses. It is most important to point out that the continuing research efforts significantly widened the range of dental treatments where dental composites can be employed – and each new application of dental composites results in the need for a thorough evaluation and subsequent improvement of their mechanical properties.

11.2 Experimental and modelling approaches to study residual stresses in dental composites

11.2.1 Experimental techniques for measuring polymerization shrinkage and shrinkage strains

The basic cause of the residual stresses which develop in dental composites during the curing reaction is the difference between the density of the starting material and the density of the product of the chemical reaction. The resin exhibits a volumetric shrinkage during the curing reaction. The polymerization shrinkage of the material can be superimposed by a temporal thermal expansion, which is caused by the heat of the reaction and the input of heat by the light source used to trigger the photo-initiation. The polymerization reaction not only gives rise to volumetric changes of the material, it also alters its mechanical characteristics.

The increase of the molecular weight of the polymers and the subsequent transition from a sol to a gel increases the modulus and viscosity of the material. The interplay of volumetric changes, increasing stiffness and decreasing flowability of the resin in a confined geometry determines the build-up of residual stresses.

Finding parameters which are experimentally easy to determine and are suitable for the assessment of different dental composites with respect to their tendency to build up harmful internal stresses is highly desirable. The polymerization shrinkage is a parameter which is commonly used to assess the tendency of dental composites to lose the marginal integrity of a restoration. The free volumetric polymerization shrinkage can be determined with the buoyancy method. A specimen is suspended in a buoyant liquid and its apparent weight (i.e. its weight in air minus the buoyant force) is determined by an accurate balance. When the polymerization reaction is initiated, the volume and – as a consequence – the buoyancy force acting on the specimen will change. The buoyancy measurement yields the time-dependent volumetric changes caused by the thermal expansion and the polymerization shrinkage. Other techniques involve dilatometric measurements or measurements on disc-shaped, flat specimens that predominantly shrink in one dimension.

The advantage of the buoyancy method is its accuracy and repeatability compared with other techniques for determining the polymerization shrinkage. Furthermore, when employing the buoyancy method, the shrinking process is not hindered by any external constraints and no internal stresses will build up. For a systematic investigation of the polymerization shrinkage, the mechanical properties of the composite and their influence on the stress development, the maximal free shrinkage is a crucial input parameter.

Although the polymerization shrinkage is the initial cause for the internal stresses, it is not possible to rely solely on this parameter to rank different dental composites with respect to their tendency to build up internal stresses. Two dental composites with identical polymerization shrinkage but different elastic modulus will exhibit different internal stresses when cured in identical confining geometries. Furthermore, the complex dynamic character of the build-up of internal stresses cannot be described by a single parameter, which characterizes only the final state of the cured dental composite. A dental composite that predominantly shrinks in an early state of the polymerization reaction will be able to reduce internal stresses by viscous flow and elastic responses to strains at a lower elastic modulus. A dental composite with identical mechanical characteristics during the curing reaction and the same final polymerization shrinkage will exhibit much higher internal stresses if it predominantly shrinks at a later stage of the polymerization reaction. The latter dental composite has fewer possibilities to reduce internal stresses during the curing reaction.

As a consequence, experimental techniques were developed which take into account the dynamic nature of the build-up of shrinkage stresses (Watts and Cash, 1991; Watts *et al*., 2003). Measuring the kinetics of the build-up of internal

stresses involves in most cases a testing geometry, which results in a one-dimensional (1D) hindered flow of the curing composite, for example the 'bonded disk' technique. The dental composite is confined between a solid block and a glass slide. The rim of the glass slide is kept at a constant distance by a spacer. The development of shrinkage stresses can be determined by measuring the elastic deformation of the glass slide.

Stress kinetic measurements provide a better insight into the tendency of composites to build up critical stresses than the measurements of the polymerization shrinkage. However, the simplified linear testing geometry is only an approximation of the clinical situation. Testing set-ups when a dental composite is cured in a cavity provide a better representation of the clinical situation. These experimental approaches often involve studying the stresses that are present in the mold, which surrounds the cured dental composite. Based on the stresses in the mold, the magnitude of the residual stresses in the composite is estimated that cause the stresses in the surrounding material. An example of this approach is the photo-elastic studies of stresses in the vicinity of model cavities by Ernst *et al.* (2004) or other researchers (Kinomoto *et al.*, 2000).

Since the polymerization shrinkage results in a complex spatial stress distribution within the composite, and stresses typically concentrate at the margin of the filling, recent developments in experimental techniques focus on studying these highly localized stresses. Yamamoto *et al.* observed the growth of a crack into a glass ceramic mold from the interface between filling and mold under the influence of the local stresses.

The variety of dedicated experimental techniques to study residual stresses in dental composites underlines both their importance for the safe performance of dental restorations and their complexity. Since residual stresses evolve in time and show a complex spatial distribution within the filling, finite element simulations are a suitable tool to gain further insight into residual stresses.

11.2.2 Modelling techniques for the assessment of residual stresses

The development of internal stresses is determined by the progress of the polymerization reaction, which can be viewed as an 'internal clock' for the build-up of stresses. Therefore, the progress of the polymerization reaction can be used as a basis for modelling the thermal, volumetric and mechanical behaviours of dental composites during the curing process.

The underlying phenomena of the volume behaviour of dental composites can be described on a microscopic level with percolation-type models or by studying the gelation and vitrification processes that occur due increasing chain length and cross-link density. The curing process is a spatially heterogeneous process, since the polymerization is initiated at several centers. During the course of the reaction, the molecular weight of the polymers and the cross-link density increases around

these nuclei. This phenomenon results temporarily in a spatially heterogeneous structure: vitrified areas around nuclei of the polymerization reaction are embedded in a matrix, which consists of material that has not reached yet the same degree of conversion.

The 'microscopic' models yield valuable insights into fundamental aspects of the structure formation during the curing reaction. However, it is difficult or costly to use the fundamental models to describe more practical aspects of the handling of dental composites, for example the effect of different photo-initiation modes or layering techniques of dental composites on the development of internal stresses. In order to do so, a suitable approach has to be chosen, which includes physical, material and processing parameters and, as a result, is able to describe the entire process. A description of the polymerization kinetics makes it possible to include many process-specific parameters into a model – like specifics of polymerization reaction or the mode of photo-initiation. The polymerization reaction, which is the underlying mechanism of the volumetric changes, and the development of mechanical characteristics, are therefore a suitable starting point for obtaining an integral description of the process.

The majority of the currently used materials for the polymeric matrix of the dental composites are based on the viscous dimethacrylate monomer 2,2-bis[4-(2-hydroxy-3-methacryloyloxypropoxy)-phenyl] propane (BIS-GMA). BIS-GMA is in general mixed with lower viscosity monomers (e.g. diethylene glycol dimethacrylate (DEGMA) and triethylene glycol dimethacrylate (TEGDMA)), in order to adjust the viscosity of the resin and facilitate the handling of the uncured material. In addition, low concentrations of activators, initiators and stabilizers needed for the polymerization reaction are added to the resin. The resin undergoes a radical cross-linking reaction upon photo-initiation, which leads to the cured dental composite.

Different models are available in order to describe the kinetics of the polymerization reaction. Kinetic models discussed in the literature include the auto-catalytic model, the 'fully integrated mixed termination model' and the photo-thermal-kinetic model. Due to the complex chemical formulation of dental composites, all models for the reaction kinetics describe simplified systems. In general, the period between initiation and activation of monomers and the depletion of initiation and inhibitor molecules are not included into the models. Furthermore, the models do not describe the change in translucency and scattering of light into the depth during ongoing polymerization. We should add that models which describe the radical polymerization and models for the cationic polymerization of epoxy resins are similar. Due to the widespread application of epoxy resins, the modelling of the curing behaviour of epoxy resins is well documented in the scientific literature.

The auto-catalytic model describes the reaction by diffusion processes that change in time. The differential conversion equation yields results, which show a maximum value of the conversion rate in the course of the reaction. However, the

auto-catalytic model does not distinguish between the initiation phase (i.e. the time period where the system is exposed to light, which initiated the photo-reaction) and the 'dark phase' (i.e. the time period after the photo-initiation).

The 'mixed termination model' describes the development of the monomer conversion and the 'radical-activated centers'. Three rate constants are used to characterize the system. One rate constant describes the monomer conversion; two rate constants are used to describe two different termination mechanisms, the monomolecular and the bimolecular termination. It is possible to include initiation and dark phase into the model. An analytical expression for the development of the monomer conversion during initiation and dark phase can be obtained, when some simplifying assumptions regarding initiation and termination in the initiation phase are made.

A photo-thermal-kinetic model (Matias *et al.*, 2009) integrates the Lambert–Beer type absorption of the light and the thermal activation to the conversion coefficient. This approach combines the semi-mechanical description of the diffusion-driven termination processes with a phenomenological model of the self-acceleration of an autocatalytic model. This results in a complex continuum model, which can take different light intensity profiles and the heat of reaction and thermal conduction during the polymerization into account.

The modelling of the reaction kinetic requires experimental methods, which can provide the required model parameters. Several experimental techniques can be used to monitor the progress of the polymerization reaction. These techniques have in common that they average over the heterogeneous microscopic processes, which characterize the curing reaction and yield a 'macroscopic' value for the conversion. Spectroscopic techniques are able to measure the mean microscopic conversion of double bonds and to determine the material-specific degree of conversion. Spectroscopic measurements can be combined with macroscopic stress kinetic measurements (Lu *et al.*, 2004; Stansbury *et al.*, 2005).

Differential scanning calorimetry analyzes the heat of reaction generated during the curing process. When analyzing the reaction kinetics with calorimetric methods, the effect of the heat conduction on the time development of the measured signal has to be taken into account. As outlined above, measurements of the evolution of the volume of a specimen during curing can also be used to study the reaction kinetics (Koplin *et al.*, 2008). The set-up of experimental studies, which take the heterogeneous nature of the reaction into account, remains challenging. A possible approach is to compare the results of simulations on the microscopic scale with macroscopic experimental observations.

The volumetric and thermal behaviour of the curing composites can be linked to the 'relevant' monomer conversion, M(t), which is obtained from the kinetic models of the polymerization reaction. Each conversion of a monomer results in a volume shrinkage Δv and a release of thermal energy ΔE. The relevant monomer conversion reaches 100% when the material-specific maximal degree of conversion of approximately 60% is reached. A description of the development of

the specific volume of a curing composite includes the contribution of the polymer shrinkage and the thermal expansion. The thermal expansion is governed by the heat of the reaction, the heat input of the polymerization lamp and the heat dissipation to the surroundings of the material.

The development of the mechanical characteristics can be linked to the models for the reaction kinetics in a similar way, as it is possible for the volumetric behaviour of the composites. The progressing monomer conversion will result in longer polymer chains and a cross-linked structure, which is able to exhibit an elastic response to external forces. Elastic moduli and viscosities are expressed as a function of a parameter that describes the development of the reaction, for example, the time-dependent degree of cross-linking, $\Phi(t)$.

In order to describe the development of residual stresses, the models describing the volumetric behaviour need to be combined with mechanical models of the curing resins. Only small strains are observed in dental composites under typical clinical conditions. As a consequence, their mechanical behaviour can be described by linear viscoelasticity. The modelling of the mechanical behaviour therefore typically includes a combination of 'spring elements' and 'dashpot elements', which can be used to describe the elastic, viscous and viscoelastic deformation response of the material to external forces. The 'standard linear solid' model and the Burgers model (Burgers, 1935) are examples for viscoelastic models, which are used to model dental composites (Dauvillier *et al.*, 2000, 2003; Hubsch *et al.*, 1999; Hubsch and Middleton, 2000; Koplin *et al.*, 2009). The development of the mechanical characteristics of a curing resin needs to be modelled by the evolution of the corresponding parameters of the viscoelastic models. The viscoelastic models can subsequently be implemented in 3D finite-element models, which are used to simulate shrinkage stresses (Barink *et al.*, 2003; Hubsch *et al.*, 2000).

Different experimental and numerical approaches are available to study the development of the mechanical characteristics during the curing reaction. An incremental approach for the time development combined with an additive strain assumption (e.g. Maxwell + shrinkage) require that the strain rate equations have to include not only the strain and stress rates but also the rate of the increase of moduli. Although this procedure is numerically costly, it is the method of choice if the experimental characterisation involves an incremental strategy. A less costly procedure is based on an integral approach, which uses the polymerisation models discussed above as an 'internal clock' for the development of moduli and shrinkage. A versatile implementation of this concept was demonstrated by integrating the autocatalytic model with the Maxwell model or hypoelastic models (Eschl, 2002; Gambin, 2010). This approach was implemented by using a model function that links the changes in moduli with the degree of conversion. An experimentally and numerically more costly approach combines the increase of the glass transition temperature, the mechanical characteristics and the diffusion driven polymerization constant with the ongoing conversion (Blumenstock, 2003).

The experimental determination of the model parameters holds the key to good agreement between composite behaviour and model prediction. The inherent time-dependence of the viscoelastic response of polymers and the development of the mechanical characteristics of curing resins pose a challenge for the measurement of the parameters of the viscoelastic models. Polymers exhibit in general a spectrum of relaxation times. Slow relaxation processes with long time constants, like the flow of the composite, contribute to the relaxation of internal stresses. These processes are therefore important for obtaining an accurate description of the development of internal stresses. In contrast to fast relaxation processes, which can be determined by dynamic rheological measurements at high frequencies (Lee *et al.*, 2003) or ultra-sonic spectroscopy (Whiting and Jacobsen, 1980) on short time scales, the slow processes need to be probed on a time scale that is similar to the time scale on which the changes of the composite due to the curing process occur. The results of stress relaxation or creep measurements, which are suitable for characterizing slow relaxation processes, are also influenced by the progressive changes of the mechanical characteristics which are caused by the curing process. A correct determination of the parameters of the viscoelastic models therefore requires a separation of the time-dependent changes in the viscosity and modulus, which are caused by the curing process from the time-dependent viscoelastic response of the composite to external stresses or strains.

Two different strategies are available for the experimental determination for a mechanical model using a uni-directional loading set-up. Tensile tests would be preferable, since internal stresses in dental composites are typically tensile stresses and not compressive stresses. Due to the nature of the specimens (small specimens, which are initially compliant), tensile tests are challenging. The sample fixation is difficult and a possible necking of the specimens would complicate the analysis of the data. Compressive tests are far easier to realize. However, we have to assume that the results of stress relaxation and creep experiments in tension and compression in the range of the measured strains are the same.

The experimental and modelling approaches for describing the build-up of residual stresses in dental fillings, which potentially result in a loss of the marginal integrity, can be summarized as follows.

Several experimental techniques – including polymerization shrinkage measurements, stress kinetic measurements or photo-elastic studies of stresses – are available and established to obtain parameters that characterize a contributing factor to the build-up of residual stresses. In addition, experimental techniques, such as spectroscopy or differential scanning calorimetry, are available for analyzing the overall progress of the polymerization reaction, which causes the stress development. These techniques provide a valuable input for understanding the general framework in which stresses in dental fillings develop during the curing reaction. However, considering the highly localized distribution of stresses, which initiate the failure of the bond between filling and tooth, the development

of suitable experimental techniques that focus on the origin of the failure remains a formidable experimental task. Most of the established experimental techniques provide an overall value for a characteristic value related to the build-up of stresses, but fail to analyse the specific stress situation at the origin of the failure of fillings. The approach of Yamamoto who utilizes crack growth as a probe for studying highly localized stresses is a first step towards developing experimental model systems, which are able to capture the real situation under which dental fillings fail.

An alternative approach provides modelling techniques, which are able to simulate the build-up of localized stresses. A combination of suitable materials models and experimental techniques, which provide the model parameters in order to describe the behaviour of a specific dental composite, is essential for reliable results of the simulations. The experimental techniques, which are used for determining the model parameters, generally focus on measuring average 'bulk characteristics' of the material. However, finite element analysis provides a means to analyse local stresses. Again, it remains a challenge to include the local structure of the enamel to which the composite bonds or the spatially heterogeneous structure of a curing resin into the simulations.

11.3 Case study: the development of local stresses in four different dental composites

The mechanical characterization of four different dental composites and the subsequent simulation of the development of localized internal stresses are shown in order to demonstrate the complexity phenomena and their dependency on the characteristics of the specific material.

The volumetric and mechanical behaviours during the curing process of four dental composites were experimentally studied in order to derive model parameters for the materials model and the model that describes the reaction kinetics. The materials model is then used to simulate the development and the spatial distribution of residual stresses. Four dental composites were included into the study:

1. a classical, acrylate-based resin (composite 1, squares);
2. an acrylate-based 'flowable' composite, i.e. a low-viscosity resin (composite 2, triangles);
3. an Ormocer®-based composite (composite 3, crosses);
4. an experimental Ormocer®-based resin (composite 4, diamonds).

The different chemical composition of the four materials causes differences in their volumetric behaviour during the curing reaction (Fig. 11.1) and different final volumetric shrinkage values (Table 11.1). The flowable exhibits the strongest thermal expansion in the initial phase of the curing and the highest final shrinkage of the four tested composites. Flowables contain in general a higher percentage of

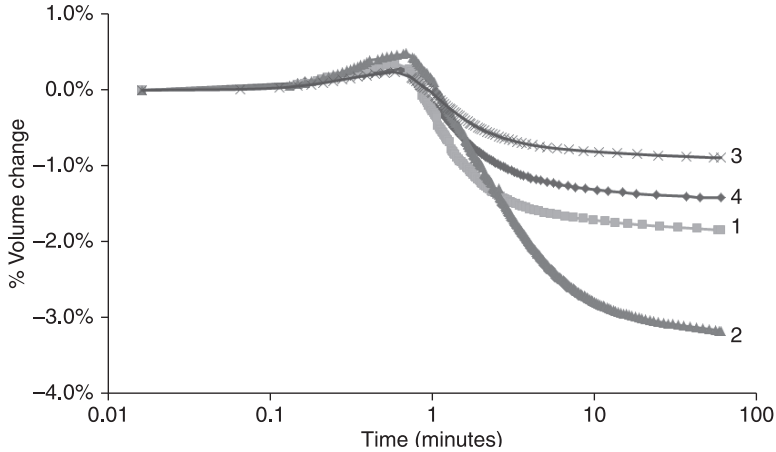

11.1 Volumetric behaviour of the four composites (1–4) measured with the buoyancy method.

Table 11.1 The polymerization shrinkage of the composites after 60 min measured by the buoyancy method

Composite	Volume shrinkage
Composite 1	–1.83% ± 0.02%
Composite 2	–3.13 % ± 0.02%
Composite 3	–1.2 % ± 0.1%
Composite 4	–1.39% ± 0.02%

low viscosity starter material compared with standard composites. The specific formulation of the flowables results in their lower viscosity, but also gives rise to a higher amount of thermal energy, which is released during the reaction and higher polymerization shrinkage. Compared with the other resins, a relatively higher percentage of the initial material polymerizes. The mechanical model requires that the thermal contribution to the volumetric behaviour is separated from the contribution to the volumetric behaviour, which is solely related to the polymerization shrinkage. Additional measurements on the thermal behaviour of the composites are carried out In order to separate the two contributions to the volumetric behaviour. Figure 11.2 shows the contribution of the polymerization shrinkage to the volumetric behaviour.

The chemical composition of the composites influence the development of the polymerization shrinkage: the two bis-GMA-based materials (composites 1 and 2) show a development in time, which differs qualitatively from the Ormocer-based resins (composites 3 and 4). A continuous decrease of the specific

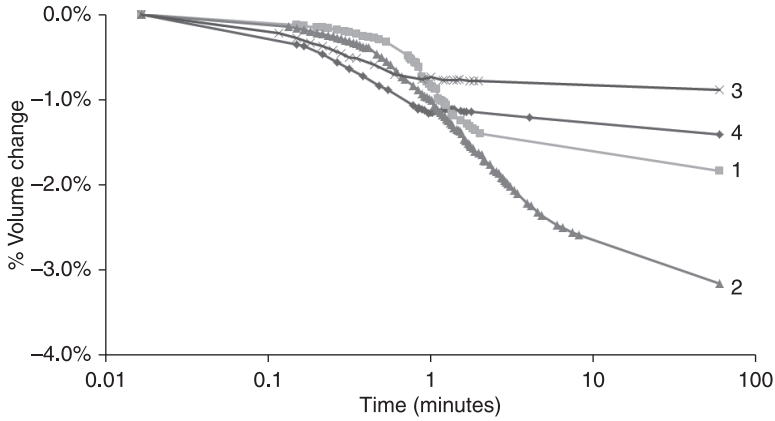

11.2 Contribution of the 'pure' polymerization shrinkage to the volumetric behaviour of the four composites (1–4).

volume is observed for all composites; composite 2 (the 'flowable' composite) exhibits the strongest shrinkage. Parameters for the 'mixed termination model' for the reaction kinetics can be determined based on the shrinkage and thermal measurements.

The mechanical characteristics of the four materials were determined by applying uni-axial compressive stresses on specimens while the curing reaction was progressing. A sequence of load steps was applied in order to study the elastic, viscous and viscoelastic response as a function of time (Fig. 11.3). These experimental data are used to determine the parameters of a Burgers model (Fig. 11.4). The progressing monomer conversion results in longer polymer chains and ultimately in a cross-linked structure. The initially compliant and viscous material transforms initially into a gel-like structure, which is able to exhibit an elastic response to external forces and ultimately into a stiff solid. The level and the duration of the load steps are adjusted to the momentary state of the specimen. In order to separate the inherent time dependency of the viscous and viscoelastic response from the development of the mechanical characteristics due to the progressing curing reaction, elastic moduli and viscosities are expressed as a function of the time-dependent degree of cross-linking, $\Phi(t)$, which varies between 0 and 1: $E = E_{max} \cdot \Phi^a$, and $\eta = \eta_{max} \cdot \Phi^b$.

The models for the polymerization kinetics used to describe the development of the polymerization shrinkage can also be used to describe the development of the degree of cross-linking, $\Phi(t)$ (Koplin *et al.*, 2009). The non-linear regression of the experimental data with the mechanical model, which includes an implicit dependence of the model parameters on the degree of cross-linking, $\Phi(t)$, yields the time dependence mechanical characteristics of the dental composite during the curing process (Fig. 11.3b). Figure 11.5 shows the strain response of the four

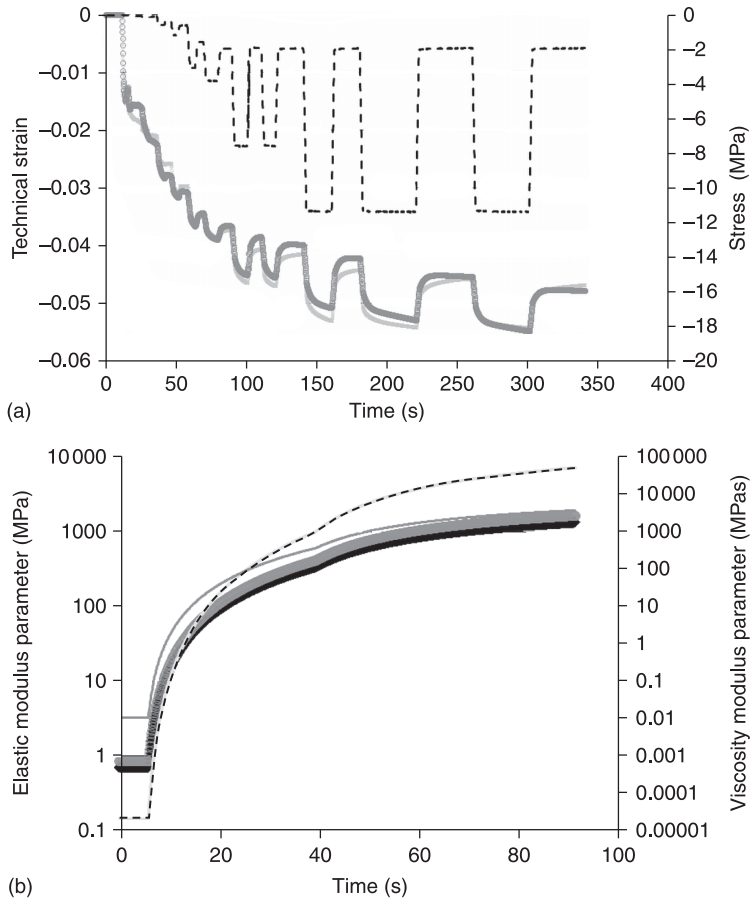

11.3 (a) Determining the mechanical characteristics of composites during the curing reaction: black dashed line, loading stress; light grey line, experimental strain response; dark grey line, model function for the strain response based on a Burgers model. (b) Time development of the model parameters of the Burgers model during the curing reaction: stiffness parameters are elastic modulus (thick black line) and viscoelastic modulus (thick grey line), but viscosity parameters are irreversible viscosity (black dashed line) and viscoelastic viscosity (dark grey thin line).

dental composites. The different strain responses of the composites in the initial phase of the curing reaction reflect their ability to reduce stresses by viscous flow.

Towards the end of the curing reaction, the compliance and the shrinkage of the composites is an indication of the build-up of internal stresses. The behaviour of the four composites differs: composite 2, the 'flowable' composite, shows a large strain response at the beginning of the curing reaction due to its rather viscous character. Towards the end of the reaction, composite 2 remains the most compliant composite. Composite 4 shows the smallest strain response of all the composites

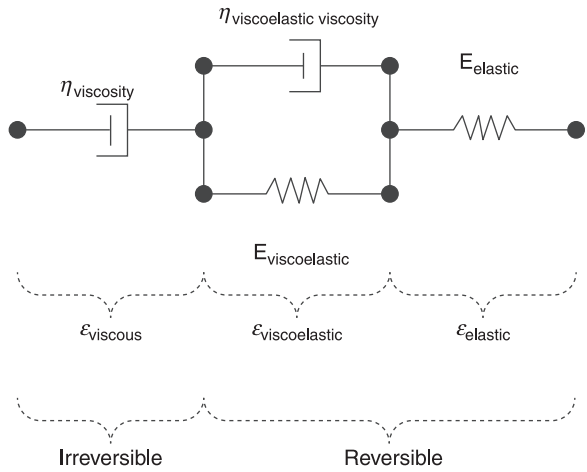

11.4 Symbolic representation of the Burgers model. Left: viscous component; right: elastic component; centre: viscoelastic components.

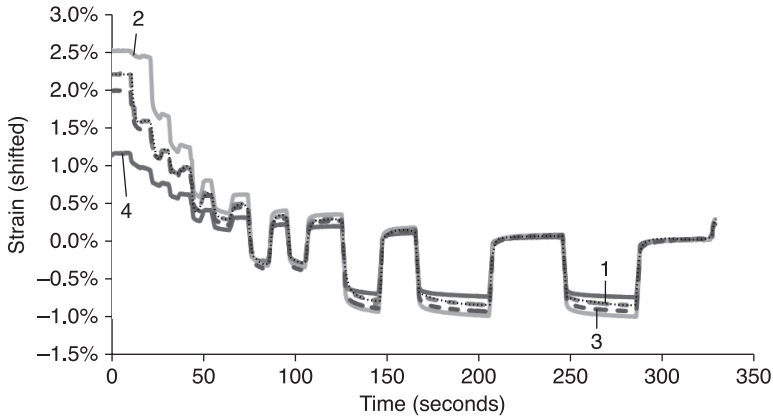

11.5 Strain response of the four composites (1–4).

during the curing reaction: it is the least compliant composite at the beginning and towards the end of the curing reaction. In order to determine the residual stresses that develop during the curing reaction, the interplay between increasing stiffness, decreasing flowability, volumetric behaviour and geometry of the cavity have to be taken into account. Finite element calculations were used to determine the temporal and spatial development of stresses and strains of a filling contained in a cylindrical model cavity. The experimental data shown above yielded the

time-dependent model parameters of a modified Burgers model, which was used to describe the mechanical behaviour of the composite.

Figure 11.6 shows the distribution of stresses and strains of composite 4 after 300 s. The stresses are localized at the 'edge' of the filling. The polymerization shrinkage results in a caving in of the filling. The finite element simulations of the stress distributions make it possible to compare the magnitude of the stresses for different composites. Figure 11.7 shows the development of the maximum values

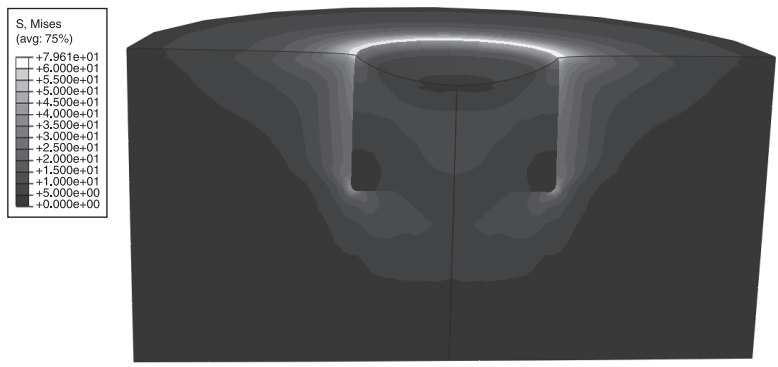

11.6 Finite element simulation of stress distribution (von Mises in MPa) and caving in of composite 1 in a cylindrical model geometry. For a better representation of the shape changes, the strains are exaggerated by a factor of 20. Black: low von Mises stress; white: high von Mises stress.

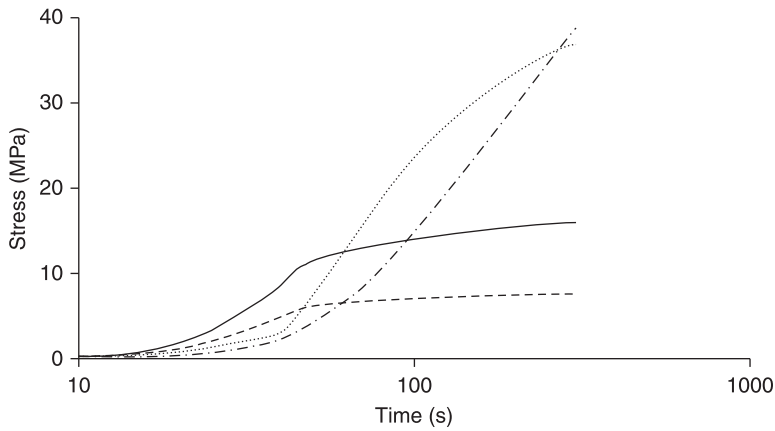

11.7 Development of the maximum values of normal stresses for the four composites. Dot-dash line: composite 1; dotted line: composite 2; dashed line: composite 3; black solid line: composite 4.

(i.e. the values at the rim of the filling) of the normal stresses and the shear stresses for the four different composites.

The analysis of the mechanical characteristics and the stress development yields some insight into the behaviour of the composites:

- Composite 2, the 'flowable' composite develops the highest stresses at the final state of the curing process. The extended flowability in the initial phase of the curing and the higher compliance of the composite, two characteristics which can result in lower residual stresses, partially compensate for the high polymerization shrinkage of the composite. Composite 1, which exhibits significantly lower polymerisation shrinkage, develops comparable stresses, since it is in general less compliant than composite 2.
- Composites 3 and 4, the two Ormocer®-based composites, exhibit a quicker increase of the stresses in an early phase of the reaction, due to a lower initial flowability. However, the increase of the stresses begins to level off at a time when the stresses of the acrylate-based composites are still increasing rapidly. The qualitatively different evolution of the polymerization shrinkage of the two types of composites results in a qualitatively different development of the residual stresses.
- The experimental composite 4 exhibits higher residual stresses than the other composites in the initial phase of the curing process and this difference remains until the end of cure. This agrees with the low flowability of this composite during the initial phase.

The order of the maximum residual stresses of the four composites at $t = 300\,s$ agrees with the order of the values for the polymerization shrinkage: the composites with the lower polymerization shrinkage also exhibit lower residual stresses. In general it would be possible that a composite with a lower polymerization shrinkage exhibits higher residual stresses than a composite with higher polymerization shrinkage. The development of the residual stresses is also determined by the development of the mechanical characteristics.

11.4 Further applications of the modelling approach

Simulations can complement experimental techniques in studying internal stresses in dental composites. Models can be used comparable to a 'magnifying glass', in order to investigate the highly localized stresses and are able to 'visualize' the development of residual stresses in time and in space. In addition, parameter studies can be used to estimate the influence of individual parameters (e.g. parameters describing the progress of the polymerization reaction or the shape of the cavity) on the build-up of stresses.

A prerequisite for reliable model prediction are suitable experimental techniques for determining the model parameters. When discussing the results of simulations, we should keep in mind that they are often extrapolations. When stress distributions

are studied by finite element calculations, results for high stresses in localized regions are frequently based on model parameters, which were derived experimentally from the bulk behaviour of the material tested often under more moderate stresses and homogeneous stress distributions. Local variations of the composite structure (fillers or variations of the material properties due to spatially inhomogeneous curing reactions), or an increased tendency to creep under high stresses, are typically not included into the models. We should proceed with the necessary caution when interpreting the results of simulations. The high potential of numerical techniques for studying phenomena, which are difficult to investigate experimentally, underlines the necessity that progress in modelling of the mechanical behaviour of composites is accompanied by progress in experimental techniques which can be used to support the results of simulations.

Keeping the limitations of the modelling approach in mind, the combination of experiments and simulations can is a useful tool for studying internal stresses in dental composites. As an example:

- Finite element simulations can be used to assess the development of internal stresses in cavities of different geometrical shape. As an example, the influence of a slanted edge of a cavity on the development of localized stresses can be determined.
- Dentists use a layering technique when preparing restoration with a larger volume. The effect of different layering techniques can be compared using finite element simulations.

An example for a layering technique is displayed in Fig. 11.8. The cavity is filled by wedge-shaped or triangular shaped layers. This technique is able to reduce the residual stresses in some regions of the filling, but will leave a small area with unaltered high critical stress. This technique used the flowability of the composite to reduce stresses by a higher shear flow.

Materials models, which include models for the reaction kinetics, can give some insight how the chemical processes (i.e. different chemical formulations of

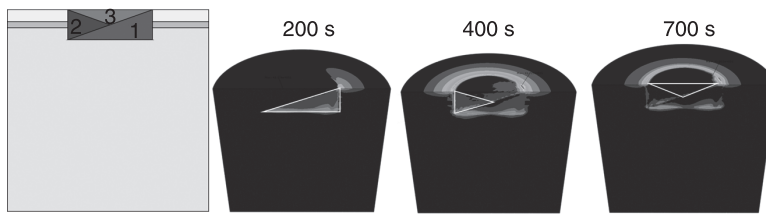

11.8 Sequence (from 1 to 3) of the triangular layers used to fill the cavity. The 1st principal stresses which build up after the curing of each filling sequence of the cavity are shown. Black: low 1st principal stress; white: high 1st principal stress.

the initial material or variations of the reaction kinetics triggered by different photo initiation modes) can influence the build-up of stresses:

- The reaction kinetics is determined by the chemical formulation of the starting material. Changes in the composition of the composite or a fundamentally different polymerization reaction will influence the development of the polymerization reaction and can influence the build-up of stresses. Parameter studies can give some insight into how changes in the chemical formulation can result in higher or lower residual stresses.
- Different modes of photo initiation can result in changes in the reaction kinetics (Koplin *et al.*, 2009). The effect of the intensity and the duration of the photo-initiation on the reaction kinetics and on the development of residual stresses can be studied with models that include a dedicated model of the reaction kinetics.

Considering the on-going development of dental composites, a combination of modelling techniques and novel experimental techniques can contribute to systematically improving the mechanical performance of the materials.

11.5 References

Barink, M., Van Der Mark, P. C., Fennis, W. M., Kuijs, R. H., Kreulen, C. M. and Verdonschot, N. (2003) A three-dimensional finite element model of the polymerization process in dental restorations, *Biomaterials*, **24**, 1427–35.

Blumenstock, T. (2003) *Analyse der Eigenspannungen während der Aushärtung von Epoxidharzmassen*, Universitätsbibliothek der Universität Stuttgart.

Burgers, J. M. 1935. Mechanical considerations, model systems, phenomenological theories of relaxation and of viscosity, *Verh. K. Akad. Wet. Amsterdam*, **15**, 5–72.

Dauvillier, B. S., Feilzer, A. J., De Gee, A. J. and Davidson, C. L. (2000) Visco-elastic parameters of dental restorative materials during setting, *J. Dent. Res.*, **79**, 818–23.

Dauvillier, B. S., Aarnts, M. P. and Feilzer, A. J. (2003) Modeling of the viscoelastic behaviour of dental light-activated resin composites during curing, *Dent. Mater.*, **19**, 277–85.

Ernst, C. P., Meyer, G. R., Klocker, K. and Willershausen, B. (2004) Determination of polymerization shrinkage stress by means of a photoelastic investigation, *Dent. Mater.*, **20**, 313–21.

Eschl, J. (2002) *Die mechanischen Eigenschaften von Stereolithographiematerialien während der Aushärtung*, Dr.-Ing., Universität Stuttgart.

Gambin, W. (2010) Visco-hypoelastic model of photo-polymerization process for small changes of temperature, *Arch. Mech.*, **62**, 379–403.

Hubsch, P. F. and Middleton, J. (2000) Asymptotic analysis of the stress field in adhering dental restorations, *J. Biomech. Eng.*, **122**, 408–15.

Hubsch, P. F., Middleton, J. and Feilzer, A. J. (1999) Identification of the constitutive behaviour of dental composite cements during curing, *Comput. Methods Biomech. Biomed. Engin.*, **2**, 245–56.

Hubsch, P. F., Middleton, J. and Knox, J. (2000) A finite element analysis of the stress at the restoration-tooth interface, comparing inlays and bulk fillings, *Biomaterials*, **21**, 1015–9.

Kinomoto, Y., Torii, M., Takeshige, F. and Ebisu, S. (2000) Polymerization contraction stress of resin composite restorations in a model Class I cavity configuration using photoelastic analysis, *J. Esthet. Dent.*, **12**, 309–19.

Koplin, C., Jaeger, R. and Hahn, P. (2008) Kinetic model for the coupled volumetric and thermal behaviour of dental composites, *Dent. Mater.*, **24**, 1017–24.

Koplin, C., Jaeger, R. and Hahn, P. (2009) A material model for internal stress of dental composites caused by the curing process, *Dent. Mater.*, **25**, 331–8.

Lee, I. B., Son, H. H. and Um, C. M. (2003) Rheologic properties of flowable, conventional hybrid, and condensable composite resins, *Dent. Mater.*, **19**, 298–307.

Lu, H., Stansbury, J. W., Dickens, S. H., Eichmiller, F. C. and Bowman, C. N. (2004) Probing the origins and control of shrinkage stress in dental resin composites. Part II: Novel method of simultaneous measurement of polymerization shrinkage stress and conversion, *J. Biomed. Mater. Res. B Appl. Biomater.*, **71**, 206–13.

Matias, J. M., Bartolo, P. J. and Pontes, A. V. (2009) Modeling and simulation of photofabrication processes using unsaturated polyester resins, *Journal of Applied Polymer Science*, **114**, 3673–85.

Stansbury, J. W., Trujillo-Lemon, M., Lu, H., Ding, X., Lin, Y. and Ge, J. (2005) Conversion-dependent shrinkage stress and strain in dental resins and composites, *Dent. Mater.*, **21**, 56–67.

Watts, D. C. and Cash, A. J. (1991) Determination of polymerization shrinkage kinetics in visible-light-cured materials: methods development, *Dent. Mater.*, **7**, 281–7.

Watts, D. C., Marouf, A. S. and Al-Hindi, A. M. (2003) Photo-polymerization shrinkage-stress kinetics in resin-composites: methods development, *Dent. Mater.*, **19**, 1–11.

Whiting, R. and Jacobsen, P. H. (1980) A non-destructive method of evaluating the elastic properties of anterior restorative materials, *J. Dent. Res.*, **59**, 1978–84.

Yamamoto T, Nishide A, Swain MV, Ferracane JL, Sakaguchi RL, Mornoi Y. Contraction stresses in dental composites adjacent to and at the bonded interface as measured by crack analysis. Acta Biomaterialia 2011; 7(1): 417–23.

12

Understanding residual stresses in thick polymer composite laminates

F. DAI, Harbin Institute of Technology, People's Republic of China

DOI: 10.1533/9780857098597.2.311

Abstract: The process conditions of thick thermoset matrix composite laminates are complicated by adverse effects involving large out-of-plane temperature gradients and internal heat generation. This chapter introduces the method to analyse the transient heat transfer and the curing process of thick laminates, by combining the finite element method with thermo-chemical and self-consistent field micro-mechanical models. The methods of measurement of residual stresses in thick laminates are introduced. Some experimental results are demonstrated. The techniques discussed are applicable not only to the study of thermal residual stresses, but also stresses induced by environmentally induced internal stresses, such as caused by moisture, temperature gradient, solvents, etc.

Key words: thick composite laminate, temperature gradient, residual stress, curing process.

12.1 Introduction

Thick composite laminates have found several applications in aerospace, military, marine and civil structures. Future growth in the usage of thick composites relies heavily on the successful fabrication of parts with dependable quality and at low cost. Unfortunately, process conditions for thick composites are not well defined. The manufacturer's recommended cycle (MRC) is often inadequate for thick composites, because of adverse effects involving large out-of-plane temperature gradient and mid-plane heat generation. Processing concerns associated with thermosetting composites have become increasingly important for components of appreciable thickness. The most common problem is an increase in temperature resulting from the resin exothermic chemical reaction (polymerization) that may raise internal temperatures to levels inducing material degradation. A second concern is the complex gradients in temperature and degree of cure accentuated by increased thickness (Guo *et al.*, 2005; Patricia *et al.*, 2007a,b). Examples can be seen in Fig. 12.1 and 12.2. The complex distribution can lead to unexpected residual deformation (Dai and Zhang, 2007).

There have been many studies on the curing of thick thermoset matrix composites. Oh and Lee (2002) studied the cure cycle for glass/epoxy composite laminate using three-dimensional (3D) finite element (FE) analysis. An optimized cure cycle with the cooling and reheating steps was developed by minimizing the

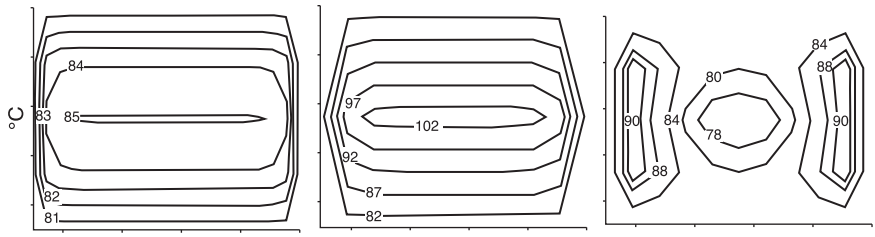

12.1 The distribution of temperature on the mid-plane for different thickness laminates.

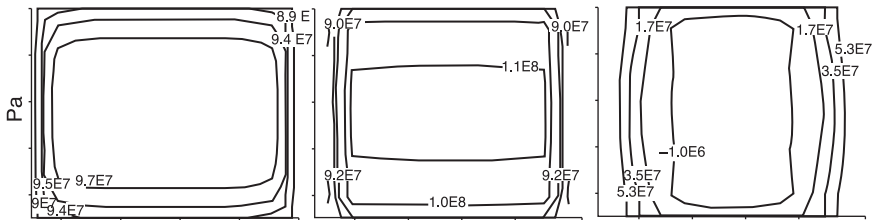

12.2 The distribution of transverse stress on mid-plane for different thickness laminates.

objective function to reduce the temperature overshoot in the composite. Bogetti and Gillespie (1991) developed a two-dimensional (2D) cure simulation analysis of thick thermoset composites and predicted the temperature and degree of cure distributions within an arbitrary cross-sectional geometry. Ciriscioli *et al.* (1992) measured the temperature, ionic conductivity and compaction in 16~200 ply thick graphite/epoxy laminates. They also compared the data to the results calculated by the Loos–Springer CURE model (Loos and Springer, 1983).

Twardowski (1993) compared the experimental temperature profiles of a thick part with the results predicted by a one-dimensional (1D) computer simulation, from which the effect of initial degree of cure and consolidation were investigated. Hojjati and Hoa (1994) constructed model laws based on dimensionless parameters for cure of thermoset composites and predicted the temperature and degree of cure distributions of a thick composite based on the model. Michaud *et al.* (1998, 2002) predicted the cure behavior of a thick vinyl ester matrix composite manufactured by resin transfer molding and investigated the effect of cure inhibitors and fibers on the cure kinetics. White and Kim (1996) developed the stage cure technique for fabricating thick composites and investigated the effect of the stage cure on the mode I interlaminar fracture toughness and shear strength. Yi *et al.* (1997) conducted the transient heat transfer FE analysis by assuming thermal properties such as density, heat capacity and thermal conductivity as a function of temperature and degree of cure. Kim and Lee (1997) developed an autoclave cure cycle with cooling and reheating steps using finite difference

analysis and experiment. They showed that the developed cure cycle was effective for the reduction of temperature overshoot.

Blest (1999) studied the modeling and simulation of resin flow, heat transfer and the cure of multiplayer thermoset composite laminates during an autoclave processing. They showed the approximate validity of the model by comparing the numerical results with the known experimental data. Joshi *et al.* (1999) presented a procedure to use a general-purpose FE package for cure modeling and demonstrated the modeling of cure of a thick laminate, a honeycomb sandwich panel and an I-beam. Martinez (1991) used a 1D finite difference analysis and an error function defined by the temperature difference between the target temperature and the laminate temperature to calculate the time-optimal autoclave cure schedule with minimum error. Park and Lee (2001) developed a 2D cure simulation by a finite element method (FEM). They calculated through-the-thickness temperature distributions of composite structures including mandrels. Melnik (2002) studied the thermoset composite applied to biochemical engineering. He studied the thermal degradation by heat transfer and cure kinetics. Loos and Springer (1983) developed a 1D model to simulation the cure process of a flat-plate by solving the governing equation using the finite difference method. Rai and Pitchumani (1997) have used mixed PDE/ODE methods to solve for coupled temperature and cure fields.

The residual stress analysis is necessary if we want to evaluate how these gradients of temperature and degree of cure influence the quality of parts. Chen *et al.* (2001) used a viscoelastic micro-mechanical model to study the effect of the cooling rate on the curing process induced residual stress. Johnston *et al.* (2001) proposed a plane strain FE model for simulation of the process-induced deformation during autoclave processing. Kheir *et al.* (2002) investigated the influence of autoclave pressure on curing stresses in carbon/epoxy laminates and showed that the initial size of laminates and autoclave pressure can significantly affect the residual deformation. The resin volume shrinkage is another important mechanism contributing to process-induced stress, besides thermal expansion mismatch. The effective mechanical properties of resin can change drastically when associated with the cross-link polymerization reaction. Therefore, thermal and chemical strains and the cure-dependent material properties should be included in the analysis of residual stress. It was pointed out that the complex spatially varying thermal and degree of cure gradients can lead to residual stress development greatly. White and Hahn (1992a,b) employed a 2D simulation and viscoelastic model to study the curing process and residual stress. Teplinsky and Gutman (1996) combined the 1D simulation with incremental laminate theory to predict the process-induced stress.

For determination of curing residual stresses, possible techniques are embedded sensors (Breglio *et al.*, 2000; Leng and Asundi *et al.*, 2002; Mulle *et al.*, 2009; Wu *et al*, 2004), deep-hole (Batemana *et al.*, 2005; Kim and Lee, 2007), first-ply failure and curvature measurements, etc. For the *in situ* and continuous monitoring

of residual strains development, some interesting results from interrupted cures of asymmetrical laminates are presented (Garstka *et al.*, 2007; Wisnom *et al.*, 2006). However, this method does not seem adapted to the autoclave process, because of the time required to remove and cool the specimens. Other techniques are used, such as fiber sensors (Garstka *et al.*, 2007; Karalekas *et al.*, 2008; Khoun *et al.*, 2011), dielectric analysis (Bartolomeo *et al.*, 2000) or electric gages instrumentation. Some studies showed that the chemical phenomena of contraction are present, but that their influence on the laminate properties is badly identified. A resent review of experimental techniques for residual stress can be found in Patricia *et al.*, (2007a,b).

In this chapter, the developments of temperature field of thick thermoset matrix laminates are measured and compared with the numerically calculated results. The finite element formulation of the transient heat transfer problem is carried out for polymeric matrix composite materials from the heat transfer differential equations, including internal heat generation produced by exothermic chemical reactions. Next, it focuses on developing a 3D FE program to simulate the curing process and analyze process-induced stress within thick section parts. A 3D FE formulation is developed to avoid limitations of 1- and 2D analyses. The self-consistent field micro-mechanics model is used to predict cure dependent mechanical properties. Then the methods of measurement of residual stresses are introduced, such as Fiber Bragg Grating (FBG) monitoring and the deep-hole method. Some experimental results are demonstrated.

12.2 Modelling the curing process in thick laminated composites

Because general-purpose FE modelling packages have well-developed pre- and post-processors, it is beneficial if they can be used for the cure model. The objective of this study is to gain a fundamental understanding of the cure process unique to thick composite laminates. One-dimensional transient heat transfer FE analysis during autoclave cure cycle for a 2 cm thick carbon fiber/epoxy laminate is analyzed by commercial FE software, ANSYS. The simulation of the cure process accounts for thermal and chemical interactions associated with the curing process. The FE model, composed of the tooling and vacuum bag assembly as well as the laminate, is used to investigate the effect of the geometry of the tooling and bagging materials on the temperature profiles.

12.2.1 Thermo-chemical model

It is assumed that the convective heat transfer effect by the resin flow is negligible and the resin and fiber are at the same temperature at any specific time. With these assumptions, the 1D model of heat transfer, including the governing equation, can be expressed as (Hojjati and Hoa, 1994; Loos and Springer, 1983; Yi *et al.*, 1997)

$$\rho C_P \frac{\partial T}{\partial t} = \frac{\partial}{\partial z}\left(k\frac{\partial T}{\partial z}\right) + \rho H_u \frac{d\alpha}{dt} \quad [12.1]$$

$$\frac{d\alpha}{dt} = g(\alpha, T) = K(T)\alpha^m (1-\alpha)^n \quad [12.2]$$

$$K(T) = A\exp\left(-\frac{E}{RT}\right) \quad [12.3]$$

$$m = C_1 \exp(-C_2 T) \quad [12.4]$$

$$n = C_3 \exp(-C_4 T) \quad [12.5]$$

where T is temperature; ρ, C_p and k are density, specific heat and thermal conductivity of composites, respectively; $d\alpha/dt$ is the cure rate; H_u is heat of reaction generated during dynamic scanning; A is pre-exponential factor; E is activation energy; R is universal gas constant; and C_1, C_2, C_3 and C_4 are constants, respectively.

The cure kinetic model of the carbon/epoxy prepreg (T300/HD03) was obtained using the PE DSC-7 (Fig. 12.3). The isothermal scanning tests were conducted with constant temperatures of 413, 423, 433, 443, 453, 463 and 473 K. The dynamic scanning tests were also performed at a constant rate of 10 K/min. Figure 12.1 shows a comparison between the rate of heat generation measured

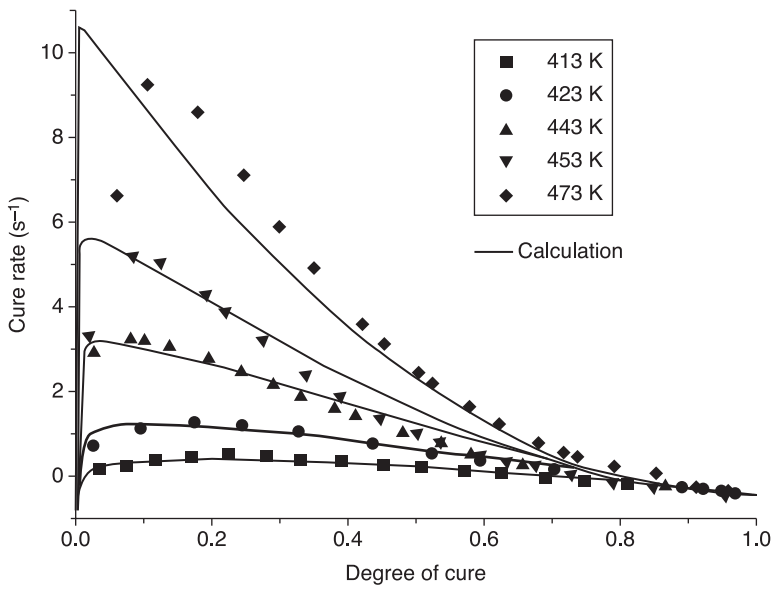

12.3 Rate of heat generation of T300/HD03 prepreg during the isothermal scanning.

Table 12.1 Cure kinetic parameters of the carbon/epoxy composite

Constant for m	C_1	1.879e10	Pre-exponential factor	A (min^{-1})	2.263e7
	C_2	6.06e-2	Activation energy	E (J/mol)	5.682e4
Constant for n	C_3	1.94e-3	Heat of reaction	H_u (J/g)	313.84
	C_4	–1.49e-2			

during the isothermal scanning and those calculated by the cure kinetic model of Eq. 12.2. The developed cure kinetic model agreed well with the experimental results. The cure kinetic parameters of the carbon/epoxy composites are presented in Table 12.1.

The internal heat generation rate was calculated using Eqs 12.2 to 12.5. The simple rule of mixture was assumed to be valid for the physical and thermal properties of the composite such as density, specific heat and longitudinal conductivity. The transverse conductivity was calculated using the following Tsai–Halpin model:

$$\frac{k}{k_m} = \frac{k_f + k_m + \left(k_f - k_m\right)V_f}{k_f + k_m - \left(k_f - k_m\right)V_f} \qquad [12.6]$$

where k_m is the conductivity of resin; k_f is the fiber conductivity in the transverse direction of fiber; and V_f is the fiber volume fraction of the composite.

12.2.2 One-dimensional finite element formulation

The temperature profiles in the laminate during the cure process can be obtained through a transient heat transfer analysis, including the internal heat generation. The combined thermal and cure problem for a given temperature cycle, $T_\infty(t)$, is referred to as the primal thermo-chemical analysis. We will derive the FE formulations for the thermal problem and cure problem separately, and then combine these two to obtain the complete FE equations for the thermo-chemical model. We will solve the temperatures and degree of cure simultaneously and accurately.

The FE formulation of Eq. 12.1 is well documented. We choose the FE shape functions $\boldsymbol{N}(z)$ for nodal solution vectors $\mathbf{T}$ (temperature) and $\boldsymbol{\alpha}$ (degree of cure), and approximate the nodal solutions as

$$T(z,t) \approx \boldsymbol{N}\{z\}\,\mathbf{T}(\mathbf{t}) \qquad \alpha(z,t) \approx \boldsymbol{N}\{z\}\,\boldsymbol{\alpha}(\mathbf{t}) \qquad [12.7]$$

So the FE equations for an element are obtained as

$$\left[\mathbf{K}_\mathbf{T}^\mathbf{e} + \mathbf{K}_\mathbf{h}^\mathbf{e}\right]\left\{T^e\right\} + \left[\mathbf{M}_\mathbf{T}^\mathbf{e}\right]\left\{\frac{\partial \mathbf{T}^\mathbf{e}}{\partial t}\right\} = \left\{\mathbf{F}^\mathbf{e}\right\} + \left\{\mathbf{Q}^\mathbf{e}\right\} \qquad [12.8]$$

$$\mathbf{M}_\alpha^\mathbf{e}\left\{\frac{d\boldsymbol{\alpha}}{dt}\right\} = \left\{\mathbf{F}_\alpha^e\right\} \qquad [12.9]$$

with

$$\mathbf{K}_{\mathbf{T}}^{\mathbf{e}} = \int_z \left(\frac{\partial \mathbf{N}^{\mathrm{T}}}{\partial x} k_x \frac{\partial \mathbf{N}}{\partial x} \right) dz \quad \mathbf{K}_{\mathbf{h}}^{\mathbf{e}} = \mathbf{N}^{\mathrm{T}} h \mathbf{N} \quad \mathbf{M}_{\mathbf{T}}^{\mathbf{e}} = \int_z \mathbf{N}^{\mathrm{T}} \rho C_p \mathbf{N} dz \quad \mathbf{M}_{\alpha}^{\mathbf{e}} = \int_z \mathbf{N}^{\mathrm{T}} \mathbf{N} \, dz$$

$$\mathbf{F}^{\mathbf{e}} = \int_z \mathbf{N}^{\mathrm{T}} \rho H_u \frac{d\alpha}{dt} dz \qquad \mathbf{F}_{\alpha}^{\mathbf{e}} = \int_z \mathbf{N}^{\mathrm{T}} \frac{d\alpha}{dt} dz \quad \mathbf{Q}^{\mathbf{e}} = hT_{\infty}$$

where $\mathbf{K}_{\mathbf{T}}^{\mathbf{e}}$ and $\mathbf{K}_{\mathbf{h}}^{\mathbf{e}}$ are element conductance and element convection matrices due to conduction and convection, respectively; $\mathbf{M}_{T}^{\mathbf{e}}$ and $\mathbf{M}_{\alpha}^{\mathbf{e}}$ are the element capacitance matrices, respectively; and $\mathbf{F}^{\mathbf{e}}$,$\mathbf{F}_{\alpha}^{\mathbf{e}}$ and $\mathbf{Q}^{\mathbf{e}}$ are heat load vectors arising from internal heat generation, cure reaction and surface convection, respectively. Since both $\mathbf{F}^{\mathbf{e}}$ and $\mathbf{F}_{\alpha}^{\mathbf{e}}$ depend on $\mathbf{T}$ and $\boldsymbol{\alpha}$, Eqs 12.8 and 12.9 comprise a transient coupled problem.

Assembly of the elemental contribution and combined with Eq. 12.9 results in the global system equations:

$$[\mathbf{K}]\boldsymbol{U} + [\mathbf{M}]\dot{\boldsymbol{U}} = \mathbf{F} \qquad [12.10]$$

with

$$\mathbf{M} = \begin{bmatrix} \mathbf{M}_{\mathbf{T}} & -\rho \mathbf{H}_{\mathbf{u}} \mathbf{M}_{\alpha} \\ \mathbf{0} & \mathbf{M}_{\alpha} \end{bmatrix} \quad \mathbf{K} = \begin{bmatrix} \mathbf{K}_{\mathbf{T}} + \mathbf{K}_{\mathbf{h}} & \mathbf{0} \\ \mathbf{0} & \mathbf{0} \end{bmatrix} \quad \boldsymbol{U} = \begin{Bmatrix} \mathbf{T} \\ \boldsymbol{\alpha} \end{Bmatrix} \quad \boldsymbol{F} = \begin{Bmatrix} \mathbf{Q} \\ \mathbf{F}_{\alpha} \end{Bmatrix}$$

To solve Eq. 12.10, the time domain is discretized using the θ method. The solution at the next time step uses:

$$\boldsymbol{U}^{n} = \boldsymbol{U}^{n-1} + \left[(1-\theta)\dot{\boldsymbol{U}}^{n-1} + \theta \dot{\boldsymbol{U}}^{n} \right] \Delta t \qquad [12.11]$$

where $\boldsymbol{U}^{n}$ and $\boldsymbol{U}^{n-1}$ are the solution at the previous and current time steps respectively; and Δt is the time step. The parameter θ is an adjustable parameter varying between 0 and 1 and the algorithm depends on the chosen value of θ. If θ is between 0.5 and 1, the integration procedures are known as implicit methods. Equation 12.10 can be discretized as

$$\left[\frac{\mathbf{M}}{\Delta t} + \theta \mathbf{K}^{\mathbf{n}} \right] \boldsymbol{U}^{n} = \left[\frac{\mathbf{M}}{\Delta t} + (\mathbf{1} - \theta) \boldsymbol{K}^{n-1} \right] \boldsymbol{U}^{n-1} + \theta \mathbf{F}^{\mathbf{n}} + (\mathbf{1} - \theta) \mathbf{F}^{\mathbf{n-1}} \qquad [12.12]$$

Since nonlinearities occur from thermal properties and internal heat generation, which are dependent on temperature and degree of cure, an iterative procedure is necessary to solve the system of equations. The Newton–Raphson algorithm, due to its quadratic convergence characteristics, is employed and the tangent stiffness matrix is updated at each iteration step.

12.2.3 Curing process experiments to validate the model

Experiments were conducted to verify the validation of simulation as well as to investigate the effectiveness of the convectional cure cycle recommended by the prepreg manufacturer. The unidirectional carbon/epoxy prepreg used in this

work was T300/HD03. The laminate was stacked to the dimensions of 300 mm × 300 mm × 20 mm. After the stacked prepreg was paced on the tool plate (thickness = 15 mm) and covered by the release film, the caul plate (thickness = 5 mm) and dams (thickness = 25 mm) covered by the release film were placed on the top and four edges of the laminate. Then the assembly was bagged with a standard nylon bagging film and cured in an autoclave using the convectional cure cycle. The typical lay-up of autoclave-cured composites scheme and experimental apparatus are shown in Figs 12.4 and 12.5, respectively. The individual material properties are shown in Table 12.2.

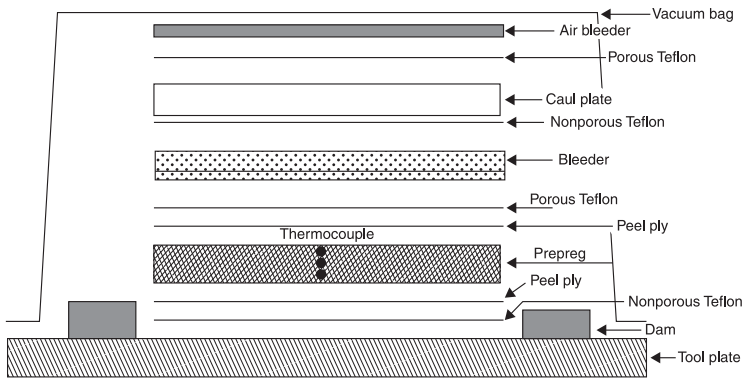

12.4 The typical lay-up of autoclave-cured composites.

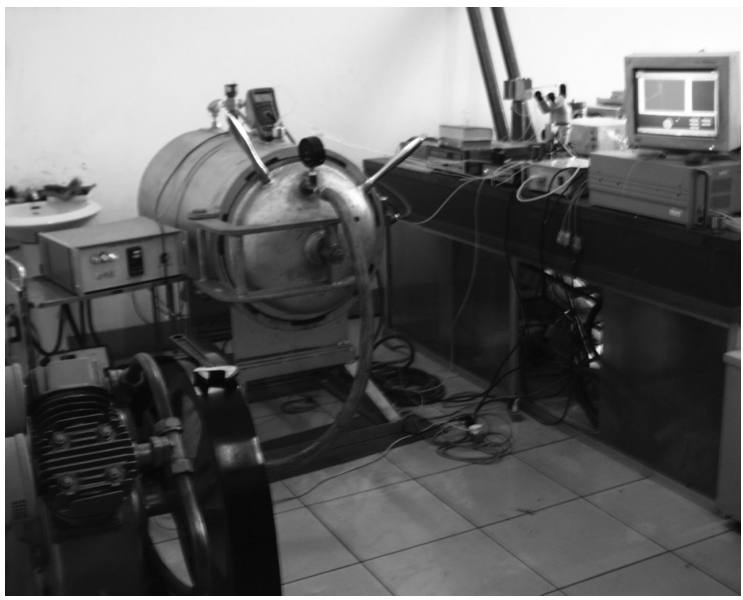

12.5 The experimental apparatus.

Table 12.2 Physical and thermal properties of the used materials (Guo *et al.*, 2005)

Properties	Value	Properties	Value
Density of resin (g/cm^3)	1.25	Conductivity of Teflon film (W/m.K)	0.40
Density of fiber (g/cm^3)	1.80	Conductivity of bag (W/m.K)	0.24
Density of aluminum (g/cm^3)	2.72	Conductivity of bleeder (W/m.K)	0.07
Density of Teflon film (g/cm^3)	2.2	Specific heat of resin (J/g.K)	1.260
Density of bag (g/cm^3)	1.14	Specific heat of fiber (J/g.K)	0.712
Density of bleeder (g/cm^3)	0.26	Specific heat of aluminum (J/g.K)	0.903
Conductivity of resin (W/m.K)	0.24	Specific heat of Teflon film (J/g.K)	1.05
Conductivity of fiber (W/m.K)	2.51	Specific heat of bag (J/g.K)	1.67
Conductivity of aluminum (W/m.K)	220	Specific heat of bleeder (J/g.K)	1.35

The convectional cure cycle is composed of two stages, first stage for consolidation and second stage for full cure. In the first stage, the autoclave temperature is increased to 130 °C with the rate of 2 °C/min and kept at this temperature for 60 min. During the first stage, the excess resin is squeezed out of the laminate. In the second stage, the temperature is increased to 170 °C, which is the cure temperature of the resin, with the same heat rate and maintained at 170 °C for 180 min to complete the cure. The thermal contact resistance was assumed to be negligible, and the convective heat transfer coefficient of 70 W/m^2.K was used between the autoclave air and vacuum bag. In order to investigate the variation of temperature inside the laminate during the cure process, three thermocouples were placed at 40-ply above the bottom, center of laminate, and 40-ply below the top of the laminate. The locations of the thermocouples are shown in Fig. 12.4.

12.3 Understanding the curing process

Figure 12.6 shows that temperature profiles through the thickness are not symmetrical along the center of the laminate. This is due to the fact that the thickness of the tool plate is different from that of the caul plate. Furthermore, thermal conductivities of bleeder materials are smaller than those of composites. Increasing the thickness of the bleeder is expected to significantly alter the temperature distribution in laminates.

The temperature profiles at the three points in laminates were obtained through the experiment and compared with the numerical simulation results. Figure 12.7 shows the comparison of the temperature profiles obtained by the simulation and experiment, in which the predicted temperature profiles were in good agreement with the experimental results. A temperature overshoot at the center of the laminate was observed from the experimental results. The maximum temperature at the mid-point of the center section was 191.7 °C. From Fig. 12.7, it was found that

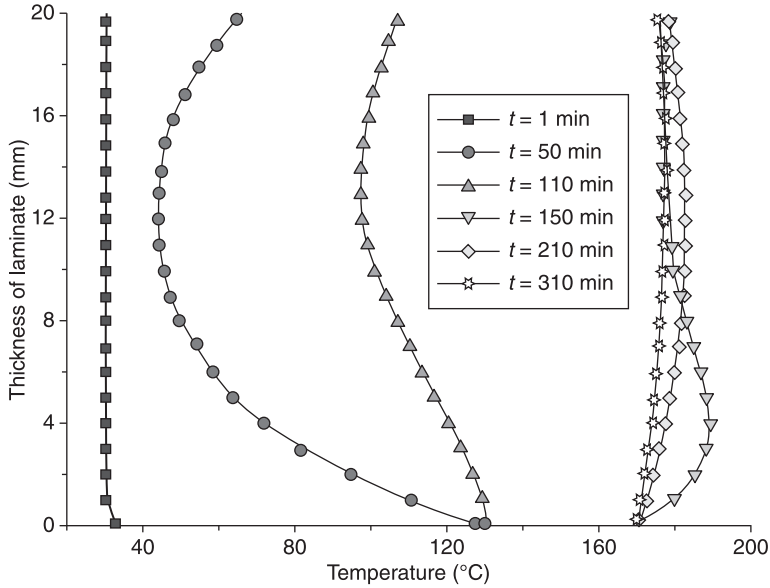

12.6 Temperature distribution.

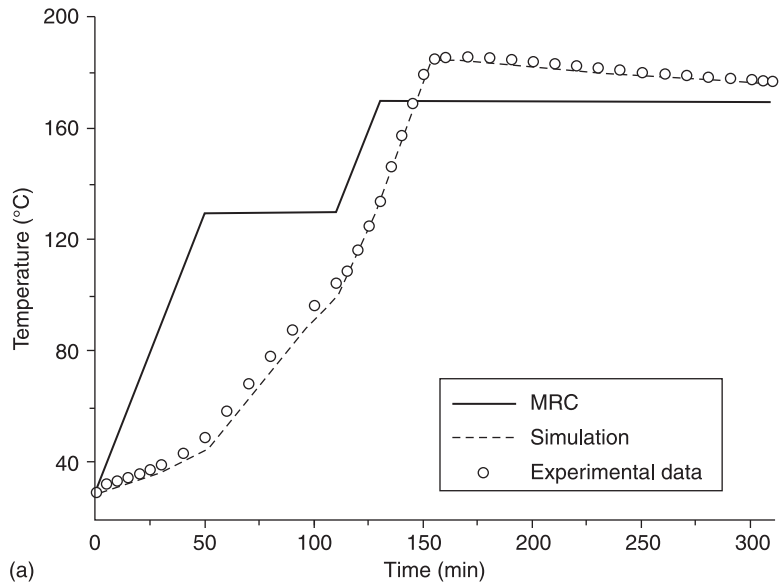

12.7 Temperature profiles of the carbon/epoxy laminate cure by the convectional cure cycle: (a) bottom temperature; (b) middle temperature; and (c) top temperature.

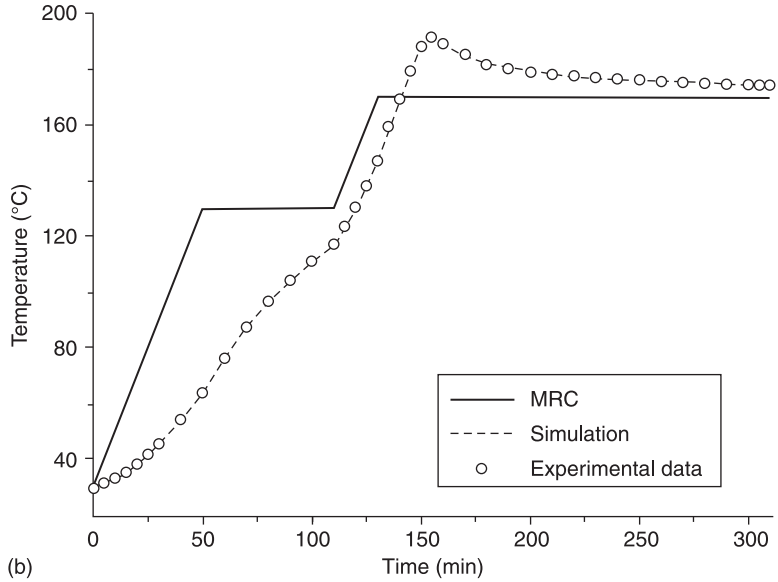

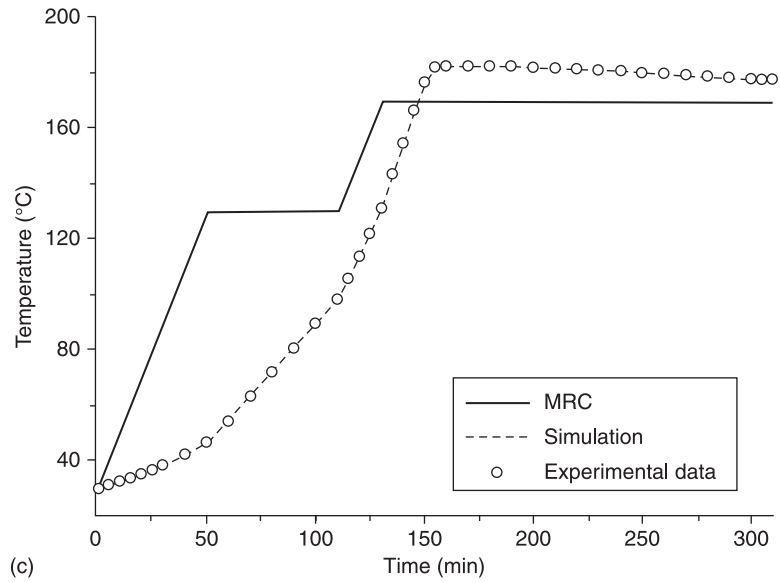

12.7 Continued.

resin degradation would occur, because the maximum temperature of the laminate exceeded 182 °C, which was the glass transition temperature of the fully cured resin. At the beginning, the maximum temperature occurs on the outside and the minimum temperature is at the center of the plate. When exothermic heat is generated from chemical reactions inside the composite, temperatures at the center increase and become higher than the autoclave temperature. Higher temperatures also result in a faster cure.

The profiles of degree of cure at the center section are presented in Fig. 12.8. At the initial stage of curing, a lower degree of cure was observed at the mid-point of the center section due to the low thermal conductivity of laminate; however, the degree of cure increased abruptly due to the internal exothermic reaction as the autoclave temperature increased.

The temperature profiles of the laminate are influenced by the convective heat transfer coefficients between the vacuum bag and the autoclave air, the thickness of bleeder, and the geometry of mold assembly such as thickness of the tooling and caul plate. In order to investigate the effect of the convective heat transfer coefficient on the temperature profile, a 1D FEM analysis was performed varying the coefficients. The temperature profiles at the center of laminate are presented in Fig. 12.9. As the coefficient decreased, the temperature overshoot decreased, while the time to reach the maximum temperature and the temperature difference from the autoclave air increased. The low convective heat transfer makes the internal exothermic reaction occur at a slow rate, which reduces the temperature overshoot. However, the high convective heat transfer coefficient promotes the fast exothermic reaction, which increases the temperature overshoot.

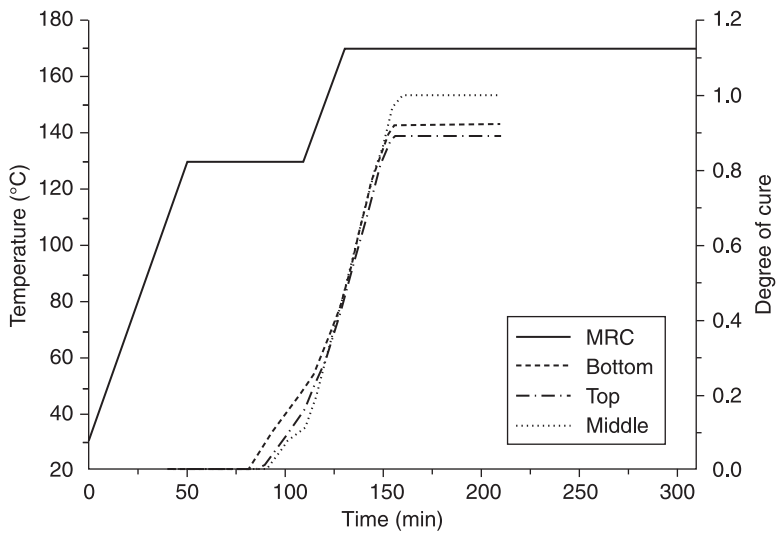

12.8 Degree of cure profiles of the carbon/epoxy laminate cured by the conventional cure cycle.

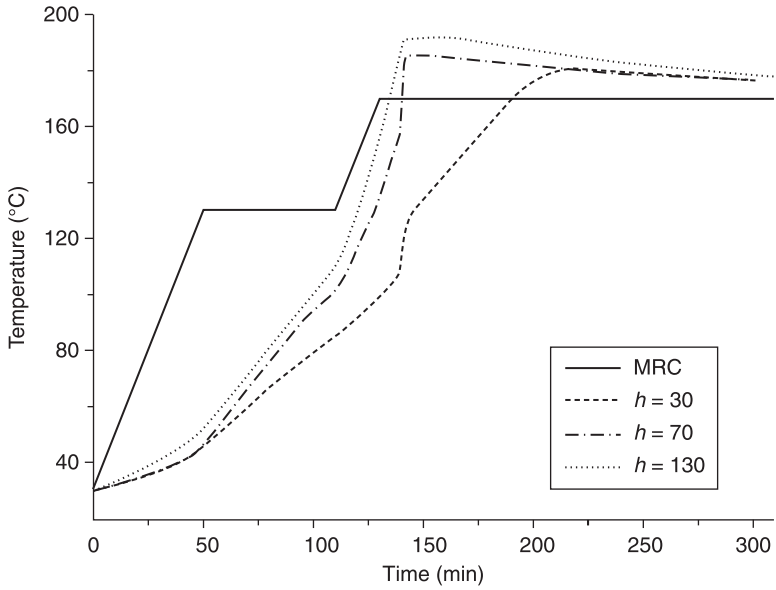

12.9 Effect of convective heat transfer coefficients (unit: W/m^2.K) on the midpoint temperature.

Figure 12.10 shows the maximum temperature at the center of the laminate and corresponding times for various thickness of the mold assembly such as the tool plate and caul plate. As the thickness of mold assembly increased, the maximum temperature decreased a little, while the corresponding time increased a little because the thickness increase of the mold assembly increased the thermal resistance between the laminate and autoclave air, which caused the slow heating of the laminate. Figures 12.9 and 12.10 show that the convective heat transfer coefficient between the vacuum bag and autoclave air had a great influence on the temperature profiles in the laminate, while the thickness of mold assembly seldom affected them.

12.4 Residual stresses in thick laminated composites

A number of studies on curing residual stress have been conducted based on a shell model. It may be successful in predicting residual stresses in thin laminates. The temperature, degree of cure and residual stress can change from point to point within composite materials for thick section parts. It is necessary to develop a 3D model to achieve the spatially varying distributions of temperature and degree of cure and evaluate the residual stresses at any point. To perform more accurate simulations, temperature and cure dependent thermal properties, and heat transport due to resin flow, should be included in the FE model.

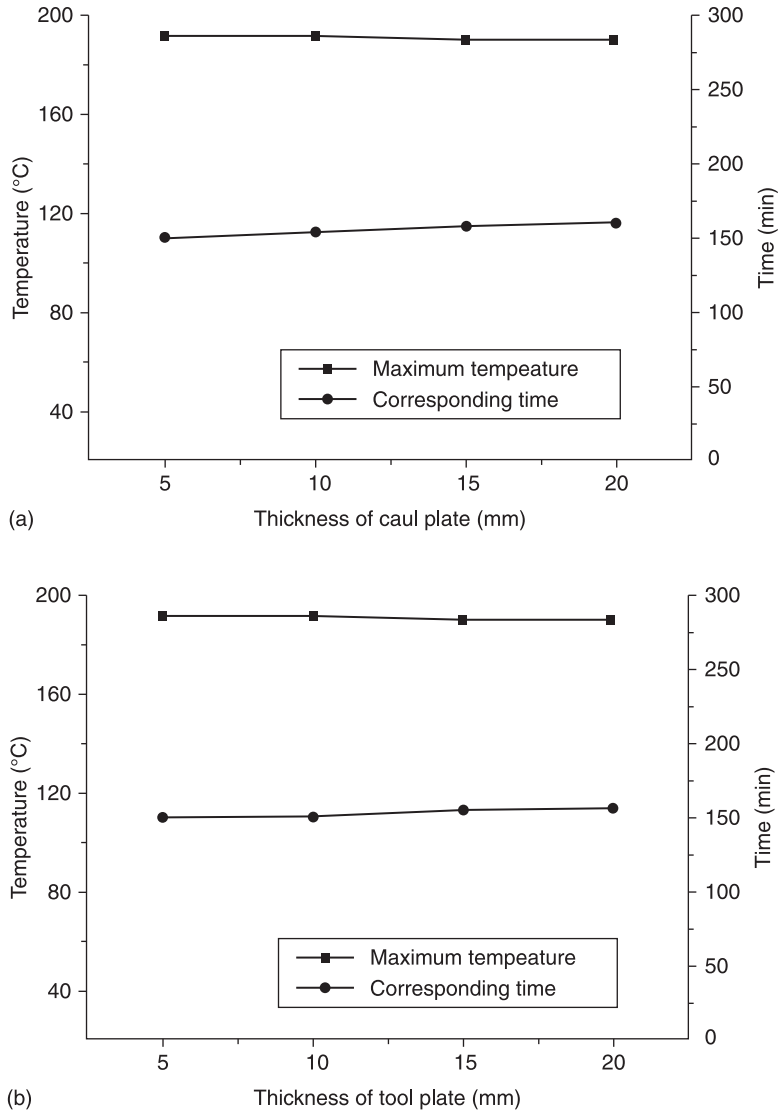

12.10 Maximum temperatures and corresponding times for various thickneses of: (a) tool plate; and (b) caul plate.

12.4.1 Thermo-chemical model

The thermal curing process of resin matrix composites is a thermo-chemo coupled process. The resin is taken as not flowing in the stage of curing and the convection thermal conduction is neglected. Thus the thermal conduction equation with chemical reaction, as written in Eq. 12.1, can be used to describe a full 3D cure process.

The cure kinetics of the resin in this chapter are listed as

$$\frac{d\alpha}{dt} = k_0 \exp(-\Delta E_c / RT)\alpha^m(1-\alpha^n) \quad [12.13]$$

$$\frac{d\alpha}{dt} = (k_1 + k_2\alpha^m)(1-\alpha^n) \quad [12.14]$$

where $k_1 = A_1 \exp(-\Delta E_1/RT)$

$k_2 = A_2 \exp(-\Delta E_2/RT)$

where R is the universal gas constant, T is temperature, and k_0, A_1, A_2, ΔE_c, ΔE_1, ΔE_2 are experimental constants.

12.4.2 Material model: cure dependent resin modulus

The modulus of resin is assumed to follow a simple rule of mixture:

$$E_r = (1-\alpha_{\text{mod}})E_r^0 + \alpha_{\text{mod}} E_r^\infty \quad [12.15]$$

$$\alpha_{\text{mod}} = \frac{\alpha - \alpha_{gel}}{\alpha_{end} - \alpha_{gel}} \quad [12.16]$$

where E_r^0 and E_r^∞ are the assumed fully uncured and fully cured temperature dependent resin modulus, respectively. The simple expression is used, since it was shown to offer a good representation of the modulus for the resin considered in this study (Batemana *et al.*, 2005). The present model assumes the Poisson's ratio and the fiber properties are constant during cure. The instantaneous resin shear modulus during cure is determined based on the isotropic material relation:

$$G_r = \frac{E_r}{2(1+\nu_r)} \quad [12.17]$$

12.4.3 Resin volumetric shrinkage model

Resin shrinkage occurs during cure and provides an important source of internal loading. Assuming a uniform strain contraction for all principal strain components, the incremental isotropic resin shrinkage strain of a unit volume element, $\Delta\varepsilon^{sh}$, and the incremental resin volumetric shrinkage have a relationship given by

$$\Delta\varepsilon^{sh} = (\sqrt[3]{1+\Delta V_r}) - 1 \quad [12.18]$$

A given incremental change in the degree of cure, $\Delta\alpha$, and the associated incremental change in specific volume of resin, ΔV_r, can be related to the total specific volume shrinkage of the completely cured resin, V_{sh}^T, as

$$\Delta V_r = \Delta\alpha V_{sh}^T \quad [12.19]$$

The cure shrinkage strain in the resin during cure is the cumulative sum of all the incremental contributions. The fiber itself is assumed not to undergo any chemical contraction during cure.

12.4.4 Effective elastic modulus of composite unit cell

The composite mechanical properties strongly depend on the fiber and resin constituent properties, and fiber volume fraction. The self-consistent field micro-mechanical model is widely used to compute the instantaneous mechanical properties for uni-directional fiber reinforced composites (Mulle *et al.*, 2009). Garstka *et al.* (2007) used the TEXCAD model to predict the effective unit cell modulus. We adopt the similar method in this chapter. At first, the composite unit cell is classified into N sorts of uni-directional reinforced composite (if necessary, the resin is also treated as one sort of such composites). Then the self-consistent model is employed to obtain effective mechanical properties of an N_{th} sort composite. Finally, the effective of unit cell is taken to be the superposition of total N sorts of composite mechanical properties, on the basis of their spatial directions:

$$\left[C_{eff}\right] = \sum_{m=1}^{N} (f_m [T]_m^T [C_m][T]_m) \qquad [12.20]$$

where $[C_{eff}]$ is the effective stiffness matrix of unit cell, f_m is fiber volume fraction of m_{th} sort composite, and $[T]_m$ is the coordinate transfer matrix of stress and strain between the local coordinate system of m_{th} sort composite and the global unit cell coordinate system.

12.4.5 Effective thermal expansion coefficients and shrinkage strain of composites

The thermal expansion and shrinkage stains are also dependent on the fiber and resin constituent properties, and fiber volume fraction. A simple model on the basis of a rule of mixture is used to predict the effective thermal expansion coefficients and shrinkage strain of composites (Leng and Asundi, 2002):

$$\varepsilon_1 = \frac{\varepsilon_{1f} E_{1f} f + \varepsilon_{1r} E_{1r} (1-f)}{E_{1f} f + E_{1r} (1-f)} \qquad [12.21]$$

$$\varepsilon_2 = \varepsilon_3 = (\varepsilon_{2f} + v_{12f}\varepsilon_{1f}) f + (\varepsilon_{2r} + v_{12r}\varepsilon_{1r})(1-f) - \left[v_{12f} f + v_{12r}(1-f)\right] \left[\frac{\varepsilon_{1f} E_{1f} f + \varepsilon_{1r} E_{1r} (1-f)}{E_{1f} f + E_{1r} (1-f)}\right] \qquad [12.22]$$

where subscript 1 stands for the longitudinal direction and 2 stands for the transverse direction. When the effective thermal expansion coefficients are

evaluated, the formula $\alpha_1 = \varepsilon_1$, $\alpha_2 = \varepsilon_2$ is taken, and when the effective shrinkage strains are evaluated, the formula $\varepsilon_1^{sh} = \varepsilon_1, \varepsilon_2^{sh} = \varepsilon_2$ is taken. The fiber is assumed to be zero shrinkage strain in this study.

12.4.6 Finite element formula for residual stress

The cure simulation yields the temperature and degree of cure distributions within the composite parts in a single time increment before the stress and deformation are calculated. The instantaneous effective material properties and the resin shrinkage load are computed according to these distributions, as discussed above. These results are taken as the input parameters for residual stress calculations at the current time step.

The total incremental strain, $\Delta\varepsilon$, is given by

$$\Delta\varepsilon = \Delta\varepsilon^e + \Delta\varepsilon^{th} + \Delta\varepsilon^{sh} \quad [12.23]$$

where ε^e is strain induced by mechanical load. The thermal strain, $\Delta\varepsilon^{th}$, can be expressed as

$$\Delta\varepsilon^{th} = \alpha \cdot \Delta T \quad [12.24]$$

The incremental form of stress and strain relationship is given by

$$[\Delta\sigma] = [C_{eff}]\ \{[\Delta\varepsilon^e] + [\Delta\varepsilon^{th}] + [\Delta\varepsilon^{sh}]\} \quad [12.25]$$

Equation 12.21 is solved with the use of the FEM at each time step. The total strain can be obtained taking the cumulative sum of incremental strain of each time step. The details can be found elsewhere (Leng and Asundi, 2002; Mulle *et al.*, 2009).

12.4.7 Numerical examples

The first example is selected for Bogetti and Gillespie (1991) to validate the present program; the material system is about glass/polyester. Table 12.3 gives the composite thermal properties and Table 12.4 gives the cure kinetic parameters. The characteristic values of polyester resin during cure are shown in Table 12.5 and the mechanical properties of glass and polyester are listed as Table 12.8. The example consists of a uni-directional laminate with the dimensions of $0.1524 \times 0.1524 \times 0.0254$ m. The model of cure kinetic is as shown in Eq. 12.13).

Table 12.3 Thermal properties of glass/polyester for 2D example

ρ_c (kg/m^3)	C_{pc} (J/(W°C))	$K_{c22} = K_{c33}$ (W/(m°C))	K_{c11}/K_{c33}
1890	1260	0.2163	2

Table 12.4 Cure kinetic parameters of glass/polyester for 2D example

m	n	$k_0(s^{-1})$	ΔE_c (J/mol)	Hr (J/kg)
0.524	1.476	6.1667×10^{20}	1.674×10^{5}	77500

Hr is heat reaction.

Table 12.5 Resin characteristic elastic modulus during cure

Properties	Polyester	Epoxy
E_m^0(MPa)	2.757	3.447
E_m^∞(MPa)	2.757×10^{3}	3.447×10^{3}

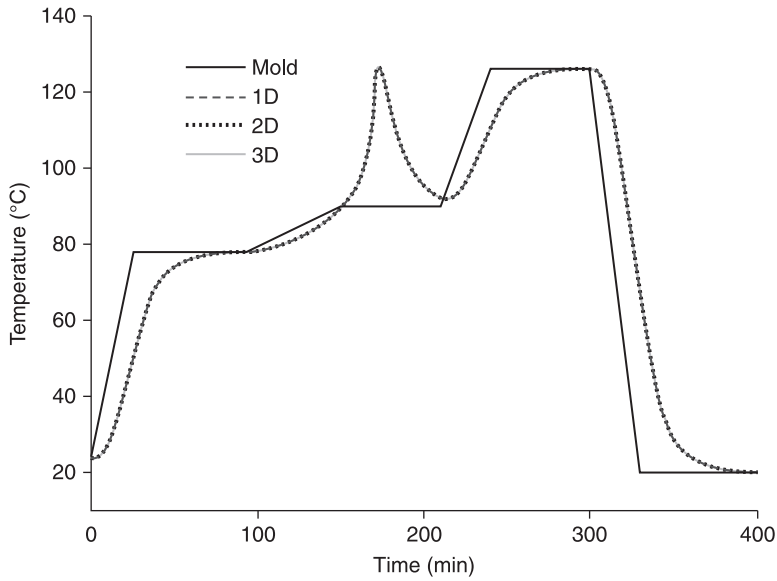

12.11 The history of temperature of Example 1.

The same boundary conditions are used in the example, namely the mold temperature is applied at the top and bottom surface of the part and the isolate heat condition is applied at the lateral surfaces. The temperature history at the centroid of the part is as shown in Fig. 12.11. The results agree well with the Bogetti's results. The present predicted temperature peak is 126.9 °C, whereas Bogetti's is 126 °C or so. Since the exact cure cycle curve cannot be obtained, the inflexion of the time in the cure cycle curve may be a little different from its original value of the Bogetti's value. The error leads to the time when the temperature peak occurs at 168 minute (Bogetti's is 164 minute) for the present simulations.

The in-plane transverse stress for three different volume shrinkage rates 6, 3, 1 and 0% are shown in Fig. 12.12. A small difference between the present solutions and Bogetti's solution is observed, especially near the mid-plane of the part. The maximum error between the present solutions and Bogetti's is 8%. The reason is that Bogetti used the laminated theory, while the 3D FEs are used in the present analysis. The significant self-equilibrating stresses remain after complete cure. The magnitude of the resin volumetric shrinkage strongly affects the stress development. These results are in agreement with Bogetti's results.

The second example is developed to illustrate the influence of thickness on residual stress. Material system is glass/epoxy, and fiber volume fraction is 60%. Table 12.6 gives the composite thermal properties and Table 12.7 gives the cure kinetic parameters. The characteristic values of epoxy resin during cure are seen in Table 12.5 and the mechanical properties of glass and epoxy are listed as Table 12.8. The model of cure kinetic is as shown in Eq. 12.14. The second example is a composites plate with different thickness (Fig. 12.13).

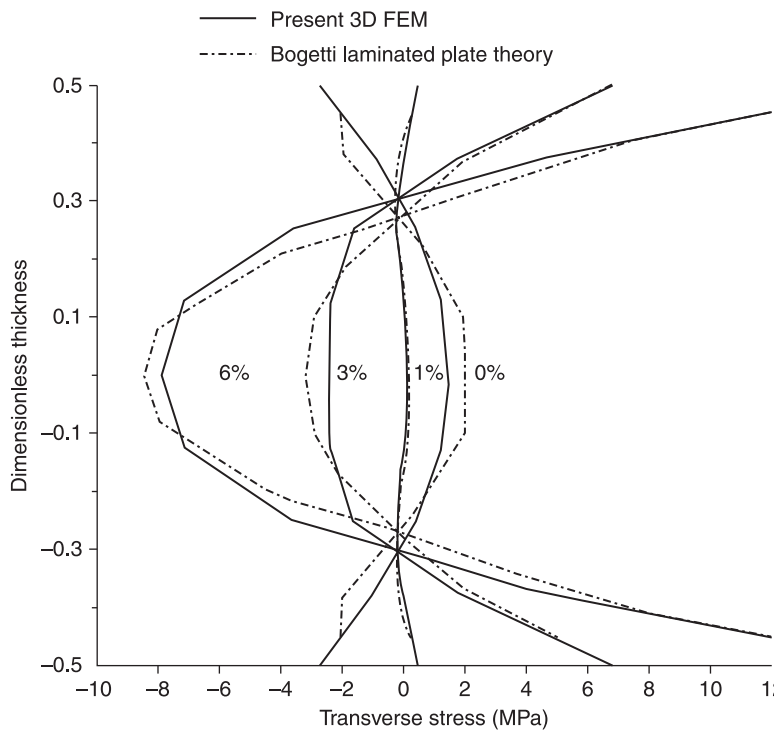

12.12 Comparison between the present analysis with the Bogetti's results for Example 1.

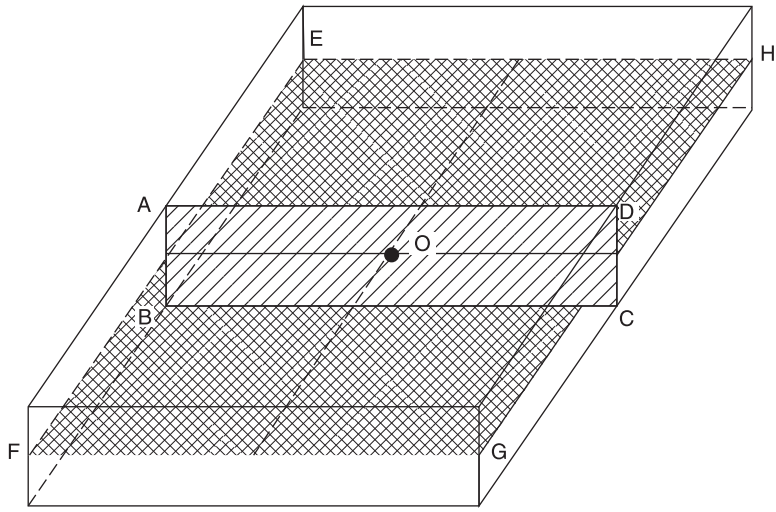

12.13 Three-dimensional composite plate for Example 2.

Table 12.6 Thermal properties of glass/epoxy for Example 2

	ρ (kg/m^3)	C_p (J/(W°C))	K (W/(m°C))
Glass	2560	712.35	0.137
Epoxy	1150	8210	8.673

Table 12.7 Cure kinetic parameters of glass/epoxy for Example 2

m	n	A_1 (s^{-1})	A_2 (s^{-1})	ΔE_1 (J/mol)	ΔE_2 (J/mol)	Hr (J/kg)
0.958	0.841	1.759×10^5	3.888×10^5	6.513×10^4	5.408×10^4	459224

The temperature history and the curing degree history at the center of the plate are shown in Figs 12.14 and 12.15, respectively. The temperature peak is delayed as the thickness increases and the different thickness plates have temperature overshoots of 7, 25 and 56 °C. Figures 12.16 to 12.19 show the temperature distribution and the curing degree distribution at the time of 2300 s. It can be

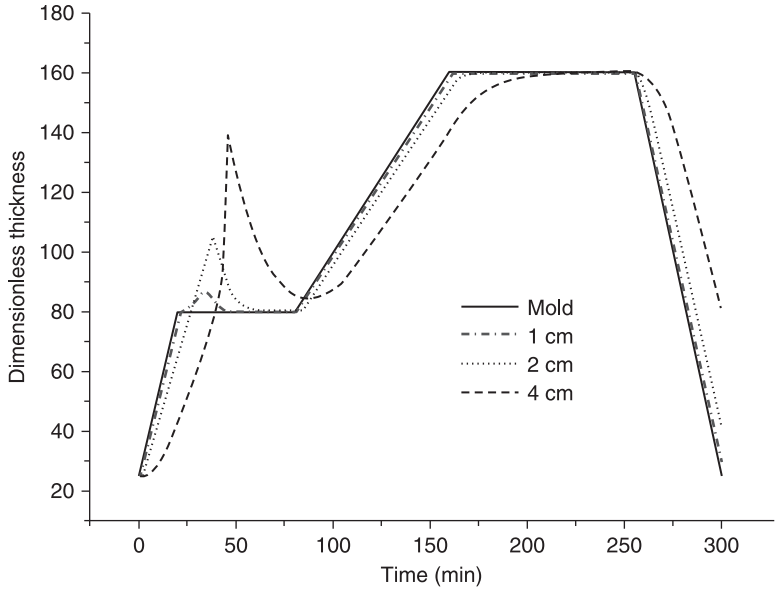

12.14 The history of temperature for the thick plate example.

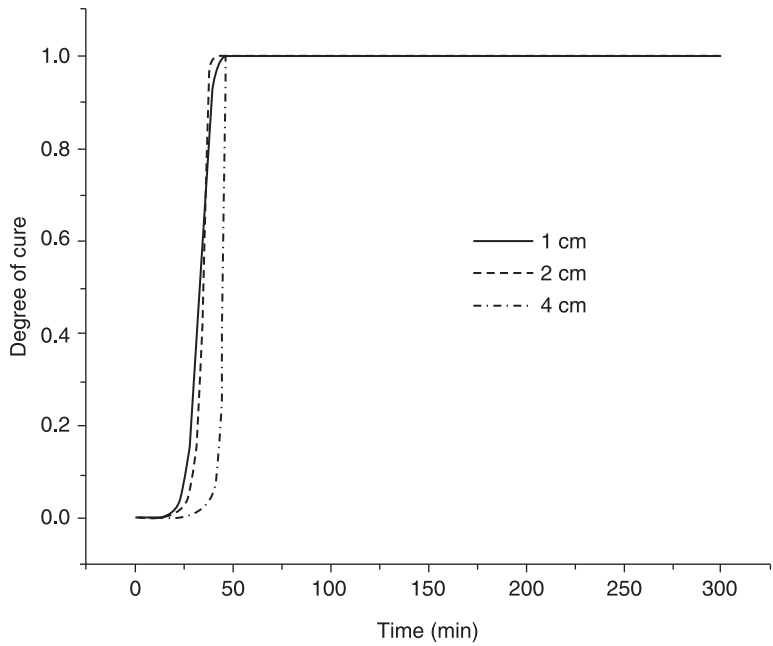

12.15 The history of cure degree for the thick plate example.

Table 12.8 Fiber and resin constituent mechanical properties

Properties	Glass	Polyester	Epoxy
E_1 (MPa)	7.308×10^4	Eq. 12.6	Eq. 12.6
E_2 (MPa)	7.308×10^4	Eq. 12.6	Eq. 12.6
ν_{12}	0.22	0.40	0.35
ν_{13}	0.22	0.40	0.35
ν_{23}	0.22	0.40	0.35
G_{12} (MPa)	2.992×10^4	Eq. 12.6	Eq. 12.6
G_{13} (MPa)	2.992×10^4	Eq. 12.6	Eq. 12.6
G_{23} (MPa)	2.992×10^4	Eq. 12.6	Eq. 12.6
α_1 (1/°C)	5.04×10^{-6}	7.20×10^{-5}	5.76×10^{-5}
α_2 (1/°C)	5.04×10^{-6}	7.20×10^{-5}	5.76×10^{-5}

found that the curing degree distribution for 1 cm thickness plate is almost uniform. The resin at the center of the 2 cm thickness plate has cured and it indicates the curing process developed from the inside to the outside; while it indicates the curing process developed from the outside to the inside for the 4 cm thickness plate. It also demonstrates a more complex distribution in the thick plate.

Stress increases with the increase in thickness and shrinkage stress is greater than thermal stress. The compression thermal stress remains before the cooling. The shrinkage tension stress remains during the curing degree. The combination of thermal and shrinkage action leads to stress change from the compression stress at the beginning to tension stress at the end. Figures 12.20 to 12.23 show the distribution of curing induced transverse stresses at the time 2300 s. The complex stress distribution is also found in the thicker plates.

12.5 Methods of measurement of residual stresses in laminated composites

Various measurement techniques for residual stress determination in polymer matrix composites have been developed in the past (Batemana *et al.*, 2005; Kim and Lee, 2007; Leng and Asundi, 2002; Mulle *et al.*, 2009). In general, experimental techniques were categorized into two classes, destructive techniques and non-destructive. Tables 12.9 and 12.10 give the overview of these techniques (Patricia *et al.*, 2007a,b). Some non-destructive techniques such as the embedded sensors, in particular the fiber optic sensors, can be applied to measure residual stresses in thick section parts. The destructive techniques, including layer removal and hole drilling, are available to evaluate the residual stress in thick composites.

A work using deep-hole method to measure residual stress can be found in Batemana *et al.* (2005). The technique is first used in large metallic components, and is extended to evaluate the residual stresses in thick section composite laminated. The method involves first drilling a small hole through the laminate

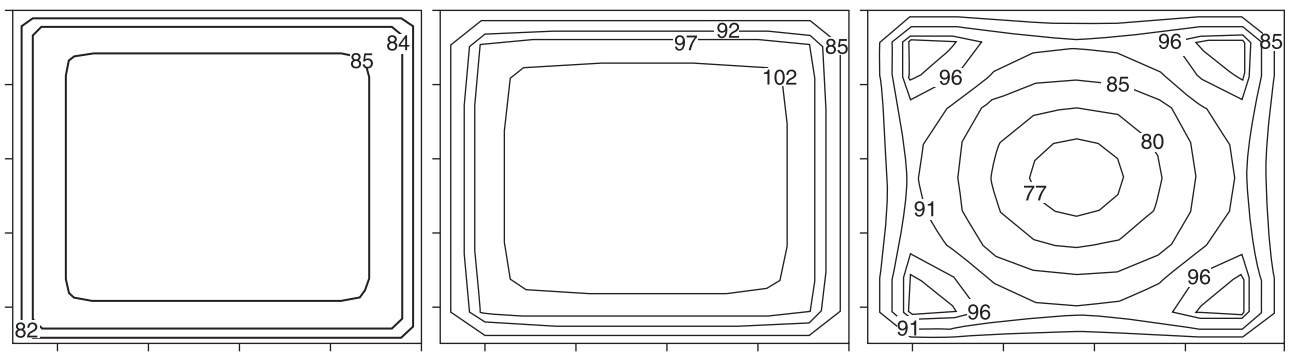

12.16 The distribution of temperature (°C) on the plane EFGH for thick plates (2300s).

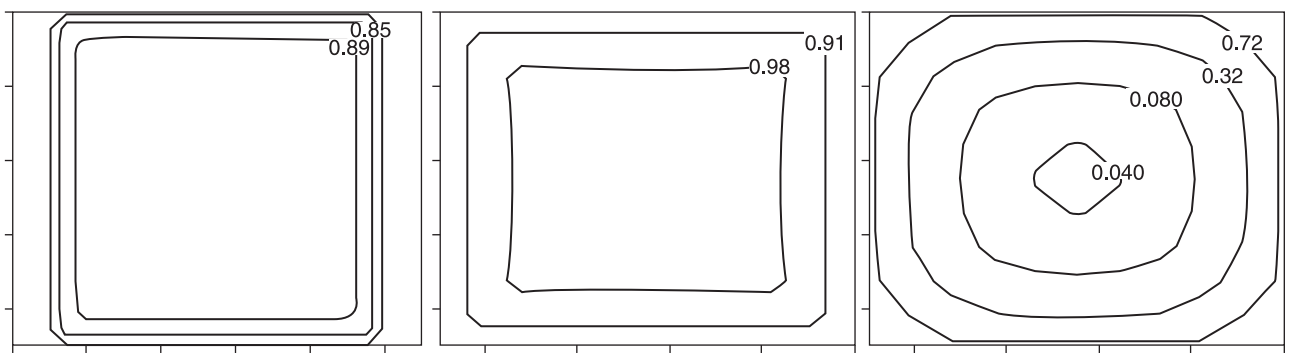

12.17 The distribution of cure degree on the plane EFGH for thick plates (2300s).

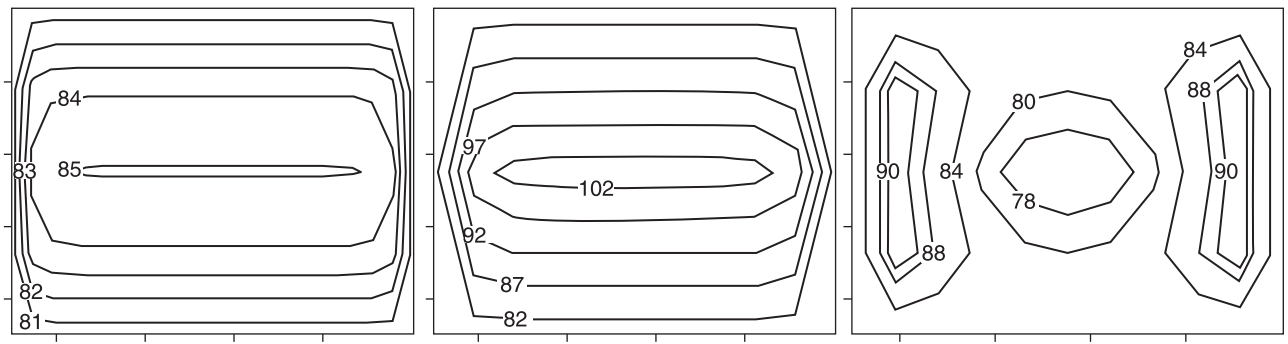

12.18 The distribution of temperature (°C) on the plane ABCD for thick plates (2300s).

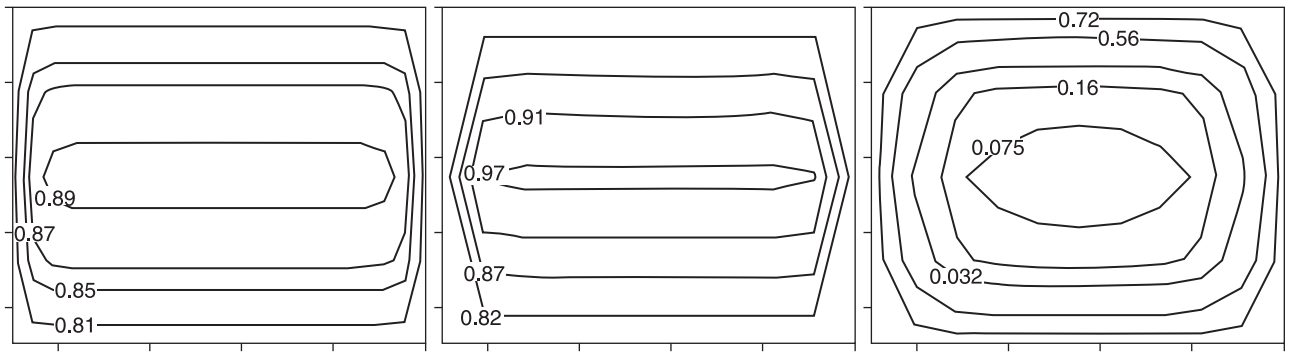

12.19 The distribution of cure degree on the plane ABCD for thick plates (2300s).

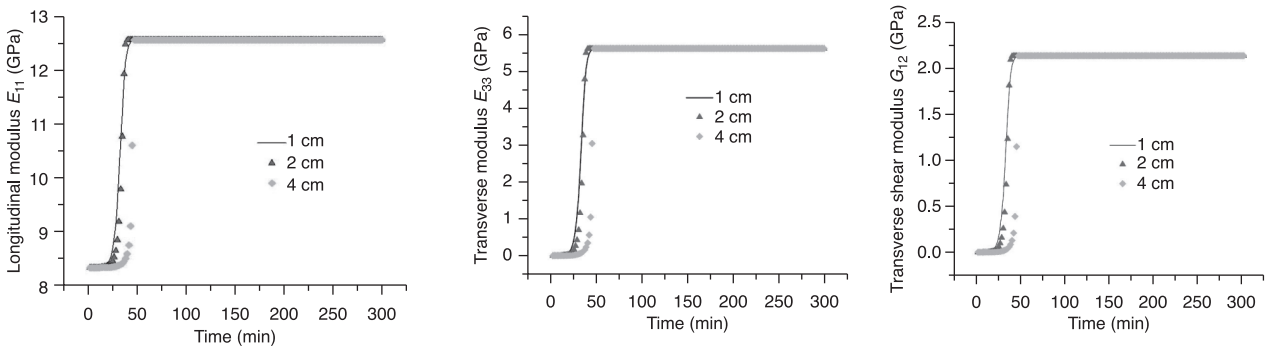

12.20 Effective modulus of composite material cell at point O.

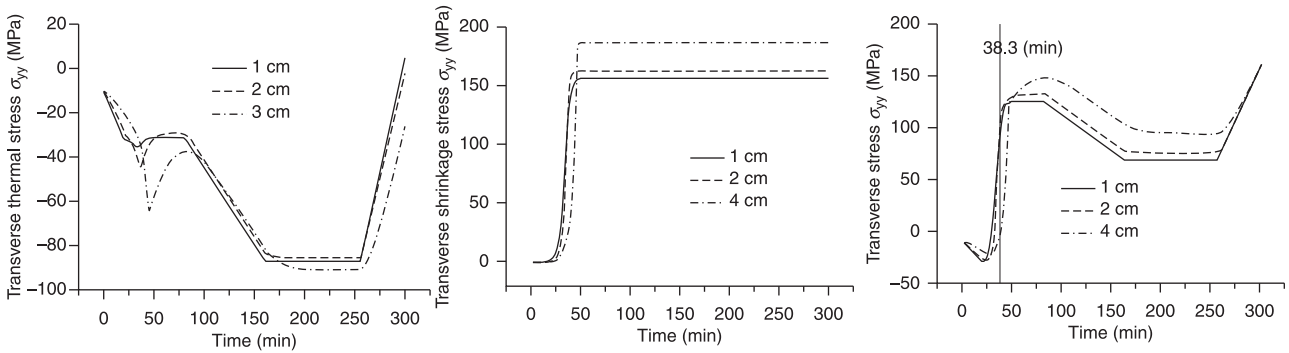

12.21 The history of transverse stresses (Pa) for thick plates.

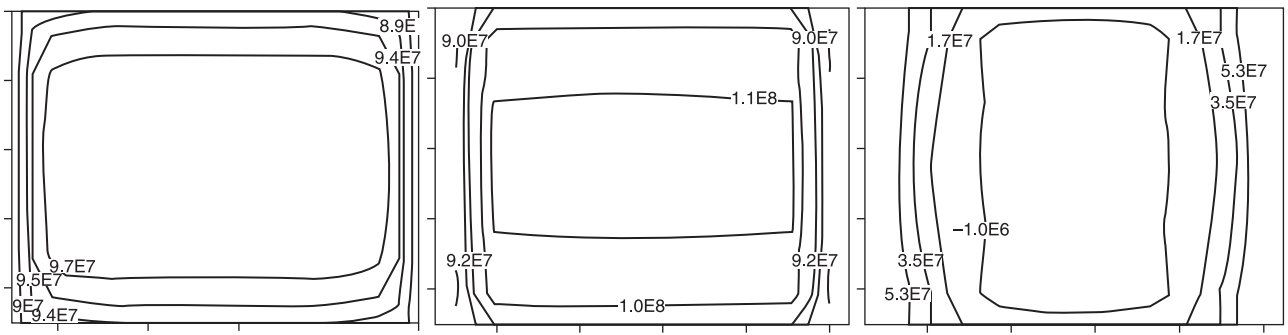

12.22 The distribution of transverse stress (Pa) on plane ABCD for thick plates (2300s).

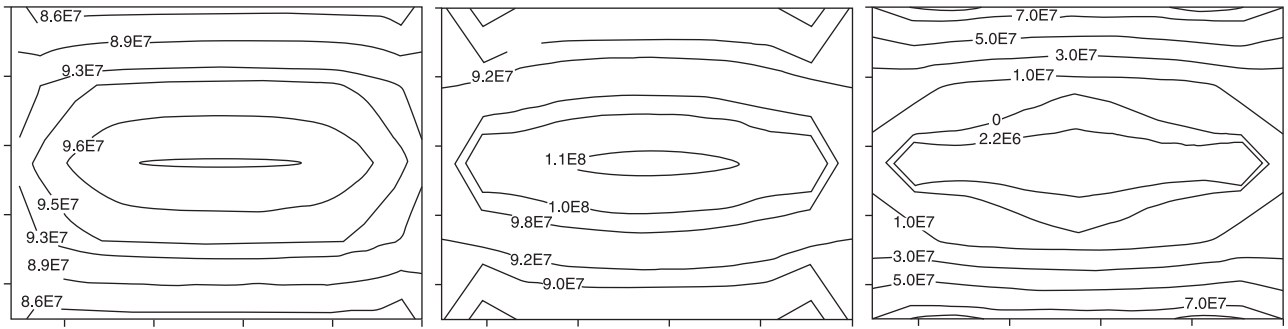

12.23 The distribution of transverse stress (Pa) on plane EFGH for the thick plate example (2300s).

Table 12.9 Overview of non-destructive experimental techniques for residual stress determination in composites (Patricia *et al.*, 2007)

Techniques	Level of residual stress			Type of specimen					Specimen requirements/ drawbacks
	Intra ply stresses	Inter ply stresses	Laminate stresses	Micro-composites	UD prepregs	Cross-ply prepregs	UD laminates	Angle ply laminates	
Photo-elasticity	X			X	X				Transparent matrix, low V_f
Raman spectroscopy	X	X		X	X		X		Transparent matrix, measures only fiber surface
Electrical conductance		X				X			In composites with electrically conducting fibers
Embedded strain gages	X	X					X	X	Compensation needed for gage CTE
Embedded FOS	X	X	X				X	X	Polarisation effects
Embedded metallic particles		X					X	X	Particles need to be close to surface
Interferometry		X					X	X	Only surface information, grid is necessary
Warpage		X			X	X	X	X	No high accuracy

CTE, coefficient of thermal expansion. FOS, fiber optical sensor.

Table 12.10 Overview of destructive techniques for residual stress determination in composites (Patricia *et al.*, 2007)

Techniques	Level of residual stress			Type of specimen					Specimen requirements/ drawbacks
	Intra ply stresses	Inter ply stresses	Laminate stresses	Micro-composites	UD prepregs	Cross-ply prepregs	UD laminates	Angle ply laminates	
First ply failure		X				X		X	Works best for [0/90] laminates
Layer removal		X	X				X	X	No high accuracy
Blind-hole drilling		X	X				X	X	Low accuracy
Successive grooving technique		X	X				X	X	Low accuracy, time consuming

perpendicular to the surface. The material around the hole is then machined away, resulting in a change in diameter of the hole due to the release of residual stress. This change in diameter is measured and used to calculate the residual stress. The calculation requires the evaluation of coefficients that depend on the properties of the composite.

12.5.1 Residual stress monitoring using Fiber Bragg Grating (FBG)

The experimental techniques that seem most feasible for monitoring residual stress development in structural components are embedded fiber optic sensors and possibly strain gages. The FBG sensor system is most promising, since it seems capable of providing a 3D profile of the stress distribution in composites. However, this system has not yet reached maturity for application in composites structures and is rather expensive. Fortunately, much effort on further development is spent on this experimental technique and it is to be expected that in a few years this is going to be a widely accepted technique. One drawback is still that if a foreign body is embedded in composites, it will give rise to possible stress concentrations.

The response to strain and temperature differences is characterized by a change in Bragg wavelength. An experimental study using FBG to monitoring residual stresses is presented as follows. The material used in the study is the T300/HD03 prepreg. The elementary specimen concerned here is a $[0_{16}]$ and $[0/90]_{4s}$ laminate (dimensions: 300 mm × 300 mm). The specimen is instrumented with optical fiber Bragg grating sensors. This operation consists of embedding the sensors in between layers during the stacking operation..

Figures 12.24 to 12.26 give the results of temperature and strains during the curing cycle in the laminates. It can be seen that the first phase corresponds to the vacuum and pressurization settlement. Encapsulated FBGs respond by small strain peaks, which do not exceed 200 micro-strains. The second phase is that of the rise in temperature. The strain change during this phase is rather problematical. The third phase is that of the isothermal dwell at 180 °C. Strains of different origins (chemical, thermal, mold–part interaction) are partially locked in as gelation and vitrification progresses. The fourth phase concerns the part of the cooling. The information delivered by the two FBGs is a little different. Strains delivered by the FBG decrease faster than temperature.

The results also indicate the heterogeneity of composite laminates. At the end of curing cycle, the longitudinal strain in $[0_{16}]$ laminate is $-84\,\mu\varepsilon$, whereas the transverse strain is $-3230\,\mu\varepsilon$. The final residual strain in cross-ply $[0/90]_{4s}$ laminate is $-663\,\mu\varepsilon$, which is in between the longitudinal and transverse strain in unidirectional laminate (Fig. 12.27). A comparison with an analytical model would have been of interest. Table 12.11 shows the comparisons between the calculated and the results by FBG. The instructive results are obtained, although a large error can be found.

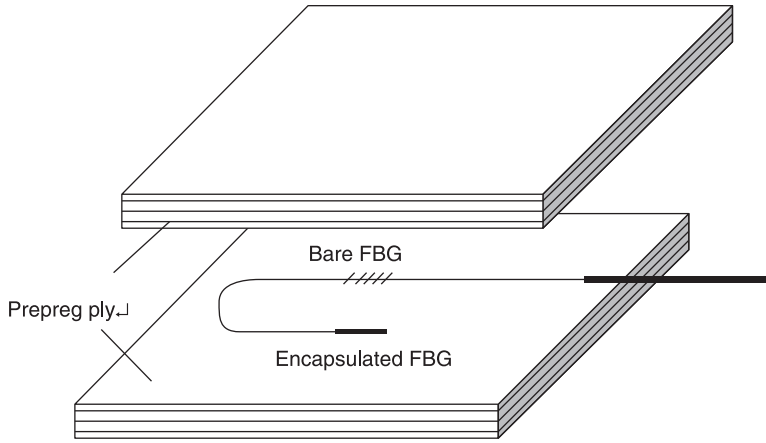

12.24 T300 laminate instrumented with FBG sensors.

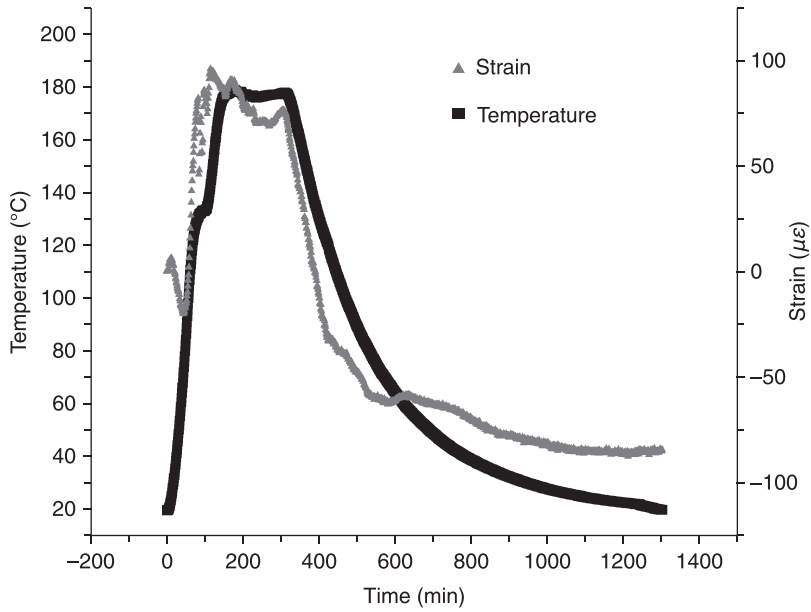

12.25 Process induced strain evolution in the longitudinal direction of $[0_{16}]$ laminate.

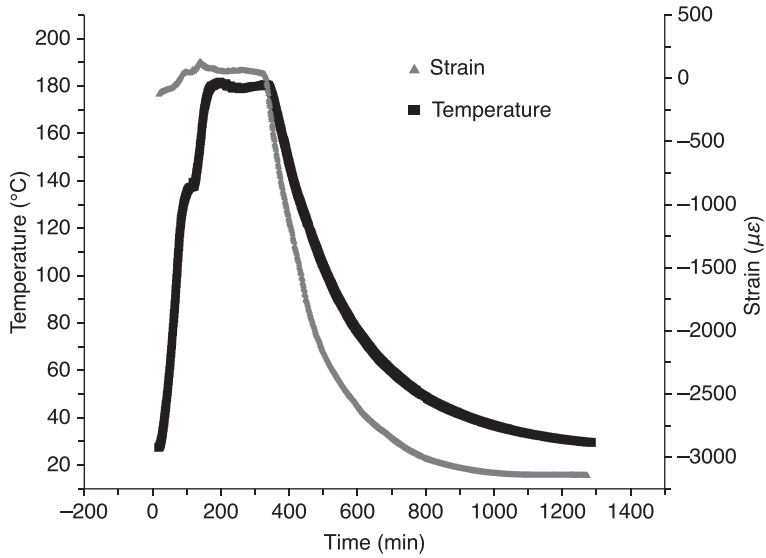

12.26 Process induced strain evolution in transverse direction of $[0_{16}]$ laminate.

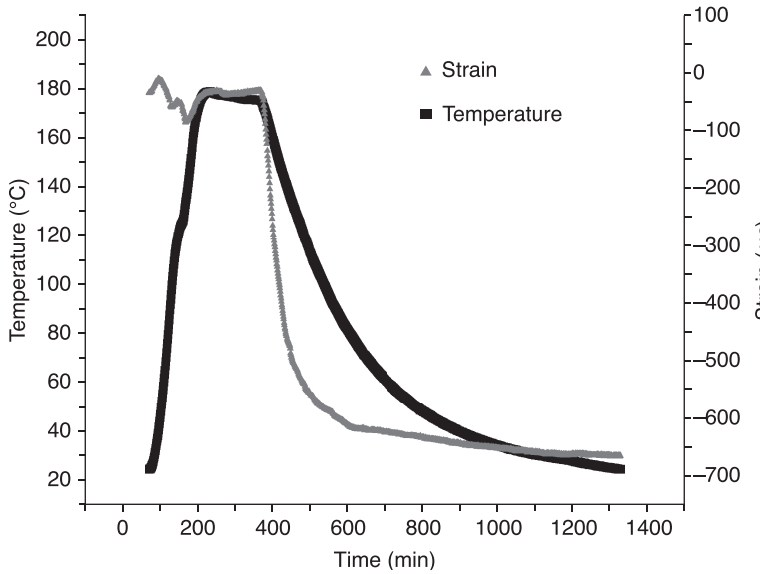

12.27 Process induced strain evolution in $[0/90]_{4S}$ laminate.

Table 12.11 Process induced residual strain and stress in $[0/90]_{4S}$ laminate

Orientation	Residual strain (με)		Residual stress (MPa)	
	Calculated	By FBG	Calculated	By FBG
0	–319.7	–579	–35.72	–73.93
90	3606.9	2567	35.72	24.6

12.6 Future trends

Some research has indicated that the nonlinear transient heat transfer FEM is successfully employed to simulate the cure processes of polymer matrix composites in thick laminates. The MRC produced a large temperature overshoot at the mid-point of the laminate, because of exothermic reaction and low thermal conductivity of matrix. This can lead to matrix degradation, non-uniform cure and consolidation, and residual stress. The temperature profiles in the laminate were much affected by the bleeder materials and the convective heat transfer coefficient between the vacuum bag and autoclave air, while they were little influenced by the thickness of mold assembly.

A 3D FE analysis of curing and process induced residual stress in thick section parts is necessary due to the complex temperature and stress distribution. The finite element method (FEM) should be to solve the coupled equations involved in the transient heat transfer and the cure kinetics of the resin and the distributions of internal temperature and curing degree within the composite at any instant time. Here the self-consistent field micro-mechanics model is used to predict the cure dependent composite mechanical properties. The other micro-mechanics model may be also used according to the materials property. The successful prediction of the process induced stresses and deformation is still a challenging problem. It is difficult to find the accurate models such as thermal-chemical dynamics, curing-dependent materials properties, the micro-mechanics models and the well-defined boundary condition. The techniques discussed are applicable not only to study thermal residual stresses, but also stresses induced by environmentally induced internal stresses, such as caused by moisture, temperature gradient, solvents, etc.

Since the 1980s, many experimental techniques have investigated residual stresses in composites. For validation of models regarding the thermal residual stress magnitude and distribution, it is necessary to obtain experimental data during the process of residual stress development (e.g. during cooling). It is important that representative processing environments are utilized, such as appropriate tooling, pressure, etc. The experimental techniques that seem most feasible for monitoring residual stress development in structural components are

embedded fiber optic sensors and possibly strain gages. New experimental techniques that directly measure the residual stress magnitude and distribution in composite laminates and structures, without affecting the composites, are still a challenging work.

12.7 Acknowledgments

The author would like to thank Zhansheng Guo who contributed to Section 12.2 'Modelling the curing process in thick laminated composites' and Hao Li, who contributed to the revision and graphic editing. The support by National Natural Science Foundation of China (Grant No.10872058) and the Major State Basic Research Development Program of China (973 Program) under grant No. 2010CB631100 is gratefully acknowledged.

12.8 References

Bartolomeo, P., Chaillant, J. F. and Vernet, J. K. L. (2000) Dielectric investigation of interphase formation in composite materials. Part I: Ionic conductivity and permittivity exploration. *J. Polym. Sci. B*, **38**(16), 2154–61.

Batemana, M. G., Millera, O. H. and Palmera, T. J. *et al.* (2005) Measurement of residual stress in thick section composite laminates using the deep-hole method, *International Journal of Mechanical Sci*ences, **47**, 1718–39.

Blest, D. C., Duffy, B. R., McKee, S. and Zulkifle, A. K. (1999), Curing simulation of thermoset composites, *Composites: Part A*, **30**, 1289–309.

Bogetti, T. A. and Gillespie, Jr. J. W. (1991) Two-dimensional cure simulation of thick thermosetting composite, *J. Compos. Mater*, **25**, 239–73.

Breglio, G., Cusano, A., Cutolo, A., Calabro, A. M., Cantoni, S. *et al.* (2000) *In-situ* measurement of thermoset resin degree of cure using embedded fiber optic, in: S. C. Liu (ed.), *Proceedings of SPIE, Smart Structures and Materials: Smart Systems for Bridges, Structures and Highways*, **3988**, 380–91.

Chen, Y., Xia, Z. and Ellyin, F. (2001) Evolution of residual stresses induced during curing processing using a viscoelastic micromechanical model, *Journal of Composite Materials*, **35**(6), 522–42.

Ciriscioli, P. R., Wang, Q. and Springer, G. S. (1992) Autoclave curing – Comparison of model and test results, *J. Compos. Mater*, **26**, 90–102.

Dai, F. and Zhang, B. (2007) A three-dimensional finite element analysis of process-induced residual stress in resin transfer molding process, *16th International Conference on Composite Materials*, Kyoto, Japan.

Fibre Bragg Grating Technology, available at: *http://www.fos-s.be/fos%2Ds/*

Garstka, T, Ersoy, N, Potter, K. D. and Wisnom, M. R. (2007) *In situ* measurements of through-the-thickness strains during processing of AS4/8552 composite, *Composites: Part A*, **38**(12), 2517–26.

Guo, Z., Du, S. and Zhang, B. (2005) Temperature field of thick thermoset composite laminates during cure process, *Composites Science and Technology*, **65**, 517–23.

Hojjati, M. and Hoa, S. V. (1994) Curing simulation of thick thermosetting composites, *Composites Manufacturing*, **5**(3), 159–69.

Johnston, A. J., Reza V. and Anoush, P. (2001) A plane strain model for process-induced deformation of laminated composite structures, *Journal of Composite Materials*, **35**(16), 1435–69.

Joshi, S. C., Liu, X. L. and Lam, Y. C. (1999) A numerical approach to the modeling of polymer curing in fiber-reinforced composites, *Composites Science and Technology*, **59**, 1003–13.

Karalekas, D., Cugnoni, J. and Botsis, J. (2008) Monitoring of process induced strains in a single fibre composite using FBG sensor: a methodological study, *Composites: Part A*, **39**, 1118–27.

Kheir, E., Tarsha, K. and Philippe, O. (2002) Thermoviscoelastic analysis of residual curing stresses and the influence of autoclave pressure on these stresses in carbon/epoxy laminates, *Composites Science and Technology*, **62**, 559–65.

Khoun, L., Oliveira, R., Michaud, V. and Hubert, P. (2011) Investigation of process-induced strains development by fine Bragg grating sensors in resin transfer moulded composites, *Composites: Part A*, **42**, 274–82.

Kim, J. S. and Lee, D. G. (1997) Development of an autoclave cure cycle with cooling and reheating steps for thick thermoset composite laminates, *J. Compos. Mater.*, **31**(22), 2264–82.

Kim, J. W. and Lee, D. G. (2007) Measurement of residual stresses in thick composite cylinders by the radial-cut-cylinder-bending method, *Composite Structures*, **77**, 444–56.

Leng, J. S. and Asundi, A. (2002) Real-time cure monitoring of smart composite materials using extrinsic Fabry Perot interferometer and fiber Bragg grating sensor, *Smart Mater. Struct.*, **11**, 249–55.

Loos, A. C. and Springer, G. S. (1983) Curing of epoxy matrix composites, *J. Compos. Mater.*, **17**, 135–69.

Martinez, G. M. (1991) Fast cure for thick laminated organic matrix composites, *Chemical Engineering Science*, **46**, 439–50.

Melnik, R. V. N. (2002) Models for coupled kinetics and heat transfer in processing polymeric materials with applications to biochemical engineering, *Modelling and Simulation in Materials Science and Engineering*, **10**, 341–57.

Michaud, D. J., Beris, A. N and Dhurjati, P. S. (1998), Cure Behavior of Thick-Sectioned RTM Composites, *J. Compos. Mater.*, **32**, 1273–96.

Michaud, D. J., Beris, A. N. and Dhurjati, P. S. (2002) Thick-sectioned RTM composite manufacturing, Part I: *In situ* cure, model parameter identification and sensing, *J. Compos. Mater.*, **36**(10), 1179–200.

Mulle, M., Collombet, F., Olivier P. and Grunevald, Y. H. (2009) Assessment of cure residual strains through the thickness of carbon–epoxy laminates using FBGs, Part I: Elementary specimen, *Composites: Part A*, **40**, 94–104.

Oh, J. H. and Lee, D. G. (2002) Cure cycle for thick glass/epoxy composite laminates, *J. Compos. Mater*, **36**(1), 19–45.

Park, H. C. and Lee, S. W. (2001) Cure simulation of thick composite structures using the finite element method, *J. Compos. Mater.*, **35**(3), 188–201.

Patricia, P., Harald, E. N. and Adriaan, B. (2007a) Residual stresses in thermoplastic composites – a study of the literature. Part II: Experimental techniques, *Composites: Part A*, **38**, 651–66.

Patricia, P. P., Harald, E. N. B. and Adriaan, B. (2007b) Residual stresses in thermoplastic composites – a study of the literature. Part III: Effects of thermal residual stresses, *Composites: Part A*, **38**, 1581–96.

Rai, N. and Pitchumani, R. (1997) Optimal cure cycle for the fabrication of thermosetting-matrix composites, *Polym. Compos.*, **18**(4), 566–81.

Teplinsky, S. and Gutman, E. M. (1996) Computer simulation of process induced stress and strain development during cure of thick-section thermosetting composites, *Computational Materials Science*, **6**, 71–6.

Twardowski, T. E., Lin, S. E. and Gell, P. H. (1993) Curing in thick composite laminates: experiment and simulation, *J. Compos. Mater.*, **27**(3), 216–50.

White, S. R. and Hahn, H. T. (1992a) Process modeling of composite materials: residual stress development during cure. Part I: Model formulation, *Journal of Composite Materials*, **26**(16), 2402–22.

White, S. R. and Hahn, H. T. (1992b) Process modeling of composite materials: residual stress development during cure. Part II: Experimental validation, *Journal of Composite Materials*, **26**(16), 2423–53.

White, S. R. and Kim, Y. K. (1996) Staged curing of composite materials, *Composites: Part A*, **27**, 219–27.

Wisnom, M. R., Gigliotti, M., Ersoy, N., Campbell, M. and Potter, K. D. (2006) Mechanisms generating residual stresses and distortion during manufacture of polymer–matrix composite structures, *Composites: Part A*, **37**, 522–9.

Wu, Z., Guo, Z., Wan, L., Zhang, B. and Du, S. (2004) *Measurement of Process-induced Stresses in Composite Laminates by FBG Sensors, SAMPE Conference Proceedings – Materials And Processing Technology – 60 Years of SAMPE Progress*, 3194–201.

Yi, S., Hilton, H. H. and Ahmad, M. F. (1997), A finite element approach for cure simulation of thermosetting matrix composite, *Computers and Structures*, **64**(1–4), 383–8.

13

Reduction of residual stresses in polymer composites using nano-additives

M. M. SHOKRIEH, S. AKBARI and A. DANESHVAR,
Iran University of Science and Technology, Iran

DOI: 10.1533/9780857098597.2.350

Abstract: This chapter discusses the reduction of residual stresses in polymer composites using nano-additives, especially carbon nanofibres (CNFs) and carbon nanotubes (CNTs). First, a review of conventional nano-additives and their mechanical and thermal properties was carried out. The main thermal and mechanical factors affecting the values of residual stresses were studied. Then the effects of nano-additives on the coefficient of thermal expansion and Young's modulus of the matrix as the main factors in the formation of residual stresses were discussed. The last section of this chapter presents the experimental results of adding CNFs on residual stresses distribution in carbon-fibre/epoxy laminated composites.

Key words: residual stress, polymer composites, coefficient of thermal expansion, Young's modulus, nano-additives.

13.1 Introduction

Residual stresses in fibre reinforced composites are introduced during the curing and cooling stages of fabrication, due to a high contraction of polymer matrix in comparison with fibres. This phenomenon is observed in almost any composites, as a result of natural inconsistency of physical and mechanical properties of the fibre and matrix. Generally, these stresses are studied from the macroscopic and microscopic points of view. The residual stress in micro-scale is a result of the mismatch in the coefficient of thermal expansion (CTE) and Young's modulus between the fibres and the matrix and interphase (Quek, 2004; Shokrieh and Safarabadi, 2012a,b). On the macro-mechanical level or layers, the non-uniform shrinkage and mismatch in CTE between different layers is the governing parameter (Borges de Almeida, 2005; Kim and Mai, 1998).

The greater the difference between thermal and mechanical properties of the fibre and matrix, the more residual stress is created. Nevertheless, the amount of residual stress depends on the layers structure, laminate lay-up and the fabrication process. In addition to the contraction of polymer during curing cycles, polymerization creates a kind of contraction induced by cross-linking of polymer molecules and therefore intensifies the residual stress creation. Such a phenomenon is important and must be taken into account (Callister, 1994).

Residual stresses negatively affect the performance of composite structures and cause several defects at the micro-mechanical and macro-mechanical levels. Some adverse effects include transverse cracks (Gentz *et al.*, 2004), delamination (Nairn, 1997), fibre buckling (Bhalerao, 1996), deformation in non-symmetrical laminates (Lawrence *et al.*, 1990; Shokrieh and Kamali, 2005), fibre-matrix debonding (Sjogren *et al.*, 1999) and loss of strength of composite components.

For instance, out-of-plane deformation occurring in non-symmetrical laminates could reduce dimensional stability and tolerance control of composite parts, which are important parameters in constructing large structures or even small ones. One reason, which can result in such a problem, is the residual stress created during the curing process of composites, which may lead to the deformation of a component after being exited from the mould (Hsiao and Gangireddy, 2008). Thus residual stress may lead to undesirable dimensional changes. Considering the effect of residual stress on the performance or even designing a composite structure, it is important to develop techniques to reduce such stresses.

Nowadays, nanotechnology has remarkably changed the materials engineering and has provided a new approach to fabricate novel materials with incredible properties. Advanced nanocomposites, which are combinations of a matrix and nano-fillers (Thostenson *et al.*, 2005), have attracted much attention over the past several years. Nano-fillers are introduced into the conventional composites to enhance their mechanical, electrical, chemical and thermal properties.

A new method to decrease the residual stresses is by using nano-fillers, which is the subject of this chapter. Until now, a few research projects have been performed to reduce residual stresses in this way. This method aims to decrease the mismatch between the properties of fibres and matrix, so as to decrease the residual stresses. As mentioned before, different thermal and mechanical properties of different layers are the major reason of introduction of residual stresses in laminated composites. The residual stress in such materials depends on the CTE, Young's modulus (E) and Poisson's ratio (ν) of constituents. Therefore, modification in any of the above properties belongs to either the matrix or fibre to decrease the dissimilarity between properties, which could result in a reduction of residual stresses. The first two factors, the CTE and Young's modulus, are more important due to their thermal and mechanical influences, respectively (Shokrieh and Safarabadi, 2011).

Since it is not intended to alter the fibre properties, the nano-fillers are added to the polymeric matrix to make its properties closer to those of the fibre. Compared with the fibre, the matrix has much higher CTE and smaller Young's modulus. Therefore, adding nano-fillers to the matrix could decrease its CTE and increase its Young's modulus.

Although many researchers have reported the increase in Young's modulus and decrease in CTE of polymers due to addition of nano-fillers, few studies have so far been carried out to experimentally to investigate the effects of nano-fillers on the values of residual stresses in polymer composites. Nishino *et al.* (2009)

considered the effect of tangusten zirconium phosphate ($Zr_2(WO_4)(PO_4)_2$) (ZWP) particles on CTE of polyetheretherketone (PEEK) polymers and experimentally showed that these particles significantly reduce residual stresses in the PEEK/Al plate. They showed that by incorporating 40 vol% ZWP particles (with negative CTE), the CTE of the PEEK composite can be reduced by about 62%. Also, Hsiao and Gangireddy (2008) utilized CNFs to control dimensional tolerance of glass/polyester laminated composites. They presented an integrated modelling and experimental investigation about the effect of CNFs on the spring-in phenomenon in L-shaped composite parts. Their analytical model and experimental results clearly explain how the CNF-enhanced dimensional tolerance control is accomplished through the reductions in the CTE of the polymeric matrix, resulting in reduction of spring-in angle in L-shaped composites.

Because of negative effects of thermal residual stresses, it is important to develop techniques to reduce these stresses. Most of the approaches employed so far for this purpose are confined to modifying curing cycles (Hodges *et al.*, 1989; Kim *et al.*, 2006; White and Hahn, 1993). Modifying curing cycles do not affect thermal and mechanical properties of fibre and resin and the inherent mismatch between these properties remains unchanged. But nano-additives could reduce inherent mismatch between the properties and consequently could inherently reduce the thermal residual stresses.

13.2 Application of nano-additives to enhance the thermal and mechanical properties of polymer composites

Residual stresses in composites, based on their resources, are studied on two levels, micro-residual stresses (single matrix-fibre composite) and macro-residual stress (in laminated composites). Total residual stresses are determined by adding micro- and macro-residual stresses.

At the macro-mechanical level, classical laminated theory (CLT) is the simplest and commonest method for analytical study of macro-residual stress in laminated composites (Hahn and Pagano, 1975). In addition, the CLT and the energy method can be used to predict the shape of the asymmetrical laminates after the curing process (Shokrieh and Kamali, 2005; Wang *et al.*, 1992). It is important to note that CLT can only present an initial estimation of macro-residual stresses, because the CLT does not consider several important factors affecting the formation of residual stresses, such as cooling rate and the change in matrix CTE during the curing process. The exact determination of residual stresses at the macro-level is only possible using destructible methods such as hole drilling or slitting (Ersoy and Vardar, 2000; Sicot *et al.*, 2003).

At the micro-mechanical level, several micro-mechanical methods have been presented by researchers to determine micro-residual stress in single fibre-matrix composites. Among them, the energy method is the most useful. This method does

not have the limiting assumptions of the other methods and provides a direct approach to obtain the micro-residual stresses. Also this method clearly shows the influence of effective parameters (CTE, Young's modulus) on micro-residual stresses (Shokrieh and Safarabadi, 2011).

In order to study nano-additives effects on residual stress in composites, it is necessary to know the main parameters affecting residual stress formation and then study the effect of nano-fillers on these parameters. As mentioned in the previous section, thermal residual stress is a function of physical and mechanical properties of the matrix and reinforcement, so effective parameters are CTE, elastic modulus (E) and Poisson's ratio (ν) of constituents. Analytical study of these elements in composites shows that residual stress fields are independent of Poisson's ratio and the effects of Poisson's ratio are negligible (Shokrieh and Safarabadi, 2011). In addition to the matrix and reinforcement properties, there are other parameters that affect residual stress formation in composites, such as fibre volume fraction, cure conditions, glass transition temperature (T_g), post-cure process and environmental conditions. But, nano-fillers effects on environmental and cure conditions are not the subject of this chapter and therefore the study of nano-filler effects on the residual stress in composites are limited to study of their effects on the CTE and Young's modulus of the matrix.

Through a systematic study of nano-filler effects on the major parameters in the formation of residual stress and the use of the CLT analysis and energy method for calculation of macro- and micro-residual stresses in laminated composites, it is possible to approximate how much the use of nano-fillers in the matrix of laminated composites can be effective for the reduction of residual stresses.

13.2.1 Conventional nano-additives

The current interest in nanocomposites began in 1991. Toyota achieved dispersion of layered silicate clays in Nylon-6, which increased highly the heat distortion temperature (HDT) and mechanical properties of Nylon-6 composites. Simultaneously in 1991, Iijima (1991) discovered carbon nanotubes (CNTs), which have attracted much attention from researchers during the past 20 years.

Nowadays, a large number of nano-additives are available, classified into four general categories: nanoparticles, nanoplatelets, nanofibres and nanotubes. These nano-additives differ in morphology, geometry, chemistry, aspect ratio and aggregate size. The type of the nano-additive chosen for dispersion in a matrix is dependent on the intended application.

Some common nanoparticles used in composites include SiO_2, alumina, ZWP and metals oxides at the nanometer scale. Nanoparticle additives result in higher stiffness, lower CTE and comparable or lower strength and elongation of the matrix (Naganuma and Kagawa, 2002; Nishino *et al.*, 2009).

Nano-clay, graphite and graphene are types of nanoplatelet nano-additives that exist as layered materials in their bulk states. It is important to employ the most

efficient method to ensure that layers are sufficiently separated and dispersed throughout the matrix. A layer of nano-clay is about 1 nm in thickness and consists of platelets of around 100 nm in width. The thickness of graphene and graphite is about 0.34 and 10 nm, respectively. Graphene is just a single layer of graphite. It is basically a single layer of sp^2-hybridized carbon with a delocalized π-bonded network. The theoretical Young's modulus of an individual graphene layer is 1600 GPa. It also has a negative CTE similar to other carbon-based nano-fillers. The polymer-based nanoplatelets nanocomposites show improved stiffness, toughness, strength and thermal stability, as well as reduced CTE (Alexandre and Dubois, 2000; Miller, 2008).

Carbon nanofibres (CNFs) are used to reinforce a variety of polymers, including polypropylene, polycarbonate, nylon, polyethersulfone (PES), polyethyleneterephthalate (PET), polyphenylenesulfide (PPS), acrylonitrile-butadiene-styrene (ABS) and epoxy. CNFs typically have diameters in the order of 50 to 200 nm, Young's modulus of about 246 to 600 GPa and a negative CTE of about $-1 \times 10^{-6}\,°C^{-1}$. Therefore, CNFs could be utilized to decrease CTE and increase the Young's modulus of polymers. Several research groups experimentally reported the CTE and Young's modulus improvement in polymer/CNF nanocomposites (Chaos-Mora *et al.*, 2011; Cho *et al.*, 2011; Hine *et al.*, 2005; Iwahoria *et al.*, 2005; Wang *et al.*, 2010).

Since their observation, numerous investigators have reported remarkable physical and mechanical properties for CNTs. The density of a SWCNT is about 1.33 to 1.40 g/cm^3, which is just one-half of the density of aluminium. The elastic and strength properties of SWCNT and MWCNTs have been extensively studied, both analytically and experimentally. Theoretically, the CNT Young's modulus is up to 1 TPa. The reported longitudinal CTE of the CNT is $-1.5 \times 10^{-6}\,°C^{-1}$. Despite this, the CNT radial CTE is about $15 \times 10^{-6}\,°C^{-1}$. The reported tensile strength of SWCNT is much larger than that of the high-strength steel. A review on the mechanical tensile properties showed an approximately linear increase in composite stiffness, but a reduction in strength and strain to failure for filler weight fractions of about 1 wt%. It has already been experimentally and theoretically proved by a number of researchers that because of the high modulus and negative CTE of CNTs, a matrix even with very low weight fraction of CNTs (<1 wt%) has much lower CTE in comparison with the pure matrix (Deng *et al.*, 2008; Xu *et al.*, 2006).

13.2.2 Nano-additive effects on coefficient of thermal expansion of the matrix

Most of materials show increase in their dimensions when encountering a thermal flux under constant pressure. However, some materials contract under heat and show negative thermal expansion. Besides, if a solid material shows different thermal properties along different directions, thermal expansion can be anisotropic.

Especially, this phenomenon takes place in reinforced composites, in which the reinforcement has different thermal properties from those of the matrix. Polymers like epoxy, generally have higher CTE in comparison with fibres and metals. In polymers, CTE is divided into two parts, before and after glass transient temperature (T_g). Polymers and composites lose most of their mechanical properties after the glass transition temperature.

As mentioned before, residual stresses are generated due to mismatch of mechanical and thermal properties of fibres and matrix. It seems that residual stresses amplitude is more dependent on CTE of composite components. At a macro-mechanical level, expansion and contraction of different layers with different orientations is the major source of residual stresses. Especially, CTE of a uni-directional ply along the longitudinal direction is much lower than the CTE in the transverse direction, because of the thermal property difference of fibres along these directions. So during the curing and cooling processes, layout of layers with different CTE to each other, results in macro-residual stress induction in composites. In polymer composites, fibres have lower CTE in comparison with the matrix; and during the curing and cooling processes, the matrix has more contraction, therefore a compressive residual stress through fibres and a tensile stress through the matrix are generated at the micro-scale.

In the CLT analysis of multi-layered laminated composites, it is shown that the closer longitudinal and transverse CTE of uni-directional ply results in lower macro-residual stresses. At the micro-mechanics level, the less difference between the CTE of fibres and matrix also leads to less micro-residual stresses induction (Shokrieh and Safarabadi, 2012a,b). There are lots of experimental studies conducted around the effect of nano-fillers on polymers CTE. Because of unique properties of nano-fillers and significant characteristics of nanocomposites through which the contact area of the matrix and reinforcement increases, in spite of nano-additives extremely low weight fraction, matrix CTE decreases considerably (Xu *et al.*, 2006).

Little data about CTE of nano-fillers are available. Determining nano-filler CTE is generally a complicated process. However, according to their high Young's modulus, it is expected that their CTE be much less than that of polymeric matrixes. Because of carbon sp^2 atomic lattices, it is expected that CNTs and CNFs have a negative CTE. Longitudinal CTE values are reported as about -1.5×10^{-6} °C^{-1} and -1×10^{-6} °C^{-1} for CNTs and CNFs, respectively. This value in the transverse direction is reported for 15×10^{-6} °C^{-1}.

There are no clear equations for exact modelling of CTE of the matrix with nano-fillers at the nano-scale. But simulations such as molecular dynamics can approximate the CTE of nanofiller/matrix composites. Nevertheless, in order to determine the CTE of polymeric composites reinforced with CNTs and CNFs, few researchers consider these nano-fillers as short fibres and use the CTE equation in micro-scale and estimate CTE of the nanocomposites (Gonnet, 2004; Hsiao and Gangireddy, 2008).

In the last section of this chapter, using thermo-mechanical analysis (TMA), it is shown that CNFs can considerably affect the thermal behaviour of epoxy polymers. As a result, the transverse CTE of the uni-directional ply decreases dramatically.

13.2.3 Nano-additive effects on Young's modulus of the matrix

In addition to the discrepancy in thermal properties, mechanical property dissimilarity of composite components affects the residual stresses. Also it results in discontinuity of stresses across layers boundaries.

In this section, the effect of nano-fillers on the Young's modulus of the matrix and consequently on uni-directional fibrous composites is studied. The dispersion of CNTs and CNFs restricts the mobility of polymer chains under loading and could improve the modulus and strength under small loadings. Based on the conducted studies, it is proved that adding nano-fillers to the matrix leads to an increase in composites Young's modulus, while the quantity of this increase depends on the type of nano-filler, matrix and methods of nano-filler dispersion in the matrix. Through matrix Young's modulus increase, due to the nano-fillers distribution within it, residual stresses of composites decrease.

Usually the nano-fillers Young's modulus is high. For example, the CNT modulus is theoretically higher than 1 Tpa. In order to present an appropriate explanation for excellent properties of composites reinforced with nano-fillers, two major factors must be investigated, distribution of nano-fillers in the matrix and interactions between the matrix and nano-fillers. Experimental results about CNTs show that as weight loading of CNTs in the matrix increases, Young's modulus of the matrix increases in a linear manner. With an increase in nano-filler content to the higher weight loadings, the rate of increasing Young's modulus decreases. This is because of difficulties of nano-fillers dispersion in the matrix and agglomeration generation when weight loadings are too high. Generally, elastic modulus of polymer reinforced with nano-filler is calculated by the use of elastic characteristics of components (nanofiller and matrix), aspect ratio and nanofiller volume fraction.

For modelling the matrix reinforced with nano-fillers, there are different experimental and semi-experimental methods in use. Most studies have been conducted on matrixes reinforced with CNTs and CNFs. Depending on the geometry and structure of the nano-fillers, it is possible to use modified micro-mechanics equations for determining the Young's modulus of composites reinforced with these nano-fillers. Elastic characteristics determination of materials reinforced with discontinuous fibres as a function of fibres volume fraction has attracted great attention.

In the next section, through the characterization of nanocomposites, it is experimentally shown that using CNFs can increase the Young's modulus of epoxy polymer and also transverse Young's modulus of the uni-directional ply.

13.3 Case study: reduction of residual stresses in carbon/epoxy laminates using carbon nanofibres (CNFs)

In this section, the effect of CNFs on thermal residual stresses in carbon fibre (CF)-reinforced epoxy composites is investigated. First, two-phase CNF/epoxy composites and three-phase CNF/CF/epoxy composites were fabricated and characterized. CNFs were dispersed into the epoxy matrix with three weight ratios of 0.1, 0.5 and 1%, and then reinforced with uni-directional CFs to fabricate laminated composites with cross-ply configuration. The slitting method was employed for the determination of residual stresses in these laminates. A detailed description of these experiments is presented in this section.

13.3.1 Fabrication and preparation of specimens

The epoxy resin ML-506 and the curing agent Aradur-830 used in this research were supplied by Mokarrar Engineering Materials and Huntsman Co., respectively. The average length and the diameter of CNFs, supplied by Grupo Antolin, were 30 μm and 20 to 80 nm, respectively.

The neat resin specimens were prepared by mixing pre-calculated amounts of ML-506 epoxy and Aradur-830 hardener thoroughly. The mixture was stirred for 30 min at 2000 rpm. Then the mixture was placed under vacuum for 30 min to remove air bubbles.

Epoxy/CNF composite specimens reinforced with three different contents of CNF were fabricated using sonication technique. First, resin was mixed with the desired CNF contents and stirred for 30 min at 2000 rpm. Then, in order to break the residual aggregates and obtain a homogeneous mixture of epoxy resin and CNFs, the mixtures containing 0.1, 0.5 and 1 wt% CNFs were sonicated (Bandelin HD3200, 20 kHz) for 40, 60 and 80 min, respectively. During sonication, the mixture container was submerged in water to keep it cool. Once sonication was complete, the curing agent was added to the mixture and stirred for 20 min at 250 rpm. Next, air bubbles and reaction volatiles were removed by degassing the solution in a vacuum chamber for 30 min. Finally, the bubble-free mixtures of CNF/epoxy and neat resin were cast on metal moulds and cured for 6 h at 100 °C, followed by 6 h at 120 °C. A mould-releasing agent was added to the mould surface to allow an easy release of the cured specimens.

Three-phase CNF/CF/epoxy composites were manufactured using the hand lay-up method. Uni-directional T300 carbon fibres (CFs), supplied by Toray Co., were used as reinforcement of the matrix. The CNF dispersed resin used in the manufacturing of CNF/CF/epoxy composites was prepared as identically as possible with the two-phase CNF/epoxy composites. The same cure process as the two-phase composites was employed for the three-phase composites.

13.3.2 Experimental characterization

Young's modulus of CNF/epoxy composites

This section focuses on characterizing the thermo/mechanical behaviour of the neat resin and CNF/epoxy composites. The Young's modulus of the fabricated specimens was obtained using tensile tests performed according to ASTM D638 (ASTM D638). The dimensions of the specimens were about 250 mm in length, 20 mm in width and 3.9 mm in thickness.

In order to perform the tensile tests, Santam STM-150 universal apparatus with a 50 kN load cell was employed. The machine was run under displacement control mode at a crosshead speed of 1.0 mm/min. The strain data was obtained using an extensometer of 50 mm gauge length. Prior to the tensile test, all the samples were mechanically polished to minimize the influence of surface flaws, especially the porosity.

At least four samples were tested for every nanocomposite specimen; the final property was the average result of the four tests. Two neat epoxy and CNF/epoxy specimens prepared for tensile test are shown in Fig. 13.1.

Figure 13.2 shows the averaged tensile test results for all three types of nanocomposites, as well as for neat resin. It is observed in this figure that the dispersion of CNF into the epoxy has a moderate effect on the Young's modulus of the two-phase composites. At 1% loading, the Young's modulus of CNF/epoxy composite was 11% larger than that of the neat resin.

In this research, dispersion of CNFs in epoxy was carried out using the sonication technique, which is one of the most effective methods of dispersing nano-additives with small loading into the pure materials.

Figure 13.3 shows the SEM micrographs for different weight fractions of the CNF corresponding with the fracture surfaces of the specimens broken by tensile tests. The fracture surface of the neat epoxy is smooth. However, by addition of CNF, the fracture surface roughness increases and the CNF broken stem can be seen.

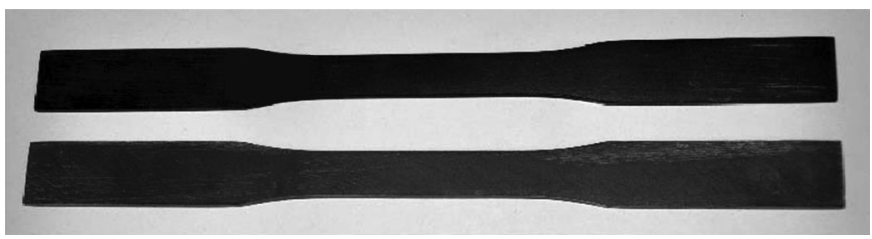

13.1 Neat epoxy and CNF/epoxy specimens used for tensile tests.

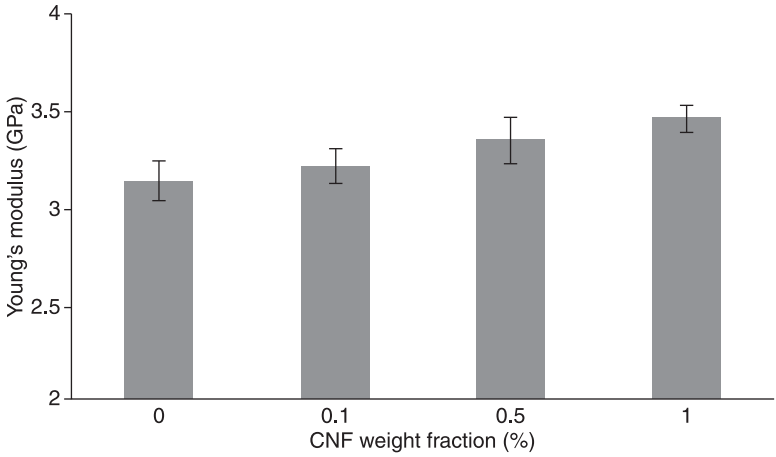

13.2 Young's modulus comparisons for CNF/epoxy composites with three different weight fractions of CNFs.

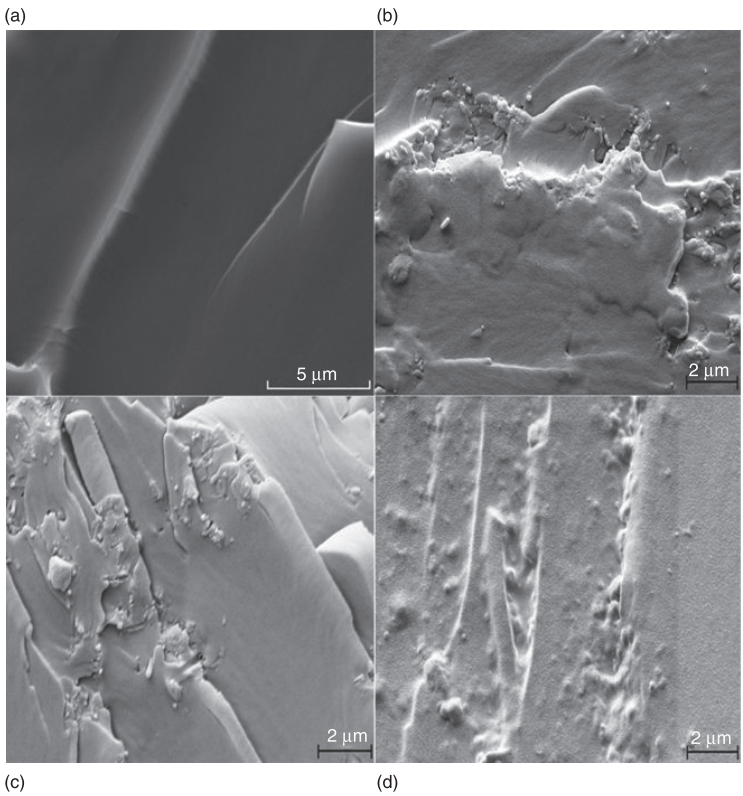

13.3 SEM micrographs showing the fracture surfaces of: (a) neat epoxy, and CNF/epoxy with (b) 0.1 wt%; (c) 0.5 wt%; and (d) 1 wt% CNF.

Coefficient of thermal expansion (CTE) of CNF/epoxy composites

In order to investigate the CNFs effects on the CTE of epoxy, CTE of the neat resin and CNF/epoxy specimens were studied by thermo-mechanical analysis (TMA). The CTE values were determined by measuring the inclination of thermal strains versus the temperature, according to ASTM E831 (ASTM E831):

$$\alpha = \Delta L / L_0 \Delta T \qquad [13.1]$$

where, ΔL is the change in the length of the composite specimen due to heating, L_0 is the initial length of test specimen and ΔT is temperature difference, over which the change in the specimen length is determined. Thermo-mechanical analysis was carried out using a thermo-mechanical analyser (SSC/5200 TMA 120 CU, Seiko Instruments). The effect of the weight fraction of CNF was assessed by measuring the CTE of CNF/epoxy composites at three different weight fractions of 0.1, 0.5 and 1%. The specimens tested had dimensions of $7 \times 7 \times 6$ mm. The test was run for up to 140 °C at a constant heating rate of approximately 0.1 °C/sec.

Figure 13.4 represents the CTE values for the composite specimens at three different weight fractions, as well as for the pure epoxy. For CNF weight fractions of 0.1, 0.5 and 1%, resin CTE decreased by 6.3, 26.0 and 32.5%, respectively. It is observed that the CTE values of all the composites significantly decreases with an increase in the weight fraction of CNF.

According to the CF data sheet, CFs have a Young's modulus of 230 GPa and a CTE of -0.41×10^{-6}/°C. The neat epoxy has a Young's modulus of 3.13 GPa and a CTE of 62.46×10^{-6}/°C. The incorporation of 1 wt% CNF into the epoxy

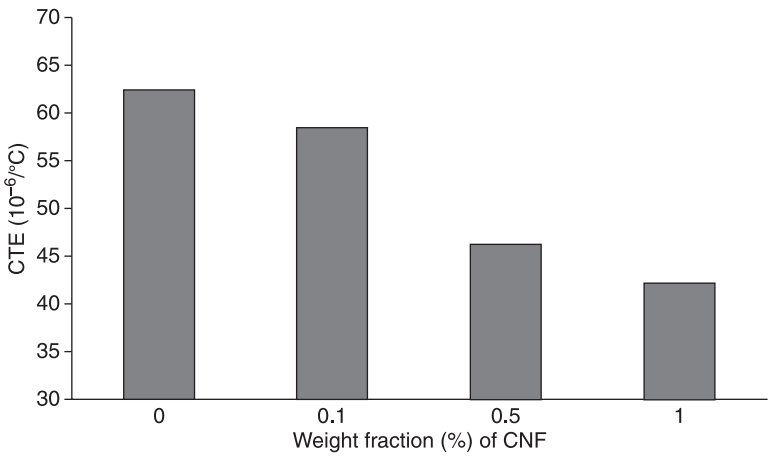

13.4 CTE comparisons for CNF/epoxy composites with three different weight fractions of CNFs.

increases its Young's modulus to 3.46 GPa and reduces its CTE to 42.17×10^{-6}/°C. Therefore, 1 wt% CNF loading results in 0.14 and 32.3% reduction in the Young's modulus and CTE mismatch between the fibre and matrix, respectively. Thus, any reduction in the residual stresses in CNF/CF/epoxy composites could be attributed to the reduction of the matrix CTE.

Young's modulus of CNF/carbon fibre (CF)/epoxy composites

Static strength tests in the longitudinal and transverse directions were performed for uni-directional CNF/CF/epoxy laminates as three-phase composites, according to ASTM D3039 (ASTM D3039). The dimensions of 0-degree uni-directional specimens were about 250 mm in length, 15 mm in width and 1 mm in thickness. The dimensions of 90-degree uni-directional specimens were about 175 mm in length, 25 mm in width and 2 mm in thickness. Two 0-degree and 90-degree uni-directional samples are shown in Fig. 13.5. For each weight fraction of CNF, three specimens were tested.

The shapes of stress–strain curves for three phase composites were almost linear. Table 13.1 shows the averaged test results of modulus for all types of CNF/CF/epoxy composites. It was found that the longitudinal modulus is not seriously affected by the CNF dispersion. On the contrary, transverse modulus is more affected by CNF dispersion. Three-phase composites with 0.5 and 1 wt% of CNF showed increases in transverse modulus of about 10.8 and 14.9%, respectively.

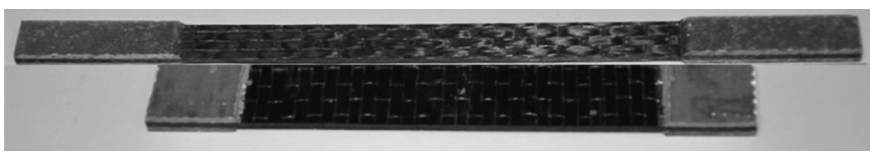

13.5 Two uni-directional composite specimens used for longitudinal and transverse tensile tests.

Table 13.1 Longitudinal and transverse Young's modulus of unidirectional CNF/CF/epoxy composite specimens with different contents of CNFs

	CNF wt%			
Young's modulus	0	0.1	0.5	1
E_x (GPa)	104.6	104.1	104.9	105.1
E_y (GPa)	7.4	7.6	8.2	8.5

13.3.3 Residual stress measurement

The residual stress measurement of composite specimens was carried out using the slitting method, which consists of cutting a narrow slit in successive increments from the surface of the specimen and measuring the released strains using a strain gauge bonded to the other surface.

Principles of slitting method

Figure 13.6 shows the typical geometry of the slitting method with a back surface strain gauge. The strain gauges bonded on the back surface of the stressed part directly opposite the slit are sensitive to all residual stress within the specimen thickness and thus generally used for through-thickness measurements. However, the strain gauges bonded on the top surface near the slit are only sensitive to near surface residual stress (usually up to 20–25% of the thickness) and therefore are appropriate for near surface measurements. In this research, back surface strain gauges were used.

The slit starts from the top surface of the specimen and is extended in successive increments towards the back surface. For the configuration shown in Fig. 13.7, the slitting method will determine unknown normal residual stress components perpendicular to the slit plane, $\sigma_{yy}(x)$, using y-strain measured by back surface or top surface strain gauges.

Because of the spatial separation of the location of the strain measurement and the location of calculated residual stress, the relationship between the residual

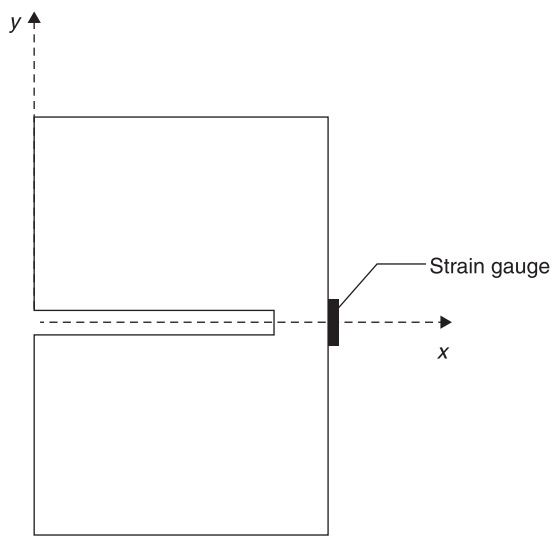

13.6 Slitting method schematic (Lee and Hill, 2007).

stresses released along the slit face and the measured strains does not have a simple one-to-one form. In fact, this relationship has the following integral form:

$$\varepsilon_{yy}(a_i) = \int_0^{a_i} C(x, a_i)\sigma_{yy}(x)dx \qquad [13.2]$$

where $\varepsilon_{yy}(a_i)$ is the measured y-strain when the slit depth is a_i. The Kernel function $C(x, a_i)$ is equal to the measured strain due to a unit stress at depth x within a slit of depth a_i.

To solve Eq. 13.2, an initial distribution for residual stress must be considered. Two conventional methods of approximation of residual stresses in slitting method include the 'Series Expansion Method' and the 'Pulse Method' (Prime, 1999). In the application of the series expansion method to the isotropic materials, the residual stress profile along the specimen thickness is often approximated by a continuous polynomial (typically Legendre polynomials) with unknown coefficients. Then the unknown coefficients are determined from compliance coefficients and the measured strain data. In layered materials like laminated composites, because of discontinuity of material properties across layers boundaries, the stress profile is not continuous. Therefore, the series expansion method cannot be used for laminated composites.

The second common approach for estimating stress profile is the pulse method. In this method, a uniform stress for each increment of slit depth is considered. The main feature of the pulse method approximation is that it requires no initial assumption about the continuity of the residual stress distribution and thus can be used for laminated composites. A brief description of this method is presented below.

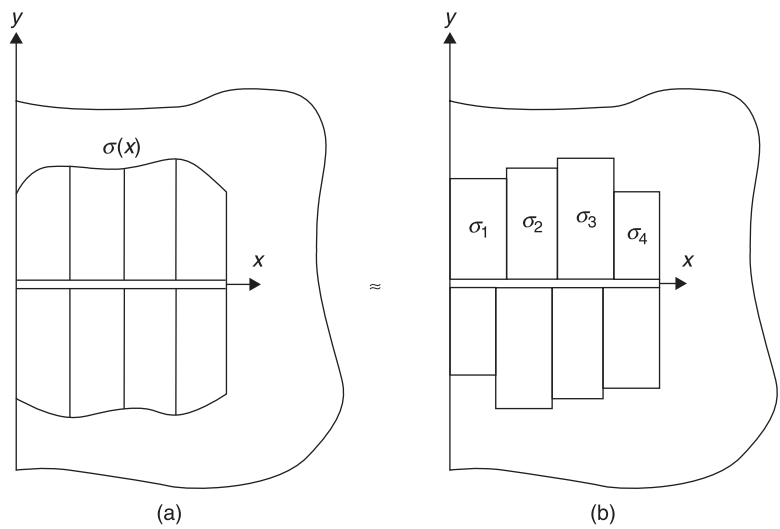

13.7 (a) An unknown residual stress distribution on slit faces; and (b) a series of uniform strip loads.

Consider a residual stress profile acting on the faces of a slit of increasing depth, as shown in Fig. 13.7(a). In the pulse method, the stress profile is estimated by a series of strip or pulse loads over each increment of the slit (Fig. 13.7(b). Therefore, in the pulse method the residual stress is estimated by

$$\sigma(x_j) = \sum_{j=1}^{n} \sigma_j U_j(x) \qquad [13.3]$$

where σ_j corresponds to the stress value in the jth increment and n is the total number of increments. The pulse functions are defined as

$$U_j(x) = \begin{cases} 1 & a_{j-1} \le x \le a_j \\ 0 & x \le a_{j-1}, x \ge a_j \end{cases} \qquad [13.4]$$

Substituting Eq. 13.3 into Eq. 13.4 results in

$$\varepsilon(a_i) = \int_0^{a_i} C(x,a_i) \sum_{j=1}^{n} \sigma_j U_j(x) dx = \sum_{j=1}^{n} \sigma_j \int_0^{a_i} C(x,a_i) U_j(x) dx = \sum_{j=1}^{n} \sigma_j C_{ij} \qquad [13.5]$$

Therefore, C_{ij} or the elements of compliance matrix are expressed by

$$C_{ij} = \int_0^{a_i} C(x,a_i) U_j(x) dx = \int_{a_{j-1}}^{a_j} C(x,a_i)\, dx \qquad [13.6]$$

Comparing with Eq. 13.2 indicates that a specific element of the compliance matrix, C_{ij}, represents the measured strain at the strain gauge location for a slit of depth a_i, when residual normal stress distribution at the domain $a_{j-1} \le x \le a_j$ is equal to the unit load:

$$C_{ij} = \varepsilon(a = a_i,\ \sigma(x) = U_j(x)) \qquad [13.7]$$

Figure 13.8 shows the physical interpretation of the compliance coefficients for the pulse method. In this work, elements of the compliance matrix are calculated using a finite element method described in Shokrieh and Akbari (2012a,b). The relationship between the measured strain data and the stresses within each depth increment can be expressed as

$$[C]\{\sigma\} = \{\varepsilon\} \qquad [13.8]$$

Therefore, the procedure of the residual stress determination involves computing the elements of the compliance matrix, measuring the released strains during the slitting and finally solving Eq. 13.8.

Experimental procedure

Residual stress measurement was performed by the slitting method on a coupon of the cured nanocomposite plates. Dimensions of the specimens are given in Table 13.2. Figure 13.9 shows the prepared specimens for the slitting test.

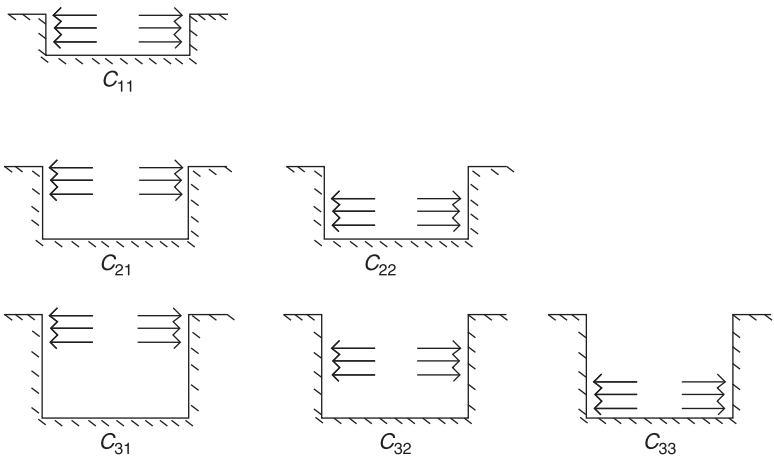

13.8 Physical interpretation of compliance coefficients of the pulse method.

13.9 Untested CNF/CF/epoxy nanocomposite specimens.

Table 13.2 Dimensions of the nanocomposite specimens (mm)

Width (B)	Length (L)	Thickness (t)	Slit width (w)
15	50	4.8	0.25

Slitting experiments were carried out in a CNC milling machine (Emco Concept Mill 155). The specimens were clamped from one side away from slit and gauge, so the other side could deform freely and recorded strains were correct (Fig. 13.10). A circular cutter 0.2 mm thick and 23 mm in diameter was used. The rotation speed of the saw blade was 5000 rpm. The slitting was carried out in successive depth increments of 0.3 mm to a final depth of 2.4 mm, which is equal to the half thickness of the specimens. The depth increment was equal to the thickness of each layer of the laminate. Figure 13.10 shows the relative position of strain gauge and cutter in the slitting experiment.

In order to measure the relaxed strains associated with incremental slitting, a type UBFLA-03 strain gauge with a gauge length of 0.3 mm, supplied from TML Co., was used. In order to minimize the effect of averaging of the strain over the gauge length and to increase the precision of strain readings at the desired location, a small gauge was selected.

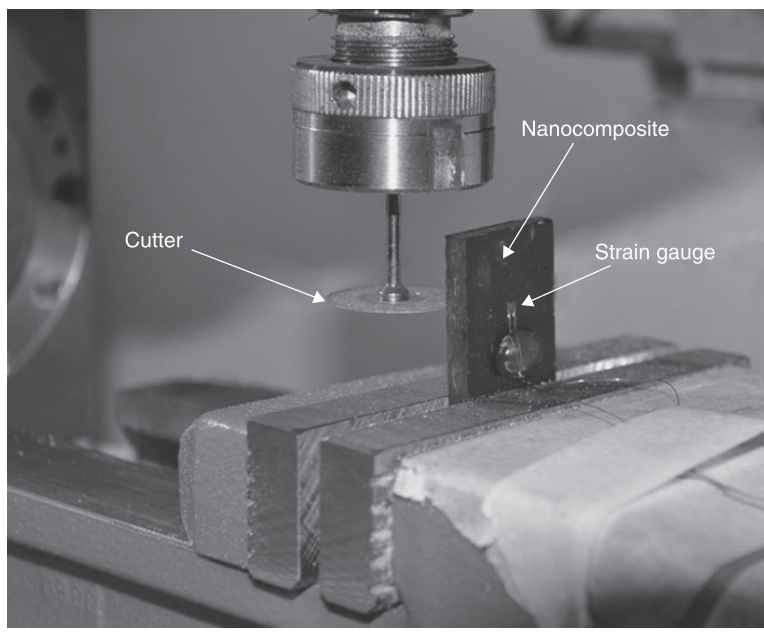

13.10 Experimental set-up of slitting test.

Prior to bonding strain gauges, the surface of the specimens was degreased with acetone. Enough care should be taken to ensure that the strain gauge is bonded directly opposite the slit. This is because this area experiences the largest deformation on the surface and the amplitude of the released strains declines rapidly from this point.

After each slitting step, the cutter was withdrawn from the specimen and the CNC machine was turned off. The released strains were measured using a computerized data acquisition system. Strain measurement was performed 3 min after each slitting step. This time allowed stabilization of any temperature fluctuations resulted from the slitting process.

13.3.4 Results and discussion

The slitting experiment was repeated for four coupons of each nanocomposite specimen. The average strains measured during the slitting experiments for each weight fraction of CNFs are reported in Table 13.3.

In order to calculate the required compliance coefficients, ANSYS finite element software was used. The mesh was constructed using 8-node 3D layered elements, Solid46 (Fig. 13.11). In this model, the magnitude of the unit load (pulse load) in each load step was considered as 1 MPa. For each nanocomposite specimen, the elastic constants obtained from characterization tests were used (Table 13.1).

In order to compute gauge-averaged strain ($\mu\varepsilon$) at the strain gauge location, displacements at nodes located at the boundaries of the strain gauge can be used with the initial gauge length (distance between the nodes) to compute C_{ij}, which is the gauge-averaged strain resulting from applying the pulse load U_j to the slit of depth a_i (Schajer, 1993). The resulting compliance matrix for CF/epoxy composite

Table 13.3 Average recorded strain $\mu\varepsilon$ for CNF/CF/epoxy nanocomposite specimens with different contents of CNFs

	CNF wt%			
Slit depth (mm)	0	0.1	0.5	1
0	0	0	0	0
0.3	–56	–53	–44	–38
0.6	–148	–139	–114	–106
0.9	–244	–235	–196	–188
1.2	–360	–344	–289	–272
1.5	–512	–495	–415	–395
1.8	–666	–646	–541	–526
2.1	–837	–816	–686	–679
2.4	–1040	–1028	–867	–877

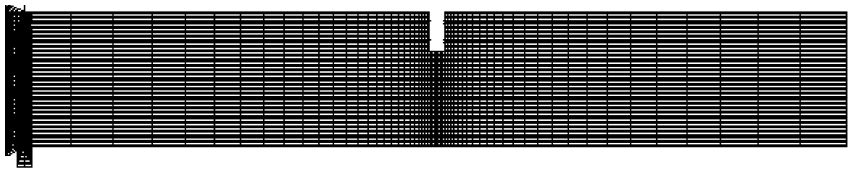

13.11 Side view of finite element model.

with no CNF content is reported below. The compliance coefficients for CNF/CF/epoxy composites are slightly different.

$$[C] = \begin{bmatrix} -3.054 & 0 & 0 & 0 & 0 & 0 & 0 & 0 \\ -5.869 & -3.507 & 0 & 0 & 0 & 0 & 0 & 0 \\ -8.163 & -6.019 & -3.444 & 0 & 0 & 0 & 0 & 0 \\ -9.683 & -7.461 & -5.152 & -2.511 & 0 & 0 & 0 & 0 \\ -13.737 & -11.250 & -8.774 & -6.289 & -3.485 & 0 & 0 & 0 \\ -19.697 & -16.707 & -13.749 & -10.826 & -7.9020 & -4.309 & 0 & 0 \\ -28.478 & -24.720 & -21.000 & -17.329 & -13.717 & -9.910 & -5.374 & 0 \\ -42.314 & -37.353 & -32.429 & -27.558 & -22.760 & -17.880 & -12.840 & -6.881 \end{bmatrix}$$

As shown in Fig. 13.12, the stresses are tensile through the 0-degree layers and compressive through the 90-degree layers. It is observed that the residual stress in almost all layers decreases by increasing the CNF content. In the third layer, the amount of residual stress increases. Generally, residual stress has more reduction in the layers that have more residual stress. The maximum tensile and compressive residual stress occurs at the fourth and fifth layers, respectively. Comparing the values of residual stresses at the fourth and fifth layers of 1 wt% CNF-reinforced CF/epoxy composite with CF/epoxy composite indicates that the residual stress in these layers decreases by about 38%.

In addition to reduction of residual stress in most layers, increase in the CNF content leads to more uniformity in the residual stress distribution. The uniformity of residual stress distribution can reduce the stress concentration across layers boundaries and delay the matrix cracking.

The change in residual stresses in different layers of CNF/CF/epoxy composites due to addition of CNFs is reported in Table 13.4. An average decrease of about 4.4, 18.8 and 25.1% in residual stress was observed with an addition of 0.1, 0.5 and 1 wt% of CNF, respectively.

Further investigations are required for higher weight fractions of CNF. However, attaining acceptable quality of the dispersion of the CNFs in higher weight fractions could create serious practical challenges. This is because when the content of CNFs reaches a certain limit, the possibility of CNFs aggregation

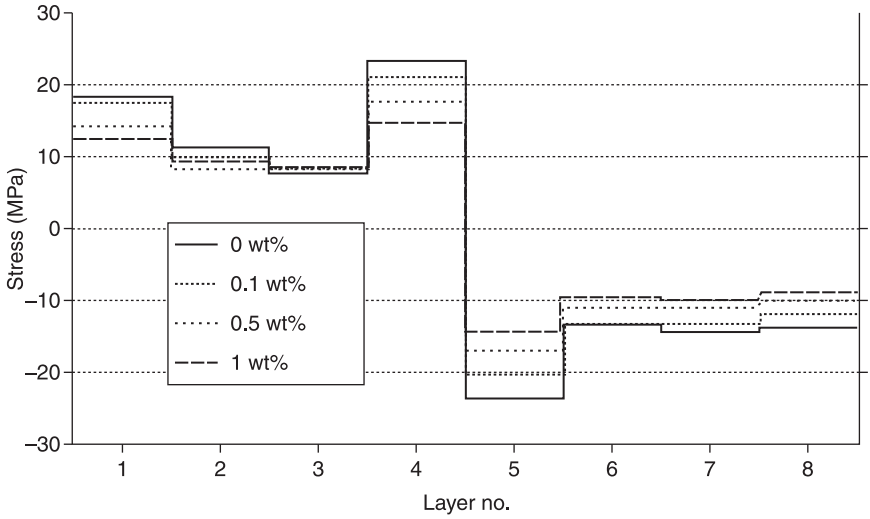

13.12 Residual stress distribution in $[0_4/90_4]_s$ CNF/CF/epoxy composites for different contents of CNFs.

Table 13.4 Change in residual stress (%) due to adding CNFs in different layers of $[0_4/90_4]_s$ CNF/CF/epoxy nanocomposites compared with CF/epoxy composites

	CNF wt%		
Layer no.	0.1	0.5	1
1	–4.3	–21.7	–32.6
2	–10.6	–26.5	–17.7
3	18.9	13.5	20.3
4	–10.2	–25.4	–38.1
5	–12.8	–25.6	–38.5
6	–2.2	–14.9	–29.9
7	–7.0	–23.8	–30.8
8	–11.6	–26.1	–33.3
Average	–4.4	–18.8	–25.1

significantly increases and the CNFs dispersion becomes inhomogeneous in the matrix.

13.4 Conclusions and future trends

Residual stresses in composites results from high contraction of the polymeric matrix in comparison with fibres during the curing and cooling processes of

fabrication. Such stresses are often ignored or neglected in the design of composites. As a result, misinterpretation may occur in characterizing the mechanical properties of the composites. There have already been some techniques to decrease residual stress in composites. However, all these approaches are confined to changing the layers arrangement or curing cycles. Thus, investigation of a practical method to decrease residual stresses in composites can be beneficial. A novel approach is to utilize the outstanding properties of nano-fillers. High Young's modulus and very low thermal coefficient expansion of nano-fillers make them appropriate to reduce residual stress in polymer composites.

This chapter has shown that decrease in thermal expansion and increase in tensile modulus of polymer matrix resulting from adding nano-fillers leads to the reduction of the residual stresses in laminated composites. It has been observed that adding nano-fillers to the epoxy matrix leads to an increase of Young's modulus and a decrease of the CTE of the matrix. Furthermore, nano-fillers effects on micro- and macro-residual stresses of laminated composites could be determined by using energy based models and CLT analysis. However, in order to exactly determine nano-filler effects on residual stresses in laminated composites, experimental methods should be employed.

In the final section of this chapter, the results of adding CNFs to $[0_4/90_4]_s$ carbon/epoxy laminates were experimentally investigated. First, the CNF/epoxy and CNF/CF/epoxy composites with desired contents of the CNF were fabricated. Then experimental characterization tests were carried out. It was observed that adding CNFs does not have a significant effect on the Young's modulus of epoxy, but extremely reduces its CTE. For CNF weight fractions of 0.1, 0.5 and 1%, matrix, CTE decreased by 6.3, 26.0 and 32.5%, respectively. The weight fraction of CNF was limited to 1 wt% due to the manufacturing challenges. Finally, the slitting method was employed to measure the residual stress in nanocomposite specimens with three different weight fractions of CNFs. An average decrease of about 4.4, 18.8 and 25.1% in residual stress was observed with an addition of 0.1, 0.5 and 1 wt% of CNF, respectively. Therefore, the incorporation of small values of CNFs into CF/epoxy laminates results in the significant reduction in residual stress. This is a direct result of the reduction of matrix CTE due to addition of CNFs.

The results described in this chapter indicate the significant effects of nano-additives in reducing residual stress in fibrous composites. This is because nano-fillers could reduce the mismatch between the fibre and matrix. However, it should be noted that the nano-fillers' influences on inter-phase properties and reaction of nano-fillers with the matrix have not been discussed in this chapter. Such phenomena may lead to the presence of the residual stress at the nano-scale.

Determining the effects of nano-fillers on residual stresses of composites needs further experimental investigations. Experimental studies on other matrices like metals and ceramics containing other conventional nano-fillers such as nanoclay and graphene is recommended. Also, this chapter only discussed the effects of nano-fillers on two main factors in the formation of residual stress, CTE and

Young's modulus. But nano-fillers can influence other parameters, such as glass transition temperature (T_g), moisture and chemical shrinkage of polymeric matrices. A deeper understanding of the 'nano-fillers' effects on such parameters is required. However, these parameters are generally less important in comparison with CTE and Young's modulus.

13.5 References

Alexandre, M. and Dubois, Ph. (2000) Polymer-layered silicate nanocomposites: preparation, properties and uses of a new class of materials, *Materials Science and Engineering*, **28**(1–2), 1–63.

American Society for Testing and Materials. *ASTM D638 Standard Test Method for Tensile Properties of Plastics*.

American Society for Testing and Materials. *ASTM D3039 Standard Test Method for Tensile Properties of Polymer Matrix Composite Materials*.

American Society for Testing and Materials. *ASTM E831 Standard Test Method for Linear Thermal Expansion of Solid Materials by Thermomechanical Analysis*.

ANSYS Help System, *Analysis Guide and Theory Reference*, Ver. 12.

Bhalerao, M. S. (1996) *On Process-induced Fibre Waviness in Composites: Theory and Experiments*, The University of Texas at Austin.

Borges de Almeida, J. (2005) *Analytical and Experimental Study on the Evolution of Residual Stresses in Composite Materials*, MSc Thesis, University of Porto.

Callister, W. D. J. (1994) *Materials Science and Engineering: An Introduction*, New York, John Wiley and Sons, Inc.

Chaos-Mora, R., Salazar, A. and Uren, A. (2011) Mechanical analysis of carbon nanofibre/epoxy resin composites, *Polymer Composites*, **32**(10), 1640–51.

Cho, M., Jang, J. and Suhr, J. (2011) Effect of filler geometry on coefficient of thermal expansion in carbon nanofibre reinforced epoxy composites, *Journal of Nanoscience and Nanotechnology*, **11**(2), 1098–102.

Deng, C. F., Ma, Y. X., Zhang, P., Zhang, X. X. and Wang, D. Z. (2008) Thermal expansion behaviors of aluminum composite reinforced with carbon nanotubes, *Materials Letters*, **62**, 2301–3.

Ersoy, N. and Vardar, O. (2000) Measurement of residual stresses in layered composites by compliance method, *Composite Materials*, **34**(7), 575–98.

Gentz, M., Armentrout, D., Rupnowski, P., Kumosa, L., Shin, E. and Sutter, J. (2004) In-plane shear testing of medium and high modulus woven graphite fibre reinforced/polyimide composites, *Composites Science and Technology*, **64**, 203–20.

Gonnet, P. (2004) *Thermal Conductivity and Coefficients of Thermal Expansion of SWNTS/Epoxy Nanocomposites*, MSc Thesis, Florida State University.

Hahn, H. T. and Pagano, H. J. (1975) Curing stresses in composite laminates, *Composite Materials*, **9**, 91–106.

Halpin, J. C. and Tsai, S. W. (1969) Effects of environmental factors on composite materials, AFML-TR-67-423, June.

Hine, P., Broome, V. and Ward, I. (2005) The incorporation of carbon nanofibres to enhance the properties of self reinforced, single polymer composites, *Polymer*, **46**, 10936–44.

Hodges, J., Yates, B., Darby, M. I., Wostenholm, G. H., Clement, J .F. and Keates, T. F. (1989) Residual stresses and the optimum cure cycle for an epoxy resin, *J. Mater. Sci.*, **24**, 1984–90.

Hsiao, K. T. and Gangireddy, S. (2008) Investigation on the spring-in phenomenon of carbon nanofibre-glass fibre/polyester composites manufactured with vacuum assisted resin transfer molding, *Composites: Part A*, **39**, 834–42.

Iijima, S. (1991) Helical microtubules of graphitic carbon, *Nature*, **354**, 56–58.

Iwahoria, Y., Ishiwatab, S., Sumizawab, T. and Ishikawa, T. (2005). Mechanical properties improvements in two-phase and three-phase composites using carbon nano-fibre dispersed resin, *Composites: Part A*, **36**(10), 1430–9.

Kim, J. K. and Mai Y. W. (1998) *Engineered Interfaces in Fibre Reinforced Composites*, Oxford, Elsevier Science Ltd, 308–20.

Kim, J. W., Lee, J. H., Kim, H. G., Kim, H.S. and Lee, D. G. (2006) Reduction of residual stresses in thick-walled composite cylinders by smart cure cycle with cooling and reheating, *Composite Structures*, **75**, 261–6.

Lawrence, W. E., Manson, J. A. E. and Seferis, J. C. (1990) Thermal and morphological skin core effects in processing of thermoplastic composites, *Composites*, **21**(6), 475–80.

Lee, M. J. and Hill, M. R. (2007) Intra-laboratory repeatability of residual stress determined by the slitting method, *Experimental Mechanics*, **47**(6), 745–52.

Miller, S. G. (2008) *Effects of Nanoparticle and Matrix Interface on Nanocomposite Properties*, DPhil Thesis, University of Akron, Polymer Science.

Naganuma, T. and Kagawa, Y. (2002) effect of particle size on the optically transparent nano meter-order glass particle-dispersed epoxy matrix composites, *Composites Science and Technology*, **62**(9), 1187–9.

Nairn, J. A. (1997) Fracture mechanics of composites with residual thermal stresses, *Applied Mechanics*, **64**, 804–15.

Nishino, T., Kotera, M. and Sugiura, Y. (2009) residual stress of particulate polymer composites with reduced thermal expansion, *Journal of Physics: Conference Series*, **184**, 12026.

Prime, M. B. (1999) Residual stress measurement by successive extension of a slot: the crack compliance method, *Journal of Applied Mechanics*, **52**(2), 75–96.

Quek, M. Y. (2004) Analysis of residual stresses in a single fibre-matrix composite, *Adhesion and Adhesives*, **24**, 379–88.

Schajer, G. S. (1993) Use of displacement data to calculate strain gauge response in non-uniform strain fields, *Strain*, **29**, 9–13.

Shokrieh, M. M. and Kamali, S. M. (2005) Theoretical and experimental studies on residual stresses in laminated polymer composites, *Composite Materials*, **39**(24), 2213–25.

Shokrieh, M. M. and Safarabadi, M. (2011) Effects of imperfect adhesion on thermal micro-residual stresses in polymer matrix composites, *Adhesion and Adhesives*, **31**(6), 490–7.

Shokrieh, M. M. and Akbari R. S. (2012a) Simulation of slitting method for alculation of compliance functions of laminated composites, *Composite Materials*, **46**(9), 1101–9.

Shokrieh, M. M. and Safarabadi, M. (2012b) Three-dimensional analysis of micro-residual stresses in fibrous composites based on the energy method: a study including interphase effects, *Composite Materials*, **46**(6), 727–35.

Sjogren, A., Joffe, R., Berglund L. and Mader, E. (1999) Effects of fibre coating (size) on properties of glass fibre vinyl ester composites, *Composites: Part A*, **30**(8), 1009–15.

Sicot, O., Gong, X. L., Cherouat, A. and Lu, J. (2003) Determination of residual stress in composite laminates using the incremental hole-drilling method, *Composite Materials*, **37**(9), 831–44.

Thostenson, E. T., Li, C. and Chou T. W. (2005) Nanocomposites in context, *Composites Science and Technology*, **65**, 491–516.

Wang, T. M., Daniel, I. M. and Gotro, J. T. (1992) Thermo-viscoelastic analysis of esidual stresses and warpage in composite laminates, *Composite Materials*, **26**(6), 883–99.

Wang, D. H., Sihn, S., Roy, A. K, Baek, J. B. and Tan, L. S. (2010) Nanocomposites based on vapor-grown carbon nanofibres and an epoxy: Functionalization, preparation and characterization, *European Polymer Journal*, **46**(7), 1404–16.

White, S. R. and Hahn, H. T. (1993) Cure cycle optimization for the reduction of processing-induced residual stresses in composite materials, *J. Comp. Mater.*, **27**, 1352–78.

Xu, Y., Ray, G. and Abdel-Magid, B. (2006) Thermal behavior of single-walled carbon nanotube polymer–matrix composites, *Composites: Part A*, **37**, 114–21.

Index